UNIVERSIDAD COMPLUTENSE DE MADRID

FACULTAD DE CIENCIAS GEOLÓGICAS

DEPARTAMENTO DE PETROLOGÍA Y GEOQUÍMICA

ROCAS EN FACIES DE ESQUISTOS AZULES DEL COMPLEJO DE MALPICA-TUY (NO DEL MACIZO IBÉRICO)

ROCHES DU FACIES DES SCHISTES BLEUS DU COMPLEXE DE MALPICA-TUY (NO DU MASSIF IBÉRIQUE)

BLUESCHIST-FACIES ROCKS FROM THE MALPICA-TUY COMPLEX (NW IBERIAN MASSIF)

TESIS DOCTORAL DE:

ALICIA LÓPEZ CARMONA

BAJO LA DIRECCIÓN DE:

JACOBO ABATI, PAVEL PITRA

Madrid, 2014

TESIS DOCTORAL

ROCAS EN FACIES DE ESQUISTOS AZULES DEL COMPLEJO DE MALPICA-TUI (NO DEL MACIZO IBÉRICO)

ROCHES DU FACIÈS DES SCHISTES BLEUS DU COMPLEXE DE MALPICA-TUI (NO DU MASSIF IBÉRIQUE)

Alicia López Carmona

2013

Departamento de Petrología y Geoquímica
Facultad de Ciencias Geológicas
Universidad Complutense de Madrid

Géosciences Rennes
UMR 6118
Université de Rennes 1

TESIS DOCTORAL

ROCAS EN FACIES DE ESQUISTOS AZULES DEL COMPLEJO DE MALPICA-TUI (NO DEL MACIZO IBÉRICO)

ROCHES DU FACIÈS DES SCHISTES BLEUS DU COMPLEXE DE MALPICA-TUI (NO DU MASSIF IBÉRIQUE)

BLUESCHIST-FACIES ROCKS FROM THE MALPICA-TUI COMPLEX (NW IBERIAN MASSIF)

Alicia López Carmona

Madrid, 2013

Departamento de Petrología y Geoquímica
Facultad de Ciencias Geológicas
Universidad Complutense de Madrid

Géosciences Rennes
UMR 6118
Université de Rennes 1

TESIS DOCTORAL *presentada por:*

ALICIA LÓPEZ CARMONA

para obtener el grado de: DOCTOR EN GEOLOGÍA POR LA UNIVERSIDAD COMPLUTENSE DE MADRID

Mención: DOCTOR EUROPEO

ROCAS EN FACIES DE ESQUISTOS AZULES DEL COMPLEJO DE MALPICA-TUI (NO DEL MACIZO IBÉRICO)

TESIS DOCTORAL *dirigida por:*

JACOBO ABATI	Profesor Titular, Université Complutense de Madrid
PAVEL PITRA	Profesor Titular, Université de Rennes 1

Jacobo Abati

Pavel Pitra

Departamento de Petrología y Geoquímica
Facultad de Ciencias Geológicas
Universidad Complutense de Madrid

Géosciences Rennes
UMR 6118
Université de Rennes 1

THÉSE présentée par:

ALICIA LÓPEZ CARMONA

pur obtenir le grade de: DOCTEUR DE L'UNIVERSITÉ DE RENNES 1

Mention: SCIENCIES DE LA TERRE–GÉOLOGIE

ROCHES DU FACIÈS DES SCHISTES BLEUS DU COMPLEXE DE MALPICA-TUI (NO DU MASSIF IBÉRIQUE)

THÉSE dirigée par:

JACOBO ABATI	Maître de conférences, Université Complutense de Madrid
PAVEL PITRA	Maître de conférences, Université de Rennes 1

Jacobo Abati

Pavel Pitra

Departamento de Petrología y Geoquímica
Facultad de Ciencias Geológicas
Universidad Complutense de Madrid

Géosciences Rennes
UMR 6118
Université de Rennes 1

Esta Tesis Doctoral ha sido realizada en el Departamento de Petrología y Geoquímica de la Universidad Complutense de Madrid y en el Departamento de Géosciences Rennes-UMR 6118 de la Universidad de Rennes 1 en el marco de un convenio de codirección firmado por ambas universidades.

Cette thèse de doctorat a été réalisée au Département de Pétrologie et Géochimie de l'Université Complutense de Madrid et au Département de Géosciences Rennes-UMR 6118, Université de Rennes 1 en vertu d'un accord de cotutelle signé par les deux universités.

Esta tesis se ha realizado durante el disfrute de una Ayuda de Formación de Personal Invesigador (BES-2008-002410) del Ministerio de Ciencia e Innovación y ha sido financiada por el PROYECTO COORDINADO CONSOLIDER CGL2007-65338-C02-01 "De Rodinia a Pangea: 1100 Ma de historia geológica en el basamento del NW de Iberia" financiado por la Dirección General de Investigación dentro del Plan Estatal de I+D+i del Ministerio de Ciencia e Innovación.

A mis padres y a mi hermano

José Miguel, Pilar y David

Agradecimientos

Tras estos años de trabajo tengo mucho que agradecer…

A mis directores, Jacobo Abati y Pavel Pitra, thank you both for all you have taught me, for your effort and experience. Without your guidance this PhD thesis won't be the same, and me neither.

Jacobo, gracias por tu apoyo y orientación a lo largo de este tiempo, por permitirme aprender con tanta libertad y por haber respetado siempre mis planteamientos. Te estoy muy agradecida por haberme cedido un "cachito de tu Malpica" y por tu intuición para muestrear, sin la que aún no se habría descrito la glaucofana en la Unidad de Ceán. Ticher, gracias por todos los buenos momentos.

Pavel, thanks for transmitting me your always unsatisfied curiosity that allows one to go further and further...For all your advices and for showing me the guts of that lovely science…physicochemistry. With you all things seemed easier. I´m very grateful for your care during my stays at Rennes, not only in the scientific aspects, but also personally. It was great!.

Ricardo, gracias por aquella llamada sin la que esta tesis no existiría. Nunca te estaré lo suficientemente agradecida por haberme ofrecido la oportunidad de hacer lo que más me gusta y por poner todos los medios para que haya salido bien.

He tenido el privilegio de contar con el apoyo de José Ramón Martínez Catalán y Michel Ballévre, que han contribuido de manera decisiva en las distintas etapas de desarrollo de este trabajo. Thanks to them I have been involved in a correlation study during which I learned from the best. Priceless!.

José Ramón, es muy difícil agradecerte sólo con unas líneas el respeto y cariño con el que siempre me has tratado. Tu inestimable ayuda en el campo, en las interpretaciones, cada discusión, y sobre todo tu constante apoyo tanto en lo personal como en lo profesional. Aunque sé que no estamos de acuerdo, siempre te he sentido como otro director más de este trabajo. Muchas gracias por todo.

Michel, visiting Ile de Groix with you each year, knowing each of its hidden corners, from the hand of a naturalist, has been more than a privilege. However, it is not necessary to travel to learn with you. Simply staying at your office is enough gazing at your huge library

or sampling in the rock museum hidden in your drawers. Thanks for kindly sharing your knowledge with me.

I am very grateful to James K.W. Lee for his supervision during my stay at Queen's University and for our subsequent collaboration. The $^{40}Ar/^{39}Ar$ contribution of this PhD thesis is owed to his teaching. I also wish to thank the technical assistance of D.A. Archibald and H. Fournier from the Queen's University $^{40}Ar/^{39}Ar$ Geochronology Laboratory. Jim, during my stay at Kingston I felt as another member of your family, thanks to you, Sally, Ashley and Carolyn for your warm welcome and for the great time we spent together!.

Very special thanks to M. Santosh and Timothy M. Kusky for giving me the opportunity to study such beautiful rocks. With you both I learned much more than the geology of the Chugach terrain. I enjoyed a lot!...hope to meet you soon!.

A Javier (sólo) Rodríguez y Antonio García Casco les agradezco mucho el generoso esfuerzo que han hecho revisando el manuscrito tan exhaustivamente.

A Javier le doy las gracias por sus siempre constructivas críticas, por aquel muestreo en el que compartimos tantas ideas y que supuso un giro al planteamiento de este trabajo, por haber sido tan accesible y haber compartido su conocimiento conmigo, sin tapujos, estos años.

A Antonio mis más cariñosas gracias por su altruismo científico, por sus sabios y respetuosos consejos y por sus enérgicos y motivadores planteamientos en las discusiones.

I greatly appreciate Francisco Pereira and Romain Bousquet big free-effort reviewing this manuscript. Thanks to both for your constructive comments.

Agradezco a Joan Reche, mi codirector durante el DEA, que me introdujese en algo tan complejo y apasionante como las pseudosecciones.

Gracias a los compañeros del equipo de investigación, de la Universidad Complutense y de la Universidad de Salamanca, en el que he crecido: Pedro, Rubén, Alejandro, Emilio, Pilar, Sonia, Icaro y Chema.

Gracias a los miembros del Departamento de Petrología y Geoquímica por tratarme con tantísimo cariño estos años y haber hecho que me encuentre tan a gusto. Si os nombro a todos me excederé aún más, y me resulta imposible no escribir cada nombre. Pero quiero dar unas gracias muy especiales a Mª José, gracias por esos momentos, que en ocasiones

se exceden de lo estrictamente académico, y que son tan necesarios y gratificantes. A Mercedes por haberme seguido tan de cerca estos años. A Jose Andrés y Fale, por estar siempre pendientes de todos los detalles. José Andrés, qué habría hecho estos años sin ti?. A los compis de despacho con los que he compartido taaaantas horas, Rebeca, Andrea, Maricarmen, Silvia…

Sin vuestro apoyo administrativo y técnico…Bea, ¡mi Bea!, y Miguel Ángel siempre ahí, pendientes de todo. Carmen, Pedro y Marian, gracias a los tres. Carmen, ni tu ayuda en la separación mineral ni las sesiones de "terapia" tienen precio!. Hago unas láminas estupendas gracias a Pedro, que me enseñó con mucha paciencia. Alfredo y Pepe, sin palabras. Qué sería de mí sin vosotros en esas interminables sesiones de microsonda. Xavi, muchísimas gracias por tu ayuda con el SEM. Jose Antonio, muchas gracias por tu dedicación y detalladas explicaciones en el tratamiento químico de las muestras para Sm/Nd. Gracias a todos.

Merci aux membres du Département de Géosciences Rennes pour son accueil chaque année. Particulièrement, je me souviens avec émotion des moments passés avec Lorraine et Camille.

Son muchas más las personas que han contribuido a que esta tesis se haya completado felizmente, sobre todo en el ámbito personal: amigos y familia, GRACIAS!.

Javier, has estado ahí desde el principio. Jamás dudaste. Gracias por esos cofis mágicos que lo curan casi todo… Gabi, gracias por todo y más, pero sobre todo por tu generosidad y por enseñarme a tener paciencia…Mi Mari guapa!, sin tu apoyo todo habría sido mucho más difícil. Gracias por escucharme, aconsejarme, consolarme y por estar siempre para mí. Pepa y Jose, gracias pareja!, qué suerte haberos conocido. A mis chicas, Cristina, Belén, Nuria, Paloma, Mairena, Almudena y a David, habéis sido una constante estos años. Gracias por todos los buenos ratos de diversión, charla, lloros, confidencias…y lo que nos queda!. Dani e Inés, infinitas gracias por vuestro apoyo. Nos vemos en Utrecht!. A mis "sintesis", Ángela, Kike, Richard, Davi, Álvaro, por endulzarme la recta final de la tesis con tanto optimismo y tantísimos buenos momentos. Amigos así no hay muchos y he tenido la suerte de encontrar el tesoro!.

Por último, quiero agradecer a mi familia su apoyo incondicional. Esta tesis se la debo a mis padres, que siempre me han dejado elegir y me han apoyado en todas y cada una de mis decisiones. Mamá, hemos hecho la tesis a la vez. Has sido mi amiga, mi confidente, mi consejera…lo has sido todo. Sin tu apoyo no lo habría conseguido. Mamá, Papá y David, vuestro cariño y comprensión han sido fundamentales. Muchas gracias a los tres.

ABSTRACT

Blueschist-facies terranes in the Ibero-Armorican Arc are restricted to scarce and relatively small areas. One of these examples is the Ceán Unit that constitutes the westernmost exposure of the Middle Allochthon in the NW Iberian Massif, and in the Variscan belt of Western Europe. The Ceán Unit is interpreted as a volcano-sedimentary sequence that probably represents part of the cover of a transitional to oceanic crust, associated with the outermost sections of the north Gondwana margin during its subduction below Laurussia. Thus, constraints on the P–T paths of rocks from this terrain are essential to understand the characteristics and mechanisms of the subduction of this margin. The Ceán Unit forms the upper tectonic sheet of the Malpica-Tui Complex and comprises variable proportions of glaucophane-chloritoid-bearing metapelites (Ceán pelitic schists) and mafic rocks with abundant well-preserved pseudomorphs after euhedral lawsonite (Cambre metabasic rocks). The main objective of this research consists in a detailed study of the metamorphic evolution of these lithologies using pseudosection approach.

Petrological analysis involving P–T–X pseudosections in the MnNCKFMASHTO chemical system in both metapelitic and metabasic rocks shows that the Ceán Unit recorded a three-stage metamorphic evolution involving (i) early subduction-related MP/LT metamorphism (M_1) roughly constrained at 350–380 °C and 12–14 kbar, which is only preserved in the basal part of the sequence. (ii) Subduction-related blueschist/LT-eclogite-facies prograde metamorphism (M_2) characterized by a H_2O-undersaturated prograde P–T path peaking at 19–22 kbar, corresponding to a maximum burial of ca. 65–70 km. (iii) Exhumation-related metamorphism (M_3/post- M_3) occurred in two stages (1) a nearly isothermal decompression from ca. 70 to ca. 30 km, characteristic of slow and long-lasting accretionary-wedge subdution type and (2) a phase of fast cooling once the rocks have reached an upper crustal level.

The results obtained from numerical modelling calculations on the effects of H_2O and Fe_2O_3 in the metamorphic evolution of blueschist-facies rocks yielded first-order constraints for geodynamic models that may have a general application in the investigation of rocks with similar composition. (i) This research proposes that subduction zone metamorphism may occur in H_2O-undersaturated conditions induced by the crystallization of a significant modal amount of lawsonite. Then, the transition from lawsonite blueschist-facies to amphibolite-greenschist facies may involve significant hydration, principally as a result of lawsonite breakdown. (ii) The proportion of ferric iron has a strong influence on phase equilibrium. The analysed values of Fe_2O_3 may not reflect the oxidation state during the main metamorphic evolution and are probably easily modified by superficial alteration even in apparently fresh samples. Then, the use of P–T–X(H_2O/Fe_2O_3) pseudosections together a thorough petrographic investigation, and an extensive knowledge on the mineral chemistry and the textural relationships is then

necessary to estimate the extent of fluid-saturation during subduction zone metamorphism and the real oxidation state of the rocks to correctly evaluate the P–T conditions.

The age of the peak blueschist-facies metamorphism has been constrained at ca. 363±2 Ma by $^{40}Ar/^{39}Ar$ step-heating of phengitic muscovite from the pelitic schists. $^{40}Ar/^{39}Ar$ dating of muscovite from the quartzo-feldspathic mylonites of the Bembibre-Ceán detachment, at the base of the Ceán Unit, yields an age of ca. 337±3 Ma, interpreted as the age that marks the beginning of the post-nappe extensional tectonics that led to the gravitational collapse of the orogen. Differences between the HP/LT event, and the beginning of the post-nappe tectonics, suggest an exhumation rate of 2–2.5 mm/year for the Malpica-Tui Complex. These ages support the equivalence of the Ceán Unit and its counterpart in the Armorican Massif, the Upper Unit of Ile de Groix, and suggest that both terranes share a blueschist-facies event constrained at ca. 360–370 Ma, that may represent the Late Devonian-Early Carboniferous subduction of the northern margin of Gondwana beneath Laurussia, at the onset of the Variscan collision.

RESUMEN

Los afloramientos de terrenos en facies de esquistos azules en el Arco Ibero-Armoricano son escasos y se limitan a áreas relativamente pequeñas. Uno de estos ejemplos es la Unidad de Ceán, que constituye el afloramiento más occidental del Alóctono Medio en el NO del Macizo Ibérico, y en el cinturón de Varisco Europeo. La Unidad de Ceán se interpreta como una secuencia volcanosedimentaria que probablemente representa parte de la cobertera de una corteza transicional a oceánica, asociada a las secciones más externas del margen norte de Gondwana durante su subducción bajo Laurussia. Por tanto, deducir las trayectorias P–T de las litologías de la unidad de Ceán resulta esencial para comprender los mecanismos y las características de la subducción de este margen. La Unidad de Ceán constituye la lámina tectónica superior del Complejo Malpica-Tui y está formada por proporciones variables de metapelitas con glaucofana y cloritoide (esquistos de Ceán) y metabasitas con abundantes pseudomorfos de lawsonita bien preservados (metabasitas de Cambre). El principal objetivo de esta investigación consiste en un estudio detallado de la evolución metamórfica de estas litologías mediante el cálculo de pseudosecciones.

El análisis petrológico y termobarométrico utilizando pseudosecciones P–T–X en el sistema químico MnNCKFMASHTO en ambas litologías ha permitido deducir tres etapas en la evolución metamórfica de la Unidad de Céan: (i) un evento de MP/BT (M_1) asociado al comienzo de la subducción que únicamente ha quedado registrado en la parte basal de la secuencia, cuyas condiciones P–T aproximadas se han establecido en 350–380°C y 12–14 kbar. (ii) El metamorfismo prograd asociado a la subducción en facies de esquistos azules/eclogitas de

BT (M_2) se caracteriza por una evolución subsaturada en H_2O. Las condiciones del pico bárico se han establecido en 19–22 kbar, correspondientes a un enterramiento máximo de ca. 65–70 km. (iii) El metamorfismo asociado a la exhumación de la unidad (M_3/post-M_3) se desarrolló en dos etapas: (1) una etapa de descompresión casi isotérmica desde ca. 70 a ca. 30 km de profundidad, característica de una subducción lenta y prolongada, y (2) una fase de enfriamiento rápido una vez las rocas han alcanzado los niveles corticales superiores.

Los resultados obtenidos de la modelización petrológica en relación a los efectos del H_2O y del Fe_2O_3 en la evolución metamórfica de las rocas en facies de esquistos azules permiten establecer estimaciones de primer orden en los modelos geodinámicos que podrían tener una aplicación general en la investigación de rocas con una composición "similar". (i) Esta investigación propone que en presencia de una proporción modal significativa de lawsonita el metamorfismo prograd en zonas de subducción puede tener lugar en condiciones de subsaturación en in H_2O. Posteriormente, la transición entre la facies de esquistos azules con lawsonita y la facies de esquistos verdes podría implicar una importante liberación de H_2O durante la retrogradación, que procedería de la desestabilización de dicho mineral. (ii) La proporción de hierro férrico considerada en la modelización petrológica influencia notablemente el equilibrio de fases mineralógicas. El porcentaje estimado de Fe_2O_3 mediante el análisis de roca total podría no reflejar el estado de oxidación real de la roca durante la evolución metamórfica principal. Este estudio refleja que la proporción analizada podría ser el reflejo de la sensibilidad de dicho componente a variaciones ambientales tales como la alteración superficial de la roca, incluso en muestras aparentemente frescas. Por tanto, el cálculo de pseudosecciones P–T–X(H_2O/Fe_2O_3), combinado con un estudio petrográfico exhaustivo, además de un amplio conocimiento de la química mineral y las relaciones texturales, resulta necesario para establecer si existieron condiciones de subsaturación en H_2O (u otro/s fluidos) durante la etapa prograda de la evolución metamórfica de la roca, así como para determinar una aproximación razonable a su estado de oxidación real, lo que posibilitará establecer de forma precisa la evolución de las condiciones P–T.

La edad del pico metamórfico en facies de esquistos azules se ha estimado en ca. 363±2 Ma mediante $^{40}Ar/^{39}Ar$ en fengitas de los esquistos pelíticos. El mismo método aplicado en moscovitas de las milonitas cuarzo-feldespáticas que representan el despegue de Bembibre-Ceán, en la base de la Unidad de Ceán, proporcionó una edad de ca. 337±3 Ma, interpretada como la edad que marca el comienzo de la tectónica extensional, tras el apilamiento de las láminas alóctonas, y que condujo al colapso gravitacional del orógeno. Las diferencias entre el evento de AP/BT y el comienzo de la tectónica extensional, sugieren que el Complejo de Malpica-Tui se exhumó a una velocidad de 2-2.5 mm/año. Los datos obtenidos apoyan la equivalencia establecida entre la Unidad de Ceán y el terreno homólogo en el Macizo Armoricano, la Unidad Superior de la Isla de Groix. Ambos terrenos experimentaron una evolución en facies de

esquistos azules datada en ca. 360–370 Ma, que se interpreta como la subducción durante finales del Devónico-comienzos del Carbonífero del margen norte de Gondwana bajo Laurussia, al comienzo de la colisión Varisca.

RÉSUMÉ

Les terrains en faciès des schistes bleus dans l'Arc Ibéro-Armoricain sont rares et limités à de petits domaines. Un de ces exemples est l'unité de Ceán qui constitue l'affleurement le plus occidental de l'Allochtone moyen dans le NO du Massif Ibérique et dans la chaîne varisque de l'Europe occidentale. L'unité de Ceán est interprétée comme une séquence volcano-sédimentaire qui représente probablement la couverture d'une croûte transitionnelle ou océanique, associée aux parties les plus externes de la marge nord du Gondwana lors de sa subduction sous le Laurussia. Les informations sur l'évolution P–T de roches de ce terrain sont donc essentielles pour comprendre les caractéristiques et les mécanismes de la subduction de cette marge. L'unité de Ceán forme la partie supérieure du Complexe de Malpica-Tui (MTC) et comprend des proportions variables de métapélites à glaucophane-chloritoïde (les schistes pélitiques de Ceán) et de roches mafiques avec d'abondants pseudomorphes de lawsonite automorphe bien préservés (les roches métabasiques de Cambre). L'objectif principal de cette recherche est une étude détaillée de l'évolution métamorphique de ces lithologies à l'aide de diagrammes de phases (pseudosections) calculés.

L'analyse pétrologique à l'aide des pseudosections P–T–X dans le système chimique MnNCKFMASHTO appliquée à la fois aux roches métapélitiques et métabasiques montre que l'unité de Ceán a enregistré une évolution métamorphique en trois étapes. (i) Un métamorphisme précoce (M_1), lié à la subduction, contraint approximativement à 350–380°C et 12–14 kbar, est uniquement préservé dans la partie basale de la séquence. (ii) Un métamorphisme prograde dans le faciès des schistes bleus/éclogites de BT (M_2), lié à la subduction, est caractérisé par une évolution P–T prograde sous-saturée en H_2O et atteint son pic à 19–22 kbar. Cela correspond à un enfouissement d'environ 65–70 km. (iii) Un métamorphisme lié à l'exhumation (M_3, post-M_3) s'est développé en deux phases (1) une décompression sub-isotherme de 70 à 30 km, caractéristique des zones de subduction lentes, à fonctionnement prolongé et (2) une phase de refroidissement rapide lorsque les roches ont atteint les niveaux crustaux supérieurs.

Les résultats obtenus à partir de la modélisation numérique des effets du H_2O et Fe_2O_3 dans l'évolution des roches du faciès des schistes bleus ont donné des contraintes de premier ordre pour les modèles géodynamiques qui peuvent avoir une application générale. (i) Cette étude propose que le métamorphisme des zones de subduction peut se développer dans des conditions de sous-saturation en H_2O, liées à la cristallisation de la lawsonite. La transition

entre le faciès schistes bleus à lawsonite et le faciès des amphibolites / schistes verts produit une hydratation significative qui est principalement le résultat de la déstabilisation de la lawsonite. (ii) La proportion du fer ferrique à une forte influence sur les équilibres de phases. Les valeurs analysées du Fe_2O_3 ne reflètent pas nécessairement l'état d'oxydation pendant les principales étapes de l'évolution métamorphique et sont probablement facilement modifiées par l'altération superficielle, même dans les échantillons frais en apparence. L'utilisation des pseudosections P/T-X(H_2O/Fe_2O_3) avec une analyse pétrographique détaillée (incluant une bonne connaissance de la composition chimique des minéraux et de leurs relations texturales) est alors nécessaire pour estimer le degré de saturation en fluide et l'état réel oxydation afin d'évaluer correctement les conditions P-T pendant le métamorphisme de subduction.

L'âge du pic du métamorphisme dans le faciès des schistes bleus a été contraint à environ 363±2 Ma par la méthode $^{40}Ar/^{39}Ar$ sur muscovite phengitique des schistes pélitiques. Les datations sur les muscovites des mylonites quartzo-feldspathiques du détachement de Bembibre-Ceán, à la base de l'unité de Ceán a donné un âge d'environ 337±3 Ma. Cet âge est interprété comme le début de la tectonique en extension qui mène au collapse gravitationnel de l'orogène. Les différences entre l'événement HP/BT et le début de la tectonique post-nappes suggèrent une vitesse d'exhumation de 2-2,5 mm/an pour le complexe de Malpica-Tui. Ces âges supportent l'équivalence de l'unité de Ceán avec l'unité supérieure de l'Ile de Groix dans le Massif Armoricain et suggèrent que les deux terrains partagent le même événement en faciès des schistes bleus vers 360-370 Ma qui peut représenter la subduction tardi-dévonienne-carbonifère précoce de la marge nord du Gondwana sous le Laurussia, au début de la tectonique varisque.

Figures at the chapter´s header design are reproductions from the originals created by V. Vasarely (Hungary, 1906-1997)

CHAPTER 1

Introduction

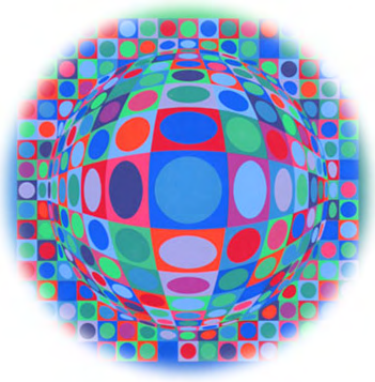

1. INTRODUCTION

1.1 *Scope of this PhD thesis*

Earth is the only known planet with subduction zones and plate tectonics (*e.g.* Stevenson, 2003). This observation indicates special thermo-mechanical conditions that led to this particular mode of planetary heat loss. Subduction zones are highly effective endogenous Earth systems of heat and mass transport of unparalleled scale and complexity. They represent our planet´s largest lithospheric recycling system, with profound implications for plate motions, the formation of continental crust or even long-term climate change (*e.g.* Ernst, 1999; Stern, 2002). Sinking of cold, dense lithosphere in subduction zones is the principal plate-driving force, triggering orogenesis at continental margins. The descent of relatively cold slabs into the mantle leads the formation of high-pressure (HP) and low (LT) to medium-temperature (MT) metamorphic rocks known as blueschists and eclogites, frequently found in the suture zones of mountain belts exhumed by tectonics from mantle depths to crustal shallow levels (*e.g.* Miyashiro, 1967; Dewey & Bird, 1970; Ernst, 1971; 1973; Coleman, 1972; Colleman *et al.*, 1974; van Keken *et al.*, 2002; Omori *et al.*, 2009).

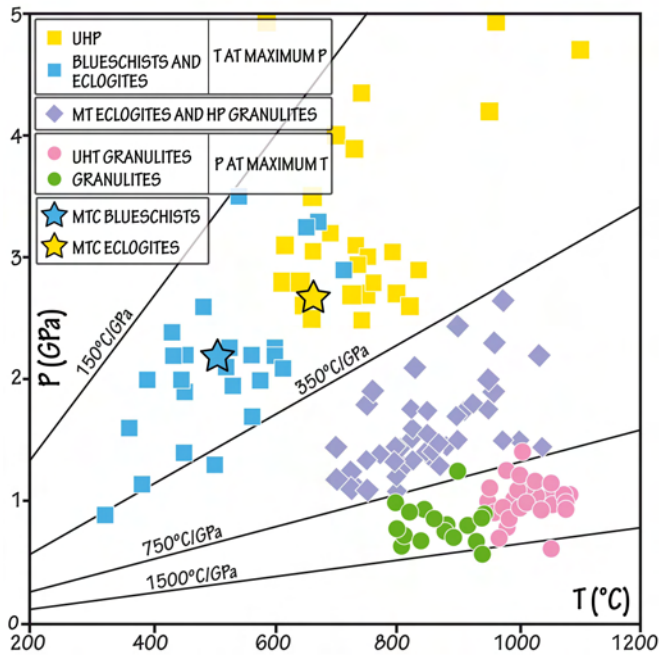

FIGURE 1. P–T diagram showing peak conditions of 140 metamorphic belts. Stars highlight the Malpica-Tui Complex (MTC) high-pressure rocks. HP–high-pressure; UHP/T–ultra-high pressure/temperature; MT–medium temperature. Modified after Brown (2010).

The tectonic significance of blueschist and eclogite assemblages, as markers of active and fossil subduction zones, has attracted great interest among Earth scientists (FIGURE 1; cf. Miyashiro, 1961; Takeuchi & Uyeda, 1965; Oxburgh & Turcotte, 1970; Hasebe *et al.*, 1970; Ernst, 1973; Fryer & Fryer, 1987; Peacock, 1989). The valuable information that can be obtained from these rocks is pivotal in unravelling important aspects regarding the thermal history of the Earth, the tectonic and metamorphic processes that take place at destructive plate boundaries or the

early stages of mountain building (e.g. Murphy & Nance, 1991; Maekawa *et al.*, 1993; Platt, 1993; Hacker, 1996; Maruyama *et al.*, 1996; Ernst, 2001; Gutiérrez-Alonso *et al.*, 2003; Hacker *et al.*, 2003; Bousquet *et al.*, 2005; Stern, 2005; Murphy *et al.*, 2009a; Pereira *et al.*, 2010; Sandiford, 2010). From the oldest HP belt, of about 700 to 800 Ma, exposed in the Pan-African Orogen (Caby, 1994; Kröner & Stern, 2004 and references therein) to the youngest one (late Miocene in age) reported in eastern Indonesia (Berry & McDougall, 1986; Maruyama *et al.*, 1996; Kadarusman *et al.*, 2010), over 250 HP belts have been documented (Maruyama *et al.*, 1996). That huge amount of information concerning the tectonic significance of blueschists and eclogites in plate tectonics has led to a better understanding of orogeny at convergent plate boundaries and the evolution of continents in the past (e.g. England & Thompson, 1984; Barber, 1982; England, 1987; Windley, 1995; Caddick & Thompson, 2008).

In this context, the study of the paleogeography and dynamics of the lithospheric plates during the Paleozoic in the peri-Gondwanan realm has been the stage for numerous works over the past decades, but many questions still remain unresolved. Particularly, the northwest section of the Iberian Massif offers a paramount example to understand the evolution of the European Variscan belt. A key aspect of this section is the presence of one of the major sutures of the belt, preserved in allegedly exotic terranes forming a huge and complex allochthonous sheet emplaced upon the Neoproterozoic to Paleozoic sequences deposited on the passive margin of northern Gondwana (Martínez Catalán *et al.*, 2009).

The research carried out in this PhD thesis consists in a detailed study of the metamorphic evolution of the HP rocks from the Middle Allochthon of the Malpica-Tui Complex (MTC; Galicia, NW Iberian Massif) through pseudosection approach. One of the main aims of this investigation, besides the contribution to the geological knowledge of the MTC, is mastering the theory and practice of building phase diagrams using scientific software tools for petrologic modelling such as THERMOCALC (Powell & Holland, 1988) and PERPLE_X (Connolly, 1990). Additionally, a comprehensive $^{40}Ar/^{39}Ar$ geochronological study in key samples has been carried out with the aim of establishing an absolute time framework for the metamorphic evolution of the studied rocks.

The MTC is an outstanding example of a subducted continental margin. This terrane is the westernmost basal unit exposed in the NW Iberian Massif, and is interpreted to represent the subduction of the most external margin of north Gondwana below the southern margin of Laurussia at the onset of the Variscan convergence (FIGURE 2; Martínez Catalán *et al.*, 1996; 2007; Arenas *et al.*, 2007a). Therefore, constraints on the P–T paths of rocks from this terrane are essential to understand the characteristics and mechanisms of the subduction of this margin.

Currently, the information about the metamorphic evolution of subducted terranes obtained through petrologic modelling is at the core of the geodynamic models and paleogeographic reconstructions of the lithospheric plates (cf. Will *et al.*, 1998). Applying pseudosection approach to bulk compositions of the HP rocks of the MTC can provide a reliable and innovative interpretation of the metamorphic evolution of the northern margin of Gondwana in Iberia, as these diagrams are at present the most suitable approach to analyse the mineral variations in a rock driven by changes in the P–T–t conditions.

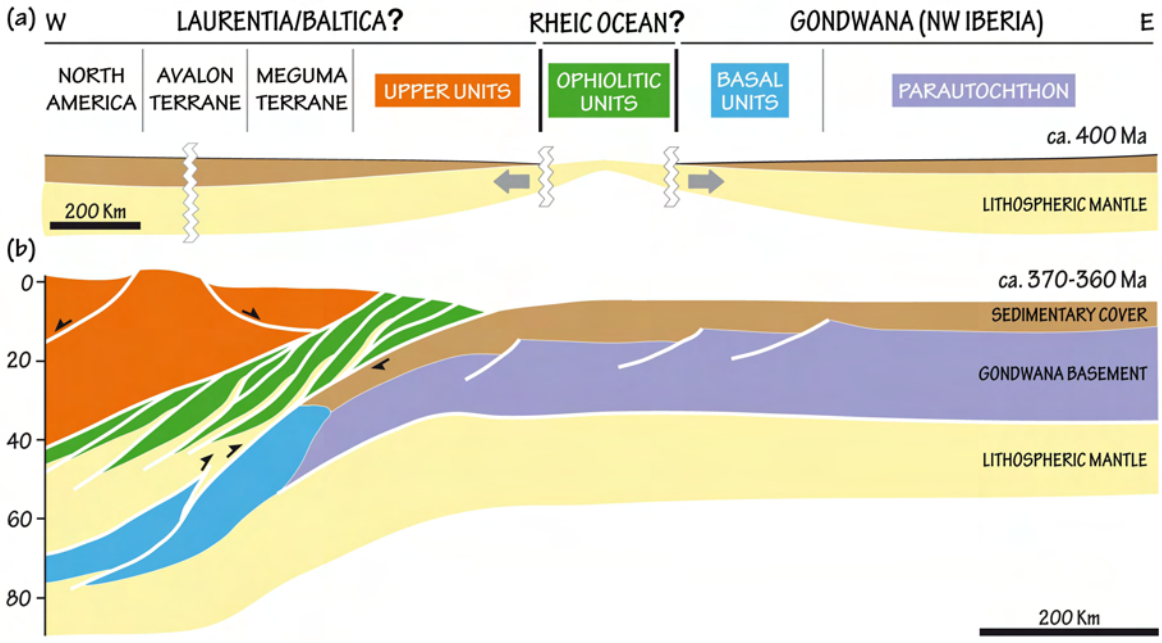

FIGURE 2. (a) Simplified paleogeographic reconstruction showing a schematic section of the terranes distribution in the Early Devonian. (b) subduction of outer margin of Gondwana and building of an accretionary wedge by underthrusting and imbrication of the allochthonous complexes of NW Iberian Massif during the Devonian . Modified from Martínez Catalán *et al.* (1996; 2007) and Arenas *et al.* (2007).

Moreover, the geology of the Iberian Peninsula can be correlated with many of the European Variscan terranes. Hence, the MTC can be correlated with similar terranes, with HP and L/MT metamorphism, from Portugal to the northern areas of Eastern Europe, such as the Kaczawa Complex in the Polish Sudetes of the Bohemian Massif (e.g. Cháb & Vrána, 1979; Guiraud & Burg, 1984; Holub & Souček, 1994; Kryza *et al.*, 1990; 2010; 2011; Smulikowski, 1995; Patočka *et al.*, 1997; Cymerman *et al.*, 1997; Záčkováet al., 2010; Faryad & Kachlík, 2013). In addition, similarities between certain geological units of the South Armorican Domain (Armorican Massif, Brittany) and the MTC allows correlation of the latter with the Île de Groix and Champtoceaux Complexes (e.g. Martínez Catalán *et al.*, 2009; Ballèvre *et al.*, 2009; 2012), particularly since the age of the HP metamorphism is the same in both terranes (Rodríguez *et al.*, 2003; Bosse *et al.*, 2005; Abati *et al.*, 2010). The investigation of the details of this correlation is another important objective of this study.

1.2 *Objectives and methodology*

The research carried out in this PhD thesis consists in: 1) a detailed petrological and thermobarometric study of the blueschist-facies rocks from the MTC using the pseudosection approach, 2) $^{40}Ar/^{39}Ar$ geochronology of the blueschist-facies rocks and 3) the correlation of the Malpica-Tui units with their counterparts in the South Armorican Domain.

The specific objectives are:

(1) Detailed petrological and thermobarometric study of the Ceán Schists and the Cambre metabasic rocks, using the following methodology:

- Bibliographic review of the study area, as well as of the rest of the allochthonous complexes of NW Iberia, in order to obtain a broad perspective of the geological background.
- Sampling and field data collection.
- Petrographic study of various thin sections for each of the selected samples.
- Mineral chemistry study using Electron Probe Micro-analyser (EPMA) and Scanning Electron Microscopy (SEM). Mineral analyses and elemental X-ray maps have been performed with a JEOL-Superprobe JXA-8900M microprobe equipped with five spectrometers at the ICTS-National Electronic Microscopy Centre at the Complutense University of Madrid (Centro Nacional de Microscopía Electrónica; http://www.cnme.es). Secondary electron images were obtained with a scanning electron microscope JEOL JSM-820 with EDX-microanalysis at the Research Assistance Centre of Geological Techniques at the Complutense University of Madrid (CAI de Técnicas Geológicas de la UCM; http://www.ucm.es/centros/webs/cai5134).
- Whole rock analysis of rock slabs of each representative sample by X-ray fluorescence spectroscopy (XRF). FeO (vs. Fe_2O_3) has been analysed by wet chemical titration. All chemical analyses were performed in Activation Laboratories Ltd. (Actlabs, Canada, http://www.actlabs.com). See further details below.
- Numerical modelling of phase equilibria through pseudosection approach using THERMOCALC (Powell & Holland, 1988) and Perple_X (Connolly, 1990).

(2) Establish a detailed P-T path for these rocks units in order to characterize the subduction process and its subsequent evolution.

(3) Provide a time frame to the thermobarometric results using $^{40}Ar/^{39}Ar$ step heating technique in white mica concentrates and single grains.

(4) Using the above data, addressing the implications of the metamorphic evolution of this unit in the evolution of the European Variscan belt and compare it with possible equivalents in the South Armorican Domain (Armorican Massif).

X-RAY FLUORESCENCE SPECTROSCOPY (XRF) was carried out using the heavy absorber fusion technique of Norrish and Hutton (1969) for major element (oxide) analysis, in order to minimize the matrix effects of the samples. The loss on ignition (LOI) is determined prior to fusion from the weight loss after roasting the sample at 1050°C for 2 hours. The fusion disk is made by mixing a 0.5 g equivalent of the roasted sample with 6.5 g of a combination of lithium metaborate (Bo_2Li) and lithium tetraborate ($Li_2B_4O_7$) with lithium bromide (LiBr) as a releasing agent. Samples were fused in Pt crucibles using an automated crucible fluxer (AFT) and automatically poured into Pt moulds for casting. Finally, samples were analysed on a PANalytical Axios Advanced wavelength dispersive XRF (WDXRF) spectrometer. The intensities are then measured and the concentrations are calculated against the standard G-16 provided by K. Norrish of CSIRO (Commonwealth Scientific and Industrial Research Organisation, Australia). Matrix corrections were done by using the oxide alpha (influence coefficients provided also by K. Norrish). In general, the limit of detection is about 0.01 wt. % for most of the major elements except for MnO and TiO_2 where is 0.001 wt. %.

FeO (vs. Fe_2O_3) was determined by TITRATION. This method is a wet chemistry technique for determining the concentration of an unknown reagent using a known concentration of another reagent (titrant) that chemically reacts completely with the unknown sample. The FeO concentration has been obtained using a variant of the method proposed by Wilson (1955). This alternative consist in a cold acid digestion of ammonium metavanadate (NH_4VO_3), and hydrofluoric acid (HF) in an open system (in order to minimize the $S_{(II)}$ tendency to reduce Fe^{3+} to Fe^{2+}) until complete decomposition of the sample. Potassium dichromate ($K_2Cr_2O_7$) was the titrating agent and a ferrous ammonium sulphate solution was added as reductometric standard after digestion. This cold digestion dissolved all silicates and most sulphides. Occasionally pyrite may be not completely dissolved. Its extent of dissolution is affected by the Fe^{3+}content; greatest concentrations of Fe^{3+} increase the solubility of pyrite. The point at which the reaction is completed is known as the end-point of the titration or the equivalence point. At the equivalence point the entire unknown sample has reacted with a quantity of the standard (known concentration) of titrant, this being determined by some kind of indicator. In this case the endpoint was determined by colour (for further details see e.g. Reichen & Fahey, 1962). Then, Fe_2O_3 is calculated stoichiometrically by the following expression Fe_2O_3 = (TOTAL IRON / 1.43 - FeO/1.286)*1.43 (for further details see section 1.5.2).

The methodology used for the petrological modelling and for the $^{40}Ar/^{39}Ar$ step heating technique is detailed in sections 1.5.2 and 3.2.2, respectively. Analytical specifications, such

as the operating parameters for punctual analyses on minerals and elemental X-ray maps, are described in detail for each rock-type in Chapter 3.

1.3 *Outline and research approach*

This PhD thesis is presented as a compilation of publications comprising multi-authored works that have been published (Articles 1, 2 and 4) or submitted for publication (Articles 3 and 5) in peer-reviewed international journals.

The research has been divided into four stages. Each of the first three stages represents a section in Chapter 3 and the fourth stage covers the entire Chapter 4.

The first stage focuses on the study of the Ceán Schists. The study of this lithology constitutes the continuation of the research initiated to obtain the MSc degree (DEA). The pelitic schists from the lower structural levels of the series contain numerous garnet porphyroblasts that include internal foliations. The mineral assemblage preserved as micro-inclusions in the first generation of garnet make this lithology ideal to study the subduction related metamorphism, deformation phases and P-T conditions. The second generation of garnet porphyroblasts contain a chloritoid-glaucophane paragenesis, which is one of the HP indicators in metapelites, as has been reported in several blueschist terranes around the world (e.g. Kiénast & Triboulet, 1972; Kryza *et al.*, 1990; Katagas, 1980; Theye *et al.*, 1992; Chopin, 1981; Song *et al.*, 2007; Wei & Song, 2008; El-Shazly & Liou, 1991; Warren & Waters, 2006). However, this mineral assemblage had not been previously described in the NW Iberian Massif. Hence, one of the goals of this study is to report the presence of choritoid-glaucophane pelitic schists and document their petrological characteristics and metamorphic P-T conditions (ARTICLE 1).

The results of the previous research include an initial approach on P-T constraints and a tentative P-T path for the Ceán Schists. Moreover, it raised interesting questions concerning uncertainties regarding the effect of key chemical components in phase equilibria, especially H_2O and Fe_2O_3. Similar to metabasic rocks, the HP assemblages of metapelitic rocks are highly sensitive to the amount of available H_2O and Fe_2O_3. In order to obtain further refinements on the petrologic modelling and the P-T evolution of the Ceán Schists, the effects of these two components has been investigated. The uncertainty associated to the role of water and the state of oxidation of Fe is mostly related to the difficulty of estimating their original proportions in the rock through quantitative analytical techniques (e.g. Guiraud *et al.*, 2001; Diener & Powell, 2010; Rebay *et al.*, 2010). Using pseudosection approach in different chemical systems it has been possible to estimate the existing proportion of both components during the prograde evolution of the Ceán Schists, and the results obtained from

pseudosection calculations yielded first-order constraints for geodynamic models that may have a general application in the investigation of rocks with similar composition (ARTICLE 2).

The second stage is centred on the investigation of the Cambre metabasic rocks. This lithology has been interpreted as strongly retrogressed blueschists containing lawsonite pseudomorphs (Rodríguez, 2005). Lawsonite is a hydrous calcium aluminium silicate mineral that crystallises at M/HP and LT conditions (e.g. Crawford & Fyfe, 1965; Liou, 1971; Pawley, 1994; Schmidt & Poli, 1994; Schmidt, 1995; Comodi *et al.*, 1996). Thus, it is another key mineral that has been reported in numerous HP belts as an indication of blueschist and, less frequently, eclogite-facies metamorphism (e.g. Maruyama *et al.*, 1996; Tsujimori *et al.*, 2006 and references therein). During decompression, lawsonite easily breaks down to secondary minerals (epidote group minerals, white micas, chlorite and albite) and hence it is more frequently found as pseudomorphs than as fresh crystals. Due to its high H_2O content lawsonite is the major water source and reservoir in the HP–LT mafic systems, playing a key role in water transport in subduction zones. When modelling HP rocks, it is commonly assumed that water saturation conditions exist during subduction metamorphism, but recent studies (Ballèvre *et al.*, 2003; Clarke *et al.*, 2006; including the one conducted in the pelitic Ceán Schists; López-Carmona *et al.*, 2013) suggests that lawsonite crystallization may lead, in some cases, to a fluid-undersaturated prograde P–T evolution. Therefore, the metamorphic evolution of the retrogressed lawsonite-bearing metabasic rocks has been explored through pseudosection approach, assessing the possibility of a prograde under-saturated evolution induced by lawsonite crystallization and investigating changes in the oxidation state on mineral assemblages affecting equilibration conditions during metamorphism. The wealth of mineral assemblages in the Cambre metabasic rocks and their complex chemistry favoured the assessment of the P–T evolution of this lithology. The results obtained are consistent and complement the data obtained for the pelitic schists, allowing to establishing a P–T history for the Middle Allochthon in the MTC. Complementarily, the $^{40}Ar/^{39}Ar$ ages obtained for the HP event in the pelitic schists and for the basal detachment separating the Lower and the Middle Allochthon in the MTC are presented in this section. Absolute time constraints on the P–T evolution of HP terranes are essential to understand the subduction-exhumation processes. Whilst the chronology of different metamorphic events of the Lower Allochthon in the MTC have been extensively studied, data for the Middle Allochthon are limited to only one $^{40}Ar/^{39}Ar$ age, and the age of the Bembibre-Ceán detachment remained unconstrained. Dating the mylonitic recrystallization associated to the detachment has contributed to the knowledge of the early extensional phases of the gravitational collapse of the orogen in the Allochthonous Complexes of NW Iberia. Finally, on the basis on their petrography, P–T conditions and age, detailed-scale correlations between similar lithologies within the Middle Allochthon across the Ibero-Armorican Arc have been proposed (ARTICLE 3).

The aim of the third stage is the study of Mesozoic blueschists from Liberty Creek (Chugach terrane, Alaska) containing abundant sodic amphiboles and fresh lawsonite. Although these units are geologically unrelated to the main study area in NW Iberia, they offer valuable insights that, as stated below, were instrumental for a better understanding of many features of the HP rocks of Galicia. Compared to the Paleozoic blueschist facies rocks from the Iberian Massif, where the original mineralogy is masked by the exhumation- and/or retrogression-related processes, or shielded in the cores of porphyroblasts, the Liberty Creek Schists preserves almost pristine textures and mineral relations, representing an outstanding complement to the previous research. The southern Alaska convergent margin contains several small belts of sedimentary and volcanic rocks metamorphosed to blueschist facies, located along the Border Ranges fault on the contact between the Wrangellia and Chugach terranes. These belts are significant in that they are the most inboard, and thus probably contain the oldest record of the Triassic–Jurassic subduction beneath Wrangellia. A description of the structural, lithological, and petrological relationships in the Liberty Creek metamorphic belt is presented, together with a detailed thermobarometric study through pseudosection modelling on the lawsonite and epidote blueschist-facies rocks from Liberty Creek. Finally, a discussion on the tectonic evolution and P–T conditions during the early stages of the subduction along the southern Alaskan convergent margin provided hypotheses that could be extrapolated to other HP terranes, for example to explain the preservation of the original geometry of some blueschist outcrops and their relation with the rate of exhumation (ARTICLE 4).

Finally, the fourth stage shows the results of a joint French-Spanish project including the work of many authors throughout several years. This project arise in the frame of this PhD joint supervision agreement between the Complutense University (UCM) of Madrid and Rennes 1 University, and has been conducted during the completion of this research, funded by a grant associated to the CONSOLIDER project (CGL2007-65338-C02-01) integrated by members of the UCM and the University of Salamanca, as well as has receiving also scientific financial support from the Geosciencies Rennes Department. The aim of this project has been to establish a correlation between the allochthonous units exposed in the NW Iberian Massif and the southern Armorican Domain, trying to unify the terminology when describing them. The correlation has been established based on lithological associations, structural position, age and geochemistry of protoliths, and tectonometamorphic evolution. Field work was undertaken by members of the French and Spanish teams to determine whether or not lithologies, structures, and the metamorphic evolution were similar. The units in both sides of the Bay of Biscay are grouped in three different ensembles called the Upper, Middle and Lower Allochthons, while an underlying allochthonous thrust sheet with stratigraphic and petrologic affinities with its relative autochthon, has been also identified in both domains, and is referred to as the Parautochthon (ARTICLE 5).

1.4 *Insights into blueschists*

1.4.1 *The concept of blueschist and blueschist facies: an overview*

During the late XIX century, V. M. Goldschmidt and P. Eskola pioneered the establishment of a sound basis for the study of the mineral composition of metamorphic rocks. Throughout the first half of the 20th century, thanks to the studies of V. M. Goldschmidt, P. Eskola, T. Vogt, T. F. W. Barth and H. Ramberg the concept of "chemical equilibrium" applied to mineral parageneses was established. Eskola (1920, 1922) realized that particular rocks (such as the eclogites from Orijärvi area, Finland) showed a specific mineralogy, recognizing the connection between metamorphic facies and progressive metamorphism (cf. Vogt, 1927; Barth, 1936).

At that time, defining the *glaucophane-schists facies* was of vital importance for the understanding of the diversity of regional metamorphism. Eskola (1929, 1939) was the first to advocate the existence of an independent metamorphic facies comprising glaucophane-bearing schists and associated rocks with an abundant modal proportion of glaucophane (> 5%) that he named *glaucophane-schist facies*. But its genetic relation with other metamorphic facies was not clear. de Roever (1955a, b), Miyashiro & Banno (1958) and Miyashiro & Seki (1958) established and consolidated the idea of the "glaucophane-schist facies" as a very distinctive facies encompassing rocks whose peculiar mineralogy suggests that they formed under HP and relatively LT conditions. Since then, the work of numerous scientists broadened knowledge of rocks of this facies (cf. van der Plas, 1959; Bearth, 1959; Bloxham, 1960; Coombs, 1960; Ellenberger, 1960; Ernst, 1963; Coleman & Lee, 1963; Kanissawa, 1964; Crawford & Fyfe, 1965; Winkler, 1965; Ghent, 1965). At odds with this interpretation, some authors ascribed the origin of blueschists to sodium (iron and magnesium) metasomatism instead of regional metamorphism (e.g. Suzuki, 1930; Harker, 1932; Taliaferro, 1943; Turner, 1948; Schürmann, 1951; 1953; 1956; Brothers, 1954). Although metasomatism has often been cited as widespread in low-grade blueschist facies conditions (e.g. Gresens, 1969; Okay, 1982), experimental petrology convincingly proved the HP stabilities of several blueschist minerals (e.g. Schreyer & Baller, 1977; Holloway & Wood, 1988; van der Laan & van Groos, 1991; Poli & Fumagalli, 2003 and references therein). Consequently, the metasomatic hypothesis was largely abandoned.

Ernst (1961) demonstrated that glaucophane on its own composition can be synthesized at a lower pressures and higher temperatures than those initially predicted, and doubts concerning the stability of this amphibole exclusively at HP conditions arose (e.g. Winkler, 1965; Turner, 1968; Hyndman, 1972; de Roever & Beunk, 1976). Consequently, glaucophane was not viewed as an index mineral of the *glaucophane-schist facies* by most

authors, although others always postulated its HP character (e.g. Miyashiro, 1973). Jadeite (cf. Bloxam, 1956; Essene & Fyfe, 1967) and/or lawsonite (cf. Ransome, 1895; Crawford & Fyfe, 1965) were considered more reliable pressure indicators. Successively, new designations like *glaucophane-lawsonite facies* (Winkler, 1965), *glaucophane-lawsonite schist facies* (Fyfe & Turner; 1966) or *lawsonite-glaucophane-jadeite facies* (Winkler, 1967) were proposed. With increasing knowledge of blueschist terranes, these names were soon considered superfluous because it was realized that the occurrence of blueschist metamorphism was not only subject to the presence of lawsonite and/or jadeite (e.g. Black, 1973) or vice versa, as reported in lawsonite-albite areas without blueschist metamorphism (e.g. de Roever, 1972).

Since Ernst´s pioneering experimental studies (1961, 1963), the stability relations of glaucophane have been the subject of a vigorous debate over the last 50 years (e.g. de Roever, 1972; Maresch, 1973; Gilbert & Popp, 1973; Carman, 1974; Koons, 1982; Carman & Gilbert, 1983; Maruyama *et al.*, 1986, Holland, 1988; Gillet *et al.*, 1989; Robie *et al.*, 1991; Corona *et al.*, submitted). It is beyond doubt that Ernst´s research spurred a thorough study, not only of this amphibole, but also of the blueschist facies rocks, in the stability of other HP minerals and its phase relations from their thermal and volume properties. Concurrently, the concept of "blueschist" was introduced into the world of metamorphic geology by E. Bailey in 1962, and was progressively adopted by petrologists. Once the term was accepted, the majority of authors used it as a synonym of Eskola´s *glaucophane-schist facies* (e.g. Liou, 1971; Coombs, 1972). Nowadays it is assumed that glaucophane is a critical mineral of the blueschist facies conditions, and that glaucophane–bearing rocks are fundamental in deciphering the tectonothermal history of HP terranes. Since the concept of "blueschist" was introduced (Bailey, 1962) numerous synonyms with minor variations of the original term have appeared and over years the nomenclature has become confusing. Currently, Eskola´s term "glaucophane schist" has recovered its former meaning, but in the meantime "blueschist" has become well accepted both, as a rock and as a facies term. As a rock term, according to the nomenclature recommended by the SCMR[1] *a blueschist* is a schist whose bluish colour is due to the presence of alkali amphibole[2] (cf. Desmons *et al.*, 1997; 2001; Desmons & Smulikowski, 2007). Particularly, schist containing the blue amphibole glaucophane can be explicitly called *glaucophane schist* with the addition of the names of other representative critical minerals such as jadeite–bearing glaucophane-phengite schists or epidote-glaucophane schist. If the term is used as a facies name, the facies context should be made clear by using "blueschist–facies rock". And the terms "glaucophane-schist facies" and "blueschist facies" are regarded as synonyms (Smulikowski *et al.*, 2007).

[1] The International Union of Geological Sciences (IUGS) Subcommission on the Systematics of Metamorphic Rocks (SCMR)

[2] The alkali-amphibole group includes three series: Glaucophane Series: $Na_2(Mg,Fe)_3Al_2Si_8O_{22}(OH)_2$; Riebeckite Series: $Na_2(Fe,Mg)_3Fe_2Si_8O_{22}(OH)_2$; Arfvedsonite Series: $Na_3(Fe,Mg)_4FeSi_8O_{22}(OH)_2$

The blueschist facies (Eskola, 1939; cf. Fyfe *et al.*, 1958) comprises a set of metamorphic mineral assemblages produced by the metamorphism of a wide range of protolith rock types under the same HP (ca. above 6 kbar) and LT (< 550°C) conditions (e.g Turner, 1981; Evans, 1990; Guiraud *et al.*, 1990; Frey *et al.*, 1991; Winter, 2001). Diagnostic minerals and mineral parageneses in such a facies would strongly depend on their protolith and its whole-rock composition. Although protoliths can be highly variable, MORB and sedimentary rocks are the most frequent. Nevertheless, common minerals in blueschist facies are not confined to mafic or pelitic compositions and, besides the above mentioned glaucophane, jadeite or lawsonite, other typical minerals are carpholite, talc or chloritoid. Characteristic mineral parageneses for various rock types compositions in the blueschist facies conditions are given in TABLE 1.

Diagnostic mineral assemblages for characteristic protolith rock-types metamorphosed in the blueschist-facies conditions. After Turner (1968; 1981), Miyashiro (1973; 1994), Spear (1993), Bucher & Frey (1994) & Kretz (1994).

TABLE 1. Blueschist–Facies	COMMON PROTOLITH TYPE	DESCRIPTION	INDEX MINERALS OR ASSEMBLAGES
MAFIC ROCKS	basalt, andesite, gabbro, diorite	Low SiO_2, moderate FeO and MgO	alkali-amphibole (mostly glaucophane), lawsonite, epidote, jadeite, phengite, chlorite, garnet, albite, titanite, quartz
ULTRAMAFIC ROCK	peridotite, serpentinite	Very low SiO_2, high MgO	serpentine group, mica group, talc, epidote (zoisite), iron oxides
PELITIC ROCKS	shale, mudstone	Rocks enriched in clay minerals High Al_2O_3, K_2O, lesser amounts CaO	alkali-amphibole, lawsonite, epidote, jadeite, carpholite, chloritoid, talc, kyanite, garnet, white mica, chlorite, albite, aragonite, quartz
CALCAREOUS ROCKS	limestone, dolomite, marls	High CaO, CO_2 Limestones and dolomite form marbles Impure limestones form Calc-silicates	aragonite/calcite, white mica
QUARTZO-FELDSPATHIC ROCKS	sandstone, rhyolite, granite, chert	High SiO_2, low FeO and MgO	jadeite, lawsonite, white mica, chlorite, kyanite garnet, aragonite, felsdpar, quartz

The blueschist facies is bounded by the zeolite, subgreenschist (pumpellyite–actinolite) and greenschist facies at low pressures, by the (epidote) amphibolite facies on the high-temperature (HT) side and the eclogite facies at high pressures and high temperatures (FIGURE 3). The blueschist facies can be subdivided into lawsonite–bearing blueschist (LT) and epidote–bearing blueschist (HT; Evans, 1990). At the same temperature range, above the quartz and graphite stability limits (> 25 kbar) the lawsonite–bearing blueschist facies is bounded by the lawsonite–eclogite facies, where the stability of coesite and diamond defines the limit between high and ultrahigh–pressure metamorphism (UHP; e.g. Chopin, 1984; Smith, 1984; Sobolev & Shatsky, 1990; Liou *et al.*, 1996; Grasemann *et al.*, 1998; Zack *et al.*, 2004; Tsujimori *et al.*, 2006). The boundaries between two facies are defined by continuous reactions and regarded as P–T intervals corresponding to transition zones with characteristic transition mineral assemblages. However, neither particular whole-rock composition nor fluids are considered in the concept of facies (e.g. Vernon & Clarke, 2008). Progressive metamorphism brings on dehydration reactions and thus, large volume changes control facies boundaries. These reactions depend on the bulk composition, which also controls the temperature at which such

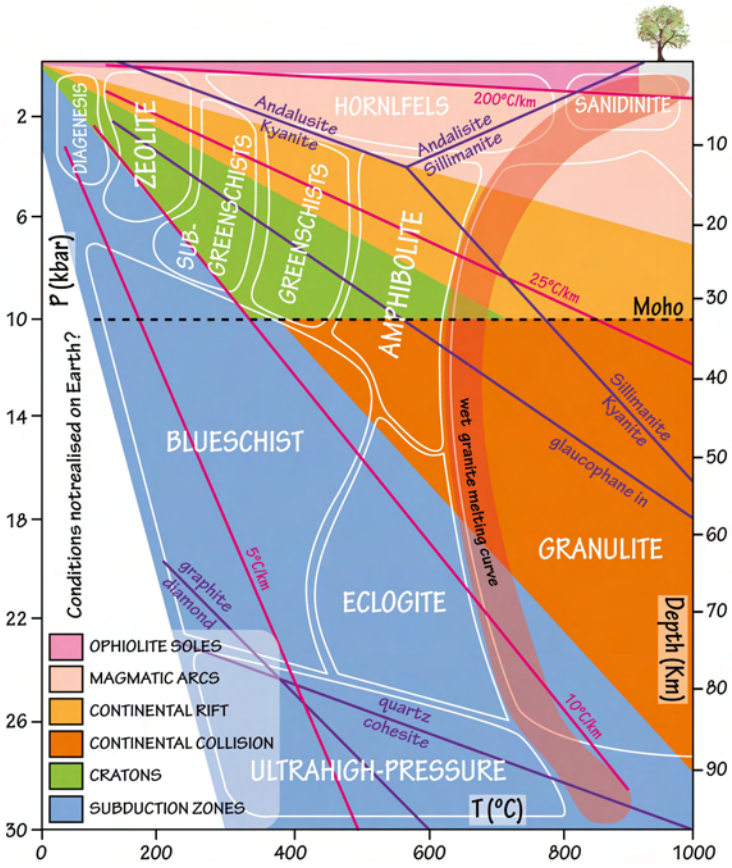

FIGURE 3. Metamorphic facies and tectonic settings in terms of pressure and temperature conditions inside the Earth. Modified after Hacker (2001 and Bentley (2010) using data from Yardley (1989), Spear (1993), Oberhänsli *et al.* (2004) and Bousquet *et al.* (2008). Diagnostic reactions are also shown for reference: aluminosilicate stability fields after Holdaway (1971); diamond=graphite after Kennedy & Kennedy (1976); coesite=quartz after Hemingway *et al.* (1998) and glaucophane-in line after Corona *et al.* (submitted). The shallowest Moho after Blackwell (1971) is also included.

reactions occur, and at the same time, these reactions are highly sensitive to fluid abundance (the tale of the *snake biting its tail*). Hence, transitions between greenschist- blueschist- eclogite-amphibolite-facies are strongly dependent on a set of intensive and extensive thermodynamic variables that determine their phase relations and specific P–T conditions (e.g. Koons & Thompson, 1985; Guiraud *et al.*, 1990, Will *et al.*, 1998). This will be discussed in more detail in section 1.5.

Summarizing, a blueschist is a fine-grained blue amphibole-bearing metamorphosed mafic igneous rock with a characteristic mineral assemblage comprising glaucophane and/or lawsonite and/or jadeite-rich pyroxene as index minerals, besides epidote, garnet, white mica (generally phengitic muscovite and paragonite), chlorite, Na-rich plagioclase (An_{0-3}), titanite and aragonite/calcite. But frequently, it is not blue or even shows schistose texture.

The nomenclature assumed in the present manuscript refers to a "blueschist" when the protolith is a metamorphosed mafic igneous rock and to a "blueschist-facies rock" for the remaining metamorphosed protoliths. However, clarifications will be made when necessary.

1.4.2 *Blueschists and subduction zones*

Experimental studies of mineral P–T stability fields indicate that regional metamorphism in blueschist–facies terranes leads to a sequence of mineral assemblages thought to be diagnostic of former subduction zone settings (e.g. Miyashiro, 1973; 1994; Harte & Hudson, 1979; Cloos, 1985) or, ephemerally, of the early stages of metamorphism related to continental convergence where the blueschist facies assemblage would re-crystallize into greenschist and/or epidote-amphibolite facies assemblages (e.g. Ernst, 1973; England &

Thompson, 1984). Thus, blueschist (and LT-eclogite) facies rocks are thought to be formed in a very special environment, at convergent plate boundaries during oceanic or continental subduction (FIGURE 4).

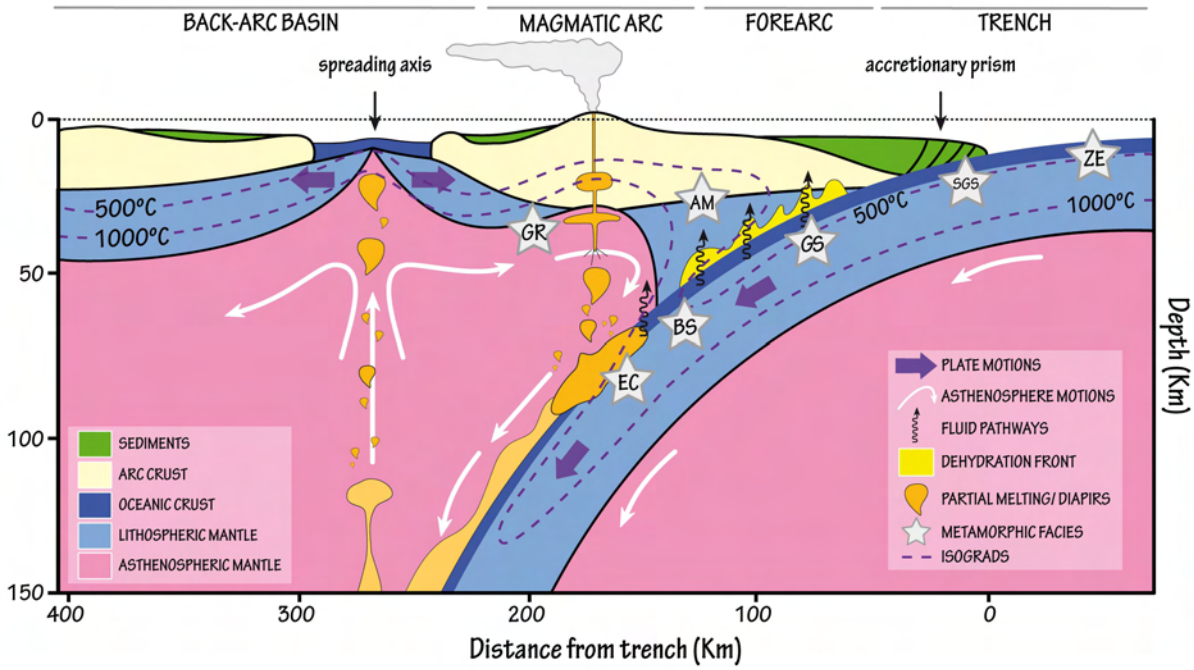

FIGURE 4. Simplified schematic section through the upper 150 km of a subduction zone. This is considered the maximum depth of subducted rocks exhumed to the Earth's surface. The metamorphic facies series of high P/T type sequence is also indicated. Facies abbreviations: ZE–zeolite; SGS–sub-greenschist; GS–greenschists; AM–amphibolites; BS–blueschists; EC–eclogites; GR–granulites. Modified from Stern (2002).

1.4.2.1 *Preservation and uplift*

Along a subduction zone, relatively cool oceanic lithosphere is pushed down to great depths yielding low geothermal gradients (<15 km/°C; temperature increases slowly with depth) and a metamorphic facies series of high P/T type (Miyashiro, 1961; 1973; 1994; Harte & Hodson, 1979; Yardley, 1989; Spear, 1993; Kornprobst, 2002) that comprises the following sequence sequence as pressure and temperature increases with prograde metamorphism: zeolite → sub-greenschist (prehnite-pumpellyite) → blueschist → eclogite (FIGURES 4 & 5a). Due to the downward dragging of the isotherms by the cold subducting plate, the thermal gradient is inverted to the top of the plate, producing inverted metamorphic isograds that sometimes are preserved in exhumed HP terranes (Arenas *et al.*, 1995; López-Carmona *et al.* 2013). During burial of the rocks of the subducted plate, the classic tectonics models predicts a metamorphism following clockwise P–T paths in which usually peak temperatures are attained closely after peak pressures (England & Thompson, 1984). Nevertheless, increasing evidences of counterclockwise P–T paths became available within this type of geotectonic regime during the past decades (e.g. Platt, 1986; Ernst, 1988; Wakabayashi, 1990; Krogh *et al.*, 1994; Pitra & Guiraud, 1996; Perchuk *et al.*, 1999; Smith

et al., 1999; Krebs *et al.*, 2001; Abati *et al.*, 2003; Willner *et al.*, 2004; García-Casco *et al.*, 2006; García-Casco, 2007; García-Casco *et al.*, 2008; van Staal *et al.*, 2008; Blanco-Quintero *et al.*, 2011a-d). It is generally agreed that counterclockwise P-T paths demands a very specific tectonic situation within the accretionary system (e.g Gerya *et al.* 2002; Gerya & Stockhert, 2006 and references therein) and most examples are described in continental subduction settings. Counterclockwise P-T paths imply a prograde metamorphism at HT, frequently together with partial melting (hot subduction) and an isobaric cooling, i.e. no change in depth (cold exhumation). In any case, the most notable differences in subduction P-T histories in blueschist-facies rocks are recorded in the retrograde paths during exhumation. Petrological constraints suggest that rocks with a high P-T ratio usually undergo decompression with little or no heating (e.g. Thompson and England, 1984; Liou *et al.*, 1996). Some exhumation histories even require a retrograde P-T path subparallel to the prograde path. In these situations commonly mineral assemblages are not (or less) overprinted by later greenschist or amphibolite facies metamorphism and peak assemblages are often well preserved (the so called "Franciscan type P-T path"; Cloos, 1982; Ernst, 1988; FIGURE 5b). Decompression with substantial heating (so called "Alpine type P-T path"; Ernst, 1988) commonly leads to an extensive greenschist or amphibolite facies overprint on the early blueschist and LT/eclogite facies assemblages.

It is widely accepted that formation and preservation of the initial mineral assemblage in blueschist and eclogite-facies rocks requires cold subduction to mantle depths and rapid exhumation (e.g. Compagnoni & Maeffo, 1973; Carswell, 1990; Poli & Schmidt, 1995; Maruyama *et al.*, 1997; Okamoto & Maruyama, 1999; Forneris & Holloway, 2004; Zack *et al.*, 2004; Zhang & Meng, 2006; Brun & Faccenna, 2008; Agard *et al.*, 2009; Ravna *et al.*, 2010; Zucali & Spalla, 2011). As mentioned above, if the geothermal gradient prevailing during exhumation is sufficiently high, these rocks will pass through the greenschist, epidote-amphibolite or amphibolite facies upon exhumation. Then, if exhumation rate is not rapid enough, these rocks will be overprinted by later assemblages to such an extent that they may not preserve any trace of the original mineralogy and significant hydration-recrystallization processes may obliterate almost all progressive assemblages, especially at high grade, before rising back to the surface (e.g. García-Casco & Torres Roldán, 1996; Duchêne *et al.*, 1997; Bousquet, 2008). Nevertheless, fortunately, in many occasions the metastable persistence of mechanically resistant host minerals, such as garnet or zircon, preserve the remnants of the (U)HP event as inclusions, which have been brought to the surface being insulated from retrogression, being the only witnesses of the early metamorphic events (e.g. Chopin, 2003).

Regionally extensive HP terranes with well-exposed synmetamorphic structures and pristine blueschist and eclogite facies assemblages are very rare (e.g. Davis & Whitney, 2006 and references therein). Most blueschist terranes are not structurally coherent or regionally

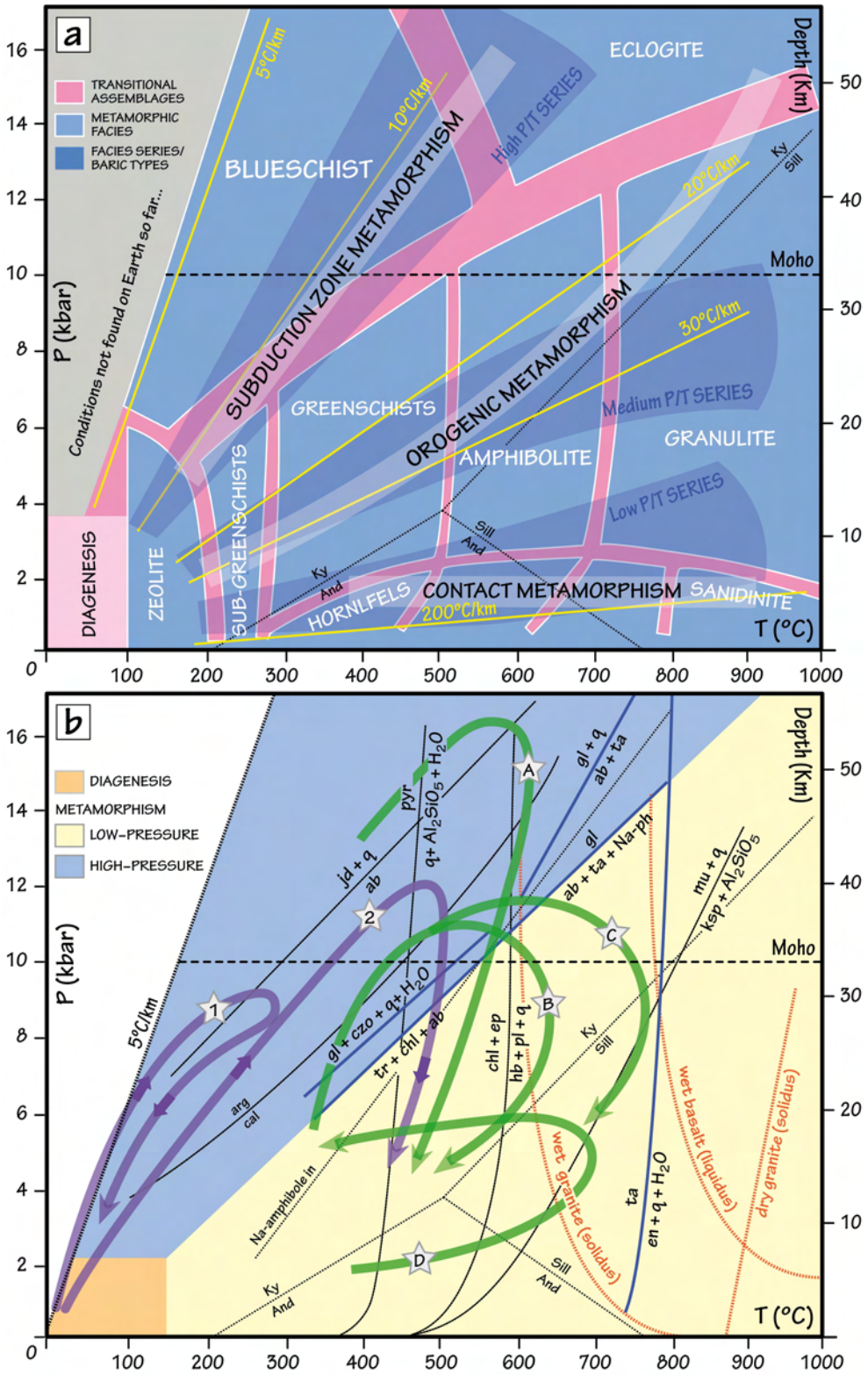

FIGURE 5. (a) P-T diagram showing principal metamorphic facies, facies series and the corresponding tectonic environment. Modified from Miyashiro (1961) and Yardley (1989). (b) P-T diagram showing characteristic P-T paths from subduction zones and other contrasting geologic environments. 1- Franciscan type showing that the rocks are cooled as they are exhumed. 2- Alpine type (western Alps) characterized by a nearly isothermal decompression caused by rapid exhumation. After Ernst (1988). Other P-T paths in compressive settings are shown for reference; A- Tauern Window (eastern Alps) representing continental collision metamorphism. The metamorphic peak is synchronous with the maximum P in the Eclogite facies. After Selverstone (1985). B&C- granulite isothermal decompression producing tectonic thickening. After England &Richardson (1977), England & Thompson (1984) and Harley (1989); D- granulite isobaric cooling that may arise from counterclockwise P-T loops. After Bohlen, (1987) and Spear (1991). Glaucophane stability field defining high-P conditions (blue reaction lines, based in Corona *et al.*, submitted). Diagnostic reactions are also shown as reference: calcite-aragonite after Johannes & Puhan (1971); pyr→q+Al_2SiO_5+H_2O and aluminosilicate stability fields after Holdaway (1971); Na-amphibole in (Maresch, 1977); jd+q→ab (Holland, 1980); The shallowest Moho after Blackwell (1971) is also included.

widespread because of their tectonic setting and mode of exhumation, or because effects of collision following subduction disrupt the original stratigraphy and structure of the subducted plate.

Thermo-mechanical numerical models on subduction zones indicate that oceanic subduction orogeny (Bally's type-B subduction, 1975), also named Pacific-type (Matsuda & Uyeda, 1971) or Miyashiro-type (Maruyama, 1997), is characterized by the formation of subduction–accretion complexes with HP/LT metamorphic belts involving blueschists (B-type blueschist; Maruyama *et al.*, 1996) and eclogites, and extensive calc-alkaline magmatism due to the long-lasting subduction of oceanic lithosphere that produces a voluminous increase of continental crust. In contrast, intracontinental orogenic belts, Alpine-type (Bally's type-A subduction, 1975) are recognized as representing ocean-margin suture zones formed by continental collision (Dewey & Bird, 1970; Molnar & Tapponnier, 1975). Collision-type orogeny results in regional HP/HT metamorphic belts including A-type blueschist (Maruyama *et al.*, 1996) and relics of UHP metamorphic rocks. This type of subduction first involves the consumption of an oceanic domain, similar to the Pacific-type subduction, followed by the subduction of the continental margin. In this case, continental growth is very limited or negligible, because it mainly involves reworking of pre-existing continental material (*e.g.* Ota & Kaneko, 2010).

Subduction is assumed to be responsible for the process by which crustal rocks reach depths in excess of 100 km (Chopin, 1984; 2003; Hacker & Peacock, 1994; Bousquets *et al.*, 1997; Ring *et al.*, 1999). A large part of the research within the last decades has been focused on elucidating the mechanisms of exhumation of HP and UHP rocks in this setting (*e.g.* Burov *et al.*, 2012). Blueschists and eclogites exhumed in oceanic subduction settings commonly indicate burials of 40–70 km whereas continental collision scenarios usually imply depths greater than 70 km (*e.g.* Platt, 1993).

The exhumation of HP rocks involves both, a horizontal and a vertical displacement of deeply buried material whose return back to the surface must be accommodated by some type of mechanism. Despite the growing amount of data on surface horizontal displacement, the vertical movements of the lithosphere and exhumation processes are still a subject of intense debate (*e.g.* Tsujimori *et al.* 2006; Agard *et al.*, 2009; Guillot *et al.*, 2009; van Dinther *et al.*, 2012; Burov *et al.*, 2012; Warren, 2013). Proposed mechanisms for exhumation include the classical channel flow (Cloos, 1982; Burov *et al.*, 2001; Gerya *et al.*, 2002), corner flow circulation within an accretionary wedge (Platt, 1986, 1993; Allemand & Lardeaux, 1997; Gerya & Stockhert, 2006; Warren *et al.*, 2008b), extensional collapse (Dewey *et al.*, 1993; Thompson *et al.*, 1997), crust–mantle delamination, i.e. buoyancy assisted by erosion and tectonic processes (Chemenda *et al.*, 1995), slab break-off (Ernst *et al.*, 1997), compression of a soft zone between two rigid blocks (Thompson *et al.*, 1997), thrusting towards the

foreland (Steck *et al.*, 1998), serpentinite channel (Guillot *et al.*, 2001), coaxial extension associated with a decoupling fault (Jolivet *et al.*, 2003), plunger exhumation involving the insertion of stronger crust into a channel of weaker material (Warren *et al.*, 2008b), vertical extrusion and horizontal channel flow (Schulmann *et al.*, 2008) or caterpillar-walk (Tirel *et al.*, 2013). All these mechanisms require low viscosity of the exhuming material and/or high erosion rates (*e.g.* Keppie *et al.*, 2009). It has been suggested that terrane buoyancy is a pre-requisite for exhumation (*e.g.* Ernst *et al.*, 1997; Warren *et al.*, 2008a, b, c). However, physical mechanisms of HP–LT rock exhumation still remain largely enigmatic, and one of the main ambiguities lies in coupling the P–T conditions inferred from petrological data and the results deduced from numerical modelling.

As an attempt to simplify the general understanding of the major processes and associated settings that can explain the worldwide exhumation of HP (and UHP) rocks, according to Guillot *et al.* (2009) three main groups of crustal materials are subducted, metamorphosed under (U)HP conditions and subsequently returned to the surface: accretionary wedge sediments (producing mainly blueschists), oceanic crust (producing mainly quartz-eclogites in serpentinite-rich subduction channels) and continental crust (producing quartz- and coesite-eclogites during continent–continent collisions). The subduction of such materials corresponds to the so called, accretionary-type, serpentinite-type and continental-type subduction, respectively. However, a subduction zone may evolve from one type to the others during its life and two different types may coexist along one subduction zone. The types of subduction are summarized in TABLE 2.

What follows is a short description of types A and B blueschist-facies rocks in orogenic belts according to their protholith-origin (Maruyama *et al.*, 1996). A-type blueschists comprises passive-margin protoliths including continental basement complexes and their overlying sediment such as platform-type carbonates, bimodal volcanics, and peraluminous sediments. B-type consists of active continental-margin protoliths in accretionary complexes prior to their subduction characterized by bedded chert, MORB, OIB, reef limestones, and graywackes. So that, A-type blueschist belts are formed by the subduction of A-type protoliths, whereas the B-type blueschist belts are produced by the subduction of B-type protoliths. Based on this classification Maruyama *et al.*, (1996) established that among the 250 recognized high-P/T belts, about 20% belong to the A-type and the rest to the B-type. Most A-type zones lie in Europe and the Tethyan domain, including UHP metamorphic terranes, and show peak pressures up to 45 kbar. B-type zones occur mainly in the circum-Pacific orogenic belts and intracontinental orogens in Asia, and were recrystallized at P <12 kbar. Modern analogues of A-type blueschists occur at the Timor-Tanimbar-Seram forearc north of Australia, and of the B-type blueschists on the Olympic Peninsula of Washington (boxed as "A" and "B", respectively in FIGURE 6).

TABLE 2. Subduction Types	ACCRETIONARY WEDGE-TYPE	SERPENTINITE CHANNEL-TYPE	CONTINENTAL-TYPE
SUBDUCTION CONTEXT	forearc accretionary wedges (or prisms) in intra-oceanic or continental arcs	intra-oceanic arc or continental margin	continental (margin) subduction and rarely oceanic subduction
EXHUMED ROCKS	oceanic sediments stacked by offscraping of the lower plate or arc rocks eroded from the upper plate (clastic sedimentary rocks with no-mantle-derived material) and already exhumed HP-LT rocks whose protoliths were sea-floor sediments	mafic blocks are interpreted to derive from the subducted oceanic plate were serpentinites are originated from abysal peridotites and their hydration likely took place during the ridge hydrotermal activity	continental and oceanic rocks derived from upper continental crust protoliths (granite, gneisess and metasedimentary rocks) and commonly peridotites and felsic amphibolitic rocks
TECTONICS OF EXHUMED ROCKS	several units of exhumed rocks forming nappes thrusted towards the palo-trench	tectonic block within serpentinite melange through the subduction channel	several units of exhumed rocks forming nappes and less frecuently core complexes
MAXIMUM P-T CONDITIONS	7-24 kbar; 350-650 °C	18-25 kbar;400-700 °C (average) up to 40 kbar at 1550 °C	26-75 kbar;700-1200 °C
METAMORPHISM	high-pressure rocks blueschist to greenschist facies conditions	high to ultrahigh-pressure rocks blueschist and eclogite facies conditions	ultrahigh-pressure rocks ultrahigh-pressure metamorphism
MAXIMUM DEPTH	70-80 km	70-100 km	100-230 km
TYPICAL GEOTHERM	5-14 °C / km	lower than 10 °C / km	5-10 °C / km; 3.5 °C / km in the Forbidden Zone in China (Liou *et al.*, 2000)
EXHUMATION RATE	1-5 mm / year	3-10 mm / year	6-20 mm / year; up to 80 mm/year in the Alps and the Himalaya (Parrish *et al.*, 2006)
EXHUMATION TIMING	intra-oceanic, early or active subduction, or at accretionary wedge collision. The exhumation is slow, can be long-lasting and is commonly driven by underplating	intra-oceanic, syn-subduction and more frecuently when the subduction melange collide with continent. Exhumation velocity is low to intermediate and usually driven by the buoyancy and the low-viscosity of the serpentinite	syn-collision; back-arc spreading; microcontinent subduction. Isothermal decompression until crustal depths. Exhumation is fast, short-lived and occurs at the transition from oceanic subduction to continental collision. Freceuntly driven by buoyancy forces and asthenospheric return flow

1.4.2.2 *Distribution of blueschists in orogenic belts: a window into subduction zone dynamics*

Miyashiro (1961) was the first to establish a relation between metamorphism and plate tectonics through the idea of the *paired metamorphic belts* in orogenic regions. He proposed the existence of parallel metamorphic belts, with similar absolute ages, but different P–T conditions: low dT/dP type metamorphism outboard, on the subducting oceanic slab and high dT/dP type metamorphism inboard, on the continental margin (cf. Takeuchi & Uyeda, 1965; Oxburgh & Turcotte, 1970; Hasebe *et al.*, 1970; Ernst, 1973; Fryer & Fryer, 1987; Ernst, 1988; Peacock, 1989). However, currently it is known that paired metamorphic belts commonly result from the juxtaposition of terranes with different metamorphic facies series that may or may not be exactly contemporaneous and that may or may not come from afar (see review by Brown, 2010). Thus, the original term of Miyashiro was extended by Brown (2009) who proposed that *paired metamorphic belts* may be defined as "penecontemporaneous belts of contrasting type of metamorphism that record different apparent thermal gradients, one warmer and the other colder, juxtaposed by plate tectonics processes".

Nevertheless, Miyashiro's hypothesis was arguably one of the important advances in metamorphic petrology within last century and currently this idea has been recognized as a concept of major importance in global tectonics.

Ophiolites, blueschists and UHP metamorphic terranes can be used as subduction-proxies (FIGURE 6; e.g. Chopin, 1984; 2003; Smith, 1984; Ernst *et al.*, 1997, Stern, 2005). Ophiolite sequences evidence two modes of lithospheric motion, seafloor spreading and obduction, and are interpreted to represent the suture of former oceans. Whereas blueschist (and LT eclogites) and UHP terranes indicate subduction to mantle depths of oceanic (low dT/dP type) and continental crust (high dT/dP type), respectively. Then, HP and UHP rocks provide the insights into the long-term dynamics inside subduction and continental collision zones, in that order.

Three peak periods of blueschist formation have been identified at 80 to 130 Ma, 400 to 500 Ma, and 700 Ma (Maruyama *et al.*, 1996). Thus, most blueschists are Mesozoic (Cretaceous) in age, with some Paleozoic (Cambrian-Devonian) examples, and only a few are of Precambrian (Neoproterozoic) age. This distribution poses some queries regarding the operating mechanisms in Plate Tectonics during these periods and on the behaviour of the thermal regime of orogenic belts through time. But also a question of preservation of the geological record, biased towards younger occurrences (regarding the Earth's formation), as blueschists are most common in post-Paleozoic orogenic belts (Liou *et al.*, 1990; Ota & Kaneko, 2010). These issues have been the subject of many discussions (see e.g. Kusky & Polat 1999; Sengör 1999; Stern, 2004; 2005; Bousquet *et al.*, 2008; Brown, 2010; Santosh & Kusky, 2010; Ota & Kaneko, 2010) and somehow still remain enigmatic.

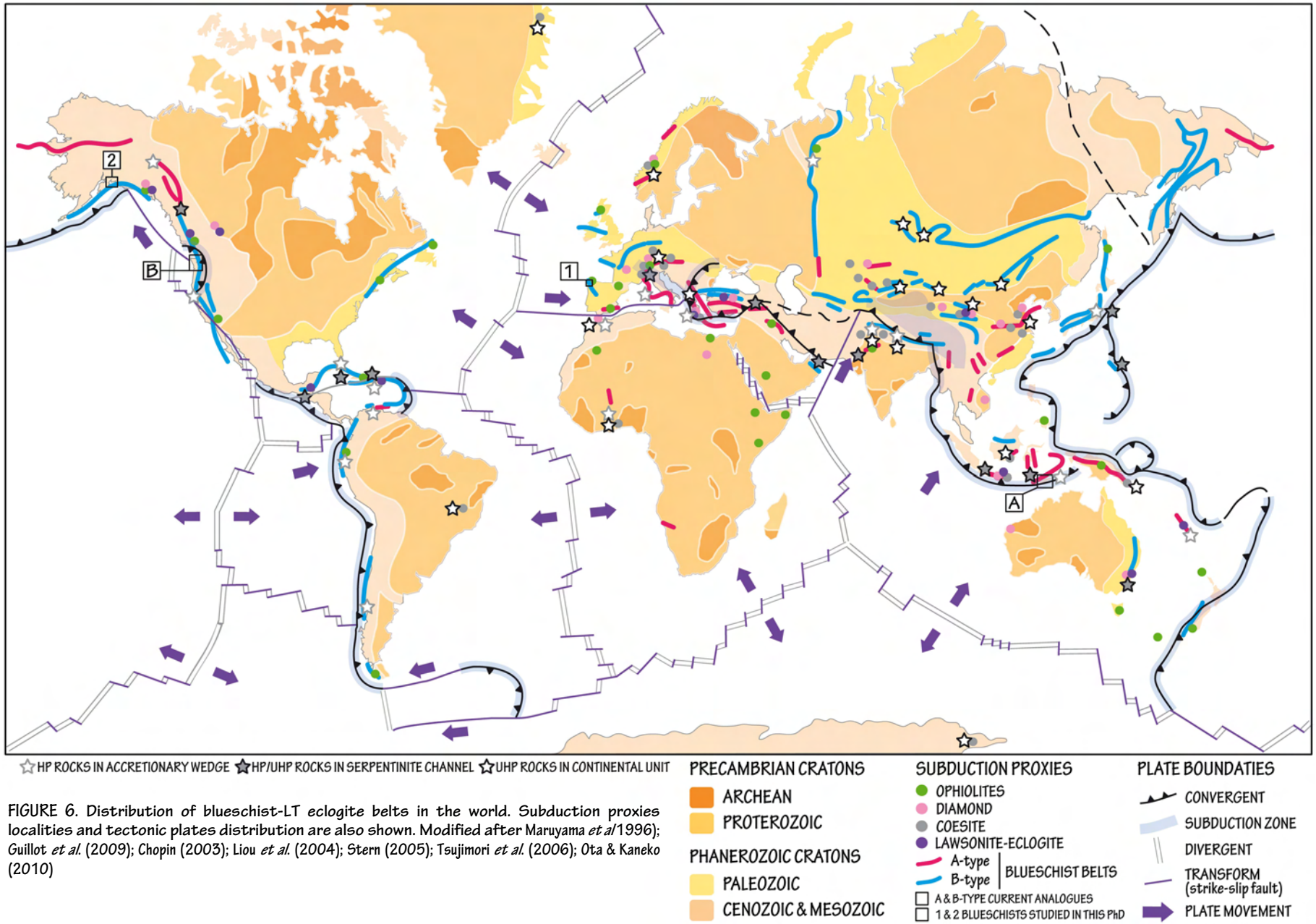

FIGURE 6. Distribution of blueschist-LT eclogite belts in the world. Subduction proxies localities and tectonic plates distribution are also shown. Modified after Maruyama *et al*/1996); Guillot *et al.* (2009); Chopin (2003); Liou *et al.* (2004); Stern (2005); Tsujimori *et al.* (2006); Ota & Kaneko (2010)

High geothermal gradients and a thinner lithosphere in the Precambrian are widely thought to have disfavoured blueschist formation. The rare preservation of Precambrian blueschist could be attributed to greenschist overprinting when the heat flow and geothermal gradient was high, rather than reflecting lack of production. However, their presence in China and Africa demonstrates that requisite conditions for blueschist facies metamorphism existed, at least, 700 Ma ago (Liou *et al.*, 1990).

Turning back toward the oldest known terranes on the Earth, reviews on the subduction and collision processes at crustal scale leading to the formation of Archean continents show two trends of understanding on the tectonothermal processes on Earth at that time (*e.g.* Liou *et al.*, 1990; Maruyama *et al.*, 1996; Möller *et al.*, 1995, 1998; Maruyama & Liou, 1998; Kusky & Polat 1999; Reddy *et al*, 2003; O'Brien & Rötzler, 2003; Stern, 2004; 2005; Bousquet *et al.*, 2008). Such trends try to unravel how Earth dynamics has evolved till present days. Some authors postulate that the crust-mantel thermal state responsible of subduction and collisional processes was quite different in the Archean, too hot to permit downgoing coherent crustal slabs, and subduction may not occurred until post-Archean times, whereas other authors suggest that a long-term protracted subduction may have operated on Earth since Archean. Nevertheless, regardless of when they started, there is an almost general agreement on the supposition that operating mechanisms of accretion within the wedge-structure have changed through time (*e.g.* Kusky & Polat 1999; Stern 2004).

On one hand, based on the blueschists distribution and on the age of the oldest UHP rocks known, reported in the Pan-African belt in Mali (Caby, 1994) and dated at ca. 620 Ma (Jahn *et al.*, 2001), some authors propose that the absence of (U)HP rocks in Archean belts may indicate that subduction was not active at that time. Liou *et al.* (1990), Maruyama *et al.* (1996), Maruyama & Liou (1998) and Stern (2005) suggests that blueschists/LT-eclogites distribution (FIGURE 6) show that, by Neoproterozoic time, subduction of lithospheric plates was efficient enough to refrigerate the hanging wall of a subduction complex generating blueschists and eclogites.

The existence of these rocks is interpreted to reflect a cooling Earth. Subduction-proxies distribution suggests a cold Precambrian Earth, sufficiently cool to allow subduction begin during Neoproterozoic time (*e.g.* de Roever, 1956; Ernst, 1972; Miyashiro, 1981). Thus, these authors postulate that there may be a drastic change of P–T conditions at ca. 800 to 700 Ma, after which an abnormally high dT/dP metamorphism began. The relationship between the total length of blueschist belts and their age correlates with the time of sea-level change, at least in the Phanerozoic, i.e. worldwide major periods of transgression correspond to extensive blueschist/LT-eclogite facies events and those of worldwide major regression to less active periods of blueschist/LT-eclogite formation. This relationship suggests that more rapid ocean-floor spreading, and hence higher subduction rates, tend to favour the formation and

exhumation of blueschist/LT-eclogite belts. Then, similarities between the patterns of blueschist/LT-eclogite and ophiolite formation support speculation concerning the control of periodic blueschist formation by the Wilson plate-tectonic cycle (Maruyama *et al.*, 1996). For example, the period of less extensive blueschist formation between 200 and 300 Ma is the time of amalgamation of the supercontinent Pangea. During that period extensive continental collisions might have reduced the activity of ocean-floor spreading on a worldwide scale.

On the other hand, the second trend is based on the analogies between the duality of thermal environments, one representing the subduction zone (low-to-intermediate dT/dP environment) and the other representing the arc–backarc system or orogenic hinterland (high dT/dP type), in old and modern plate tectonics regimes. Numerous examples of wedge-structures displaying blueschist/LT-eclogite facies conditions have been recognised in active mountain belts such as the Central Alps, the Apennines, the Shikoku Island (Japan), the Franciscan Complex or the Aleutians in the southern of Alaska. This, together with the broadly contemporaneous occurrence of MT eclogites and HP granulites from both old and young metamorphic terranes in the geological record since the Archean, indicate that thermal and tectonic lithospheric processes have not changed significantly, since at least the Neoarchean Era, and that HP conditions could have existed during Archean times (*e.g.* Möller *et al.*, 1995, 1998; Reddy *et al*, 2003; O'Brien & Rötzler, 2003; Haissen *et al.*, 2004; Pereira *et al.*, 2007; Pitra *et al.*, 2010b).

The duality of thermal environments may be a consequence of both globally continuous subduction and metamorphic imprints in the geological record that represent discrete "events" due to changes in plate kinematics or subduction boundary dynamics, or as a result of collision of ridges, arcs or continents with the upper plate at the trench (Brown, 2010). Moreover, many new occurrences of UHP rocks are found as relics in HP-granulite terranes (*e.g.* Liou *et al.*, 2004 with more references therein) and is suspected that UHP-eclogite conditions may have been present even when the Earth was much hotter (see Bousquet *et al.*, 2008). Additionally, experimental constrains on partial melting of hydrous basalt under eclogite facies conditions produces granitoid liquids with major (and trace) element revealing equivalent compositions to those of Archean TTG[3] (Rapp *et al.* 2003). Thus, the apparent Phanerozoic-ubiquitously of (U)HP may not be such restricted.

[3] tonalite–trondhjemite–granodiorite (TTG) series comprising silicic and sodic rocks that form a major component of preserved Archaean crust, and are widely considered to have formed during subduction by partial melting of hydrated oceanic crust

1.5 *Numerical modelling on phase equilibria*

1.5.1. *From inverse to forward modelling: a short review*

Knowledge on thermodynamics is a key to understand physicochemical changes occurring in Earth's crust, producing metamorphic rocks. All systems naturally tend to the minimum energetic configuration, i.e. equilibrium. Chemical equilibrium implies no change over time. Thus, equilibration conditions attained by a mineral assemblage would preserve the characteristics of the phases involved in the system at a certain moment, e.g. the P–T formation conditions of a metamorphic rock. As soon as the conditions (e.g. P or T) change, the system will immediately tend to a new equilibrium state. But since diffusion is involved, the scale at which the equilibrium will be achieved depends on the particular conditions (especially the temperature), on the character of the phases involved (e.g. diffusion in fluids is much faster than in solids), and on the available time. If the conditions change rapidly, the scale of equilibration will be small. However, it can be argued that even in this case the system will develop local equilibria – small domains where equilibrium is achieved or approached (e.g. Korzhinskii 1959; Thompson 1959). The equilibrium phase (mineral) assemblages and compositions can then be identified through a rigorous petrological analysis and the principles of equilibrium thermodynamics may be applied in order to understand the rock and determine the conditions of formation (cf. Powell, 1978; Pitra, 2011).

As mentioned above, the first to apply the concept of *chemical equilibrium* in metamorphic rocks was Goldschmidt (1911), suggesting through his research that thermodynamics was an essential tool for the study of metamorphism, and that the development of characteristic minerals in each type of metamorphic rock could be influenced by variations in pressure (depth), temperature and on changes in the bulk rock chemical composition. For long it has only been possible to infer qualitative comparisons on the P–T formation conditions of metamorphic rocks through the presence of index minerals or based on the assemblages resulting by the metamorphism of a wide range of protoliths under a particular facies.

Chemical thermodynamics is the formal mathematical framework that links measurable variables (i.e. mineral composition) with those that cannot be directly measured (i.e. chemical potential, pressure, temperature or fluid composition; e.g. Wood & Fraser, 1977; Powell, 1978; Ferry, 1982; Nordstrom & Munoz, 1994; Patiño Douce, 2011), using mathematical expressions based on the application of three laws: the ideal gas equation and the first two laws of thermodynamics. This enables deciphering the P–T history of metamorphic rocks, which is the main aim of the geothermobarometry. Experimentally determined phase equilibrium lie at the heart of nearly all thermobarometric methods. The experimental calibration of metamorphic reactions is the so called *conventional or classical inverse modelling*

thermobarometry, and was the only numerical method used until the late 80s for the quantification of P–T formation conditions of a metamorphic rock (e.g. Bohlen, 1987; Bohlen & Lindsley, 1987; Hodges, 1991; Spear, 1993; Philpotts & Ague, 2009). It involves the use of two (end-members) mineral reactions, ideally one highly pressure-dependent (geobarometer) and another strongly dependent on temperature (geothermometer). The simultaneous solution of both reactions in the P–T space provides a quantitative estimation to be valid only if minerals are in equilibrium. Although this technique may provide reasonable results, likewise requires important simplifications and show several limitations (errors derived from thermodynamic consistency, from the experimental calibrations or from the assumed equilibrium condition; e.g. Holland & Powell, 1985; Berman, 1991). One of the most important limitations is the use of single sets of equilibria to calculate the P–T conditions under which a rock equilibrated. A rock contains multiple minerals and is affected by several reactions. Then, increasing these information increases the accuracy on the estimations. Thus, to overcome these issues, and allow calculation of all equilibriums between a set of not only mineral end-member data, but also to activity–composition data (together with calorimetric or heat capacity and volume data among others), thermodynamic databases were created (e.g. Powell & Holland, 2008).

The so called *multi-equilibrium thermobarometry* begins to develop during the 90s for this purpose. It involves the use of internally consistent thermodynamic datasets for a wide range of minerals and chemical systems, implying a breakthrough on the research of phase relationship for mineral assemblages. These datasets are known as *internally consistent* because the thermodynamic parameters regressed for each phase depend on the others to produce equilibria which best fit the experimental determinations. The two most commonly used internally consistent databases in metamorphic petrology are those compiled by Holland and Powell (1985; 1990; 1998 updated 2003; 2011) and Berman (1988; 1991; 2007). Currently, there are several thermodynamic calculation softwares that use internally-consistent datasets for modelling phase equilibrium in petrological systems. THERMOCALC (Powell & Holland, 1988), Perple_X (Connolly, 1987) and Theriak-Domino (de Capitani, 1987) are most commonly used in metamorphic petrology. Generally speaking, at their heart these softwares are an internally consistent thermodynamic dataset that allows using thermodynamic data in a variety of ways solving how to handle multiple dimensions represented in two.

Perple_X is a command-line-driven software package that performs Gibbs energy minimization to create phase diagrams and pseudosections. Theriak-Domino is a suite of programs to calculate and plot thermodynamic functions, equilibrium assemblages and rock-specific equilibrium assemblage diagrams (pseudosections). Straightforward application is granted by both Perple_X and Theriak-Domino, which are based on fast computing algorithms

and has the ability to calculate and plot "ready to use" phase diagrams in reasonably short times without user intervention, performing calculations with a wide range of thermodynamic databases.

On the other hand, THERMOCALC uses a nonlinear equation solver to calculate user-specified equilibria using only its own internally-consistent thermodynamic dataset (Holland & Powell, 1985; 1990; 1998 updated 2003; 2011). It handles mineral equilibria through *inverse modelling* (geobarometry/thermometry using average P–T), and *forward modelling* (calculating phase diagrams for model systems, i.e. P–T–X pseudosections). The average P–T method of THERMOCALC considers an independent set of equilibria (from which all the other possible equilibria can be calculated) and a robust statistical treatment to indicate quantitatively the uncertainty on the result (Powell & Holland 1994; Powell & Holland 2008; Pitra, 2011). Create a diagram in THERMOCALC is laborious as curves must be built up one by one, and manually combined and can be extremely time-consuming without granting success. On the other hand, it allows understanding how phase diagrams are constructed (user monitors the Phase Rule, Schreinemaker's analysis, and how variance changes across field boundaries). Summarizing, numerical modelling of phase relations requires a set of thermodynamic data for mineral end-members (e.g. Berman 1988; Holland & Powell 1990; Holland & Powell 1998; Holland & Powell 2011), a description of the activity-composition (a-x) relations (the solid- (or liquid-) solution models or mixing models) and a software to perform the calculations. Among the most frequently used softwares in metamorphic petrology, the rapidity and relative easiness of use, together with the possibility of using multiple datasets, make Perple_X and Theriak-Domino interesting alternatives for calculating phase diagrams in relatively simple chemical systems, or as an initial approach prior to the use of THERMOCALC. THERMOCALC may be the best choice for calculating accurate phase diagrams in complex chemical systems or with phases requiring complex mixing models.

1.5.2 *Pseudosection approach*

The advantage of multi-equilibrium thermodynamic calculation softwares resides in the possibility of understanding observed rock data such as mineral assemblages, mineral proportions and mineral compositions, which is a much more sophisticated approach than plugging numbers into formulas (cf. Essene, 1982, 1989; Powell *et al.*, 1998; Powell & Holland, 2008). But their great progress is their ability to generate pseudosections. The petrological modelling through pseudosection approach of mineralogical phase equilibria in this PhD thesis has been performed using the software THERMOCALC, although other multi-equilibrium tools have been used as complements. This section therefore focuses on the use and management, as well as in the applications, advantages and problematic aspects of such

CALCULATING PSEUDOSECTIONS:
AN EXAMPLE IN THE KFMASH SYSTEM
FOR THE CEÁN SCHISTS

THERMOCALC is software that implements a method capable of generating various types of phase diagrams through sections, pseudosections or projections of a multicomponent heterogeneous system (cf. Powel et al., 1998).

Phase diagrams involving solid solutions are calculated by solving sets of non-linear equations (Powell & Holland 1990) representing equilibrium in a field or phase region (Hillert, 1985).

Thermobarometry using pseudosections is essentially qualitative, once the composition of the equilibration volume is chosen, and the diagram drawn (the "forward" part of the modelling). The "inverse" part of the modelling involves a qualitative comparison of the observed mineral compositions and proportions with the calculated equilibria. On the other hand, conventional thermobarometry is pure inverse modelling, but only using the observed mineral compositions, not the composition of the equilibration volume or the mineral proportions (Holland & Powell, 2008). Inverse modelling in THERMOCALC implies that it consider as unknowns the intensive variables pressure (P), temperature (T) and composition (X).

Calculating pseudosections involves the following steps:

(1) Choosing the model chemical system: KFMASH
(2) Defining the right bulk-rock composition: K_2O:3.34;FeO:7.04;MgO:4.78;Al_2O_3:13.42;SiO_2:71.42
(4) Selecting the mixing models for solid solutions of the phases: biotite, carfolite, chlorite, chlorithoid, coesite, garnet, kyanite, muscovite, quartz, sillimanite, staurolite and talc
(3) Calculating the P-T pseudosection between 5-35 kbar; and 400-800 °C considering q, mu and H_2O in excess

Based on Gibbs Phase Rule, the theoretical setting for equilibrium thermodynamic equations (Table I; Φ–phases; Cs–system components):

- when Φ = Cs + 2 = zero. The solution for such a system will provide P, T and X variables values at an invariant point

software for the construction of pseudosections. However, both the theoretical concepts and the uncertainties resulting from its use can be extrapolated to other softwares.

After the pioneering work of Hensen (1971), and subsequent inquiries by some isolated workers (e.g. Hudson 1980; Hudson & Harte 1985) it was the development of the internally-consistent thermodynamic dataset and the associated software THERMOCALC at the end of the 1980s (Powell & Holland 1985, 1988; Guiraud *et al.* 1990; Powell & Holland 1990) what allowed the widespread use of pseudosections for metamorphic rocks.

PSEUDOSECTIONS are phase diagrams that show stability fields of different equilibrium mineral assemblages for a particular bulk-rock composition (e.g. Powell & Holland, 1988; Spear & Menard, 1989; Connelly & Petrini, 2002). Considering the rock chemical composition (X) provides added constraints on the P–T conditions, unavailable in conventional thermobarometry, such as phase's coexistence, when phases (minerals, fluids or liquids) in the mineral assemblage are no longer stable, or when additional phases join the mineral assemblage. Through the comparison between the natural observations and the results of the numerical model, pseudosections

Table I. Gibbs Phase Rule in the KFMASH system (SiO_2, H_2O in excess); L–variance; Cs–system components; Φ–phases; n >3

L = Cs + 2– Φ Cs=4 (KFMA)	Phases		Varience	graphical representation	P, T, X variables
L = 4 + 2 – 6	Φ = Cs + 2	Φ =6	L =0	invariant point	P, T ,X values are obtained
L = 4 + 2 – 5	Φ = Cs + 1	Φ =5	L =1	univariant reaction	P, T or X value has to be set
L = 4 + 2 –4	Φ = Cs	Φ =4	L =2	divariant field	2 of the 3 variables ought to be set
L = 4 + 2 – 3	Φ = Cs – 3	Φ =3	L =3	trivariant field	the 3 variables ought to be set
L = 4 + 2 – Φ	Φ = Cs – n	Φ <3	L =n	n-variance field	n variables ought to be set

allow understanding the metamorphic evolution of a specific rock as P, T and X change. Pseudosections have the power to provide valuable additional thermobarometric information and do not depend on measurements of mineral composition. Likewise, even partly preserved assemblages (e.g. inclusions or partly pseudomorphed minerals) may be useful to infer segments of the P–T path of a rock, before and after the main equilibration stage (cf. Guiraud *et al.* 1990; 2001; Powell & Holland 1990; 2008; Powell *et al.* 1998; 2005; White *et al.* 2001; White & Powell 2002; Evans, 2004a; Guiraud & Powell 2006; Pitra, 2011).

Moreover, at each point of a pseudosection the composition and proportion of all phases may be calculated. Then, pseudosections allow estimating specific equilibria by calculating the P–T stability of particular mineral compositions with respect to the bulk rock composition, i.e. allows calculating mineral composition (and proportion, expressed in relative molar abundance) isopleths. The value set for the isopleth compositional variable derives from the EPMA analysis of that particular mineral in a specific sample (cf. Evans, 2004a, b). Isopleths then are used to further constrain equilibration conditions. But isopleths are particularly useful when applied on understanding chemical zoning of minerals, allowing to quantitatively investigate the effects of crystal fractionation on phase stability (e.g. Vance & Holland, 1993; Stüwe & Powell 1995; Ayres & Vance, 1997; Spear & Markussen, 1997; Vance & Mahar 1998; Marmo *et al.*, 2002; Evans, 2004a; Tinkham

- when $\Phi = Cs + 2 = 1$. The solution for such a system will be indeterminate. Providing a random value of P, T or X the value of the other two unknowns will be known. This enable the P–T–X location of any univariant equilibrium

- when $\Phi = Cs + 2 = 2$ any compositional isopleth in a divariant field could be sketched just by fixing the X value together with P or T

- when $\Phi = Cs + 2 > 2$ the number of variables set needs to be similar to the variance of the mineral assemblage

Starting from a previous petrogenetic grid (Wei & Powell, 2003) calculated for several HP-metapelites with similar composition to the Ceán Schists (FIGURE I) the first step is establishing the invariant points (i1-i5, i7, i8) and univariant reactions that the Ceán Schists composition "sees":

g + chl ↔ bi + ky [5]; ctd ↔ g + chl + ky [8]; g + car + ky ↔ ctd + coe [10]; g + car ↔ chl + ctd [17]; ctd ↔ g + chl + st [20]; g + chl ↔ bi + st [23]; g + ky ↔ bi + st [26]; chl + st ↔ g + ky [27]

THERMOCALC does not discriminate the relative stability of each mineral assemblage. However, the "dogmin" code allows Gibbs energy minimisation that enable deducing which is the assemblage with the lowest free energy within all possibilities

Sketch an outline of each reaction would help to understand the calculations (and future labelling) when trying to guess which phases may appear. Finally, the crafted scheme would represent a drawing of the P-T pseudosection in the range of interest (FIGURES II–IV).

e.g. CALCULATION OF LINE [17]

Line [17] is "seen" by the Ceán Schists between 24.26 to 23.46 kbar and 480 to 540°C, respectively (numbers highlighted in blue in FIGURE II). The reaction is actually "seen" from (24.56, 470), being metastable at those conditions (grey numbers; note that phase's mode does not change). Mode variations allow deducing which phases are on the L/HT side of the equation. Usually the low-T side is represented by the first line (in purple). But the software may switch the lines depending on the characteristics of each reaction. Reliable indicators are fluids, which systematically appear in the high-T side. Line [17] is almost subhorizontal (negative slope; FIGURE III), what suggests that the reaction is strongly pressure dependent. Then, the mode lines need to be interpreted in terms of low/high-P side of the equation. In line [17] carpholite and garnet "goes into" the equation (2nd mode line highlighted in green; high-P side) and chlorite and chloritoid "comes out" (1st mode line in purple), in the H_2O- bearing side, which is the highest volume side and thus low-P side. After deducting products and reagents location in the sketch, the following fields are established depending on the variations on the modal proportion of each phase. At 23.52 kbar and 520°C (orange values/squares) carpholite disappears and garnet appears in the low-P side of the reaction, which beyond 23.46 kbar and 540°c is no-longer stable (see FIGURE III).

& Ghent, 2005; Štípská *et al.* 2006; Pitra *et al.*, 2010a; López-Carmona *et al.*, 2013). Therefore, applying pseudosections to real rocks provides P-T estimates at which particular minerals grew within a rock. The qualitative information about the relative equilibration conditions or about the evolution of a rock may be the major strength of the pseudosection approach (Pitra, 2011). However, pseudosections are not fool proof and show certain drawbacks that are shortly addressed below.

When calculated using a thermodynamic dataset, pseudosections represent the result of a forward numerical modelling and are independent on the petrographic observations that can be done in the specific rock. An important restriction when using multi-equilibrium tools is implicit in *the internally consistent thermodynamic dataset*. Knowledge on the thermodynamic parameters for mineral phases used in thermobarometry has largely improved since databases appeared, but there is still much to be done. Occasionally, the use of *provisional data* in the

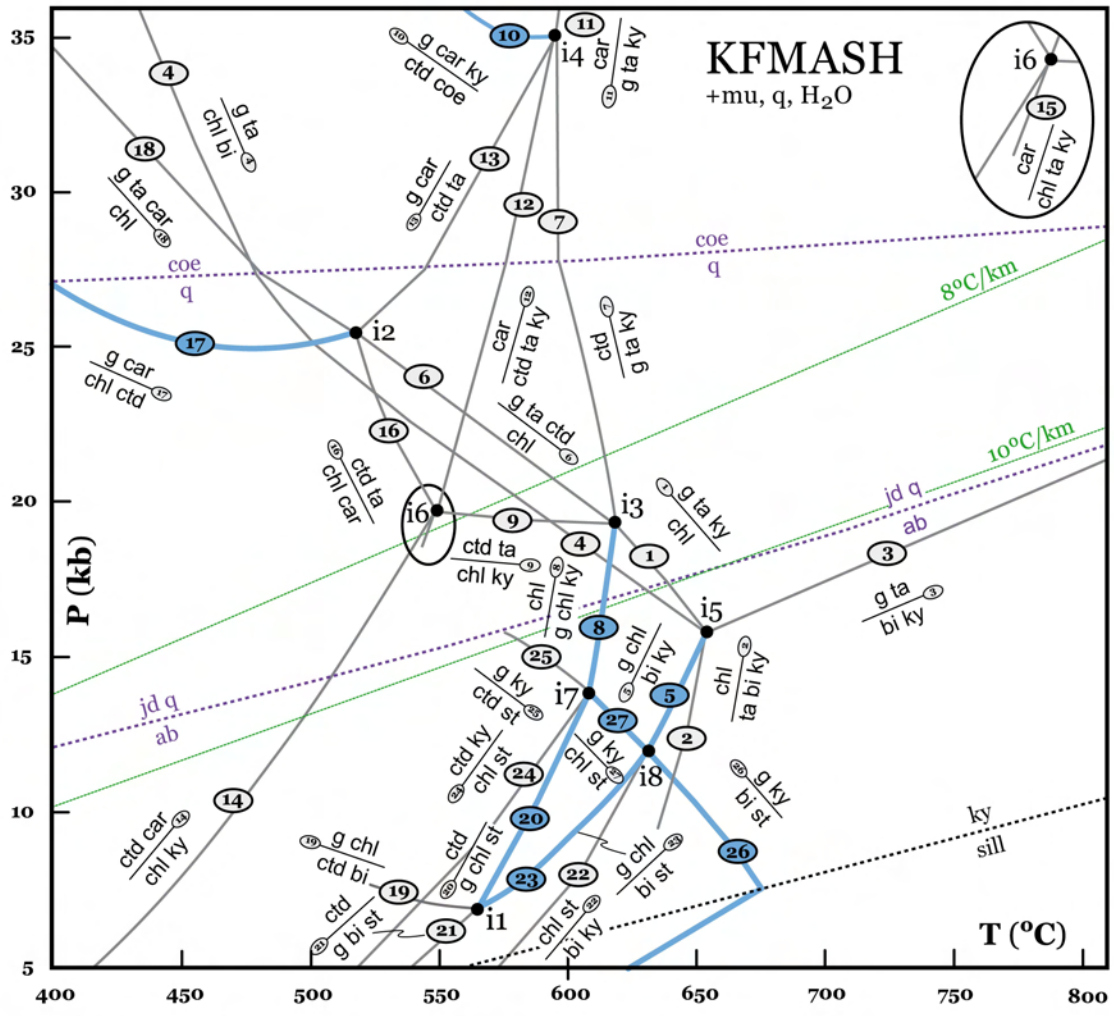

FIGURE 1. Petrogenetic grid for various HP-metapelites. Black dots and blue lines represent the invariant points and univariant reactions "seen" by the Ceán Schists composition, respectively. Modified after Wei & Powell (2003)

internally consistent database is subject to unknown errors that can slightly alter phase's stability, and thus the P–T estimates. Nevertheless, even the best software cannot overcome problems arising from missing or unconfident thermodynamic data (e.g. Petrakakis & de Capitani, 2005; Manon, 2008).

Two crucial elections have to be carefully considered before start working with THERMOCALC: choosing the chemical system and the *right* bulk rock composition. The elected CHEMICAL SYSTEM must be as close as possible to nature, because ignoring a phase component (such as e.g. apatite) can artificially alter the bulk rock composition. This is avoidable if proper correction is made (e.g. Ca in apatite [$Ca_5(PO_4)_3(F,Cl,OH)$] correction $CaO=CaO-3{,}33*P_2O_5$). The available chemical system usually depends on the available solid solution models for minerals. In general, simpler systems may be used to forward modelling theoretical scenarios, whereas inverse modelling requires larger systems. However, complex systems imply complex mixing models for solid-solution phases that may be a source of additional errors. Choosing the *right* BULK ROCK COMPOSITION (expressed in mol %) is decisive since the pseudosection would be only valid for such election. Nevertheless, as many minor elements are systematically ignored (e.g. P_2O_5 or BO_3), bulk rock compositions in THERMOCALC are always (fairly reliable) approximations to real rocks. The effects of overlooking these components depend on the sensitivity with which the adjustments on the bulk composition have been done, which relies on the petrographic user-knowledge of the sample considered. THERMOCALC manages the so called EFFECTIVE BULK ROCK COMPOSITION, which is that available to the reacting assemblage of phases

phases : cr, chl, ctd, g, (mu, q, H_2O)

P(kbar)	T(°C)	x(cr)	x(chl)	y(chl)	N(chl)	x(ctd)	x(g)	x(mu)	y(mu)
24.56	470	0.62	0.64	0.50	0.49	0.89	0.94	0.55	0.38

$76cr + 27g = 13chl + 89ct + 103q + 10H2O$

P(kbar)	T(°C)	x(cr)	x(chl)	y(chl)	N(chl)	x(ctd)	x(g)	x(mu)	y(mu)
24.26	480	0.59	0.59	0.50	0.49	0.87	0.93	0.51	0.40

$61cr + 20g = 10chl + 71ctd + 81q + 11H_2O$

mode	cr	chl	ctd	g	mu	q	
	0.29	0.01	0.05		0.37	0.28	→[↓P]
	0.32		0.02	0.01	0.36	0.27	→[↑P]

P(kbar)	T(°C)	x(cr)	x(chl)	y(chl)	N(chl)	x(ctd)	x(g)	x(mu)	y(mu)
23.52	520	0.45	0.42	0.51	0.49	0.75	0.86	0.37	0.48

$76cr + 20g = 10chl + 86ctd + 96q + 27H_2O$

mode	cr	chl	ctd	g	mu	q
		0.04	0.23	0.01	0.38	0.35
	0.13		0.12	0.05	0.37	0.32

P(kbar)	T(°C)	x(cr)	x(chl)	y(chl)	N(chl)	x(ctd)	x(g)	x(mu)	y(mu)
23.46	540	0.39	0.35	0.51	0.49	0.67	0.81	0.31	0.51

$87cr + 20g = 10chl + 97ctd + 107q + 37H_2O$

mode	cr	chl	ctd	g	mu	q
		0.00	0.20	0.05	0.38	0.35
	0.02		0.19	0.06	0.38	0.35

P(kbar)	T(°C)	x(cr)	x(chl)	y(chl)	N(chl)	x(ctd)	x(g)	x(mu)	y(mu)
23.51	550	0.36	0.31	0.51	0.49	0.62	0.77	0.28	0.52

$94cr + 20g = 10chl + 103ctd + 114q + 44H_2O$

FIGURE II. THERMOCALC "output" for reaction [17]

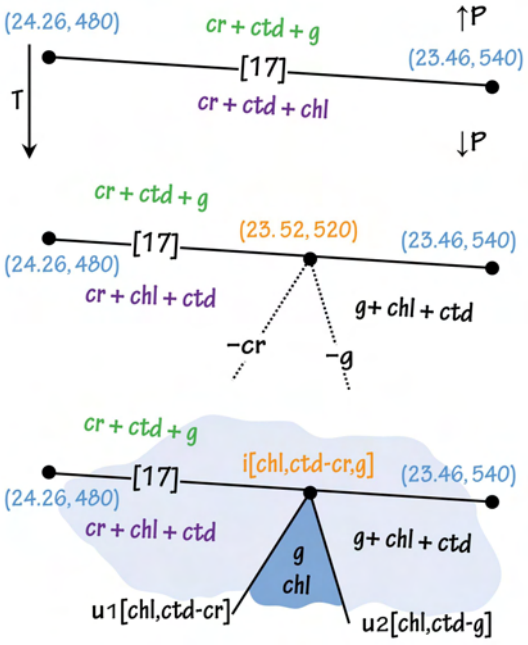

FIGURE III. Sketch for reaction [17]

(see Stüwe, 1997). Metamorphic rocks are commonly heterogeneous; this effective composition then may change throughout the history of metamorphic recrystallization and largely depends on the EQUILIBRATION VOLUMES. Two mechanisms can alter the effective bulk-composition of a rock during metamorphism, the open system behaviour (e.g. deformation or fluid effects) and the successive (re)equilibrations (e.g. Evans, 2004a). The occurrence of CHEMICALLY ZONED PHASES (typically garnet) in a sample implies crystal fractionation, thus the chemical reservoir from which minerals are growing (i.e. whole-rock bulk composition before garnet crystallization) would change into a new rock composition devoid of the components that reacted while the zoned crystal was growing (i.e. effective rock composition after garnet crystallization) (cf. Hollister, 1966; Atherton, 1968; Spear, 1988; Spear *et al.*, 1990; Frost & Tracy, 1991; Vance & Mahar, 1998; Marmo *et al.*, 2002; Evans, 2004a).

Thus, the effective bulk-composition of a rock through its metamorphic history may be characterised by a multitude of relatively small equilibration volumes (e.g. Stüwe, 1997; Tinkham & Ghent, 2005; Pitra, 2011). Currently two main approaches are used to obtain the effective-bulk composition, but the method used depends on the scale and accuracy of the problem to be solved. Small compositional domains may be analysed by quantitative X-ray mapping with an EPMA over a selected area of the sample (e.g. Clarke *et al.*, 2001; Marmo *et*

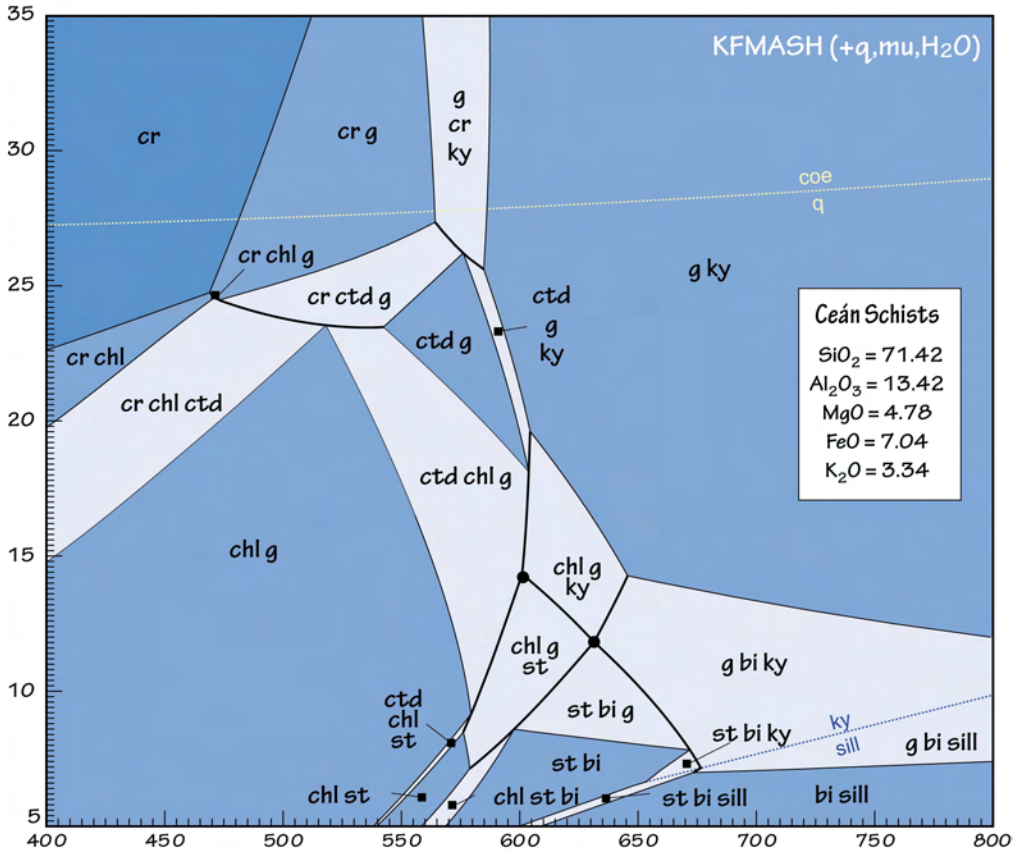

FIGURE IV. P–T pseudosection in the KFMASH system for the Ceán Schists. References of the mixing models for solid solutions are those from Wei & Powell (2004). Black dots and highlighted black lines represent the invariant points and univariant reactions "seen" by the Ceán Schists composition Modified after López-Carmona *et al.* (2010)

al., 2002). This method allows both the possibility to selectively eliminate individual phases that are interpreted not to have been reacting during recrystallization of surrounding phases, and the chance to eliminate compositional domains that are distinctly different from that of the region of primary interest in compositionally layered samples (see Tinkham & Ghent, 2005). Equilibrium is generally thought to be attained at the hand-sample scale provided that no clear evidence to the contrary is found (Chernoff & Carlson, 1997; Hirsch *et al.*, 2003). Theoretically, if the compositional domains of interest are on the order of 1 cm wide or greater, up to hand-sample scale, individual domains can be separated and analysed with X-ray fluorescence spectroscopy (XRF). THERMOCALC is provided of a facility (the rbi "read bulk info" code) that allows defining or changing a bulk rock composition through the mode and composition of phases. This application can be used to investigate the internal buffering of fluids or the fractionation of bulk rock compositions due to porphyroblast growth, as well as to assess the loss of melt from a bulk rock composition or to make an approximate protolith composition from a melt depleted rock.

Finally, the lack or difficulty to determine the proportion of significant components such as H_2O and Fe_2O_3 ("O" in THERMOCALC) in the bulk composition by routine analytical techniques raises important uncertainties when modelling phase equilibria, and can largely influence phase relations and hence P-T estimates. The amount of H_2O has to generally be guessed if not in excess, whereas the Fe_2O_3 can be determined. Total iron (as $Fe_2O_{3(T)}$) can be measured by XRF and FeO can be analysed by wet chemical titration. Then, the amount of Fe_2O_3 is calculated stoichiometrically as $[(Fe_2O_{3(T)}/1.43\text{-}FeO/1.286)*1.43]$ (for further details on the analytical technique see section 1.2).

CALCULATING FeO, Fe_2O_3 & "O"

In standard analytical techniques, all elements are oxidised when analysed. Then in:

$Fe_2O_{3(R)} = [(\text{TOTAL IRON}/1.43) - (FeO/1.286)]*1.43$
$Fe_2O_{3(R)} = [\text{TOTAL IRON} - FeO]*1.43$

the total iron measured by XRF is $Fe_2O_{3(T)}$, FeO is measured by titration and $Fe_2O_{3(R)}$ is that reported by the lab. The $Fe_2O_{3(T)}$ is converted to Fe and then subtracted from the converted FeO to Fe. This gives the Fe left in the sample that is then multiplied by the conversion factor 1.43 to get the $Fe_2O_{3(R)}$. The FeO is subtracted from TOTAL IRON using the conversion factor given by the ratio of the molecular weights: $Fe_2O_3/2*FeO=1.1113$ because in FeO there is an oxygen for one iron (1:1), whereas in Fe_2O_3 the proportion is 3:2 (=1.5). So, converting FeO to Fe_2O_3 (in wt%) is done $FeO=1.1113*Fe_2O_3$
In THERMOCALC The $Fe_2O_{3(R)}$ recalculated to mol % (=wt %/molecular weight) in the appropriate chemical system would be the "O" parameter (i.e. $O=1.5*Fe_2O_3$).

1.5.3 *Guessing Fe_2O_3 and H_2O*

On Earth, iron exists in two oxidation states: reduced ferrous iron, depicted as Fe^{2+}, or oxidized ferric iron, depicted as Fe^{3+}. These states can be found in nature as solids in the form of Fe^{2+}- and Fe^{3+}-bearing minerals (or as ions dissolved in fluids). Ferric iron is present in significant amounts in some of the most common silicates (e.g. epidote, amphibole, garnet, chloritoid, clinopiroxene or biotite) and in accessory minerals (e.g. rutile or ilmenite) in both

metapelitic and metabasic rocks. For long it has been considered that the oxidation state may be significantly affected by alteration, and became a common practice dealing with "total iron" instead of analysing FeO and Fe_2O_3. Whereas this may be acceptable from the geochemical point of view, it hinders non-negligible effects when modelling phase relations in metamorphic rocks. Low and high-grade pelitic lithologies are thought to be form under relatively reducing conditions and calculations indicate that in typical metapelitic bulk compositions small (to moderate) amounts of Fe_2O_3 have little effect on silicate mineral equilibria (e.g. White *et al.* 2000; White *et al.*, 2002). However, the Fe^{3+}-influence in HP pelitic rocks is less contrasted and recent studies reveals that its effects cannot be overlooked (e.g. López-Carmona *et al.*, 2013). The situation is different in metabasic rocks since through years studies attention has been focused on the effects of ferric iron in the modelling of mafic systems. Since the formulation of satisfactory solid-solution models including ferric iron for amphiboles and pyroxenes (Dale *et al.* 2005; Diener *et al.* 2007; Green *et al.* 2007), it became clear that the amount of ferric iron in metabasic rocks needs to be taken into account. In the absence of reliable data on the oxidation state of metabasic rocks, the amount of ferric iron can be estimated from the chemical composition and the mode of the minerals present (e.g. Ballèvre *et al.* 2003; Warren & Waters 2006). Nevertheless, in this case a supplementary uncertainty arises from the problematic estimation of the ferric iron content from microprobe analyses (e.g. Droop 1987). When working with THERMOCALC the most reliable way to keep the consistency between EPMA and numerical modelling is calculating the mineral formulae of phases using the software AX (Holland & Powell, 2000 in Powell & Holland 2002; http://www.esc.cam.ac.uk/research/research-groups/holland/ax). The AX is an activity-composition calculation program for rock-forming minerals in which the amount of ferric iron is calculated from stoichiometric constraints.

It is assumed that water content of pelites is high. Therefore, it can be expected that the proportion of water released during metamorphism help to keep the rock in chemical equilibrium. Prograde metamorphism of pelitic sediments starts with rocks at a maximum hydrated state (e.g. Bucher & Frey, 2002). Although this is a good approximation in most metapelites, in some cases, the proportion of water in the rocks when burial begins may vary due to many factors such as the available amount of water external to the system, or whether if this system was closed or not. Therefore, is justified assuming water-saturated conditions systematically for petrologic modelling?. The possibility of reduced water availability in certain geodynamic scenarios allows rocks to experience a fluid-absent prograde evolution during subduction. Then, guessing the appropriate H_2O content is a critical issue when modelling phase equilibria.

A vast majority of metamorphic reactions have a dehydration character and produce H_2O fluid when crossed upon heating, during the prograde evolution. Accordingly, most rocks are

saturated in H_2O, which is then commonly considered in excess for petrological modelling. Whereas this approach yields correct results in most cases, several exceptions merit highlighting: polycyclic evolution, partial melting, retrograde evolution and subduction metamorphism. The latter is the one that concerns this PhD thesis. Metamorphism in subduction zones is characterized by low geothermal gradients (steep in a P–T diagram). Rocks following these gradients may cross some dehydration reactions in the "wrong", H_2O-consuming direction. This is the case of the reactions involving lawsonite, which have a relatively "flat" slope with lawsonite being stable at the HP–LT side. Consequently, rocks become H_2O undersaturated with important implications for the phase relations and mineral assemblages encountered in such environments (e.g. Ballèvre *et al.*, 2003; Clarke *et al.*, 2006; López-Carmona *et al.*, 2013). Unlike their metabasic counterparts, pelitic rocks are depleted in Ca and can only form limited quantities of lawsonite. It is then not common for a metapelite to experience a fluid-absent prograde metamorphism, which can be expected in metabasic rocks.

Summarising, phase relations in mafic systems for blueschists (and eclogites) are being widely investigated in the last decades (e.g. Clarke *et al.*, 1997, 2006; Will *et al.*, 1998; Carson *et al.*, 1999; Ballèvre *et al.*, 2003; Fitzherbert *et al.*, 2003; Wei *et al.*, 2003; Štípská & Powell, 2005) with particular attention on the effects/influence of H_2O (e.g. Guiraud *et al.*, 2001; Ballèvre *et al.*, 2003; Clarke *et al.*, 2006; Konrad-Schmolke *et al.*, 2011) and Fe_2O_3 (e.g. Proyer *et al.*, 2004; Warren & Waters 2006; Diener *et al.* 2007; Rebay *et al.*, 2010; Diener & Powell, 2010; Korhonen *et al.*, 2012). Recent improvements in solid solution models for Fe^{3+}-bearing mineral end-members (e.g. White *et al.*, 2000; Tajčmanova *et al.*, 2009; Diener & Powell, 2012) has given way to more precise phase diagram calculations in model chemical systems closer to real rocks (e.g. Warren & Waters, 2006; Wei *et al.*, 2009; Groppo & Castelli, 2010; López-Carmona *et al.*, 2011, 2012; Vitale Brovarone *et al.*, 2011). However, the effects/influence of H_2O and Fe_2O_3 in blueschist (and eclogites) facies rocks in pelitic systems need to be further refined.

CHAPTER 2

The Malpica-Tui Complex

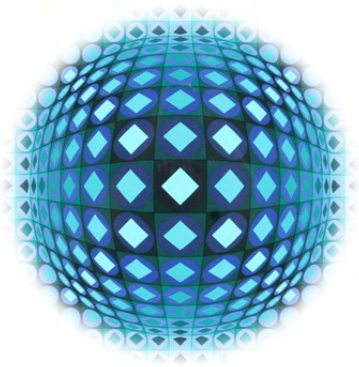

2. THE MALPICA-TUI COMPLEX

2.1 *Geological background*

The Malpica-Tui Complex is located in the NW section of the Iberian Massif, in the Galicia-Trás-os-Montes Zone (Farias *et al.*, 1987; Arenas *et al.*, 1988), constituting the westernmost outcrop of the internal areas of the European Variscan Belt. The Galicia-Trás-os-Montes Zone is a large allochthonous sheet thrusted over the Central Iberian Zone (Julivert *et al.*, 1972, 1980) that comprises two domains: the Schistose Domain (so called the Parauthocthon) and the overlying Allochthonous Complexes Domain (FIGURE 7). The Schistose Domain is interpreted as a section of the most distal margin of Gondwana, tectonically transported towards the internal areas of the continent (Arenas *et al.*, 1986; Farias *et al.*, 1987; Ribeiro *et al.*, 1990; Martínez Catalán *et al.*, 1997, 1999; Marcos & Farias, 1999; Martínez Catalán *et al.*, 2007). The Allochthonous Complexes are, in turn, thrusted over the Schistose Domain, and consist on a succession of units with different affinities that have undergone large displacements becoming part of a huge nappe stack during the Variscan collision (Ries & Shackeleton, 1971). In the initial orogenic pile these units were separated by thrusts and extensional detachments, but commonly their tectonic relations were subsequently modified by later strike-slip and brittle tectonics (see Martínez Catalán *et al.*, 2002; Gómez Barreiro *et al.*, 2007; Díez Fernández *et al.*, 2011). From bottom to top in the structural pile these units are grouped as basal, ophiolitic and upper units, and can be correlated between the different complexes, although not all units are always present. Both the basal and upper units show continental affinity. However,

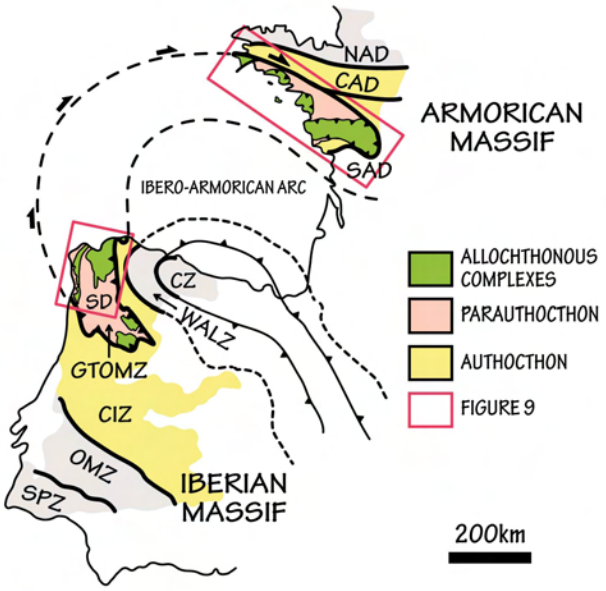

FIGURE 7. Simplified sketch showing the distribution of the different domains in the Iberian and Armorican Massifs through the Ibero-Armorican Arc. CZ–Cantabrian Zone; WALZ–West Asturoccidental-leonese Zone; SD–Schistose Domain; GTOMZ–Galicia-Tras-os-Montes Zone; CIZ–Central Iberian Zone; OMZ–Ossa-Morena Zone; SPZ–South Portuguese Zone; NAD–North Armorican Domain; CAD–Central Armorican Domain; SAD– South Armorican Domain. Modified after Julivert *et al* (1972); Farias *et al.* (1987); Martínez Catalán *et al.* (2002; 2007; 2009) and Ballèvre *et al.*, (2009).

they are very different. The basal units record a Cambrian-Ordovician rifting event including alkaline and peralkaline magmatism (Pin *et al.*, 1992) and passive margin sequences, whereas the upper units represent a Cambro-Ordovician continental island arc (Abati *et al.*, 1999; Abati, 2002). The basal units experienced a relatively simple monocyclic tectonothermal evolution of Variscan age (Martinez Catalan *et al.* 1996), and the upper units record a pre-Variscan and Variscan polimetamorphic tectonothermal evolution. Because the basal units are not separated from the parauthochthon by ophiolites, they are assumed to belong to Gondwana, and because the ophiolitic units overlie them, they are viewed as fragments of the most external margin of this continent. On the other hand, the ophiolitic units contain lithologic associations and geochemical signatures characteristic of oceanic domains, including a variety of geodynamic environments (e.g. Sánchez Martínez, 2009). In this sense the nomenclature is confusing. The allochthonous terranes, sensu stricto, different and exotic, are the so called ophiolitic and upper units, whereas the basal units are part of Gondwana's margin toghether with the parautochthon.

The allochthonous nappes experienced a complex tectonothermal evolution that concluded in their exhumation by crustal-scale thrusting, accompanied by recumbent folding and tectonic denudation (Martínez Catalán *et al.*, 1996, 1997; Díez Fernández & Martínez Catalán, 2009; Gómez Barreiro *et al.*, 2010; Díez Fernández *et al.*, 2010), together with a strong thinning of the original ensemble and the dismemberment of the different units (e.g. Martínez Catalán *et al.*, 2009).

Currently, the Allochthonous Complexes represent residual mega-klippen of the initial stacking preserved within the core of late synformal folds that outcrop in the NW Iberian Massif between Spain (Cabo Ortegal, Órdenes and Malpica-Tui complexes) and Portugal (Bragança and Morais complexes) and in different massifs across western and central Europe into Poland, where the Variscan Belt is shifted by a tectonic line known as Tornquist Fault (FIGURE 8). For this reason, and to facilitate the terminology in the view of correlations across the European Variscan Belt, the classical nomenclature for the different units forming the Allochthonous Complexes of the NW Iberian Massif consisting on basal, ophiolitic and upper units, has been recently extended to Lower, Middle and Upper Allochthons (Ballèvre *et al*, submitted), and this recent most nomenclature is the one used in the present research. Both divisions are roughly equivalent so that the upper units and the Upper Allochthon are counterparts, whereas the basal and ophiolitic units have been redistributed within the Lower and Middle Allochthon. The major difference concerns the "basal units", where two tectonically juxtaposed sequences of different affinity, metamorphism and tectonostratigraphy have been identified in the Galician Allochthonous Complexes (c.f. Martínez Catalán 2002; 2007; 2009; Rodríguez, 2005; Díez Fernández *et al.*, 2010; Gómez Barreiro *et al.*, 2010; López-Carmona *et al.*, 2010). The lower sequence, the one located structurally below, corresponds to

the Lower Allochthon, whereas the upper sequence has been included in the so called Middle Allochthon, together with the ophiolitic units. All the details of the correlation are extensively described in Chapter 4. In addition, throughout this chapter, each of the allochthonous units will be shortly described, and all what concerns the Malpica-Tui Complex will be detailed.

The Variscan Orogen resulted from the collision of the continental margins of Laurussia and Gondwana during the Late Paleozoic (Devonian-Permian), prior to the formation of the last Supercontinent Pangea. This collision involved Gondwana-derived intermediate continental blocks (so called peri-Gondwanan terranes) that were amalgamated upon Gondwana forming a large orogenic wedge through the Devonian-Carboniferous before its final accretion to Laurussia (Martínez Catalán *et al.*, 2007; 2009; von Raumer & Stampfli, 2008). During the Paleozoic the Iberian Peninsula was located close to the confluence of the three most important Paleozoic orogenic belts: Appalachian, Caledonian and Variscan (FIGURE8). For this

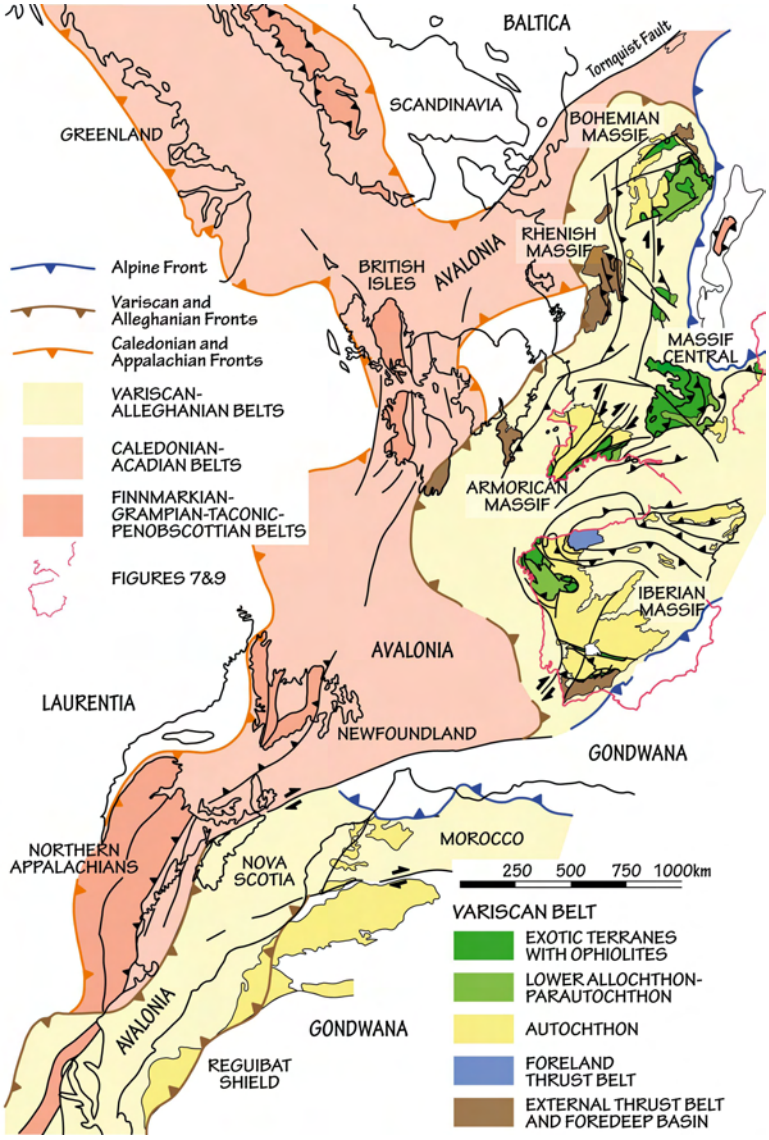

FIGURE 8. Scheme showing the position of the Iberian Peninsula and France in relation to the Appalachian, Caledonian and Variscan belts at the end of the Variscan Orogeny. Modified from Neuman & Max (1989) and Martínez Catalán *et al.*, (2007).

reason, the Iberian Variscan orogen is one of the key geological frameworks to study the latest Precambrian and Paleozoic evolution of the Earth (e.g. Martínez Catalán *et al.*, 2002). At the end of the Paleozoic the NW Iberian Peninsula and the SW of France shared a marked curvature known as the Ibero-Armorican Arc (e.g. Brun & Burg., 1982; Ribeiro *et al.* 1995).

2.1.1 *The Allochthonous Complexes throughout the Ibero-Armorican Arc*

The Ibero-Armorican Arc is considered one of the main macrostructures of the Variscan belt in Western Europe (e.g. Suess, 1888; Stille, 1924; Lotze, 1929; Bard *et al.* 1971; Ribeiro *et al.* 1995). The arc can be followed from Brittany, across the Bay of Biscay, to western Iberia (FIGURE 7), where it is bounded by a coupled orocline system with two linked bends: the Cantabrian Orocline to the north (e.g. Suess, 1909; Julivert, 1971; Weil *et al.*, 2000, 2001, 2013; Gutiérrez-Alonso *et al.*, 2004, 2011a, 2011b; Weil *et al.*, 2013) and the Central Iberian Orocline to the south (e.g. Staub, 1926, du Toi, 1937; Aerden, 2004; Martínez-Catalán, 2010, 2011; Shaw *et al.*, 2012). The orogenic-scale folding is interpreted as a late feature, developed essentially during the late Carboniferous-early Permian (c. 310–295 Ma) (Weil *et al.*, 2010; Pastor-Galán *et al.*, 2011), resulting from the rotation around a vertical axis of the initially linear orogen (e.g. Brun & Burg., 1982; Weil *et al.*, 2001; Martínez-Catalán, 2011; Weil *et al.*, 2013) and is thought to be formed at a lithospheric scale (Gutiérrez-Alonso *et al.*, 2004; Pastor-Galán *et al.*, 2012).

As mentioned above, previously, during the early phases of the Varican orogeny, a huge nappe stack was built on both sides of the Bay of Biscay forming a complex allochthonous sheet emplaced upon the sequences deposited on the passive margin of north Gondwana. The remnants of this ensemble exist as allegedly exotic terranes that can be separated into three lithostratigraphic units, Upper, Middle and Lower Allochthons, stacked above an underlying thrust sheet, with stratigraphic and petrologic affinities with its relative autochthon, which is referred to as the Parautochthon and has been identified in both domains. These units bear the imprint of the Paleozoic subduction and can be correlated across north-west Iberia and the southern Armorican Massif throughout the Ibero-Armorican Arc (FIGURE 9; Ballèvre *et al.*, 2009; Martínez Catalán *et al.*, 2009; Ballèvre *et al.*, submitted; López-Carmona *et al.*, submitted).

The Upper Allochthon includes fragments of a Cambro-Ordovician continental (ensialic) island arc (Arenas *et al.*, 1986; Jégouzo *et al.*, 1986; Janjou, 1998; Abati *et al.*, 1999; Andonaegui *et al.*, 2002; Santos Zalduegui *et al.*, 2002; Abati *et al.* 2003; Castiñeiras, 2005; Gómez Barreiro *et al.* 2006; Le Hébel *et al.*, 2007; Castiñeiras *et al.* 2010; Fuenlabrada *et al.*, 2010; Albert *et al.*, 2012). The arc was developed at ca. 500 Ma in an active part of the northern margin of Gondwana and the related back-arc extension probably helped to open the (Rheic?) ocean/s (see e.g. Murphy *et al.*, 2009b). This arc was subsequently accreted to

Laurentia or Baltica between 440 and 410 Ma (age of the high-pressure and high-temperature metamorphism; Fernández-Suárez *et al.*, 2007). The Middle Allochthon consists of dismembered slices of oceanic derivation that locally display a blueschist-to eclogite-facies imprint during the Variscan orogeny. These units contain the remnants of a Cambro-Ordovician back-arc (Arenas *et al.*, 2007a; Sánchez Martínez *et al.*, 2007a), possible evidence of Ordovician oceanic crust (Pin *et al.*, 2006), and suprasubduction type, Early-Middle Devonian ophiolites (Peucat, 1973; Hanmer, 1977; Bernard-Griffiths & Cornichet, 1985; Paquette, 1987; Díaz García *et al.* 1999; Lucks *et al.*, 2002; Arenas *et al.*, 2004a, b; Pin *et al.*, 2006; Faure *et al.*, 2005; 2008; Sánchez Martínez *et al.*, 2007b; 2009; Gómez Barreiro *et al.* 2010). Among these oceanic complexes, some are true ophiolitic units, while others are interpreted as accretionary prisms derived from an Early Ordovician ocean/s, or an ocean-continent transitional domain related either to the Lower or the Upper Allochthon. True ophiolites are considered to be remnants of the (Rheic?) ocean/s accreted below the Upper Allochthon at ca. 385 Ma (Sánchez Martínez, 2009).

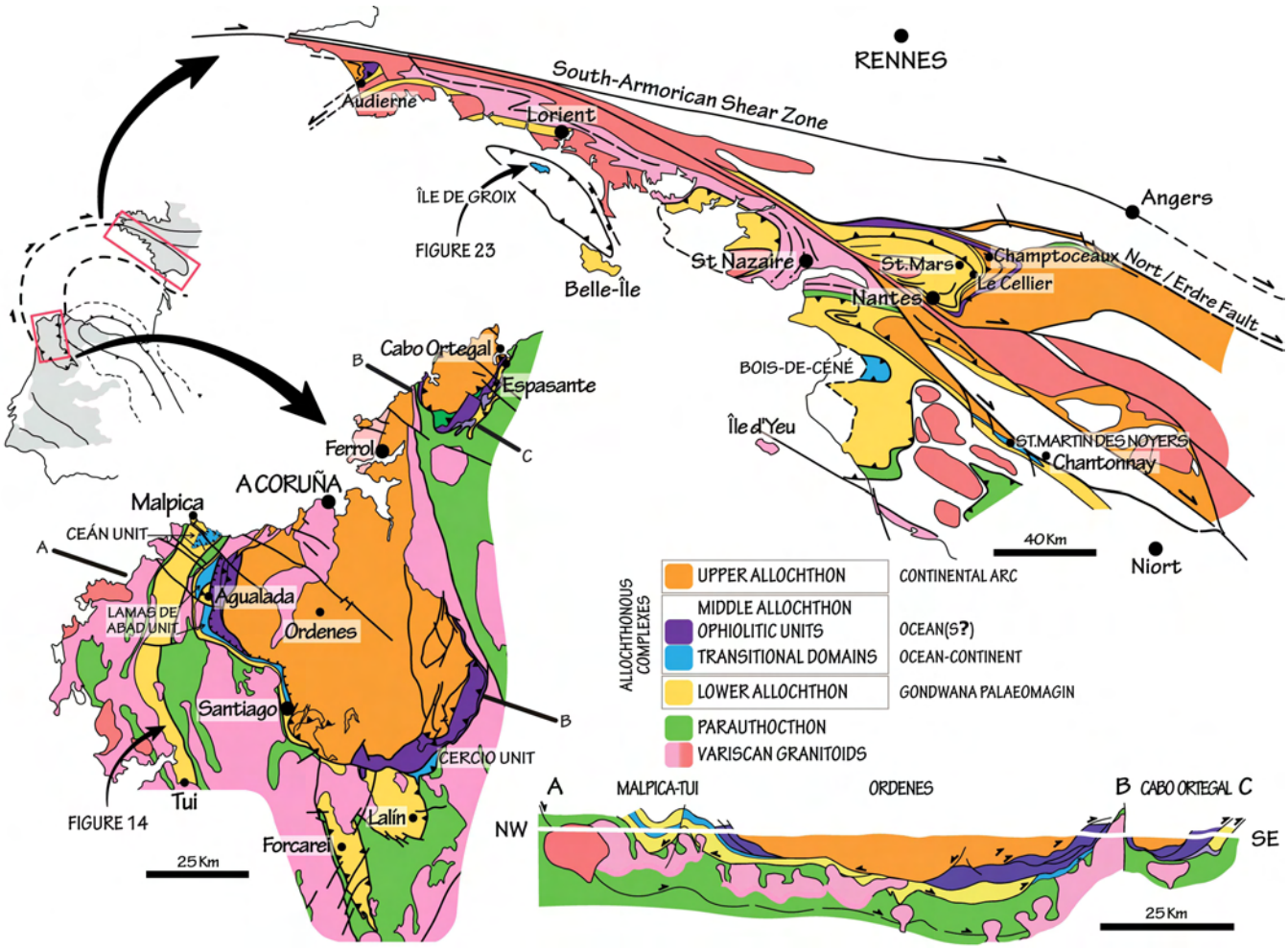

FIGURE 9. Simplified geological maps of NW Iberia and the Southern Armorican Massif showing the distribution and correlation of the allochthonous domains. The cross-section displays the general structure of the Malpica-Tui, Órdenes and Cabo Ortegal complexes in NW Spain. Modified from Gómez Barreiro *et al.* (2007); Ballévre *et al.* (2009); Martínez Catalán *et al.*,(2009); Díez Fernández *et al.* (2010); Ballévre *et al.* (submitted) and López-Carmona *et al.* (submitted)

Finally, the Lower Allochthon represents the outermost sections of the north Gondwana continental margin subducted beneath the southern margin of Laurussia during late Devonian, at the beginning of the Variscan collision (Martínez Catalán *et al.*, 1996; 1997; Arenas *et al.*, 1997; Ballèvre *et al.*, 2009; Martínez Catalán *et al.*, 2009; Ballèvre *et al.*, submitted). Subsequently, the Lower Allochthon was accreted to the Variscan orogenic wedge as a thin, imbricated thrust sheet. The early-Variscan high-pressure and low-temperature metamorphism affecting the Lower and Middle allochthon has been interpreted as a result of this subduction, that marked the final closure of the existing Cambro-Ordovician ocean/s (Rheic?) and the last stages of the assembly of Pangea (Matte, 1986; Scotese, 1997; Stampfli & Borel, 2002; Gutiérrez-Alonso *et al.*, 2008; Martinez Catalan *et al.*, 2009; Díez Fernández *et al.* 2012). The polarity of the subduction has been deduced by the presence of a pressure gradient along the sheet, where pressure increases from east to west indicating that the subduction had a significant westward component in present coordinates (Martínez Catalán *et al.*, 1996). The paleodip of the subduction zone has been estimated from P-T conditions and thermal modelling at 15° to 20° (Alcock *et al.*, 2005), and kinematic indicators in high-pressure fabrics are in agreement with this reconstruction suggesting top to the northwest movement (Díez Fernández *et al.*, 2012).

2.2.2 *Metamorphism in the Lower Allochthon and the basal part of the Middle Allochthon*

This section concerns the description of the metamorphism in the Lower Allochthon and the basal part of the Middle Allochthon (the transitional domains in FIGURE 9), which share a relatively similar tectonothermal evolution, leaving aside the ophiolitic units, with very different lithological associations and metamorphic evolution.

In the Iberian Massif, according to their tectonostratigraphy and metamorphism, the Lower and Middle Allochthons form two tectonically juxtaposed sequences composed mainly of magmatic and metasedimentary rocks, respectively (FIGURE 9). Knowing the northwest-directed component of subduction, the characteristics of each sequence suggests that the Middle Allochthon would occupy an oceanward position compared to the Lower Allochthon before the Variscan collision (cf. Martínez Catalán 2002; 2007; 2009; Rodríguez, 2005; Díez Fernández *et al.*, 2010; Gómez Barreiro *et al.*, 2010; López-Carmona *et al.*, 2010). Thus, the Lower Allochthon is interpreted as a slice of continental crust, where felsic orthogneisses and terrigenous metasediments predominate (cf. Rodríguez, 2005; Díez Fernández, 2011), whereas the Middle Allochthon is interpreted to represent a volcano-sedimentary sequence viewed as a more distal part of the same continental margin transitional to an oceanic domain (cf. Rodríguez, 2005; Díez Fernández *et al.*, 2010; López-Carmona *et al.*, 2010). Although their outcrops in the different Allochthonous Complexes

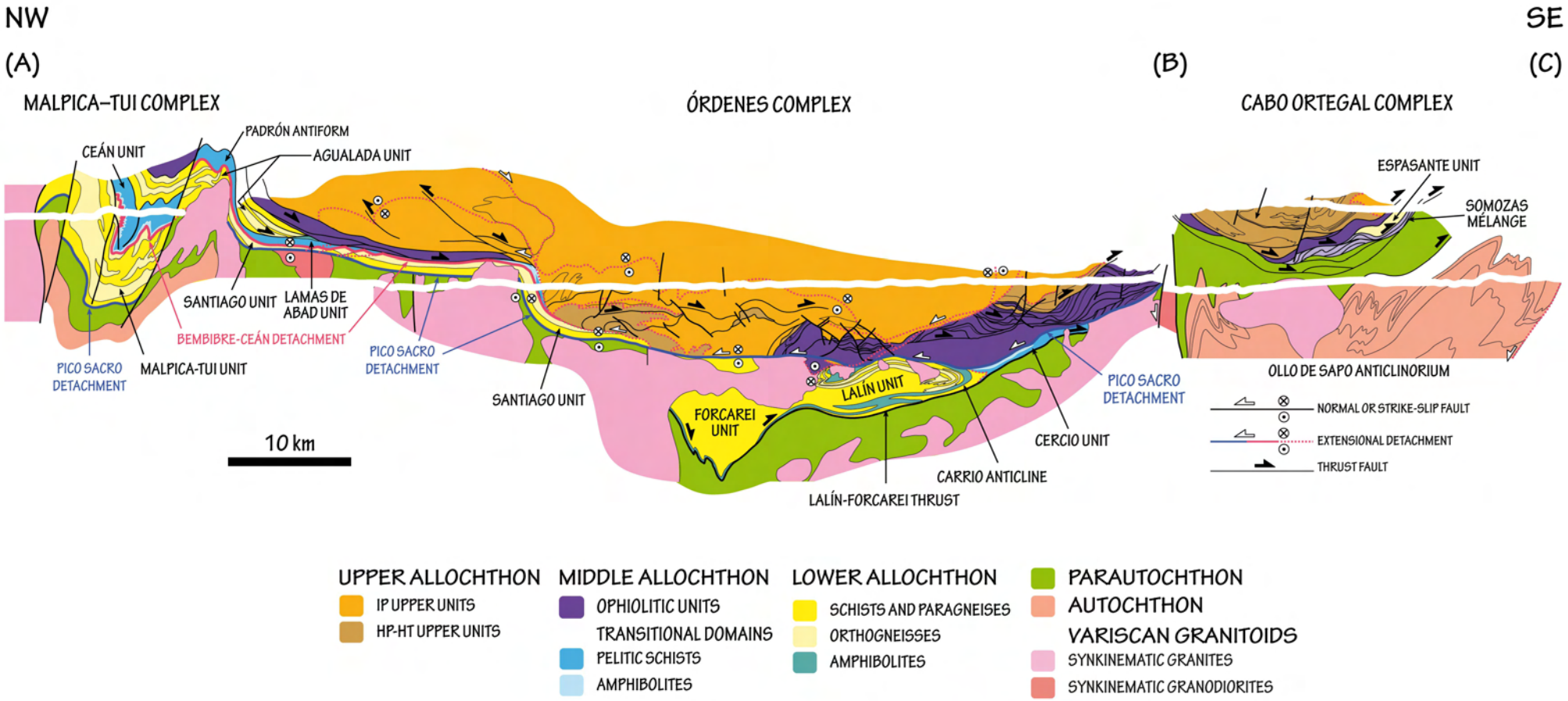

FIGURE 10. Representative cross section showing the general structure of the Allochthonous Complexes (Malpica-Tui, Órdenes and Cabo Ortegal) in NW Spain. Location of each cross section (A–B–C) is indicated in FIGURE 9. Modified from Martínez Catalán *et al.* (2007) and Díez Fernández *et al.* (2011).

are separated by relatively large distances and show certain particularities, structural reconstructions indicates that both allochthons formed a coherent and continuous sheet of continental and transitional to oceanic lithosphere (FIGURE 10; Martínez Catalán *et al.*, 2007; Díez Fernández *et al.*, 2011).

The Lower Allochthon forms the lower part of the Malpica-Tui Complex (i.e. the Malpica-Tui Unit), Santiago, Agualada, Lalín, Forcarei (Órdenes Complex) and Espasante (Cabo Ortegal Complex) units (PHOTO SHEETS 1-3; Arenas *et al.*, 1995; Martínez Catalán *et al.*, 1996; 2009; Rubio Pascual *et al.*, 2002; Rodríguez, 2005; Gómez Barreiro *et al.*, 2010).

Possible equivalents in the South Armorican Domain are the Cellier, Saint-Mars, Mauves (Champtoceaux Complex) and Sainte-Pazanne (Essarts Complex, Vendée) units (FIGURE 9; Ballèvre *et al.*, submitted; López-Carmona *et al.*, submitted). The Ceán (Malpica-Tui Complex), Lamas de Abad and Cercio (Órdenes Complex) units in the Iberian Massif (PHOTO SHEET 1(a-c); Rodríguez *et al.*, 2003; López-Carmona *et al.*, 2010; 2013; submitted; Gómez Barreiro *et al.*, 2010; Díez Fernández *et al.*, 2011; Fuenlabrada *et al.*, 2012), and Groix and Bois-de-Cené in the Armorican Massif (Ballèvre *et al.*, 2009: and references therein) are related to the Middle Allochthon (FIGURE 9; PHOTO SHEET 4; Ballèvre *et al.*, submitted; López-Carmona *et al.*, submitted).

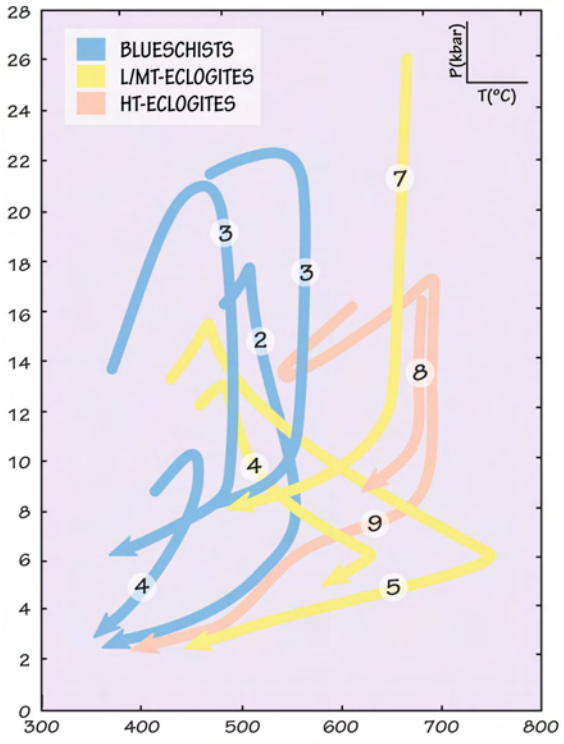

FIGURE 11. P-T diagram showing the tectono-metamorphic episodes experienced by several units from the Lower and Middle Allochthonous terranes in the NW Iberian Massif. In the Middle Allochthon: 2-Lamas de Abad; 3-Ceán, 4-Forcarei (basal part). In the Lower Allochthon: 4-Forcarei; 5-Lalín; 7- Malpica-Tui; 8-Espasante; 9-Agualada. Modified from Martínez Catalán *et al.* (1996) and López-Carmona *et al.* (2013; submitted).

Three main tectonometamorphic episodes have been established in the Lower and Middle Allochthons of the NW Iberian Massif (FIGURE 11; Martínez Catalán *et al.*, 1996; Gómez Barreiro *et al.*, 2010): a high-pressure event related to continental subduction (D_1/M_1-M_2), a decompression event driven by thrust and recumbent folding (D_2/M_2-M_3) and a final exhumation due to late orogenic readjustments during the gravitational extension of the orogenic pile (D_3/M_3-post/M_3), comprising: an out of sequence thrust system originated during the obduction of the ophiolitic sequences (Middle Allochthon) and the Upper Allochthon (Martínez Catalán *et al.* 2002), the orogenic collapse driven by ductile to ductile-brittle extensional shearing and a final strike-slip tectonics that bended all previous fabrics into open to tight upright folds subsequently cut by transcurrent shear bands (Gómez Barreiro *et al.*, 2010; Díez Fernández *et al.*, 2012).

Both the Lower and Middle Allochthon share a first high-pressure metamorphic event during the continental subduction (M_1–M_2) and the subsequent collisional deformation (M_2–M_3) through the Variscan orogeny. However, their peak P–T conditions vary from blueschist- to high-temperature eclogite-facies, according to their initial location in the subducting slab within the subduction complex (FIGURES 12 & 13). In general, the Lower Allochthon developed eclogite-facies metamorphism (Gil Ibarguchi & Ortega Gironés 1985; Arenas *et al.*, 1997; Rubio Pascual *et al.*, 2002; Rodríguez *et al.*, 2003; Rodríguez, 2005), whereas the overlying Middle Allochthon, separated by a major tectonic contact (i.e. the Bembibre-Ceán detachment), reached blueschist-facies conditions (Arenas *et al.*, 1995; Rodríguez *et al.*, 2003; López-Carmona *et al.*, 2010; 2013; submitted). In the eastern part of the Lower Allochthon (Forcarei unit; see FIGURES 9 & 10 for location) the metamorphic conditions are in the blueschist/low-temperature eclogite-facies, and going to the west the peak P and T increases progressively up to medium-temperature eclogite facies in the Malpica-Tui Complex (Martínez Catalán *et al.*, 1996; Rubio Pascual *et al.*, 2002).

The second tectonothermal episode (M_2–M_3) affecting these allochthons is related to their early exhumation, driven by a combination of recumbent folding and thrusting with a general top-to-the east movement (Martínez Catalán *et al.*, 2002). A major ductile reverse fault, the Fervenza thrust, followed by the propagation toward the foreland of a train of recumbent folds drove the early exhumation of the Lower and Middle Allochthons (Díez Fernández *et al.* 2011; 2012). D_2-nappe tectonics culminated with the Lalín-Forcarei thrusts fault, which separates the Lower and Middle Allochthons from the Parautochthon in the southeast area of the Órdenes Complex (FIGURE 10; Forcarei, Lalín and Cercio units). During D_2 some of the units of the Lower Allochthon were thrusted over the units of the Middle Allochthon, resulting in the formation of an inverted metamorphic zoning, from high-temperature amphibolite-facies conditions at the top (FIGURE 10; e.g. Agualada unit) to low-temperature amphibolite to greenschist-facies conditions below (e.g. Ceán unit; Arenas *et al.* 1995; Rubio Pascual *et al.* 2002; Gómez Barreiro,

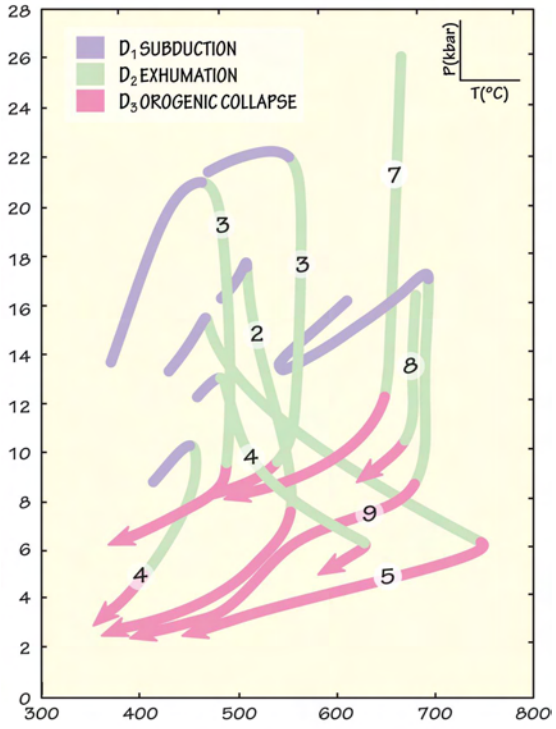

FIGURE 12. Diagram showing a summary of the peak P-T-conditions and the trajectories from the units of the Lower and Middle Allochthons in the NW Iberian Massif. In the Middle Allochthon: 2–Lamas de Abad; 3–Ceán, 4–Forcarei (basal part). In the Lower Allochthon: 4–Forcarei; 5–Lalín; 7– Malpica-Tui; 8–Espasante; 9–Agualada. Modified from Martínez Catalán *et al.* (1996) and López-Carmona *et al.* (2013; submitted).

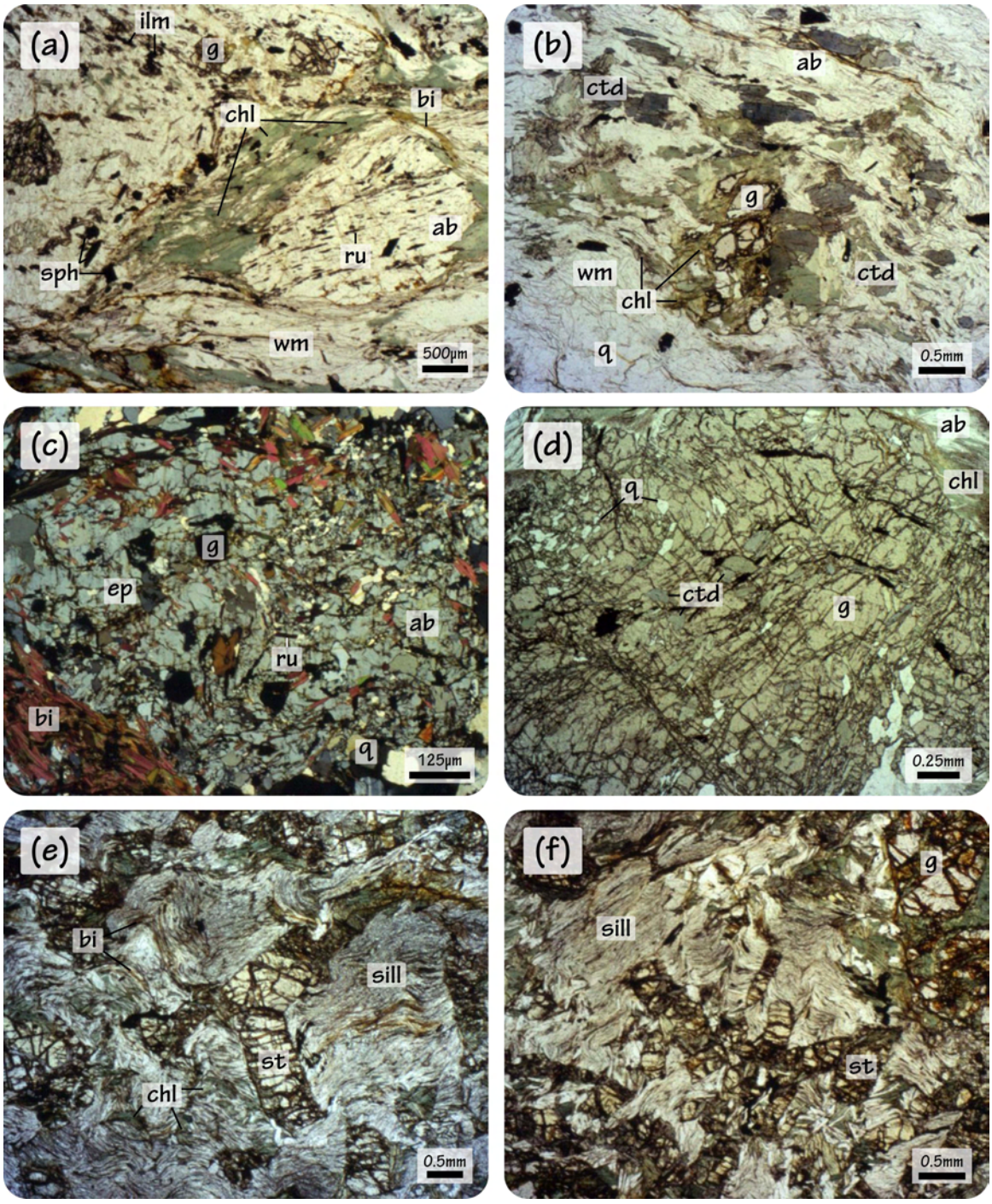

PHOTO SHEET 1. Thin-section images from the metasediments in the Middle (a-b) and Lower (c-f) Allochthon of the Órdenes Complex. In the Lamas de Abad Unit: (a-b) garnet mica-schist displaying a foliation composed of white mica [wm], biotite [bi], titanite [sph], rutile [ru], ilmenite [ilm], chlorite [chl], chloritoid [ctd] and quartz [q] wrapping around syntectonic albite [ab] porphyroblasts. In the Santiago Unit (in the semipelitic Santiago Schists) (c) Albite porphyroblast with oriented inclusion trails of white mica, epidote [ep], rutile, ilmenite, chlorite, quartz and subhedral to anhedral garnet (g) grains. (d) Garnet porphyroblast displaying concentric clorithoid-rutile-quartz inclusions. (e-f) Regional foliation at the base of the unit composed of sillimanite [sill], estaurolite [st], garnet, muscovite, biotite, chlorite, plagioclase and quartz. These photos were provided by Ricardo Arenas.

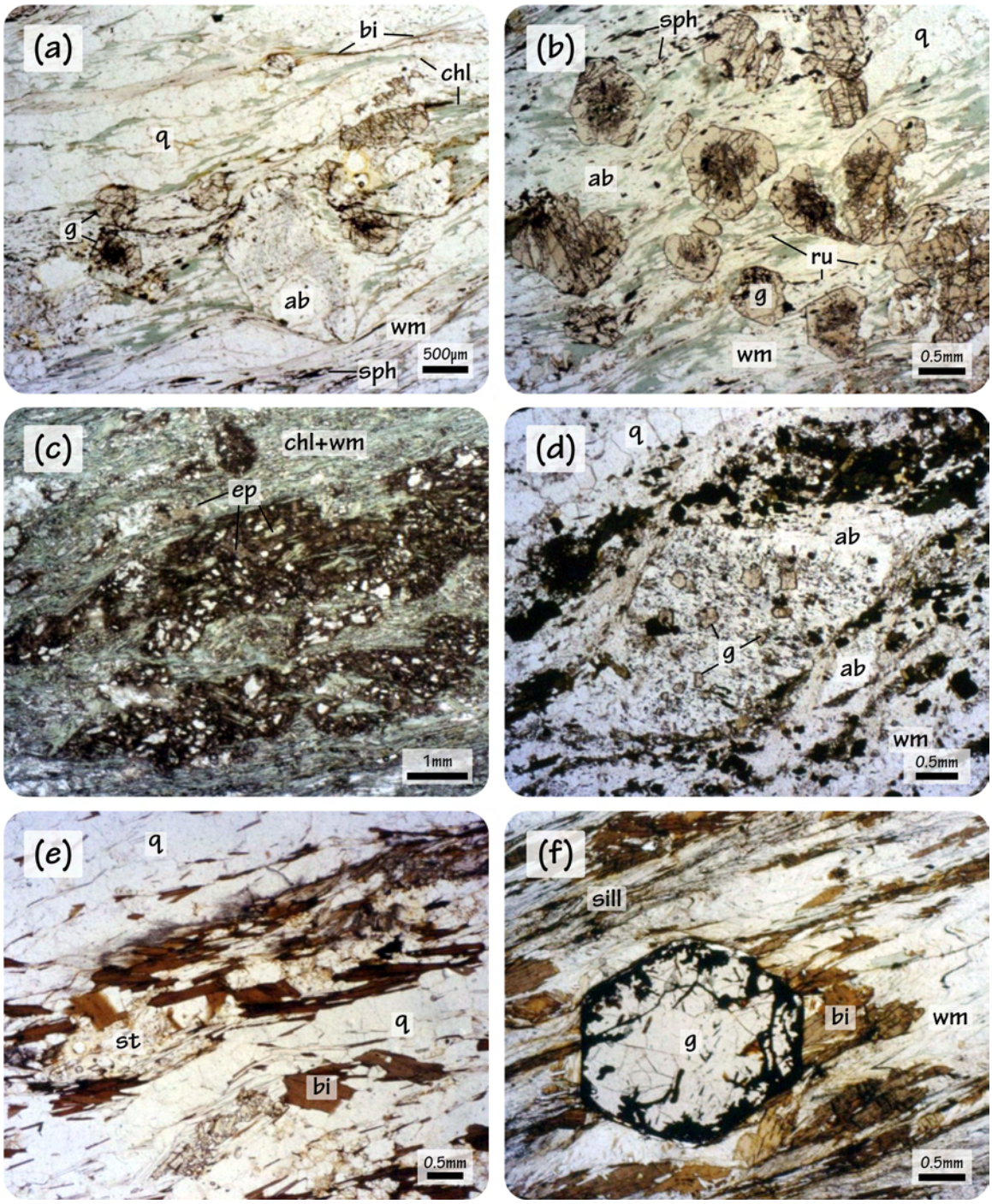

PHOTO SHEET 2. Thin-section images from the Forcarei (a-d) and Lalín (e-f) units in the Lower Allochthon of the Órdenes Complex. Metapelites: (a-b) fine-grained micaschist with albite porphyroblasts [ab] surrounded by the regional schistosity that comprises garnet [g], white mica [wm], chlorite [chl], biotite [bi], rutile [ru], titanite [sph] and quartz [q]. The porphyroblasts include a microfolded internal schistosity containing white mica, chlorite, rutile, ilmenite, quartz and, rarely, garnet. Metabasic rocks: (c) rhomboidal polycrystalline aggregates of epidote-clinozoisite interpreted as pseudomorphs after lawsonite (Martínez Catalán *et al.*, 1996) surrounded by the main foliation in the greenschist-facies conditions; (d) albite porphyroblasts with garnet inclusions and stretched polycrystalline aggregates. (e) Metapelitic rocks from the Lalín unit showing a main foliation comprising garnet, staurolite [st], white mica, biotite and quartz. These photos were provided by Ricardo Arenas.

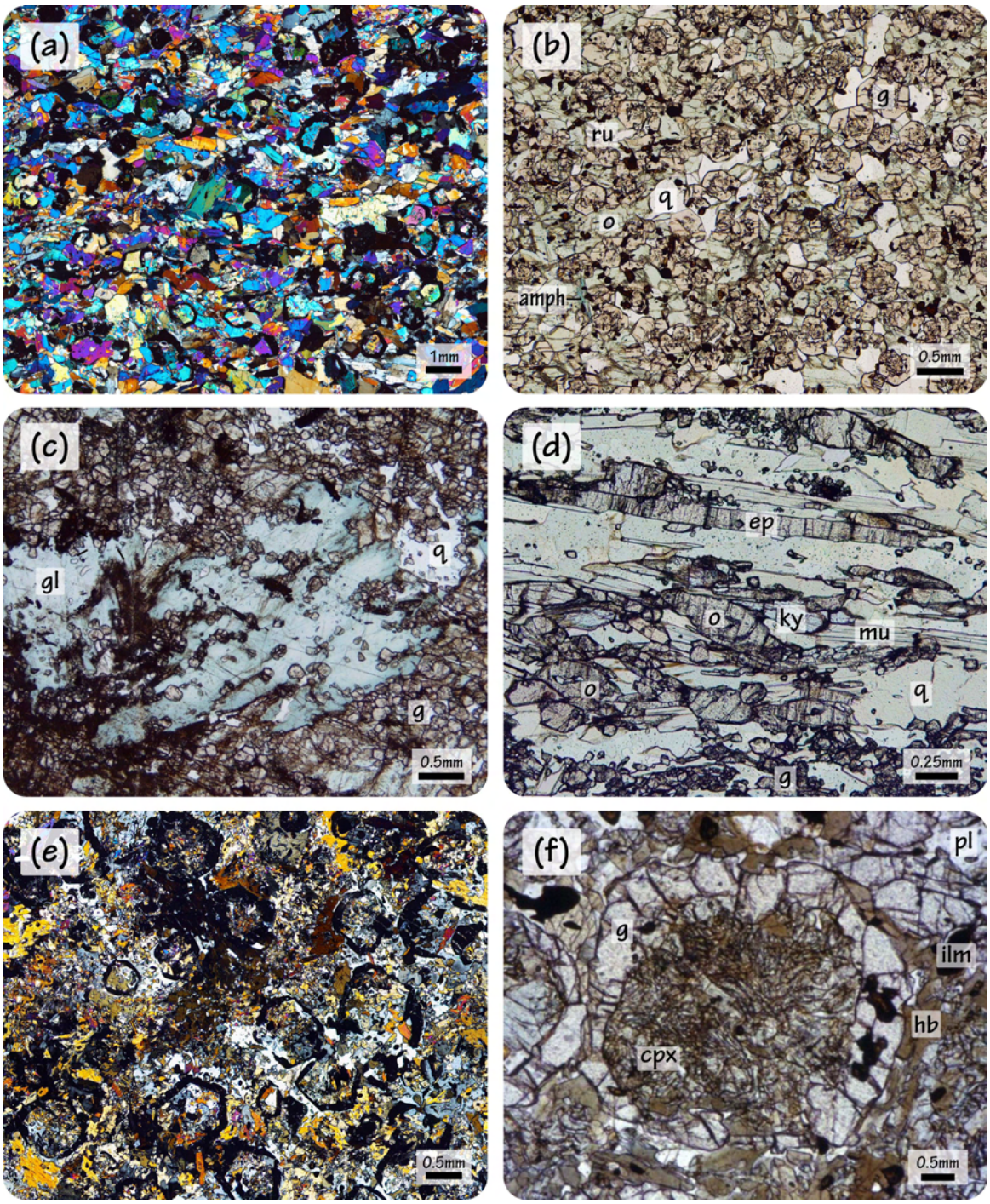

PHOTO SHEET 3. Thin-section images from the eclogites in the Middle Allochthon of the Malpica-Tui Unit (a-d; MTU; Malpica-Tui Complex) and the Agualada Unit (e-f; Órdenes Complex). Eclogites from the MTU (a-b) showing honeycomb textures including garnet [g], omphacite [o], rutile [ru], clinozoisite, and white mica. (c) A later generation of poikiloblastic sodic amphiboles [gl; amph] is occasionally observed. (d) Tonalitic ortogneises in the eclogite-facies conditions displaying similar assemblages but with a higher proportion of white mica [wm] and epidote [ep] and abundant kyanite [ky]. (e) Retrogressed eclogite showing primary honeycomb texture formed by omphacite (later transformed to a symplectitic aggregate) surrounding garnet. The eclogitic assemblage is formed by garnet, omphacite, rutile, and quartz. Post-eclogitic parageneses in the amphibolite-facies conditions include hornblende [hb], plagioclase [pl], and epidote. (f) Detail of a symplectite showing the intergrowth between clinopyroxene [cpx] and the host garnet producing interstitial plagioclase. After Arenas *et al.* (1997) and Abati *et al.* (2010).

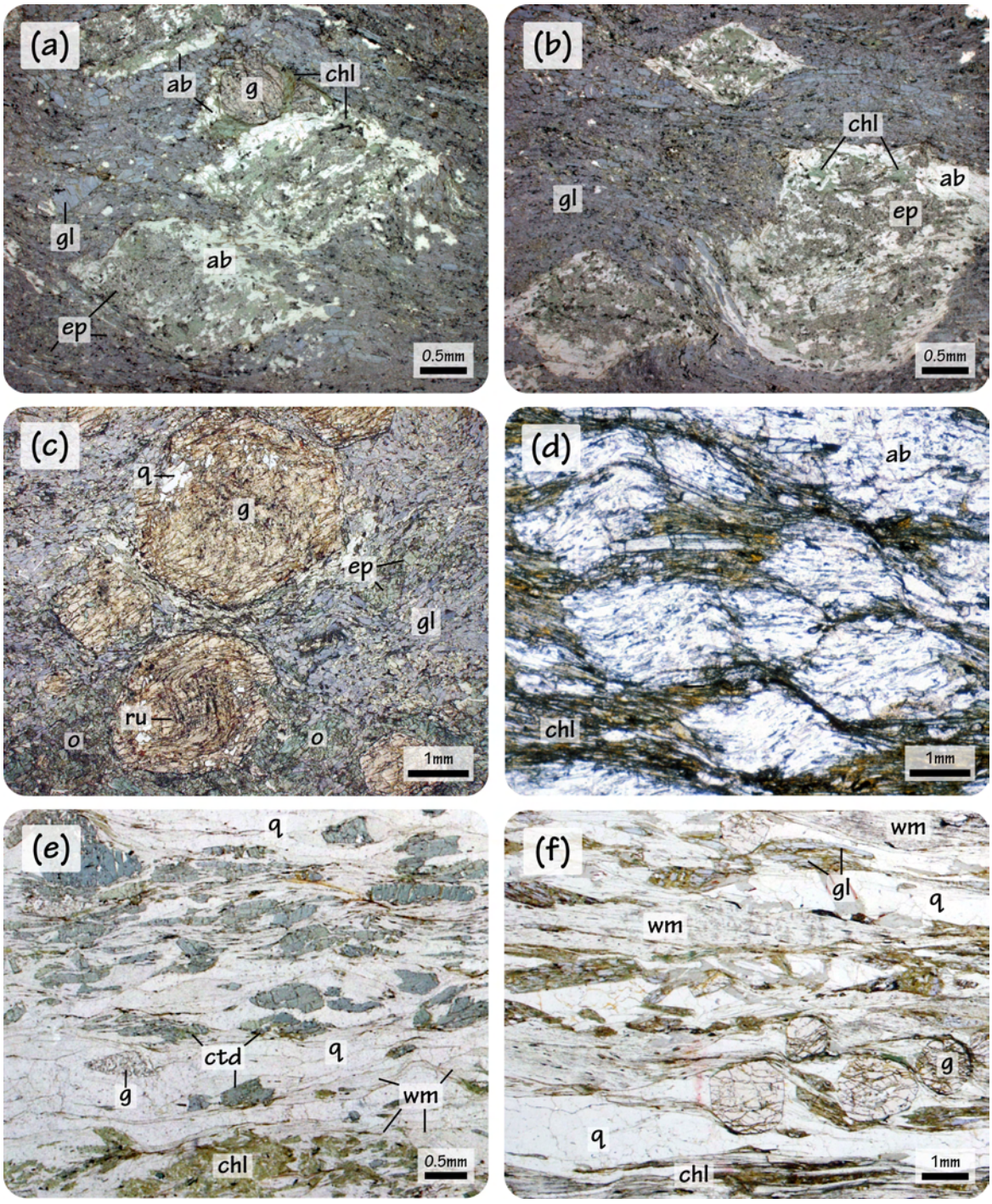

PHOTO SHEET 4. Thin-section images from the Upper Unit of Ile de Groix in the south Armorican Domain of the Armorican Massif. In the metabasic rocks (a-b) lawsonite pseudomorph-bearing blueschists overgrowing a garnet [g], glaucophane [gl], epidote [ep], titanite foliation; (c) omphacite [o]-glaucophane [gl]-bearing blueschists; (d) greenschists containing abundant syntectonic albite porphyroblasts. In the metapelitic rocks; (e) chloritoid [ctd]-garnet micaschist; (f) glaucophane-garnet micaschist.

2007; Gómez Barreiro *et al.*, 2010; López-Carmona *et al.*, 2013). The interlayering of a blueschist-facies unit (e.g. Ceán) in between two eclogite-facies units (e.g. Malpica-Tui and the Agualada units) is interpreted as an original feature of the subducted complex, related with the typical geometry of the isotherms in subduction zones (e.g. Gómez Barreiro *et al.*, 2010; López-Carmona *et al.*, 2013). Subsequently, the D_2 shortening associated with the underthrusting of the Gondwana basement generate an out-of-sequence thrust system that scarcely dismembered the Lower and Middle Allochthons (Gómez Barreiro *et al.*, 2007; Martínez Catalán *et al.*, 2009).

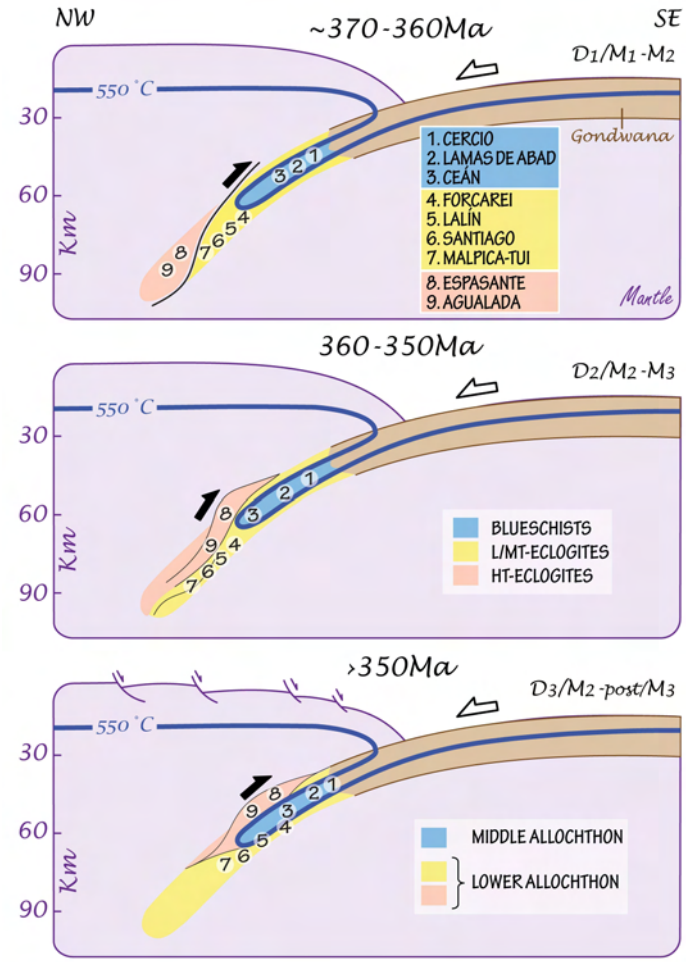

FIGURE 13. Schematic cross-section of the evolution of the subduction zone operating in the NW Iberian Massif from 370 to 350 Ma. L/MT–low to medium temperature; HT–high temperature. Based on Martínez Catalán *et al.* (1996) and López-Carmona *et al.* (2013; submitted).

During D_3, thermal relaxation lead to widespread magmatism by melting of the thickened lower and middle crust. The orogenic pile became mechanically unstable and resulted in an extensional collapse. Whereas domes (such as the Padrón migmatitic dome; FIGURE 10) and viscous flow developed at depth, regional-scale extensional detachments were nucleated at the base of the rigid crustal segments reactivating feeble pre-existing shear zones that favoured the nucleation of the detachments. Shear zones associated with the detachments overprinted the previous tectonic fabrics under conditions ranging from lower amphibolite to

greenschist facies (M_3-post/M_3), and with heterogeneously distributed ductile to brittle deformation (Gómez Barreiro *et al.*, 2010). Three extensional faults dismembered the D_2 macrostructure of the Lower and Middle Allochthon around the Padrón dome: Redondela-Beariz, Pico Sacro, and Bembibre-Ceán detachments (FIGURE 10), the two first forming a divergent system of conjugated shear zones (Díez fernández *et al.*, 2012). The Bembibre-Ceán detachement marks the contact between the Lower and Middle Allochthons. The Pico Sacro detachement marks the contact between the whole allochthonous pile and the Parauthocthon in the northern half of the complexes, and similarly, the Redondela-Bearriz detachment in the southern half (cf. Gómez Barreiro *et al.*, 2010; Díez Fernández *et al.*, 2012). On the basis of the estimated age of the Lalín-Forcarei thrust (ca. 340 Ma; Martínez Catalán *et al.*, 1996; Dallmeyer *et al.*, 1997) and on the age of synkinematic leucogranites intruding the relative autochthon (Rodríguez *et al.*, 2003), their motion took place between 340 and 317 ± 3 Ma, with the Bembibre-Ceán detachment being older than the Pico Sacro detachment (Gómez Barreiro, 2007; Gómez Barreiro *et al.*, 2010).

2.2 *Geology of the Malpica-Tui Complex*

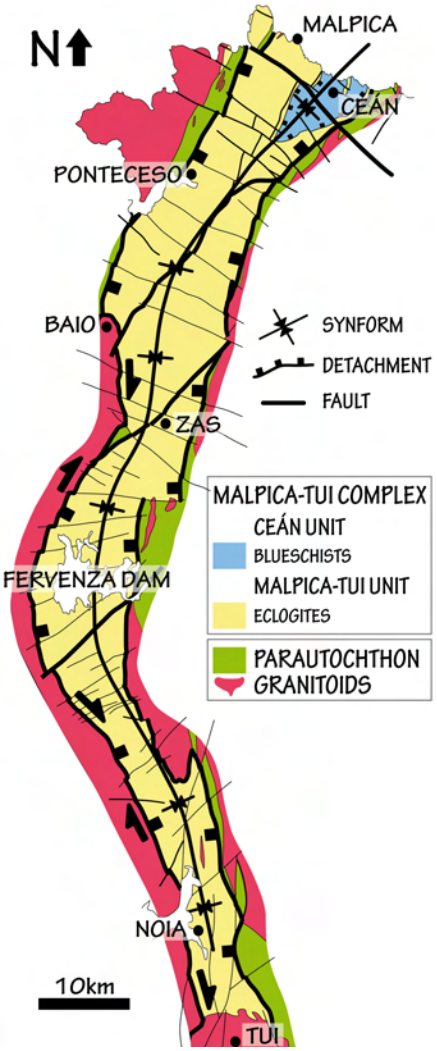

The Malpica-Tui Complex was first identified in 1945 as an "*amphibolite-gneiss band between Malpica and Vigo*" (Carle, 1945) but it was not recognized as a tectonic domain until 1953, defined then as the "*Old Complex* " by Isidro Parga Pondal (1953a, b and c, 1956). Years later, geologists of the "Leiden School" (The Netherlands) called it "*Blastomilonitic Graben*" (den Tex & Floor, 1966). They identified that it was a polimetamorphic unit, which was originally located at higher cortical levels, and that after the migmatization process collapsed by extension being sunken with respect to the adjacent migmatitic materials (den Tex & Floor, 1966; den Tex, 1981a, b). The translation into Spanish of this term is the reason why, for a long time, even nowadays, the geologists of the NW Iberian Massif have referred to this area with the colloquial name of "*La Fosa*" ("*The Trench* ").

While the prolific "Dutch school" begins to develop different researches in this area, other authors raised the allochthonous character of the unit (Ries & Shackleton, 1971; Anthonioz & Ferragne, 1978; Lefort

FIGURE 14. Simplified geological map of the Malpica-Tui Complex highlighting its structure, its relation with the Parautochthon and the distribution of the metamorphic conditions. Modified from Díez Fernández, 2011.

& Ribeiro, 1980). But the term partially valid today to refer to this zone was established in the early 80´s as "*Malpica-Tui Unit*" (Ortega Gironés & Gil Ibarguchi, 1983). This denomination has no genetic connotations, as it refers strictly to its geographical boundaries.

Rodríguez (2005) postulated the existence of two distinct lithological domains within this unit comprising a sequence of oceanic affinity (N- MORB) overlaying a set of continental materials. This lead to the consideration of a new nomenclature for the Malpica-Tui Unit, which according to the guidelines used in the rest of the allochthonous complexes of NW Iberia, would adopt the name of "*Malpica-Tui Complex*".

At the beginning of this research the author opted for the nomenclature proposed by Ortega Gironés & Gil Ibarguchi (1983) finding that the division proposed by Rodríguez (2005) did not imply the existence of two different units, because both associations would have been part of the same continental margin and the oceanic unit does not represent an ophiolitic sequence comparable to those described in the rest of the Allochthonous Complexes (e.g. Sánchez Martínez, 2009; Sánchez Martínez *et al.*, 2009). The N-MORB affinity of the Cambre metabasic rocks, together with the interbedded sediments, suggests a transitional context, rather than a "pure" oceanic or continental environment. However, as the two concepts are not mutually exclusive, and with the aim of unify the terminology, especially in the view of correlations with similar European terranes, based on the division proposed by Rodríguez (2005), the denomination of *Malpica-Tui Complex* is the one assumed in the present research.

Over the following years, within the "IGME-MAGNA Plan" (Instituto Geológico y Minero de España) the entire complex was mapped at 1:50.000 scale. All this information, together with the research of the "Leiden School" (Collée, 1964; Avé Lallemant, 1965; Floor, 1966; den Tex & Floor, 1967; Arps, 1970; van Calsteren, 1977; van der Wegen, 1978; den Tex, 1981a), the PhD´s of Llana-Fúnez (2001) and Díez Fernández (2011), dealing with the structural geology of the Malpica-Tui Complex, and the PhD of Rodríguez (2005), focused primarily on the metamorphism of orthoderived lithologies, have been the references and the starting point for setting the objectives of this research.

Cartographically the Malpica-Tui Complex defines an elongated structure of about 150 km long and 10 km wide, oriented N165º in the southern area and N15º-N30º in the northern zone, above the Fervenza Dam (Díez Fernández, 2011). It extends from Malpica, in A Coruña, to Tui, in Pontevedra, outcropping in the core of a synformal structure whose axis dips slightly towards the north (FIGURE 14). Structurally, this synform is located on the western flank of the Padrón Antiform, a migmatitic dome originated during the extensional collapse of the Variscan orogen (FIGURE 10; Martínez Catalán *et al.*, 2009; Díez Fernández & Martínez Catalán., 2009). To the east it is bounded by a basal shear zone overlying the Parauthocthon

(i.e. the Schistose Domain of Galicia-Trás os-Montes; Gil Gironés Ibarguchi & Ortega, 1985; Llana-Fúnez & Marcos, 2002) and to the west by a subvertical dextral shear zone (Coke & Ribeiro, 2000; Llana-Fúnez, 2001).

The Malpica-Tui Complex (MTC) can be separated in two tectonically juxtaposed sequences (FIGURES 14 &15):

(i) a lower sequence of continental affinity that corresponds to the Lower Allochthon, the so called Malpica-Tui Unit (MTU), dominated by felsic orthogneisses and turbiditic metasedimentary rocks and

(ii) an upper sequence that corresponds to the Middle Allochthon and comprises pelitic schists and N-MORB metabasic rocks. It is known as the Ceán Unit and constitutes the study area of this research.

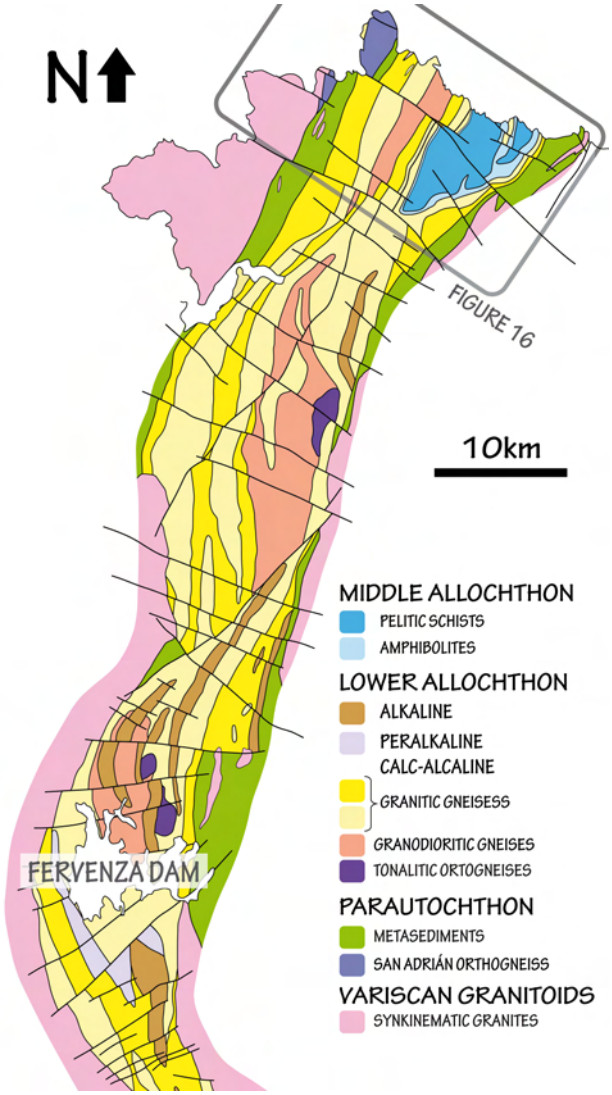

FIGURE 15. Geological map of the Malpica-Tui Complex showing the magmatic series from the Lower Allochthon. The lowermost section of the complex is not shown. Modified from Llana-Fúnez (2001); Rodríguez (2005) and Díez Fernández (2011).

The contact between the upper and the lower sequences (i.e. between the Lower and the Middle Allochthon) is marked by a several metres thick layer of mylonites and ultramylonites located at the base of the metabasic rocks known as the Bembibre-Ceán Detachment (Gómez Barreiro *et al.*, 2010; Díez Fernández *et al.*, 2012). Peak metamorphic conditions in the MTU are in the intermediate temperature eclogite facies (P = 25 kbar and T = 610 °C; Rodríguez, 2005) whereas the Ceán Unit can be considered as a highly condensed metamorphic succession with a lower part in the blueschist facies and an uppermost part without high-pressure relicts (López-Carmona *et al.*, 2007; 2010; 2013). The significant difference in metamorphic grade between the Lower and the Middle Allochthons, and between the upper and lower part of the Ceán Unit suggests that the mylonites that mark the contacts are related to an extensional deformation (López-Carmona *et al.*, 2007).

The lower Allochthon in the MTC consists on a monotonous pile of terrigenous sediments

and igneous rocks with a minimum present thickness of 4 km, which probably represents less than a half of the original (Díez Fernández, 2011; Díez Fernández *et al.*, 2012). The MTU is heterogeneously deformed. The less deformed domain consists on meso- to macro scale boudins that may preserve original stratigraphic features. The sedimentary sequence comprises immature sandstones (greywakes) preserving sedimentary structures such as cross-bedding or Bouma sequences alternating with minor layers or lenses of pelites, graphite-bearing schists, calc-silicate rocks and quartzites. Besides the intrusions of mafic dikes (alkali basalts; Marquínez García, 1984; Rodríguez, 2005), two different igneous associations intruding the sediments have been identified: (1) a calc-alkaline suit formed by high-K granites, granodiorites and tonalities and (2) an alkaline to peralkaline suit including metaluminous alkali-feldspar quartz-syenites and granites, peraluminous alkali-feldspar granites, and peralkaline granites (FIGURE 15; Rodríguez, 2005). During the Variscan Orogeny both magmatic series were metamorphosed into the eclogite facies conditions (FIGURE 14; Rodríguez, 2005). The age of the oldest calc-alkaline orthogneises establish a minimum depositional age of 495-500 Ma (Abati *et al.*, 2010) for the Lower Allochthon in the MTC. The peralkaline series (including A-type granitoids) is related to an extensional event interpreted to reflect the Early (to Middle?) Ordovician rifting (Floor, 1966; Ribeiro & Floor, 1987; Pin *et al.*, 1992). However, its relation with the calc-alkaline magmatism is not completely clear, and some authors correlate both magmatic events with post-collisional process (Rodríguez, 2005). Nevertheless, recent studies suggests that calc-alkaline magmatic suite is ca. 20 Ma older than the alkaline to peralkaline plutonic suite (dated at ca. 470-475 Ma; Rodríguez *et al.*, 2007), and thus probably represents a distinct geologic event (Abati *et al.*, 2010).

2.2.1 *The Middle Allochthon: the Pazos Synform*

The Middle Allochthon of the MTC comprises the entire study area, which is located in the northwest of Galicia, in the region of *Bergantiños* (A Coruña), to the SE of the vicinity of *Malpica*, at the eastern end of the coastal section popularly known as *Costa da Morte*. The area is completely covered by the 1:25.000 topographic map 44-1 of the Spanish National Geographic Institute (IGN). The study area includes part of the coastal section of the MTC extending, from west to east, from *los Molinos de Ceán* to the *Riás beach*. To the north it is limited by the Atlantic Ocean and to the south by the village of *Pazos de Abaixo* (FIGURE 16).

Geologically, the study area covers the so called Pazos Synform (Alonso & González, 1982), which is a north-plunging late Variscan fold that crops out in the highest structural level of the MTC. The Pazos Synform comprises two synformal structures of different proportions. The broader structure occupies the area bounded, from west to east, between *los Molinos de Ceán* and *San Miro beach*, and the smallest one extends from the *San Miro* to the *Riás beach*. The entire synform is composed by the materials forming the Upper Group of the Ceán-

Razo Series (Ortega, 1980) consisting on (1) a sequence of variable thickness of finely foliated amphibolites and greenschists with N-MORB chemistry that define the cartographic limit of the structure (the so called Cambre Amphibolites; Llana-Fúnez, 2001), and (2) a thicker metasedimentary sequence of pelitic schists (the so called Ceán Schists; Rodríguez, 2005) with minor intercalations of bituminous schist, cherts and carbonates. The transition between the two lithologies is gradual and locally both are interbedded (Arps, 1981).

This sequence is known as the Ceán Unit (see above), and represents the westernmost exposure of the Middle Allochthon in the NW Iberian Massif and in the Variscan Belt of Western Europe. It forms the upper tectonic sheet of the MTC and is constituted by the Ceán pelitic schists and the Cambre metabasic rocks, which are interpreted as a volcano-sedimentary sequence that probably represents part of the cover of a transitional to oceanic crust associated with the outermost sections of the north Gondwana margin during the Variscan collision (Martínez Catalán *et al.*, 1996; Ballèvre *et al.*, submitted; López-Carmona *et al.*, submitted). The lithologies that constitute the Ceán Unit are the subject of this PhD thesis.

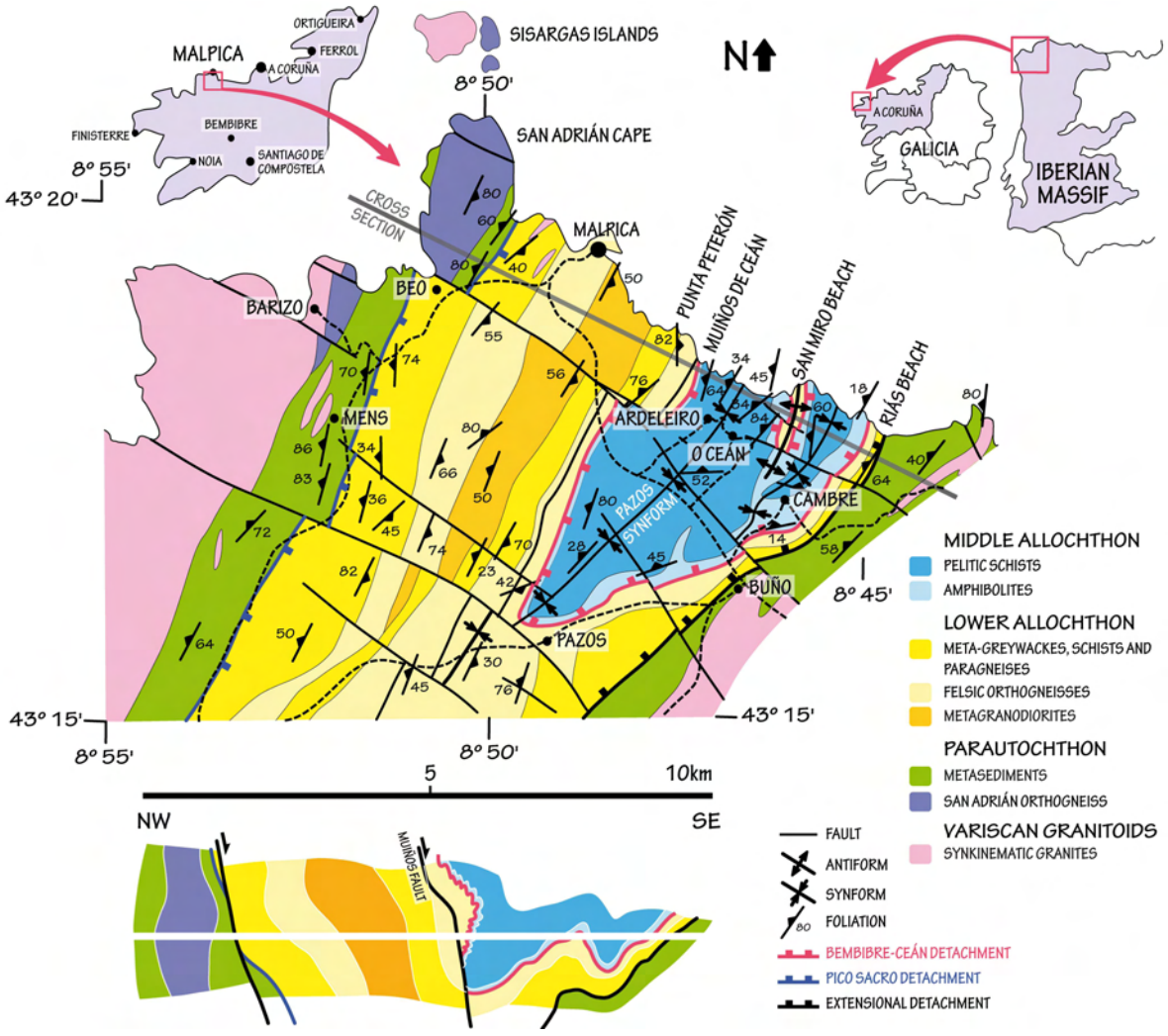

FIGURE 16. Geological map and cross section of the study area showing the relation between the Middle and Lower Allochthons in the Malpica-Tui Complex. The maps include data from Ortega (1980); Alonso & González (1982); Llana-Fúnez (2001); Rodríguez (2005), Díez Fernández (2011) and our own data.

2.2.1.1 *The Ceán pelitic schists*

The Ceán Schists constitute a rather monotonous succession of fine-grained pelitic micaschists with an apparent minimum thickness of 170 m (Llana-Fúnez, 2001) and have a chemical composition of typical pelites (FIGURE 17; *e.g.* Atherton & Brotherton, 1982). However, to the base of the sequence, metapelitic rocks are interbedded with the Cambre metabasic rocks and most samples show compositions that move away from the field of pure pelites in the direction of N-MORB, indicating either some mixing between both lithologies during primary volcano-sedimentary processes, or mechanical assimilation during the deformation. The different whole-rock chemistry between the samples selected for this study results in slightly different mineral associations (TABLE 3).

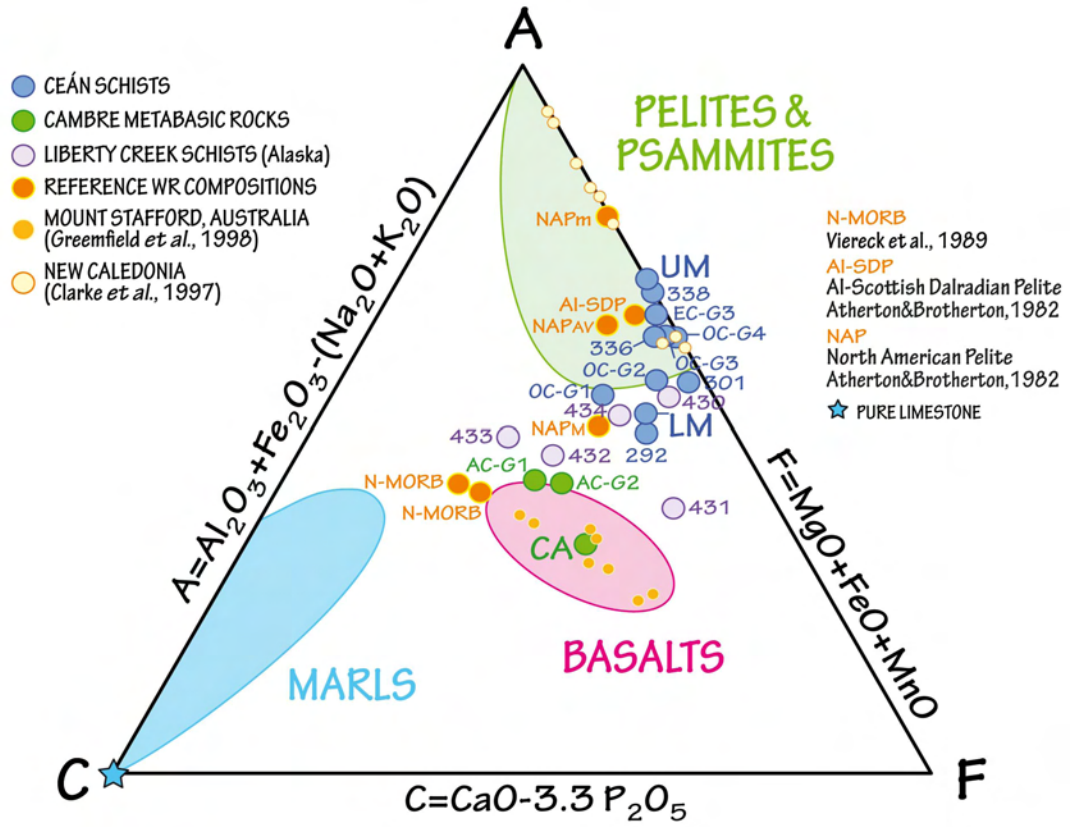

FIGURE 17. ACF ternary diagram plotting the compositional variations of the whole-rock (WR) chemical analyses of the studied samples. Samples LM and UM are classified as pelites and sample CA as basalt. Shaded fields are obtained by plotting a range of claystones (pelites), sandstones (psammites), marls and basalts. The Mount Stafford series of metamorphosed turbidites and the high-pressure metabasalts from new Caledonia are shown as reference. Modified from Turner (1981) and Vernon & Clarke (2008).

To the base of the sequence the metapelites are chloritoid–glaucophane-bearing micaschist (López-Carmona *et al.*, 2010) that gradually transits to a garnet micaschist, which are the dominant rock-type. Locally, predominantly in the upper levels of the series, a pervasive growth of albite porphyroblasts occurs. Albites either define a parallel banding or display a random distribution without orientation, whose origin was initially related to compositional differences in the sedimentary protolith (Alonso & González, 1982; Gil Ibarguchi & Ortega

Gironés, 1985). Upwards in the sequence the content of mica decreases, garnet disappears, and a gradual increase of opaque phases and quartzite beds occur. The paragenesis becomes restricted to fine-grained white mica, chlorite and quartz, giving the rocks a slaty texture and suggesting that the metamorphic gradient decreases rapidly upwards. The transition occurs at approximately 500 m from the base of the sequence, indicating important telescoping of metamorphic isograds compatible with extensional detachment faulting (López-Carmona *et al.*, 2008).

TABLE 3. Whole-rock compositions of the Ceán pelitic schists (highlighted in blue) and the Cambre metabasic rocks (highlighted in green)

	LM	UM	336	338	292	301	ECG3	OCG1	OCG2	OCG3	OCG4	CA	ACG1	ACG2
SiO_2	57.54	57.67	56.18	50.45	57.10	67.12	61.29	58.36	57.62	60.50	57.53	47.89	48.29	47.46
TiO_2	1.01	0.74	1.09	1.20	0.76	0.55	1.06	0.75	0.96	1.06	0.87	1.92	1.24	1.24
Al_2O_3	17.04	20.96	19.09	26.40	16.82	14.10	17.83	17.02	18.21	18.20	19.57	13.36	15.83	15.86
FeO	6.78	5.93	6.83	7.56	6.72	5.83	5.22	5.67	6.69	6.40	6.07	7.90	6.11	6.18
MnO	0.17	0.26	0.42	0.32	0.28	0.33	0.36	0.19	0.19	0.35	0.22	0.22	0.18	0.18
MgO	2.92	1.72	1.94	2.33	2.68	1.72	2.14	2.38	3.26	2.11	2.52	7.11	6.91	8.18
CaO	2.75	0.36	1.32	0.41	3.04	1.05	1.02	3.66	2.03	1.02	1.14	10.00	12.09	10.26
Na_2O	1.26	0.85	1.88	1.25	2.01	0.93	1.10	1.46	0.87	1.12	1.20	2.92	2.47	2.44
K_2O	4.59	3.83	3.97	4.34	3.30	2.91	4.04	3.47	4.27	4.17	4.42	0.07	0.16	0.19
NiO	0.00	0.00	0.00	0.00	0.00	0.00	0.00	0.00	0.00	0.00	0.00	0.00	0.06	0.05
P_2O_5	0.14	0.13	0.31	0.11	0.18	0.18	0.25	0.13	0.17	0.29	0.14	0.13	0.00	0.00
Cr_2O_3	0.05	0.04	0.02	0.04	0.03	0.02	0.01	0.00	0.00	0.00	0.00	0.00	0.03	0.05
Fe_2O_3	1.39	1.98	2.15	1.46	0.09	0.09	2.03	1.27	1.50	1.43	1.36	1.76	4.92	4.76
A	12.58	18.26	15.39	22.27	11.60	10.35	14.72	13.36	14.57	14.34	15.31	12.13	18.12	17.99
C	2.29	-0.07	0.30	0.05	2.45	0.46	0.20	3.23	1.47	0.06	0.68	9.57	12.09	10.26
F	9.87	7.91	9.19	10.21	9.68	7.88	7.72	8.23	10.14	8.85	8.81	15.23	13.20	14.54

The Ceán schists show a medium-grained porphyro-lepidoblastic texture and a well-developed planar to plano-linear fabric. White mica and quartz constitute >50%, and locally up to 80%, of the modal proportion of each sample. The alternation of both minerals defines a banding preserved between extensional shear bands. The foliation is defined by the shape preferred orientation of phengitic muscovite, paragonite and chlorite, and is parallel to the banding. The deformation in the Ceán Schists is generally strong and relatively heterogeneous, with irregular development of foliations and deformation phases in different domains and, in discrete areas, the regional foliation is transitional to mylonitic types. Quartz grains commonly show undulate extinction, subgrain boundaries, recrystallization to smaller grain aggregates and ribbons around the porphyroblasts. Late C´ shear bands and kink-band structures are also common.

Their deformation history includes several compressive, extensional and strike-slip phases (Díez Fernández *et al.*, 2011). The fabric from the earliest deformational event (S_1) is preserved exclusively as inclusion trails in a first generation of garnet porphyroblasts (g1). S_2

is preserved in a second generation of garnet (g2) and chloritoid porphyroblasts (ctd 1). The matrix foliation (S_3) usually obliterates the previous fabric, resulting in a composite foliation S_2 + S_3 and includes the pervasive development of spaced extensional shear bands and meso-scale folds, related with a first extensional event (Díez Fernández *et al.*, 2011).

Subsequent deformations are associated with the development of late-Variscan folds (such as Pazos Synform) and to a final superposed dextral strike-slip tectonics. The effects of post-S_3 deformations associated with vertical folding are particularly evident in the core of the synformal structure, where an axial planar foliation S_4 is usually developed. In these areas, the schists are highly altered and the main foliation consists of alternations of quartz and phyllosilicate-rich layers.

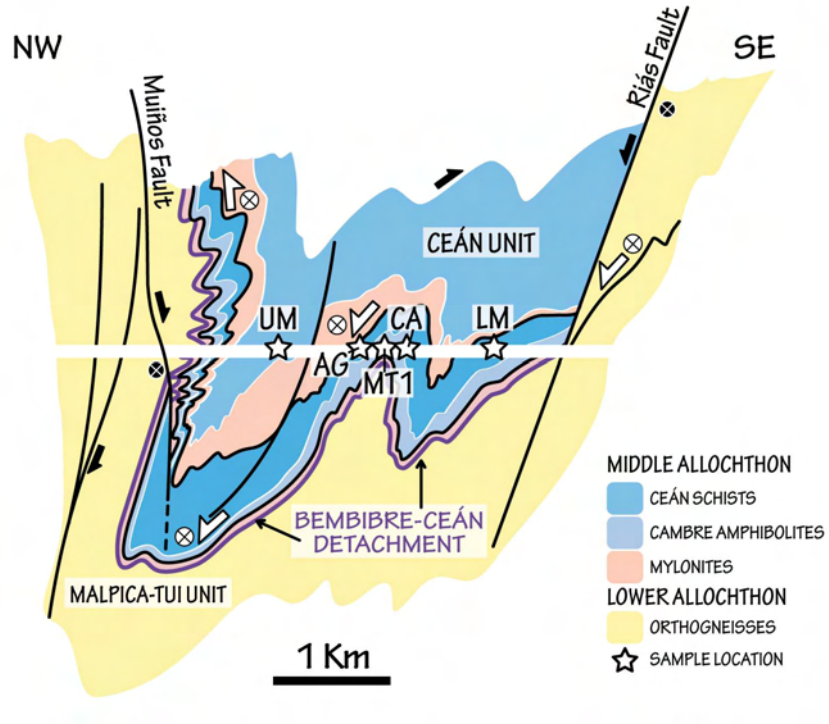

FIGURE 18. Cross-section for the Ceán Unit (Pazos Synform) of the Malpica–Tui Complex showing the location of the studied samples. Modified from Díez Fernández, 2011; López-Carmona *et al.* (2013; submitted).

Two representative rock-types within the thick metasedimentary sequence of pelitic schists have been studied in detail. The first rock-type, referred to hereafter as LM (for Lower metapelites) is located at the base of the synformal structure, and interbedded within the Cambre metabasic rocks. The presence of numerous garnet porphyroblasts rich in S_1 and S_2 inclusions makes this sample ideal to study the first subduction-related deformation phases. The second rock-type, referred to hereafter as UM (for upper metapelites) is located structurally above the LM, in the middle part of the synformal structure, in an upper structural domain separated from the first by a mylonitic band (FIGURE 18).

In the LM the first metamorphic stage (M_1) is recorded by aligned inclusions of ep, ru, sph, q (mineral abbreviations[4] are after Holland & Powell, 1998) in the cores of large garnet porphyroblasts. M_2 is characterized by the inclusions of ctd, chl, gl, ru, ilm, mu, q preserved in the rim of garnet porfiroblasts. The third stage (M_3) is recorded by the matrix foliation (S_3), comprising the assemblage chl, ep, mu, pa, bi, ru/ilm, sph, q ± g, win/bar. Finally, post-M_3 crystallization includes phases such as chl, hb/ts, ab, ser, stp, carb, sul (FIGURE 19).

In the UM it is inferred that the preserved mineral assemblages correspond to the sequence of two metamorphic stages, M_2 and M_3, according to their mineralogy and textural position. The M_1 event (recorded in the LM) has not been identified in the UM. The M_1 event represents the early stages of subduction, and it has not been possible to deduce if it was not preserved in these rocks, or if they never recorded it. Evidences for M_2 are achieved by the assemblage g, ctd, mu, pa, ru ± ilm. These minerals occur preserved as inclusions in garnet and in chloritoid porphyroblasts and define the internal fabric S_2. M_3 corresponds to the matrix foliation (S_3) and is composed of g, chl, mu, pa, ru, ilm, q ± ctd. The post-M_3 event includes post-S_3 phases such as chlorite and Fe/Ti-oxides (FIGURE 20).

The Ceán pelitic schists are extensively studied in section 3.1 of Chapter 3.

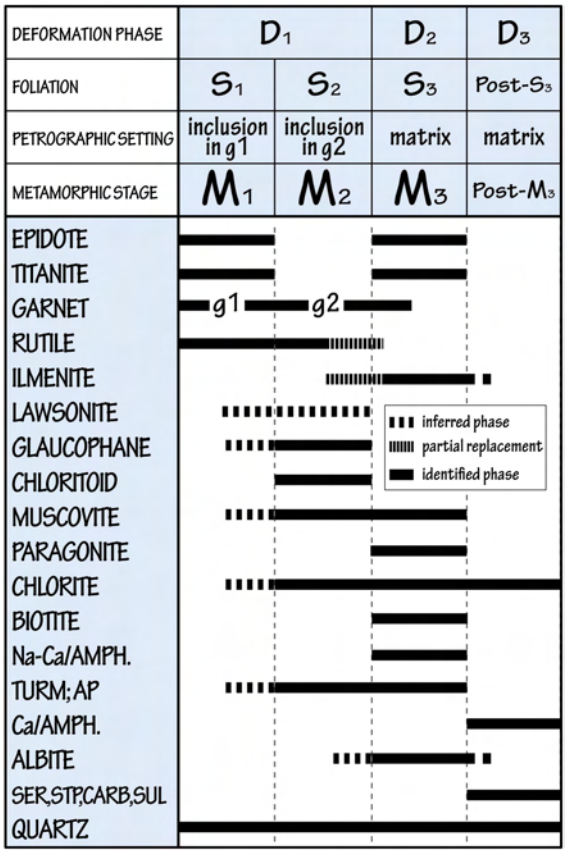

FIGURE 19. Crystallization–deformation relations for the LM. Modified from López-Carmona *et al.* (2010; 2013).

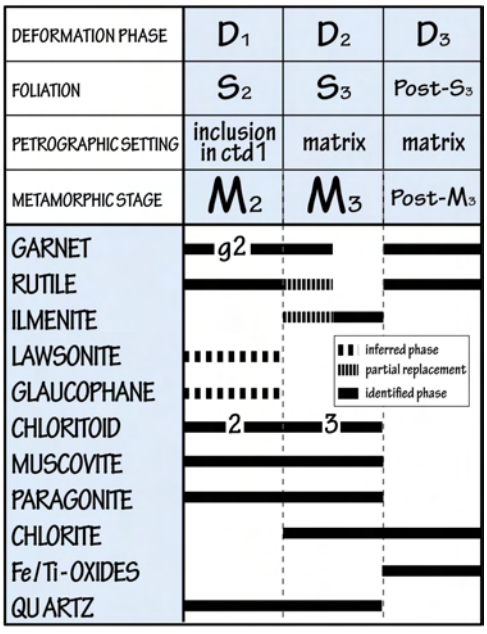

FIGURE 20. Crystallization–deformation relations for the UM. Modified from López-Carmona *et al.* (2010; 2013).

[4] Mineral abbreviations are those used by THERMOCALC (Holland & Powell, 1998): ab-albite; act-actinolite, bi-biotite, chl-chlorite, ep-epidote, g-garnet, gl-glaucophane, hb-hornblende, hem-hematite, ilm-ilmenite, jd-jadeite, law-lawsonite, mt-magnetite, mu-muscovite, o-omphacite, pa-paragonite, pl-plagioclase, q-quartz, ru-rutile and sph-titanite (sphene). Other abbreviations: bar-barroisite, carb-carbonates, ser-sericite; stp-stilpnomelane; sul-sulphides, ts- tschermakite, win-winchite.

2.2.1.2 *The Cambre metabasic rocks*

The Cambre metabasic rocks are intensely foliated amphibolites and greenschists with N-MORB chemical composition (FIGURE 17; Arps, 1981; González Lodeiro *et al.*, 1984; Rodríguez, 2005) that outcrop at the base of the Pazos Synform.

The Cambre metabasic rocks are immediately overlying the so-called Bembibre-Ceán detachment, which marks the limit between the Lower and the Middle Allochthon in the MTC. The dominant rock type is teal/bluish-green fine to medium-grained garnet-bearing amphibolite with frequent levels containing pseudomorphs after lawsonite, usually less than 10 m thick. Going upwards in the sequence, lawsonite pseudomorphs disappear gradually, but quickly, and amphibolites grade into greenschists with garnet porphyroblasts dispersed in a dark green matrix. The greenschists contain epidote-rich layers several centimetres up to 1–2 metres thick. Finally, the top of the succession is dominated by greenschists with albite porphyroblasts ("prasinites";Rodríguez, 2005) and fine-grained pelitic schists without garnet (FIGURE 21).

Deformation in the Cambre metabasic rocks is highly heterogeneous. Whereas in some levels the lawsonite pseudomorphs preserve the euhedral shape, towards the top of the sequence the pseudomorphs are strongly stretched and almost indistinguishable from the matrix. Mylonitic to ultra-mylonitic layers are localized in the basal part, at the contact with the gneisses of the Lower Allochthon, along the Bembibre-Ceán detachment. However, deformation history in the Cambre metabasic rocks would include several compressive, extensional and strike-slip phases (Díez Fernández *et al.*, 2011). Three foliations, with uneven development at different structural levels, have been identified. The main foliation in the lower part of the sequence is defined by the shape preferred orientation of amphibole, epidote, albite, chorite and muscovite. This foliation wraps gently around mostly euhedral crystals of garnet and lozenge-shaped aggregates containing epidote, chlorite, albite and white micas, interpreted as pseudomorphs after lawsonite (Rodríguez *et al.*, 2003).

Unoriented, or partially oriented, relicts of an early assemblage preserved in the core of garnet porphyroblasts are related to an incipient foliation S_1. A second foliation, S_2, develops in the garnet rim and is continuous with the matrix foliation, suggesting syntectonic growth of garnet. Pseudomorphs after lawsonite comprise oriented crystals of epidote and stretched clusters interpreted as inclusions in the original lawsonite crystals. Stretched clusters define a slightly curved internal foliation, generally oblique to but continuous with the matrix foliation, suggesting that the crystallisation of lawsonite is also contemporaneous with the initial development of S_2. Clusters are compoused of rutile/ilmenite and titanite and of chlorite-albite aggregates. Their mineralogy indicates that chlorite-albite aggregates may represent pseudomorphs after a former phase, most likely, glaucophane (cf. Le Bayon *et al.*, 2006;

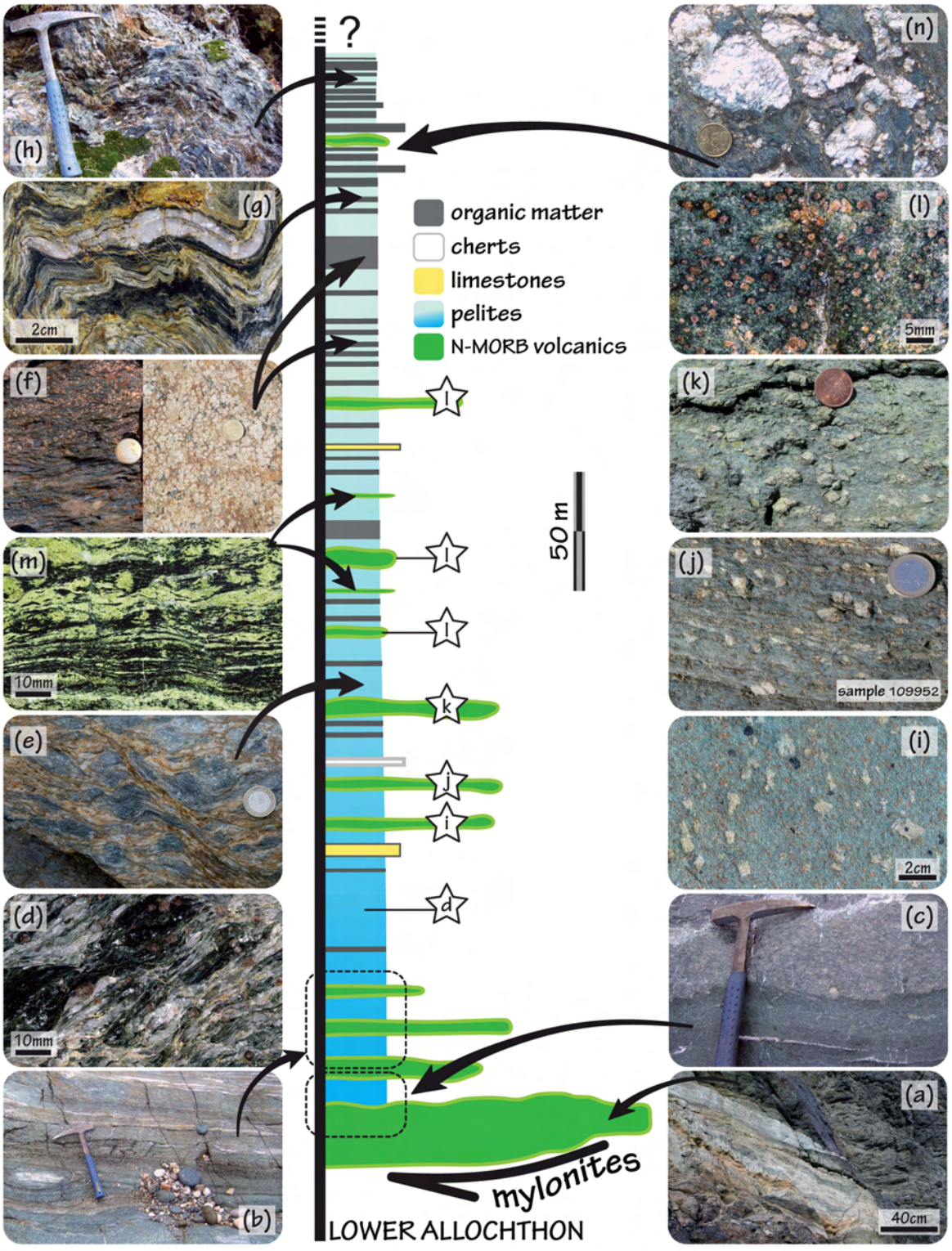

FIGURE 21. Idealized stratigraphic column of the Ceán Unit in the MTC. Photographs showing field aspects of (a) the Bembibre-Ceán Detachment; (b-c) metasediments intercalated with metavolcanics; (d-h) Ceán pelitic schists and (i-n) Cambre metabasic rocks. (d-j). Stars and arrows indicate the location of the photographs in each level. See details in the text. The stratigraphic column is modified from Díez Fernández (2011).

Rodríguez, 2005). The preservation in certain domains of the euhedral shape of the former lawsonite crystals suggests that pseudomorphism occurred as a static process and these domains were not affected by any further ductile deformation (cf. Ballèvre *et al.*, 2003; Philippon *et al.*, 2013).

To the top of the succession the main foliation is defined by the shape preferred orientation of amphibole, epidote, chlorite, albite and minor amounts of muscovite, and is parallel to boudined layers of quartz and, locally, epidote. This foliation, S_3, wraps around garnet and strongly deformed pseudomorphs after lawsonite. In intensely deformed samples lawsonite pseudomorphs are absent and porphyroblasts of albite dominate.

Albites contain anhedral crystals of garnet and sigmoidal inclusion trails, continuous with the matrix foliation, suggesting the syntectonic growth of albite. The development of S_3 is stronger to the upper part of the sequence and is limited to highly deformed or mylonitic levels in the middle and lower areas. Thus, the associated deformation was concentrated at this structural level. However, this foliation reworks S_2, as evidenced by the relics in lawsonite pseudomorphs and garnet inclusions in albite porphyroblasts.

Two representative samples of the Cambre metabasic rocks have been chosen for detailed study. The first rock type, referred to hereafter as CA (for Cambre Amphibolites), is located in the intermediate part of the sequence. The presence of numerous garnet porphyroblasts, rich in S_1 and S_2 inclusions, and the abundant well-preserved pseudomorphs of euhedral lawsonite, makes this sample ideal to study the early deformation phases. The second rock-type, referred to hereafter as AG (for Albite Greenschists), represent albite-bearing samples located at the top of the succession. The occurrence of syn-S_3 albite porphyroblasts allows investigating the late exhumation-related stage.

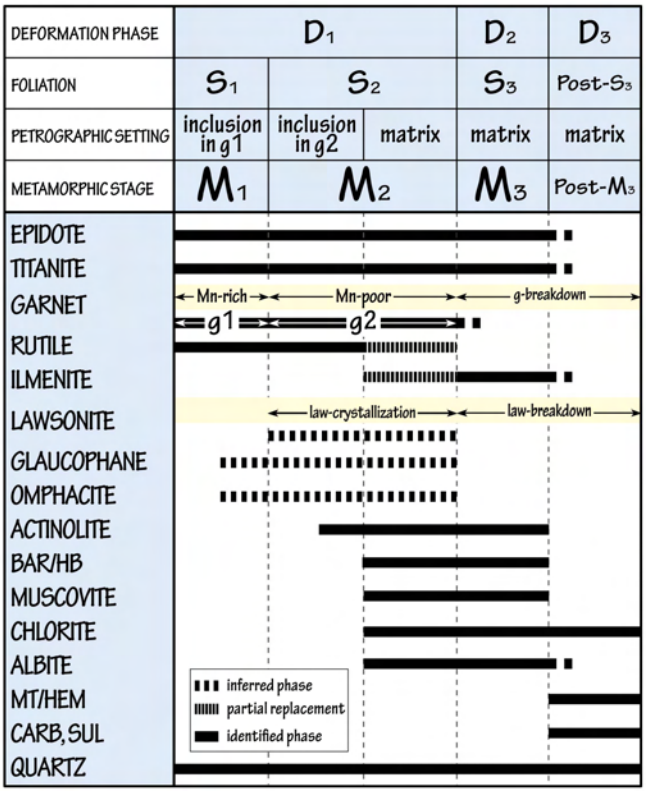

FIGURE 22. Crystallization–deformation relations for the CA. Modified from López-Carmona *et al.* (submitted).

Three stages of blastesis are distinguished in the evolution of the Cambre metabasic rocks (M_1, M_2 and M_3). The M_1 episode is preserved as a relict S_1 assemblage

that comprises inclusions of ep-sph-ru-q within the first generation of garnet (g1). It is followed by a second metamorphic stage, M_2, characterized by the syntectonic development of an assemblage including lawsonite, a second generation of garnet (g2) and a foliation (S_2) consisting of law-ep-act/bar±gl-o-mu-ru/ilm-sph-q. This assemblage is preserved at the base of the upper sequence of the MTC. The third stage M_3 is best developed at the top of the sequence. It is characterized by the growth of syntectonic albite porphyroblasts and a foliation S_3 containing ep-act-hb-mu-chl±ilm-sph-q. Whereas both, S_2 and S_3, have the same orientation, first order petrographic observations suggest that they developed at distinct P-T conditions. Finally, post-M_3 crystallization includes post-S_3 phases such as mt, hem, chl, carb, sul, q, variably present in most samples of the Cambre metabasic rocks (FIGURE 22).

The Cambre metabasic rocks are extensively studied in section 3.2 of Chapter 3.

2.3 *Blueschists from the Middle Allochthon of the IAA*

Over the last decade several correlations between the Malpica-Tui Complex and equivalent units in the south of the Armorican Massif have been suggested (c.f. Rodríguez *et al.,* 2003; Ballèvre *et al.*, 2009; Martínez Catalán *et al.*, 2009; Abati *et al.*, 2010). From their age and tectonometamorphic evolution, correlations between the upper sequence of the Malpica-Tui Complex (the Ceán Unit), and the Upper Unit of Ile de Groix are widely accepted. Both terranes show similar lithologic associations constituted by variable proportions of glaucophane-chloritoid-bearing metapelites and mafic rocks with pseudomorphs after lawsonite. The Upper Unit of Ile de Groix and the Ceán Unit share a blueschist-facies event constrained by $^{40}Ar/^{39}Ar$ dating of phengitic muscovite at 360-370 Ma in both the metapelites from Ile de Groix (Bosse *et al.*, 2005) and the metapelites from the Ceán Unit (Rodríguez *et al.,* 2003; López-Carmona *et al.,* submitted).

Ile de Groix is a classical blueschists Variscan outcrop. The island is located 10 km off the southern coast of Brittany (France; FIGURE 9), and is well-known by the European geologists because of the nice exposures of well-preserved blueschists, whose first petrographic descriptions date back to the 19th century (Barrois, 1883). Geophysical and offshore geological studies revealed that the island represents a small emerged part of a much larger NW-SE blueschists unit (of about 40 km long and 10 km wide; Delanoë *et al.*, 1972; Audren & Lefort, 1977). According to modern studies, blueschist-facies rocks from the Ile de Groix consist of around 80% pelitic and 20% mafic rocks intercalated at all scales (Audren *et al.*, 1993; Bosse *et al.*, 2005). In the higher grade, east part of the island, blueschists typically consist of a foliated matrix of glaucophane (± omphacite), epidote and titanite, with dispersed idioblastic garnets and numerous rhomboidal shaped pseudomorphs formed by aggregates of epidote, chlorite and paragonite, replacing former lawsonite (Cogné *et al.*, 1966; Ballèvre *et al.*, 2003). Although the existence of lawsonite remnants was suggested by Felix (1972), clear

evidence has not subsequently been found. Blueschist-facies rocks in the south Armorican domain also outcrop further to the SE of Ile de Groix, in the Bois-de-Cené units in the Vendée area (Triboulet, 1974; 1991; Guiraud *et al.*, 1987) and the Saint-Martin des Noyers formation (Thieblemont *et al.*, 1988). Bois-de-Cené blueschist-facies rocks are characterized by garnet-chloritoid-chlorite to chloritoid-chlorite-bearing pelitic micaschists and are considered the eastern equivalent of Ile de Groix (Guiraud *et al.*, 1987). The Saint-Martin des Noyers formation consists on highly retrogresed amphibolites ranging in composition from ultramafic to rhyolitic (Thieblemont *et al.*, 1988). Basaltic compositions show a relict garnet-barroisite assemblage and complex amphibole chemistry. Although it would require a comprehensive petrographic and thermobarometric study, this formation could be equivalent to the Cambre metabasic rocks.

The Ile de Groix and Bois-de-Cené blueschists and blueschist-facies rocks are interpreted to derive from tholeiitic to alkali-basalt types, i.e. oceanic island basalts (OIB), and oceanic sediments, respectively (Bernard-Griffiths *et al.*, 1986; El Korh *et al.* 2009, 2012). As in the NW Iberian Massif, both units occur as a ~ 1km thickness klippe of ocean-derived material thrusted over the Parautochthon (Ile de Groix), or are preserved within the core of late synformal folds (Bois-de-Cené; Brun & Burg, 1982; Lefort & Vigneresse, 1992). These blueschists are interpreted either as an accretionary prism developed at an early stage of the subduction or to be part of a suture rooted along the contact at the base of les Folies-Siffait (Champtoceaux Complex) or Saint-Martin-des-Noyers (Vendée) units (Ballèvre *et al.*, submitted; FIGURE 9).

In the Iberian Massif, equivalent blueschists are usually highly retrogressed, and they were not described until much later, firstly in the Trás-os-Montes region of north Portugal (Ribeiro, 1976; Munhá & Ribeiro, 1984; Gil Ibarguchi & Dallmeyer, 1991). Paradoxically, although fresh lawsonite has never been found in the well-preserved blueschists from Ile de Groix, it has been described in the Morais Complex of north Portugal (Schermerhorn & Kotsch, 1984). Blueschists-facies metapelites and highly retrogressed blueschists have been also reported in the middle allochthonous units of Galicia, in the Órdenes Complex (Forcarei unit; Martínez Catalán *et al.*, 1996) and in the Ceán Unit of the Malpica-Tui Complex (Rodríguez *et al*, 2003; López-Carmona *et al.*, 2010). The following chapter comprises a detailed petrological and thermobarometric study of the blueschist-facies rocks from the Ceán Unit, which is the main objective of this PhD thesis.

2.3.1 *The metamorphic gap: greenschist-facies overprint or a preservation problem*?

Since the first mapping by Lamouche (1929), the large-scale structure of Ile de Groix has often been described as a NW–SE trending upright anticline (Cogné, 1954; Quinquis & Choukroune, 1981; Bosse *et al.*, 2002; Ballèvre *et al.*, 2003). According to their

metamorphism, the modal proportion of garnet and the deformation history, two domains, eastern and western, have been classically distinguished in Ile de Groix (Cogné *et al.*, 1966; Boudier & Nicolas, 1976; Carpenter, 1976; Quinquis, 1980; Bosse *et al.*, 2002; Ballèvre *et al.*, 2003). In the eastern domain, the so called Upper Unit, with abundant Mn-rich garnet, peak P-T conditions are related to a first defomation stage in the blueschist-facies conditions, and are estimated at 16-20 kbar and 500 °C (Bosse *et al.*, 2002; Ballèvre *et al.*, 2003; Bosse *et al.*, 2005), whereas in the western domain, in the so called Lower Unit, with very low modal proportion of garnet, peak P-T conditions has been constrained at 14-16 kbar and 450 °C in metapelitic rocks (Bosse *et al.*, 2002), and are attributed to a second deformation event in the greenschist-facies conditions. Thus, metamorphic grade increases from the Lower to the Upper Unit and the garnet isograd trending NNE-SSW (FIGURE 23; Carpenter, 1976; Quinquis, 1980), considered the limit between the two units, has been interpreted in different ways. Cannat (1985) and Bosse *et al.* (2002) interpret it as a greenschist facies ductile thrust that superimposes the higher grade over the lower grade unit after the high-pressure event, i.e. during the exhumation of both units, suggesting that the exhumation was not only controlled by crustal-scale extension. The inverted gradient is then interpreted as a result of the superposition of the two blueschist-facies units that have experienced different P-T paths. Moreover, Ballèvre *et al.* (2003) supports this interpretation with new metamorphic data, suggesting that the distribution of the lawsonite pseudomorphs at the scale of the island is also controlled by a difference in P-T conditions during the blueschist-facies event. They conclude that peak pressures in the Lower Unit did not exceed those permitting lawsonite growth in mafic rocks of basaltic composition. This would confirm that peak pressures were lower in the Lower Unit than in the Upper Unit, supporting the existence of a thrust contact between the two units (Bosse *et al.*, 2002). The blueschist-facies event has been dated by $^{40}Ar/^{39}Ar$ in phengitic muscovite at 360-370 Ma, whereas the greenschist-facies event has been constrained at 345-353 by Rb-Sr (whole rock) and $^{40}Ar/^{39}Ar$ (muscovite) in both well-preserved blueschist-facies rocks and strongly overprinted samples from both units (Bosse *et al.*, 2005).

On the other hand, some authors describe the structure of the island as a succession of west verging inclined folds with a 100-300 m wavelength, instead of a single kilometre-scale anticline (Jeannette, 1965; Boudier & Nicolas, 1976; Philippon *et al.*, 2009). The existence of shear bands with opposite senses of shear was deduced by the analysis of snowball garnets rotation (Quinquis, 1980) and quartz c-axes fabrics (Cannat, 1985). At that time intense deformations, and the associated ductile fabrics, in mountain belts were attributed to thrusting and therefore, the exhumation of metamorphic rocks was implicitly explained by erosion. Shelley and Bossière (1999) observed top-to-NW and top-to-SE shearing in similar proportions (pure shear deformation) at both sides of the island, and described the whole lithological pile as a unique metamorphic series, that reached peak eclogite-facies conditions

and experienced a later greenschist facies overprint during (extensional) exhumation, without any internal discontinuity. Thus, they propose that the Ile de Groix blueschists were exhumed by crustal thinning rather than by ductile thrusting.

Recent studies by Philippon *et al.* (2009) describe two associated senses of shear showing a systematic relation with rock-types occurring in shear bands of 10-100 m heterogeneously distributed: a southeast directed shear (top-to-the N140°E) only observed in the well-shaped lawsonite pseudomorphs-bearing metabasic rocks in the eastern part of the island, synchronous with a prograde high-pressure metamorphism, and preceding the quasi-opposite northwest (top-to-N350°E) directed shear, synchronous to the retrograde greenschist-facies overprint. The lack of clear evidence for N140°E shear criteria at the island-scale suggest that it might be erased by the top-to-N350°E shearing, what is in agreement with the lack of lawsonite pseudomorphs-bearing metabasic rocks in the western part of the island. In the frame of the Variscan Belt of southern Brittany, the southeast directed shear is attributed to thrusting related to a northward dipping subduction and the northwest directed shear to an exhumation controlled by a northward dipping extensional detachment.

In any case, the models proposed for the tectonometamorphic evolution of Ile de Groix cannot consider its relation with other units, because of its limited extension and the lack of exposed contacts. nevertheless, in the westernmost equivalent terrane of Ile de Groix, the Ceán Unit, is possible to observe the contact with a lower eclogitic unit of continental nature (the Lower Allochthon) that allow complementing the interpretation of the tectonometamorphic evolution (by comparision) of both units. The Ceán Unit developed a metamorphism in the blueschist-facies conditions (López-Carmona *et al.*, 2010; 2013).

Nevertheless, deformation in the upper sequence of the MTC is highly heterogeneous and the blueschist-facies fabrics are preserved at specific levels of the series. In general, strain intensity increases towards the top of the succession. Whereas in some levels the lawsonite pseudomorphs preserve the euhedral shape, towards the top of the lithological sequence the pseudomorphs become more deformed, strongly stretched and progressively incorporated into the matrix of the metabasic rocks (López-Carmona *et al.*, submitted). To the base of the sequence the metapelites are chloritoid–glaucophane-bearing micaschist whereas upwards the content of mica decreases, garnet disappears, and a gradual increase of opaque phases and quartzite beds occur (López-Carmona *et al.*, 2010). The paragenesis becomes restricted to fine-grained white mica, chlorite and quartz, giving the rocks a slaty texture and suggesting that the metamorphic gradient decreases rapidly to the top of the succession. Therefore, the lower structural levels of the sequence preserve evidence of the subduction-related metamorphism, whereas the upper structural levels contain indications of the exhumative

evolution (López-Carmona *et al.*, 2013; submitted), and metapelites and metabasic rocks show systematic changes in texture and mineral composition that are spatially related.

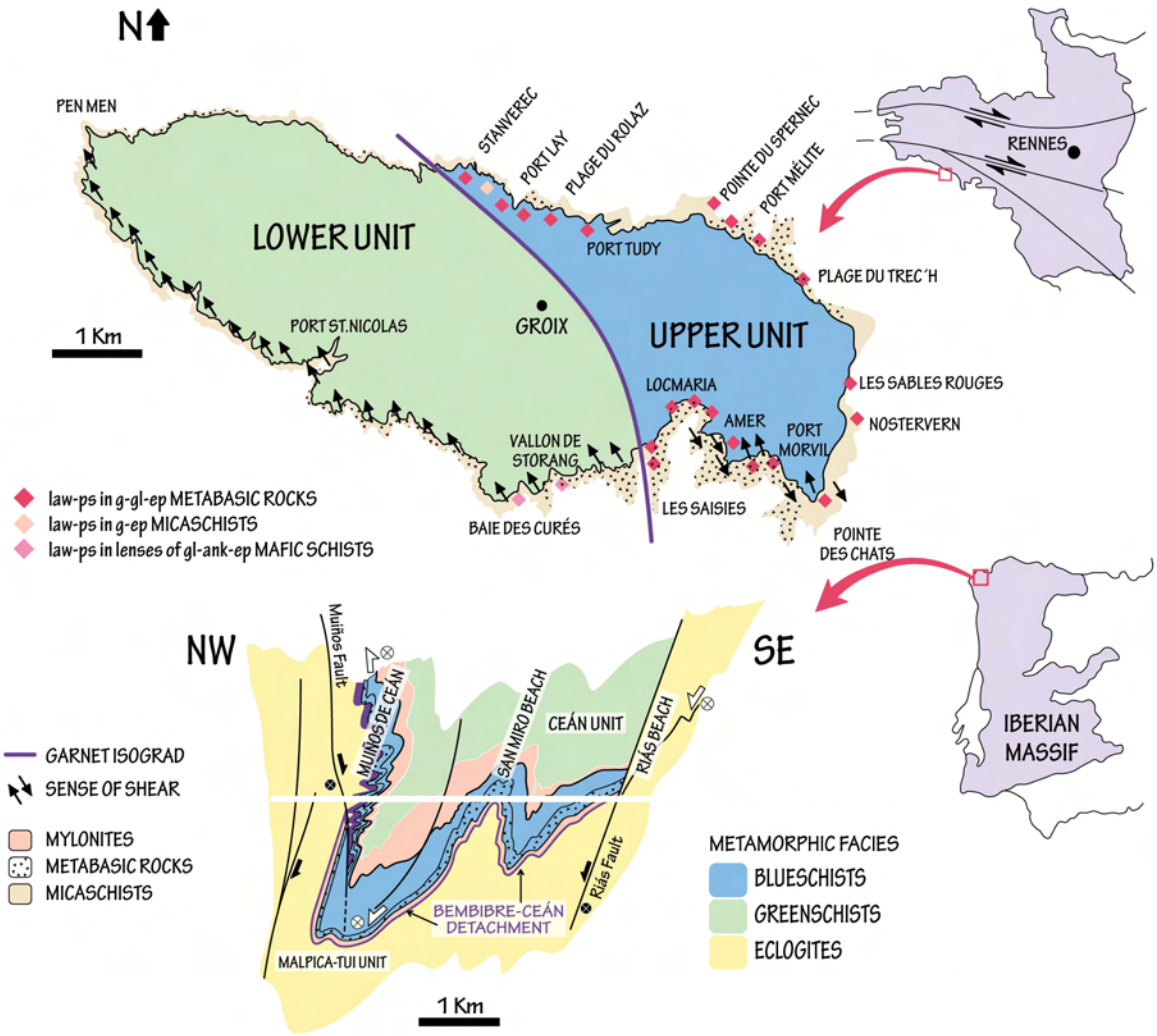

FIGURE 23. Simplified geological map and cross section of the Ile de Groix and the Pazos Synform, respectively, showing the distribution of metamorphic facies in both terranes. Modified from Bosse *et al.* (2002), Ballèvre *et al.* (2003), Philippon *et al.* (2009); Díez Fernández (2011) and López-Carmona *et al.* (2013; submitted).

The Ceán Unit is considered a as a highly condensed metamorphic succession with a lower part in the blueschist-facies and an uppermost part without high-pressure relicts (López-Carmona *et al.*, 2007; 2010; 2013; submitted). Peak conditions in the Ceán Unit are constrained between 19–22 kbar in the lower structural levels of the sequence. Nevertheless, the temperatures recorded by the metapelitic and the metabasic rocks differ slightly. From the bottom to the top of the sequence, the sample of the Cambre metabasic rocks (CA) is the lowermost one, overlying the mylonites (sample MT1). The lower metapelites (sample LM) are located immediately above CA, whereas the upper metapelites (sample UM) are situated in the middle part of the synformal structure, in an upper structural domain separated from the

lower domain by a mylonitic band (FIGURES 18 & 23). Within the Ceán schists, the temperature of the pressure peak is of ca. 460°C at the base (LM) and of ca. 520°C in the intermediate part of the sequence (UM). The temperature estimated for the Cambre metabasic rocks is slightly higher and constrained at ca. 560 °C. Both metapelites and metabasic rocks have recorded similar P–T histories. Then, the temperature gap, that varies from slight variations to a difference of 100 °C, could be attributed to different processes; (1) The temperature gap could reflect the different location of the samples in the orogenic wedge, as the original position of the different units during subduction was preserved despite the subsequent post-high-P history (cf. Martínez Catalán et al., 1996; Gómez Barreiro et al., 2010; López-Carmona et al., 2013). (2) It could be attributed to the thermal effects of fluid migration during metamorphism. In numerous orogens it has been reported that metamorphic hydration reactions represent a possible mechanism that may lead to a localized increase in temperature due to fluid flow (e.g. Peacock, 1987; Yakovlev, 1993; Stober & Bucher, 2004; Dipple & Ferry, 1992; Wing & Ferry, 2002, 2007; Lyubetskaya & Ague, 2009). Nevertheless, crustal fluid flow models are not easy to evaluate and are beyond the scope of this PhD tesis. (3) Another possibility for these temperature variations may be due to the deformation gradient related to the contact between the Lower and the Middle Allochthons. This gradient decreases both upward and downward. The conversion of mechanical energy into heat is a well know processes, commonly referred to as shear heating (e.g. Souche et al., 2013; Gottardi et al., 2013). Accordingly, the two samples with the highest equilibration temperature (CA and UM) are located immediately above a shear zone. Sample CA, showing the highest temperature (560 °C) is located just above the main shear zone, and sample UM is located just above a secondary mylonitic band (FIGURES 18 & 23). Thus, temperature seems to increase with deformation.

However, it should also be stressed out that the absolute accuracy of the P-T estimation based on pseudosections should not be overestimated. The main advantage of this approach is the determination of the qualitative evolution of the rocks. The absolute values are subject to a certain degree of uncertainty, related among others to the accurate estimation of the effective bulk rock composition (and its possible evolution along the P-T path) and the accuracy of the mixing models for solid solutions. It is therefore possible that the difference in the absolute P-T conditions recorded by the metapelitic and metabasic samples may be within an acceptable error.

The significant difference in metamorphic grade between the lower sequence (i.e. MTU in the eclogite-facies) and the upper sequence (i.e. Ceán Unit, in the blueschist-facies) of the MTC, and between the upper and lower part of the Ceán Unit suggests that the mylonites that mark the contacts are related to an extensional deformation (López-Carmona *et al.*, 2007). The transition occurs at approximately 500 m from the base of the sequence, indicating important telescoping of metamorphic isograds compatible with extensional detachment

faulting (López-Carmona *et al.*, 2008). The pressure gap between the two domains of the Ceán Unit is interpreted as a result of the greenschist facies overprint that occurred during decompression driven by crustal-scale extension.

Exhumation models for the Lower and Middle Allochthon of NW Iberia (Martínez Catalán *et al.*, 1996; Díez Fernández *et al.*, 2011) include geological data and mutual relationships of all the units described in the Allochthonous Complexes. These models propose a complex evolution of the subduction-exhumation channel starting with buoyancy driven large thrusts and recumbent folds, partly simultaneous with the development of extensional detachments in upper crustal levels. Out of sequence thrusts also play an important role in the present disposition of the units (Martínez Catalán *et al.*, 2002). Thus, the models proposed for Ile de Groix can be easily inserted in the general model proposed for the lower and middle allochthons in the NW Iberian Massif.

CHAPTER 3

P-T Conditions

3. P–T CONDITIONS

3.1 *Ceán pelitic schists*

3.1.1 *Introduction*

HP–LT rocks in orogenic belts constitute the main markers of paleo-subduction zones, and knowledge of their P–T conditions can provide useful information about the mechanisms of subduction and the maximum burial reached (*e.g.* Ernst, 1973; Platt, 1993; Maruyama *et al.*, 1996; Ernst, 2001; Babist *et al.*, 2006; Warren & Miller, 2007; Warren *et al.*, 2008b; Masago *et al.*, 2009; Omori *et al.*, 2009; Santosh *et al.*, 2009).

Data about the metamorphic evolution of subducted terranes obtained through petrologic modeling are at the core of geodynamic models and paleogeographic reconstructions of the lithospheric plates. These models, and the plate relationships and paleogeography of the Paleozoic, are the key to unraveling the evolution of the peri-Gondwanan terranes during the Variscan orogeny. In this context, the northwestern section of the Iberian Massif offers an important clue to understanding the evolution of the European Variscan belt. A key aspect of this section is the presence of exotic terranes emplaced as large, complex allochthonous sheets upon sequences deposited on the passive margin of northern Gondwana (Martínez Catalán *et al.*, 2007). The different exotic units can be grouped into three main terranes. The upper terrane is viewed as a piece of an island arc developed at ca. 500 Ma in an active part of the northern Gondwana margin, the related back-arc extension of which probably helped to open the Rheic Ocean. This arc was subsequently accreted to Laurentia or Baltica between 440 and 410 Ma (age of the high-P metamorphism; Fernández-Suárez *et al.*, 2007). The intermediate terrane includes two associated ophiolitic units that are considered to be remnants of the Rheic Ocean accreted below the upper units at ca. 385 Ma. Finally, in the lower structural position, the Basal Units are interpreted to represent a large, complex sheet emplaced upon sequences deposited on the most external passive margin of northern Gondwana (Martínez Catalán *et al.*, 2009). The Basal Units show the imprints of a late Devonian HP metamorphism that has been interpreted to be related to its subduction beneath the southern margin of Laurussia at the onset of Variscan convergence (Arenas *et al.*, 1995; 1997; Martínez Catalán, *et al.*, 1996). In this study, we use the thermodynamic modeling software THERMOCALC (Powell & Holland, 1988) and PERPLE_X (Connolly, 2005) to constrain the metamorphic evolution of chloritoid–glaucophane pelitic schists from the HP Malpica–Tui

Unit in Galicia (NW Spain). This unit is the westernmost exposure of the Basal Units of the Allochthonous Complexes of the NW Iberian Massif. The HP pelitic schists (Ceán schists; FIGURE 1) crop out in the northern coastal section of the Malpica-Tui Unit and contain an initial chloritoid-glaucophane paragenesis, which is one of the HP indicators for metapelites that has been reported in several HP terranes around the world (e.g. Ile de Groix, Kiénast & Triboulet, 1972; the Kaczawa Complex, Kryza *et al.*, 1990; the Peloponnese, Katagas, 1980; Theye *et al.*, 1992; the Gran Paradiso Massif, Chopin, 1981; north Qilian Orogen, Song *et al.*, 2007, Wei & Song, 2008; Oman, El-Shazly & Liou, 1991, Warren & Waters, 2006). The geological significance that can be inferred from the presence of glaucophane has been considered by several authors to explain Siluro-Devonian subduction and collision processes in the majority of the geotectonic models proposed for the Variscan orogeny (Behr *et al.*, 1984; Matte, 1986; Pin & Vielzeulf, 1988).

The presence of rocks with comparable mineral associations is common in many of the European Variscan outcrops. Hence, the Basal Units of the NW Iberian Massif can be correlated with similar terranes with HP-LT/MT metamorphism from Portugal to the northern areas of eastern Europe, such as the Kaczawa Complex in the Polish Sudetes of the Bohemian Massif (Kryza *et al.*, 1990; Cymerman *et al.*, 1997). In addition, similarities between certain geological units of the Armorican Massif (Brittany) and the Malpica-Tui Unit allows correlation of the latter with the Ile de Groix (Kiénast & Triboulet, 1972; Shelley & Bossière, 1999; Ballevre *et al.*, 2003) and Champtoceaux Complex (Ballèvre *et al.*, 2009), particularly since the age of the HP metamorphism is the same in both terranes (Bosse *et al.*, 2005). This age has been tightly constrained to around 371 Ma in NW Iberia by $^{40}Ar/^{39}Ar$ geochronology on white micas from different lithologies, including eclogites (Van Calsteren *et al.*, 1979; Rodríguez *et al.*, 2003), and by U-Pb zircon ages (Abati *et al.*, 2009). However, chloritoid-glaucophane mineral assemblages have not been previously described in the NW Iberian Massif. Hence, one of the goals of this study is to record the presence of choritoid-glaucophane pelitic schists and document their petrological characteristics and metamorphic P-T conditions.

3.1.2 *Petrologic modelling of chloritoid–glaucophane schists from the NW Iberian Massif*

LÓPEZ-CARMONA, A., ABATI, J. & RECHE, J. (2010) GONDWANA RESEARCH 17, 377–391

Gondwana Research 17 (2010) 377–391

Contents lists available at ScienceDirect

Gondwana Research

journal homepage: www.elsevier.com/locate/gr

Petrologic modeling of chloritoid–glaucophane schists from the NW Iberian Massif

A. López-Carmona [a,b,*], J. Abati [a,b], J. Reche [c]

[a] Departamento de Petrología y Geoquímica, Universidad Complutense de Madrid, 28040 Madrid, Spain
[b] Instituto de Geología Económica-Consejo Superior de Investigaciones Científicas, 28040 Madrid, Spain
[c] Unitat de Petrología i Geoquímica, Facultat de Ciències, Universitat Autònoma de Barcelona, 08193 Bellaterra (Barcelona), Spain

ARTICLE INFO

Article history:
Received 29 April 2009
Received in revised form 24 September 2009
Accepted 1 October 2009
Available online 17 October 2009

Keywords:
Malpica–Tui unit
High-pressure terranes
Blueschist
Glaucophane–chloritoid
P–T pseudosection

ABSTRACT

Two *P–T* pseudosections computed with Thermocalc and Perplex software for high-pressure pelitic Ceán Schists from the NW Iberian Massif show that the paragenesis chloritoid + glaucophane, preserved as relict micro-inclusions in garnet porphyroblasts, is stable above 17–18 kbar, indicating a first stage of subduction with 65–70 km of burial. The subsequent growth of biotite and albite porphyroblasts, according to their stability fields in a MnNCKFMASH *P–T* phase diagram, indicates strong decompression accompanied by slight heating to reach a metamorphic peak at ~500 °C. This mineral association, described in many subduction-related terranes around the world as one of the high-pressure indicators for metapelites, has not been reported previously in the NW Iberian Massif. The schists contains an initial high-pressure assemblage formed by chloritoid + garnet ($Alm_{0.58}$ $Prp0_{0.03}$ $Grs_{0.38}$ $Sps_{0.09}$) ± glaucophane + phengite (3.5–3.4 Si p.f.u.) + paragonite + chlorite + epidote + rutile + ilmenite + quartz, preserved as micro-inclusions in garnet, chloritoid and albite porphyroblasts defining an S_1 internal fabric. The matrix foliation (S_2) additionally contains a high-pressure association formed by garnet ($Alm_{0.68}$ $Prp_{0.04}$ $Grs_{0.25}$ $Sps_{0.03}$) + phengite (3.4–3.3 Si p.f.u.) + paragonite + winchite + barroisite + hornblende + chloritoid + chlorite + epidote + rutile + ilmenite + albite + quartz ± biotite. An initial pseudosection calculated in the KFMASH system with Thermocalc 3.26 gives pressure estimates through Si-content in phengite barometry that are in agreement with conventional thermobarometry and Thermocalc average *P–T* calculations, but is unable to describe the full complexity of the mineral assemblages of the schists. For this reason, a more complete *P–T* pseudosection in the model system MnNCKFMASH was calculated with Perplex 07. This provides a reliable succession of mineral assemblages that are consistent with the petrographic observations and allows a mineralogical sequence to be set for each metamorphic event in the *P–T* evolution of the high-*P* pelitic Ceán Schists.

1. Introduction

High-pressure (high-*P*) and low-temperature (low-T) rocks in orogenic belts constitute the main markers of paleo-subduction zones, and knowledge of their *P–T* conditions can provide useful information about the mechanisms of subduction and the maximum burial reached (e.g. Ernst, 1973; Platt, 1993; Maruyama et al., 1996; Ernst, 2001; Babist et al., 2006; Warren and Miller, 2007; Warren et al., 2008; Masago et al., 2009; Omori et al., 2009; Santosh et al., 2009).

Data about the metamorphic evolution of subducted terranes obtained through petrologic modeling are at the core of geodynamic models and paleogeographic reconstructions of the lithospheric plates. These models, and the plate relationships and paleogeography of the Paleozoic, are the key to unraveling the evolution of the peri-Gondwanan terranes during the Variscan orogeny. In this context, the northwestern section of the Iberian Massif offers an important clue to understanding the evolution of the European Variscan belt. A key aspect of this section is the presence of exotic terranes emplaced as large, complex allochthonous sheets upon sequences deposited on the passive margin of northern Gondwana (Martínez Catalán et al., 2007). The different exotic units can be grouped into three main terranes. The upper terrane is viewed as a piece of an island arc developed at *ca.* 500 Ma in an active part of the northern Gondwana margin, the related back-arc extension of which probably helped to open the Rheic Ocean. This arc was subsequently accreted to Laurentia or Baltica between 440 and 410 Ma (age of the high-pressure metamorphism; Fernández-Suárez et al., 2007). The intermediate terrane includes two associated ophiolitic units that are considered to be remnants of the Rheic Ocean accreted below the upper units at *ca.* 385 Ma. Finally, in the lower structural position, the Basal Units are interpreted to represent a large, complex sheet emplaced upon sequences deposited on the most external passive margin of northern

* Corresponding author. Departamento de Petrología y Geoquímica, Facultad de Ciencias Geológicas, C/ Jose Antonio Novais, 2, 28040 Madrid, Spain. Tel.: +34 913944903; fax: +34 915442535.
E-mail addresses: alcarmona@geo.ucm.es (A. López-Carmona), abati@geo.ucm.es (J. Abati), Joan.Reche@uab.cat (J. Reche).

1342-937X/$ – see front matter © 2009 International Association for Gondwana Research. Published by Elsevier B.V. All rights reserved.
doi:10.1016/j.gr.2009.10.003

Gondwana (Martínez Catalán et al., 2009). The Basal Units show the imprints of a late Devonian high-*P* metamorphism that has been interpreted to be related to its subduction beneath the southern margin of Laurussia at the onset of Variscan convergence (Arenas et al., 1995; Martínez Catalán, et al., 1996; Arenas, et al., 1997). In this study, we use the thermodynamic modeling software Thermocalc (Powell and Holland, 1988) and Perplex (Connolly, 2005) to constrain the metamorphic evolution of chloritoid–glaucophane pelitic schists from the high-*P* Malpica–Tui Unit in Galicia (NW Spain). This unit is the westernmost exposure of the Basal Units of the Allochthonous Complexes of the NW Iberian Massif. The high-*P* pelitic schists (Ceán schists, Fig. 1) crop out in the northern coastal section of the Malpica–Tui Unit and contain an initial chloritoid–glaucophane paragenesis, which is one of the high pressure indicators for metapelites that has been reported in several high-*P* terranes around the world (e.g. Île de Groix, Kiénast and Triboulet, 1972; the Kaczawa Complex, Kryza et al., 1990; the Peloponnese, Katagas, 1980; Theye et al., 1992; the Gran Paradiso Massif, Chopin, 1981; north Qilian Orogen, Song et al., 2007, Wei and Song, 2008; Oman, El-Shazly and Liou, 1991, Warren and Waters, 2006). The geological significance that can be inferred from the presence of glaucophane has been considered by several authors to explain Siluro–Devonian subduction and collision processes in the majority of the geotectonic models proposed for the Variscan orogen (Behr et al., 1984; Matte, 1986; Pin and Vielzeulf, 1988).

The presence of rocks with comparable mineral associations is common in many of the European Variscan outcrops. Hence, the Basal Units of the NW Iberian Massif can be correlated with similar terranes with high-*P* and low- to intermediate-temperature metamorphism from Portugal to the northern areas of eastern Europe, such as the Kaczawa Complex in the Polish Sudetes of the Bohemian Massif (Kryza et al., 1990; Cymerman et al., 1997). In addition, similarities between certain geological units of the Armorican Massif (Brittany)

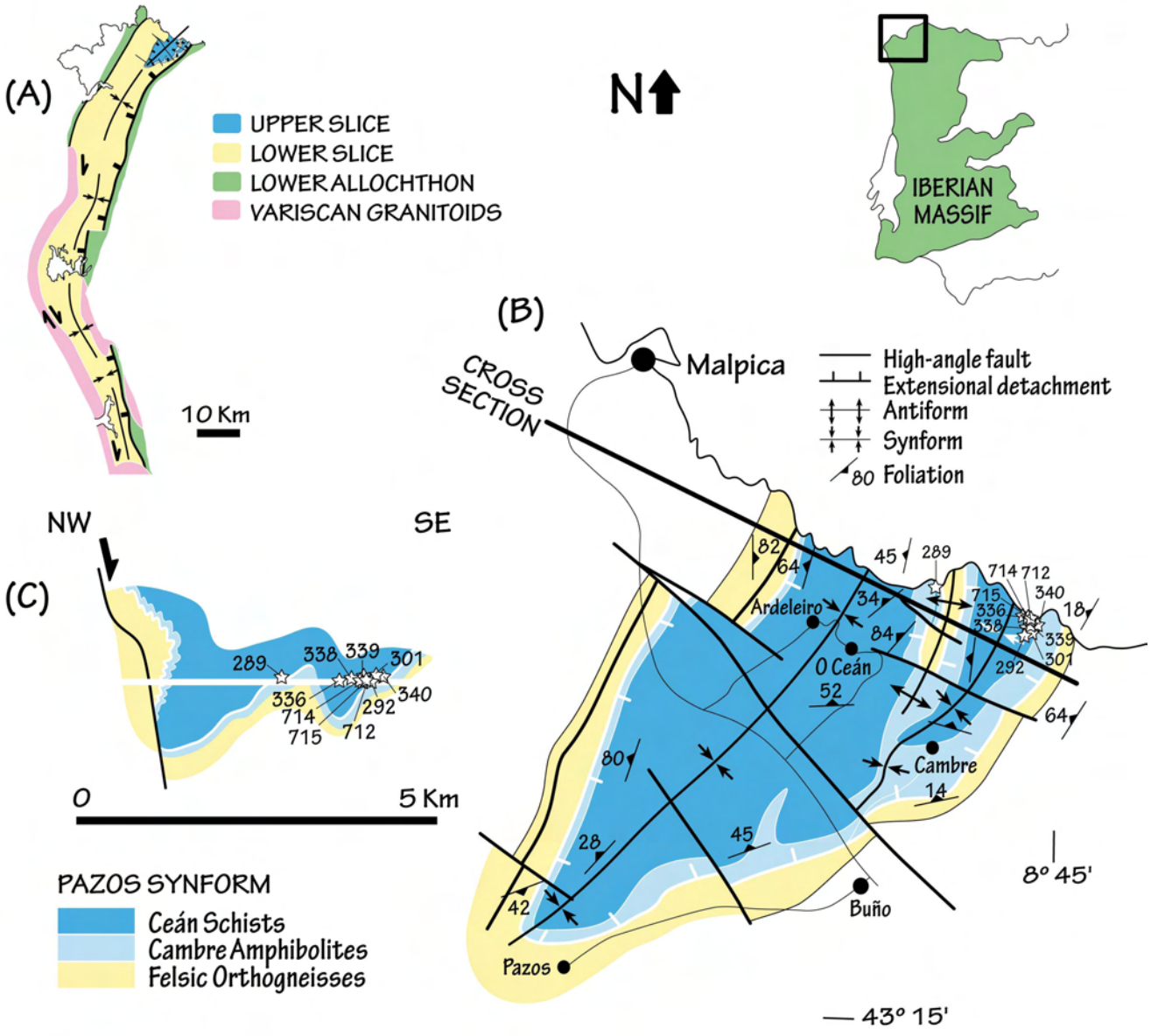

Fig. 1. Schematic geological maps and cross section of the Malpica–Tui Unit. (A) Large scale map of the unit; (B) Detailed map of the upper slice showing only the Pazos Synform; and (C) Cross section across the upper slice. The maps include data from Ortega (1980); Alonso and González (1982); Llana-Fúnez (2001); Rodríguez Aller (2005) and our own data.

and the Malpica–Tui Unit allows correlation of the latter with the Île de Groix (Kiénast and Triboulet, 1972; Shelley and Bossière, 1999; Ballevre et al., 2003) and Champtoceaux Complex (Ballèvre et al., 2009), particularly since the age of the high-*P* metamorphism is the same in both terranes (Bosse et al., 2005). This age has been tightly constrained to around 371 Ma in NW Iberia by $^{40}Ar/^{39}Ar$ geochronology on white micas from different lithologies, including eclogites (Van Calsteren et al., 1979; Rodríguez et al., 2003), and by U–Pb zircon ages (Abati et al., 2009).

However, chloritoid–glaucophane mineral assemblages has not been previously described in the NW Iberian Massif. Hence, one of the goals of this study is to record the presence of choritoid–glaucophane pelitic schists and document their petrological characteristics and metamorphic *P*–*T* conditions.

2. Geological setting

The Malpica–Tui Unit is the westernmost exposure of the Basal Units in the Allochthonous Complexes of NW Iberia. It crops out as an elongated synformal structure oriented N–S, the axis of which plunges slightly to the north. It is about 150 km long and 10 km wide, stretching from Malpica in A Coruña, to Tui in Pontevedra (Fig. 1). To the east, it is bordered by a basal shear zone that overlies the Schistose Domain of the Galicia Trás-os-Montes Zone (Gil Ibarguchi and Ortega Gironés, 1985; Llana-Fúnez and Marcos, 2002). To the west, is bordered by a subvertical dextral strike–slip fault known as the Malpica-Lamego shear zone (Coke and Ribeiro, 2000; Llana-Fúnez, 2001).

The Ceán schists outcrop in the coastal strip of the Malpica–Tui Unit, in the core of the north-plunging, late Variscan Pazos synform (Alonso and González, 1982), and so occupies the highest structural level of the unit (Fig. 1). The unit is entirely composed of rocks belonging to the Ceán-Razo Series (Ortega, 1980), which consists of: (1) a sequence of massive finely foliated amphibolites with lawsonite-pseudomorphs and variable thickness that define the cartographic limit of the structure, and (2) a thicker metasedimentary sequence consisting of pelitic schists (Ceán Schists) and minor intercalations of ampelites, lydites and carbonates. The transition between the two lithologies is gradual (Arps, 1981) (Fig. 2), and locally there are horizons where both are interbedded. This volcanosedimentary sequence shows a metamorphic evolution developed almost entirely under blueschist facies conditions, whereas the rest of the Malpica–Tui Unit records the existence of metamorphism developed in eclogites facies conditions. Therefore, two lithologic assemblages with different tectonothermal evolution can be differentiated; a structurally lower assemblage consisting of metasediments and granitic to granodioritic orthogneisses with abundant mafic enclaves, and an upper assemblage composed of amphibolites with lawsonite pseudomorphs and pelitic schists (Fig. 1).

Peak conditions of metamorphism in the lower assemblage were approximately $P = 25$ kbar and $T = 610$ °C (Rodríguez Aller, 2005), whereas in the upper assemblage metamorphism is of lower grade, with an initial blueschist facies event highly overprinted by epidote-amphibolite and greenschist facies metamorphism. This gap in the *P*–*T* conditions of metamorphism, together with the telescoping of isograds, are compatible with an extensional detachment separating the two slices (López-Carmona et al., 2008).

The geochemistry of the mafic rocks is also different in the two assemblages, with continental alkali basalts in the lower slice and N-MORB basalts in the upper slice. The lithologic association and geochemistry of the lower slice is clearly of continental affinity, whereas the upper slice represents a volcanosedimentary sequence that is viewed as representing the more distal, extremely extended part of the same continental margin, transitional to an oceanic domain (Rodríguez Aller, 2005).

3. Petrography and field occurrence

The Ceán Schists have a composition of typical pelites (Fig. 8; Table 4) (e.g. Atherton and Brotherton, 1982), showing a medium-grained porphyro-lepidoblastic texture and a highly developed planar to plano-linear fabric. The deformation is generally strong and, in discrete areas, the regional foliation is transitional to mylonitic types, with the development of subgrains and quartz ribbons around the porphyroblasts, and marked undular extinction of quartz and white micas. Late C′ shear bands and kink-band structures are also common (Fig. 2).

The blueschist facies mineral assemblage is formed by Grt + Phn + Pg ± Gln + Ctd + Chl + Ep + Rt-Ilm + Qtz (mineral abbreviations are after Kretz, 1983; Holland and Powell, 1998). These minerals occur preserved as micro-inclusions in garnet and chloritoid porphyroblasts, and define an internal fabric (S_1) that frequently shows cross-cutting relationships with the external foliation (S_2) (Fig. 3). The matrix foliation (S_2) is formed by the mineral association Grt + Phn + Pg ± Win ± Bar ± Hb-Ts + Ctd + Chl + Ep + Rt-Ilm + Ap + Tur + Qtz ± Bt ± Ab (Fig. 3), which probably represents an evolution of the S_1 assemblage to slightly higher temperature and lower pressures, but still within blueschist facies. Post-S_2 deformations include the restricted development of spaced C' shear bands, tight and straight D_3 folds, and a later gentle subhorizontal crenulation. The occurrence of retrograde minerals, such as chlorite, sericite, stilpnomelane, carbonates and sulfurs and sphene, in the C′ planes indicates very low-grade greenschist facies conditions.

The presence of garnet and phengite in the absence of biotite is typical of pelites in high-*P* belts (Kurata and Banno, 1974; Råheim, 1977; Hynes and Forest, 1988; Arenas et al., 1995). In the Ceán Schists, biotite is absent in the S_1 micro-inclusions fabric, but is a common mineral in some of the samples. It tends to grow as orientated lepidoblasts in the matrix foliation, and as a late S_2 mineral, essentially replacing garnet and white mica. Petrographic observation suggests that biotite grew partly as a stable S_2 mineral in favorable compositional types (Fig. 3). Glaucophane has not been identified in the matrix of the schists, but in some samples accessory amounts of sodic–calcic and calcic amphiboles occur, probably after glaucophane. They include bluish-green winchite and barroisite, and smaller amounts of green hornblende and tschermakite. Sodic–calcic amphiboles are typically developed during exhumation of high-*P* rocks at the expense of peak phases (e.g. Hirajima and Compagnoni, 1993).

From the bottom to the top of the sequence, the schists show a marked variation in mineralogy and texture. In the basal part, they are interbedded with the lawsonite–pseudomorph amphibolites (samples 336, 338, 339, 340, 289, 292, 301, 712, 714, and 715), and the most complete and best preserved blueschist facies parageneses are found here (referred to hereafter as the "lower schists"). Locally, a pervasive growth of late albite porphyroblasts occurs, either defining a parallel banding (sample F-03) or without orientation (and F-04), and with a random distribution that can be related to compositional differences in the sedimentary protolith (Alonso and González, 1982; Gil Ibarguchi and Ortega Gironés, 1985). Upwards in the sequence the content of mica decreases, garnet disappears, and a gradual increase of opaque phases and quartzite beds occur (samples F-07 and F-08). The paragenesis becomes restricted to fine-grained white mica + Chl + Qtz, giving this rock a slaty texture in the upper part of the sequence (referred to hereafter as the "upper schists") and suggesting that the metamorphic gradient decreases rapidly upwards (Fig. 2). The transition occurs at approximately 500 m from the base of the sequence, indicating important telescoping of metamorphic isograds compatible with extensional detachment faulting (López-Carmona et al., 2008).

The most abundant porphyroblasts are garnets. According to their textural and chemical characteristics, these can be divided into two different types: texturally zoned garnets with inclusion-rich cores and

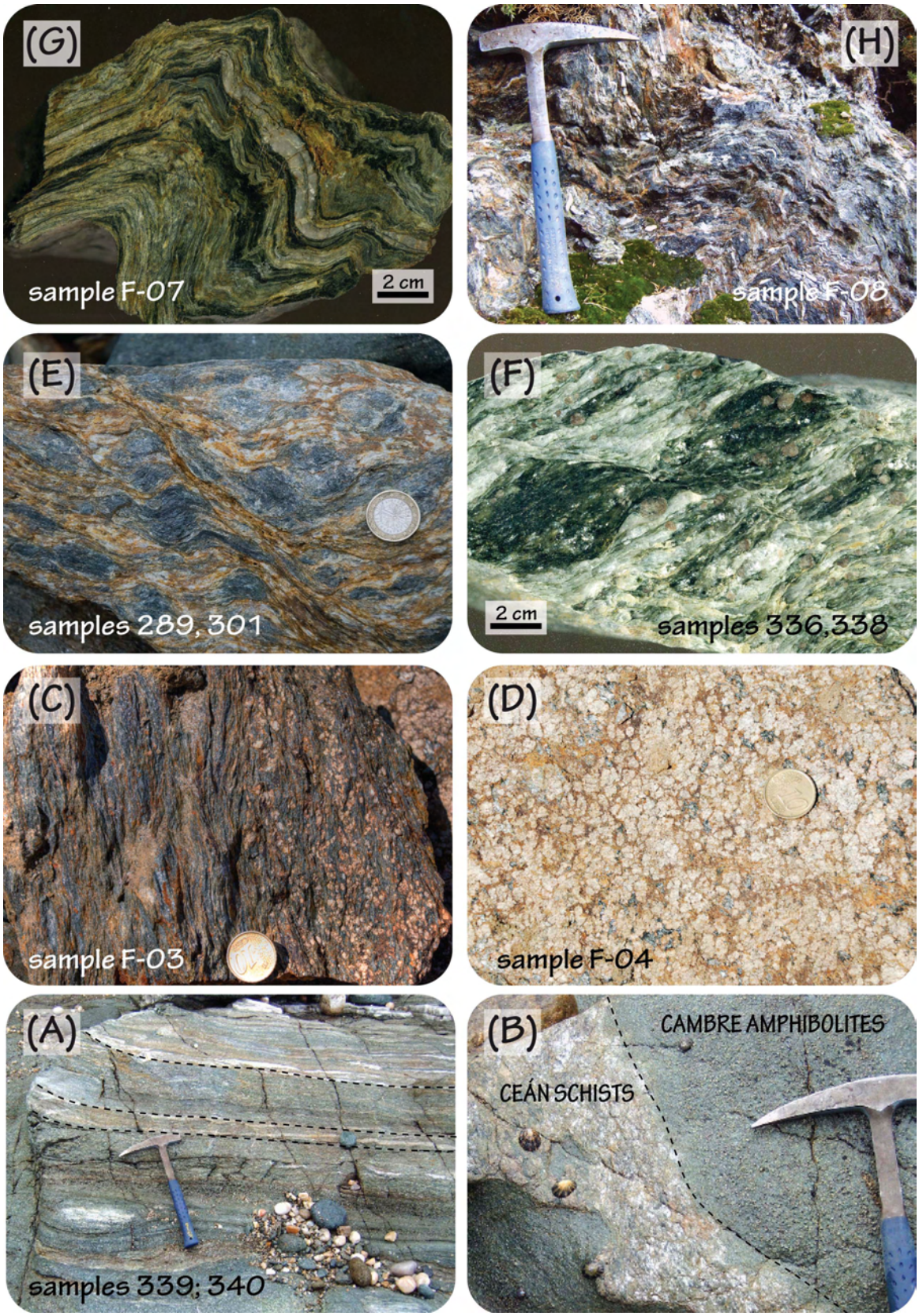

Fig. 2. Photographs showing field aspects of the Ceán Schists. (A–B) Ceán Schists interbedded with amphibolites with lawsonite pseudomorphs (Cambre amphibolites) at the base of the sequence; (C–D) schists with albite porphyroblasts defining a parallel banding (sample F-03) or without orientation (and F-04); (E–F) chloritoid–glaucophane bearing schists of the lower structural levels of the series showing the typical bluish grey color and late C′ shear bands; and (G–H) schists without garnet at the higher structural levels of the series showing the gradual increase of opaque phases and quartzite beds.

rims of variable thickness with fewer inclusions (type I garnets), and smaller, homogeneous garnets scattered in the matrix and commonly included in albite porphyroblasts (type II garnets). Both types of garnet can occur in the same rock. The type I garnets are coarse grained (4–7 mm) and sub- to idiomorphic. Their central areas are also idiomorphic and the identified micro-inclusions are of Gln, Ctd, Chl, Phn-Pg, Rt-Ilm and Qtz. The core-rim texture suggests two stages of growth. The external zone is synkinematic with respect to the S_2 fabric. In detail, some differences in the chemical composition of type I garnet can be observed depending on the structural position of the samples. In the lower structural levels of the series, type I garnets appear as inclusions in chloritoid porphyroblasts, reaching a maximum size of 0.10–0.20 mm. Type II garnets are generally smaller (1–4 mm in diameter) and idiomorphic. They show simple textures containing only a few inclusions that tend to concentrate in the cores. They usually form bands parallel to S_2, scattered in the white mica-rich levels, or as inclusions in albite porphyroblasts no larger than 0.20–0.30 mm (Fig. 3). If inclusions are present, they consist of fine rutile needles (frequently partially replaced by ilmenite), acicular chlorite aggregates, small prismatic epidote crystals, polycrystalline quartz aggregates and rare apatite. Samples containing type I garnets with glaucophane inclusions crop out in the lower structural levels of the sequence, interbedded with the lawsonite-pseudomorph amphibolites. Hence, their mineral chemical composition reflects the maximum burial conditions.

As with the garnets, white mica, chloritoid, chlorite and epidote each occur in two textural types. Type I white micas are fine crystals with grain sizes ranging from 0.25 to 0.75 mm and define S_1 as inclusions in garnet and chloritoid porphyroblasts. Type II white micas are present as micro-inclusions in the late albite porphiroblasts and as S_2 lepidoblasts in the matrix. Chloritoid appears as micro-inclusions in garnets (type I chloritoid) as an S_1 mineral, and as coarse prisms with no core-rim zonation that reach more than 9 mm in length in the S_2 matrix foliation (type II chloritoids). It is not possible to determine whether the latter chloritoid is in equilibrium with the rest of the M_2 phases or is a relict phase from the M_1 stage. However, the petrographic features suggest that type II chloritoids were stable at least until the early M_2 stage. Type I chlorites grains occur as micro-inclusions in garnet and albite porphyroblasts, whereas type II chlorites occur in the quartz-mica matrix domains, and in the pressure shadows of other porphyroblasts. Type I epidotes are acicular or prismatic crystals (<0.4 mm long) forming micro-inclusions in type II garnets, whereas type II epidotes are larger prismatic crystals (>2 mm) in the matrix. Apatite occurs as idiomorphic prisms of variable length up to 2 mm, and rarely as small (0.5–1 mm long) prisms included in type II garnets. In some cases apatite contains rutile inclusions that define a straight schistosity, suggesting a metamorphic origin.

A summary of the petrographic data is shown in Fig. 4, in which the observed mineral associations have been grouped according to their relationship to the two metamorphic events, M_1 and M_2.

4. Mineral chemistry

Six representative samples of the Ceán Schists were analysed with a JEOL-Superprobe JXA-8900 M microprobe equipped with five spectrometers at the Luis Bru Electronic Microscopy Centre (Universidad Complutense de Madrid). The operating parameters were: 15 kV accelerating voltage, 20 nA beam current, between 1 and 5 μm of beam diameter and 10 s counting time. The selected samples were the least retrograded with the best preserved parageneses. A selection of analyses is shown in Tables 1 and 2.

4.1. Garnet

Both type I and type II garnets are almandine (Table 3). Type I garnet profiles (Fig. 5) show, from core to rim: (1) a slight increase in pyrope and a more pronounced increase of almandine, (2) a compensating decrease in grossular and spessartine, and (3) a relatively constant Fe/(Fe + Mg) ratio. The central plateau with maximum X_{Ca} and X_{Mn} matches the idiomorphic core and represents a first stage of growth, in which grossular and spessartine reach a maximum, almandine shows the opposite trend, and pyrope remains almost constant.

As mentioned previously, some differences in type I garnet chemical composition occur with structural position. Type I garnets from the lower part are richer in X_{Ca} and poorer in X_{Fe}, X_{Mg} and X_{Mn} with respect to those in the upper part of the series. The most marked difference is in the grossular content, which varies from ~0.30 to ~0.15 between the lower and upper part, suggesting significantly lower pressure at the upper levels, assuming a higher grossular content implies higher pressures (see Hollister, 1966; Atherton, 1968; Thompson et al., 1982; Chakraborty and Ganguly, 1991; Spear, 1995; Holdaway, 2001; Zuluaga et al., 2005).

Type II garnet chemical profiles (Fig. 5) show, from core to rim, a slightly increase in pyrope and almandine. Grossular and spesartine contents decrease significantly and the ratio Fe/(Fe + Mg) remains almost constant, decreasing slightly towards the rims. At the same structural level, type I garnets rims and type II garnets cores have similar compositions, suggesting that they grew at the same time.

4.2. Amphibole

Three types of amphiboles can be distinguished. The blue amphibole that appears as micro-inclusions (0.25–0.5 mm) in type I garnets is a sodic amphibole with an Si content above 7.8 and a Na/(Na + Ca) ratio above 0.97, which corresponds to glaucophane with a mean X_{Fe} of 0.05 [$X_{Fe} = Fe^{3+}/(Fe^{3+} + Al)$]. The matrix green-blue amphiboles belong to the sodic–calcic group, and comprise winchite and barroisite with $X_{Mg} \approx 0.48–0.63$ [$X_{Mg} = Mg/(Mg + Fe)$] and $X_{Fe} \approx 0.29$. Finally, the green amphiboles found in the matrix of the schists range in composition from Mg-hornblende to Fe-hornblende and tschermakite, with $X_{Mg} \approx 0.49–0.62$ and $X_{Fe} \approx 0.07–0.22$.Their Al_2O_3 and Na_2O contents are relatively high (Table 2), which is consistent with their coexistence at relatively high pressures with glaucophane (Reynard and Ballèvre, 1988; Smelik and Veblen, 1992).

4.3. White Mica

The composition of both types of micas (type I and type II) corresponds to either phengite or paragonite. The Si content of type I phengites lies in the range of 3.4–3.5 cations p.f.u. (on a basis of 11 oxygen), and the range of 3.3–3.4 cations p.f.u. for type II phengites (Tables 1 and 2). X_{Fe} increases from 0.46 in type I to 0.48 in type II. The composition of type I and II paragonites, on the other hand, is relatively constant, with very low variation in X_{Fe} and a high Na/(Na + K) ratio (0.97 and 0.80 for type I and type II, respectively). In the diagram FeO_T–Al_2O_3 (Fig. 6), the majority of the white micas are classified as metamorphic micas from glaucophane schists (Miyashiro, 1973). Some of the analyses corresponding to type II white micas plot in the chlorite–biotite–almandine zone, suggesting that they grew under slightly different *P*–*T* conditions (lower pressure and higher temperature). The six analyses that plot at the limit or within this field correspond to the biotite-bearing schists. Comparison of the phengite chemistry with other high-*P* pelites of the Basal Units shows a marked similarity between the type II phengites from the Ceán Schists and the type I phengites from the Santiago Schists (Fig. 6), outcropping to the east in the Ordenes Complex. The phengites of the Santiago Schists are part of a high-pressure foliation preserved as inclusions in albite porphyroblasts, whereas the regional foliation is developed at medium pressure (Arenas et al., 1995). However, the high silica

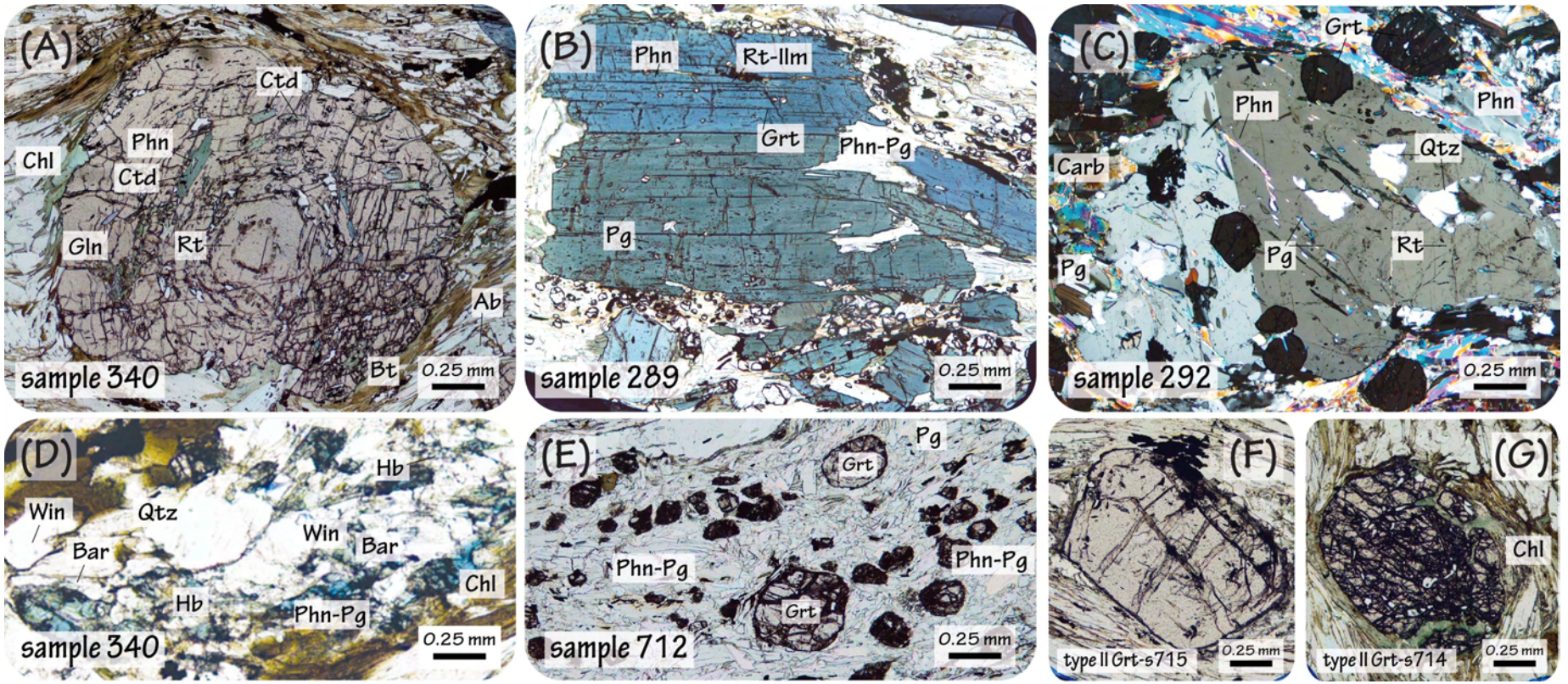

Fig. 3. Thin section images showing the textural relationships in the Ceán Schists. (A) Type I garnet porphyroblast corresponding to profile A in Fig. 5, showing complex textural zoning and a high-pressure internal foliation (S_1) formed by gln, ctd, phn, rt, ilm and qtz; (B) Albite porphyroblast containing an internal foliation developed under high-pressure conditions that is discordant to the external foliation. The internal foliation is formed by type II grt, type II phn, pg, rt and qtz; (C) Unzoned chloritoid porphyroblast showing an internal foliation still developed under high-pressure conditions formed by type II grt, rt ilm, type II phn, pg and qtz. (D) Matrix foliation of the lower schists showing the three amphibole types in samples with glaucophane. The foliation is formed by Ca-amph, Na/Ca-amph, type II grt, type II phn, pg, chl, bt and qtz; (E) Porphyro-lepidoblastic texture in the matrix of the upper schists. The foliation is formed by type II grt, type II phn, pg, chl, bt, tur and qtz; and (F–G) Different aspects of type II garnets. Gln: glaucophane; win: winchite; bar: barroisite; hb: hornblende; ctd: chloritoid; phn: phengite; rt: rutile; ilm: ilmenite; qtz: cuartz; grt: garnet; bt: bitite; ab: albite; tur: tourmaline.

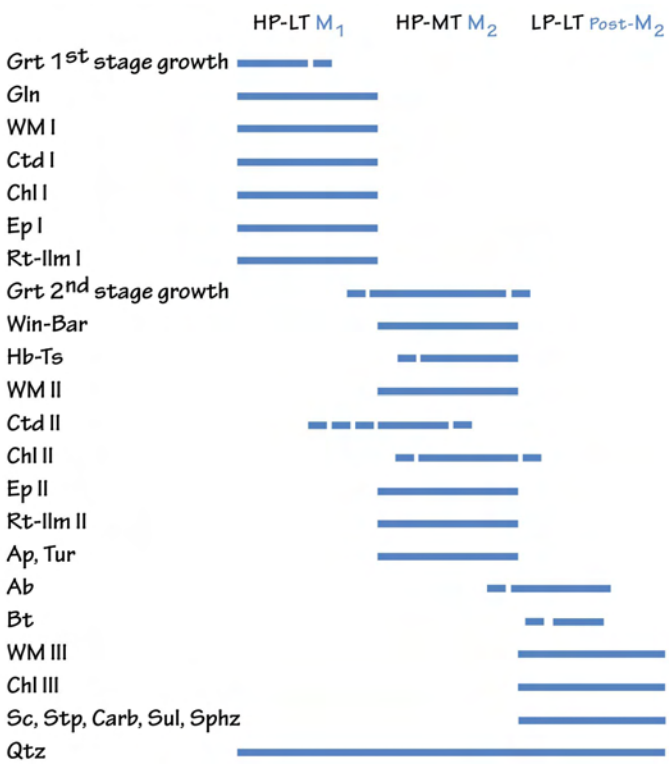

Fig. 4. Mineral crystallization diagram for the Ceán Schists.

content in the type I phengites of the Cean Schists is not found in the Santiago Schists, suggesting that the pressure peak was higher in the Ceán Schists.

Table 1
Representative microprobe analysis of coexisting M_1 minerals.

Sample	340	340	339	340	340	340	340
Mineral	Grt Core	Phn	Pg	Gln	Ctd	Chl	Ep
Analysis	146	4	3	2	3	43	9
SiO_2	37.96	50.92	45.75	56.79	23.81	25.93	38.13
TiO_2	0.25	0.19	0.05	0.03	0.02	0.07	0.04
Al_2O_3	22.77	27.44	38.97	11.78	39.06	21.23	26.26
Cr_2O_3	0.07	0.05	0.06	0.01	0.05	0.04	0.11
Fe_2O_3	0.00	0.00	0.00	0.98	1.97	0.00	11.07
FeO	24.22	3.51	1.07	11.86	22.27	21.82	0.10
MnO	3.87	0.03	0.00	0.04	0.36	0.15	0.19
MgO	0.60	2.35	0.22	10.04	3.20	16.44	0.00
CaO	9.95	0.00	0.05	0.41	0.01	0.04	22.21
Na_2O	0.05	0.28	7.61	6.43	0.03	0.03	0.00
K_2O	0.02	10.20	0.41	0.02	0.00	0.02	0.00
Total	99.76	94.97	94.19	98.39	90.78	85.77	98.11
Data calculated with AX software (Holland and Powell, 1998)							
Si	3.00	3.42	2.97	7.81	1.00	2.74	2.99
Ti	0.01	0.01	0.00	0.00	0.00	0.01	0.00
Al	2.12	2.17	2.98	1.91	1.94	2.64	2.43
Cr	0.00	0.00	0.00	0.00	0.00	0.00	0.01
Fe^{3+}	0.00	0.00	0.00	0.10	0.06	0.00	0.65
Fe^{2+}	1.60	0.19	0.06	1.37	0.78	1.93	0.01
Mn	0.26	0.00	0.00	0.01	0.01	0.01	0.01
Mg	0.07	0.23	0.02	2.06	0.20	2.59	0.00
Ca	0.84	0.00	0.00	0.06	0.00	0.01	1.87
Na	0.01	0.04	0.96	1.72	0.00	0.01	0.00
K	0.00	0.87	0.03	0.00	0.00	0.00	0.00
X_{Mg}	0.02	0.54	0.26	0.60	0.20	0.57	
X_{Na}		0.04	0.97	0.97			
X_{Fe}		0.46	0.73	0.05	0.79	0.43	0.21

$X_{Mg} = Mg/(Mg + Fe)$ (Phn, Pg, Gln, Ctd, Chl); $X_{Mg} = Mg/(Fe + Mn + Mg + Ca)$ (Grt); $X_{Fe} = Fe^{3+}/(Fe^{3+} + Al)$ (Gln, Ep); $X_{Na} = Na/(Na + K)$ (Phn, Pg); $X_{Na} = Na/(Na + Ca)$ (Gln).

4.4. Biotite

Biotites appear as small bundles, 3–4 mm in length, with compositions intermediate between annite and phlogopite (calculated using the method of Holdaway et al., 1988) and low TiO_2 contents (<2 w%). The wide range in X_{Fe} and TiO_2 values suggests a relatively wide margin for their crystallization.

4.5. Chlorite

Type I chlorites are notably more magnesian ($X_{Mg} \approx 0.57$) than type II chlorites ($X_{Mg} \approx 0.40$).

4.6. Chloritoid

Both chloritoid types are moderately rich in FeO, with X_{Fe} ranging from 0.80 to 0.84 in type I and type II respectively, and no core-rim zonation. Their compositions are characteristic of medium pressure chloritoids in paragenesis with garnet, staurolite and/or kyanite (Deer et al., 1992). The observed decrease in X_{Mg} between type I chloritoid inclusions ($X_{Mg} \approx 0.20$) and type II chloritoid porphyroblasts ($X_{Mg} \approx 0.16$) suggest a slight increase in temperature from M_1 to M_2.

4.7. Epidote

Epidote shows a restricted range of composition and no core-rim zonation with $X_{Fe} \approx 0.20$ for both type I and type II.

4.8. Plagioclase

Plagioclase is nearly pure albite with maximum anorthite and orthose contents of 0.28 and 0.16 wt.%, respectively, in samples without glaucophane, and 3.84 and 0.42 wt.% in samples with glaucophane.

4.9. Sphene and Fe-Ti oxides

Sphene is not chemically zoned and shows low Al_2O_3 contents that reach a maximum (2.04 wt.%) in the samples without glaucophane. Rutile is nearly pure and ilmenite shows a wide range of chemical variation.

5. Phase equilibria and *P–T* evolution

Three metamorphic episodes corresponding to the paragenetic events M_1, M_2 and post-M_2 have been established from the petrography of the Ceán Schists. Only the first two can be quantified provided since the mineralogy corresponding to the third episode is insufficient for evaluating the *P–T* conditions.

M_1 is recorded in the oldest paragenesis observed in the schists, represented by a relict schistosity preserved as micro-inclusions in garnet, albite and chloritoid porphyroblasts, and defined by a mineral assemblage Grt + Phn + Pg + Gln + Ctd + Chl + Ep + Rt-Ilm + Qtz. This assemblage defines a fine-grained foliation (S_1) developed under high-*P* and low-T conditions. M_2 correspond to the main foliation (S_2) and represents an evolution of S_1 to slightly higher temperatures and lower pressures, as indicated by the mineral paragenesis Grt + Phn + Pg + Win + Bar + Hb-Ts + Ctd + Chl + Ep/Czo + Rt-Ilm + Ap + Tur + Qtz ± Ab.

Different methods were applied to the quantification of the M_1 and M_2 metamorphic events in the chloritoid–glaucophane Ceán pelitic schists, including conventional thermobarometric techniques, average *P–T* multiequilibrium thermobarometry, and thermodynamic modelling in appropriate chemical systems. A data summary showing the techniques applied and the results obtained is listed in Table 4.

Table 2
Representative microprobe analysis of coexisting M_2 minerals.

Samples	340	336	336	340	340	340	340	340	289	340	340	340	340
Mineral	Grt Rim	Phn	Pg	Fe-Hb	Mg-Hb	Ts	Win	Bar	Ctd	Chl	Bt	Ep	Ab
Analysis	207	215	59	16	17	24	11	26	134	67	13	18	85
SiO_2	37.95	49.04	46.7	44.54	44.94	47.23	53.96	46.75	24.28	24.61	36.54	38.04	67.25
TiO_2	0.06	0.28	0.07	0.27	0.26	0.23	0.14	0.10	0.06	0.06	1.55	0.15	0.00
Al_2O_3	21.78	28.25	39.38	12.48	12.74	10.40	13.28	9.43	41.69	23.15	16.71	26.68	19.87
Cr_2O_3	0.00	0.00	0.00	0.08	0.04	0.12	0.04	0.00	0.05	0.00	0.10	0.09	0.00
Fe_2O_3	0.00	0.00	0.08	1.56	5.61	4.51	0.00	6.05	0.00	0.00	0.00	9.75	0.03
FeO	32.71	3.68	1.09	15.13	11.63	11.93	14.01	11.99	22.18	29.14	18.36	0.09	0.00
MnO	0.46	0.00	0.01	0.44	0.45	0.51	0.47	0.42	0.15	0.41	0.18	0.08	0.03
MgO	1.55	2.26	0.25	8.28	10.74	11.20	7.32	11.29	2.30	10.84	11.57	0.04	0.00
CaO	6.58	0.02	0.08	9.68	10.19	9.80	6.14	8.88	0.00	0.00	0.00	23.20	0.06
Na_2O	0.01	0.36	6.02	1.06	1.59	1.77	1.63	2.40	0.01	0.01	0.02	0.02	10.92
K_2O	0.00	10.29	2.23	0.39	0.37	0.30	0.62	0.25	0.03	0.01	9.79	0.02	0.03
Total	101.1	94.18	95.91	93.92	98.55	98.01	97.61	97.57	90.75	88.23	94.82	98.16	98.19
Data calculated with AX software (Holland and Powell, 1998)													
Si	3.00	3.33	2.99	6.81	6.54	6.88	7.60	6.88	1.01	2.63	2.79	2.98	2.98
Ti	0.00	0.01	0.00	0.03	0.03	0.03	0.01	0.01	0.00	0.00	0.09	0.01	0.00
Al	2.03	2.26	2.97	2.25	2.19	1.79	2.21	1.64	2.04	2.91	1.50	2.46	1.04
Cr	0.00	0.00	0.00	0.01	0.00	0.01	0.01	0.00	0.00	0.00	0.00	0.00	0.00
Fe^{3+}	0.00	0.00	0.00	0.18	0.61	0.49	0.00	0.67	0.00	0.00	0.00	0.57	0.00
Fe^{2+}	2.16	0.21	0.06	1.94	1.42	1.45	1.65	1.48	0.77	2.60	1.17	0.01	0.00
Mn	0.03	0.00	0.00	0.06	0.06	0.06	0.06	0.05	0.00	0.04	0.01	0.01	0.00
Mg	0.18	0.23	0.02	1.89	2.33	2.43	1.54	2.48	0.14	1.72	1.32	0.00	0.00
Ca	0.56	0.00	0.00	1.56	1.59	1.52	0.93	1.40	0.00	0.00	0.00	1.95	0.00
Na	0.00	0.05	0.75	0.32	0.45	0.50	0.45	0.69	0.00	0.00	0.00	0.00	0.94
K	0.00	0.89	0.18	0.08	0.07	0.06	0.11	0.05	0.00	0.00	0.95	0.00	0.00
X_{Mg}	0.06	0.52	0.29	0.49	0.62	0.63	0.48	0.63	0.16	0.39	0.53		
X_{Na}		0.05	0.80	0.17	0.22	0.25	0.33	0.33					
X_{Fe}		0.48	0.71	0.07	0.22	0.21	0.00	0.29	0.84	0.60	0.47	0.19	
An													0.28
Ab													99.57
Or													0.16

$X_{Mg} = Mg/(Mg + Fe)$ (Phn, Pg, Amph, Ctd, Chl, Bt); $X_{Mg} = Mg/(Fe + Mn + Mg + Ca)$ (Grt); $X_{Fe} = Fe^{3+}/(Fe^{3+} + Al)$ (Amph, Ep); $X_{Na} = Na/(Na + K)$ (Phn, Pg); $X_{Na} = Na/(Na + Ca)$ (Amph); $An = [Ca/(Ca + Na + K)]100$, $Ab = [Na/(Ca + Na + K)]100$, $Or = [K/(Ca + Na + K)]100$.

Garnet-Phengite thermometry (Hynes and Forest, 1988), and GRIPS (Bohlen and Liotta, 1986) and GASP (Koziol, 1989; Holdaway, 2001) barometry calculations using micro-inclusion compositions, indicate peak conditions around $P = 19$–22 kbar and $T = 420$–500 °C. The same calculations using the S_2 fabric minerals yield approximate values of $P = 16$-20 kbar and $T = 440$–515 °C (Fig. 7).

The average *P–T* multiequilibrium thermobarometry using THERMOCALC 3.26 (Powell and Holland, 1988) with the internally consistent thermodynamic dataset of Holland and Powell (1998; updated 22 Nov. 2003), provides more consistent *P–T* values. These are essentially in agreement with the conventional thermobarometry results, but show significantly lower pressures for the M_2 stage. Average *P–T* calculations using micro-inclusion compositions indicate peak conditions between $P = 19$–20 kbar and $T = 425$–430 °C. The values obtained using the matrix mineral compositions are $P = 13$–14 kbar and $T = 495$–500 °C (Fig. 7.). In general, we consider the estimates obtained using the average *P–T* calculations to be more reliable because the same thermodynamic data and activity-composition models are used for all the calculations (Powell and Holland, 2008). However, the results of conventional thermobarometry show a similar range of *P–T* values, suggesting that this technique is not without merit.

Thermodynamic modeling of rocks or compositional volumes in rocks (effective bulk composition or equilibration volume) has been shown to be one of the most powerful methods for obtaining information about the metamorphic evolution of terranes. *P–T* pseudosections, in particular, allow a system to be modeled for the composition of interest and the parageneses observed in the rock to be compared with the ones predicted by the phase diagram. Pseudosections also let the observed parageneses in a particular

Table 3
Stages of garnet growth according to the structural position of the samples in which they occur.

Samples	1st stage		2nd stage	
Lower structural levels	Grt IC		Grt IR Grt IIC	Grt IIR Grt IIAb
Higher structural levels		Grt ICtd		Grt IR
End-member components		Grt IC		
	$Alm_{[0.58]}Py_{[0.03]}Grs_{[0.38]}Sps_{[0.09]}$		$Alm_{[0.68]}Py_{[0.04]}Grs_{[0.25]}Sps_{[0.03]}$ $Alm_{[0.67]}Py_{[0.04]}Grs_{[0.24]}Sps_{[0.05]}$	$Alm_{[0.73]}Py_{[0.06]}Grs_{[0.15]}Sps_{[0.06]}$ $Alm_{[0.73]}Py_{[0.07]}Grs_{[0.14]}Sps_{[0.07]}$
		$Alm_{[0.61]}Py_{[0.05]}Grs_{[0.18]}Sps_{[0.16]}$ $Alm_{[0.57]}Py_{[0.04]}Grs_{[0.15]}Sps_{[0.23]}$		$Alm_{[0.70]}Py_{[0.07]}Grs_{[0.15]}Sps_{[0.08]}$

Grt I C; garnets type I cores. Grt I R; garnets type I rims. Grt II C: garnets type II cores. Grt II R: garnets type II rims. Grt II_{Ab}: garnets type II cores-rims included as micro-inclusions in albite porphyroblasts. Grt I_{Ctd}: garnets type I cores-rims included as micro-inclusions in chloritoid porphyroblasts. End-members average compositions: $X_{Alm} = Fe/(Fe + Mg + Mn + Ca)$; $X_{Py} = Mg/(Fe + Mg + Mn + Ca)$; $XGrs = Ca/(Fe + Mg + Mn + Ca)$; $XSps = Mn/(Fe + Mg + Mn + Ca)$.

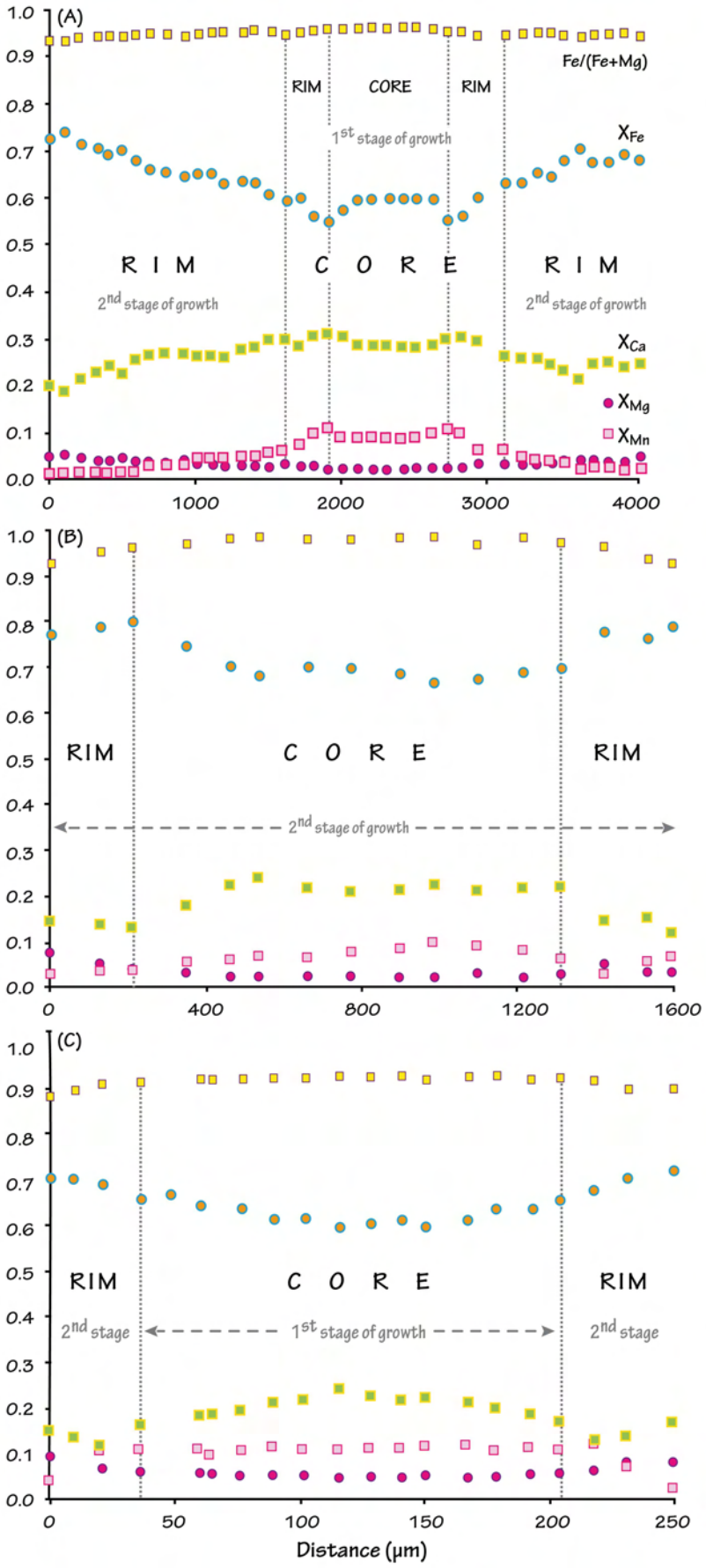

Fig. 5. Garnet profiles. (A) Type I garnet in samples from the lower structural levels; (B) Type II garnet in samples from the lower structural levels; and (C) Type I garnet in samples from the upper structural levels.

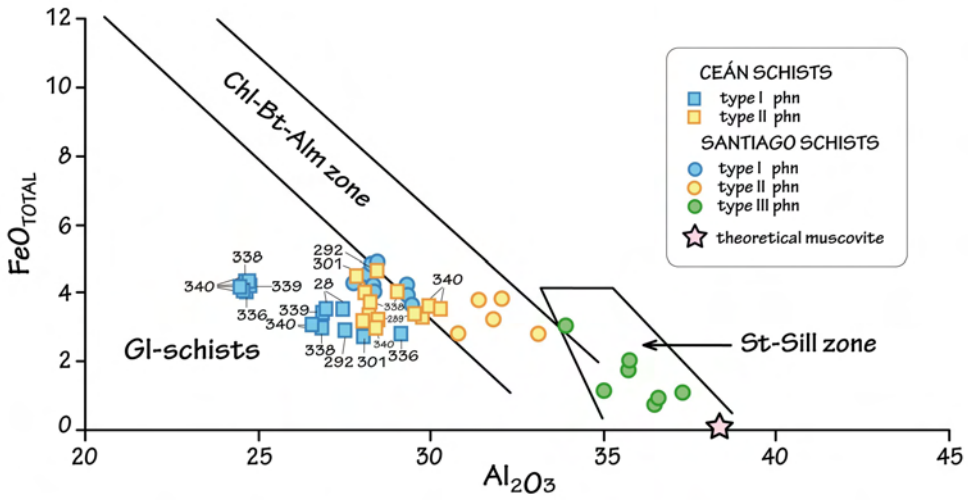

Fig. 6. White mica classification diagram based on metamorphic origin (Miyashiro, 1973).

Table 4
Summary of the thermobarometric techniques.

	M_1	P_1(kbar);T_1(°C)	M_2	P_2(kbar);T_2(°C)	Chemical composition	
Conventional thermobarometry	Peak paragenesis (S_1)	19–22;420–500	Matrix paragenesis (S_2)	16–20;440–515	M_1 S_1 minerals Table 1	M_2 S_2 minerals Table 2
Average *P–T* calculations	Peak paragenesis (S_1)	19.3; 454 ($\sigma=1.5$)	Matrix paragenesis (S_2)	13.7; 493 ($\sigma=1.5$)	M_1 S_1 minerals Table 1	M_2 S_2 minerals Table 2

n-variant fields			Bulk composition
Theoretic major elements pelites composition (Atherton and Brotherton, 1982)		KFMASH	[SiO_2:72.91; Al_2O_3:13.74; MgO:4.25; FeO:6.38; K_2O:2.72]
		MnNCKFMASH	[SiO_2:70.14; Al_2O_3:13.22; CaO:1.29; MgO:4.08; FeO:6.14; K_2O:2.62; Na_2O:2.38; MnO:0.12]
KFMASH pseudosection	Cr Chl Ctd	Chl Grt	[SiO_2:71.42; Al_2O_3:13.42; MgO:4.78; FeO:7.04; K_2O:3.34]
MnNCKFMASH pseudosection	Gl Chl Ctd Grt Lw	Gl Chl Grt Pa	[SiO_2:68.73; Al_2O3:13.78; CaO:1.46; MgO:4.49; FeO:6.55; K_2O:3.37; Na_2O:1.39; MnO:0.23]

rock be placed in the context of alternative mineral assemblages, such as when phases are no longer stable, or when additional minerals join the parageneses. In addition, pseudosections are not dependent on establishing original mineral compositions, which is an important advantage, especially in texturally complex rocks (Powell and Holland, 2008) like those considered here.

We computed two pseudosections using the average bulk rock composition of the Ceán Schists (samples EC-G3 and EC-G4) obtained by whole-rock analysis as the equilibration volume (Fig. 8; Table 4) since, in fluid-saturated rocks, this is generally a good approximation of the effective bulk composition (Tajčmanová et al., 2007). Fig. 8 is an ACF ternary diagram that shows the protolith composition. Samples EC-G3 and EC-G4 are classified as pelites (Turner, 1981; Vernon and Clarke, 2008). The first pseudosection was computed in the KFMASH system, widely used for pelitic rocks. However, while this proved useful as a first approximation, the importance of Na-bearing minerals in these rocks made it necessary the widening the system to one involving at least Na. For this reason we computed a second pseudosection in the MnNCKFMASH system.

The KFMASH pseudosection was calculated using Thermocalc 3.26 (Powell and Holland, 1988) and the internally consistent thermodynamic dataset (Holland and Powell, 1998; updated Nov. 2003). It is based on the petrogenetic grid proposed by Wei and Powell (2003) for a synopsis of high-*P* metapelites with similar bulk rock compositions to those of the Ceán Schists. The most obvious limitations of the pseudosection obtained, which are primarily due to the absence of Mn, Na and Ca components, and: (1) the limited mineral associations that can be computed, and (2) the unrealistic stability field predicted for garnet, which appears only above 550 °C. This makes the comparison of the mineral assemblages present in the schists with the predicted associations in the *P–T* diagram almost useless, as some of the key minerals relevant to these rocks, such as amphiboles, paragonite and albite, are not represented (Fig. 9).

However, the comparison between both phase diagrams is useful for visualizing the influence of Ca and Mn, small amounts of which can strongly influence garnet stability (Spear and Cheney, 1989; Symmes and Ferry, 1992; Mahar et al., 1997). The effect of adding these components generally results in a dramatic widening of the garnet stability field (see e.g. Tinkham et al., 2003; Proyer, 2003; Boger and Hansen, 2004; Zuluaga et al., 2005). The most useful aspect of this pseudosection is in the ability to plot isopleths for silica content in phengite in the different stability fields (dashed lines in Fig. 9), which provides an accurate barometer (e.g. Massone and Schreyer, 1987) that is essentially in agreement with the pressure values obtained from average *P–T* calculations at the same temperatures.

The *P–T* pseudosection in the model MnNCKFMASH system has been calculated with Perplex vs. 07 (Connolly, 2005; http://www.perplex.ethz.ch/) using the internally consistent thermodynamic dataset (Holland and Powell. 1998; updated Nov. 2003) for the same bulk rock composition (Table 4). The solution models used (see details and references in the file solut08.dat; PERPLEX 07; database hp02ver.dat) are Gt(HP), Mica(CH2), Bio(HP), Chl(HP), Ctd(HP), Pl (h), Gl, and Carp. The *P–T* pseudosection obtained shows several low-sloped limits between key mineral associations, which can be used as sensitive pressure indicators. The low-*P* limit of the paragenesis

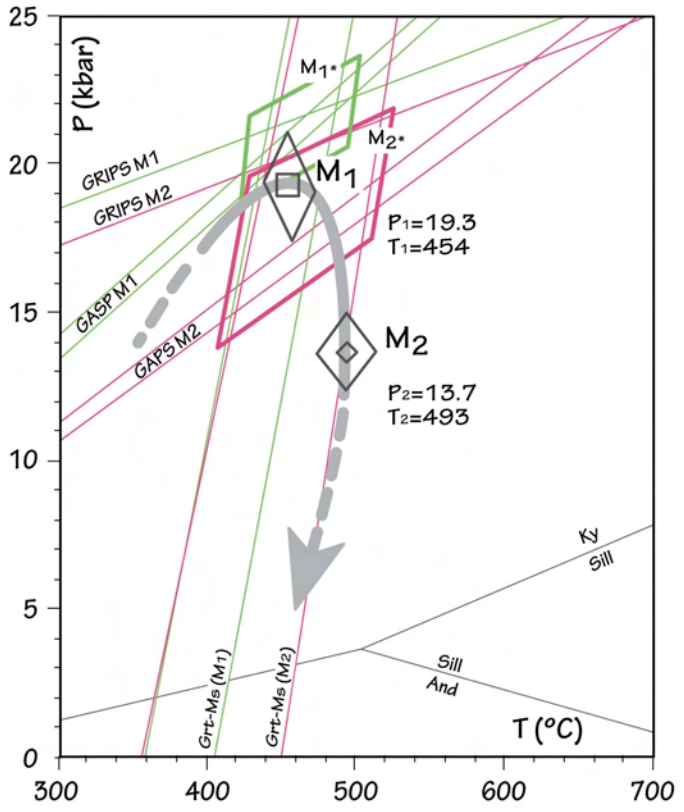

Fig. 7. Conventional thermobarometry results and Average *P–T* calculation. For Thermocalc, the 1.5σ errors are automatically calculated. For the conventional thermobarometers, errors were estimated on the basis of their upper and lower limits based on compositional variations.

chloritoid + glaucophane at ≈17 kbar (Fig. 10) constrains the conditions for the M_1 event and confirms the high-*P* character of this association. The stable phases accompanying chloritoid and glaucophane are garnet, lawsonite and chlorite, whereas paragonite appears at these pressures only above 500 °C. Lawsonite is the only high-*P* phase predicted that has not been observed either as inclusions in garnet or in the matrix. However, pseudomorphs of this mineral are not uncommon in the interbedded mafic rocks, and some of the abundant crystals of zoisite/clinozoisite found in the matrix of the schists are likely to have formed at the expense of lawsonite. The limit of the stability field of plagioclase is another useful indicator. The growth of late albite porphyroblasts in some levels indicates a dramatic decompression from the fields with chloritoid + glaucophane to the fields with stable albite. We can place further constrains from the fact that part of the samples contain biotite in S_2, indicating that the *P–T* path should first go through fields with biotite and then through those with albite. The path that best fits the petrographic data starts in the field Chl, Ctd, Gl, Law (Fig. 10) and evolves through Chl, Ctd, Gl, Gt, Law, Pa and Chl, Gl, Gt, Pa (with the formation of new paragonite and the disappearance of lawsonite), to enters the field Bt, Chl, Gt, Zo, Pa to form biotite (Fig. 10) and, finally, to Chl, Gt, Zo, Pa, Ab (pervasive albite porphyroblast growth). This *P–T* path suggests strong decompression, from more than 17 to 7 kbar, with moderate heating to a peak around 500–525 °C. The isopleths of silica content in phengite are also valuable pressure indicators (Fig. 10-B). The mean content in the S_1 phengites is close to 3.4 cations p.f.u., whereas it is slightly lower (3.3 cations p.f.u.) in the S_2 phengites. This indicates pressures above 17–18 kbar for M_1 and around 12–13 kbar for M_2, assuming the temperature ranges indicated by the stability field of the parageneses and the average *P–T* Thermocalc multiequilibrium thermobarometry.

	Al-SDP	Average
SiO_2	61.87	61.32
TiO_2	1.06	1.01
Al_2O_3	19.79	19.54
FeO_T	7.89	8.04
MnO	0.12	0.26
MgO	2.42	2.75
CaO	1.06	1.46
Na_2O	2.17	1.11
K_2O	3.62	4.49
Total	100	100

	EC-G3	EC-G4
SiO_2	62.88	60.71
TiO_2	1.10	0.91
Al_2O_3	18.91	20.65
FeO_T	7.99	7.69
MnO	0.36	0.24
MgO	2.19	2.66
CaO	1.06	1.20
Na_2O	1.16	1.27
K_2O	4.33	4.66
Total	100	100

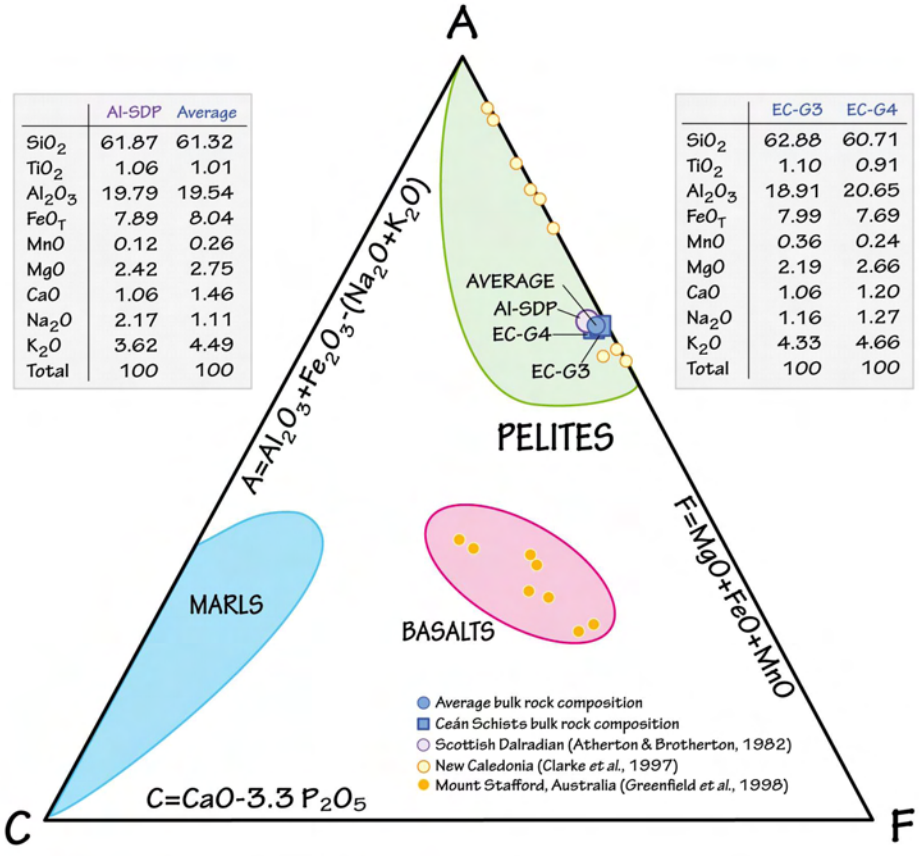

Fig. 8. ACF ternary diagram showing the protolith composition. Samples EC-G3 and EC-G4 are classified as pelites (Turner, 1981; Vernon and Clarke, 2008). EC; Ceán Schists. Al-SDP; aluminous Scottish Dalradian Pelite.

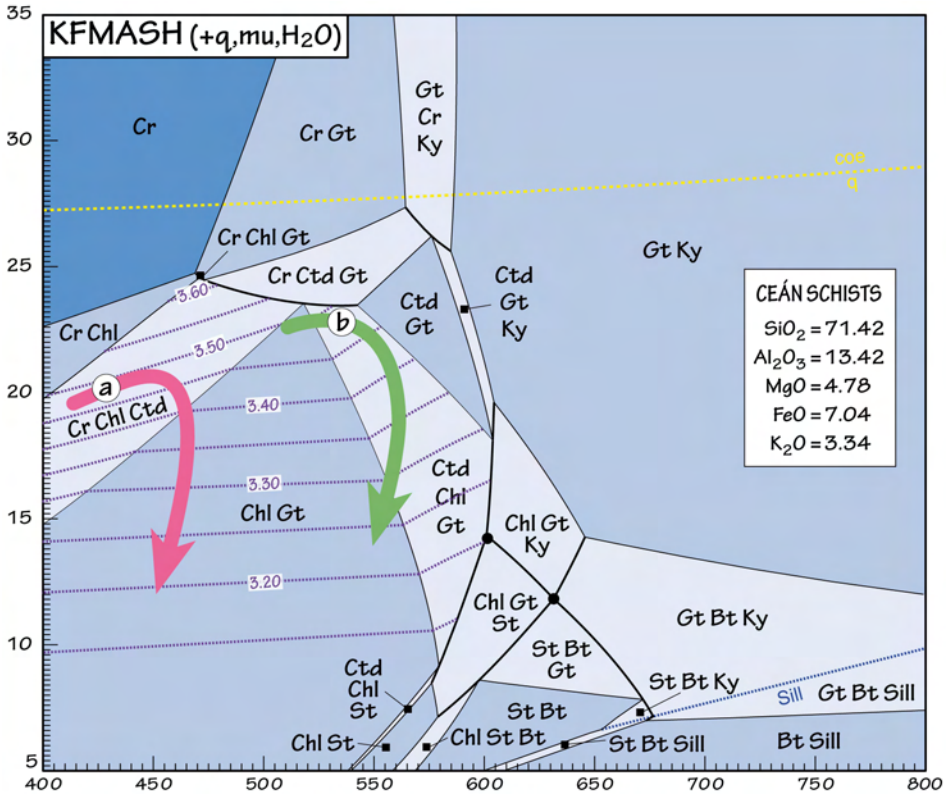

Fig. 9. KFMASH pseudosection calculated with Thermocalc program v.3.26. The dashed lines show the silica content in phengite (c.p.f.u).

6. Conclusions

The main conclusions of this study are:

1. The stability field of the M_1 paragenesis containing glaucophane + chloritoid is located, for the composition of the pelitic Ceán Schists, above 17–18 kbar. Hence, the *P–T* path deduced from all the data obtained in this study indicates an initial stage of subduction burial to a depth of 65–70 km. Maximum burial was followed by dramatic exhumation with slight heating, reaching a metamorphic peak at ~500 °C. This slight increase in temperature during decompression is supported by the presence of late biotite in chemical imbalance with the rest of the M_2 minerals, suggesting an origin related to a localized heating that could have taken place during the exhumation of the unit.
2. The secondary growth of Na–Ca amphiboles, most likely after glaucophane, indicate that, although it has not been identified in the matrix of the schists, it was a stable phase during the second high-pressure event. The sodic–calcic amphiboles and coexisting hornblende occur as intergrowths and occur only in the matrix of samples containing glaucophane as garnet inclusions. This intergrowth texture can be interpreted in two ways: as an amphibole miscibility gap and as a disequilibrium growth texture. Reynard and Ballèvre (1988) demostrated the existence of a miscibility gap between sodic and calcic amphiboles at $T = 500–550$ °C, which suggests that glaucophane and hornblende could have coexisted during M_2. However, textural observations in the Na–Ca amphiboles of the Ceán Schist show chemical zonation indicating disequilibrium growth. Therefore, these amphiboles cannot be considered as an intermediate stage between the two end-members (Reynard and Ballèvre, 1988). They are compatible with amphibole formation during retrograde fluid infiltration under high-*P* conditions, as described, for example, by Menold et al. (2001) and Shi et al. (2003).
3. A preliminary pseudosection in the basic pelitic KFMASH shows the significant influence of Mn and Ca components on the stability of garnet, leading to an overestimation of the temperature. However, the pressure calculated with silica isopleths in the same diagram corresponds well with the other barometric calculations.
4. The MnNCKFMASH system pseudosection fully describes the succession of mineral assemblages in the schists, and produces results that are consistent with the petrographic observations.
5. There are several studies focused on the metamorphic evolution of different parts of the Basal Units, a compilation of which is given in Martínez Catalán et al. (1996). These authors see the Basal Units as a coherent terrane and propose that the differences in the *P–T* conditions and geometry of the *P–T* paths observed in the diverse sub-units are essentially related to their position in the subduction complex. The consistent increase in the pressure peak registered from east to west (present coordinates) in the Basal Units was used to deduce a westward polarity for the subduction that is consistent with the east-vergence of the nappes and folds in the internal zones of the orogen in the NW Iberian Massif. In this context, the *P–T* path obtained for the Ceán Schists is consistent with their location in the western part of the basal sheet, registering the highest pressures obtained in the entire Basal Units. Their low-T evolution in the blueschist facies contrasts with the rest of the Malpica–Tui unit, where the metamorphic peak is developed in the medium-T eclogite facies. However, their evolution is quite similar to the nearby Santiago Schists in the Ordenes Complex (Arenas et al., 1995). The peak pressure of the Ceán Schists is 20 kbar, whereas in the Santiago Schists, located to the east of Malpica, it is 16 kbar. Thus, it is possible to separate the Basal Units in two different types according to their metamorphic evolution and position: an upper blueschist type and a lower eclogite facies type.

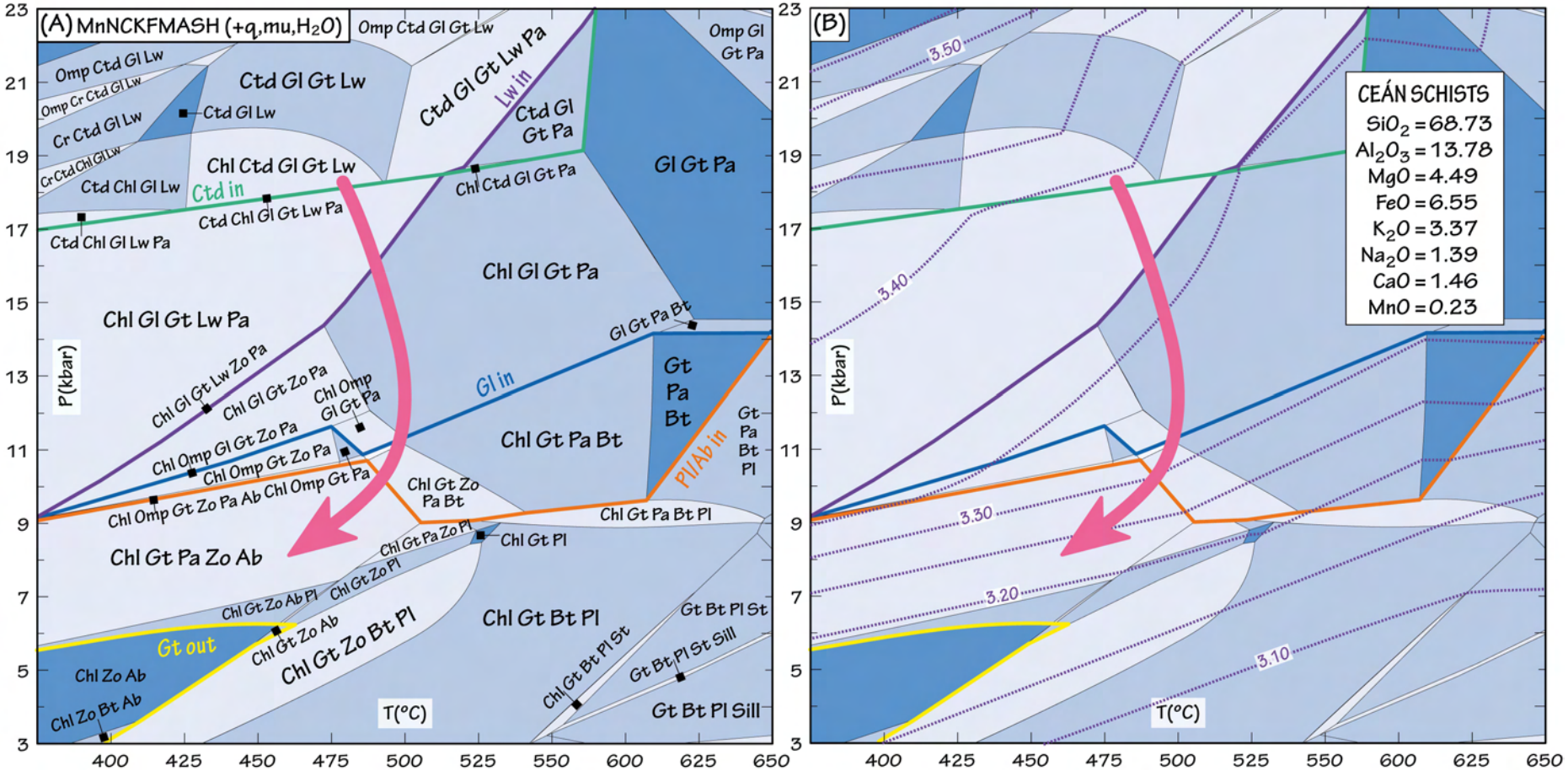

Fig. 10. (A) MnNCKFMASH pseudosection calculated with Perplex 07 software, and (B) Isopleths for Si-content in phengite (c.p.f.u).

Acknowledgements

This work was financially supported by the CGL2007-65338-C02-01 project. We thank Dr. Pavel Pitra and Dr. Michel Ballèvre for broadening our perspectives. We also thank the Guest Editor Dr. Damian Nance, Dr. Ricardo Arenas and two anonymous reviewers for their constructive comments and suggestions that significantly improved the final manuscript. We also wish to thank A. Larios and J. Tánago, from the Luis Bru Electronic Microscopy Centre, for their technical support.

References

Abati, L.L., Gerdes, A., Fernández Suárez, J., Arenas, R., Whitehouse, M.J., Díez Fernández, R., 2009. Magmatism and early-Variscan continental subduction in the northern Gondwana margin recorded in zircons from the basal units of Galicia, NW Spain. Geological Society of America Bulletin 122 (1–2), 219–235.

Alonso, L.L., González, J.C., 1982. Mapa Geológico Nacional Sisargas-Carballo. Instituto Geológico y Minero de España, Hoja 44, scale 1:50.000.

Arenas, R., Rubio Pascual, F., Díaz-García, F., Martínez Catalán, J.R., 1995. High-pressure micro-inclusions and development o fan inverted metamorphic gradient in the Santiago Schists (Órdenes Complex, NW Iberian Massif, Spain): evidence of subduction and syncollisional decompression. Journal of Metamorphic Geology 13, 141–164.

Arenas, R., Abati, J., Martínez Catalan, J.R., Díaz Garcia, F., Rubio Pascual, F.J., 1997. *P–T* evolution of eclogites from the Agualada Unit (Ordenes Complex, northwest Iberian Massif, Spain): Implications for crustal subduction. Lithos 40, 221–242.

Arps, C.E.S., 1981. Amphibolites and other mafic rocks of the Blastomylonitic Graben in Western Galicia, NW Spain: Field relations and petrography. Leidse Geologische Mededelingen 52, 57–71.

Atherton, M.P., 1968. The variation in garnet, biotite and chlorite composition in medium grade pelitic rocks from the Dalradian, Scotland, with particular reference to the zonation in garnet. Contributions to Mineralogy and Petrology 18, 347–371.

Atherton, M.P., Brotherton, M.S., 1982. Major element composition of the pelites of the Scottish Dalradian. Geological Journal 17, 185–221.

Babist, J., Handy, M.R., Konrad-Schmolke, M., Hammerschmidt, K., 2006. Precollisional, multistage exhumation of subducted continental crust: the Sesia Zone, western Alps. Tectonics 25, TC6008. doi:10.1029/2005TC001927.

Ballevre, M., Pitra, P., Bohn, M., 2003. Lawsonite growth in the epidote blueschists from the Ile de Groix (Armorican Massif, France): a potential geobarometer. Journal of Metamorphic Geology 21, 723–735.

Ballèvre, M., Bosse, V., Ducassou, C., Pitra, P., 2009. Palaeozoic history of the Armorican Massif: models for the tectonic evolution of the suture zones. Comptes Rendus Geosciences 34, 174–201.

Behr, H.J., Engel, W., Franke, W., Giese, P., Weber, K., 1984. The Variscan Belt in Central Europe: main structures, geodynamic implications, open questions. Tectonophysics 109, 15–40.

Boger, S.D., Hansen, D., 2004. Metamorphic evolution of the Georgetown Inlier, northeast Queensland, Australia; evidence for an accreted Palaeoproterozoic terrane? Journal of Metamorphic Geology 22, 511–527.

Bohlen, S.R., Liotta, J.J., 1986. A barometer for garnet amphibolites and garnet granulites. Jounal of Petrology 27, 1025–1034.

Bosse, V., Feraud, G., Ballevre, M., Peucat, J.-J., Corsini, M., 2005. Rb-Sr and $^{40}Ar/^{39}Ar$ ages in blueschists from the Ile de Groix (Armorican Massif, France): implications for closure mechanisms in isotopic systems. Chemical Geology 220, 21–45.

Chakraborty, S., Ganguly, J., 1991. Compositional zoning and cation diffusion in aluminosilicate garnets. In: Ganguly, J. (Ed.), Diffusion atomic ordering and mass transport: selected problems in geochemistry. Springer-Verlag, New York, pp. 120–170.

Chopin, C., 1981. Talc-phengite: a widespread assemblage in high-grade pelitic blueschists of the Western Alps. Journal of Petrology 22, 628–650.

Coke, C., Ribeiro, A., 2000. Malpica-Lamego shear zone: a major crustal discontinuity in the Iberian Variscan fold belt. In: Arenas, et al. (Ed.), Excursion guidebook, Program and Abstracts. Galicia 2000: 15th International Conference on Basement Tectonics: Variscan-Appalachian dynamics: The building of the Upper Paleozoic Basement. A Coruña, Spain, pp. 208–210.

Connolly, J.A.D., 2005. Computation of phase equilibria by linear programming: a tool for geodynamic modeling and its application to subduction zone decarbonation. Earth and Planetary Science Letters 236, 524–541.

Cymerman, Z., Piasecki, M.A.J., Seston, R., 1997. Terranes and terrane boundaries in the Sudetes, Northeast Bohemian Massif. Geological Magazine 134, 717–725.

Deer, W.A., Howie, R.A., Zussman, J., 1992. An introduction to the rock-forming minerals. Prentice Hall, London.

El-Shazly, A.K., Liou, J.G., 1991. Glaucophane–chloriotid-bearing assemblages from NE Oman: petrologic significance and petrogenetic grid for HP metapelites. Contributions to Mineralogy and Petrology 107, 180–201.

Ernst, W.G., 1973. Blueschists metamorphism and *P–T* regimes in active subduction zones. Tectonophysics 17, 255–272.

Ernst, W.G., 2001. Subduction, ultrahigh-pressure metamorphism, and regurgitation of buoyant crustal slices-implications for arcs and continental growth. Physics of the Earth and Planetary Interiors 127, 253–275.

Fernández-Suárez, J., Arenas, R., Abati, J., Martínez Catalán, J.R., Whitehouse, M.J., Jeffries, T., 2007. U–Pb Chronometry of polimetamorphic high-pressure granulites: an example from the allochthonous terranes of the NW Iberian Variscan belt. In: HatcherJr. Jr., R.D., Carlson, M.P., McBride, J.H., Martínez Catalán, J.R. (Eds.), 4-D framework of continental crust: Geological Society of America Memoir, vol. 200, pp. 469–488.

Gil Ibarguchi, J.I., Ortega Gironés, E., 1985. Petrology, structure and geotectonic implications of glaucophane-bearing eclogites and related rocks from the Malpica-Tuy unit, Galicia, northwest Spain. Chemical Geology 50, 145–162.

Hirajima, T., Compagnoni, R., 1993. Petrology of a jadeite-quartz/coesite almandine–phengite fels with retrograde ferro-nyböite from the Dora-Maira Massif, Western Alps. European Journal of Mineralogy 5, 943–955.

Holdaway, M.J., 2001. Recalibration of the GASP geobarometer in light of recent garnet and plagioclase activity models and versions of the garnet–biotite geothermometer. American Mineralogist 86, 1117–1129.

Holdaway, M.J., Dutrow, B.L., Hinton, R.W., 1988. Devonian and carboniferous metamorphism in west-central Maine; the muscovite-almandine geobarometer and the staurolite problem revisited. American Mineralogist 73, 20–47.

Holland, T.J.B., Powell, R., 1998. An internally consistent thermodynamic data set for phases of petrological interest. Journal of Metamorphic Geology 16, 309–343.

Hollister, L.S., 1966. Garnet zoning: an interpretation based on the Rayleigh fractionation model. Science 154, 1647–1651.

Hynes, A., Forest, R.C., 1988. Empirical garnet–muscovite geothermometry in low-grade metapelites, Selwyn Range (Canadian Rockies). Journal of Metamorphic Geology 6, 297–309.

Katagas, C., 1980. Ferroglaucophane and chloritoid-bearing metapelites from the phyllite series, southern Peloponnes, Greece. Mineralogical Magazine 43, 975–978.

Kiénast, J.R., Triboulet, C., 1972. Le chloritoïde dans les paragenèses à glaucophane, albite ou paragonite. Bulletin de la Societe Francaise Minéralogie et de Cristallographie 95, 565–573.

Koziol, A.M., 1989. Recalibration of the garnet-plagioclase-Al_2SiO_5-quartz (GASP) geobarometer and application to natural parageneses. American Geophysical Union Spring Meeting, vol. 70. EOS, Baltimore, Maryland, p. 493.

Kretz, R., 1983. Symbols for rock-forming minerals. American Mineralogist 68, 277–279.

Kryza, R., Muszynski, A., Vielzeuf, D., 1990. Glaucophane-bearing assemblage overprinted by greenschist-facies metamorphism in the Variscan Kaczawa complex, Sudetes, Poland. Journal of Metamorphic Geology 8, 345–355.

Kurata, H., Banno, S., 1974. Low-grade progressive metamorphism of Pelitic Schists of the Sazare area, Sanbagawa Metamorphic Terrain in central Sikoku, Japan. Journal of Petrology 15, 361–382.

Llana-Fúnez, S., 2001. La estructura de la unidad de Malpica–Tui (Cordillera varisca en Iberia). Ph.D. thesis, Instituto Geológico y Minero de España, Madrid.

Llana-Fúnez, S., Marcos, A., 2002. Structural record during exhumation and emplacement of high-pressure-low-to intermediate-temperature rocks in the Malpica–Tui unit (Variscan Belt of Iberia). In: Martínez Catalán, J.R., HatcherJr Jr, R.D., Arenas, R., Díaz García, F. (Eds.), Variscan-Appalachian dynamics: The building of the late Paleozoic bassamen: Geological Society of America-Special Paper, vol. 364, pp. 125–142.

López-Carmona, A., Abati, J., Reche, J., 2008. Evolución Metamórfica de los Esquistos de AP/BT de Ceán (Unidad de Malpica–Tui, NW del Macizo Ibérico). Geogaceta 43, 3–6.

Mahar, E.M., Baker, J.M., Powell, R., Holland, T.J.B., Howell, N., 1997. The effect of Mn on mineral stability in metapelites. Journal of Metamorphic Geology 15, 223–238.

Martínez Catalán, J.R., Arenas, R., Díaz García, F., Rubio Pascual, F.J., Abati, J., Marquínez, J., 1996. Variscan exhumation of a subducted Paleozoic continental margin: the basal units of the Ordenes Complex, Galicia, NW Spain. Tectonics 15, 106–121.

Martínez Catalán, J.R., Arenas, R., Díaz García, F., Gómez Barreiro, J., González Cuadra, P., Abati, J., Castiñeiras, P., Fernández Suárez, J., Sánchez Martínez, S., Andonaegui, P., González Clavijo, E., Díez Montes, A., Rubio Pascual, F.J., Valle Agudo, B., 2007. Space and time in the tectonic evolution of the northwestern Iberian Massif. Implications for the comprehension of the Variscan belt. In: Hatcher, R.D.J., Carlson, M.P., McBride, J.H., Martínez Catalán, J.R. (Eds.), 4-D framework of continental crust: The Geological Society of America Memoir, vol. 200, pp. 403–423.

Martínez Catalán, J.R., Arenas, R., Abati, J., Sánchez Martínez, S., Díaz García, F., Fernández Suárez, J., González Cuadra, P., Castiñeiras, P., Gómez Barreiro, J., Díez Montes, A., González Clavijo, E., Rubio Pascual, F.J., Andonaegui, P., Jeffries, T.E., Alcock, J.E., Díez Fernández, R., López-Carmona, A., 2009. A rootless suture and the loss of the roots of a mountain chain: the Variscan belt of NW Iberia. Comptes Rendus Geosciences 341, 114–126.

Maruyama, S., Liou, G., Terabayashi, M., 1996. Blueschists and eclogites of the world. International Geology Review 38, 485–594.

Masago, H., Omori, S., Maruyama, S., 2009. Counter-clockwise prograde *P–T* path in collisional orogeny and water subduction at the Precambrian–Cambrian boundary: the ultrahigh-pressure pelitic schist in the Kokchetav massif, northern Kazakhstan. Gondwana Research 15, 137–150.

Massone, H.J., Schreyer, W., 1987. Phengite geobarometry based on the limiting assemblage with K-feldspar, phlogopite and quartz. Contributions to Mineralogy and Petrology 96, 212–214.

Matte, P.H., 1986. Tectonics and plate tectonics model for the Variscan belt of Europe. Tectonophysics 126, 329–374.

Menold, C.A., Manning, C.E., Yin, A., Chen, X., 2001. Metamorphism and Exhumation of Very High-Pressure Eclogites, North Qaidam, China. 2001 AGU Fall Meeting, San Francisco: American Geophysical Union.

Miyashiro, A., 1973. Metamorphism and metamorphic belts. G. Allen and Unwin Publications, London.

Omori, S., Kita, S., Maruyama, S., Santosh, M., 2009. Pressure-temperature conditions of ongoing regional metamorphism beneath the Japanese Islands. Gondwana Research 16, 458–469.

Ortega, E., 1980. Aportaciones a la estructura geológica de los alrededores de Malpica, extremo septentrional de la Fosa Blastomilonítica, La Coruña. Cuadernos del Laboratorio Xeológico de Laxe 1, 177–186.

Pin, C., Vielzeulf, D., 1988. Les granulites de haute pression d´Europe moyenne témoins d´une subuctionéo-hercynienne. Implications surl´orgine des groupes leptyno- amphiboliques. Bulletin de la Societé Géologique de France 1, 13–20.
Platt, J.P., 1993. Exhumation of high-pressure rocks: a review of concepts and processes. Terra Nova 5, 119–133.
Powell, R., Holland, T.J.B., 1988. An internally consistent dataset with uncertainties and correlations: 3. Applications to geobarometry, worked examples and a computer program. Journal of Metamorphic Geology 6, 173–204.
Powell, R., Holland, T.J.B., 2008. On thermobarometry. Journal of Metamorphic Geology 26, 155–179.
Proyer, A., 2003. Metamorphism of pelites in NKFMASH-a new petrogenetic grid with implications for the preservation of high-pressure mineral assemblages during exhumation. Journal of Metamorphic Geology 21, 493–509.
Råheim, A., 1977. Petrology of the Strathgordon area, western Tasmania: Si^{4+}-content of phengite mica as a monitor of metamorphic grade. Journal of the Geological Society of Australia 24, 329–338.
Reynard, B., Ballèvre, M., 1988. Coexisting amphiboles in an eclogite from the Western Alps: new constraints on the miscibility gap between sodic and calcic amphiboles. Journal of Metamorphic Geology 6, 333–350.
Rodríguez Aller, J., 2005. Recristalización y deformación de litologías supracorticales sometidas a metamorfismo de alta presión (Complejo de Malpica–Tui, NO del Macizo Ibérico). Nova Terra, vol. 29. A Coruña.
Rodríguez, J., Cosca, M.A., Gil Ibarguchi, J.I., Dallmeyer, R.D., 2003. Strain partitioning and preservation of $^{40}Ar/^{39}Ar$ ages during Variscan exhumation of a subducted crust (Malpica–Tui complex, NW Spain). Lithos 70, 111–139.
Santosh, M., Maruyama, S., Sato, K., 2009. Anatomy of a Cambrian suture in Gondwana: Pacific-type orogeny in southern India? Gondwana Research 16, 321–341.
Shelley, D., Bossière, G., 1999. Ile de Groix: retrogression and structural developments in an extensional régime. Journal of Structural Geology 21, 1441–1455.
Shi, G.-H., Cui, W.-Y., Tropper, P., Wang, C.-Q., Shu, G.-M., Yu, H., 2003. The petrology of a complex sodic and sodic–calcic amphibole association and its implications for the metasomatic processes in the jadeitite area in northwestern Myanmar, formerly Burma. Contributions to Mineralogy and Petrology 145, 355–376.
Smelik, E.A., Veblen, D.R., 1992. Exsolution of Ca-amphibole from glaucophane and the miscibility gap between sodic and calcic amphiboles. Contributions to Mineralogy and Petrology 112, 178–195.
Song, S.-G., Zhang, L.-F., Niu, Y., Wei, C.-J., Liou, J.-G., Shu, G.-M., 2007. Eclogite and carpholite-bearing metasedimentary rocks in the North Qilian suture zone, NW China: implications for Early Palaeozoic cold oceanic subduction and water transport into mantle. Journal of Metamorphic Geology 25, 547–563.
Spear, F.S., 1995. Metamorphic phase equilibria and pressure–temperature–time paths. Mineralogical Society of America Monograph, Washington.
Spear, F., Cheney, J., 1989. A petrogenetic grid for pelitic schists in the system SiO_2–Al_2O_3–FeO–MgO–K_2O–H_2O. Contributions to Mineralogy and Petrology 101, 149–164.
Symmes, G.H., Ferry, J.M., 1992. The effect of whole-rock MnO content on the stability of garnet in pelitic schists during metamorphism. Journal of Metamorphic Geology 10, 221–237.
Tajčmanová, L., Konopásek, J., Connolly, J., 2007. Diffusion-controlled development of silica-undersaturated domains in felsic granulites of the Bohemian Massif (Variscan belt of Central Europe). Contributions to Mineralogy and Petrology 153, 237–250.
Theye, T., Seiidel, E., Vidal, O., 1992. Carpholite, sudoite and chloritoid in low-grade high-pressure metapelites from Crete and the Peloponnese, Greece. European Journal of Mineralogy 4, 487–507.
Thompson, J.B.J., Laird, J., Thompson, A.B., 1982. Reactions in amphibolite, greenschist and blueschist. Journal of Petrology 23, 1–27.
Tinkham, D.K., Zuluaga, C.A., Stowell, H.H., 2003. Metapelite phase equilibria modeling in MnNCKFMASH: The effect of variable Al2O3 and MgO/(MgO + FeO) on mineral stability. American Mineralogist 88, 1174.
Turner, F.J., 1981. Metamorphic petrology, Mineralogical and Field Aspects, Second edition. McGraw-Hill, New York.
Van Calsteren, P.W.C., Boelrijk, N.A.I.M., Hebeda, E.H., Priem, H.N.A., Tex, E. Den, Verdurmen, E.A.T.H., Verschure, R.H., 1979. Isotopic dating of older elements (including the Cabo Ortegal mafic-ultramafic complex) in the Hercynian Orogen of NW Spain: manifestations of a presumed Early Paleozoic Mantle-plume. Chemical Geology 24, 35–56.
Vernon, R.H., Clarke, G.L., 2008. Principles of metamorphic petrology. Cambridge University Press, New York.
Warren, C.J., Miller, J.M., 2007. Structural and stratigraphic controls on the origin and tectonic history of a subducted continental margin, Oman. Journal of Structural Geology 29, 541–558.
Warren, C.J., Waters, D.J., 2006. Oxidized eclogites and garnet-blueschists from Oman: *P–T* path modeling in the NCFMASHO system. Journal of Metamorphic Geology 24, 783–802.
Warren, C.J., Beaumont, C., Jamieson, R.A., 2008. Modelling tectonic styles and ultra-high pressure (UHP) rock exhumation during the transition from oceanic subduction to continental collision. Earth and Planetary Science Letters 267, 129–145.
Wei, C.-J., Powell, R., 2003. Phase relations in high-pressure metapelites in the system KFMASH (K_2O–FeO–MgO–Al_2O_3–SiO_2–H_2O) with application to natural rocks. Contributions to Mineralogy and Petrology 145, 301–315.
Wei, C.-J., Song, S.-G., 2008. Chloritoid–glaucophane schist in the north Qilian orogen, NW China: phase equilibria and *P–T* path from garnet zonation. Journal of Metamorphic Geology 26, 301–316.
Zuluaga, C.A., Stowell, H.H., Tinkham, D.K., 2005. The effect of zoned garnet on metapelite pseudosection topology and calculated metamorphic *P–T* paths. American Mineralogist 90, 1619–1628.

3.1.3 *Partial Conclusions*

The main conclusions of this study are:

1. The stability field of the M_1 paragenesis containing glaucophane+chloritoid is located, for the composition of the pelitic Ceán schists, above 17-18 kbar. Hence, the P-T path deduced from all the data obtained in this study indicates an initial stage of subduction burial to a depth of 65-70 km. Maximum burial was followed by dramatic exhumation with slight heating, reaching a metamorphic peak at ~500 °C. This slight increase in temperature during decompression is supported by the presence of late biotite in chemical imbalance with the rest of the M_2 minerals, suggesting an origin related to a localized heating that could have taken place during the exhumation of the unit.

2. The secondary growth of Na-Ca amphiboles, most likely after glaucophane, indicates that, although it has not been identified in the matrix of the schists, it was a stable phase during the second HP event. The sodic-calcic amphiboles and coexisting hornblende occur as intergrowths and occur only in the matrix of samples containing glaucophane as garnet inclusions. This intergrowth texture can be interpreted in two ways: as an amphibole miscibility gap and as a disequilibrium growth texture. Reynard & Ballèvre (1988) demostrated the existence of a miscibility gap between sodic and calcic amphiboles at T=500-550 °C, which suggests that glaucophane and hornblende could have coexisted during M_2. However, textural observations in the Na-Ca amphiboles of the Ceán Schist show chemical zonation indicating disequilibrium growth. Therefore, these amphiboles cannot be considered as an intermediate stage between the two end-members (Reynard & Ballèvre, 1988). They are compatible with amphibole formation during retrograde fluid infiltration under HP conditions, as described, for example, by Menold *et al.* (2001) and Shi *et al.* (2003).

3. A preliminary pseudosection in the basic pelitic KFMASH shows the significant influence of Mn and Ca components on the stability of garnet, leading to an overestimation of the temperature. However, the pressure calculated with silica isopleths in the same diagram corresponds well with the other barometric calculations.

4. The MnNCKFMASH system pseudosection fully describes the succession of mineral assemblages in the schists, and produces results that are consistent with the petrographic observations.

5. There are several studies focused on the metamorphic evolution of different parts of the basal units, a compilation of which is given in Martínez Catalán *et al.* (1996). These authors see the basal units as a coherent terrane and propose that the differences in the P–T conditions and geometry of the P–T paths observed in the diverse sub-units are essentially related to their position in the subduction complex. The consistent increase in the pressure peak registered from east to west (present coordinates) in the basal units was used to deduce a westward polarity for the subduction that is consistent with the east-vergence of the nappes and folds in the internal zones of the orogen in the NW Iberian Massif. In this context, the P–T path obtained for the Ceán schists is consistent with their location in the western part of the basal sheet, registering the highest pressures obtained in the entire basal units. Their LT evolution in the blueschist-facies contrasts with the rest of the Malpica–Tui Unit, where the metamorphic peak is developed in the MT eclogite-facies. However, their evolution is quite similar to the nearby Santiago Schists in the Ordenes Complex (Arenas *et al.*, 1995). The peak pressure of the Ceán schists is 20 kbar, whereas in the Santiago schists, located to the east of Malpica, it is 16 kbar. Thus, it is possible to separate the basal units in two different types according to their metamorphic evolution and position: an upper blueschist type and a lower eclogite-facies type.

3.1.4 *Introduction*

Sinking of cold, dense lithosphere in subduction zones is the principal plate-driving force, causing orogénesis along continental margins. The descent of a relatively cold crustal slab to mantle depths leads to the formation of HP-LT/MT metamorphic rocks, like blueschists and eclogites, frequently found in the suture zones of orogenic belts (e.g. Miyashiro, 1961; Ernst, 1971; Maruyama *et al.*, 1996). Blueschist- and eclogite-facies assemblages, as markers of fossil and active subduction zones, store much information concerning processes at convergent plate boundaries, and provide important clues to the understanding of the thermal history of the evolving Earth (e.g. Ernst, 1973, 2001; Platt, 1993; Stern, 2005).

Data about the metamorphic evolution of subducted terranes, obtained through petrological analysis and thermodynamic modelling, are fundamental to geodynamic models and palaeogeographical reconstructions of the lithospheric plates. In this context, the northwest section of the Iberian Massif provides information that helps to understand the evolution of the European Variscan belt. This region comprises exotic terranes forming a huge and complex Allochthonous sheet emplaced upon the sequences deposited on the passive margin of north Gondwana (Martínez Catalán *et al.*, 2009). They include a HP-LT/MT belt that can be discontinuously traced throughout the Variscan belt, located below several rock units with ophiolitic associations, probably having originated in the Rheic Ocean. This HP belt is a coherent piece of continental crust formed by different rock units known in the NW Iberian Massif as the basal units.

The goal of this work is to analyse phase equilibria of blueschist-facies metapelites (Ceán Schists) from the upper sequence of the westernmost basal unit, the Malpica–Tui Unit, with particular attention to the effects of H_2O and Fe_2O_3. This lithology preserves the chloritoid–glaucophane paragénesis (López-Carmona *et al.*, 2010), which is one of the classic HP indicators in metapelites (e.g. Kiénast & Triboulet, 1972; Katagas, 1980; Chopin, 1981; El-Shazly & Liou, 1991; Wei & Song, 2008). Phase equilibria of pelitic rocks at high pressures do not attract as much attention as metabasic rocks, probably because the mineral associations are less spectacular. Yet, metapelitic rocks are common in HP terranes (e.g. Bosse *et al.*, 2002; Wei & Powell, 2003 and references therein), and are suitable for constraining P–T evolution. However, similar to metabasic rocks, the assemblages are sensitive to the amount of available H_2O and Fe_2O_3 (cf. Korhonen *et al.*, 2012).

3.1.5 *Blueschist facies metapelites from the Malpica-Tui Unit (NW Iberian Massif): phase equilibria modelling and H_2O and Fe_2O_3 influence in high–pressure assemblages*

LÓPEZ-CARMONA, A., PITRA, P. & ABATI, J. (2013) JOURNAL OF METAMORPHIC GEOLOGY, 31, 263–280

Journal of
METAMORPHIC GEOLOGY

J. metamorphic Geol., 2013, **31,** 263–280 doi:10.1111/jmg.12018

Blueschist-facies metapelites from the Malpica–Tui Unit (NW Iberian Massif): phase equilibria modelling and H_2O and Fe_2O_3 influence in high-pressure assemblages

A. LÓPEZ-CARMONA,[1,2] P. PITRA[2] AND J. ABATI[1]
[1]*Departamento de Petrología y Geoquímica (UCM) and Instituto de Geociencias (IGEO-CSIC), 28040 Madrid, Spain (alcarmona@geo.ucm.es)*
[2]*Géosciences Rennes, UMR 6118, Université Rennes 1 & CNRS, 35042 Rennes cedex, France*

ABSTRACT The Malpica–Tui Unit (Galicia, NW Spain) records eclogite- and blueschist-facies metamorphism during the onset of the Variscan orogeny in Europe. Petrological analysis involving pseudosections calculated using THERMOCALC shows that the Upper Sheet of this unit, the Ceán Schists, recorded a three-stage metamorphic evolution involving (i) Early subduction-related medium-pressure/low-temperature metamorphism (M_1) constrained at ~350–380 °C, 12–14 kbar, which is only recorded in the basal part (lower metapelites, LM) of the Ceán Schists. (ii) Subduction-related blueschist facies prograde metamorphism (M_2) going from ~19 kbar, 420 °C to 21 kbar, 460 °C in the LM, and from 16 kbar 430 °C to 21–22 kbar, 520 °C in the structurally upper metapelites (UM). (iii) Exhumation-related metamorphism (M_3) is characterized by a decompression to 8–10 kbar, 470–490 °C in the LM. This decompression is also recorded in the UM, but it was not possible to estimate precise *P–T* conditions. The calculations indicate that (i) the prograde evolution in subduction zones may occur in fluid-undersaturated conditions due to the crystallization of lawsonite, even in metapelitic rocks. This significantly influences phase equilibria and hence the *P–T* estimates. (ii) The proportion of ferric iron also has a strong influence on phase equilibria, even in metapelites. However, the analysed values of Fe_2O_3 may not reflect the oxidation state during the main metamorphic evolution and are probably easily modified by superficial alteration even in apparently fresh samples. The use of P–T–$X(Fe_2O_3)$ pseudosections together with petrographic observations is then necessary to estimate the real oxidation state of the rocks and correctly evaluate the *P–T* conditions.

Key words: blueschist-facies metapelites, H_2O content, Iberian Massif, MnNCKFMASHTO, Variscan subduction

INTRODUCTION

Sinking of cold, dense lithosphere in subduction zones is the principal plate-driving force, causing orogenesis along continental margins. The descent of a relatively cold crustal slab to mantle depths leads to the formation of high-pressure (HP) and low- (LT) to medium-temperature (MT) metamorphic rocks, like blueschists and eclogites, frequently found in the suture zones of orogenic belts (e.g. Miyashiro, 1961; Ernst, 1971; Maruyama *et al.*, 1996). Blueschist- and eclogite-facies assemblages, as markers of fossil and active subduction zones, store much information concerning processes at convergent plate boundaries, and provide important clues to the understanding of the thermal history of the evolving Earth (e.g. Ernst, 1973, 2001; Platt, 1993; Stern, 2005).

Data about the metamorphic evolution of subducted terranes, obtained through petrological analysis and thermodynamic modelling, are fundamental to geodynamic models and palaeogeographical reconstructions of the lithospheric plates. In this context, the northwest section of the Iberian Massif provides information that helps to understand the evolution of the European Variscan belt. This region comprises exotic terranes forming a huge and complex allochthonous sheet emplaced upon the sequences deposited on the passive margin of north Gondwana (Martínez Catalán *et al.*, 2009). They include a HP and LT–MT belt that can be discontinuously traced throughout the Variscan belt, located below several rock units with ophiolitic associations, probably having originated in the Rheic Ocean. This HP belt is a coherent piece of continental crust formed by different rock units known in the NW Iberian Massif as the Basal Units (Fig. 1). The goal of this work is to analyse phase equilibria of blueschist-facies metapelites (Ceán Schists) from the upper sequence of the westernmost basal unit, the Malpica–Tui Unit (MTU; Fig. 1), with particular attention to the effects of H_2O and Fe_2O_3. This lithology preserves the chloritoid–glaucophane paragenesis (López-Carmona *et al.*, 2010), which is one of the classic HP indicators in metapelites (e.g. Kiénast & Triboulet, 1972; Katagas, 1980; Chopin, 1981; El-Shazly & Liou, 1991; Wei & Song, 2008).

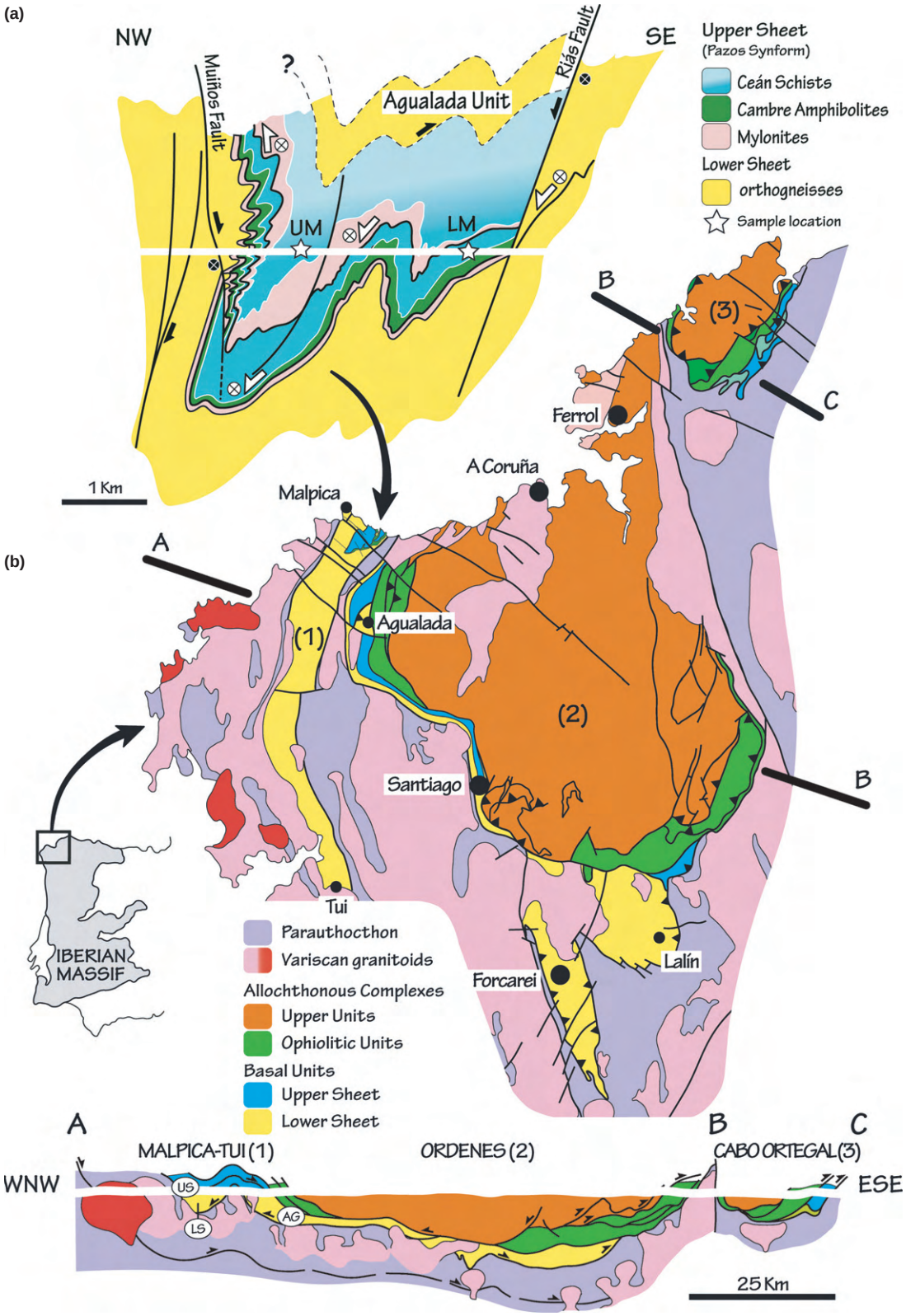

Figure 1. (a) Cross-section for the Upper Sheet (Pazos Synform) of the Malpica–Tui Unit. The gradation of colours indicates the decrease in the metamorphic grade. Sample locations are indicated. Modified from Díez Fernández (2011). (b) Geological map of the Allochthonous Complexes of the NW Iberian Massif. A–B and B–C correspond to cross-sections along the different units. US, upper sheet; LS, lower sheet; AG, Agualada Unit. Modified from Martínez Catalán *et al.* (2009).

Phase equilibria of pelitic rocks at high pressures do not attract as much attention as metabasic rocks, probably because the mineral associations are less spectacular. Yet, metapelitic rocks are common in HP terranes (e.g. Bosse *et al*., 2002; Wei & Powell, 2003 and references therein), and are suitable for constraining *P–T* evolution. However, similar to metabasic rocks, the assemblages are sensitive to the amount of available H_2O and Fe_2O_3 (cf. Korhonen *et al*., 2012).

HIGH-PRESSURE ROCKS IN THE BASAL UNITS OF NW IBERIA

Pods and relicts of HP rocks, well preserved in the NW Iberian massif, with widespread distribution along the so-called Basal Units, are the best record of the Variscan subduction of the north Gondwana margin during the Late Devonian. Their petrological and structural study has constrained the *P–T* paths and the kinematics of the subduction (e.g. Martínez Catalán *et al*., 1996; Arenas *et al*., 1997; López-Carmona *et al*., 2010; Díez Fernández *et al*., 2011), concluding that Basal Units formed part of a subducting slab buried beneath Laurussia at the onset of the Variscan collision (Arenas *et al*., 1995, 1997; Santos Zalduegui *et al*., 1995; Rodríguez Aller *et al*., 2003; Abati *et al*., 2010). They were rapidly exhumed by crustal-scale thrusting accompanied by recumbent folding and tectonic denudation (Martínez Catalán *et al*., 1996, 1997; Díez Fernández & Martínez Catalán, 2009; Díez Fernández *et al*., 2011). The original polarity of the subducting slab was reconstructed on the basis of the palaeo-pressures inferred from metamorphic parageneses, indicating that the subduction had a significant westward component in present coordinates (Martínez Catalán *et al*., 1996). Kinematic indicators in HP fabrics are in agreement with this reconstruction, indicating top to the northwest movement (Díez Fernández *et al*., 2012).

According to their metamorphism and tectonostratigraphy, the Basal Units can be separated into two sheets (Fig. 1). In the MTU: (i) a Lower Sheet of continental affinity, where felsic orthogneisses and turbiditic metasedimentary rocks predominate; and (ii) an Upper Sheet that represents a volcano-sedimentary sequence viewed as a more distal part of the same continental margin, extremely attenuated and transitional to an oceanic domain (Rodríguez Aller, 2005). The Upper Sheet is preserved in a small synformal structure (the Pazos Synform) and is formed by a basal layer of finely foliated amphibolites and greenschists with N-MORB chemistry (Cambre Amphibolites), and an overlying sequence of pelitic schists (Ceán Schists) with minor intercalations of bituminous schist, cherts and carbonates. The mafic rocks are strongly retrogressed blueschists that locally preserve lawsonite pesudomorphs dominated by epidote/clinozoisite and paragonite (Rodríguez Aller *et al*., 2003; López-Carmona *et al*., 2010). The contact between the Upper and the Lower Sheets is marked by a several metres thick layer of mylonites and ultramylonites located at the base of the Cambre Amphibolites (Díez Fernández, 2011). Another layer of mylonites occurs in the middle of the Upper Sheet, within the Ceán Schists, separating them in a lower and an upper part (Fig. 1a).

Peak metamorphic conditions in the Lower Sheet of the MTU are in the intermediate temperature eclogite facies (Rodríguez *et al*., 2005), with a progressive transition to the blueschist facies in the eastern sections of the same units in the remaining allochthonous complexes (Martínez Catalán *et al*., 1996; Rubio Pascual *et al*., 2002). The Upper Sheet can be considered as a highly condensed metamorphic sequence with a lower part in the blueschist facies and an uppermost part without HP relicts (Fig. 1a). The significant difference in metamorphic grade between the Upper and the Lower Sheets, and between the upper and lower part of the Upper Sheet suggests that the mylonites that mark the contacts are related to extensional deformation (López-Carmona *et al*., 2007; Fig. 1).

Previous *P–T* estimates

The metamorphic evolution of the Ceán Schists has been previously studied by conventional thermobarometric techniques, multiequilibrium thermobarometry (THERMOCALC average *P–T*) and thermodynamic modelling, using pseudosections in the KFMASH and MnNCKFMASH chemical systems (López-Carmona *et al*., 2010). Conventional thermobarometry calculations using microinclusion compositions indicate peak conditions of ~19–22 kbar and 500 °C. The same calculations using the matrix minerals yield approximate values of 16–20 kbar and 440–515 °C. *P–T* values obtained with the average *P–T* multiequilibrium thermobarometry are compatible with the conventional thermobarometry results, but show significantly lower pressures for the matrix foliation (13–14 kbar and 495–500 °C). Petrological modelling in the MnNCKFMASH system provided a minimum pressure limit for the paragenesis chloritoid + glaucophane at ~17 kbar, confirming the HP stability of this assemblage.

SAMPLE DESCRIPTION AND MINERAL CHEMISTRY

The deformation in the Ceán Schists is relatively heterogeneous, with irregular development of foliations and deformation phases in different domains. Their deformation history includes several compressive, extensional and strike-slip phases (Díez Fernández *et al*., 2011). However, only three of the deformation phases have a direct link with relevant metamorphic associations. Two blueschist facies deformation phases have been identified (D_1–D_2), followed by the development of the main foliation in blueschist-amphibolite facies conditions (D_3) and an amphibolite–greenschist facies overprint (post-D_3) (Fig. 2). The fabric from the

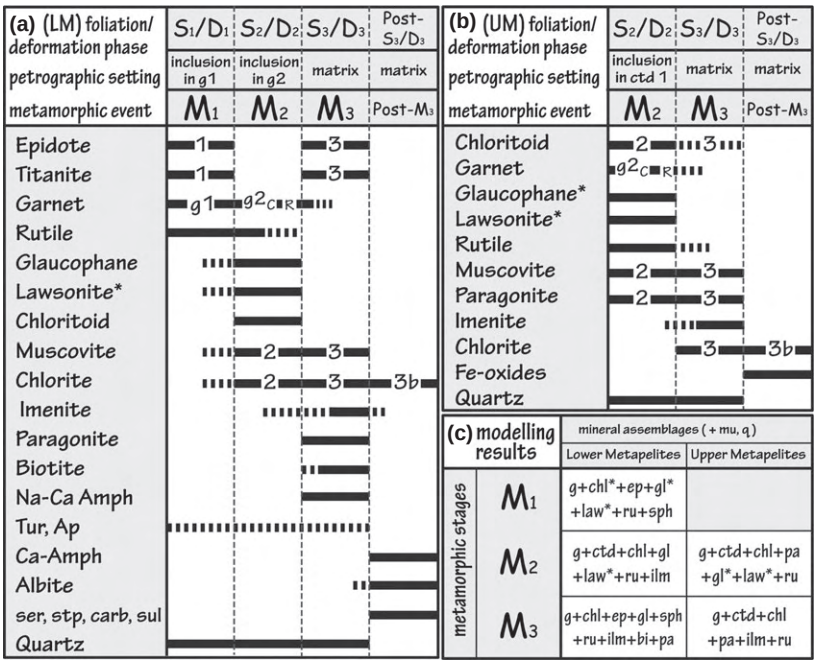

Figure 2. Diagram showing the crystallization–deformation relations of the Ceán Schists in the lower (a) and upper metapelites (b). (c) Summary of the modelling results showing the mineral assemblages predicted in the metamorphic events. *Inferred phases that have not been observed petrographically.

Table 1. (a) Bulk-rock composition from XRF analyses of samples LM and UM expressed in wt%. (b) Bulk-rock compositions normalized with THERMOCALC expressed in mol.%. $Fe_2O_{3(T)}$ was measured by the XRF and FeO by wet chemical titration. The amount Fe_2O_3 is calculated stoichiometrically as: [total iron/1.43–(FeO/1.286)*1.43].

	Studied samples			MnNCKFMASHTO					CKFMASH
(a)	LM (wt%)	UM (wt%)	(b)	LM (mol.%)		UM (mol.%)			UM (mol.%)
SiO_2	57.54	57.67	SiO_2	66.15	66.15	68.63	68.63	49.73	81.04
TiO_2	1.01	0.74	TiO_2	0.87	0.87	0.66	0.66	0.53	
Al_2O_3	17.04	20.96	Al_2O_3	11.55	11.55	14.70	14.70	7.17	8.66
FeO	6.78	5.93	FeO	7.72	7.72	7.68	7.68	2.01	3.02
Fe_2O_3	1.39	1.98	O	0.60	0.60	0.89	0.05	0.04	
MnO	0.17	0.26	MnO	0.17	0.17	0.26	0.26	0.01	
MgO	2.92	1.72	MgO	5.00	5.00	3.05	3.05	1.68	3.03
CaO	2.75	0.36	CaO	3.16	3.16	0.24	0.24	0.04	0.07
Na_2O	1.26	0.85	Na_2O	1.40	1.40	0.98	0.98	0.79	
K_2O	4.59	3.83	K_2O	3.37	3.37	2.91	2.91	2.33	4.19
P_2O_5	0.14	0.13	H_2O	In excess	14.38	In excess	In excess	35.69	In excess
Cr_2O_3	0.05	0.04	Figure	5a;5c	5b;5d	6a;c	6d	6e	6f

earliest deformational event (S_1) is preserved exclusively as inclusion trails in a first generation of garnet porphyroblasts. S_2 is preserved in a second generation of garnet and chloritoid porphyroblasts. The matrix foliation (S_3) usually obliterates the previous fabric, resulting in a composite foliation $S_2 + S_3$ and includes the pervasive development of spaced extensional shear bands and meso-scale folds, related with a first extensional event (Díez Fernández *et al.*, 2011). Subsequent deformations are associated with the development of late-Variscan folds (such as Pazos Synform, Fig. 1) and to a final superposed dextral strike-slip tectonics. The effects of post-S_3 deformations associated with vertical folding are particularly evident in the core of the synformal structure, where an axial-planar foliation S_4 is usually developed. In these areas, the schists are highly altered and the main foliation consists of alternations of quartz and phyllosilicate-rich layers.

The dominant rock type of the Ceán series is a typical pelite (e.g. Atherton & Brotherton, 1982). However, to the base of the sequence, metapelitic rocks are interbedded with the Cambre Amphibolites and most samples show compositions that move away from the field of pure pelites in the direction of N-MORB, indicating either some mixing between both lithologies during primary volcano-sedimentary processes, or mechanical assimilation during the deformation. The different whole-rock chemistry between the samples selected for this study results in slightly different mineral associations (Table 1).

The Ceán Schists show a medium-grained porphyro–lepidoblastic texture and a well-developed planar to planar–linear fabric (Fig. 3). White mica and quartz constitute > 50%, and locally up to 80%, of the modal proportion of each sample. The alternation of both minerals defines a banding preserved between extensional shear bands. The foliation is defined by the shape preferred orientation of phengitic muscovite, paragonite and chlorite, and is parallel to the banding. Quartz grains commonly show undulate extinction, subgrain boundaries and recrystallization to smaller grain aggregates (Fig. 3).

Two representative samples of the Ceán Schists from the Upper Sheet of the MTU (Fig. 1) were studied. Sample 106340, referred to hereafter as LM

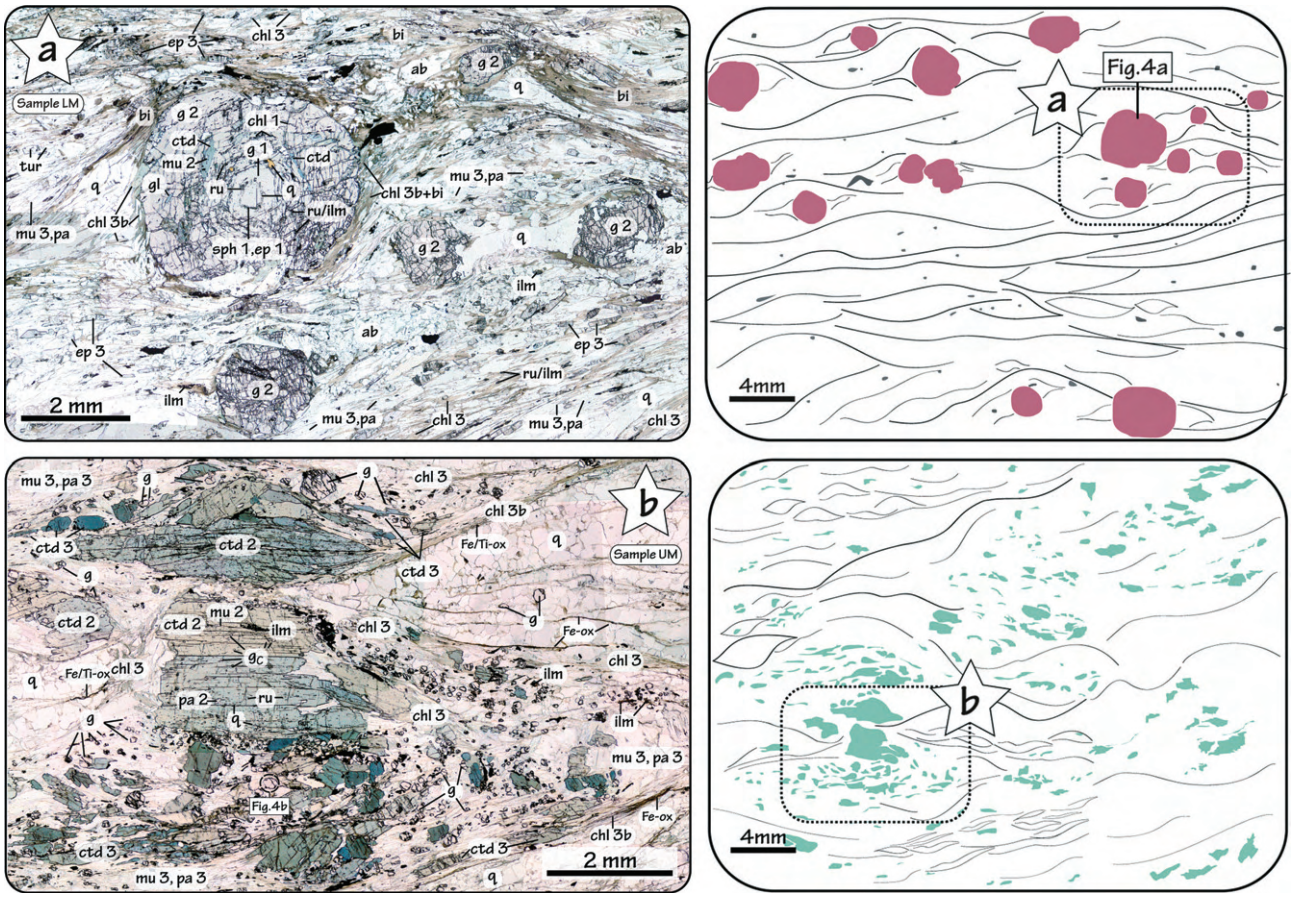

Figure 3. Microphotographs of the Ceán Schists. Photomontages of thin-section images displaying the porphyro–lepidoblastic texture and the highly deformed fabrics. (a) Sample LM showing garnet porphyroblasts filled with concentric inclusions. (b) Sample UM – cluster of highly pleochroic chloritoid porphyroblasts and numerous small garnets. Sample locations are indicated in Fig. 1. Mineral abbreviations are after Holland & Powell (1998). Other abbreviations: tur, tourmaline; Fe/Ti-ox, Fe/Ti-bearing oxides.

(for lower metapelites), is located at the base of the synformal structure, and interbedded within the Cambre Amphibolites. The presence of numerous garnet porphyroblasts rich in S_1 and S_2 inclusions makes this sample ideal to study the first subduction-related deformation phases. Sample 108289, referred to hereafter as UM (for upper metapelites), is located structurally above the sample 106340, in the middle part of the synformal structure, in an upper structural domain separated from the first by a mylonitic band (Fig. 1a).

Mineral analyses and elemental X-ray maps have been performed with a JEOL-Superprobe JXA-8900M microprobe equipped with five spectrometers at the ICTS-National Electronic Microscopy Centre at the Complutense University of Madrid (Spain; http://www.cnme.es). The operating parameters for punctual analyses were 15 kV accelerating voltage, 20 nA beam current, between 1 and 5 μm beam diameter (1 μm for the microinclusions) and 10 s counting time. X-ray maps were operated at 20 kV and 150 nA. Representative analyses of selected minerals are listed in Tables 2 and 3. Mineral abbreviations are those used by THERMOCALC (Holland & Powell, 1998): albite (ab), biotite (bi), chlorite (chl), chloritoid (ctd), clinozoisite (cz), epidote (ep), garnet (g), glaucophane (gl), ilmenite (ilm), jadeite (jd), lawsonite (law), muscovite (mu), omphacite (o), paragonite (pa), plagioclase (pl), quartz (q), rutile (ru) and titanite (sph). Other abbreviations: apatite (ap), barroisite (bar), carbonates (carb), Fe/Ti-bearing oxides (Fe/Ti-ox), hornblende (hb), sericite (ser), stilpnomelane (stp), sulphides (sul), tschermakite (ts), tourmaline (tur) and winchite (win). Other symbols: $X_{Fe} = Fe^{2+}/(Fe^{2+} + Mg)$; $X_{Fe3+} = Fe^{3+}/(Fe^{3+} + Al–2)$ (epidote); $X_{Fe3+} = Fe^{3+}/(Fe^{3+} + Al)$ (amphibole) $X_{Na} = Na/(Na + K)$ (white mica); $X_{Na} = Na/(Na + Ca)$ (amphibole); Alm = Fe/(Fe + Mg + Ca + Mn), Prp = Mg/(Fe + Mg + Ca + Mn), Grs = Ca/(Fe + Mg + Ca + Mn), Sps = Mn/(Fe + Mg + Ca + Mn); per formula unit (pfu); weight per cent (wt%); ' → ' denotes core-to-rim evolution, and '*' indicates phases inferred from the petrological modelling that have not been identified petrographically.

Table 2. Representative microprobe analyses from sample LM.

	S_1				S_2						S_3									Post-S_3			
Mineral	ep 1	sph 1	g 1_C	g 1_R	gl	ctd	mu 2	chl 2	$g2_C$	$g2_R$	ilm	ep 3	mu 3	bi	pa	chl 3	sph 3	win	bar	chl 3b	hb	ts	ab
Analysis	9	1	2	196	2	3	160	43	179	183	18	18	4	13	59	67	8	11	26	96	17	24	85
SiO_2	38.13	30.46	36.98	37.36	56.79	23.81	51.29	25.93	37.47	37.92	0.05	38.04	50.92	36.54	46.70	24.61	30.16	53.96	46.75	24.52	44.94	47.23	67.25
TiO_2	0.04	35.81	0.31	0.05	0.03	0.02	0.15	0.07	0.12	0.09	53.38	0.15	0.19	1.55	0.07	0.06	35.51	0.14	0.10	0.09	0.26	0.23	0.00
Al_2O_3	26.26	1.41	20.81	22.08	11.78	39.06	24.73	21.23	22.16	22.01	0.34	26.68	27.44	16.71	39.38	23.15	1.83	13.28	9.43	22.50	12.74	10.40	19.87
Cr_2O_3	0.11	0.03	0.01	0.05	0.01	0.05	0.06	0.04	0.00	0.03	0.08	0.09	0.05	0.10	0.00	0.00	0.00	0.04	0.00	0.01	0.04	0.12	0.00
Fe_2O_3	11.07	0.00	0.82	0.00	0.98	1.97	1.19	0.00	0.00	0.00	0.00	9.75	0.00	0.00	0.08	0.00	0.00	3.61	6.05	0.00	5.61	4.51	0.03
FeO	0.10	0.76	22.46	27.51	11.86	22.27	3.17	21.82	23.61	27.06	42.24	0.09	3.51	18.36	1.09	29.14	1.23	14.01	11.99	27.72	11.63	11.93	0.00
MnO	0.19	0.18	7.95	2.46	0.04	0.36	0.00	0.15	4.55	1.66	3.75	0.08	0.03	0.18	0.01	0.41	0.32	0.47	0.42	0.26	0.45	0.51	0.03
MgO	0.00	0.00	0.54	0.88	10.04	3.20	3.33	16.44	0.56	0.80	0.00	0.04	2.35	11.57	0.25	10.84	0.00	7.32	11.29	12.00	10.74	11.20	0.00
CaO	22.21	30.06	10.03	8.37	0.41	0.01	0.03	0.04	10.24	9.36	0.00	23.20	0.00	0.00	0.08	0.00	29.40	6.14	8.88	0.08	10.19	9.80	0.06
Na_2O	0.00	0.02	0.05	0.03	6.43	0.03	0.22	0.03	0.00	0.03	0.00	0.02	0.28	0.02	6.02	0.01	0.04	1.63	2.40	0.01	1.59	1.77	10.92
K_2O	0.00	0.02	0.00	0.00	0.02	0.00	9.73	0.02	0.00	0.01	0.01	0.02	10.20	9.79	2.23	0.01	0.00	0.62	0.25	0.06	0.37	0.30	0.03
Total	98.11	98.75	99.96	98.8	98.39	90.78	93.90	85.77	98.71	98.97	99.85	98.16	94.97	94.82	95.91	88.23	98.49	101.2	97.56	87.25	98.56	98.00	98.19
Si	2.99	1.01	2.97	3.00	7.81	1.00	3.48	2.74	3.00	3.03	0.00	2.98	3.42	2.79	2.99	2.63	1.25	7.42	6.88	2.63	6.54	6.88	2.98
Ti	0.00	0.90	0.02	0.00	0.00	0.00	0.01	0.01	0.01	0.01	1.01	0.01	0.01	0.09	0.00	0.00	0.00	0.01	0.01	0.01	0.03	0.03	0.00
Al	2.43	0.06	1.97	2.09	1.91	1.94	1.98	2.64	2.09	2.07	0.01	2.46	2.17	1.50	2.97	2.91	0.84	2.15	1.62	2.85	2.19	1.79	1.04
Cr	0.01	0.00	0.00	0.00	0.00	0.00	0.00	0.00	0.00	0.00	0.00	0.00	0.00	0.00	0.00	0.00	0.00	0.00	0.00	0.00	0.00	0.01	0.00
Fe^{3+}	0.65	0.00	0.05	0.00	0.10	0.06	0.06	0.00	0.00	0.00	0.00	0.57	0.00	0.00	0.00	0.00	0.89	0.37	0.67	0.00	0.61	0.49	0.00
Fe^{2+}	0.01	0.02	1.51	1.85	1.37	0.78	0.18	1.93	1.58	1.81	0.89	0.01	0.19	1.17	0.06	2.60	0.00	1.61	1.48	2.49	1.42	1.45	0.00
Mn	0.01	0.01	0.54	0.17	0.01	0.01	0.00	0.01	0.31	0.11	0.08	0.01	0.00	0.01	0.00	0.04	0.05	0.06	0.05	0.02	0.06	0.06	0.00
Mg	0.00	0.00	0.06	0.11	2.06	0.20	0.34	2.59	0.07	0.10	0.00	0.00	0.23	1.32	0.02	1.72	0.09	1.50	2.45	1.92	2.33	2.43	0.00
Ca	1.87	1.07	0.86	0.72	0.06	0.00	0.00	0.01	0.88	0.80	0.00	1.95	0.00	0.00	0.00	0.00	0.20	0.91	1.38	0.01	1.59	1.52	0.00
Na	0.00	0.00	0.01	0.01	1.72	0.00	0.03	0.01	0.00	0.01	0.00	0.00	0.04	0.00	0.75	0.00	0.00	0.44	0.68	0.00	0.45	0.50	0.94
K	0.00	0.00	0.00	0.00	0.00	0.00	0.84	0.00	0.00	0.00	0.00	0.00	0.87	0.95	0.18	0.00	0.00	0.11	0.05	0.01	0.07	0.06	0.00
Sum	7.97	3.06	8.00	7.95	15.04	3.99	6.92	9.94	7.94	7.93	1.99	7.99	6.93	7.83	6.97	9.90	3.33	14.58	15.26	9.94	15.29	15.22	4.96
X_{Fe}			0.96	0.95	0.40	0.80	0.35	0.43	0.96	0.95			0.45	0.47	0.75	0.60		0.52	0.38	0.56	0.38	0.37	
X_{Na}					0.97		0.03						0.04		0.81			0.32	0.33		0.22	0.25	
X_{Fe3+}	0.60				0.05	0.03						0.55						0.15	0.29		0.22	0.21	

C, core; R, rim. Data calculated using AX software (Holland & Powell, 2000 in Powell & Holland 2002 http:/www.esc.cam.ac.uk/research/research-groups/holland/ax). The amount of ferric iron was calculated from stoichiometric constraints using the programme AX (Powell & Holland, 2002). For amphibole, the Fe3+ content corresponds to the average from minimum and maximum constraints (Holland & Blundy, 1994).

Table 3. Representative microprobe analyses from sample UM.

	S_2						S_3					Post-S_3
Mineral	mu 2	pa 2	ctd 2	$g_{C\text{-INCL}}$	$g_{C\text{-MTX}}$	g_R	mu 3	pa 3	ctd 3	chl 3	ilm	chl 3b
Analysis	33	100	134	116	82	70	52	53	40	35	4	13
SiO_2	49.98	46.55	24.28	37.00	37.26	38.24	49.15	47.45	24.51	24.14	0.05	23.92
TiO_2	0.15	0.07	0.06	0.13	0.09	0.02	0.24	0.09	0.02	0.07	53.37	0.11
Al_2O_3	28.09	39.36	41.69	20.35	20.72	21.29	28.10	40.29	41.24	23.00	0.00	23.27
Cr_2O_3	0.02	0.06	0.05	0.00	0.04	0.03	0.00	0.00	0.00	0.00	0.00	0.05
Fe_2O_3	1.81	0.00	0.00	0.00	0.00	0.00	1.18	0.23	0.80	0.00	0.00	0.10
FeO	4.14	0.96	22.18	24.26	18.76	31.44	3.98	0.86	23.35	29.84	42.34	29.31
MnO	0.05	0.01	0.15	11.20	16.54	2.55	0.00	0.04	0.34	0.23	3.11	0.32
MgO	2.75	0.07	2.30	1.14	0.57	1.70	2.52	0.09	3.16	11.05	0.00	12.08
CaO	0.00	0.12	0.00	6.06	6.98	5.08	0.01	0.08	0.00	0.02	0.00	0.02
Na_2O	0.29	6.84	0.01	0.04	0.01	0.05	0.44	6.71	0.00	0.00	0.00	0.00
K_2O	10.48	0.58	0.03	0.00	0.00	0.00	10.16	0.82	0.00	0.00	0.00	0.03
Total	97.76	94.62	90.75	100.18	100.97	100.40	95.78	96.66	93.42	88.35	98.87	89.21
Si	3.33	3.00	1.01	2.99	2.99	3.05	3.32	2.99	1.00	2.59	0.00	2.53
Ti	0.01	0.00	0.00	0.01	0.01	0.00	0.01	0.00	0.00	0.01	1.02	0.01
Al	2.21	2.99	2.04	1.94	1.96	2.00	2.24	3.00	1.98	2.91	0.00	2.91
Cr	0.00	0.00	0.00	0.00	0.00	0.00	0.00	0.00	0.00	0.00	0.00	0.00
Fe^{3+}	0.09	0.00	0.00	0.08	0.06	0.00	0.06	0.01	0.03	0.00	0.00	0.01
Fe^{2+}	0.14	0.05	0.77	1.56	1.20	2.09	0.16	0.04	0.80	2.67	0.90	2.60
Mn	0.00	0.00	0.01	0.77	1.12	0.17	0.00	0.00	0.01	0.02	0.07	0.03
Mg	0.27	0.01	0.14	0.14	0.07	0.20	0.25	0.01	0.19	1.76	0.00	1.91
Ca	0.00	0.01	0.00	0.52	0.60	0.43	0.00	0.01	0.00	0.00	0.00	0.00
Na	0.04	0.85	0.00	0.01	0.00	0.01	0.06	0.82	0.00	0.00	0.00	0.00
K	0.89	0.05	0.00	0.00	0.00	0.00	0.88	0.07	0.00	0.00	0.00	0.00
Sum	6.98	6.96	3.97	8.00	8.00	7.96	6.99	6.94	4.00	9.96	1.98	10.00
X_{Fe}	0.34	0.88	0.84	0.92	0.95	0.91	0.39	0.81	0.81	0.60		0.58
X_{Fe3+}			0.84						0.81			
X_{Na}	0.04	0.95					0.06	0.93				

C, core; R, rim; INCL, inclusion in ctd 2; MTX, matrix. Data calculated using AX software (Holland & Powell, 2000 in Powell & Holland 2002 http:/www.esc.cam.ac.uk/research/research-groups/holland/ax). The amount of ferric iron was calculated from stoichiometric constraints using the programme AX (Powell & Holland, 2002). For amphibole, the Fe3+ content corresponds to the average from minimum and maximum constraints (Holland & Blundy, 1994).

Structurally lower metapelites

Sample LM is a micaschist that contains a main foliation (S_3) defined by white mica (type 3 phengite with 3.40–3.45 Si pfu, X_{Na} = 0.04 and paragonite, X_{Na} = 0.81), biotite (X_{Fe} = 0.47), epidote (type 3; X_{Fe3+} = 0.55), minor chlorite (type 3; X_{Fe} = 0.60) and quartz. The dominant Ti-bearing minerals in the matrix are Mn-rich ilmenite (MnO = 3.7 wt%, i.e. ~9% pyrophanite) and titanite (type 3), which contains up to 1.8 wt% Al_2O_3, up to 1.2 wt% FeO and up to 0.4 wt% F. S_3 parageneses also include minor proportions of bluish Ca–Na amphiboles such as winchite (Si = 7.4 pfu; X_{Na} = 0.30–0.32; X_{Fe} = 0.51–0.52) and barroisite (Si = 6.9 pfu; X_{Na} = 0.33–0.36; X_{Fe} = 0.45–0.5), and relatively abundant small crystals of dravite-rich tourmaline and apatite (Fig. 3a; Table 2).

This foliation wraps around subhedral crystals of garnet (0.5–4 mm) concentrated in the micaceous domains of the matrix, and locally included in albite porphyroblasts. Garnet is rich in inclusions, which commonly display a concentric arrangement (Figs 3a & 4a). Locally, however, they define curved or sigmoidal patterns or, more rarely, markedly rotational paths arranged as spirals (snowball garnet). Large garnet crystals display an optical zoning. The cores, referred to as garnet 1 (g1), usually lack fractures and contain very fine-grained inclusions (< 0.06 mm) of epidote (type 1, X_{Fe3+} = 0.60), titanite (type 1), rutile needles and quartz (Fig. 3a; Table 2). In general, the inclusions define a very fine foliation, S_1. The outer parts of large garnet, referred to as garnet 2 (g2), are commonly fractured and rich in coarser-grained (up to 0.7 mm) inclusions of glaucophane (Si = 7.8 pfu; X_{Na} = 0.97; X_{Fe} = 0.4; X_{Fe3+} = 0.05–0.1), chloritoid (X_{Fe} = 0.80), phengitic muscovite (type 2, Si up to 3.5 pfu) that is locally also included in chloritoid (an inclusion in an inclusion), chlorite (type 2, X_{Fe} = 0.43), rutile (locally partly replaced by ilmenite), ilmenite and quartz (Fig. 3a; Table 2). In most cases, these inclusions define a curved or sigmoidal foliation (S_2) discordant with the external foliation, S_3. The optical zoning can be correlated with the chemical zoning (Fig. 4a). Type 1 garnet core displays zoning characterized by an increase in almandine and pyrope (Alm51 → 60, Prp2 → 3) and a decrease in spessartine (Sps18 → 9). X_{Fe} remains constant (X_{Fe} = 0.96) and the proportion of grossular varies irregularly between 28 and 31%. The apparent absence of zoning in garnet 1 core in Fig. 4a is caused by the profile running slightly off the centre of the crystal; the core values were obtained by point analysis (Table 2). The garnet 1 zoned rim (Fig. 4a; profile 1) is characterized by an increase in the amount of both grossular and spessartine, compensated by the decrease of the proportion of almandine (Grs28 → 32, Sps9 → 11, Alm61 → 55). In type 2 garnet, the rimward evolution is characterized by a decrease in grossular, spessartine and X_{Fe} (Grs31 → 19, Sps11 → 1, X_{Fe} = 0.96 → 0.93), accompanied by an increase in almandine and pyrope (Alm55 → 73, Prp3 → 6).

Finally, post-S_3 minerals are locally present around garnet and are commonly composed by intergrowths of chlorite (type 3b), albite and quartz. Garnet rim is nearby replaced by chlorite flakes (type 3b; X_{Fe} = 0.56). Rare bluish-green Ca-amphibole such as Fe/Mg-hornblende (Si = 6.5–6.8 pfu; X_{Na} = 0.17–0.22; X_{Fe} = 0.51–0.38; X_{Fe3+} = 0.07–0.22) and tschermakite (Si = 6.9 pfu; X_{Na} = 0.24–0.25; X_{Fe} = 0.36–0.37; X_{Fe3+} = 0.21) grow in optical continuity on the rims of the Na–Ca amphibole. Locally, hornblende develops large crystals (> 0.3 mm long), which are arranged parallel to type 3b chlorite (Fig. 3a; Table 2). Minor proportions of sericite, stilpnomelane, carbonates and sulphides are commonly concentrated along the extensional shear planes and in some samples a pervasive growth of albite porphyroblasts occurs.

In summary, three metamorphic stages (M_1–M_3) can be distinguished in the evolution of this sample (Fig. 2). Evidence for M_1 is recorded by aligned inclusions (ep, ru, sph, q) in the cores of large garnet (g1) (Fig. 3a). M_2 is characterized by the inclusions of ctd, chl, gl, ru, ilm, mu, q preserved in garnet 2. The third stage (M_3) is recorded by the matrix foliation (S_3), comprising the assemblage chl-ep-mu-pa-bi-ru/ilm-sph-q ± g ± win/bar (Figs 2a & 3a). Finally, post-M_3 crystallization includes post-S_3 phases such as chl, hb/ts, ab, ser, stp, carb, sul.

Structurally upper metapelites

Sample UM consists essentially of quartz, white mica, chloritoid porphyroblasts and garnet. It displays layers dominated by quartz and white mica respectively. Chloritoid and garnet are concentrated in the micaceous domains. The matrix foliation (S_3) is parallel to the layering and contains quartz, muscovite (type 3, 3.06–3.08 Si pfu, X_{Na} = 0.06), paragonite (type 3; X_{Na} = 0.93), chlorite (type 3; X_{Fe} = 0.60), garnet (0.1–0.4 mm in average, locally up to 1 mm), ilmenite (MnO = 3.11 wt%, i.e. ~9% pyrophanite) and rare elongated crystals of chloritoid (type 3; 0.5–1 mm long, X_{Fe} = 0.81–0.82). It is not clear whether these chloritoid crystals really belong to the foliation or represent reoriented crystals of an older generation of chloritoid (type 2). Small crystals of tourmaline are relatively widespread in the foliation. The foliation wraps around clusters containing abundant large stubby crystals of chloritoid (type 2; up to 4 mm long, X_{Fe} = 0.80–0.84), commonly lacking a preferred orientation. Garnet, white mica and minor chlorite, quartz, rutile and ilmenite are also present in these clusters. Chloritoid porphyroblasts contain numerous tiny inclusions of tourmaline, rutile, phengitic muscovite (type 2; Si = 3.33–3.34 pfu, X_{Na} = 0.04), paragonite (type 2; X_{Na} = 0.95), garnet and locally ilmenite

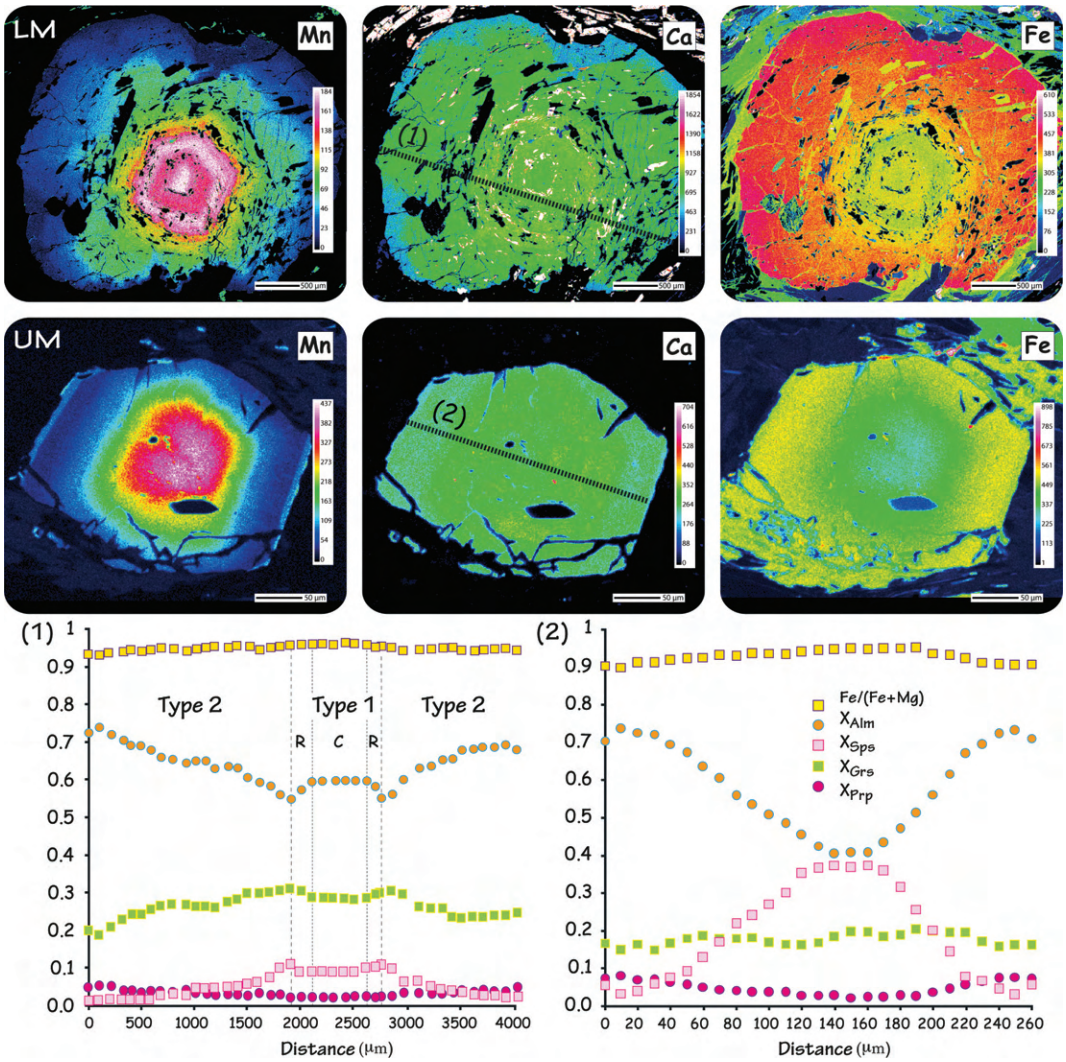

Figure 4. X-Ray maps and chemical profiles illustrating zoning of garnet porphyroblasts from the Ceán Schists. (a) Types 1–2 garnet from the lower metapelites (profile 1). (b) Garnet from the upper metapelites (profile 2). Thick dashed lines on the X-ray maps indicate the position of the profiles. The location of each garnet is indicated in Fig. 3.

that define an internal foliation, S_2. Garnet inclusions are euhedral and significantly smaller (0.02–0.06 mm) than the matrix crystals (Fig. 3b). Chemical zoning of garnet (Fig. 4; profile 2) is characterized, from core to rim, by a decrease in spessartine (Sps38 → 5), balanced by an increase in almandine (Alm41 → 73) and pyrope (Prp2 → 9). X_{Fe} decreases regularly from 0.96 to 0.93. The grossular content varies irregularly between Grs20 and Grs16, with a tendency to decrease towards the rim. Finally, an increase in spessartine (Sps5 → 7) and X_{Fe} (0.90 → 0.93) is observed in the outermost rim, together with an inversion of the general zoning pattern of pyrope (Prp9 → 8) and almandine (Alm73 → 70). Garnet inclusions in chloritoid display the same type of zoning. However, the rims lack the reversal in spessartine zoning and their composition (Alm61 Prp4 Grs18–20 Sps18) suggests that they correspond to the matrix crystals, the growth of which was arrested by the inclusion in the chloritoid (type 2). Finally, post-S_3 phases include tiny crystals of chlorite (type 3b; X_{Fe} = 0.58) and Fe–Ti-bearing oxides and hydroxides concentrated along the shear planes (Figs 2b & 3b).

In summary, it is inferred that the preserved mineral assemblages correspond to the sequence of two metamorphic stages, named M_2 and M_3, according to their textural position. The M_1 event (recorded in the LM) was not identified as inclusions in garnet cores in sample UM. This event represents the early stages of subduction, and it is not possible to infer if it was not preserved in these rocks, or if they never recorded it. Evidence for M_2 is achieved by the assemblage g-ctd-mu-pa-ru ± ilm. These minerals occur preserved as inclusions in garnet and in chloritoid porphyroblasts (type 2), and define the internal fabric S_2. M_3 corresponds to the matrix foliation S_3 and is composed of

g-chl-mu-pa-ru-ilm-q ± ctd. The post-M_3 event includes post-S_3 phases such as chlorite and Fe/Ti-oxide.

P–T ESTIMATES

Pseudosections were calculated for the *P–T* domain of interest, between 350 and 600 °C and 5–25 kbar. The diagrams have been computed using THERMOCALC 3.33–3.35 (Powell & Holland, 1988) and the internally consistent thermodynamic data set 5.5 (Holland & Powell, 1998; updated Nov. 2003). References of the mixing models for solid solutions of the phases considered in the calculations are amphibole (Diener *et al.*, 2007), clinopyroxene (Green *et al.*, 2007), chloritoid (Mahar *et al.*, 1997; White *et al.*, 2000), chlorite (Le Bayon *et al.*, 2006; based on Holland *et al.*, 1998), white mica (Coggon & Holland, 2002), plagioclase (Holland & Powell, 2003), epidote (Holland & Powell, 1998), magnetite (White *et al.*, 2002), garnet, biotite, ilmenite and hematite (White *et al.*, 2005).

The rock slab of each sample used to make the thin section was crushed and analysed by XRF to obtain the bulk composition. FeO (*v.* Fe_2O_3) was analysed by wet chemical titration. Phase relations were modelled in the chemical system MnO–Na_2O–CaO–K_2O–FeO–MgO–Al_2O_3–SiO_2–H_2O–TiO_2–Fe_2O_3 (MnNCKFMASHTO). The original compositions of the studied rocks were simplified to fit this system (Table 1). Bulk-rock compositions indicated in brackets in figure captions are those recalculated using THERMOCALC. The fluid phase was fixed as pure H_2O, initially in excess. The diagrams are shown in Figs 5 & 6. Thick lines indicate the stability field of diagnostic phases, and the thickest semitransparent lines represent the proposed *P–T* paths. White fields are divariant and increasing variance is shown with progressively darker shades. Mineral abbreviations are those used by THERMOCALC (see above).

Lower metapelites

A *P–T* pseudosection calculated in the system MnNCKFMASHTO for the analysed bulk composition with H_2O considered in excess is presented in Fig. 5a. The stability domains corresponding to the observed relicts of mineral assemblages M_1 (g, ep, sph, ru, q) and M_2 (g, ctd, chl, gl, ru, ilm, mu, q) are modelled in the HP and LT part of the pseudosection. However, most assemblages containing these phases are predicted to also contain lawsonite, which has not been observed either as inclusions in garnet or in the matrix. This hydrous mineral is stable over a wide *P–T* range in the LT blueschist facies, but rarely preserved. Pseudomorphs of this mineral can be found in the interbedded mafic rocks, so it seems possible that some of the abundant crystals of epidote present in the matrix of the schists could be the product of destabilization of lawsonite, although unquestionable pseudomorphs of this mineral were not found.

The ctd + gl paragenesis, preserved in the second generation of garnet (g2), and characteristic of this lithology, is present in the uppermost part of the diagram between 20 and 22 kbar, and 400 and 500 °C. However, in this field, the calculated composition of garnet does not correspond to that observed in g2. The isopleth values corresponding to type 2 garnet cores ($g2_C$) (Grs = 28–32% and Sps = 5–11%) intersect in the lower pressure chloritoid-absent field (at 18 kbar and 470 °C; see shaded star (1) in Fig. 5a). The isopleths that represent the garnet rim ($g2_R$) (Grs = 28–19% and Sps = 5–1%) intersect in the same field at higher pressures (~20 kbar and 490 °C; see shaded star (2) in Fig. 5a). Therefore, it is not possible to infer a reasonable *P–T* evolution for this sample because garnet zoning does not fit with the petrographic observations.

Although considering water in excess for the petrological modelling is a good approximation in most metapelites along the prograde path, crystallization of strongly hydrous minerals, like lawsonite, at high pressures and low temperatures may lead to H_2O-undersaturation as metamorphism progresses (e.g. Guiraud *et al.*, 2001; Ballèvre *et al.*, 2003; Clarke *et al.*, 2006). The available amount of H_2O also has an influence on the position of the compositional isopleths. To estimate the amount of H_2O available in the system at peak conditions, a *P–X*(H_2O) pseudosection has been calculated at 480 °C (Fig. 5b). The temperature corresponds to that estimated for the peak conditions from pseudosection approach (Fig. 5). However, other temperature values have been tested and the exact value does not have a significant effect on the result. The assemblage corresponding to the crystallization of the second generation of garnet (g-ctd-chl-gl-law*-ru-ilm + mu,q) is stable between 21 and 23 kbar under H_2O-saturated conditions, but extends to slightly lower pressures (down to 20.5 kbar) with the decreasing amount of H_2O. In this four-variant field, the isopleths corresponding to the composition of the outer part of garnet 2 ($g2_R$) (Grs = 28–19%, Sps = 5–1%) intersect between X_{H_2O} of 13.75 and 15%. Therefore, the available amount of H_2O was set to 14.375 mol.% (~14.4 mol.%), corresponding to the average of these values (see shaded area in Fig. 5b). In addition, with the estimated amount of water (14.4 mol.%), a *P–X* (Fe_2O_3) pseudosection at 480 °C has been calculated to explore the effect of varying the Fe_2O_3 content for sample LM (Fig. 5c). According to this diagram, the isopleths of interest intersect in a wide area between the Fe_2O_3 values analysed and the double of it (see shaded area in Fig. 5c). Therefore, this diagram yields no constraints on the amount of Fe_2O_3 present in the rock, although it excludes values significantly lower than the analysed one. A new *P–T* pseudosection has been computed in the MnNCKFMASHTO system for the analysed bulk composition and the amount of H_2O fixed at 14.4% (Fig. 5d; Table 1b). The diagram shows that the rock

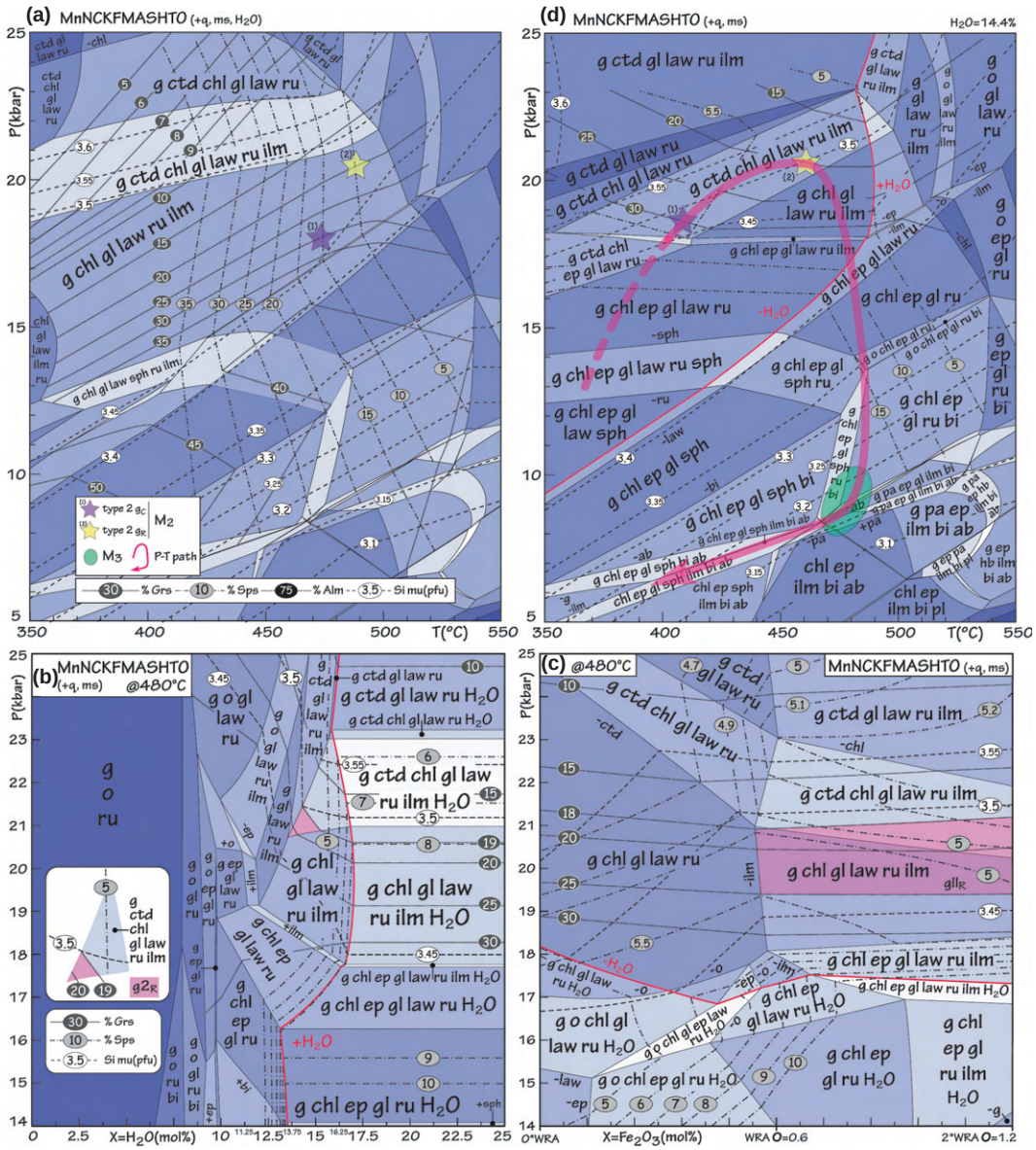

Figure 5. Sample LM [SiO_2:66.15; TiO_2:0.87; Al_2O_3:11.55; FeO:7.72; O:0.60; MnO:0.17; MgO:5.00; CaO:3.16; Na_2O:1.40; K_2O:3.37]. (a) *P–T* pseudosection with H_2O in excess. (b) *P–X*(H_2O) pseudosection calculated at 480 °C. White box in the left shows a detail of the area of interest. (c) *P–T* pseudosection with H_2O = 14.4%. (d) *P–X*(Fe_2O_3) pseudosection calculated at 480 °C with H_2O = 14.4%. WRA – original whole-rock analysis from XRF. See text and Table 1 for details.

is water saturated at LPs and HTs, but fluid absent under HP–LT conditions. The HP part of the diagram (> 18 kbar) is characterized by the presence of gl + ctd and the absence of epidote (stable at < 18 kbar). Titanite is present at pressures lower than ~15 kbar and temperatures lower than 480 °C. Rutile is stable at pressures higher than ~12 kbar or temperatures in excess of 470 °C. Biotite is stable in the LP, HT part of the diagram. The stability of paragonite is modelled only at > 470 °C and < 11 kbar (Fig. 5d).

The type 1 garnet inclusions (ep, sph, ru, q) are inferred to represent relicts of the former full assemblage g-chl*-ep-gl*-law*-ru-sph-mu*-q, suggesting that the rock passed through the corresponding stability field at 350–380 °C, 12–14 kbar. Garnet 2 cores equilibrated then in the field g-ctd-chl-gl-law*-ru-ilm + mu,q. This area is a relatively wide field at ~360–480 °C, 18–22 kbar. *P–T* conditions corresponding to the growth of garnet 2 have been refined based on the intersection between different isopleths. The isopleths corresponding to the composition of type 2 garnet core ($g2_C$) (Sps5-11, Grs28-32) and muscovite inclusions (mu2, Si = 3.45–3.50 pfu) intersect between ~18 and 19 kbar, and ~400 and 420 °C (shaded star (1) in Fig. 5d). Continuous decrease in grossular and spessartine

towards garnet 2 rims ($g2_R$) (Grs28 → 19; Sps5 → 1) suggests further heating at increasing pressure up to ~460 °C, 21 kbar (shaded star (2) in Fig. 5d). The matrix foliation (M_3) assemblage is defined by the occurrence of muscovite, paragonite, biotite, chlorite, epidote, Na–Ca amphibole, ilmenite and titanite, and the absence of chloritoid. The appearance of epidote indicates < 18 kbar for the M_3 event. Biotite is stable at < 16 kbar, ilmenite and paragonite at < 11 kbar. The presence of paragonite suggests temperatures higher than 470 °C, whereas titanite is stable at < 480 °C. Although all these phases are not stable together in a single field of the pseudosection, their stability domains are extremely close in the region ~8–10 kbar, 470–490 °C, which is inferred to represent the approximate conditions of development of the main foliation S_3 (green ellipse in Fig. 5d). This point is further discussed below. In any case, this suggests significant subisothermal decompression between M_2 and M_3. Finally, the late crystallization of albite (post-M_3) indicates pressures lower than ~8 kbar and a probable further evolution towards lower *P–T* (Fig. 5d). Although this pseudosection accounts quite well for the petrographic evolution of sample LM in general terms, the modelled composition of amphibole along the post-M_2 path does not agree with that of the observed Na–Ca amphiboles. This issue will also be discussed below.

Upper metapelites

A *P–T* pseudosection has been calculated in the MnNCKFMASHTO model system for the bulk composition obtained by XRF and the amount of FeO (*v.* Fe_2O_3) obtained by titration (Fig. 6). To check that the bulk composition does not reach H_2O-undersaturated conditions during the prograde evolution, the amount of H_2O was set so that the rock is just fluid saturated in the HP part of the field ctd-chl-pa-ep-ilm-ru + q,ms, along the LP stability limit of lawsonite. This field corresponds to a *P–T* domain through which the rock would pass, when following a hypothetical, but probable *P–T* path, before entering the stability domain of lawsonite. Indeed, as discussed above (see also Ballèvre *et al.*, 2003; Clarke *et al.*, 2006), the formation of lawsonite commonly leads to H_2O undersaturation. However, in this low-Ca metapelite, the modelled modal amount of lawsonite is very low. As a result, using this approach, the assemblages are H_2O undersaturated at low pressures and temperatures, with aqueous fluid stabilized at higher conditions (Fig. 6b). Consequently, the entire prograde evolution of this rock occurs under H_2O-saturated conditions and water is considered in excess in the following calculations.

In this *P–T* pseudosection (Fig. 6a), garnet is stable at > 500 °C, epidote is stable at < 520 °C and < 18 kbar and glaucophane is predicted to be stable from 15 to 21 kbar, at < 590 °C. Epidote and glaucophane have not been found either as inclusions or in the matrix. Therefore, based on the petrographic observations the four-variant field g-ctd-chl-pa-ilm-ru + q,ms located between 12 and 15 kbar and at > 510 °C reflects the paragenesis corresponding to the matrix foliation. However, this pseudosection cannot be used to infer the equilibration conditions of the garnet core, as the observed amount of spessartine in the garnet core (Sps38-40; Fig. 4b) is not modelled anywhere in the diagram. The maximum values predicted in the diagram are Sps15. One reason may be the relatively high amount of Fe_2O_3 analysed in this sample, uncommon in typical pelites. Although sample UM does not appear to be altered in hand specimen or in thin section, the concentration of Fe-bearing oxides/hydroxides along shear planes (Fig. 3b) suggests that the Fe_2O_3 proportion in the original rock may have been significantly lower compared with the result of the analysed bulk composition, possibly due to the circulation of oxidizing fluids. A series of pseudosections was recalculated with progressively lower amounts of Fe_2O_3 ('O' in the bulk composition), with significant changes only being observed when the amount of Fe_2O_3 was close to zero. The highest values predicted in the diagram for the spessartine and grossular isopleths calculated for the garnet core composition intersect at ~16 kbar in the three-variant field g-ctd-pa-ep-gl-ilm-ru + q,ms (shaded star in Fig. 6a). Therefore, this domain seemed the most suitable for obtaining spessartine values closer to the observed ones by modifying the amount of Fe_2O_3 in the bulk composition. Trying to estimate a reliable amount of Fe_2O_3 for this sample, a T–$X(Fe_2O_3)$ pseudosection was calculated at 16 kbar (Fig. 6c). This diagram shows that the isopleths corresponding to the composition of the garnet core intersect between 425 and 440 °C in the four-variant field g-ctd-chl-pa-gl-law-ru + q,ms for Fe_2O_3 = 0.05 (shaded star in Fig. 6c). Consequently, a *P–T* pseudosection has been recalculated with this value, O = 0.05 (Fig. 6d; Table 1b).

Compared with the original diagram, in this *P–T* pseudosection, garnet stability increases notably towards lower temperatures (from 510 to 420 °C) and glaucophane is stable at pressures higher than 11 kbar. The syn-S_3 matrix assemblage, g-ctd-chl-pa-ilm-ru + mu,q is modelled in the relatively LP and HT part of the diagram. The analysed composition of muscovite (Si < 3.1 pfu) is compatible with the equilibration of the matrix in the LP part (< 11 kbar) of this field. The isopleths corresponding to the proportions of grossular and spessartine in the garnet cores (18–20 and 38–40% respectively) intersect in the four-variant field g-ctd-chl-pa-gl-law-ru + q,ms at ~15–16 kbar, 430 °C (shaded star (1) in Fig. 6d). One of the principal characteristics of the garnet zoning observed in the sample is a continuous decrease of spessartine, whereas the grossular content remains at an approximately stable value. This evolution may only be explained if a Ca-rich phase – like epidote or lawsonite – coexists with garnet (shaded star (2) in Fig. 6d). Beyond, both

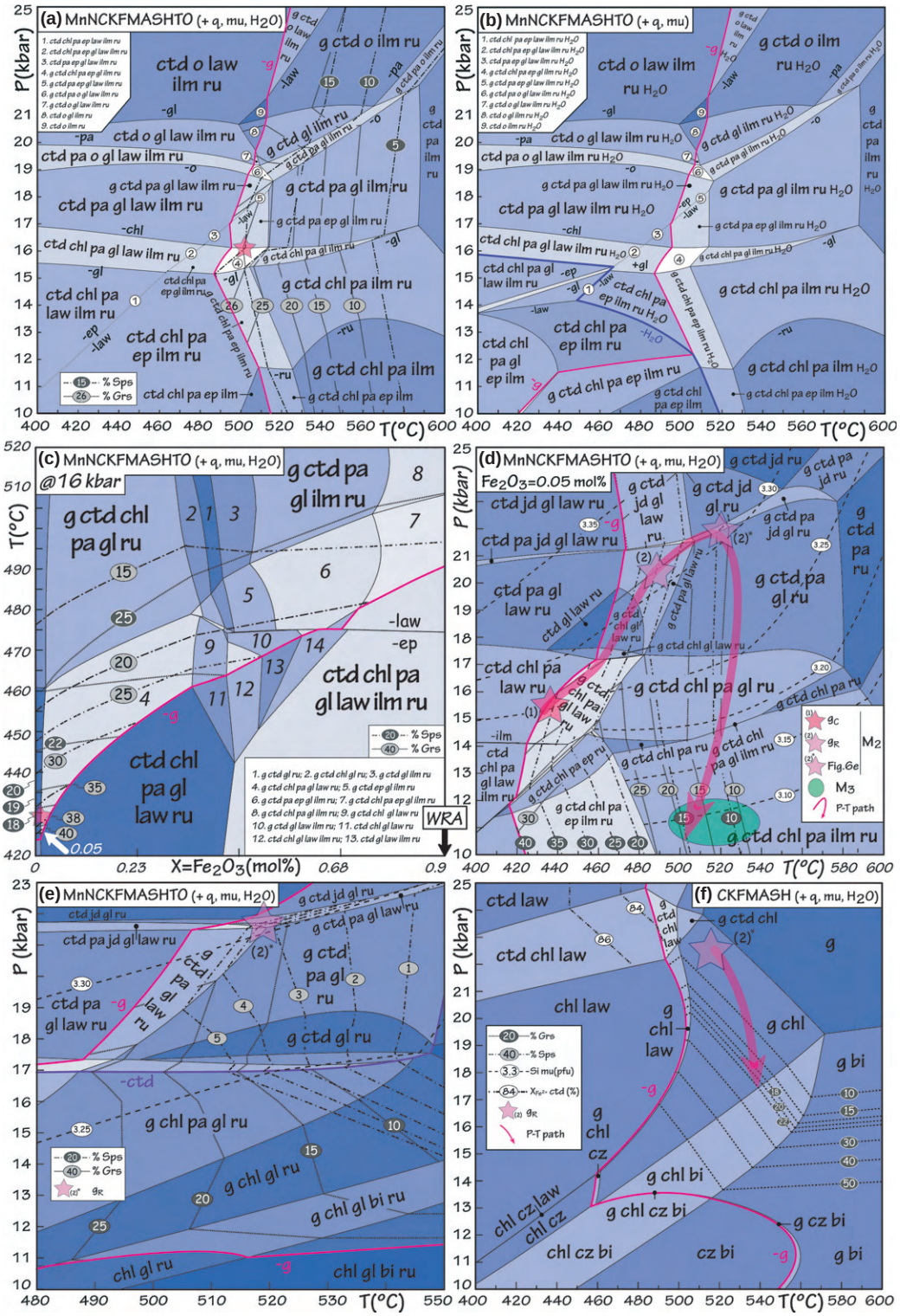

Figure 6. Sample UM [SiO_2:68.63; TiO_2:0.66; Al_2O_3:14.70; FeO: 7.68; O:0.89; MnO:0.26; MgO:3.05; CaO:0.24; Na_2O:0.98; K_2O:2.91] (a) *P–T* pseudosection with H_2O in excess. (b) *P–T* pseudosection calculated for the analysed bulk-rock composition showing dehydration along the stability limit of lawsonite. (c) *T–X*(Fe_2O_3) pseudosection calculated at 16 kbar between 420 and 520 °C; WRA – original whole-rock analysis from XRF. (d) *P–T* pseudosection with Fe_2O_3 = 0.05 mol.%. The star (2)* is inferred from Fig. 6e. (e) *P–T* pseudosection calculated for the bulk-rock composition after fractionation of garnet and chloritoid. (f) *P–T* pseudosection calculated in the CKFMASH system for the bulk-rock composition after fractionation. The star (2)* is inferred from (e). See text and Table 1 for details.

isopleths become nearly parallel and a decrease in spessartine is accompanied by a decrease in grossular, which is not observed in the sample. However, at the lawsonite-out line of the field g-ctd-pa-gl-law-ru + q,ms, for grossular contents between 15 and 20%, corresponding to those observed in the sample, the spessartine content is ~15%, whereas the value observed in the garnet rim is ~3% (Fig. 4b).

As Mn is mostly stored in garnet cores during prograde metamorphism, this inconsistency could be related to the fractionation of whole-rock composition due to the garnet growth. However, progressive removal of even all crystallizing garnet from the bulk composition does not reproduce the observed garnet rim compositions. Although much poorer in Mn than garnet, chloritoid does contain Mn and is present in significant quantities in the sample (and the model pseudosection). Furthermore, clusters of large chloritoid crystals in the sample appear shielded from the deformation associated with the development of the main foliation and could be effectively inert during the recrystallization of the rock matrix (and the crystallization of the rims of matrix garnet). Progressive fractionation of garnet and the removal of 95% of chloritoid at the point when the modelled crystallizing garnet has the composition of the rims of the garnet inclusions in chloritoid results in a Mn-poor bulk composition (Table 1b) and a corresponding *P–T* pseudosection depicted in Fig. 6e. This model reproduces the observed garnet zoning, with the garnet rims crystallizing at the lawsonite-out limit of the field g-ctd-pa-gl-law-ru + q,mu at ~21.5 kbar, 510–520 °C.

The composition of muscovite (Si ~3.3 pfu) modelled along the path inferred for the garnet growth is compatible with the values observed in the muscovite inclusions in the chloritoid porphyroblasts. Consequently, the preserved garnet zoning constrains the prograde *P–T* evolution of the sample from ~16 kbar and 430 °C to ~21 kbar and 510 °C.

The lack of further garnet growth suggests that the subsequent evolution must have occurred at constant or decreasing garnet mode. Indeed, partial garnet resorption is suggested by the local increase of spessartine at the very rim of the matrix crystals (Fig. 4). The isopleths of garnet mode (not represented) are essentially parallel to the isopleths of the spessartine content. Their position suggests an evolution dominated by decompression at approximately constant or decreasing temperature. Nevertheless, in Fig. 6e, such an evolution systematically passes through fields containing glaucophane, which is not present in sample UM. Glaucophane disappears from the model mineral assemblages at pressures lower than 8 kbar (not represented). But, all fields at pressures lower than 10–13 kbar contain biotite, which is not present in the sample either (Fig. 6e). However, it cannot actually be excluded that the rock passed although biotite-bearing fields because during cooling rocks become dry and diffusion inefficient (e.g. Guiraud *et al.*, 2001). Consequently, it is not possible to interpret the formation of the matrix assemblage using this pseudosection.

Trying to overcome these problems, the chemical system was simplified to CKFMASH using the following assumptions based on the petrographic observations. Sodium was removed from the bulk composition in the form of paragonite (which is the only Na-bearing mineral in the matrix), MnO was subtracted in the form of ilmenite containing 10% pyrophanite and the remaining TiO_2 was removed as 40% rutile and 60% ilmenite (according to the modal proportions observed in thin section). These minerals are therefore considered de facto in excess. The resulting *P–T* pseudosection (Fig. 6f) has chloritoid in the HP–LT corner of the diagram, whereas biotite is stable in the LP–HT part. The stability field that approaches best the observed matrix assemblage is g-chl (+ mu-q; + pa-ilm-ru), stable at temperatures between 460 and 560 °C and $13 < P < 23$ kbar. The *P–T* conditions of the formation of the matrix remain therefore largely unconstrained.

DISCUSSION

The two samples representative, respectively, of the lower and upper level of the Ceán Schists in the Upper Sheet of the MTU have recorded similar *P–T* evolutions characterized by a prograde *P–T* path in blueschist facies conditions, peaking at 21–22 kbar. The temperatures recorded in the UM are slightly higher than those from the LM (Fig. 7a). Both samples could have experienced a slightly different evolution due to their different position in the orogenic wedge (Fig. 7b). In the LM, the blueschist facies assemblages were overprinted by the regional foliation developed at significantly lower pressures (8–10kbar, 470–490 °C). Whereas the calculated phase diagrams and the proposed metamorphic evolution account reasonably well for the first-order petrographic observations, and are in agreement with the mineral chemistry in both the LM and the UM, several details need to be discussed.

Phase diagrams

For both rock types, the first step was to calculate a *P–T* pseudosection using the water-saturated analysed bulk composition. Confronted with the lack of compatibility between the observations and the modelling results, various compositional parameters that may significantly modify the appearance of the pseudosection have been investigated (calculating parts of *P–T* or *P/T–X* pseudosections), to obtain coherent results. For the LM, the H_2O content appeared to be the critical factor. Fe^{3+} appeared to play the major role for UM, whereas the low mode of lawsonite in this low-Ca pelite did not lead to H_2O-depletion and the rock remained H_2O saturated during the prograde evolution.

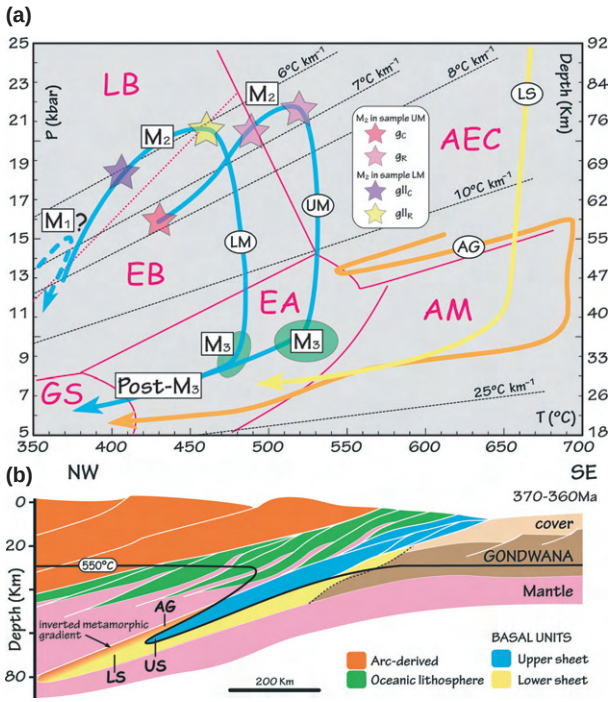

Figure 7. (a) *P–T* diagram showing the metamorphic paths of the Ceán Schists (LM and UM). The *P–T* paths for the Lower Sheet of the Malpica–Tui Unit (unpublished data) and for the Agualada Unit (Arenas *et al.*, 1997) are also included. Metamorphic facies field abbreviations: GS, greenschist facies; EA, epidote, amphibolite facies; AM, amphibolite facies; LB, lawsonite blueschist facies; EB, epidote blueschist facies and AEC, amphibole–eclogite facies (Evans, 1990 (dashed line); Maruyama *et al.*, 1996). (b) Schematic cross-section of the subduction zone operating in the NW Iberian Massif at 370–360 Ma. US, upper sheet; LS, lower sheet; AG, Agualada Unit. Based on Martínez Catalán *et al.* (1996).

In both samples, the modelling accounts quite well for the observed paragenetic sequence. It can be objected that all the phases inferred to be stable during the prograde part of the *P–T* evolution, in particular lawsonite and glaucophane, are not observed in the thin sections (with the exception of the M_2 glaucophane inclusion in garnet of the LM). However, inclusions typically only represent *remnants* of the initial full assemblages. In more detail, in the LM, the absence of lawsonite has already been discussed above and can be explained by the classic replacement by epidote during decompression. In the UM, the modelled proportion of both lawsonite and glaucophane is very low (max. 0.9 and 3–5% respectively) making their preservation improbable.

In the LM, no stability field can account for the presence of all the M_3 minerals in the S_3 foliation. The stability domains of the M_3 minerals, in particular paragonite, chlorite and titanite are extremely close to one another in the topologically complex region at around 8 kbar, 470 °C, but do not overlap. Nevertheless, it can be argued that along a *P–T* path crossing this region, a rock could develop these minerals sequentially, giving the impression of an equilibrium assemblage. Alternatively, minor changes in the parameters of the mixing models for solid solutions could change the topology sufficiently to obtain the observed assemblage in one field in this *P–T* domain.

Similarly, only small and scattered crystals of chemically heterogeneous Na–Ca amphibole are observed in the matrix foliation. However, the amphibole predicted in the pseudosection has systematically a high-glaucophane content and is relatively abundant (18–14 mol.%) down to pressures of ~8 kbar, when albite becomes stable. When reaching the field g-chl-ep-gl-sph-bi-ab + q,ms at 7 kbar, an abrupt decrease in the mode of amphibole (from 14 to 3 mol.%) coincides with an increase of the proportion of hornblende. This increase is compatible with the presence of Ca-amphiboles, such as hornblende and tschermakite, observed in the post-S_3 textural position. Although the amphibole chemical composition along the proposed *P–T* path never coincides with the analysed compositions, this qualitative evolution is compatible with the crystallization of the post-S_3 phases under relatively LP conditions, of the order of 7–8 kbar, <480 °C.

In sample UM, it is difficult to estimate reliably the equilibration conditions of the matrix foliation (S_3). In the *P–T* pseudosection calculated for the analysed bulk composition (Fig. 6a,b), the syn-S_3 matrix assemblage, g-ctd-chl-pa-ilm-ru + q,ms and the composition of the matrix muscovite (Si $<$ 3.1 pfu) suggest equilibration of the matrix in the LP and HT part of the diagram (<11 kbar, >480 °C). However, this diagram does not account for the observed garnet zoning. This can only be explained if significant fractionation of garnet and chloritoid takes place (Fig. 6e). Then, however, any reasonable *P–T* evolution systematically passes through fields containing glaucophane, which is not present in the sample, unless paragonite is forced in excess in a model system reduced effectively to CKF-MASH (Fig. 6f).

The first reason for this can be a problem with the solid-solution models. Unfortunately, even using the most recent glaucophane (Diener & Powell, 2012) and white mica (Smye *et al.*, 2010) models only results in minor differences in the pseudosection and does not solve the problem. It appears that glaucophane is 'too stable', in particular with respect to paragonite. A second reason may be related to problems with the identification of the effective bulk composition. This can be related to the deformation-enhanced fractionation of the bulk composition in a layered rock. In certain layers, the initial bulk composition undergoes fractionation during the growth of garnet and chloritoid porphyroblasts. During the subsequent deformation, a certain proportion of these porphyroblasts is preserved in undeformed domains, forming the observed chloritoid + garnet-rich clusters (Fig. 3b). Other layers and a part of the garnet–chloritoid clusters recrystallize during the formation of the S_3 foliation.

For these domains, the unfractionated composition and hence the original pseudosection (Fig. 6a,b) is still applicable. Alternatively, problems may also be related to the presence in the sample of some minerals that should have been removed from the effective bulk composition, like tourmaline. However, the crystallization of such minerals is generally related to fluid circulation, which may occur at different stages of the metamorphic evolution, resulting in the modification of the bulk composition at a point that may be difficult to estimate. Finally, a major change in the oxidation conditions during the evolution of the rock cannot be excluded, with important consequences on the stable mineral assemblages, as discussed before.

Fluid-absent prograde metamorphism

The possibility of reduced water availability in certain geodynamic scenarios allows rocks to experience a fluid-absent prograde evolution during subduction. A vast majority of metamorphic reactions have a dehydration character and produce H_2O fluid when crossed upon heating, during the prograde evolution. Accordingly, most rocks are saturated in H_2O, which is then commonly considered in excess for petrological modelling. Whereas this approach yields correct results in most cases, several exceptions merit highlighting: polycyclic evolution, partial melting, retrograde evolution and subduction metamorphism. The latter is the one that concerns this study. Metamorphism in subduction zones is characterized by low geothermal gradients (steep in a *P–T* diagram). Rocks following these gradients may cross some dehydration reactions in the 'wrong', H_2O-consuming direction. This is the case of the reactions involving lawsonite, which have a relatively 'flat' slope with lawsonite being stable at the HP, LT side. Consequently, rocks become H_2O undersaturated with important implications for the phase relations and mineral assemblages encountered in such environments (e.g. Ballèvre *et al.*, 2003; Clarke *et al.*, 2006). Unlike their metabasic counterparts, pelitic rocks are depleted in Ca and can only form limited quantities of lawsonite. It is then not common for a metapelite to experience a fluid-absent prograde metamorphism, which can be expected in metabasic rocks. Sample LM, with a composition intermediate between a pelitic and a basic one, is more likely to have undergone a fluid-absent prograde metamorphism than a pure pelite. On the contrary, sample UM, with a true pelitic composition, experienced a fluid-bearing prograde metamorphism.

Tectonic implications inferred from garnet zoning

The zoning of type 1 garnet in sample LM is not accounted for satisfactorily by the phase diagrams, as the predicted garnet composition does not match the observed one in the appropriate assemblage fields. This may have several reasons including problems with activity–composition relations in Mn-bearing systems, inappropriate estimation of the effective bulk composition or the oxidation state of the rock, or problems with the degree of H_2O (under)saturation of the mineral assemblages. However, the preserved zoning can be used to draw some qualitative inferences about the evolution of the rock. Whereas the core of garnet 1 displays a decrease in spessartine (Sps18 $\rightarrow$ 09), the rim displays a reverse trend (Sps9 $\rightarrow$ 11) to reach values characteristic of the core of garnet 2 (Sps11) (Fig. 4). Because of the strong fractionation of Mn into garnet, garnet growth is systematically associated with the decrease in the proportion of spessartine. Similarly, an increase of spessartine is typically related to a decrease in pressure and/or temperature (cf. Fig. 5). Consequently, the decrease of spessartine in the garnet 1 core can be interpreted in terms of a prograde growth. Higher spessartine content preserved in the core of garnet 2 suggests that it began to crystallize at *P–T* conditions lower than those reached by the rim of garnet 1. This suggests a slightly more complex metamorphic evolution characterized by a stage of partial exhumation during the subduction process (Fig. 7a). The reverse zoning in the garnet 1 rim may be related either to partial resorption or to a diffusional reequilibration with the garnet 2 core (e.g. Banno & Chii, 1978; Tracy, 1982). Moreover, type 1 garnet contains the earliest foliation (S_1) preserved in the Ceán Schists, which is not observed in samples from the higher structural levels. Therefore, the M_1 event was recorded at least by the LM and the first subduction-related stage is only preserved in the lower structural levels of the series (Fig. 7a).

Implications for the Variscan subduction in NW Iberia

The *P–T* results obtained from pseudosection calculations yield first-order constraints for geodynamic models: the maximum depth reached by the Upper Sheet of the MTU during subduction and the geothermal gradient. *P–T* conditions of 21–22 kbar and 460 and 520 °C in the lower and UM, respectively, correspond to an approximate depth of $\sim$76–80 km and a geothermal gradient of 6–7 °C km^{-1}, typical of relatively cold subduction zones (Fig. 7a). The relative present-day tectonostratigraphic position of the MTU (blueschist facies Upper Sheet and eclogite facies Lower Sheet) and the Basal Units of the neighbouring Ordenes Complex (Agualada Unit in Fig. 1) suggests that the original position of the different units during subduction was preserved despite the subsequent post-HP history (see e.g. Martínez Catalán *et al.*, 1996). The important relative movements between the Upper and the Lower Sheet, reflected by their tectonic extensional contact, produced the superposition of sheets located at different depths in the subduction complex, but their relative position in the subducting slab was probably not altered. The differences in the *P–T* paths (Fig. 7a) between the MTU and the Agualada Unit can be

explained on a schematic cross-section of the subduction zone at the moment when peak pressures were reached (Fig. 7b). The blueschist sheet of this study (Ceán Schists) is sandwiched between two eclogitic units: the Lower Sheet of MTU below and the Agualada Unit above. The highest temperatures during subduction are found in Agualada, where the temperature peak is ~720 °C and pressure is >14 kbar (Arenas *et al.*, 1997). The fact that highest temperatures have been recorded on the top of the subducting slab demonstrates the existence of an inverted metamorphic gradient at the top of the subducting slab. The presence of a blueschist sheet sandwiched between two eclogite facies sheets is interpreted as a consequence of the geometry of the isotherms (Fig. 7b).

CONCLUSIONS

From this study we can conclude that:

1 The Upper Sheet of the MTU recorded a three-stage metamorphic evolution involving (i) Early subduction-related medium-pressure/LT metamorphism (M_1) roughly constrained at ~ 350–380 °C, 12–14 kbar, which is only preserved in the basal part (LM) of the Ceán Schists. (ii) Subduction-related blueschist facies prograde metamorphism (M_2) going from ~19 kbar, 400 °C to 21 kbar, 460 °C in the structurally LM, and from 16 kbar 430 °C to 21–22 kbar, 520 °C in the UM. (iii) Exhumation-related metamorphism (M_3) is characterized by a decompression to 8–10 kbar, ~470–490 °C in the LM. This decompression is also recorded in the UM, but it was not possible to estimate precise *P–T* conditions.

2 The pseudosection calculations indicate that the prograde evolution in subduction zones may occur in H_2O-undersaturated conditions due to the crystallization of lawsonite, even in metapelitic rocks. This significantly influences phase equilibria and hence the *P–T* estimates.

3 The proportion of ferric iron has a strong influence on the phase equilibria of HP metapelites. However, the analysed values of Fe_2O_3 may not reflect the oxidation state during the main metamorphic evolution and are probably easily modified by superficial alteration even in apparently fresh samples. The use of P/T–$X(Fe_2O_3)$ pseudosections together with petrographic observations is then necessary to estimate the real oxidation state of the rocks and correctly evaluate the *P–T* conditions.

4 The Basal Units of the NW Iberian Massif formed part of a slab subducted beneath Laurussia at the onset of the Variscan collision. The units are separated and displaced by tectonic contacts. However, the succession of the *P–T* conditions recorded by the different basal units preserves the original thermal structure of the subduction zone in the northern margin of Gondwana.

ACKNOWLEDGEMENTS

This work was financially supported by the Spanish Project CGL2007-65338-CO2-01 (Ministerio de Ciencia e Innovación). We thank A. Fernández Larios and J. González del Tanago from the Spanish National Electronic Microscopy Centre (ICTS/CNME-UCM), and P. Lozano from the UCM, for their technical support. We are grateful to M. Ballèvre for stimulating discussions. This manuscript was significantly improved by the careful and constructive reviews from F. Korhonen and an anonymous referee. Editorial handling by R. Powell is gratefully appreciated.

REFERENCES

Abati, J., Gerdes, A., Fernández Suárez, J. *et al.*, 2010. Magmatism and early–Variscan continental subduction in the northern Gondwana margin recorded in zircons from the Basal Units of Galicia, NW Spain. *Geological Society of America Bulletin*, **122,** 219–235.

Arenas, R., Rubio Pascual, F.J., Diaz Garcia, F. & Martínez Catalan, J.R., 1995. High-pressure micro–inclusions and development of an inverted metamorphic gradient in the Santiago Schists (Ordenes Complex, NW Iberian Massif, Spain): evidence of subduction and syncollisional decompression. *Journal of Metamorphic Geology*, **13,** 141–164.

Arenas, R., Abati, J., Catalan, J.R.M., Garcia, F.D. & Pascual, F.J.R., 1997. *P–T* evolution of eclogites from the Agualada Unit (Ordenes Complex, northwest Iberian Massif, Spain): implications for crustal subduction. *Lithos*, **40,** 221–242.

Atherton, M.P. & Brotherton, M.S., 1982. Major element composition of the pelites of the Scottish Dalradian. *Geological Journal*, **17,** 185–221.

Ballèvre, M., Pitra, P. & Bohn, M., 2003. Lawsonite growth in the epidote blueschists from the Ile de Groix (Armorican Massif, France): a potential geobarometer. *Journal of Metamorphic Geology*, **21,** 723–735.

Banno, S. & Chii, S., 1978. A model to explain the Mn–enrichment in the rim of zoned garnet. *Geochemical Journal*, **12,** 253–257.

Bosse, V., Ballèvre, M. & Vidal, O., 2002. Ductile thrusting recorded by the garnet isograd from blueschist-facies metapelites of the Ile de Groix, Armorican Massif, France. *Journal of Petrology*, **12,** 485–510.

Chopin, C., 1981. Talc–Phengite: a widespread assemblage in high-grade pelitic Blueschists of the Western Alps. *Journal of Petrology*, **22,** 628–650.

Clarke, G.L., Powell, R. & Fitzherbert, J.A., 2006. The lawsonite paradox: a comparison of field evidence and mineral equilibria modelling. *Journal of Metamorphic Geology*, **24,** 715–725.

Coggon, R. & Holland, T.J.B., 2002. Mixing properties of phengitic micas and revised garnet–phengite thermobarometers. *Journal of Metamorphic Geology*, **20,** 683–696.

Diener, J.F.A. & Powell, R., 2012. Revised activity–composition models for clinopyroxene and amphibole. *Journal of Metamorphic Geology*, **30,** 131–142.

Diener, J.F.A., Powell, R., White, R.W. & Holland, T.J.B., 2007. A new thermodynamic model for clino– and orthoamphiboles in the system Na_2O–CaO–FeO–MgO–Al_2O_3–SiO_2–H_2O–O. *Journal of Metamorphic Geology*, **25,** 631–656.

Díez Fernández, R., Martínez Catalán, J.R., Arenas Martín, R. & Abati Gómez, J., 2011. Tectonic evolution of a continental subduction–exhumation channel: variscan structure of the basal allochthonous units in NW Spain. *Tectonics*, **30,** TC3009.

Díez Fernández, R., 2011. *Evolución estructural y cinemática de una corteza continental subducida: la Unidad de Malpica–Tui (NO del Macizo Ibérico)*. Nova Terra, A Coruña.

Díez Fernández, R. & Martínez Catalán, J.R., 2009. 3D Analysis of an Ordovician igneous ensemble: a complex magmatic structure hidden in a polydeformed allochthonous Variscan unit. *Journal of Structural Geology*, **31,** 222–236.

Díez Fernández, R., Martínez-Catalán, J.R., Arenas, R. & Abati, J., 2012. The onset of the assembly of Pangaea in NW Iberia: constraints on the kinematics of continental subduction. *Gondwana Research*, **22,** 20–25.

El-Shazly, A.K. & Liou, J.G., 1991. Glaucophane chloritoid–bearing assemblages from NE Oman: petrologic significance and a petrogenetic grid for high P metapelites. *Contributions to Mineralogy and Petrology*, **107,** 180–201.

Ernst, W., 1971. Metamorphic zonations on presumably subducted lithospheric plates from Japan, California and the Alps. *Contributions to Mineralogy and Petrology*, **34,** 43–59.

Ernst, W.G., 1973. Blueschists metamorphism and *P–T* Regimes in active subduction zones. *Tectonophysics*, **17,** 255–272.

Ernst, W.G., 2001. Subduction, ultrahigh-pressure metamorphism, and regurgitation of buoyant crustal slices–implications for arcs and continental growth. *Physics of the Earth and Planetary Interiors*, **127,** 253–275.

Evans, B.W., 1990. Phase relations of epidote–blueschists. *Lithos*, **25,** 3–23.

Green, E., Holland, T. & Powell, R., 2007. An order–disorder model for omphacitic pyroxenes in the system jadeite–diopside–hedenbergite–acmite, with applications to eclogitic rocks. *American Mineralogist*, **92,** 1181–1189.

Guiraud, M., Powell, R. & Rebay, G., 2001. H_2O in metamorphism and unexpected behaviour in the preservation of metamorphic mineral assemblages. *Journal of Metamorphic Geology*, **19,** 445–454.

Holland, T.J.B. & Blundy, J.D., 1994. Non-ideal interactions in calcic amphiboles and their bearing on amphibole-plagioclase thermometry. *Contributions to Mineralogy and Petrology*, **116,** 433–447.

Holland, T.J.B. & Powell, R., 1998. An internally consistent thermodynamic data set for phases of petrological interest. *Journal of Metamorphic Geology*, **16,** 309–343.

Holland, T., Baker, J. & Powell, R., 1998. Mixing properties and activity–composition and relationships of chlorites in the system $MgO–FeO–Al_2O_3–SiO_2–H_2O$. *European Journal of Mineralogy*, **10,** 395–406.

Holland, T. J. B. & Powell, R., 2003. Activity-composition relations for phases in petrological calculations: an asymmetric multicomponent formulation. *Contributions to Mineralogy and Petrology*, **145,** 492–501.

Katagas, C., 1980. Ferroglaucophane and chloritoid–bearing metapelites from the phyllite series, southern Peloponnes, Greece. *Mineralogical Magazine*, **43,** 975–978.

Kiénast, J.R. & Triboulet, C., 1972. Le chloritoïde dans les paragenèses à glaucophane, albite ou paragonite. *Bulletin de la Societe Francaise Minéralogie et de Cristallographie*, **95,** 565–573.

Korhonen, F.J., Powell, R. & Stout, J.H., 2012. Stability of sapphirine + quartz in the oxidized rocks of the Wilson Lake terrane, Labrador: calculated equilibria in NCKFMASHTO. *Journal of Metamorphic Geology*, **30,** 21–36.

Le Bayon, B., Pitra, P., Ballèvre, M. & Bohn, M., 2006. Reconstructing *P–T* paths during continental collision using multi–stage garnet (Gran Paradiso nappe, Western Alps). *Journal of Metamorphic Geology*, **24,** 477–496.

López-Carmona, A., Abati, J. & Reche, J., 2007. Metamorphic evolution of the H*P*/L*T* Ceán Schists (Malpica–Tui Unit, NW Iberian Massif). *Geogaceta*, **43,** 3–6.

López-Carmona, A., Abati, J. & Reche, J., 2010. Petrologic modelling of chloritoid–glaucophane schists from the NW Iberian Massif. *Gondwana Research*, **17,** 377–391.

Mahar, E.M., Baker, J.M., Powell, R., Holland, T.J.B. & Howell, N., 1997. The effect of Mn on mineral stability in metapelites. *Journal of Metamorphic Geology*, **15,** 223–238.

Martínez Catalán, J.R., Arenas, R., Díaz García, F., Rubio Pascual, F.J., Abati, J. & Marquínez, J., 1996. Variscan exhumation of a subducted Paleozoic continental margin: the Basal Units of the Ordenes Complex, Galicia, NW Spain. *Tectonics*, **15,** 106–121.

Martínez Catalán, J.R., Arenas, R., Díaz García, F. & Abati, J., 1997. Variscan acretionary complex of northwest Iberia: terrane correlation and succession of tectonothermal events. *Geology*, **27,** 1103–1106.

Martínez Catalán, J.R., Arenas, R., Abati, J. *et al*., 2009. A rootless suture and the loss of the roots of a mountain chain: the Variscan belt of NW Iberia. *Comptes Rendus Geosciences*, **341,** 114–126.

Maruyama, S., Liou, G. & Terabayashi, M., 1996. Blueschists and eclogites of the world. *International Geology Review*, **38,** 485–594.

Miyashiro, A., 1961. Evolution of metamorphic belts. *Journal of Petrology*, **2,** 277–311.

Platt, J.P., 1993. Exhumation of high-pressure rocks: a review of concepts and processes. *Terra Nova*, **5,** 119–133.

Powell, R. & Holland, T.J.B., 1988. An internally consistent dataset with uncertainties and correlations: 3. Applications to geobarometry, worked examples and a computer program. *Journal of Metamorphic Geology*, **6,** 173–204.

Powell, R. & Holland, T.J.B., 2002. Course Notes for THERMOCALC Workshop 2002: Calculating Metamorphic Phase Equilibria (Barcelona). CD-ROM.

Rodríguez Aller, J., 2005. *Recristalización y deformación de litologías supracorticales sometidas a metamorfismo de alta presión (Complejo de Malpica–Tui, NO del Macizo Ibérico)*. O Castro, A Coruña.

Rodríguez Aller, J., Cosca, M.A., Gil Ibarguchi, J.I. & Dallmeyer, R.D., 2003. Strain partitioning and preservation of $^{40}Ar/^{39}Ar$ ages during Variscan exhumation of a subducted crust (Malpica–Tui complex, NW Spain). *Lithos*, **70,** 111–139.

Rubio Pascual, F.J., Arenas, R., Díaz García, F., Martínez Catalán, J.R. & Abati, J., 2002. Eclogites and eclogite–amphibolites from the Santiago Unit (Ordenes Complex, NW Iberian Massif, Spain): a case study of contrasting high-pressure metabasites in a context of crustal subduction. In: *Variscan–Appalachian Dynamics: the Building of the Late Paleozoic Basement* (eds Martínez Catalán, J.R., Hatcher, R.D., Arenas, R. & Díaz García, F.). *Geological Society of America Special Paper*, **364,** 105–124.

Santos Zalduegui, J.F., Schärer, U. & Gil Ibarguchi, J.I., 1995. Isotope constraints on the age and origin of magmatism and metamorphism in the Malpica–Tuy allochthon, Galicia, NW–Spain. *Chemical Geology*, **121,** 91–103.

Smye, A.J., Greenwood, L.V. & Holland, T.J.B., 2010. Garnet–chloritoid–kyanite assemblages: eclogite facies indicators of subduction constraints in orogenic belts. *Journal of Metamorphic Geology*, **28,** 753–768.

Stern, R.J., 2005. Evidence from ophiolites, blueschists, and ultra–high pressuremetamorphic terranes that the modern episode of subduction tectonics began in Neoproterozoic time. *Geology*, **33,** 557–560.

Tracy, R.J., 1982. Compositional zoning and inclusions in metamorphic minerals. In: *Characterization of metamorphism through mineral equilibria* (ed Ferry, J. M.), Reviews in Mineralogy, **Vol. 10,** pp. 355–397, Mineralogical Society of America, Washington, DC.

Wei, C. & Powell, R., 2003. Phase relations in high-pressure metapelites in the system KFMASH ($K_2O–FeO–MgO–Al_2O_3–SiO_2–H_2O$) with application to natural rocks. *Contributions to Mineralogy and Petrology*, **145,** 301–315.

Wei, C.-J. & Song, S.-G., 2008. Chloritoid–glaucophane schist in the north Qilian orogen, NW China: phase equilibria and *P–T* path from garnet zonation. *Journal of Metamorphic Geology*, **26,** 301–316.

White, R.W., Powell, R., Holland, T.J.B. & Worley, B., 2000. The effect of TiO_2 and Fe_2O_3 on metapelitic assemblages at greenschist and amphibolite facies conditions: mineral equilibria calculations in the system K_2O–FeO–MgO–Al_2O_3–SiO_2–H_2O–TiO_2–Fe_2O_3. *Journal of Metamorphic Geology*, **18,** 497–511.

White, R.W., Powell, R. & Clarke, G.L., 2002. The interpretation of reaction textures in Fe–rich metapelitic granulites of the Musgrave Block, central Australia: constraints from mineral equilibria calculations in the system K_2O–FeO–MgO–Al_2O_3–SiO_2–H_2O–TiO_2–Fe_2O_3. *Journal of Metamorphic Geology*, **20,** 41–55.

White, R.W., Pomroy, N.E. & Powell, R., 2005. An in-situ metatexite–diatexite transition in upper amphibolite facies rocks from Broken Hill, Australia. *Journal of Metamorphic Geology*, **23,** 579–602.

Received 25 February 2012; revision accepted 24 October 2012.

3.1.6 *Partial Conclusions*

From this study we can conclude that:

1. The Upper Sheet of the Malpica-Tui Unit recorded a three-stage metamorphic evolution involving (i) Early subduction-related MP-LT metamorphism (M_1) roughly constrained at ~ 350–380ºC, 12–14 kbar, which is only preserved in the basal part (LM) of the Ceán Schists. (ii) Subduction-related blueschist-facies prograde metamorphism (M_2) going from ~19 kbar, 400ºC to 21 kbar, 460 ºC in the structurally LM, and from 16 kbar 430ºC to 21–22 kbar, 520ºC in the UM. (iii) Exhumation-related metamorphism (M_3) is characterized by a decompression to 8–10 kbar, ~ 470–490ºC in the LM. This decompression is also recorded in the UM, but it was not possible to estimate precise P–T conditions.

2. The pseudosection calculations indicate that the prograde evolution in subduction zones may occur in H_2O-undersaturated conditions due to the crystallization of lawsonite, even in metapelitic rocks. This significantly influences phase equilibria and hence the P–T estimates.

3. The proportion of ferric iron has a strong influence on the phase equilibria of HP metapelites. However, the analysed values of Fe_2O_3 may not reflect the oxidation state during the main metamorphic evolution and are probably easily modified by superficial alteration even in apparently fresh samples. The use of P/T–X(Fe_2O_3) pseudosections together with petrographic observations is then necessary to estimate the real oxidation state of the rocks and correctly evaluate the P–T conditions.

4. The basal units of the NW Iberian Massif formed part of a slab subducted beneath Laurussia at the onset of the Variscan collision. The units are separated and displaced by tectonic contacts. However, the succession of the P–T conditions recorded by the different basal units preserves the original thermal structure of the subduction zone in the northern margin of Gondwana.

3.2 *Cambre metabasic rocks*

3.2.1 *Introduction*

Lawsonite is a hydrous calcium aluminium silicate mineral (Ransome, 1895) which crystallises at MP/HP-LT conditions (e.g. Crawford & Fyfe, 1965; Liou, 1971; Heinrich & Althaus, 1988; Pawley, 1994; Schmidt & Poli, 1994; Schmidt, 1995; Comodi & Zanazzi, 1996). It has been reported in numerous terranes as an indication of blueschist- and, less frequently, eclogite-facies metamorphism (e.g. Maruyama *et al.,* 1996; Tsujimori *et al.,* 2006, with references therein), and as a marker of ancient and present subduction zones (e.g. Miyashiro, 1961; Ernst, 1971, 1973; Platt, 1993; Poli & Schmidt, 2002; Stern, 2005). During decompression, lawsonite readily breaks down to secondary minerals (epidote group minerals, white micas, chlorite and albite) and hence it is more frequently found as pseudomorphs than as fresh crystals. Due to its high H_2O content (~11.5 wt. %) lawsonite is the major water source and reservoir in the HP–LT mafic systems playing a key role in water transport in subduction zones. When modelling HP rocks, H_2O-saturated conditions are commonly assumed during subduction metamorphism, but recent studies suggests that lawsonite crystallization may lead, in some cases, to a fluid-undersaturated prograde P–T evolution (Ballèvre *et al.,* 2003; Clarke *et al.,* 2006; López-Carmona *et al.,* 2013).

Pseudomorphs after lawsonite have been described in numerous HP belts around the world such as in the Caledonian (e.g. Wu *et al.,* 1990; Spandler *et al.,* 2003; Song *et al.,* 2003), Uralian (e.g. Dobretsov *et al.,* 1974; Schulte & Sindern, 2002; Beane & Liou, 2005), Variscan (e.g. Schermerhorn & Kotsch, 1984; Ballèvre *et al.,* 2003, Rodríguez, 2005), Alaskan (e.g. Forbes *et al.,* 1984; Patrick & Evans, 1989), Alpine (e.g. Ellenberger, 1960; Gómez-Pugnaire *et al.,* 1985; Gleissner *et al.,* 2007) and Aegean belts (e.g. Dixon, 1968; Okrusch *et al.,* 1978; Able, 2001; Philippon *et al.,* 2013); as well as in the younger Caribbean (e.g. Green *et al.,* 1968; Smith *et al.,* 1999) and New Caledonian (Lillie, 1975; Clarke *et al.,* 1997, with more references therein; Spandler *et al.,* 2003). Nevertheless, relicts of lawsonite included in the pseudomorphs have been found only in very few locations (e.g. Pognante, 1989; Sperry, 2000; Able & Brady, 2001; Schulte & Sindern, 2002; Fitzherbert *et al.,* 2003; López-Carmona *et al.,* 2011).

The MTC is located in the NW section of the Iberian Massif, constituting the westernmost outcrop of the internal areas of the European Variscan belt. The MTC can be separated in two tectonically juxtaposed sequences with different tectonometamorphic evolution: (i) a lower sequence, the so called Malpica-Tui Unit (MTU), dominated by felsic orthogneisses and turbiditic metasedimentary rocks and (ii) an upper sequence, the so called Ceán Unit, that comprises metasediments intercalated with MORB-type metavolcanic rocks (Arps, 1981).

They correspond respectively to the Lower and Middle Allochthon of the Variscan nappe stack in the Ibero-Armorican Arc (Ballèvre *et al.*, submitted). Peak metamorphic conditions in the MTU are in the intermediate temperature eclogite facies (P≈25kbar and T≈610ºC; Rodríguez, 2005) and have been constrained at ca. 370 Ma by U-Pb on zircon (Abati *et al.*, 2010). On the other hand, peak conditions in the Ceán Unit are in the blueschist-facies conditions (Rodríguez, 2005; López-Carmona *et al.*, 2010; 2013) and the HP event is constrained by a single $^{40}Ar/^{39}Ar$ age on muscovite of 348 ± 8 Ma (Rodríguez *et al.*, 2003).

Pseudomorphs after lawsonite were first reported by Rodríguez *et al.*, (2003) in the metabasic rocks of the Ceán Unit. However, a detailed petrographic and thermobarometric study of these rocks has never been done, and constitutes the main objective of this research. In order to understand the tectonic evolution and the apparent metamorphic zoning of the MTC, particular attention is paid to the relations of the metamorphic assemblages with the deformational fabrics. Preliminary studies on the metabasic rocks using conventional thermobarometric technics suggest peak conditions in the epidote-blueschist facies (minimum P = 1.4–1.8 GPa and T = 440–525 °C; Rodríguez, 2005). Numerical modelling of phase equilibrium in the interbedded metasediments indicates that this sequence developed a metamorphism in the blueschist-facies conditions constrained at ca. 1.9–2.2 GPa, 460–520 °C (López-Carmona *et al.*, 2013). Studying the P–T evolution of the retrogressed lawsonite pseudomorph-bearing metabasic rocks through pseudosection approach aims to establish a P–T evolution for the Ceán Unit in the MTC and associate it with the different stages of the subduction- vs. exhumation-related deformations.

The contact between the upper and the lower sequences of the MTC (i.e. between the Lower and the Middle Allochthon) is marked by a several metres thick layer of mylonites and ultramylonites located at the base of the metabasic rocks known as the Bembibre-Ceán Detachment. This detachment is part of the Bembibre–Pico Sacro detachment system (formed by the Bembibre-Ceán and the Pico Sacro detachments; see Gómez Barreiro *et al.*, 2010 and Díez Fernández *et al.*, 2012a) and resulted from a regional-scale extensional episode that reactivated pre-existing tectonic contacts. It is thought to be coeval with late orogenic collapse and widespread magmatism, representing its upper crustal expression (cf. Gómez Barreiro *et al.*, 2007; Díez Fernández *et al.*, 2012a). However, its precise age remains unconstrained. Dating the formation of this mylonite and the blueschist-facies fabric in the Ceán Unit by $^{40}Ar/^{39}Ar$ step heating constitutes the second purpose of this study. Considering the above objectives, an attempt to establish possible equivalences between the Lower and Middle Allochthons in the MTC and similar terranes in the southern Armorican Massif, along the Ibero-Armorican Arc, will be carried out.

3.2.2 *Retrogressed lawsonite blueschists from the NW Iberian Massif:* P–*T constraints from numerical modelling and $^{40}Ar/^{39}Ar$ geochronology*

LÓPEZ-CARMONA, A., ABATI, J., PITRA, P. & LEE, J.K.W. SUBMITTED TO CONTRIBUTIONS TO MINERALOGY AND PETROLOGY (under review)

Contributions to Mineralogy and Petrology

Retrogressed lawsonite blueschists from the NW Iberian Massif: P-T constraints from numerical modelling and 40Ar/39Ar geochronology

--Manuscript Draft--

Manuscript Number:	
Full Title:	Retrogressed lawsonite blueschists from the NW Iberian Massif: P-T constraints from numerical modelling and 40Ar/39Ar geochronology
Article Type:	Original Paper
Keywords:	lawsonite blueschist; pseudomorphs after lawsonite; H2O; Ibero-Armorican Arc
Corresponding Author:	Alicia López-Carmona, Ph.D. student Universidad Complutense de Madrid Madrid, SPAIN
Corresponding Author Secondary Information:	
Corresponding Author's Institution:	Universidad Complutense de Madrid
Corresponding Author's Secondary Institution:	
First Author:	Alicia López-Carmona, Ph.D. student
First Author Secondary Information:	
Order of Authors:	Alicia López-Carmona, Ph.D. student
	Jacobo Abati, Ph.D.
	Pavel Pitra, Ph.D.
	James K.W. Lee, Professor
Order of Authors Secondary Information:	

ABSTRACT

Blueschist-facies terranes in the Variscan Ibero-Armorican Arc are restricted to scarce and relatively small areas. One of these examples is the Ceán Unit, which is the westernmost exposure of the middle allochthonous sheet of the Variscan belt in the Malpica-Tui Complex (NW Iberian Massif). The Ceán Unit is a highly condensed metamorphic succession with a lower part in the blueschist facies and an upper part without HP relicts. It comprises variable proportions of glaucophane-chloritoid-bearing metapelites and mafic rocks with abundant well-preserved pseudomorphs after euhedral lawsonite. The metamorphic evolution of the metabasic rocks has been constrained in the P–T space through pseudosection approach and is characterized by H_2O-undersaturated prograde evolution induced by the crystallization of lawsonite. Peak conditions in the blueschist/LT-eclogite facies have been constrained at ca. 2.2 GPa and 560 °C. Exhumation-related metamorphism is characterized by a nearly isothermal decompression from the lawsonite-bearing fields to fields with stable albite at P ≈ 1 GPa. This lead to the pseudomorphism of lawsonite in the early decompression stages, and a subsequent amphibolite-greenschist facies overprint at P < 0.8 GPa and T ≈ 440–480 °C. The preservation of the lawsonite crystal shape despite complete retrogression indicates that pseudomorphism occurred as a static process and that particular levels of the blueschist host rock were not affected by penetrative deformation during exhumation. $^{40}Ar/^{39}Ar$ step-heating of phengitic muscovite from the pelitic schists interbedded with the lawsonite pseudomorph-bearing metabasic rocks yield plateau ages of ca. 363±2 Ma and 354±1 Ma. The older age is interpreted as the age of the peak blueschist-facies metamorphism. $^{40}Ar/^{39}Ar$ dating of muscovite from the quartzo-feldspathic mylonites of the Bembibre-Ceán detachment, at the base of the Ceán Unit, yields an age of ca. 337±3 Ma, interpreted as the age of the post-nappe extensional tectonics. Similar data obtained from the blueschists of Ile de Groix (Armorican Massif; Bosse *et al.,* 2005), support the equivalence of the Ceán Unit and the Upper Unit of Ile de Groix along the Ibero- Armorican Arc, and suggest that these units share a blueschist-facies event constrained at ca. 360–370 Ma, that is inferred to represent the Late Devonian-Early Carboniferous subduction of the northern margin of Gonwana beneath Laurussia.

KEY WORDS: lawsonite blueschist; pseudomorphs after lawsonite; H_2O; Ibero-Armorican Arc

INTRODUCTION

Lawsonite is a hydrous calcium aluminium silicate mineral (Ransome, 1895) which crystallises at medium- to high-pressure (HP) and low-temperature (LT) conditions (e.g. Crawford and Fyfe, 1965; Liou, 1971; Heinrich and Althaus, 1988; Pawley, 1994; Schmidt and Poli, 1994; Schmidt, 1995; Comodi and Zanazzi, 1996). It has been reported in numerous terranes as an indication of blueschist- and, less-frequently, eclogite-facies metamorphism (e.g. Maruyama *et al.,* 1996; Tsujimori *et al.,* 2006, with references therein), and as a marker of

ancient and present subduction zones (e.g. Miyashiro, 1961; Ernst, 1971, 1973; Platt, 1993; Poli and Schmidt, 2002; Stern, 2005). During decompression, lawsonite readily breaks down to secondary minerals (epidote group minerals, white micas, chlorite and albite) and hence it is more frequently found as pseudomorphs than as fresh crystals. Due to its high H_2O content (~11.5 wt. %) lawsonite is the major water source and reservoir in the HP–LT mafic systems playing a key role in water transport in subduction zones. When modelling HP rocks, H_2O-saturated conditions are commonly assumed during subduction metamorphism, but recent studies suggests that lawsonite crystallization may lead, in some cases, to a fluid-undersaturated prograde P–T evolution (Ballèvre *et al.,* 2003; Clarke *et al.,* 2006; López-Carmona *et al.,* 2013).

Pseudomorphs after lawsonite have been described in numerous HP belts around the world such as in the Caledonian (e.g. Wu *et al.,* 1990; Spandler *et al.,* 2003; Song *et al.,* 2003), Uralian (e.g. Dobretsov *et al.,* 1974; Schulte and Sindern, 2002; Beane and Liou, 2005), Variscan (e.g. Schermerhorn and Kotsch, 1984; Ballèvre *et al.,* 2003, Rodríguez, 2005), Alaskan (e.g. Forbes *et al.,* 1984; Patrick and Evans, 1989), Alpine (e.g. Ellenberger, 1960; Gómez-Pugnaire *et al.,* 1985; Gleissner *et al.,* 2007) and Aegean belts (e.g. Dixon, 1968; Okrusch *et al.,* 1978; Able, 2001; Philippon *et al.,* 2013); as well as in the younger Caribbean (e.g. Green *et al.,* 1968; Smith *et al.,* 1999) and Ne°w Caledonian (Lillie, 1975; Clarke *et al.,* 1997, with more references therein; Spandler *et al.,* 2003). Nevertheless, relicts of lawsonite included in the pseudomorphs have been found only in very few locations (e.g. Pognante, 1989; Sperry, 2000; Able and Brady, 2001; Schulte and Sindern, 2002; Fitzherbert *et al.,* 2003; López-Carmona *et al.,* 2011).

The Malpica-Tui Complex (MTC; Fig. 1) is located in the NW section of the Iberian Massif, constituting the westernmost outcrop of the internal areas of the European Variscan Belt. The MTC can be separated in two tectonically juxtaposed sequences with different tectonometamorphic evolution: (i) a lower sequence, the so called Malpica-Tui Unit (MTU), dominated by felsic orthogneisses and turbiditic metasedimentary rocks and (ii) an upper sequence, the so called Ceán Unit, that comprises metasediments intercalated with MORB-type metavolcanic rocks (Arps, 1981). They correspond respectively to the Lower and Middle Allochthon of the Variscan nappe stack in the Ibero-Armorican Arc (Ballèvre *et al.,* submitted). Peak metamorphic conditions in the MTU are in the intermediate temperature eclogite facies (P≈25kbar and T≈ 610°C; Rodríguez, 2005) and have been constrained at ca. 370 Ma by U-Pb on zircon (Abati *et al.,* 2010). On the other hand, peak conditions in the Ceán Unit are in the blueschist-facies conditions (Rodríguez, 2005; López-Carmona *et al.,* 2010; 2013) and the HP event is constrained by a single $^{40}Ar/^{39}Ar$ age on muscovite of 348±8 Ma (Rodríguez *et al.,* 2003). Pseudomorphs after lawsonite were first reported by Rodríguez *et al.,* (2003) in the metabasic rocks of the Ceán Unit. However, a detailed petrographic and thermobarometric

study of these rocks has never been done, and constitutes the main objective of this research. In order to understand the tectonic evolution and the apparent metamorphic zoning of the MTC, particular attention is paid to the relations of the metamorphic assemblages with the deformational fabrics. Preliminary studies on the metabasic rocks using conventional thermobarometric technics suggest peak conditions in the epidote-blueschist facies (minimum P = 1.4–1.8 GPa and T = 440–525 °C; Rodríguez, 2005). Numerical modelling of phase equilibrium in the interbedded metasediments indicates that this sequence developed a metamorphism in the blueschist-facies conditions constrained at ca. 1.9–2.2 GPa, 460–520 °C (López-Carmona *et al.,* 2013). Studying the P–T evolution of the retrogressed lawsonite pseudomorph-bearing metabasic rocks through pseudosection approach aims to establish a P–T evolution for the Ceán Unit in the MTC and associate it with the different stages of the subduction- vs. exhumation-related deformations.

The contact between the upper and the lower sequences of the MTC (i.e. between the Lower and the Middle Allochthon) is marked by a several metres thick layer of mylonites and ultramylonites located at the base of the metabasic rocks known as the Bembibre-Ceán Detachment. This detachment is part of the Bembibre–Pico Sacro detachment system (formed by the Bembibre-Ceán and the Pico Sacro detachments; see Gómez Barreiro *et al.,* 2010 and Díez Fernández *et al.,* 2012a) and resulted from a regional-scale extensional episode that reactivated pre-existing tectonic contacts. It is thought to be coeval with late orogenic collapse and widespread magmatism, representing its upper crustal expression (cf. Gómez Barreiro *et al.,* 2007; Díez Fernández *et al.,* 2012a). However, its precise age remains unconstrained. Dating the formation of this mylonite and the blueschist-facies fabric in the Ceán Unit by $^{40}Ar/^{39}Ar$ step heating constitutes the second purpose of this study. Considering the above objectives, an attempt to establish possible equivalences between the Lower and Middle Allochthons in the MTC and similar terranes in the southern Armorican Massif, along the Ibero-Armorican Arc, will be carried out.

GEOLOGICAL BACKGROUND

The MTC is part of the Ibero-Armorican Arc (IAA), one of the main macrostructures of the Variscan belt in Western Europe (e.g. Suess, 1888; Stille, 1924; Lotze, 1929; Bard *et al.,* 1971; Ribeiro *et al.,* 1995). The arc can be followed from Brittany, across the Cantabrian Sea (Bay of Biscay), to western Iberia (Fig. 1). The orogenic-scale folding is interpreted as a late feature, developed essentially during the late Carboniferous-early Permian (ca. 310–295 Ma) (Weil *et al.,* 2010; Pastor-Galán *et al.,* 2011), resulting from the rotation around a vertical axis of an initially linear orogen (e.g. Brun and Burg. 1982; Weil *et al.,* 2001; Martínez Catalán, 2011; Weil *et al.,* 2013) and is thought to be formed at a lithospheric scale (Gutiérrez-Alonso *et al.,* 2004; Pastor-Galán *et al.,* 2012). Previously, during the early phases of the Varican orogeny, a huge nappe stack was built forming a complex of allochthonous sheets emplaced

upon the sequences deposited on the passive margin of north Gondwana. The remnants of this ensemble exists as allegedly exotic terranes that can be separated into three lithostratigraphic units recently grouped as Upper, Middle and Lower Allochthons, stacked above an underlying Parautochthon on both sides of the Bay of Biscay (Ballèvre *et al.,* submitted). These units bear the imprint of an early Palaeozoic subduction and can be correlated across north-west Iberia and the southern Armorican Massif throughout the IAA (Ballèvre *et al.,* 2009; Martínez Catalán *et al.,* 2009; Ballèvre *et al.,* submitted; Fig. 1). The polarity of the subduction has been deduced by the presence of a pressure gradient along the basal part of the nappe stack, where pressure increases from east to west indicating that the subduction had a significant westward component in present coordinates (Martínez Catalán *et al.,* 1996). The paleodip of the subduction zone has been estimated from P–T conditions and thermal modelling at 15° to 20° (Alcock *et al.,* 2005), and kinematic indicators in HP fabrics are in agreement with this reconstruction suggesting top to the northwest movement (Díez Fernández *et al.,* 2012b).

Knowing the west-directed component of subduction, the characteristics of each terrane suggests that the Middle Allochthon would occupy an oceanward position compared to the Lower Allochthon before the Variscan collision (cf. Martínez Catalán *et al.,* 1996; 2002; 2007; 2009; Ballèvre *et al.,* submitted). Thus, the Lower Allochthon is interpreted as a slice of a continental crust, whereas the Middle Allochthon is interpreted to represent a volcano-sedimentary sequence viewed as a more distal part of the same continental margin transitional to an oceanic domain (cf. Rodríguez *et al.,* 2003; Díez Fernández *et al.,* 2010; López-Carmona *et al.,* 2010; 2013). The Lower Allochthon represents the outermost sections of the north Gondwana continental margin subducted beneath Laurussia during late Devonian (Martínez Catalán *et al.,* 1996; 1997; Arenas *et al.,* 1997; Ballèvre *et al.,* 2009; Martínez Catalán *et al.,* 2009; Ballèvre *et al.,* submitted). This subduction marked the final closure of the existing Cambro-Ordovician ocean/s (Rheic?) and the last stages of the assembly of Pangea (Matte, 1986; Scotese, 1997; Stampfli and Borel, 2002; Gutiérrez-Alonso *et al.,* 2008; Martinez Catalan *et al.,* 2009; Díez Fernández *et al.,* 2012b).

The westernmost exposure of the Middle Allochthon in the NW Iberian Massif is the Ceán Unit. It forms the upper tectonic sheet of the MTC and is constituted by the Ceán pelitic schists and the Cambre metabasic rocks, the principal objective of this paper.

BLUESCHISTS IN THE MIDDLE ALLOCHTHON OF THE IAA

Blueschist-facies rocks in the south Armorican domain are particularly well known from Ile de Groix (Barrois, 1883; Cogné *et al.,* 1966; Felix, 1972; Ballèvre *et al.,* 2003, Bosse *et al.,* 2002; 2005), but also outcrop further to the SE in the Bois-de-Cené unit in the Vendée area (Guiraud *et al.,* 1987) and the Saint-Martin des Noyers formation (Thiéblemont *et al.,* 1988).

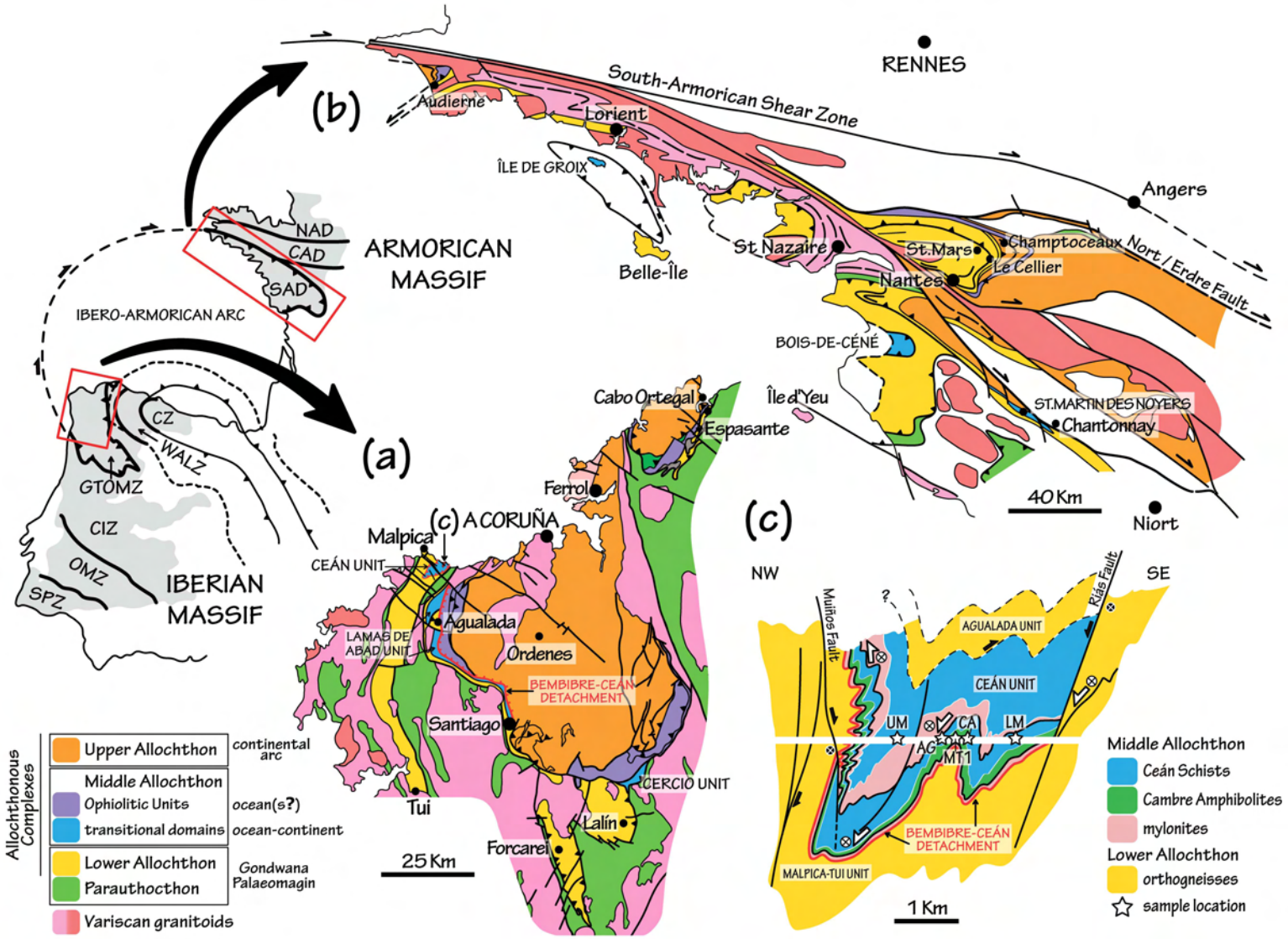

Fig. 1. Location of the Ibero-Armorican Arc in the Variscan orogen. Geological map of the Allochthonous Units in the (a) NW Iberian Massif and in the (b) South Armorican Domain. c) Cross-section for the Middle Allochthon in the Malpica-Tui Complex. The stars indicate sample location. CZ–Cantabrian Zone; WALZ–West Asturoccidental-leonese Zone; GTOMZ–Galicia-Tras-os-Montes Zone; CIZ–Central Iberian Zone; OMZ–Ossa-Morena Zone; SPZ–South Portuguese Zone; NAD–North Armorican Domain; CAD–Central Armorican Domain; SAD–South Armorican Domain. Modified from Ballèvre et al. (2009), Martínez Catalán et al. (2009) and Ballèvre et al. (submitted).

In the Iberian Massif, equivalent blueschists are usually highly retrogressed, and they were not described until much later, firstly in the Trás-os-Montes region of north Portugal (Ribeiro, 1976; Munhá and Ribeiro, 1984; Gil Ibarguchi and Dallmeyer, 1991). Paradoxically, although fresh lawsonite has never been found in the well-preserved blueschists from Ile de Groix, it has been described in the Morais Complex of north Portugal (Schermerhorn and Kotsch, 1984). Blueschist-facies metapelites and highly retrogressed blueschists have been also reported in the Middle Allochthonous units of Galicia, in the Órdenes Complex (Martínez Catalán *et al.,* 1996) and in the Ceán Unit of the MTC (Rodríguez *et al*, 2003; López-Carmona *et al.,* 2010). Within the last, the Cambre metabasic rocks (Llana-Fúnez, 2001; Rodríguez, 2005) are the subject of this study.

Over the last decade, several correlations between the MTC and equivalent units in the south of the Armorican Massif have been established (Rodríguez *et al.,* 2003; Ballèvre *et al.,* 2009; Martínez Catalán *et al.,* 2009; Abati *et al.,* 2010). From their age and tectonometamorphic evolution, correlations between the upper sequence of the MTC (the Ceán Unit), and the Ile de Groix materials are widely accepted. Both terranes show similar lithologic associations constituted by variable proportions of glaucophane-chloritoid-bearing metapelites and mafic rocks with pseudomorphs after lawsonite. The Upper Unit of Ile de Groix and the Ceán Unit share a blueschist-facies event constrained by $^{40}Ar/^{39}Ar$ dating of phengitic muscovite at 360–370 Ma in metapelites from Ile de Groix (Rodríguez *et al.,* 2003; Bosse *et al.,* 2005).

RETROGRESSED BLUESCHISTS: THE CAMBRE METABASIC ROCKS

The Cambre metabasic rocks are intensely foliated amphibolites and greenschists with N-MORB chemical composition (Table 1) (Arps, 1981; González Lodeiro *et al.,* 1984; Rodríguez, 2005). They outcrop in the upper structural levels of the MTC, at the base of the Pazos Synform, and together with the pelitic schists constitute the Ceán Unit (Fig. 1c). The Cambre metabasic rocks are immediately overlying the so-called Bembibre-Ceán detachment, which marks the limit between the Lower and the Middle Allochthon in the MTC (Díez Fernández *et al.,* 2011; Figs. 1a–b, 2a). The dominant rock type is teal/bluish-green fine to medium-grained garnet-bearing amphibolite with frequent levels containing pseudomorphs after lawsonite. At the base of the sequence, the metabasic rocks are interbedded with chloritoid–glaucophane-bearing metapelites (Fig. 2b–c) (López-Carmona *et al.,* 2010; 2013). The lawsonite pseudomorph-bearing amphibolite levels are < 10 m thick (Fig. 2d–f). Going upwards in the sequence, lawsonite pseudomorphs disappear gradually, but quickly, and amphibolites grade into greenschists with garnet porphyroblasts dispersed in a dark green matrix (Fig. 2g, i). The greenschists contain epidote-rich layers several centimetres up to 1–2 metres thick (Fig. 2h). Finally, the top of the succession is dominated by greenschists with albite porphyroblasts

("prasinites") (Rodríguez, 2005; Fig. 2j) and fine-grained pelitic schists without garnet (Fig. 2k).

TABLE 1. (a) Bulk-rock composition from XRF analyses of sample CA expressed in wt. % and mol. %. (b) Bulk-rock compositions normalized with THERMOCALC expressed in mol. %.

(a)	wt%	mol%	(b)	NCKFMASHTO (mol%)			
SiO_2	47.89	53.28	SiO_2	35.52	35.52	35.52	35.52
TiO_2	1.92	1.60	TiO_2	1.07	1.07	1.07	1.07
Al_2O_3	13.36	8.76	Al_2O_3	5.84	5.84	5.84	5.84
FeO	8.49	7.90	FeO	5.23	5.23	5.23	5.23
Fe_2O_3*	4.20	1.76	O	1.17	1.17	O-2*O	1.20
MnO	0.22		MgO	7.86	7.86	7.86	7.86
MgO	7.11	11.79	CaO	7.81	7.81	7.81	7.81
CaO	10	11.72	Na_2O	2.1	2.1	2.1	2.10
Na_2O	2.92	3.15	K_2O	0.03	0.03	0.03	0.03
K_2O	0.07	0.05	H_2O	*in excess*	O-25	7.50	7.50
P_2O_5	0.13		Fig.	9a	9b	9c	9d

* $Fe_2O_{3\,(T)}$ was measured by the XRF and FeO by wet chemical titration. The amount of Fe_2O_3 is calculated stoichiometrically as: [total iron/1.43–(FeO/1.286)*1.43].

Deformation in the Cambre metabasic rocks is highly heterogeneous. Whereas in some levels the lawsonite pseudomorphs preserve the euhedral shape (Fig. 3a-1), towards the top of the sequence the pseudomorphs are strongly stretched and almost indistinguishable from the matrix (Fig. 3a-2). Mylonitic to ultra-mylonitic layers are localized in the basal part, at the contact with the gneisses of the Lower Allochthon, along the Bembibre-Ceán detachment (Figs. 1a-b, 2a). However, deformation history in the Cambre metabasic rocks would include several compressive, extensional and strike-slip phases (Díez Fernández *et al.,* 2011).

Three foliations, with uneven development at different structural levels, have been identified. The main foliation in the lower part of the sequence is defined by the shape preferred orientation of amphibole, epidote, albite, chorite and muscovite. This foliation wraps gently around mostly euhedral crystals of garnet and lozenge-shaped aggregates containing epidote, chlorite, albite and white micas, interpreted as pseudomorphs after lawsonite (Fig. 3a-1, b; cf. Ballèvre *et al.,* 2003; Rodríguez *et al.,* 2003). Unoriented, or partially oriented, relicts of an

early assemblage preserved in the core of garnet porphyroblasts are related to an incipient foliation S_1. A second foliation, S_2, develops in the garnet rim and is continuous with the matrix foliation, suggesting syntectonic growth of garnet (Fig. 3c). Pseudomorphs after lawsonite comprise oriented crystals of epidote and stretched clusters interpreted as inclusions in the original lawsonite crystals. Stretched clusters define a slightly curved internal foliation, generally oblique to but continuous with the matrix foliation (Fig. 3b), suggesting that the crystallisation of lawsonite is also contemporaneous with the development of S_2. Clusters are compoused of rutile/ilmenite and titanite and of chlorite-albite aggregates. Their mineralogy indicates that chlorite-albite aggregates may represent pseudomorphs after a former phase, most likely, glaucophane (cf. Le Bayon *et al.*, 2006; Rodríguez, 2005). The preservation of the euhedral shape of the former lawsonite crystals suggests that pseudomorphism occurred as a static process and these rocks were not affected by any further ductile deformation (cf. Ballèvre *et al.*, 2003; Philippon *et al.*, 2013).

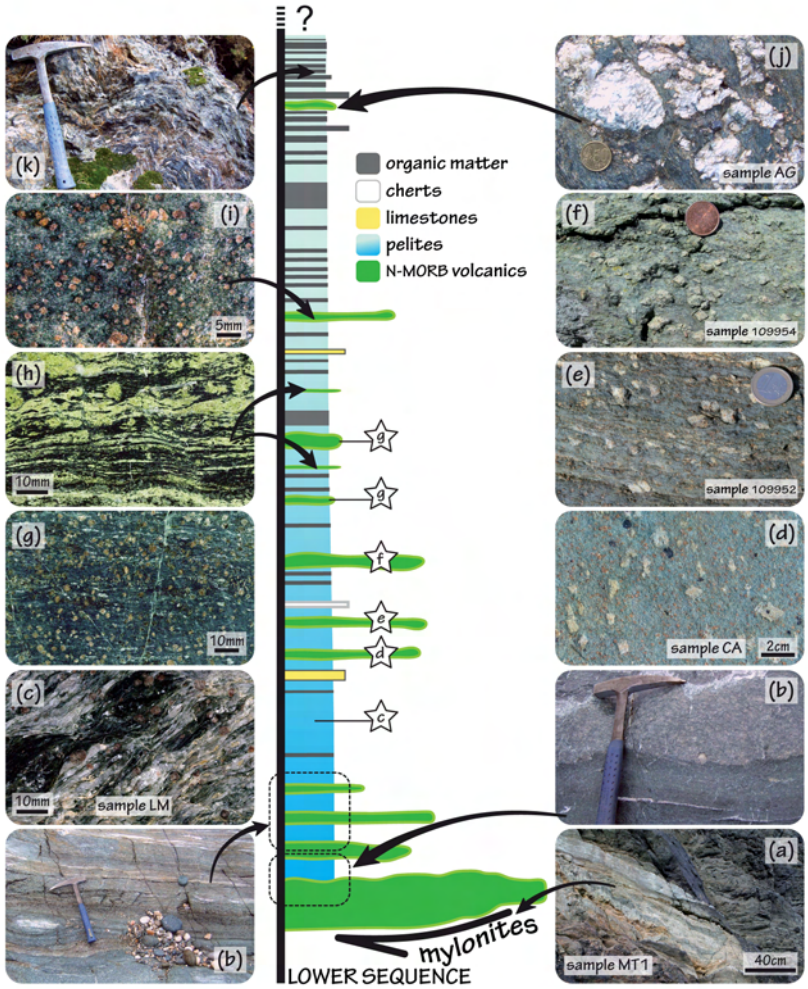

Fig 2. Idealized stratigraphic column for the Ceán Unit in the Malpica-Tui Complex. Photographs showing field aspects of the Bembibre-Ceán Detachment (a), metasediments intercalated with metavolcanics (b), Ceán pelitic schists (c and k) and Cambre metabasic rocks (d-j). The intermediate part of the sequence is dominated by lawsonite and garnet-bearing amphibolites (d-f) that going upwards grade into greenschists with garnet porphyroblasts (g, i) that contain epidote-rich layers (h). The top of the succession is dominated by greenschists with albite porphyroblasts (j) and bituminous schists without garnet (k). Stars and arrows indicate the location of the photographs in each level. Sample locations are also indicated. The stratigraphic column is modified from Díez Fernández (2011).

To the top of the succession the main foliation is defined by the shape preferred orientation of amphibole, epidote, chlorite, albite and minor amounts of muscovite, and is parallel to boudined layers of quartz and, locally, epidote. This foliation, S_3, wraps around garnet and strongly deformed pseudomorphs after lawsonite (Fig. 3a-2). In intensely deformed samples lawsonite pseudomorphs are absent and porphyroblasts of albite dominate. Albite contain anhedral crystals of garnet and sigmoidal inclusion trails, continuous with the matrix foliation, suggesting the syntectonic growth of albite (Fig. 3a-3, d). The development of S_3 is limited to the upper part of the sequence. Thus, the associated deformation was concentrated at this structural level. However, this foliation reworks S_2, as evidenced by the relics in lawsonite pseudomorphs and garnet inclusions in albite porphyroblasts.

Two representative samples of the Cambre metabasic rocks have been chosen for detailed studied. Sample 106343, referred to hereafter as CA (for Cambre Amphibolites), is located in the intermediate part of the sequence. The presence of numerous garnet porphyroblasts, rich in S_1 and S_2 inclusions, and the abundant well-preserved pseudomorphs of ehuedral lawsonite, makes this sample ideal to study the early deformation phases. Additionally, textural and chemical relations have been investigated in similar samples located at equivalent levels, and some of the petrographic images correspond to such examples (samples 109952 and 109954). Sample 106331, referred to hereafter as AG (for Albite Greenschists), represent albite-bearing samples located at the top of the succession. The occurrence of syn-S_3 albite porphyroblasts allows investigating the late exhumation-related stage.

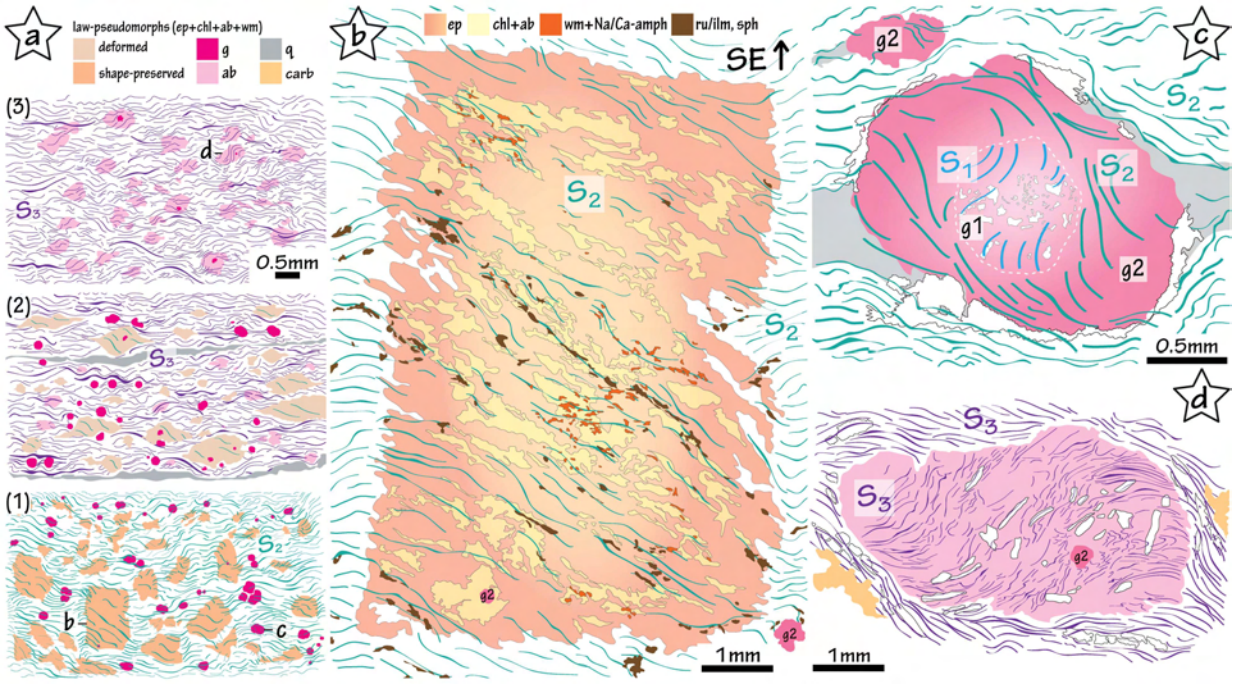

Fig 3. Schematic illustration highlighting foliations (a) at different structural levels of the sequence, from the bottom (1) to top (3) of the series; (b) in lawsonite pseudomorphs; (c) in garnet porphyroblasts; (d) in albite porphyroblasts. Mineral abbreviations are are after Holland and Powell (1998). Other abbreviations: carb-carbonates; g1-garnet 1; g2-garnet 2; Na/Ca-amph-sodic/calcic amphiboles; wm-white mica.

PETROGRAPHY AND MINERAL CHEMISTRY

Mineral analyses and elemental X-ray maps were performed with a JEOL-Superprobe JXA-8900M microprobe equipped with five spectrometers at the ICTS-National Electronic Microscopy Centre at the Complutense University of Madrid (Spain; http://www.cnme.es). The operating parameters for punctual analyses were: 15kV accelerating voltage, 20 nA beam current, between 1 and 5 μm beam diameter (1 μm for the microinclusions) and 10 s counting time on peak for each element. X-ray maps were operated at 20 kV and 150 nA. Representative analyses of selected minerals are listed in Tables 2-5. Mineral formulae have been calculated using the software AX (http:/www.esc.cam.ac.uk/research/research-groups/holland/ax). The amount of ferric iron was calculated from stoichiometric constraints.

Mineral abbreviations are those used by THERMOCALC (Holland and Powell, 1998): ab-albite, act-actinolite, bi-biotite, chl-chlorite, ep-epidote, g-garnet, gl-glaucophane, hb-hornblende, hem-hematite, ilm-ilmenite, jd-jadeite, law-lawsonite, mt-magnetite, mu-muscovite, o-omphacite, pa-paragonite, pl-plagioclase, q-quartz, ru-rutile and sph-titanite (sphene).

Other abbreviations: bar-barroisite, carb-carbonates, sul-sulphides, win-winchite. Compositional variables: $X_{Fe} = Fe^{2+}/(Fe^{2+}+Mg)$; $X_{Fe3+}(ep) = Fe^{3+}/(Fe^{3+}+Al-2)$; $X_{Na}(mu, pa) = Na/(Na+K)$; amphiboles: $y = X_{Al}^{M2}$; $z = X_{Na}^{M4}$; $a = X_{Na}^{A}$; $c = X_{Ca}^{M4}$; $f = X_{Fe3+}^{M2}$; garnet: Alm = Fe/(Fe+Mg+Ca+Mn), Prp = Mg/(Fe+Mg+Ca+Mn), Grs = Ca/(Fe+Mg+Ca+Mn), Sps = Mn/(Fe+Mg+Ca+Mn); feldspars: Ab = Na/(Na+Ca+K), An = Ca/(Na+Ca+K), Or = K/(Na+Ca+K);

Other symbols: pfu – per formula unit; wt. % – weight percent; "→" denotes core-to-rim evolution. "/" indicates partial replacement; "*" specifies phases texturally inferred from petrography or from petrologic modelling that have not been identified petrographically. "#" indicates phases described by other authors that have not been recognized in this study.

In sample CA, calcic to sodic-calcic amphiboles constitute up to 80 % in volume of each sample and define the main foliation S_2. Other matrix minerals are, in the order of decreasing abundance, epidote, chlorite, albite, phengitic muscovite, titanite, rutile/ilmenite, magnetite, hematite, apatite and quartz (Fig. 4; Table 2). Chlorite (type 2; $X_{Fe} = 0.34$), nearly pure albite (type 2; An = 0.8 % and Or = 0.2 %), titanite (type 2b; $Al_2O_3 \sim 1$ wt. %) and rutile partially or almost completely replaced by ilmenite (type 2; MnO ~ 1.2 wt. %; Fig. 5a) are relatively homogeneous, whereas epidote is strongly zoned (type 2b; $X_{Fe3+} = 0.35 \rightarrow 0.67$). Phengitic muscovite (type 2) has Si contents ranging typically between 3.38 and 3.42 pfu ($X_{Na} = 0.05$-0.06), reaching a maximum value of 3.46 ($X_{Na} = 0.02$). In the most deformed areas the Si contents are systematically lower (3.34 to 3.36 pfu).

Table 2	S_2																								
Mineral	$ep2b_C$	$ep2b_R$	sph2b	ilm2	bar2b	bar2b	$act2b_C$	$hb2b_{R1}$	$hb2b_{R2}$	$hb2b_C$	$hb2b_R$	mu2	mu2	mu2	chl2	ab2	$act2b_{C1}$	$act2b_{C2}$	$hb2b_R$	$act2b_C$	$parg_{R1}$	$hb2b_{R2}$	$act2b_C$	bar2b$_R$	$act2b_C$	$hb2b_R$
Analysis	29	30	26	12	58	60	34	36	35	21	22	40	41	35	18	217	1	2	3	18	17	19	122	123	125	126
								crystal			crystal							g P-tail			g P-tail			law/ps P-tail		law/ps P-tail	
SiO_2	38.0	37.5	30.0	0.9	52.3	52.7	54.9	52.1	51.9	47.9	46.7	51.1	50.7	51.4	28.3	67.5	55.6	52.2	49.1	54.0	43.1	44.1	55.1	49.2	54.9	47.2
TiO_2	0.2	0.1	41.9	52.9	0.1	0.1	0.1	0.2	0.2	0.2	0.3	0.2	0.3	0.2	0.0	0.0	0.0	0.1	0.1	0.0	0.3	0.3	0.0	0.1	0.1	0.2
Al_2O_3	27.5	24.6	1.0	0.3	7.6	7.2	2.9	5.3	5.1	9.1	10.4	25.3	26.7	28.7	19.7	19.9	2.7	3.8	6.2	3.7	14.3	14.0	2.4	9.4	1.7	8.9
Cr_2O_3	0.0	0.0	0.0	0.0	0.0	0.1	0.0	0.1	0.0	0.0	0.0	0.1	0.0	0.1	0.0	0.1	0.0	0.0	0.0	0.0	0.1	0.1	0.0	0.0	0.0	0.1
FeO_T	7.1	11.1	0.4	43.6	10.0	11.3	9.0	11.5	11.3	15.5	15.4	2.4	2.4	2.1	18.8	0.1	8.5	12.8	14.1	10.4	16.8	17.3	9.0	12.8	9.1	14.0
MnO	0.1	0.1	0.0	1.1	0.0	0.1	0.0	0.2	0.1	0.3	0.3	0.0	0.0	0.0	0.2	0.0	0.0	0.1	0.1	0.0	0.3	0.1	0.0	0.0	0.0	0.0
MgO	0.0	0.0	0.0	0.1	14.7	15.1	18.1	15.6	15.9	11.5	10.5	4.1	3.5	3.2	20.0	0.0	18.1	15.7	13.9	16.8	8.8	8.5	17.3	12.9	18.5	12.8
CaO	24.1	23.1	28.9	0.1	8.8	9.0	10.7	10.0	10.2	10.2	9.3	0.0	0.0	0.0	0.0	0.2	10.6	10.8	11.4	10.7	9.7	9.3	11.2	8.8	11.0	10.5
Na_2O	0.0	0.0	0.0	0.2	2.2	2.2	1.2	1.5	1.7	1.9	2.4	0.2	0.4	0.5	0.0	11.7	1.5	1.0	1.2	1.3	2.8	2.9	1.2	2.5	1.0	2.1
K_2O	0.0	0.0	0.0	0.0	0.2	0.1	0.2	0.1	0.1	0.1	0.1	10.5	10.3	9.9	0.0	0.1	0.1	0.0	0.0	0.1	0.5	0.4	0.1	0.1	0.1	0.1
Total	96.8	96.6	102	99.2	96.0	97.8	97.1	96.4	96.5	96.8	95.3	93.9	94.3	96.1	87.1	99.37	97.0	96.5	96.3	97.0	96.6	96.9	96.4	95.9	96.4	95.9
Si	3.00	3.00	0.96	0.02	7.48	7.44	7.75	7.49	7.45	7.03	6.96	3.46	3.42	3.38	2.89	2.97	7.82	7.55	7.22	7.68	6.45	6.55	7.86	7.14	7.81	6.98
Ti	0.01	0.01	1.01	1.00	0.01	0.01	0.01	0.02	0.02	0.03	0.03	0.01	0.01	0.01	0.00	0.00	0.00	0.01	0.01	0.00	0.03	0.03	0.00	0.00	0.01	0.01
Al	2.57	2.33	0.04	0.01	1.28	1.20	0.48	0.89	0.86	1.58	1.82	2.02	2.13	2.22	2.37	1.03	0.45	0.65	1.08	0.61	2.52	2.46	0.41	1.62	0.29	1.55
Cr	0.00	0.00	0.00	0.00	0.00	0.01	0.00	0.01	0.00	0.00	0.00	0.01	0.00	0.00	0.00	0.00	0.00	0.00	0.00	0.00	0.01	0.01	0.00	0.00	0.00	0.00
Fe^{3+}	0.30	0.66	0.00	0.00	0.19	0.27	0.18	0.29	0.36	0.35	0.33	0.00	0.00	0.00	0.00	0.00	0.18	0.30	0.32	0.23	0.32	0.32	0.06	0.40	0.21	0.34
Fe^{2+}	0.13	0.01	0.01	0.91	1.01	1.03	0.89	1.09	1.00	1.55	1.59	0.14	0.14	0.12	1.60	0.00	0.82	1.25	1.41	1.01	1.77	1.83	1.01	1.15	0.87	1.40
Mn	0.00	0.00	0.00	0.02	0.01	0.01	0.01	0.02	0.01	0.04	0.04	0.00	0.00	0.00	0.02	0.00	0.00	0.01	0.01	0.00	0.03	0.01	0.00	0.00	0.00	0.00
Mg	0.00	0.00	0.00	0.00	3.14	3.17	3.81	3.34	3.39	2.52	2.32	0.42	0.35	0.32	3.04	0.00	3.79	3.38	3.04	3.55	1.97	1.88	3.67	2.80	3.92	2.83
Ca	2.04	1.98	0.99	0.00	1.34	1.36	1.62	1.55	1.57	1.60	1.49	0.00	0.00	0.00	0.00	0.01	1.60	1.68	1.80	1.63	1.55	1.48	1.71	1.36	1.68	1.67
Na	0.00	0.00	0.00	0.01	0.61	0.59	0.33	0.41	0.47	0.54	0.69	0.02	0.05	0.06	0.01	1.00	0.40	0.27	0.35	0.36	0.82	0.82	0.33	0.71	0.28	0.60
K	0.00	0.00	0.00	0.00	0.03	0.02	0.04	0.02	0.02	0.01	0.02	0.91	0.88	0.83	0.00	0.00	0.02	0.00	0.01	0.02	0.10	0.08	0.01	0.02	0.01	0.01
Sum	8.06	8.00	3.01	1.98	15.1	15.1	15.1	15.1	15.2	15.3	15.3	6.98	1.43	6.94	9.93	5.02	15.1	15.1	15.3	15.1	15.6	15.5	15.1	15.2	15.1	15.4
X_{Fe}					0.24	0.25	0.19	0.25	0.23	0.36	0.41	0.25	0.28	0.27	0.34		0.18	0.27	0.32	0.22	0.47	0.49	0.22	0.29	0.18	0.33
X_{Fe3+}	0.35	0.67									X_{Na}	0.02	0.05	0.06												
y					0.38	0.32	0.11	0.19	0.16	0.31	0.38				Ab	99.1	0.13	0.10	0.15	0.14	0.48	0.51	0.14	0.38	0.05	0.26
z					0.27	0.25	0.13	0.15	0.15	0.14	0.27				An	0.79	0.17	0.08	0.05	0.14	0.16	0.20	0.13	0.26	0.11	0.11
a					0.08	0.10	0.06	0.11	0.16	0.27	0.08				Or	0.20	0.06	0.11	0.25	0.08	0.49	0.43	0.06	0.19	0.07	0.37
c					0.67	0.68	0.81	0.77	0.79	0.80	0.67						0.80	0.84	0.90	0.82	0.78	0.74	0.86	0.68	0.84	0.83
f					0.10	0.14	0.09	0.14	0.18	0.18	0.10						0.09	0.15	0.16	0.11	0.16	0.16	0.03	0.20	0.11	0.17

TABLE 2. Representative microprobe analyses in the minerals of the matrix foliation (S2) from sample CA. C-core; R-rim; g P-tail-crystallization tails; lawps pseudomorphs after lawsonite

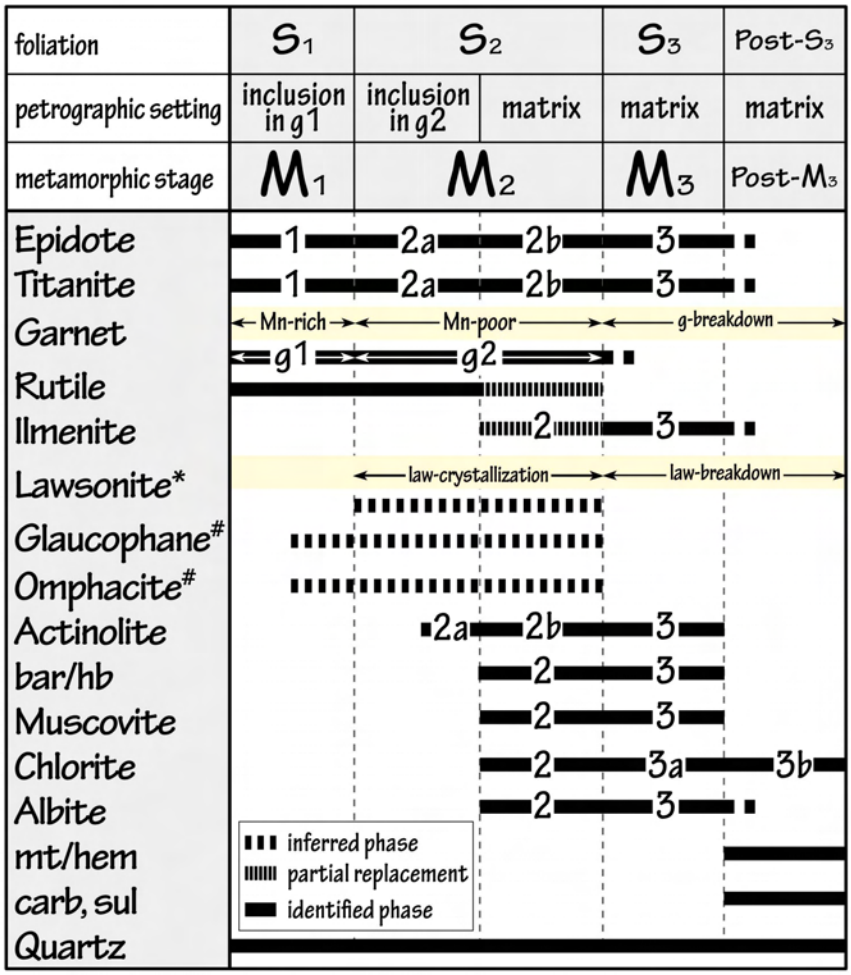

Fig 4. Diagram showing the crystallization–deformation relations of the Cambre metabasic rocks. "*" specifies phases inferred from petrography and/or from petrologic modelling that have not been identified petrographically. "#" indicates phases described by other authors that have not been recognized in this study.

AMPHIBOLES IN THE MATRIX

Calcic amphiboles are fine to medium-grained (0.025–0.3 mm) and are either actinolite (pale green hue; type 2a) with hornblende rims (green-bluish) or slightly zoned hornblende crystals (blue-green to deep green; type 2). Coexisting actinolite and hornblende are commonly found together in a patchy intergrowth. Large domains in the matrix foliation consist of very fine-grained symplectitic intergrowth of hornblende (commonly with actinolite cores) and albite (Fig. 5 b–c). Rodríguez (2005) described omphacite as very rare pre-S_3 prisms, showing irregular rims of hornblende-albite symplectites. Relicts of omphacite have not been identified in the samples of this study. However, the hornblende-albite symplectitic intergrowth possibly represents replacement of former crystals of omphacitic pyroxene (e.g. Miller *et al.,* 1980; Ortega-Gutiérrez *et al.,* 2008; Vega-Granillo *et al.,* 2007) or glaucophanic amphibole (e.g. Miller *et al.,* 1980; Liou, 1981; Engvik *et al.,* 2000). The chemical variation of the actinolitic cores is Si = 7.75–7.85 pfu; X_{Fe} = 0.18–0.20; z = 0.12–0.14; c = 0.79–0.82;

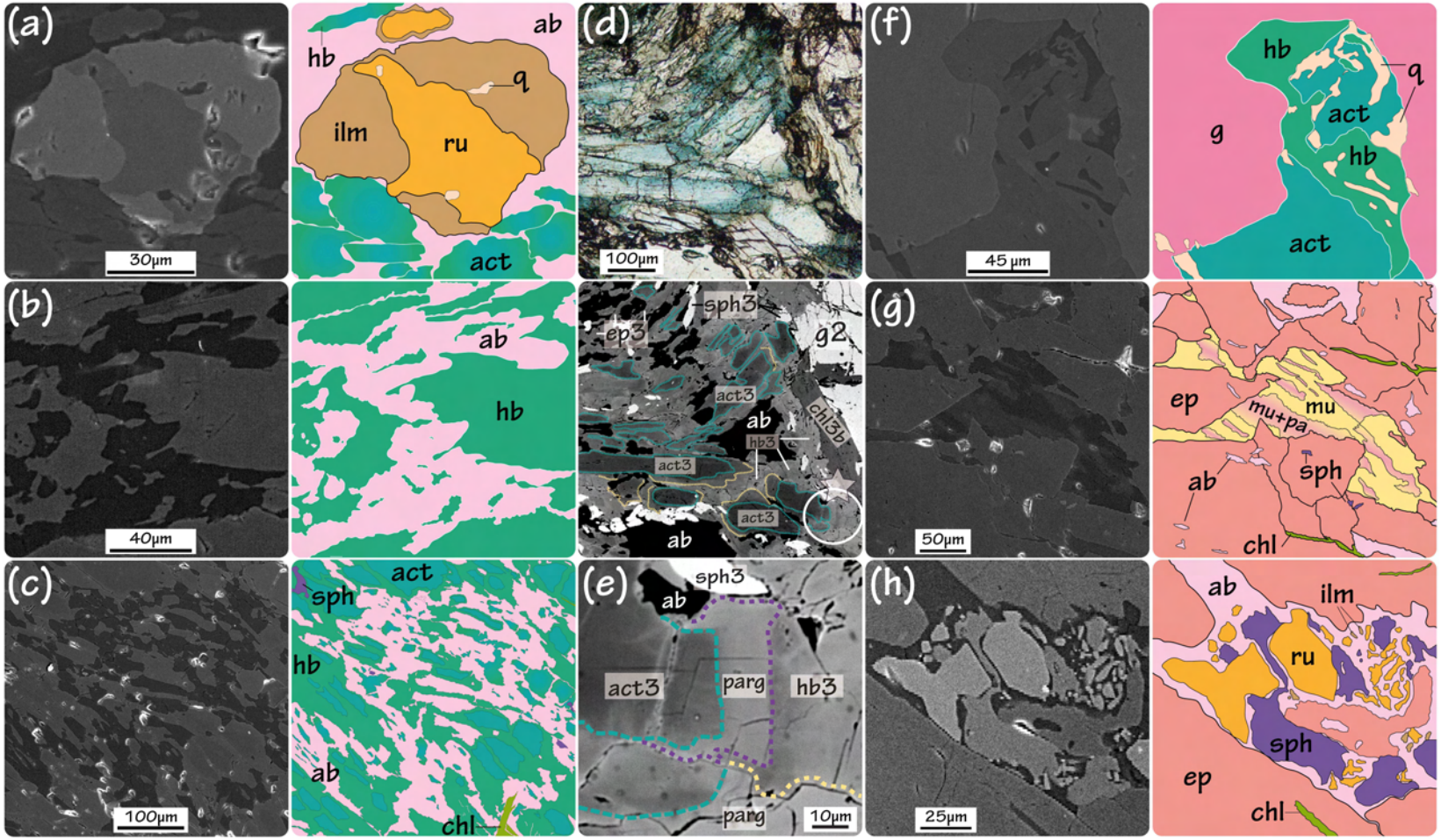

Fig 5. Back-scattered electron images showing detailed textures in the Cambre metabasic rocks. (a) ilm replacing ru in the matrix foliation; (b-c) symplectitic intergrowth of Ca-amphiboles and ab in the S2-foliation; (d-e) Zoned amphiboles in crystallization tails in garnet; (f) act grain showing exolution lamellae of hb in the outermost rim of a type 2 garnet porphyroblast; (g) pa+mu intergrowth inside a cluster in a law-pseudomorph; (h) Incipient sph coronae around ru. Mineral abbreviations are after Holland and Powell (1998).

f = 0.08–0.1. The composition of the hornblende rims is Si= 7.49→7.45 pfu; X_{Fe} = 0.25→0.23; z ~ 0.15; c = 0.77→0.79; f = 0.14→0.18. The general zonation trend, from core-to-rim, is characterised by a decrease in Ca and an increase in Na, Al, Fe^{3+} and the X_{Fe} ratio (Table 2). The chemical variation in zoned hornblende crystals is Si = 7.03→6.96 pfu; X_{Fe} = 0.38→0.41; z = 0.14→0.20; c = 0.80→0.74; f = 0.16→0.18. In all amphiboles, K and Ti proportions are always close to zero and the X_{Fe} ratio is below 0.5. In all analyses Ca_{M4} is systematically higher than total Na and a continuous range of compositions between actinolite and hornblende sensu lato is observed, the former being closer to calcic compositions, and the latter tending towards calcic-sodic compositions (Fig. 6). Only in a limited number of analyses Na_B (=Na_{M4}) > 0.5. These sodic-calcic amphiboles are small (< 0.1 mm) single prismatic to subhedral crystals of barroisitic hornblende (type 2; Si= 7.44–7.48 pfu; X_{Fe} ~ 0.25; X_{NaM4} = 0.25–0.27; X_{CaM4} ~ 0.68; $X_{Fe}{}^{3+}{}_{M2}$ = 0.10–0.14; Table 2).

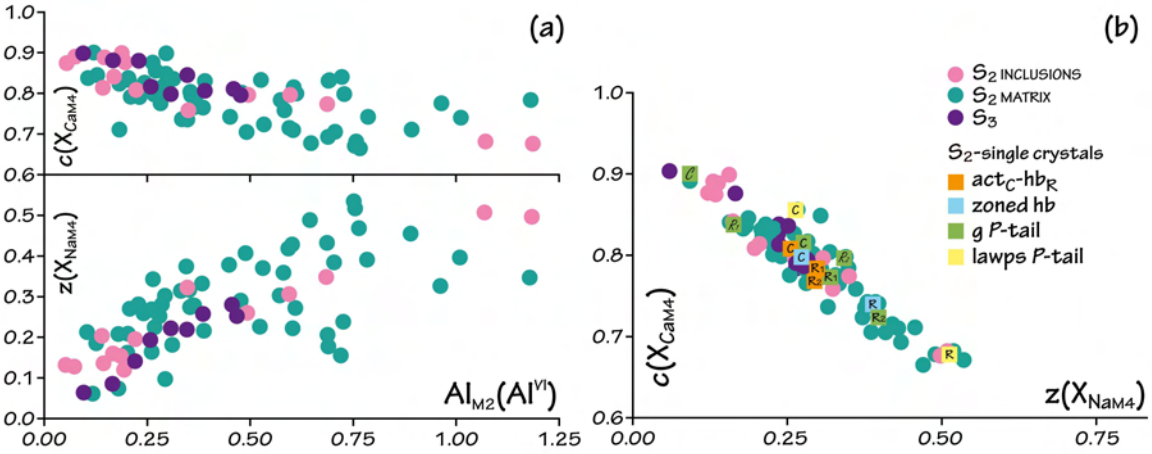

Fig 6. Compositional variations in amphiboles in the Cambre metabasic rocks. C–core; R–rim; P-tail–crystallization tail; lawps–lawsonite pseudomorph. Mineral abbreviations are after Holland and Powell (1998).

Crystallization tails around garnet porphyroblasts and lawsonite pseudomorphs typically comprise granoblastic quartz and randomly oriented chlorite flakes. Amphiboles in these areas have a slightly coarser grain size than the crystals in the matrix and are chemically zoned. Amphiboles in the crystallization tails around garnet include cores of actinolite (type 2b; Si= 7.44–7.48 pfu; X_{Fe} ~ 0.25; z = 0.25–0.27; c ~ 0.68; f = 0.10–0.14) surrounded by less magnesian hornblende (type 2; Si = 6.55–7.22 pfu; X_{Fe} = 0.32–0.49; z = 0.25–0.43; c = 0.74–0.9; f ~ 0.16) and/or pargasite (Si ~ 6.45 pfu; X_{Fe} ~ 0.47; z ~ 0.16; c ~ 0.78; f ~ 0.16) rims (Fig. 5 d–e). Amphiboles within the crystallization tails around the pseudomorphs after lawsonite consist of actinolite cores (type 2b; Si= 7.81–7.86 pfu; X_{Fe} = 0.18–0.22; z = 0.11–0.13; c = 0.84–0.86; f = 0.03–0.11) with rims of barroisitic hornblende (type 2; Si = 7.14 pfu; X_{Fe} ~ 0.3; z ~ 0.26; c ~ 0.7; f ~ 0.2) or hornblende (type 2; X_{Fe} ~ 0.33; z ~ 0.11; c ~ 0.83; f ~ 0.2; Table 2).

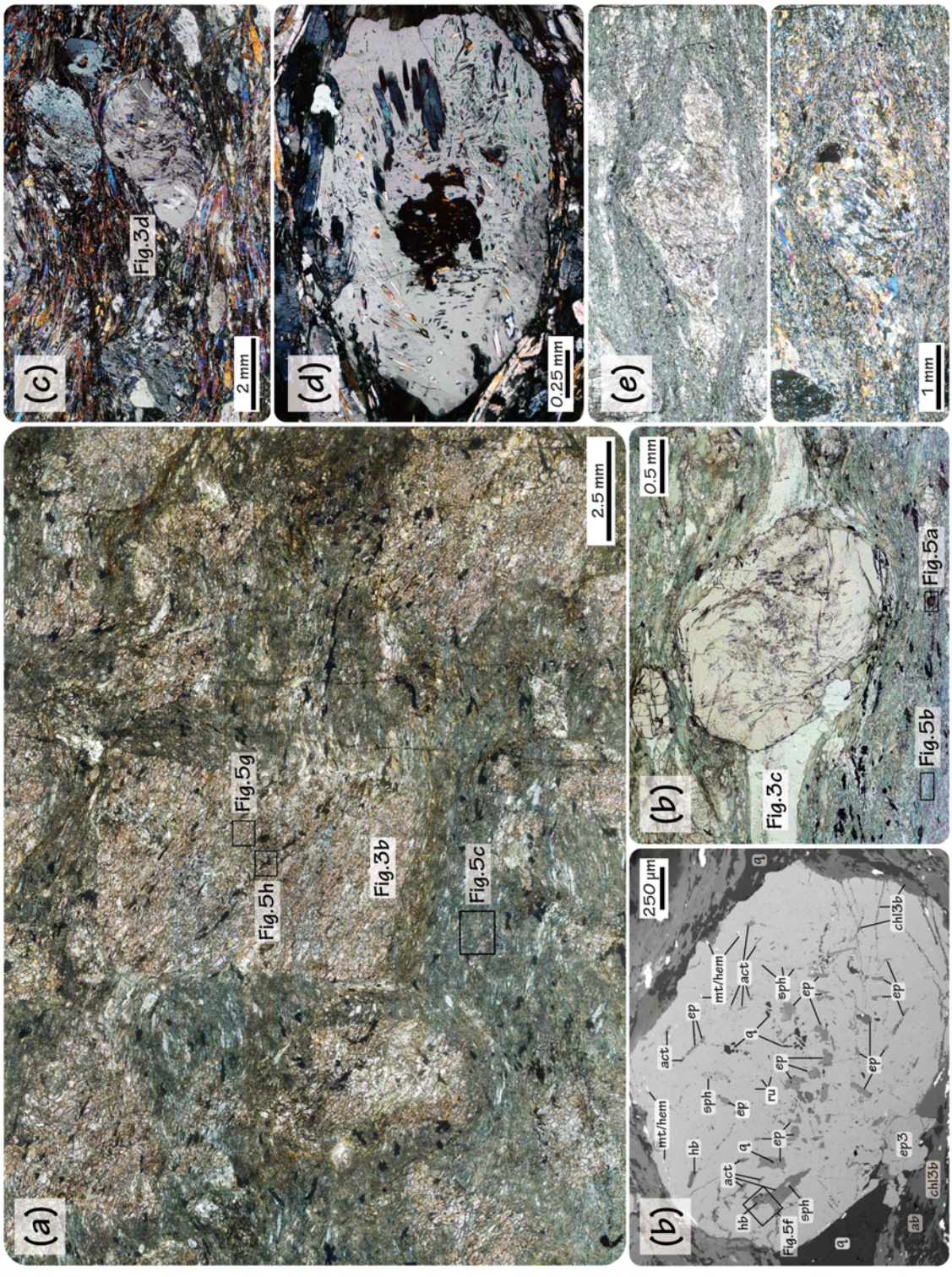

Fig 7. Microphotographs of thin-section images of the Cambre metabasic rocks showing (a) euhedral lawsonite pseudomorphs (sample CA); (b) garnet porphyroblasts displaying curved inclusions; (c) albite-bearing samples (sample AG); (d) strongly stretched pseudomorphs after lawsonite almost indistinguishable from the matrix foliation.

GARNET ZONING AND INCLUSION PATTERNS

Garnet forms subhedral to ehuedral porphyroblasts (up to 2.5 mm in diameter) that commonly display optical zoning. The cores of the porphyroblasts, referred to as garnet 1 (g1), contain very fine-grained inclusions of epidote (type 1; 5–10 μm, X_{Fe3+}= 0.51), titanite (type 1; Al_2O_3 ~ 2 wt. %), very tiny rutile needles (< 2 μm) and quartz (Figs. 4, 7b; Table 3). The inclusions define a subtle internal foliation (S_1) that has unoriented or curved patterns. In the outer part of the garnet porphyroblasts (referred here to as garnet 2, g2), S_1 turns progressively continuous towards another internal foliation (S_2), which is continuous with the matrix foliation (S_2; Fig. 3c). S_2 is formed by slightly coarser-grained inclusions (0.01–0.2 mm) of epidote (type 2a; X_{Fe3+}= 0.6), titanite (type 2a; Al_2O_3 ~ 1 wt. %), very small crystals of rutile partially replaced by ilmenite (< 4 μm), amphibole and quartz.

Amphiboles form subhedral crystals of unzoned actinolite (< 150 μm; type 2a; Si = 7.71-7.77 pfu; X_{Fe} = 0.25v0.29; z = 0.07–0.1; c = 0.81–0.89; f = 0.09–0.13) (Fig. 7b; Table 3). Additionally, single grains of actinolite (type 2a) showing exsolution lamellae of hornblende (Si = 7.14–7.17 pfu; X_{Fe} = 0.32–0.40; z = 0.18–0.23; c = 0.71–0.77; f = 0.18) are preserved in the outermost rims of some garnets (Figs. 5f, 7b; Table 3). Compared to the actinolite cores of the amphibole crystals in the matrix, the S_2-inclusions are less magnesian and aluminous, and more calcic (Fig. 6; Tables 2, 3).

Optical zoning in garnet porphyroblasts correlates with chemical zoning (Fig. 8). Garnet core ($g1_C$) is characterised by an increase in almandine (Alm43→49%) and a decrease in grossular (Grs35→31%) and spessartine (Sps20→16%). X_{Fe} remains constant (X_{Fe}=0.94–0.95) and the proportion of pyrope varies irregularly between 2 and 3% (Fig.8a–profile 1; Table 3). According to the different behaviour of grossular and spessartine it is possible to distinguish two areas. The intermediate area ($g1_R$) is characterised by an increase in the amount of both almandine and grossular, and a strong decrease of the proportion of spessartine (Alm48→56%, Grs31→37%, Sps18→5%), whereas X_{Fe} and the proportion of pyrope show only small variations with respect to the core values (Fig. 8a–profile 1; Table 3). In the external area ($g2_C$) the rimward evolution is characterised by a decrease in grossular, spessartine and X_{Fe} (Grs37→28%, Sps5→2%, X_{Fe} = 0.95→0.89%), accompanied by an increase in almandine and pyrope (Alm56→61%, Prp3→9%) (Fig. 8a–profiles 1, 2; Table 3). Finally, in the outermost rim ($g2_R$): almandine and X_{Fe} first decrease before increasing again (Alm61→59→61%, X_{Fe}=0.89→0.84→0.86%), pyrope first increases (Prp9→12) and then locally decreases (Prp12→10) grossular and spessartine decrease (Grs30→27%, Sps2→1%; Fig. 8a–profile 1; Table 3).

Garnet grains included in the pseudomorphs are in general smaller (0.25–0.65 mm) and are chemically equivalent to the inner part of garnet 2 ($g2_C$; Fig. 8b–profile 3; Table 4). Smaller garnet grains scattered in the matrix (0.5–1.5 mm; Fig. 8a–profile 2; Table 3) and the ones included in the albite porphyroblasts (< 0.5 mm) are chemically equivalent to the outer part of garnet 2 ($g2_R$).

Table 3	S_1-core					S_2-core								S_2-rim			
Mineral	*ep 1*	*sph1*	*g1C*	*g1C*	*g1R*	*ep2a*	*sph2a*	*act2a*	*act2a*	*g2C*	*g2C*	*g2R*	*g2R*	*hb2a*	*hb2a*	*g2R*	*g2R*
Analysis	*7*	*10*	*117*	*123*	*108*	*16*	*13*	*14*	*41*	*106*	*91*	*83*	*76*	*42*	*15*	*64*	*62*
SiO_2	37.4	30.5	37.6	37.8	37.4	37.1	30.2	53.8	53.7	37.6	38.0	37.2	37.4	48.8	49.5	37.8	37.7
TiO_2	0.7	37.3	0.3	0.2	0.2	0.1	39.3	0.0	0.0	0.2	0.1	0.2	0.1	0.1	0.0	0.0	0.1
Al_2O_3	23.9	2.0	21.4	21.4	21.5	24.8	1.0	1.9	2.0	21.0	21.6	21.2	21.6	8.4	8.9	21.9	21.6
Cr_2O_3	0.1	0.0	0.0	0.0	0.0	0.1	0.1	0.0	0.0	0.1	0.0	0.0	0.0	0.1	0.0	0.0	0.1
FeO_T	10.6	1.2	19.1	19.9	22.4	10.0	0.6	13.5	12.5	21.2	24.9	25.9	27.5	16.3	13.8	26.3	27.5
MnO	0.0	0.2	8.9	8.2	6.9	0.1	0.1	0.1	0.1	8.0	2.1	1.7	1.0	0.1	0.1	0.5	0.4
MgO	0.0	0.0	0.5	0.7	0.8	0.0	0.0	15.8	16.6	0.7	0.8	1.3	1.6	11.5	12.8	2.5	2.9
CaO	24.0	29.1	12.3	12.2	11.1	24.0	29.7	11.5	11.4	10.8	12.8	11.5	10.7	10.2	10.0	10.4	9.4
Na_2O	0.0	0.0	0.0	0.0	0.0	0.0	0.0	0.7	0.8	0.0	0.0	0.0	0.0	1.8	1.7	0.0	0.0
K_2O	0.0	0.0	0.0	0.0	0.0	0.0	0.0	0.1	0.1	0.0	0.0	0.0	0.0	0.3	0.1	0.0	0.0
Total	96.7	100	100	100	100	96.2	101	97.4	97.3	99.5	100	99.0	100	97.5	96.8	99.3	99.5
Si	3.03	1.00	2.98	2.99	2.97	2.98	0.98	7.75	7.71	3.01	3.00	2.98	2.97	7.14	7.17	3.00	2.99
Ti	0.04	0.92	0.02	0.01	0.01	0.01	0.96	0.00	0.00	0.01	0.01	0.01	0.01	0.01	0.00	0.00	0.00
Al	2.29	0.08	2.01	2.00	2.01	2.35	0.04	0.33	0.35	1.98	2.01	2.00	2.02	1.45	1.52	2.04	2.02
Cr	0.01	0.00	0.00	0.00	0.00	0.00	0.00	0.00	0.00	0.00	0.00	0.00	0.00	0.01	0.00	0.00	0.00
Fe^{3+}	0.30	0.00	0.00	0.00	0.02	0.49	0.00	0.22	0.27	0.00	0.00	0.01	0.02	0.30	0.35	0.00	0.00
Fe^{2+}	0.39	0.03	1.27	1.32	1.47	0.18	0.02	1.38	1.23	1.42	1.65	1.73	1.81	1.65	1.29	1.74	1.82
Mn	0.00	0.00	0.60	0.55	0.46	0.01	0.00	0.01	0.01	0.54	0.14	0.12	0.07	0.01	0.01	0.03	0.02
Mg	0.00	0.00	0.06	0.09	0.10	0.00	0.00	3.40	3.56	0.09	0.09	0.16	0.19	2.50	2.76	0.29	0.34
Ca	2.09	1.02	1.05	1.03	0.95	2.07	1.03	1.78	1.75	0.93	1.09	0.98	0.91	1.59	1.55	0.88	0.80
Na	0.00	0.00	0.00	0.00	0.00	0.00	0.00	0.21	0.22	0.00	0.00	0.01	0.00	0.51	0.47	0.00	0.00
K	0.00	0.00	0.00	0.00	0.00	0.00	0.00	0.02	0.02	0.00	0.00	0.00	0.00	0.06	0.02	0.00	0.00
Sum	8.14	3.05	7.99	8.00	8.00	0.69	3.04	15.09	15.11	7.98	7.99	8.00	8.00	15.25	15.14	7.98	8.00
X_{Fe}			0.95	0.94	0.94			0.29	0.26	0.94	0.95	0.92	0.90	0.40	0.32	0.86	0.84
X_{Fe3+}	0.51					0.59											
y *Alm*			43	44	49			0.04	0.03	48	56	58	61	0.45	0.34	59	61
z *Prp*			2	3	3			0.07	0.07	3	3	5	6	0.23	0.18	10	11
a *Grs*			35	35	32			0.08	0.09	31	37	33	31	0.29	0.12	30	27
c *Sps*			20	18	16			0.89	0.87	18	5	4	2	0.71	0.77	1	1
f								0.11	0.13					0.18	0.18		

TABLE 3. Representative microprobe analyses in the inclusions in garnet (S1 and S2 foliations in g1 and g2, respectively) from sample CA. C-core; R-rim

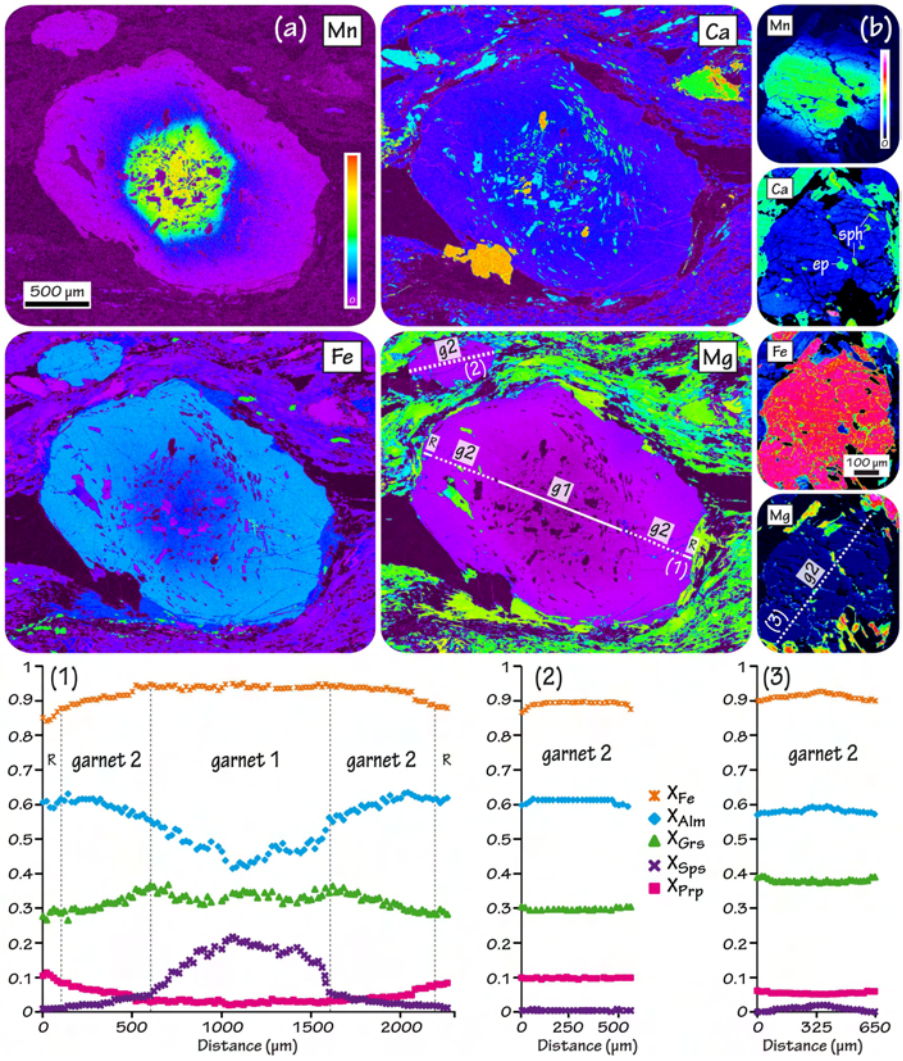

Fig 8. X-Ray maps and chemical profiles illustrating zoning of garnet porphyroblasts from the Cambre metabasic rocks. (a) Euhedral porphyroblasts displaying an optical zoning interpreted as types 1 and 2 garnets (profile 1). (b) Subidioblastic type 2 garnet grains in the matrix foliation (profile 2) and (c) included in the pseudomorphs (profiles 3). Thick dashed lines on the X-ray maps indicate the position of the profiles. C–core; R–rim.

PSEUDOMORPHS AFTER LAWSONITE

The lawsonite pseudomorphs are distinctly white in hand specimen and up to 2 cm long. The original porphyroblasts are completely replaced by aggregates showing, in the less deformed areas, the typical rectangle or rhombus shape of fresh lawsonite (Fig. 7a). Minerals forming the aggregates are typically dominated by fine-grained prisms of zoned epidote (type 2b; X_{Fe3+} = 0.24→0.45) with small titanite inclusions (type 2b; < 5µm, Al_2O_3 ~ 1.2 wt. %), rutile partially replaced by ilmenite (type 2; MnO ~ 2 wt. %), chlorite (type 2; X_{Fe} = 0.28) and albite (type 2; An = 1.3 and Or = 0.3 %). Almandine-rich garnet ($g2_C$; < 0.65 mm; Alm55→57%, Prp6→7%, Grs38→40%, Sps4→2%; Fig. 8b) is randomly scattered in the pseudomorphs and contains very fine-grained inclusions (< 0.01 mm) of epidote, titanite and quartz (Fig. 8b). Additionally, white mica and amphibole, if present, are exclusively concentrated in specific areas of the pseudomorphs (Fig. 3b; Table 4). White micas are individual crystals of phengitic muscovite (type 2; up to 3.5 Si pfu, X_{Na} = 0.03) or fine grained

intergrowths of muscovite and paragonite (< 2 μm; below electron microprobe resolution; Fig. 5g). Paragonite is not present in the matrix foliation and phengitic muscovite in the pseudomorphs shows slightly higher Si contents than the ones in the matrix foliation. Amphiboles are acicular (10–15 μm) to prismatic (< 70–100 μm) unzoned crystals of actinolite (type 2b; Si = 7.77–7.83 pfu; X_{Fe} = 0.17–0.20; z ~ 0.13; c = 0.78–0.85; f = 0.07–0.09) chemically equivalent to the crystals included in g2 (Table 3), and barroisitic hornblende (type 2; Si= 6.45–6.65 pfu; X_{Fe} = 0.32–0.35; z ~ 0.25; c ~ 0.68; f = 0.14–0.21) , which is poorer in Si and Mg and richer in Na and Ti than the crystals in the matrix foliation and in the pressure tails (Table 4). Inclusions of glaucophane have been described in the pseudomorphs by Rodríguez (2005), but have not been identified in this study. Actinolite crystals are chemically equivalent to the crystals included in garnet 2. Barroisitic hornblende from the pseudomorphs is chemically different to the crystals of the matrix foliation and the pressure tails, being poorer in Si and Mg and richer in Na and Ti (Table 3).

Table 4						S_2							
Mineral	ep2b$_C$	ep2b$_R$	sph2b	Ilm2	g2$_C$	g2$_R$	mu2	bar2b	bar2b	act2b	act2b	chl2	ab2
Analysis	15	14	17	11	61	72	20	10	13	4	9	28	198
SiO_2	38.3	38.1	30.3	0.0	38.4	38.3	51.3	45.5	44.8	54.6	55.2	26.6	67.4
TiO_2	0.1	0.1	39.7	52.8	0.0	0.1	0.2	0.5	0.2	0.0	0.1	0.1	0.0
Al_2O_3	28.8	26.3	1.2	0.0	21.5	21.5	24.7	14.1	16.1	2.0	3.1	22.5	20.0
Cr_2O_3	0.0	0.0	0.0	0.0	0.1	0.1	0.1	0.1	0.0	0.0	0.0	0.0	0.0
FeO_T	5.9	8.9	0.4	44.7	25.6	25.9	4.4	12.9	13.2	8.4	9.6	15.3	0.1
MnO	0.0	0.1	0.0	2.1	0.2	0.1	0.0	0.1	0.1	0.0	0.0	0.1	0.0
MgO	0.0	0.0	0.0	0.0	1.6	1.8	3.3	11.0	10.9	18.2	18.0	22.0	0.0
CaO	24.7	24.4	29.6	0.1	13.7	12.5	0.0	8.7	8.8	11.0	10.3	0.1	0.3
Na_2O	0.0	0.0	0.0	0.2	0.0	0.0	0.2	3.5	3.2	1.1	1.1	0.0	11.7
K_2O	0.0	0.0	0.0	0.0	0.0	0.0	9.7	0.2	0.1	0.1	0.1	0.0	0.1
Total	97.8	97.8	101	100	101	100	93.9	96.4	97.4	95.6	97.4	86.7	99.6
Si	2.99	3.01	0.98	0.00	3.00	3.02	3.48	6.65	6.45	7.83	7.77	2.68	2.96
Ti	0.00	0.00	0.97	1.00	0.00	0.00	0.01	0.05	0.03	0.00	0.01	0.00	0.00
Al	2.65	2.45	0.05	0.00	1.98	1.99	1.98	2.43	2.73	0.34	0.52	2.68	1.04
Cr	0.00	0.00	0.00	0.00	0.00	0.00	0.00	0.01	0.01	0.00	0.00	0.00	0.00
Fe^{3+}	0.20	0.38	0.00	0.01	0.02	0.00	0.06	0.27	0.43	0.18	0.14	0.00	0.00
Fe^{2+}	0.16	0.17	0.01	0.93	1.65	1.70	0.18	1.27	1.11	0.81	0.97	1.29	0.00
Mn	0.00	0.00	0.00	0.04	0.01	0.01	0.00	0.01	0.02	0.01	0.00	0.01	0.00
Mg	0.00	0.00	0.00	0.00	0.19	0.21	0.34	2.39	2.35	3.88	3.79	3.31	0.00
Ca	2.07	2.07	1.03	0.00	1.15	1.05	0.00	1.36	1.35	1.69	1.55	0.01	0.01
Na	0.00	0.00	0.00	0.01	0.00	0.01	0.03	0.98	0.90	0.32	0.31	0.00	1.00
K	0.00	0.00	0.00	0.00	0.00	0.00	0.84	0.03	0.02	0.01	0.01	0.00	0.00
Sum	8.08	8.08	3.03	2.00	8.00	7.99	6.92	15.46	15.40	15.07	15.06	9.98	5.02
X_{Fe}					0.90	0.89	0.35	0.35	0.32	0.17	0.20	0.28	
X_{Fe3+}	0.24	0.45				X_{Na}	0.03						
y Alm					55	57		0.54	0.59	0.09	0.14	Ab	98.42
z Prp					6	7		0.25	0.25	0.13	0.13	An	1.29
a Grs					38	35		0.47	0.40	0.06	0.05	Or	0.30
c Sps					4	2		0.68	0.68	0.85	0.78		
f								0.14	0.21	0.09	0.07		

TABLE 4. Representative microprobe analyses in the minerals of the lawsonite pseudomoprhs from sample CA. C-core; R-rim

As exposed above, within the aggregates forming the pseudomorphs, it is possible to distinguish two individual sets of stretched clusters defining an internal curved foliation. The first group is composed by albite, chlorite and, frequently, epidote crystals. The second type of clusters is composed of rutile, ±ilmenite and titanite. Titanite occurs as partial or complete coronas around rutile, locally replaced by ilmenite in the outermost rims (Fig. 5h). This curved pattern is oblique to the matrix foliation inside the pseudomorph, and continuous with it in their outer zones. In general, epidote prisms show an oblique orientation with respect to the pseudomorph rims. Clusters orientation is more evident as deformation increases. Finally, the outermost areas of the pseudomorphs overgrow an amphibole–epidote–titanite foliation (S_2). These features suggest that lawsonite crystals were synkinematic with the matrix foliation. Towards the top of the lithological sequence the lawsonite pseudomorphs become more deformed (Fig. 7e). Locally, the matrix of the albite-bearing rocks contains stretched and folded aggregates of epidote, white micas and albite that can be interpreted as strongly deformed lawsonite pseudomorphs by comparison to the neighbouring rocks. Hence, it can be inferred that with increasing strain intensity, lawsonite pseudomorphs were strongly deformed and became progressively incorporated into the matrix.

ALBITE PORPHYROBLASTS

Albite porphyroblasts are only present in the uppermost levels of the sequence and do not coexist with euhedral lawsonite pseudomorphs. To the top of the succession, as exemplified by sample AG, the main foliation is defined by the shape preferred orientation of Ca-amphibole, epidote (type 3; X_{Fe3+} = 0.3–0.4), chlorite (type 3a; X_{Fe}= 0.29), phengitic muscovite (type 3; with Si < 3.4 pfu, X_{Na} = 0.07–0.08), and minor amounts of titanite (type 3; Al_2O_3 ~ 1wt. %), ilmenite (type 3; MnO ~ 1 wt. %) and quartz (Fig. 7c; Table 5). Amphiboles are unzoned actinolite (type 3; Si≈ 7.5 pfu; X_{Fe} = 0.2–0.21; z = 0.08–0.15; c = 0.8–0.88; f = 0.08–0.09) and hornblende (type 3; Si = 6.8–6.9 pfu; X_{Fe} = 0.33–0.35; z = 0.12–0.23; c = 0.71–0.8; f = 0.18–0.23). This foliation wraps around coarse-grained subhedral to anhedral porphyroblasts of albite (type 3; An = 2 and Or = 0.3 %; up to 3 mm long). Porphyroblasts contain linear, curved, folded or helicitic inclusion trails well defined by minerals of variable size (5–200 μm) and continuous with the S_3 foliation (Figs. 3c, 7c). Inclusion trails comprise the same phases as the matrix foliation. Amphiboles in the S_3 foliation are slightly richer in Ca and poorer in Al and Na than S_2 amphiboles (Fig. 6). Albite also locally contains inclusions of anhedral grains of garnet ($g2_R$; Alm62→63%, Prp7→9%, Grs29→27%, Sps0; Fig. 7d) and apatite.

Finally, post-S_3 phases include magnetite, hematite and sulphides concentrated along localized shear planes and carbonates locally overgrowing the S_3 foliation. Other late features include the occurrence of chlorite in fractures and the partial to complete replacement of garnet by chlorite flakes (type 3b; X_{Fe} = 0.46–0.48, Table 5).

Table 5	S_3														Post-S_3	
Mineral	ep3	ep3	sph3	ilm3	g2	g2	$mu3_p$	$mu3_m$		$act3_m$	$hbt3_p$	$hb3_m$	chl3a	ab3	chl3b	chl3b
Analysis	65	72	216	14	13	18	56	61	69	206	42	53	67	22	10	28-1
SiO_2	38.58	38.10	30.06	0.03	37.30	37.53	50.47	50.20	53.50	53.51	46.86	46.52	27.42	67.93	25.3	25.4
TiO_2	0.11	0.15	38.31	52.03	0.08	0.20	0.28	0.32	0.05	0.06	0.19	0.28	0.05	0.00	0.1	0.0
Al_2O_3	29.43	28.47	1.00	0.06	21.75	21.65	28.09	28.20	5.56	3.54	11.74	11.22	20.93	20.30	21.3	21.1
Cr_2O_3	0.08	0.13	0.03	0.03	0.06	0.03	0.04	0.04	0.09	0.05	0.05	0.05	0.24	0.00	0.0	0.0
FeO_T	5.20	7.11	0.23	46.19	27.90	28.4	2.11	2.09	9.31	9.13	13.71	14.26	0.00	0.12	24.3	23.7
MnO	0.00	0.09	0.01	0.98	0.58	0.47	0.03	0.00	0.25	0.21	0.06	0.12	16.39	0.00	0.2	0.2
MgO	0.07	0.02	0.00	0.07	1.87	2.20	3.37	3.33	16.50	17.25	11.43	11.99	0.26	0.02	14.8	15.5
CaO	24.19	23.56	29.36	0.20	10.05	9.49	0.02	0.05	10.60	11.41	9.06	10.20	22.10	0.43	0.0	0.0
Na_2O	0.00	0.06	0.01	0.04	0.03	0.04	0.45	0.53	1.29	0.81	2.64	1.57	0.01	11.47	0.0	0.0
K_2O	0.00	0.01	0.01	0.00	0.00	0.02	9.64	9.72	0.08	0.07	0.27	0.26	0.03	0.06	0.1	0.0
Total	97.6	97.7	99.03	99.63	100	100	94.49	94.48	97.24	96.03	96.00	96.47	87.47	100.3	85.98	85.84
Si	2.98	2.97	0.99	0.00	2.97	2.98	3.37	3.36	7.55	7.67	6.86	6.79	2.79	2.96	2.70	2.71
Ti	0.01	0.01	0.95	0.96	0.01	0.01	0.01	0.02	0.01	0.01	0.02	0.03	0.00	0.00	0.00	0.00
Al	2.68	2.62	0.04	0.00	2.04	2.02	2.21	2.22	0.92	0.59	2.03	1.93	2.48	1.04	2.68	2.66
Cr	0.01	0.01	0.00	0.00	0.00	0.00	0.00	0.00	0.01	0.01	0.01	0.01	0.019	0.00	0.00	0.00
Fe^{3+}	0.29	0.41	0.00	0.08	0.01	0.01	0.04	0.02	0.17	0.16	0.35	0.46	0.00	0.00	0.00	0.00
Fe^{2+}	0.05	0.00	0.01	0.93	1.85	1.87	0.08	0.10	0.93	0.93	1.33	1.28	1.38	0.00	2.18	2.11
Mn	0.00	0.01	0.00	0.02	0.04	0.03	0.00	0.00	0.03	0.03	0.01	0.01	0.02	0.00	0.02	0.01
Mg	0.01	0.00	0.00	0.00	0.22	0.26	0.34	0.33	3.47	3.682	2.49	2.61	3.31	0.00	2.36	2.46
Ca	2.00	1.97	1.04	0.00	0.86	0.81	0.00	0.00	1.60	1.75	1.42	1.59	0.00	0.02	0.00	0.00
Na	0.00	0.01	0.00	0.00	0.01	0.01	0.06	0.07	0.35	0.22	0.75	0.45	0.01	0.97	0.00	0.00
K	0.00	0.00	0.00	0.00	0.00	0.00	0.82	0.83	0.02	0.01	0.05	0.05	0.00	0.00	0.01	0.00
Sum	8.02	8.00	3.03	2.00	8.00	8.00	6.93	6.95	15.07	15.06	15.32	15.22	9.99	5.00	9.96	9.96
X_{Fe}					0.89	0.88	0.19	0.23	0.21	0.20	0.35	0.33	0.29		0.48	0.46
X_{Fe3+}	0.30	0.40				X_{Na}	0.07	0.08								
y Alm					62	63			0.24	0.13	0.45	0.36	Ab	97.68		
z Prp					7	9			0.15	0.08	0.23	0.12	An	2.02		
a Grs					29	27			0.06	0.06	0.29	0.21	Or	0.30		
c Sps					0	0			0.80	0.88	0.71	0.80				
f									0.09	0.08	0.18	0.23				

TABLE 5. Representative microprobe analyses in the minerals of the albite porphyroblasts from sample AG. C–core; R–rim

Three stages of blastesis are distinguished in the evolution of the Cambre metabasic rocks (M_1, M_2 and M_3). The M_1 episode is preserved as a relict S_1 assemblage that comprises inclusions of ep-sph-ru-q within the first generation of garnet (g1). It is followed by a second metamorphic stage, M_2, characterized by the syntectonic development of an assemblage including lawsonite, a second generation of garnet (g2) and a foliation (S_2) consisting of law*-ep-act/bar±gl*#-o*#-mu-ru/ilm-sph-q. This assemblage is preserved at the base of the upper sequence of the MTC. The third stage M_3 is best developed at the top of the sequence. It is characterized by the growth of syntectonic albite porphyroblasts and a foliation S_3 containing ep-act-hb-mu-chl±ilm-sph-q. Whereas both, S_2 and S_3, have the same orientation, first order petrographic observations suggest that they developed at distinct P–T conditions. Finally, post-M_3 crystallization includes post-S_3 phases such as mt, hem, chl, carb, sul, q, variably present in most samples of the Cambre metabasic rocks.

P–T–X EVOLUTION: PSEUDOSECTION MODELLING

In order to constrain the P–T path for the Cambre metabasic rocks, the observed mineral assemblages and chemical compositions have been compared with the stability and compositions of phases in P–T–X pseudosections. Pseudosections were calculated using THERMOCALC 3.33 and 3.37 (Powell and Holland, 1988) and the internally consistent

thermodynamic dataset (Holland and Powell, 1998; updated Nov. 2003). References of the mixing models for solid solutions of the phases considered in the calculations are: amphibole and clinopyroxene (Diener and Powell, 2012), garnet (White *et al.*, 2007 modified by Diener *et al.*, 2008), chlorite (Holland *et al.*, 1998), white mica (Smye *et al.*, 2010), plagioclase (Holland and Powell, 2003), epidote (Holland and Powell, 1998), magnetite (White *et al.*, 2000), ilmenite and hematite (White *et al.*, 2000). Bulk-rock composition was obtained by X-ray fluorescence on a crushed rock slab of a sample of the CA. FeO (vs. Fe_2O_3) was analysed by wet chemical titration. The fluid phase was fixed as pure H_2O, initially in excess. Phase relations were modelled in the chemical system Na_2O-CaO-K_2O-FeO-MgO-Al_2O_3-SiO_2-H_2O-TiO_2-Fe_2O_3 (NCKFMASHTO) between P = 0.5–2.6 GPa and T = 350–600 °C.

The original composition of the studied rocks was simplified to fit this system (Table 1). Because activity-composition relations for Mn-bearing solid solutions are poorly constrained and the studied sample has a low MnO content (0.22 wt. %; Table 1), which is exclusively concentrated in the garnet cores, MnO was not included in the chemical model system. The diagrams are shown in Fig. 9, where white fields are divariant and increasing variance is shown with progressively darker shades. Mineral abbreviations are those used by THERMOCALC (see above).

As a first approach, a H_2O-saturated P–T pseudosection has been computed for the analysed bulk-rock composition (Fig. 9a). In the diagram, quartz is stable across the entire P–T range and TiO_2 is chiefly contained in rutile at P >1.5 GPa and in titanite for P < 1.5 GPa. Glaucophane is stable in most of the fields, with the exception of low pressures and high temperatures where hornblende is stable. Glaucophane commonly occurs with actinolite and omphacite in the HP–LT part of the diagram. Muscovite is stable at P > 6–15 kbar, depending on the temperature, whereas biotite is stable at low pressures. The equilibration conditions of the relic M_1 assemblages included in the Mn-rich garnet core cannot be quantified in this diagram because MnO has not been considered in the calculations (see above), and it extends significantly the stability of garnet towards lower P and T.

Nevertheless, garnet zoning can be used qualitatively to constrain the P–T evolution associated with the crystallisation of the garnet core (g1). The preserved zoning, in particular the decrease in the proportion of spessartine, suggests that the first generation of garnet (g1) grew along the prograde P–T path in an epidote-bearing rock (as ep is an inclusion in g1). By comparison with the interbedded pelitic rocks M_1 can be roughly constrained at ≈ 1.2–1.4 GPa, 350–380 °C (López-Carmona *et al.*, 2013).

The coexistence of lawsonite, epidote and garnet in the syn-S_2 assemblage (law*-ep-act/bar±gl*#-o*#-mu-ru/ilm-sph-q) gives strong P–T constraints in the framework of the present pseudosection. The three minerals are stable together only in a relatively narrow

domain at $T > 550°C$ and $P > 2$ GPa. The calculated amount of the phengitic substiution in muscovite in this domain (Si = 3.36–3.46 pfu; Fig. 9a) fits well that observed in the S_2 foliation (Si = 3.38–3.46 pfu). However, the measured proportion of grossular in garnet decreases in g2 from 38 to 28 mol%, whereas the maximum grossular value modelled in the pseudosection only reaches 31%, and this value is only compatible with the composition of the rim of g2. Nevertheless, this pseudosection provides a suitable starting point for assessing the effects of the components H_2O and Fe_2O_3 that are difficult to quantify reliably using chemical analyses of rocks, but that usually have significant influence on phase equilibria, and hence on the P–T estimates. Furthermore, the metamorphic study of the interbedded pelitic rocks revealed that (1) their prograde evolution occurred in fluid undersaturated conditions due to the crystallization of lawsonite and that (2) the bulk Fe_2O_3 in the metapelites did not reflect the oxidation state during the main metamorphic evolution (López-Carmona *et al.*, 2013). Given these results, a particular attention on these aspects is necessary for the modelling of CA.

The available amount of H_2O has an influence on the position of the compositional isopleths. Then, trying to estimate the amount of H_2O available in the system at peak conditions, a P–X(H_2O) pseudosection has been calculated at 550°C (Fig. 9b). The temperature corresponds to that predicted at H_2O-saturation conditions for the coexistence of epidote, lawsonite and garnet at the maximum content of grossular predicted in the pseudosection (Fig. 9a). In the new diagram the assemblage that would have been stable during the crystallization of g2 is stable above 2 GPa at H_2O-undersaturated conditions in the field gl-act-o-g-law-ep-ru-mu-q. In this area the Si content in S_2-muscovite (typically between 3.38–3.42 pfu) and the X_{Ca} isopleths for the rim composition of g2 (Grs31–28%) intersect between 2–2.1 GPa and 5–10% H_2O (shaded area in Fig. 9b). Therefore, for the subsequent calculations, the amount of H_2O has been fixed at a mean value of 7.5 mol %. The H_2O-out line and the law-out line are almost coincident within this interval, suggesting that the rock reached H_2O-undersaturation due to the crystallization of lawsonite.

With the estimated amount of H_2O (7.5 mol. %) a P–X(Fe_2O_3) pseudosection at 550°C has been calculated to evaluate the effects of varying the Fe_2O_3 content ("0" in the bulk composition; Fig. 9c). Other temperatures have been tested and the exact value does not have a significant effect on the result. Following the above mentioned procedure, in the diagram the assemblage in equilibrium with g2 (gl-act-o-g-law-ep-ru-mu-q) is stable in the H_2O-undersaturated region in a large area above 1.9 GPa, where the relevant isopleths for the rim composition of g2 and the Si content in phengitic muscovite (Grs = 31→28%; Si(mu) = 3.38–3.42 pfu) intersect between 1.9–2.2 GPa and 0.6–1.2 % Fe_2O_3 (shaded area in Fig. 9c). Therefore, this diagram yields no tight constraints on the amount of Fe_2O_3 present in the rock, although it excludes values significantly higher than the analysed one.

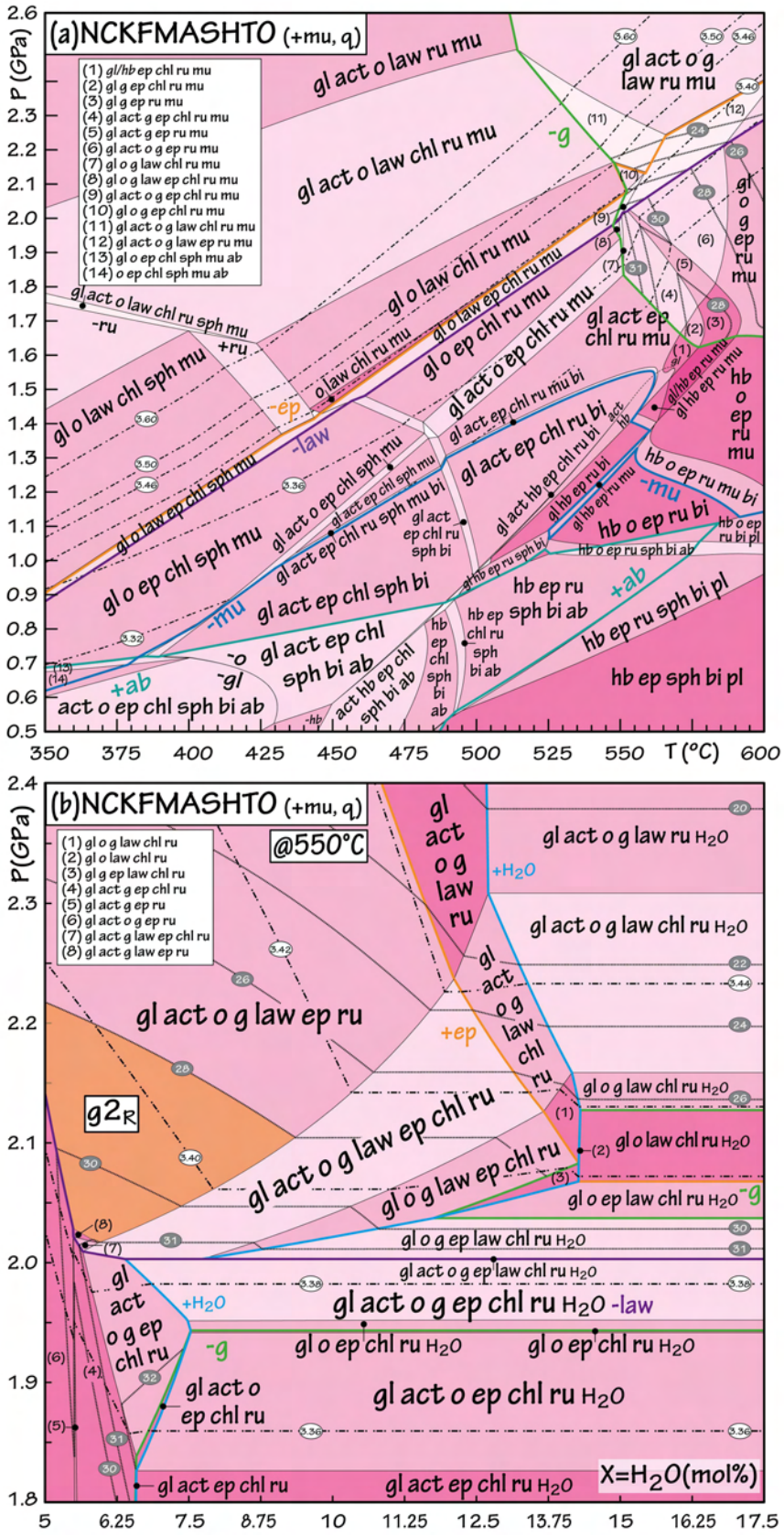

Fig 9. Sample CA [Si02:53.28; Ti02:1.60; Al203:8.76; Fe0: 7.90; Fe203:1.76; Mg0:11.79; Ca0:11.72; Na20:3.15; K20:0.05] (a) P–T pseudosection with H20 in excess; (b) P–X(H20) pseudosection calculated at 550°C for the analysed bulk–rock composition showing H20-out line;

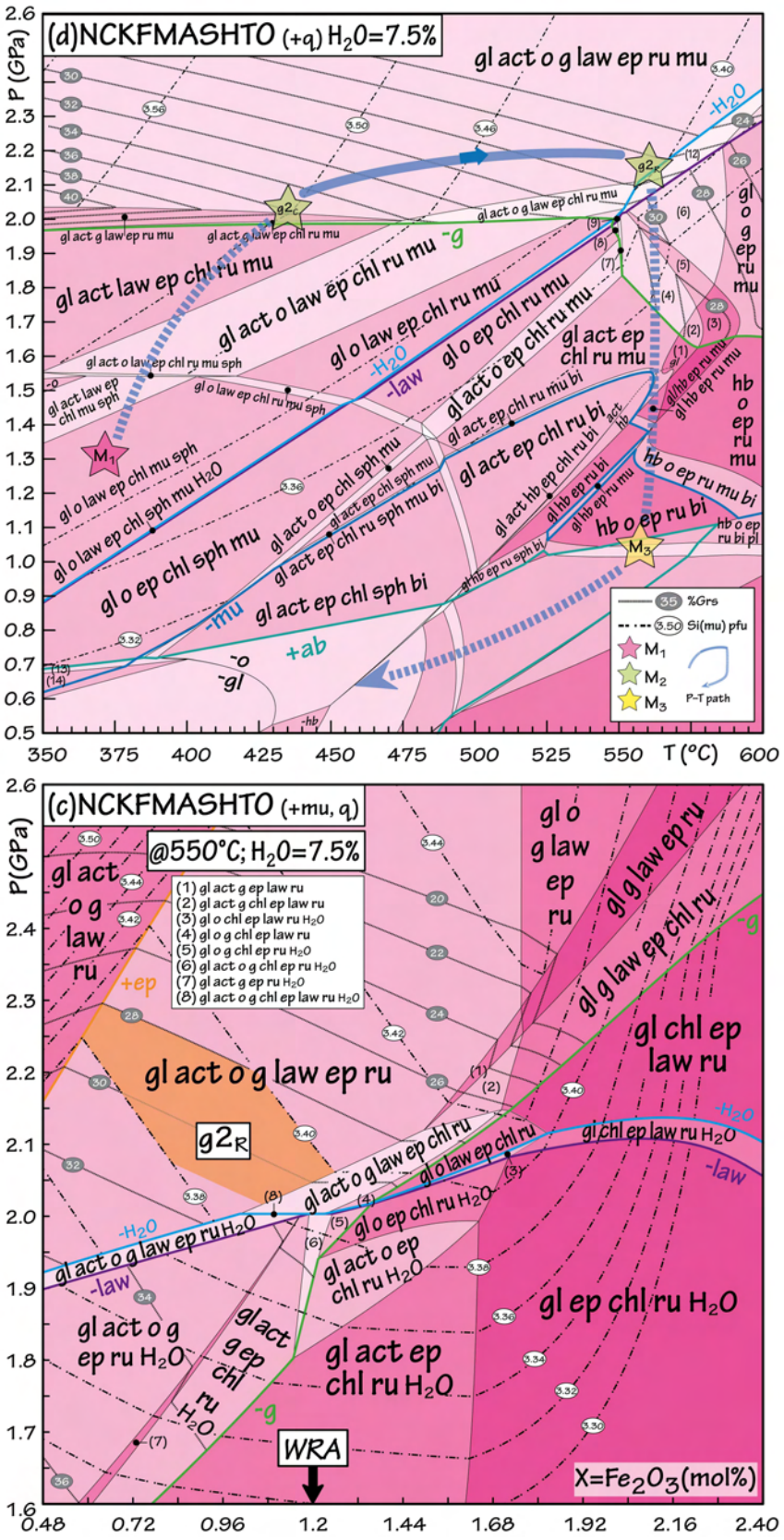

Fig 9. (c) P–X(Fe2O3) pseudosection calculated at @550°C for H2O = 7.5 mol.%; WRA – original whole rock analysis from XRF; (d) P–T pseudosection with H2O = 7.5 mol.%. See text and Table 1 for details.

Based on the inferred estimations, with the aim of establishing the *P–T* evolution for the CA at peak conditions, a new *P–T* pseudosection fixing the amount of H_2O = 7.5 mol. % has been recalculated in the NCKFMASHTO system (Fig. 9d). Compared to the original diagram (Fig. 9a), in this *P–T* pseudosection, the stability of garnet increases significantly in the H_2O-undersaturated region toward lower P (down to 2 GPa) and *T*, and epidote is stable in all the diagram. Thus, the stability of assemblages containing *g* + law + *ep* extends towards low temperature and high-pressures. The paragenesis corresponding to the M_2 stage is located at pressures higher than 2 GPa, in the trivariant fluid-absent field gl-act-o-g-law-ep-ru-mu-q, and the fluid-present equivalent field (label 12 in Fig. 9d). Based on textural observations, this stage of the metamorphic evolution involves crystallization of both lawsonite and garnet 2. In the diagram, the X_{Ca} isopleths for the core of garnet 2 and those calculated for the Si content in S_2-muscovite (Grs = 37%; Si (mu) up to 3.5 pfu) intersect between 2–2.1 GPa at 430–440 °C (shaded star, $g2_C$, in Fig. 9d). The continuous decrease in grossular (37→28%) suggests that garnet 2 rims equilibrated at 2.2 GPa and 550–565 °C. Further evolution involved decreasing pressure, leading to the destabilisation of lawsonite and crossing the solvus between Na and Ca-amphiboles. Above the solvus, the mode of glaucophane is systematically more abundant than the mode of actinolite. Close to the solvus, *z* in glaucophane decreases and *c* increases, and the opposite occurs in actinolite. Thus glaucophane becomes less sodic and more calcic, and vice versa for actinolite. On decompression, the amount of Al^{VI} (*y*) in glaucophane decreases progressively as it approaches the domain where the three amphiboles (gl, act and hb) coexist. In this region both glaucophane and hornblende have a similar *y*, which suggests that glaucophane can progressively recrystallize with compositions approaching those of hornblende. Beyond the solvus actinolite disappears and the mode of hornblende is systematically higher than the mode of glaucophane, which does not exceed 10% (whereas the mode of hornblende is 50%). From this point, the exhumative evolution can be followed in the gl-out domain. The M_3 stage is defined by the appearance of albite at P < 1.1 GP, suggesting a decompression from the law-bearing fields to the fields with stable albite at P ≈ 1–1.1 GPa and *T* ≈ 550–560 °C and a further cooling to the glaucophane and omphacite-out field act-hb-ep-chl-bi-sph-ab-mu-q at P ≈ 0.6–0.7 GPa and *T* ≈ 440–480 °C.

$^{40}Ar/^{39}Ar$ GEOCHRONOLOGY

Timing constraints on the *P–T* evolution of HP terranes are essential to understand the subduction-exhumation process. Whilst the ages of various events of the Lower Allochthon of the MTC have been extensively studied, the data for the Middle Allochthon are limited to only one $^{40}Ar/^{39}Ar$ age on muscovite of 348±8 Ma (Rodríguez *et al.*, 2003). To improve this chronological frame, one of the objectives of this study was to date the blueschist facies fabric and the mylonites of the basal contact by $^{40}Ar/^{39}Ar$ in white mica and amphibole separates. For

that purpose, three samples were selected: one mylonite developed in the felsic gneisses just below the Cambre metabasic rocks (sample MT1), a pelitic schist interbeded with the Cambre metabasic rocks (sample LM, for lower metapelites, from López-Carmona *et al.,* 2013) and one sample of the Cambre metabasic rocks with euhedral lawsonite pseudomorphs (sample CA). Location of the dated samples and their relative structural position is shown on Figs. 1c and 2.

SAMPLE SELECTION

The main goal of dating the mylonites (sample MT1) separating the Lower and the Middle Allochthon in the MTC (Bembibre-Ceán detachment; Fig. 1 a, c) is to establish the age of the early regional extensional phases that leaded to the orogenic collapse in the Allochthonous Complexes of NW Iberia (e.g. Martínez Catalán *et al.,* 2002; Gómez Barreiro *et al.,* 2010; Díez Fernández *et al.,* 2012a). Sample MT1 is a fine- to medium-grained (0.1–1mm) mylonite developed in the granitic orthogneisses of the MTU. It consists of millimeter-scale alternations of chlorite and muscovite and disrupted quartz ribbons that define a banding preserved between extensional shear bands. The phylosilicate domains contain white mica porphyroclasts (0.1–1 mm) with strong undulate extinction and kink-bands, K-feldspar phenocrysts showing partial to complete saussuritization/sericitization (0.4–0.8 mm), epidote (up to 0.5 mm long) crystals and suhedral to anhedral garnet grains (<0.3 mm). The deformation gradient related to this contact decreases both upward and downward, with secondary ultramylonitic shear zones occurring several meters above and below the main shear zone (Fig. 1c; Díez Fernández *et al.,* 2012a). Sample LM was chosen based on its textural equilibrium, characterized by a well-preserved peak mineral assemblage (S_2) mainly preserved as relict micro-inclusions in the rim of garnet porphyroblasts and in specific domains of the matrix foliation. Sample LM shows a medium-grained (0.2–4 mm) porphyro-lepidoblastic texture and a well-developed planar to plano-linear fabric. White mica and quartz constitute >50%, and locally up to 80%, of the modal proportion of each sample. The foliation is defined by the shape preferred orientation of phengitic muscovite, paragonite and chlorite. In these pelitic schists, the matrix foliation usually obliterates an early fabric resulting in a composite foliation S_2+S_3. Whereas S_2 is interpreted as the foliation preserved from the subduction-related blueschist-facies prograde metamorphism, S_3 correspond to the early exhumative event (López-Carmona *et al.,* 2013). Finally, the interbedded Cambre metabasic rocks are usually more retrogressed, and the HP fabric is commonly overprinted by the amphibolite-greenschist facies fabrics. The aim of dating both samples LM and CA is to provide better time constraints for the HP event and/or the early isothermal decompression of the Ceán Unit.

MINERAL CHARACTERIZATION AND SAMPLE PREPARATION

All sample preparation was performed at the Complutense University of Madrid. Samples were crushed and sieved, and single pristine grains of muscovite (samples MT1 and LM) and

hornblende (sample CA) were separated using conventional magnetic and gravimetric methods, followed by hand-picking using a binocular microscope.

The following K-bearing minerals were separated from the samples: 1) lens-shaped crystals of muscovite in the matrix of sample MT1, which range in size from 100 to 1000 μm and have 3.25–3.35 Si pfu and X_K = 0.94–0.98 (Table 6). The selected fraction consists of the crystals in the interval 100-200 μm because they typically have the highest K_2O contents. 2) Crystals of unzoned phengitic muscovite (300–500 μm) from the S_2 matrix foliation of sample LM, which have Si ~ 3.50 pfu and X_K = 0.93–0.99, typically close to 1 (Table 6). It was possible to separate individual unzoned grains larger than 1500 μm. A chemically homogeneous population of S_2-micas in the matrix can be distinguished from the S_3-micas because the latter usually appear in mixed grains together with paragonite, biotite and chlorite and have slightly lower Si content (Si = 3.4-3.45 pfu). In sample CA, hornblende crystals (Si= 7.03→6.96 pfu; X_{Fe} = 0.38→0.41; z = 0.14→0.20; c = 0.80→0.74; f = 0.16→0.18) from the matrix foliation in the grain-size fraction between 200 and 300 μm, were selected (Table 2).

Sample	Lithology	Fabric	Event	Mineral	Mesh(μm)	n Steps	^{39}Ar(%)	Plateau age(Ma)	2σ	MSWD
MT1	mylonite	E	post-M_3	mu	100-200	(8-17)/18	65.32	337	±2.41	1.77
LM	schist	D2	M_2	mu	300-500	(8-19)/20	71.18	354.27	±0.96	1.31
LM	schist	D2	M_2	mu	300-500	(7-19)25	67.07	354.96	±0.96	1.23
LM	schist	D1	M_1	mu	1500	(3-11)/11	98.51	362.75	±2.17	0.72

Sample	MT1					LM				
Mineral	mu	mu	mu	mu	mu	mu	mu	mu	mu	mu
Analysis	35	36	37	38	39	160	64	130	47	70
Lengh (μm)	123.05	141.51	185.54	195	200	310	480	350	420	1500
SiO_2	49.25	49.29	49.26	48.77	48.34	51.29	51.70	52.66	52.65	50.83
TiO_2	0.99	0.75	0.86	0.84	0.68	0.15	0.18	0.24	0.22	0.21
Al_2O_3	28.04	28.78	29.05	29.00	29.89	24.73	24.44	24.67	25.64	23.87
Cr_2O_3	0.02	0.01	0.04	0.01	0.01	0.06	0.07	0.07	0.06	0.03
FeO_T	2.18	2.28	2.04	2.36	2.75	4.36	4.15	4.12	3.11	4.21
MnO	0.00	0.02	0.00	0.04	0.09	0.00	0.00	0.00	0.00	0.03
MgO	2.48	2.68	2.50	2.44	2.38	3.33	3.38	3.26	3.24	3.13
CaO	0.01	0.00	0.00	0.00	0.00	0.03	0.00	0.03	0.02	0.00
Na_2O	0.40	0.39	0.42	0.35	0.12	0.22	0.07	0.48	0.50	0.07
K_2O	9.91	10.12	10.11	10.27	10.94	9.73	10.53	10.98	10.96	10.51
Total	*93.28*	*94.32*	*94.28*	*94.08*	*95.20*	*93.90*	*94.52*	*96.51*	*96.40*	*92.89*
Si	3.35	3.32	3.31	3.30	3.25	3.48	3.51	3.50	3.50	3.51
Ti	0.05	0.04	0.04	0.04	0.03	0.01	0.01	0.01	0.01	0.01
Al	2.25	2.28	2.30	2.31	2.37	1.98	1.95	1.95	2.00	1.94
Cr	0.00	0.00	0.00	0.00	0.00	0.00	0.00	0.00	0.00	0.00
Fe^{3+}	0.00	0.00	0.00	0.00	0.01	0.06	0.00	0.00	0.00	0.00
Fe^{2+}	0.12	0.13	0.12	0.13	0.14	0.18	0.24	0.24	0.17	0.24
Mn	0.00	0.00	0.00	0.00	0.01	0.00	0.00	0.00	0.00	0.00
Mg	0.25	0.27	0.25	0.25	0.24	0.34	0.34	0.34	0.32	0.32
Ca	0.00	0.00	0.00	0.00	0.00	0.00	0.00	0.00	0.00	0.00
Na	0.05	0.05	0.06	0.05	0.02	0.03	0.01	0.01	0.06	0.01
K	0.86	0.87	0.87	0.89	0.94	0.84	0.91	0.91	0.93	0.93
Sum	*6.94*	*6.96*	*6.95*	*6.97*	*7.00*	*6.92*	*6.97*	*6.97*	*7.00*	*6.97*
X_K	0.94	0.94	0.94	0.95	0.98	0.96	0.99	0.99	0.93	0.99
X_{Ca}	0.06	0.06	0.06	0.05	0.02	0.03	0.01	0.01	0.06	0.01

TABLE 6. Summary of the 40Ar/39Ar step-heating results and representative microprobe analysis on muscovites from samples MT1 and LM. XK=K/(Ca+Na+K); XCa=Ca/(Ca+Na+K). Mineral formulas has been calculated using AX software (Holland and Powell, 2000 in Powell and Holland 2002 http:/www.esc.cam.ac.uk/research/research-groups/holland/ax).

ANALYTICAL TECHNIQUES

All analyses were carried out in the ^{40}Ar-^{39}Ar Geochronology Research Laboratory of Queen's University (Kingston, Canada). All samples were ultrasonically rinsed several times in distilled water, wrapped in pure aluminium foil, and stacked vertically in an Al canister, which was then irradiated at the McMaster University Nuclear Reactor in Hamilton, Canada with the ^{40}Ar-^{39}Ar flux monitor - Hb3gr hornblende [1072 ± 11 Ma (2σ)] (Roddick, 1983). Following irradiation, the samples and monitors were placed in small pits, ~2 mm in diameter, drilled in a Cu sample holder. This was placed inside a small, bakeable, stainless steel chamber with a ZnSe viewport connected to an ultra-high vacuum purification system. Monitors were fused in a single step, using a focused New Wave MIR-10 30-watt CO_2 laser.

For the step-heating experiments, the laser beam was defocused to heat the entire sample until fusion as a glass bead in the final step. Samples were heated for ~3 minutes with increasing power increments. The evolved gases were purified using a SAES C50 getter for ~5 minutes. Argon isotopes were measured using a MAP 216 mass spectrometer, with a Bäur Signer source and an electron multiplier. All data were corrected for blanks, atmospheric contamination, and neutron-induced interferences (Onstott and Peacock, 1987; Roddick, 1983). All errors are reported as ±2σ, unless otherwise noted, and dates were calculated using the decay constants recommended by Steiger and Jager (1977).

$^{40}Ar/^{39}Ar$ STEPWISE HEATING RESULTS

$^{40}Ar/^{39}Ar$ step-heating analyses on single grains and concentrates of muscovite and hornblende were performed on each of the selected samples. In this paper it is considered that a reliable plateau age is obtained when the apparent ages of at least three consecutive steps, comprising a minimum of 60% of the $^{39}Ar_k$ released, agree within 2σ error with the integrated age of the plateau segment. The age spectra are shown in Fig. 10 and the corresponding data on Tables 7-10, where ages are reported at ±2σ (95% confidence level).

The apparent-age spectrum from sample MT1 muscovite (Fig. 10a) shows very young apparent ages in the low-temperature steps that rapidly increase to a plateau age of 337 ± 3 Ma (Steps 8-13, MSWD = 1.84) defining 56% of the ^{39}Ar released. Because the low and high-temperature steps in the age spectrum appear to be associated with both elevated Ca/K and Cl/K ratios (Table 7), these are interpreted to reflect possible very minor contamination from minute inclusions in the mica crystal. The integrated age of the sample is 325 ± 3 Ma. A replicate sample also yields similar plateau and integrated ages.

Two $^{40}Ar/^{39}Ar$ step-heating analyses on muscovite concentrates from sample LM give two excellent, identical plateau ages of 354 ± 1 Ma (71% of the ^{39}Ar released, MSWD=1.31; and 67% of the ^{39}Ar released, MSWD=1.23, respectively) (Fig. 10 b, c). A single grain analysis of a

phengite crystal (~1500µm) yielded an older age of 363 ± 2 Ma (98.5% of the ^{39}Ar released, MSWD=0.72) (Fig. 10 d).

In sample CA, the step-heating analyses of a concentrate of hornblende unfortunately yielded no reliable results. Several analyses of hornblende provided integrated ages ranging from 620-800 Ma (not shown because geologically meaningless). These amphiboles are strongly zoned and although the isotopic record of each generation do not need to be affected by the crystallization of texturally younger amphiboles (e.g. Villa *et al.*, 2000), apparently significant excess argon was present in the rock and thus stepwise heating does not yield coherent dates.

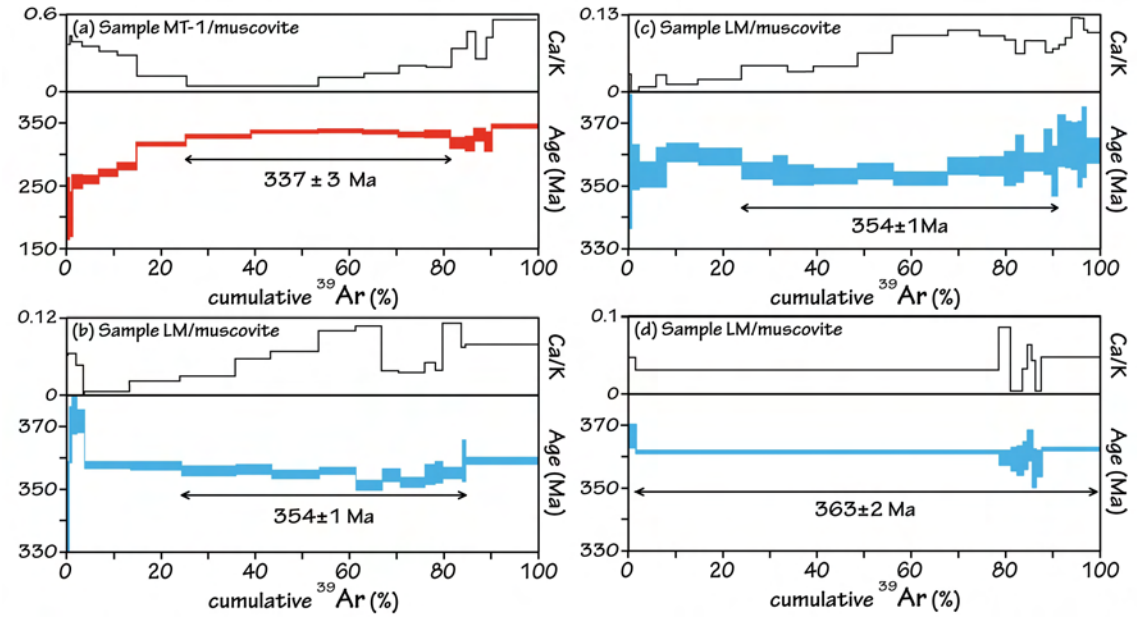

Fig 10. ^{40}Ar/^{39}Ar step-heating results from samples MT1 (a) and LM (b–d).

Ar RETENTION RECORD AND CLOSURE TEMPERATURE

Diffusive-like behaviour of Ar in micas is one of the main advantages in linking ^{40}Ar/^{39}Ar dates to P-T histories. Whereas, Dodson´s (1973) formulation has been often used to estimate the mean closure temperature in cooling geochronological systems, recent studies suggest that because there appears to be a significant pressure dependence of Ar diffusion in muscovite (Harrison *et al.*, 2009) Dodson´s closure-temperature model may not be applicable all metamorphic scenarios, especially to those that have experienced relatively rapid orogenic cycles (e.g. Warren *et al.*, 2008a, b; 2012). Therefore, linking an apparent muscovite ^{40}Ar/^{39}Ar age to a single closure temperature must be done cautiously (e.g. Warren *et al.*, 2012). The closure temperature of muscovite (and broadly, white mica) in the K-Ar isotopic system have been commonly discussed (e.g. discussion by Rodríguez *et al.*, (2003), Bosse *et al.*, (2005) and Pitra *et al.*, (2010), in similar rocks of Variscan age). Currently, several studies using ^{40}Ar/^{39}Ar dating in HP terranes show that the isotopic closure temperature for white micas in the blueschist-facies conditions may be as high as 500 °C for muscovite (Villa, 1998; Bosse *et al.*,

2005; Harrison *et al.*, 2009) or higher than 550 °C (Lister and Baldwin, 1996; Pitra *et al.*, 2010) for phengitic muscovite. This is confirmed by the temperature conditions (ca. 460 °C) established for the HP event in the Ceán Unit. In the present study, the metamorphic muscovite $^{40}Ar/^{39}Ar$ ages have been evaluated using the method proposed by Warren *et al.*, (2012).

This method enables one to determine if $^{40}Ar/^{39}Ar$ muscovite should be interpreted as either crystallization or cooling ages. Assuming a cooling rate of 20°C/Ma (common in HP–LT terranes; e.g. Ernst (1973) and Newton and Fyfe (1976), although almost similar results are obtained for a rate of 10°C/Ma) peak P–T conditions estimated for sample LM (≈ 2.1 GPa and ≈ 460 °C; López-Carmona *et al.*, 2013) and considering a grain size fraction between 0.1–1 mm radii (cf. Table 6), modelling suggests that at the estimated peak conditions, Ar diffusion follows two different trends (cf. Fig. 4 in Warren *et al.*, 2012). In the largest grains (≈ 1mm), Ar diffusion is inefficient over the short duration of heating (> 80% Ar retention) and such crystals probably preserve most of the radiogenic Ar-production, suggesting that the obtained dates may be interpreted as crystallization ages. The smallest grains (> 0.5 mm), however, plot in the region showing partial diffusive loss (> 60% Ar retention). This difference of Ar retention in chemically homogeneous muscovites reflects the influence of grain radius on Ar diffusion. On the other hand, conditions constraining the muscovites in sample MT1, inferred to represent the last stages of the exhumation (≈ 8 GPa and ≈ 460 °C; López-Carmona *et al.*, 2013), are projected in the region dominated by efficient Ar diffusion (> 20% Ar retention) and are thus interpreted as cooling ages (Fig. 11).

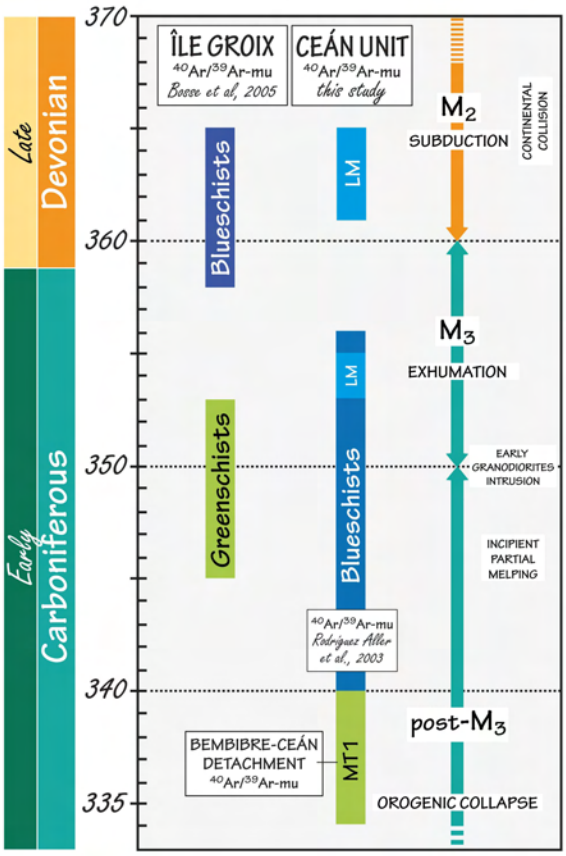

Fig 11. Synthesis of the 40Ar/39Ar ages from the blueschists in the Middle Allochthon of the Ibero-Armorican Arc. The interpretation on the age of the metamorphic stages is also indicated. Devonian–Carboniferous boundary after Walker et al (2012).

DISCUSSION AND CONCLUSIONS

The Upper Sheet of the MTC developed a metamorphism in the blueschist-facies conditions (López-Carmona *et al.*, 2010; 2013). The lower structural levels of the sequence preserve evidence of the subduction-related metamorphism, whereas the upper structural

levels contain indications of the exhumative evolution. Then, the Cambre metabasic rocks show systematic changes in texture and mineral composition that are spatially related. Their prograde metamorphic evolution has been studied through pseudosection approach in samples from the less deformed levels of the middle part of the sequence containing garnet porphyroblasts, rich in S_1 and S_2 inclusions, and abundant well-preserved pseudomorphs of euhedral lawsonite. It is characterized by a *P–T* evolution in the lawsonite blueschist/LT-eclogite-facies conditions peaking at $P \approx 2.2$ GPa and $T \approx 550–560$ °C (Fig. 12).

PHASE DIAGRAMS: CONSISTENCY BETWEEN CALCULATIONS AND NATURAL ASSEMBLAGES

Calculated phase diagrams account reasonably well for the first-order petrographic observations. Pseudosection calculations indicate that the prograde evolution would have occurred in H_2O-undersaturated conditions induced by the crystallization of lawsonite, as demonstrated for the interbedded metapelitic rocks by López-Carmona *et al.,* (2013). The transition from lawsonite blueschist/LT-eclogite to amphibolite-greenschist facies may involve significant hydration (*e.g.* Schliestedt and Matthews, 1987; Barrientos and Selverstone, 1993; Bosse *et al.,* 2002), principally as a result of lawsonite breakdown (cf. Ballèvre *et al.,* 2003; Clarke *et al.,* 2006; López-Carmona *et al.,* 2013). Thus, the H_2O content appears to be a critical factor in the metamorphic evolution of the Cambre metabasic rocks. Nevertheless, the modelling failed to reproduce some of the petrographic observations. First, the stability of titanite in the pseudosections, limited to low pressures, whereas it is a common phase in all assemblages, as inclusions and in the matrix. This may be explained by the fact that titanite is considered as a pure end-member in the model, whereas analysed titanite has small, but non negligible, substitutions of Al and Fe (ranging from 1 to 2 wt. % and up to 1.2 wt. %, respectively; Tables 2–5). This is rather common, particularly at high pressures (*e.g.* Franz and Spear 1985; Holényi and Annerstein 1987; Enami *et al.,* 1993; Tropper *et al.,* 2002; Harlov *et al.,* 2006; Manon, 2008). Althought minor, these substitutions (that commonly do not exceed a couple of weight %) could significantly extend the stability of titanite and explain this apparent incompatibility between the observations and the predictions in the calculated phase diagrams. Second, the model does not predict ilmenite and paragonite. In a hydrated MORB system ilmenite is expected to stabilize at LP–HT conditions (Liou *et al.,* 1998; Meinhold, 2010), whereas rutile or titanite are the dominant Ti-bearing minerals in the *P–T* range of the presented phase diagrams. Ilmenite occurs replacing rutile and associated with titanite coronae as a late phase during the retrograde metamorphism. Its crystallisation thus probably reflects local equilibrium and cannot be reliably modelled in a phase diagram that supposes equilibration at the scale of the entire sample. Although the coexistence of these three Ti-rich phases is well known, it has not yet been constrained experimentally (Liou *et al.,* 1998). Additionally, the modelled chemical system is Mn-free and ilmenite contains up to a 2 wt. % of MnO, which can extend its stability domain.

Similarly, paragonite is exclusively present as a product of destabilization of lawsonite (it is not present in the matrix foliation). This process cannot be accounted for appropriately in the framework of diagrams calculated for the analysed bulk composition of the sample. Indeed, the pseudomorphic replacement of lawsonite by the epidote + phengite/paragonite + chlorite + albite ± quartz aggregates reflects equilibration in volumes close to the size of the lawsonite crystals, and hence an effective bulk composition (e.g. Tracy, 1982; Stüwe, 1997) significantly different from that of the entire sample. Finally, biotite is modelled at $P < 1.4$ GPa, but not observed in the Cambre metabasic rocks. However, the proportion of biotite predicted in the diagram reaches a maximum of 0.7 % along the proposed P–T path and further decreases with decreasing temperatures. Therefore, biotite could have been stable but not observed, for example because it was chloritised during retrogression.

LAWSONITE CRYSTALLIZATION IN THE BLUESCHISTS

Lawsonite crystals in the Cambre metabasic rocks are entirely pseudomorphed by an aggregate of epidote + phengite/paragonite + chlorite + albite ± quartz. The breakdown products of lawsonite may follow a reaction g + gl + law = chl + ep + mu/pa + H_2O (cf. Will *et al.,* 1998; Ballèvre *et al.,* 2003) and may represent the onset of retrogression into the amphibolite-greenschist facies (e.g. Shelley and Bossière, 1999). Modelling suggests that the S_2 foliation was glaucophane-bearing. Due to the retrograde overprint during the transition from the blueschist/LT-eclogites to the amphibolite-greenschist facies conditions, almost all traces of the destabilisation of former phases were destroyed. However, relict textures as the recrystallized symplectitic intergrowth of hornblende and albite in the matrix foliation, and the chlorite-albite aggregates inside the pseudomorphs, may represent the replacement of former crystals of glaucophane. Moreover, in the interbedded pelitic rocks, glaucophane has been found in the S_2 foliation preserved as relict microinclusions in the rim of garnet porphyroblasts, confirming its occurrence during M_2 in the Ceán Unit.

Despite complete retrogression, the preservation of some of the lawsonite crystal shapes indicates that pseudomorphism occurred as a static process (e.g. Ballèvre *et al.,,* 2003) and particular levels of the blueschist host rock were not affected by penetrative deformation during exhumation (e.g. Philippon *et al.*, 2013). Petrographic observations and phase diagram calculations suggest that the second generation of garnet grains (g2) and lawsonite crystallized at peak conditions in the matrix assemblage (M_2), and replacement took place at decreasing pressure, in the early almost isothermal decompression stages (post-M_2) (Fig. 11). Then, communication between the garnet inclusions (g2) in the pseudomorphs and the matrix during lawsonite crystals replacement could have facilitated the development of diffusion zoning in the rim (Fig. 8). It is therefore possible that garnet resorption and the destabilisation of lawsonite were simultaneous (Fig. 4). Lawsonite would then have grown at the metamorphic peak, at the end of garnet crystallisation, but before its resorption.

METAMORPHIC EVOLUTION OF THE CEÁN UNIT

The Ceán Unit is the westernmost exposure of the Middle Allochthon in the NW Iberian Massif. It is constituted by the Ceán pelitic schists and the Cambre metabasic rocks, which are interpreted to represent a volcano-sedimentary sequence in an ocean-continent transitional domain. Both lithologies have recorded similar P-T evolutions comprising three metamorphic episodes (M_1-M_3; Fig. 12).

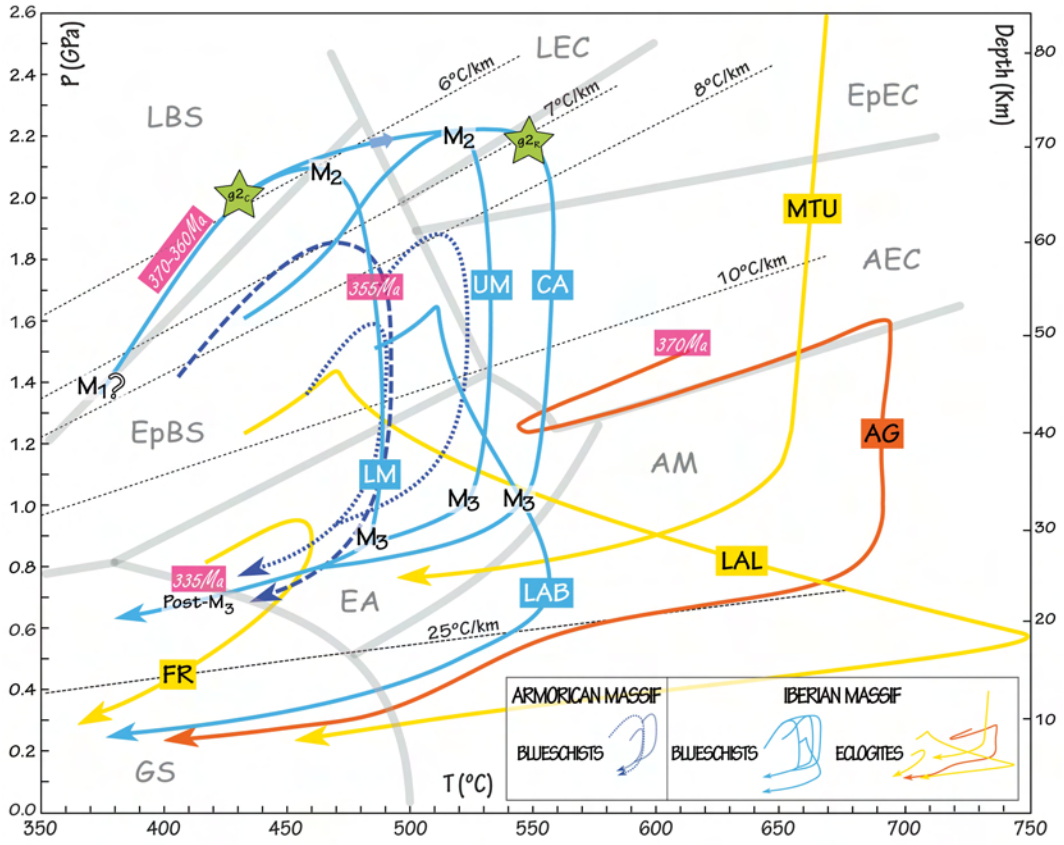

Fig 12. P-T diagram showing a summary of the metamorphic paths from the lower and middle allochthonous units in the NW Iberian Massif. In the Middle Allochthon: the Ceán (Cambre metabasic rocks-CA, Ceán schists-LM and UM) and the Lamas de Abad (LAB) units. In the Lower Allochthon: the Malpica-Tui (MTU), Agualada (AG), Lalín (LAL) and Forcarei (FR) units. For comparison, the P-T path for the Upper Unit of of Ile de Groix is also shown, after Philippon et al., (2009; thickest dashed line) and Bosse et al., (2002) and Ballèvre et al., (2003; thinnest dashed line). Metamorphic facies field abbreviations: GS, greenschist facies; EA, epidote-amphibolite facies; AM, amphibolite facies; LB, lawsonite blueschist facies; EB, epidote blueschist facies and AEC, amphibole-eclogite facies; EpBS and LBS, epidote and lawsonite blueschists, respectively; EpEc and LEC, epidote and lawsonite eclogites, respectively; after Heinrich and Althaus (1988), Evans (1990), Maruyama et al., (1996) and Okamoto and Maruyama (1999). M1, M2, M3 and post-M3-metamorphic events; M2 in the CA is indicated by the stars g2C and g2R (from Fig. 9d). g2-garnet 2; C-core; R-rim.

The first episode (M_1) represents the early subduction-related stages and is only preserved in the lower structural levels of the sequence (López-Carmona *et al.*, 2013). M_1 is characterized by the relics of a former assemblage partially preserved as S_1 inclusions (ep-sph-ru-q) in the core of large garnet porphyroblasts, and has been roughly constrained at ≈ 1.2-1.4 GPa, 350-380 °C. The second metamorphic stage, M_2, is evidenced by the syntectonic development of an assemblage including lawsonite, glaucophane, a second

generation of garnet (g2) and a foliation (S_2) consisting of ep-act/bar-o*#-mu-ru/ilm-sph-q in the metabasic rocks and ctd-chl-mu-pa-ru/ilm-q in the metapelites. This assemblage is preserved at the base and in the middle part of the Ceán Unit of the MTC. M_2 represents the subduction-related blueschist facies prograde metamorphism and is characterized by a H_2O-undersaturated prograde *P–T* path peaking at 1.9–2.2 GPa. The temperatures recorded by the metapelitic and the metabasic rocks differ slightly. From the bottom to the top of the sequence, the sample of the Cambre metabasic rocks (CA) is the lowermost one, overlying the mylonites (sample MT1). The lower metapelites (sample LM) are located immediately above CA, whereas the upper metapelites (sample UM, for upper metapelites of López-Carmona *et al.,* 2013) are situated in the middle part of the synformal structure, in an upper structural domain separated from the lower domain by a mylonitic band (Fig. 1c). Within the Ceán schists, the temperature of the pressure peak is of ca. 460°C at the base (LM) and of ca. 520°C in the intermediate part of the sequence (UM; López-Carmona *et al.,* 2013). The temperature estimated for the Cambre metabasic rocks is slightly higher and constrained at ca. 560 °C. Both metapelites and metabasic rocks have recorded similar *P–T* histories. The slight variations in temperature could reflect different position of the samples in the orogenic wedge (cf. López-Carmona *et al.,* 2013; Fig. 13), or the thermal effects of fluid migration during metamorphism. In numerous orogens it has been reported that metamorphic hydration reactions represent a possible mechanism that may lead to a localized increase in temperature due to fluid flow (e.g. Peacock, 1987; Yakovlev, 1993; Stober and Bucher, 2004; Dipple and Ferry, 1992; Wing and Ferry, 2002, 2007; Lyubetskaya and Ague, 2009). Nevertheless, crustal fluid flow models are not easy to evaluate and are beyond the scope of this paper. Another possibility for these temperature variations may be due to the deformation gradient related to the contact between the Lower and the Middle Allochthons. This gradient decreases both upward and downward. The conversion of mechanical energy into heat is a well know processes, commonly referred to as shear heating (e.g. Souche *et al.,* 2013; Gottardi *et al.,* 2013). Accordingly, the two samples with the highest equilibration temperature (CA and UM) are located immediately above a shear zone. Sample CA, showing the highest temperature (560 °C) is located just above the main shear zone, and sample UM is located just above a secondary mylonitic band (Fig. 1c). Thus, temperature seems to increase with deformation.

However, it should also be stressed out that the absolute accuracy of the *P–T* estimation based on pseudosections should not be overestimated. The main advantage of this approach is the determination of the qualitative evolution of the rocks. The absolute values are subject to a certain degree of uncertainty, related among others to the accurate estimation of the effective bulk rock composition (and its possible evolution along the P-T path) and the accuracy of the mixing models for solid solutions. It is therefore possible that the difference in the absolute P-T conditions recorded by the metapelitic and metabasic samples may be within an acceptable error.

Finally, M_3 is best developed at the top of the sequence. It is characterized by the growth of syntectonic albite porphyroblasts and a foliation S_3 containing ep-act-hb-chl-mu±ilm-sph-q in the metabasic rocks, and ep-chl-mu-pa-bi-ru/ilm-sph-q±g±win/bar in the metapelites, during the retrograde part of the *P–T* path. The exhumation-related metamorphism is characterized by a nearly-isothermal decompression to ≈ 1 GPa, 550–560 °C (M_3) and an amphibolite-greenschist facies overprint between ≈ 0.6–0.7 GPa and *T* ≈ 460–480 °C (post-M_3).

AGE OF THE METAMORPHISM IN THE MTC

An attempt of dating the age of the HP event in the upper tectonic sheet of the MTC (Ceán Unit) has been carried out on phengitic muscovite concentrates and single grains from the Ceán schists. The older age of ca. 363 ± 2 Ma obtained in this study is interpreted as a young limit on the age of the M_2 blueschists facies metamorphism in the Middle Allochthon of the MTC. Considering the age of ca. 365 Ma is interpreted as a crystallization age, and that the first blueschist-facies stage (M_1) represents the early subduction-related metamorphism, this age may be interpreted as a young limit because M_1, recorded by both metapelites and metabasic rocks, remains unconstrained. As mentioned above, M_1 is recorded by aligned inclusions in the core of garnet porphyroblasts and in-situ laser ablation analyses were not performed. This age is consistent with the other muscovite plateaus of ca. 355 Ma, which are interpreted as cooling ages and are inferred to represent some point relatively close to peak conditions at the onset of the isothermal decompression. These ages are consistent with the available geochronological data for the eclogite-facies peak metamorphism in the MTC. According to U-Pb, $^{40}Ar/^{39}Ar$ and Rb-Sr data, the age of the HP metamorphism in eclogites and eclogite-facies rocks from the MTU (i.e. lower sheet of the MTC; Fig. 1a) has been constrained at ca. 370 Ma, considered the minimum age of the subductive event that ended around ca. 365 Ma (van Calsteren *et al.,* 1979; Santos Zalduegui *et al.,* 1995; Rodríguez *et al.,* 2003; Abati *et al.,* 2010). The $^{40}Ar/^{39}Ar$ ages presented in this study and data from Rodríguez *et al.,* (2003), suggests that post-peak metamorphic evolution may be constrained between ca. 360 and 350 Ma, including the main stacking of the basal and middle allochthonous units. The beginning of post-nappe tectonics is defined by the intrusion of early I-type Variscan granodiorites at ca. 350-340 Ma, (Serrano Pinto *et al.,* 1987; Bellido *et al.,* 1992; Gallastegui, 1993; unpublished data, G. Gutiérrez-Alonso and J. Fernández-Suárez, pers. com.). This time interval would include the incipient partial melting related to decompression that took place under amphibolite-facies conditions in the Lower Allochthon (Abati, 2002), dated by U-Pb in zircon in the Agualada unit at ca. 346 Ma (Abati and Dunning 2002). Furthermore, it is consistent with the Lalín-Forcarei thrust activity constrained by $^{40}Ar/^{39}Ar$ in muscovite at around 340 Ma (Dallmeyer *et al.,* 1997) and considered as responsible of the ultimate emplacement of the Lower and Middle Allochthon nappes by the underthrusting of a new crustal sheet (the Parautochthon; Martínez Catalán *et al.,* 2002; 2007; Abati *et al.,*

2010). Subsequently, exhumation in the MTC was driven by thrusting and recumbent folding associated with the so called Bembibre-Pico Sacro detachment system. Its activity has been constrained from 340 Ma to 317 ± 15 Ma, coeval with widespread magmatism and the late orogenic collapse (Gómez Barreiro *et al.,* 2003; 2007; Martínez Catalán *et al.,* 2009; Diéz Fernández *et al.,* 2011), with the Bembibre-Ceán detachment being older than the Pico Sacro detachment (Gómez Barreiro *et al.,* 2010). Then, the extensional shearing that led to the gravitational collapse of the orogen may be constrained at ca. 337 ± 3 Ma.

The age of the HP event in the blueschist-facies conditions in the Ceán Unit can be constrained at a minimum age ca. 363 ± 2 Ma. Differences between the HP–LT event, and the beginning of the postnappe tectonics (at ca. 350-340 Ma), confirms that the exhumation of the MTC lasted ca. 15-20 Ma (Llana-Fúnez and Marcos, 2002; Rodríguez *et al.,* 2003; Abati *et al.,* 2010). Assuming a pressure peak of 2.1 GPa (and the corresponding maximum subduction depth in the blueschists; López-Carmona *et al.,* 2013), a nearly isothermal decompression from 2.1 to 0.8 GPa provides an exhumation rate of ≈ 2.5 mm/year from 60 to 24 km. Afterward, during the orogen collapse, a fast cooling may follow rapid exhumation because of the upward advection of heat (e.g. Ring *et al.,* 1999). Therefore, last stages of exhumation from 0.8 to 0.5 GPa occurred within a period of ca. 15 Ma (from 350 to 335 Ma) and from *T* =480 to 380 °C, suggesting a cooling rate of 7°C/Ma (or a geothermal gradient of 10°C/km). These rates are in agreement with well constrained natural examples and numerical thermal-mechanical models (e.g. Grasemann *et al.,* 1998; Gerya *et al.,* 2002; Kylander-Clark *et al.,* 2008; Warren *et al.,* 2008b; Burov *et al.,* 2012), which suggest that decompression occurs in two stages (1) a slower exhumation stage with little temperature change over a large depth interval and (2) a phase of fast cooling once the rocks have reached an upper crustal level (Fig. 12).

EQUIVALENCES ALONG LOWER AND MIDDLE ALLOCHTHON IN THE IAA

In the Iberian Massif, according to their metamorphism and tectonostratigraphy, the Lower and Middle Allochthons form two tectonically juxtaposed sheets (Fig. 1a). The Lower Allochthon is interpreted as a slice of a continental crust, where felsic orthogneisses and terrigenous metasediments predominate (Rodríguez, 2005). It forms the lower part of MTC (i.e. MTU), Santiago, Agualada, Lalín, Forcarei (Órdenes Complex) and Espasante (Cabo Ortegal Complex) units (Martínez Catalán *et al.,* 1996; 2009; Rubio Pascual *et al.,* 2002; Rodríguez, 2005; Gómez Barreiro *et al.,* 2010). Possible equivalents in the South Armorican Domain are the Cellier, Saint-Mars and Mauves units (Champtoceaux Complex) and Sainte-Pazanne unit (Essarts Complex, Vendée) (Ballèvre *et al.,* submitted; Fig. 1b).

The Middle Allochthon is interpreted to represent a volcano-sedimentary sequence viewed as a more distal part of the same continental margin transitional to an oceanic domain

(Rodríguez, 2005). The Ceán (MTC), Lamas de Abad and Cercio (Órdenes Complex) units in the Iberian Massif (Rodríguez *et al.*, 2003; López-Carmona, 2010; Gómez Barreiro *et al.*, 2010), and Groix and Bois-de-Cené in the Armorican Massif (Ballèvre *et al.*, 2009: and references therein) belong to the Middle Allochthon (Ballèvre *et al.*, submitted).

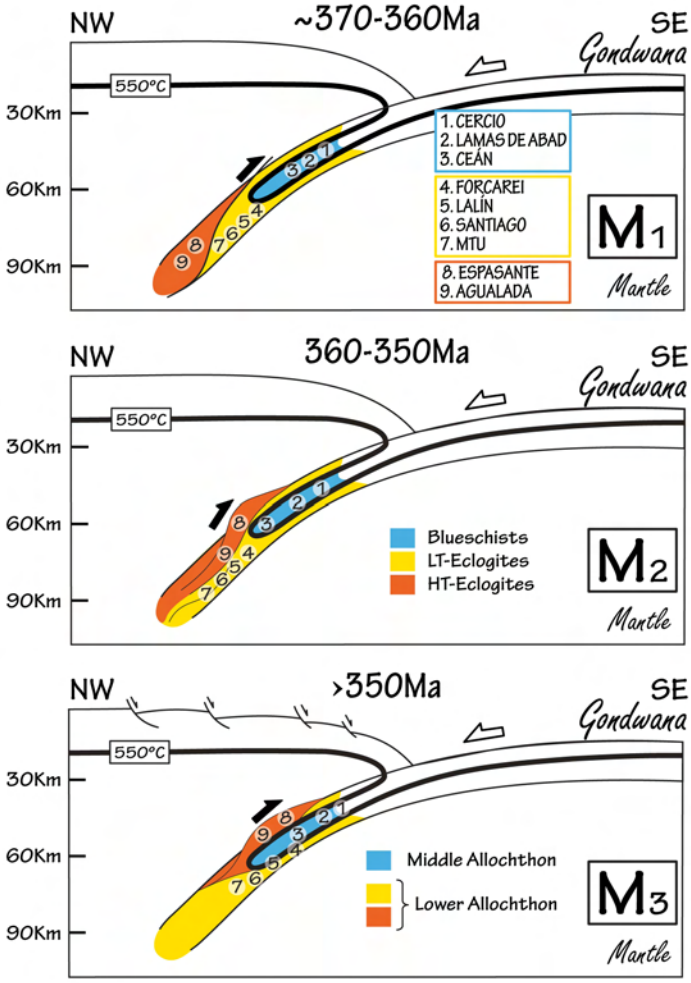

Fig 13. Schematic cross-section of the subduction zone operating in the NW Iberian Massif at 370–360 Ma, 360–350 Ma and below 350 Ma. Based on Martínez Catalán et al., (1996) and López-Carmona et al., (2013).

In the NW Iberian Massif, both sheets share a first HP metamorphic event but, according to their initial location in the subducting slab, the characteristics of this metamorphism are different. In general, the Lower Allochthon developed eclogite-facies metamorphism (Gil Ibarguchi and Ortega Gironés 1985; Arenas *et al.*, 1997; Rubio Pascual *et al.*, 2002; Rodríguez *et al.*, 2003), whereas the overlying Middle Allochthon reached blueschist-facies conditions (Arenas *et al.*, 1995; Rodríguez *et al.*, 2003; López-Carmona *et al.*, 2010). In the eastern part of the Lower Allochthon (Forcarei unit; Fig. 1a) the metamorphic conditions are in the blueschist facies, and going to the west the peak P and T increases progressively up to medium-T eclogite facies in the MTC (Figs. 1a, 13). The overlying Middle Allochthon is separated by a major tectonic contact (Bembibre-Ceán detachment) and is always in

blueschist-facies conditions. In a few places, the blueschist facies units are interlayered between two eclogite-facies units (e.g. the Ceán Unit is sandwiched between the MTU and the Agualada unit, Fig. 1c). The interlayering has been previously interpreted as an original feature of the subducted complex, related with the typical geometry of the isotherms in subduction zones (e.g. López-Carmona *et al.*, 2013; Fig. 13).

ACKNOWLEDGEMENTS

We thank C. Valdehita from the Universidad Complutense de Madrid for her technical support and advices in $^{40}Ar/^{39}Ar$ mineral separation. We appreciate the technical assistance of D.A. Archibald and H. Fournier from the Queen's University $^{40}Ar/^{39}Ar$ Geochronology Laboratory. J.R. Martínez Catalán and R. Fernández Díez are thankfully acknowledged for their help and support in sampling. We are grateful to J.Fernández-Suárez and G. Gutiérrez-Alonso that kindly allow us to use their unpublished age constraints. Stimulating discussions with A. García-Casco, M. Ballèvre and R. Arenas has significantly improved the quality of this manuscript. This work has been financially supported by the Spanish Project CGL2012-34618 (Ministerio de Ciencia e Innovación).

Sample MT1		Step	Laser Power (Wats)	$^{40}Ar/^{39}Ar$	± (1σ)	$^{38}Ar/^{39}Ar$	± (1σ)	$^{37}Ar/^{39}Ar$	± (1σ)	$^{36}Ar/^{39}Ar$	± (1σ)	$^{40}Ar^*/^{39}Ar_{(K)}$	± (1σ)	$^{40}Ar^*$(%)	Cumulative ^{39}Ar (%)	Age (Ma)	± (1σ)	Ca/K	± (1σ)	Cl/K	± (1σ)
J	0.016564	1	1.50	7.641	0.182	0.028	0.018	0.106	0.038	0.000	0.006	7.611	1.889	99.605	0.404	214.20	50.12	0.192	0.069	0.003	0.004
± (1σ)	0.000018	2	1.60	9.111	0.172	0.033	0.012	0.148	0.025	0.006	0.004	7.249	1.336	79.556	1.086	204.57	35.66	0.269	0.048	0.004	0.003
% error	0.11	3	1.70	9.312	0.090	0.022	0.004	0.119	0.009	0.000	0.001	9.283	0.419	99.676	3.170	258.04	10.85	0.216	0.019	0.002	0.001
Int Age (Ma)	325.01	4	1.80	9.716	0.075	0.017	0.002	0.100	0.007	0.001	0.001	9.415	0.247	96.892	6.729	261.44	6.39	0.181	0.015	0.001	0.000
± (2σ)	2.03	5	1.90	10.081	0.064	0.015	0.002	0.082	0.005	0.001	0.001	9.848	0.220	97.681	10.739	272.61	5.65	0.149	0.011	0.000	0.000
with ± in J	2.13	6	2.00	10.431	0.067	0.016	0.002	0.071	0.004	0.001	0.001	10.258	0.203	98.340	14.760	283.11	5.20	0.128	0.010	0.000	0.000
Plateau Age	337.17	7	2.10	11.855	0.061	0.015	0.001	0.032	0.002	0.000	0.000	11.691	0.099	98.616	25.329	319.36	2.47	0.058	0.004	0.000	0.000
± (2σ)	3.15	8	2.20	12.318	0.054	0.015	0.001	0.022	0.002	0.000	0.000	12.202	0.085	99.057	39.207	332.09	2.12	0.040	0.003	0.000	0.000
with ± in J	2.50	9	2.30	12.646	0.053	0.015	0.001	0.022	0.001	0.000	0.000	12.516	0.074	98.967	53.461	339.88	1.84	0.040	0.003	0.000	0.000
MSWD	1.84	10	2.40	12.755	0.063	0.016	0.001	0.030	0.002	0.001	0.000	12.572	0.103	98.557	63.199	341.26	2.55	0.055	0.004	0.000	0.000
% ^{39}Ar	56.00	11	2.50	12.566	0.064	0.015	0.001	0.036	0.003	0.000	0.000	12.474	0.122	99.261	70.812	338.84	3.03	0.065	0.006	0.000	0.000
		12	2.60	12.454	0.067	0.015	0.001	0.047	0.003	0.000	0.000	12.319	0.157	98.911	76.430	335.01	3.91	0.086	0.007	0.000	0.000
		13	2.70	12.531	0.078	0.014	0.002	0.046	0.004	0.001	0.001	12.357	0.220	98.605	81.754	335.94	5.45	0.083	0.008	0.000	0.000
		14	2.80	11.892	0.103	0.016	0.002	0.091	0.006	0.000	0.001	11.777	0.328	99.032	85.113	321.51	8.21	0.166	0.014	0.000	0.000
		15	2.90	11.797	0.129	0.014	0.005	0.174	0.011	0.000	0.001	11.740	0.457	99.503	86.936	320.57	11.42	0.317	0.025	0.000	0.001
		16	3.00	12.790	0.117	0.015	0.003	0.061	0.008	0.002	0.001	12.321	0.399	96.329	89.241	335.05	9.91	0.111	0.015	0.000	0.001
		17	3.10	12.608	0.140	0.018	0.005	0.139	0.013	0.002	0.002	11.863	0.612	94.076	90.653	323.64	15.29	0.253	0.027	0.001	0.001
		18	5.50	13.078	0.065	0.022	0.001	0.273	0.006	0.001	0.000	12.877	0.108	98.445	100.000	348.79	2.65	0.498	0.025	0.002	0.000

TABLE 7. (a) $^{40}Ar/^{39}Ar$ analyses on muscovite concentrates from sample MT1. The plateau has been inferred considering the steps indicated in bold italics. The age spectrum is shown in Fig. 10a. ELECTRONIC SUPPLEMENTARY MATERIAL

Sample LM		Step	Laser Power (Wats)	$^{40}Ar/^{39}Ar$	± (1σ)	$^{38}Ar/^{39}Ar$	± (1σ)	$^{37}Ar/^{39}Ar$	± (1σ)	$^{36}Ar/^{39}Ar$	± (1σ)	$^{40}Ar^{*}/^{39}Ar_{(K)}$	± (1σ)	$^{40}Ar^{*}$(%)	Cumulative ^{39}Ar (%)	Age (Ma)	± (1σ)	Ca/K	± (1σ)	Cl/K	± (1σ)
J	0.016578	1	1.60	18.554	0.329	0.036	0.006	0.043	0.020	0.026	0.005	10.809	1.387	58.254	0.190	297.36	35.18	0.079	0.037	0.004	0.001
± (1σ)	0.000018	2	1.70	15.344	0.198	0.019	0.004	0.007	0.012	0.009	0.002	12.528	0.711	81.645	0.535	340.43	17.61	0.014	0.022	0.001	0.001
% error	0.11	3	1.80	15.133	0.138	0.017	0.003	0.008	0.007	0.005	0.001	13.570	0.362	89.673	1.112	366.08	8.84	0.015	0.012	0.000	0.001
Int Age (Ma)	356.29	4	1.90	14.858	0.094	0.014	0.002	0.008	0.004	0.003	0.001	13.836	0.245	93.124	2.124	372.56	5.95	0.015	0.007	0.000	0.000
± (2σ)	1.84	5	2.00	14.793	0.086	0.013	0.001	0.004	0.003	0.003	0.000	13.752	0.143	92.966	3.811	370.52	3.47	0.007	0.005	0.000	0.000
with ± in J	1.07	6	2.10	-0.488	0.157	0.002	0.010	0.000	0.042	0.000	0.008	0.000	2.453	0.000	3.852	0.00	73.37	0.000	0.076	0.000	0.002
Plateau Age	354.27	7	2.20	13.363	0.039	0.013	0.000	0.001	0.000	0.001	0.000	13.184	0.053	98.654	13.448	356.61	1.30	0.001	0.001	0.000	0.000
± (2σ)	0.96	8	2.30	13.295	0.038	0.013	0.000	0.001	0.001	0.000	0.000	13.171	0.052	99.073	24.313	356.31	1.28	0.003	0.001	0.000	0.000
with ± in J	1.19	9	2.40	13.298	0.046	0.012	0.000	0.002	0.001	0.001	0.000	13.112	0.058	98.601	35.895	354.86	1.43	0.003	0.001	0.000	0.000
MSWD	1.31	10	2.50	13.309	0.044	0.012	0.001	0.006	0.001	0.000	0.000	13.133	0.055	98.672	43.382	355.36	1.36	0.011	0.001	0.000	0.000
% ^{39}Ar	71.18	11	2.60	13.306	0.039	0.013	0.000	0.010	0.001	0.001	0.000	13.075	0.051	98.264	53.530	353.93	1.26	0.017	0.002	0.000	0.000
		12	2.70	13.284	0.040	0.013	0.000	0.037	0.001	0.000	0.000	13.109	0.049	98.685	61.395	354.79	1.20	0.067	0.004	0.000	0.000
		13	2.80	13.169	0.039	0.012	0.001	0.050	0.002	0.001	0.000	12.931	0.054	98.189	66.906	350.39	1.32	0.091	0.005	0.000	0.000
		14	2.90	13.281	0.050	0.013	0.001	0.003	0.001	0.001	0.000	13.059	0.083	98.329	70.585	353.54	2.04	0.005	0.002	0.000	0.000
		15	3.00	13.180	0.049	0.012	0.001	0.002	0.001	0.001	0.000	12.969	0.066	98.395	76.028	351.32	1.63	0.004	0.001	0.000	0.000
		16	3.10	13.344	0.068	0.013	0.001	0.005	0.002	0.001	0.000	13.065	0.129	97.906	78.104	353.69	3.16	0.009	0.003	0.000	0.000
		17	3.20	13.362	0.066	0.013	0.001	0.003	0.002	0.001	0.000	13.091	0.138	97.966	79.759	354.32	3.39	0.005	0.003	0.000	0.000
		18	3.30	13.320	0.059	0.013	0.001	0.060	0.002	0.001	0.000	13.089	0.079	98.258	83.807	354.28	1.94	0.110	0.006	0.000	0.000
		19	3.40	13.659	0.081	0.013	0.002	0.013	0.004	0.001	0.001	13.240	0.267	96.934	84.627	358.00	6.56	0.023	0.008	0.000	0.000
		20	5.50	13.348	0.041	0.012	0.000	0.015	0.001	0.000	0.000	13.238	0.048	99.173	100.000	357.94	1.17	0.028	0.002	0.000	0.000

TABLE 8. (a) $^{40}Ar/^{39}Ar$ analyses on muscovite concentrates from sample LM. The plateau has been inferred considering the steps indicated in bold italics. The age spectrum is shown in Fig. 10b. ELECTRONIC SUPPLEMENTARY MATERIAL

Sample LM		Step	Laser Power (Watts)	$^{40}Ar/^{39}Ar$	±(1σ)	$^{36}Ar/^{39}Ar$	±(1σ)	$^{37}Ar/^{39}Ar$	±(1σ)	$^{36}Ar/^{39}Ar$	±(1σ)	$^{40}Ar^{*}/^{39}Ar_{(K)}$	±(1σ)	$^{40}Ar^{*}$(%)	Cumulative ^{39}Ar (%)	Age (Ma)	±(1σ)	Ca/K	±(1σ)	Cl/K	±(1σ)
J	0.016578	1	1.90	14.061	0.142	0.016	0.002	0.002	0.008	0.003	0.001	13.228	0.446	94.078	0.546	357.71	10.94	0.004	0.015	0.000	0.001
±(1σ)	0.000018	2	2.00	13.608	0.065	0.014	0.001	0.000	0.003	0.001	0.000	13.168	0.150	96.768	2.275	356.22	3.68	0.001	0.005	0.000	0.000
% error	0.11	3	2.10	13.302	0.048	0.013	0.001	0.001	0.001	0.001	0.000	13.074	0.083	98.286	5.814	353.93	2.04	0.001	0.002	0.000	0.000
Int Age (Ma)	356.53	4	2.20	13.516	0.077	0.013	0.001	0.002	0.002	0.001	0.000	13.171	0.131	97.451	7.966	356.30	3.23	0.004	0.004	0.000	0.000
±(2σ)	0.81	5	2.30	13.541	0.039	0.013	0.000	0.001	0.001	0.001	0.000	13.360	0.058	98.658	14.718	360.92	1.41	0.002	0.001	0.000	0.000
with ± in J	1.07	6	2.40	13.432	0.040	0.013	0.000	0.001	0.001	0.000	0.000	13.308	0.056	99.075	23.953	359.65	1.36	0.003	0.001	0.000	0.000
Plateau Age	354.96	7	2.50	13.263	0.043	0.013	0.000	0.004	0.001	0.000	0.000	13.128	0.058	98.980	30.453	355.24	1.43	0.008	0.002	0.000	0.000
±(2σ)	0.96	8	2.60	13.296	0.050	0.013	0.001	0.004	0.002	0.000	0.000	13.128	0.095	98.740	33.678	355.25	2.34	0.008	0.003	0.000	0.000
with ± in J	1.19	9	2.70	13.284	0.044	0.013	0.001	0.003	0.001	0.001	0.000	13.065	0.063	98.347	39.127	353.69	1.55	0.005	0.002	0.000	0.000
MSWD	1.23	10	2.80	13.189	0.037	0.013	0.001	0.004	0.001	0.000	0.000	13.047	0.053	98.927	48.375	353.26	1.29	0.007	0.002	0.000	0.000
% ^{39}Ar	67.07	11	2.90	13.200	0.038	0.013	0.000	0.011	0.001	0.000	0.000	13.102	0.053	99.253	55.838	354.60	1.31	0.021	0.002	0.000	0.000
		12	3.00	13.155	0.035	0.013	0.000	0.046	0.001	0.000	0.000	13.018	0.052	98.954	67.486	352.55	1.28	0.083	0.004	0.000	0.000
		13	3.10	13.311	0.040	0.013	0.001	0.069	0.002	0.000	0.000	13.179	0.057	99.005	74.189	356.51	1.41	0.126	0.007	0.000	0.000
		14	3.20	13.300	0.037	0.013	0.000	0.045	0.001	0.000	0.000	13.179	0.060	99.084	79.469	356.50	1.48	0.081	0.004	0.000	0.000
		15	3.30	13.294	0.061	0.013	0.001	0.033	0.003	0.000	0.000	13.150	0.115	98.912	81.902	355.78	2.82	0.060	0.006	0.000	0.000
		16	3.40	13.407	0.068	0.013	0.001	0.011	0.003	0.000	0.000	13.277	0.152	99.026	83.781	358.89	3.72	0.020	0.005	0.000	0.000
		17	3.70	13.368	0.046	0.013	0.001	0.031	0.001	0.000	0.000	13.240	0.064	99.045	88.123	358.00	1.58	0.056	0.003	0.000	0.000
		18	3.80	13.516	0.061	0.012	0.001	0.012	0.003	0.000	0.000	13.371	0.154	98.933	89.668	361.21	3.77	0.022	0.005	0.000	0.000
		19	4.00	13.374	0.074	0.013	0.001	0.016	0.003	0.001	0.000	13.115	0.164	98.060	91.018	354.92	4.02	0.029	0.006	0.000	0.000
		20	4.20	13.551	0.065	0.013	0.001	0.022	0.003	0.000	0.000	13.519	0.168	99.763	92.397	364.82	4.11	0.040	0.006	0.000	0.000
		21	4.40	13.621	0.072	0.012	0.001	0.038	0.003	0.000	0.000	13.466	0.155	98.857	93.742	363.52	3.79	0.069	0.007	0.000	0.000
		22	4.60	13.627	0.064	0.012	0.001	0.185	0.007	0.001	0.000	13.449	0.158	98.684	95.172	363.11	3.87	0.338	0.020	0.000	0.000
		23	4.80	13.612	0.092	0.012	0.001	0.182	0.008	0.001	0.001	13.342	0.221	98.000	96.090	360.48	5.40	0.331	0.022	0.000	0.000
		24	5.00	13.700	0.069	0.013	0.002	0.070	0.005	0.001	0.001	13.503	0.230	98.556	96.994	364.44	5.62	0.127	0.011	0.000	0.000
		25	5.50	13.526	0.048	0.013	0.001	0.058	0.003	0.000	0.000	13.379	0.087	98.903	100.000	361.39	2.12	0.106	0.007	0.000	0.000

TABLE 9. (a) $^{40}Ar/^{39}Ar$ analyses on muscovite concentrates from sample LM. The plateau has been inferred considering the steps indicated in bold italics. The age spectrum is shown in Fig. 10c. ELECTRONIC SUPPLEMENTARY MATERIAL

Sample LM		Step	Laser Power (Watts)	$^{40}Ar/^{39}Ar$	± (1σ)	$^{38}Ar/^{39}Ar$	± (1σ)	$^{37}Ar/^{39}Ar$	± (1σ)	$^{36}Ar/^{39}Ar$	± (1σ)	$^{40}Ar^*/^{39}Ar_{(K)}$	± (1σ)	$^{40}Ar^*$(%)	Cumulative ^{39}Ar (%)	Age (Ma)	± (1σ)	Ca/K	± (1σ)	Cl/K	± (1σ)
J	0.016578	1	1.50	23.967	1.092	0.016	0.028	0.000	0.089	0.046	0.023	10.436	6.814	43.500	0.110	287.88	#####	0.000	0.162	0.000	0.006
± (1σ)	0.000018	2	1.80	15.885	0.191	0.016	0.002	0.005	0.007	0.006	0.001	14.133	0.468	89.000	1.490	379.76	11.33	0.009	0.013	0.000	0.001
% error	0.11	3	2.20	13.721	0.040	0.013	0.001	0.002	0.000	0.001	0.000	13.440	0.051	98.000	78.570	362.89	1.24	0.004	0.001	0.000	0.000
Int Age (Ma)	362.91	4	2.30	14.001	0.101	0.015	0.001	0.035	0.005	0.003	0.001	13.191	0.299	94.200	81.070	356.80	7.33	0.064	0.009	0.000	0.000
± (2σ)	2.19	5	2.40	13.798	0.165	0.013	0.003	0.000	0.008	0.002	0.002	13.144	0.485	95.300	82.400	355.64	11.91	0.000	0.014	0.000	0.001
with ± in J	2.31	6	2.50	13.933	0.183	0.013	0.003	0.000	0.010	0.003	0.002	13.119	0.602	94.200	83.450	355.01	14.79	0.000	0.019	0.000	0.001
Plateau Age	362.75	7	2.60	14.164	0.162	0.012	0.004	0.002	0.010	0.003	0.002	13.309	0.586	94.000	84.450	359.68	14.37	0.004	0.019	0.000	0.001
± (2σ)	2.17	8	2.70	14.234	0.189	0.012	0.004	0.011	0.010	0.002	0.002	13.721	0.609	96.400	85.460	369.75	14.83	0.020	0.018	0.000	0.001
with ± in J	2.29	9	2.80	14.260	0.227	0.017	0.005	0.004	0.012	0.005	0.003	12.724	0.858	89.200	86.280	345.29	21.19	0.007	0.021	0.000	0.001
MSWD	0.72	10	3.00	13.900	0.129	0.010	0.003	0.000	0.007	0.003	0.002	12.989	0.526	93.500	87.640	351.83	12.94	0.000	0.013	0.000	0.001
% ^{39}Ar	98.51	11	4.00	13.682	0.049	0.012	0.001	0.005	0.001	0.000	0.000	13.589	0.073	99.300	100.000	366.52	1.78	0.009	0.002	0.000	0.000

TABLE 10. (a) $^{40}Ar/^{39}Ar$ analyses on muscovite concentrates from sample LM. The plateau has been inferred considering the steps indicated in bold italics. The age spectrum is shown in Fig. 10d. ELECTRONIC SUPPLEMENTARY MATERIAL

3.2.3 *Partial Conclusions*

The main conclusions of this study are:

1. The Cambre metabasic rocks show systematic changes in texture and mineral composition that are spatially related depending on deformation. Prograde metamorphism is characterized by a H_2O-undersaturated P–T evolution induced by the crystallization of lawsonite, in the lawsonite blueschist/LT-eclogite-facies conditions peaking at P ≈ 22 kbar and T ≈ 550–560 °C (M_2). Exhumation-related metamorphism is characterized by a nearly isothermal decompression from the lawsonite-bearing fields to fields with stable albite at P ≈ 10 kbar (M_3). This led to the pseudomorphism of lawsonite crystals in the early decompression stages, and a subsequent amphibolite-greenschist facies overprint at P < 8 kbara and T ≈ 440–480 °C (post-M_3).

2. Petrographic observations and pseudosection modelling suggest that the second generation of garnet grains (g2) and lawsonite crystallized at peak conditions in the matrix assemblage (M_2), and replacement took place at decreasing pressure, in the early almost isothermal decompression stages (post-M_2).

3. The preservation of the lawsonite crystal shape despite complete retrogression indicates that pseudomorphism occurred as a static process and that particular levels of the blueschist host rock were not affected by penetrative deformation during exhumation.

4. Differences in the temperatures recorded by the metapelitic and the metabasic rocks comprising the Ceán Unit are interpreted as a result (or a combination) of: (i) their different position in the orogenic wedge within the subduction complex, (ii) the thermal effects of fluid migration during metamorphism or (iii) related to shear heating effects that may have favoured a temperature increase with deformation.

5. $^{40}Ar/^{39}Ar$ step-heating of phengitic muscovite from the pelitic schists yield plateau ages of ca. 363±2 Ma and 354±1 Ma. The older age is interpreted as the age of the peak blueschist-facies metamorphism. The age of 355 Ma is interpreted as a cooling age and is inferred to represent some point relatively close to peak conditions at the onset of the isothermal decompression. Differences between the HP–LT event and the beginning of the postnappe tectonics, suggest an exhumation rate of ≈ 2.5 mm/year for the Malpica-Tui Complex. These ages support the equivalence of the Ceán Unit and the Upper Unit of Ile de Groix along the Ibero- Armorican Arc, and suggest that these units share a blueschist-facies event constrained at ca. 360–370 Ma, that may represent the Late Devonian-Early Carboniferous subduction of the northern margin of Gonwana beneath Laurussia.

6. $^{40}Ar/^{39}Ar$ dating of muscovite from the quartzo-feldspathic mylonites of the Bembibre-Ceán detachment, at the base of the Ceán Unit, yields an age of ca. 337±3 Ma, interpreted as the age that marks the beginning of the post-nappe extensional tectonics leading to the gravitational collapse of the orogen, characterized by a cooling rate of 7°C/Ma (10°C/km).

3.3 *Blueschists from Liberty Creek (Chugach terrane, Alaska)*

3.3.1 *Introduction*

Blueschists and related HP-LT assemblages are considered as markers of fossil subduction zones, and record the tectonic processes associated with convergent plate boundaries (e.g. Maruyama *et al.*, 1996). Recent petrological and geochronological studies of blueschist facies and associated rocks have provided important clues in understanding subduction zone metamorphism (e.g. Isozaki *et al.*, 2010; López-Carmona *et al.*, 2010), thermotectonic evolution (e.g., Z. Zhang *et al.*, 2009) and the styles of exhumation, such as the in the case of the world's youngest blueschist from Leti Island in eastern Indonesia (Kadarusman *et al.*, 2010). In a recent review, Ota and Kaneko (2010) synthesized the petrologic information from blueschist facies rocks worldwide and showed that in most cases, their P–T field is bounded on the low-pressure side by greenschist and pumpellyite–actinolite facies, on the high-temperature side by epidote–amphibolite facies, and the high-P and high-temperature sides by eclogite facies.

Among the rocks belonging to these metamorphic facies, blueschists and eclogites manifest lithospheric plate subduction, because these rocks, especially blueschists, require unusually cold upper mantle geotherms which are only found in active subduction zones (e.g., Ernst, 2010; Omori *et al.*, 2009). Thus, the space–time distribution of blueschist eclogite belts have been regarded as markers of paleosubduction zones and are hence critical in the context of tectonics associated with convergent plate boundaries, and the evolution of continents. Several studies have also demonstrated that the transformation of lawsonite, a high-density hydrous mineral with ca. 11 wt.% H2O which is stable at high pressure and low temperature, from the lawsonite-stability to epidote-stability fields leads to the release of water in the subduction channel (e.g. Poli and Schmidt, 2002; Tsujimori *et al.*, 2006). The presence of free water in the subduction channel triggers the partial melting of the mantle wedge above the subduction channel, and thus contributes to the generation of island arc volcanic rocks (Maruyama *et al.*, 2009; Poli & Schmidt, 2002).

The southern Alaska convergent margin contains several small belts of sedimentary and volcanic rocks metamorphosed to blueschist facies, located along the Border Ranges fault on the contact between the Wrangellia and Chugach terranes. These include the Raspberry Schist on Kodiak Afognak, Shuyak, and several small islands, the Seldovia blueschist on the Kenai Peninsula, and the Liberty Creek schist in the Chugach Mountains (Carden and Decker, 1977; Carden and Forbes, 1976; Roeske, 1986; Roeske *et al.*, 1989). These belts are significant in that they are the most inboard, and thus probably contain the oldest record of Triassic–Jurassic northward-directed subduction beneath Wrangellia. Here we present a description of the structural, lithological, and petrological relationships in the Seldovia and Liberty Creek metamorphic belts, and discuss what these relationships might mean for the tectonic evolution and PT conditions during early stages of subduction along the southern Alaskan convergent margin.

3.3.2 *P–T and structural constraints of lawsonite and epidote blueschists from Liberty Creek and Seldovia: Tectonic implications for early stages of subduction along the southern Alaska convergent margin.*

LÓPEZ-CARMONA, A., KUSKY, T.M., SANTOSH, M. & ABATI, J. (2011) LITHOS, 121, 100–116

Lithos 121 (2011) 100–116

Contents lists available at ScienceDirect

Lithos

journal homepage: www.elsevier.com/locate/lithos

P–T and structural constraints of lawsonite and epidote blueschists from Liberty Creek and Seldovia: Tectonic implications for early stages of subduction along the southern Alaska convergent margin

Alicia López-Carmona [a], Timothy M. Kusky [b,*], M. Santosh [c], Jacobo Abati [a]

[a] Departamento de Petrología y Geoquímica and Instituto de Geología Económica, Universidad Complutense-Consejo Superior de Investigaciones Científicas, 28040 Madrid, Spain
[b] State Key Lab for Geological Processes and Mineral Resources, and Three Gorges Center for Geohazard, Ministry of Education, China University of Geosciences, Wuhan, 388 Lumo Road, Hongshan District, Wuhan 430074, China
[c] Department of Interdisciplinary Science, Faculty of Science, Kochi University, Akebono-cho 2-5-1, Kochi 780-8520, Japan

ARTICLE INFO

Article history:
Received 14 May 2010
Accepted 17 October 2010
Available online 29 October 2010

Keywords:
Alaska
Blueschist
Subduction
Border Ranges Fault
PT pseudosections

ABSTRACT

The southern Alaska convergent margin contains several small belts of sedimentary and volcanic rocks metamorphosed to blueschist facies, located along the Border Ranges fault on the contact between the Wrangellia and Chugach terranes. These belts are significant in that they are the most inboard, and thus probably contain the oldest record of Triassic–Jurassic northward-directed subduction beneath Wrangellia. The Liberty Creek HP-LT schist belt is the oldest and the innermost section of the Chugach terrane. Within this belt lawsonite blueschists contains an initial high-pressure assemblage formed by lawsonite + phengite + chlorite + sphene + albite ± apatite ± carbonates and quartz. Epidote blueschists are composed of sodic, sodic–calcic and calcic amphiboles + epidote + phengite + chlorite + albite + sphene ± carbonates and quartz. *P–T* pseudosections computed from four representative samples constrain maximum pressures at 16 kbar and 250–280 °C for the Lawsonite-bearing blueschists, and 15 kbar and 400–500 °C for the epidote-bearing blueschists, suggesting a initial subduction stage of 50–55 km depth. The growth of late albite porphyroblasts in all samples suggests a dramatic decompression from *ca.* 9 kbar to 5 kbar. The Liberty Creek schists can be correlated with the Seldovia blueschist belt on the Kenai Peninsula. Metamorphism in both terranes took place in the Early Jurassic (191–192 Ma), recording an early stage of subduction beneath Wrangellia. In the nearby terranes of the same margin, the age of metamorphism records an early stage of subduction at 230 Ma. Based on this difference in age, a maximum of 40 Ma were necessary to subduct the protoliths of the Seldovia and Liberty Creek blueschists to depths of circa 50–55 km, suggesting a minimum vertical component of subduction of 1.2–1.5 cm/year.

1. Introduction

Blueschists and related HP/LT (high-pressure/low-temperature) assemblages are considered as markers of fossil subduction zones, and record the tectonic processes associated with convergent plate boundaries (e.g. Maruyama et al., 1996). Recent petrological and geochronological studies of blueschist facies and associated rocks have provided important clues in understanding subduction zone metamorphism (e.g. Isozaki et al., 2010; López-Carmona et al., 2010), thermotectonic evolution (e.g., Z. Zhang et al., 2009) and the styles of exhumation, such as the in the case of the world's youngest blueschist from Leti Island in eastern Indonesia (Kadarusman et al., 2010). In a recent review, Ota and Kaneko (2010) synthesized the petrologic information from blueschist facies rocks worldwide and showed that in most cases, their *P–T* field is bounded on the low-*P* side by greenschist and pumpellyite–actinolite facies, on the high-*T* side by epidote–amphibolite facies, and the high-*P* and high-*T* sides by eclogite facies. Among the rocks belonging to these metamorphic facies, blueschists and eclogites manifest lithospheric plate subduction, because these rocks, especially blueschists, require unusually cold upper mantle geotherms which are only found in active subduction zones (e.g., Ernst, 2010; Omori et al., 2009). Thus, the space–time distribution of blueschist eclogite belts have been regarded as markers of paleo-subduction zones and are hence critical in the context of tectonics associated with convergent plate boundaries, and the evolution of continents. Several studies have also demonstrated that the transformation of lawsonite, a high-density hydrous mineral with *ca.* 11 wt.% H_2O which is stable at high pressure and low temperature, from the lawsonite-stability to epidote-stability fields leads to the release of water in the subduction channel (e.g., Poli and Schmidt, 2002; Tsujimori et al., 2006). The presence of free water in the subduction channel triggers the partial melting of the mantle wedge above the subduction

* Corresponding author.
E-mail addresses: alcarmona@geo.ucm.es (A. López-Carmona), tkusky@gmail.com (T.M. Kusky), santosh@cc.kochi-u.ac.jp (M. Santosh), abati@geo.ucm.es (J. Abati).

0024-4937/$ – see front matter © 2010 Elsevier B.V. All rights reserved.
doi:10.1016/j.lithos.2010.10.007

channel, and thus contributes to the generation of island arc volcanic rocks (Maruyama et al., 2009; Poli and Schmidt, 2002).

2. Regional geology

The southern Alaska convergent margin consists of several different tectonic units, including two elongate terranes — the Wrangellia composite terrane (consisting of the Peninsular, Wrangellia, and Alexander terranes), and farther outboard, the Chugach–Prince William terrane (Fig. 1). The Wrangellia composite terrane consists of Late Proterozoic and younger magmatic arc, oceanic plateau, rifted arc, and flysch belts (Plafker and Berg, 1994). During much of the Mesozoic, the Wrangellia and Chugach–Prince William terranes formed a magmatic arc and accretionary wedge, respectively, above a circum-Pacific subduction zone (e.g., Bradley et al., 2003; Kusky and Bradley, 1999; Kusky and Glass, 2007; Kusky et al., 1997a,b, 2003; Plafker et al., 1989). The boundary between the two terranes is the Border Ranges fault system, which apparently began its history as a subduction-related thrust system, and was later reactivated in many places as a strike slip fault system.

The accretionary wedge of south-central Alaska (Fig. 1) includes both Mesozoic and Cenozoic parts. The inboard, Mesozoic part has been referred to as the Chugach terrane and the outboard, Cenozoic part as the Prince William terrane (e.g., Coney et al., 1980). On the Kenai Peninsula, the farthest inboard rocks of the subduction complex belong to the Seldovia metamorphic complex (Bradley et al., 1997, 1999), which occupies a narrow fault slice just north of Seldovia village, whereas this structural position is occupied by the Liberty Creek schists in the northern Chugach Mountains. Metamorphism took place in the Early Jurassic (191–192 Ma) under conditions of high pressure and low temperature—conditions that suggest metamorphism in a subduction zone.

The McHugh Complex is a tectonic melange (Kusky and Bradley, 1999) that flanks the metamorphic rocks on their seaward side. Its main components are argillite, graywacke, chert, and basalt; minor components are limestone, gabbro, and ultramafic rocks, structurally juxtaposed at all scales (Bradley et al., 1999; Kusky and Bradley, 1999; Kusky et al. (1997b) Prehnite–pumpellyite metamorphic facies assemblages are typical (Bradley et al., 1999). The primary melange foliation, ductile shear zones, and metamorphism are all suggested to have formed during subduction–accretion. The timing of subduction–accretion is not well known, but probably spanned much of the Jurassic and Cretaceous. Early Jurassic (191–192 Ma) metamorphism of the Seldovia metamorphic complex indicates subduction during that time. A Norian (230 Ma) age on gabbro of the Halibut Cove Complex is interpreted by Kusky and Glass (2007) to reflect formation in a suprasubduction zone spreading environment associated with early stages of subduction beneath Wrangellia. So although subduction probably was initiated in the Triassic, the subducting oceanic plate likely had Paleozoic crust.

The Valdez Group of Late Cretaceous (Campanian? to Maastrichtian) age flanks the McHugh Complex on its seaward side. It consists of medium- and thin-bedded graywacke turbidites, black argillite, and minor pebble to cobble conglomerate (Bradley et al., 1999). These strata were probably deposited on the downgoing plate in a deep-sea trench (Nilsen and Zuffa, 1982), and accreted shortly thereafter. The McHugh Complex was structurally emplaced above the Valdez Group along a thrust fault, known as the Chugach Bay thrust. Beneath the fault is a melange of partially to thoroughly disrupted Valdez Group turbidites (Kusky et al., 1997a,b).

The Border Ranges Fault forms the boundary between the Wrangellia Composite terrane and the Chugach–Prince William terranes. The Border Ranges fault has been suggested to have originated as a subduction thrust (Plafker and Berg, 1994; Plafker et al., 1989), but some critical data to test this idea is lacking (Pavlis and Roeske, 2007). However, the field relations on the Kenai Peninsula preclude the possibility that the present fault is merely a thrust that has been steepened to near vertical. For it to be a thrust, essentially unmetamorphosed, supracrustal rocks of the Wrangellia composite terrane in the hanging-wall would somehow need to have been emplaced above deep-crustal blueschists in the footwall. It seems more likely that the fault that now bounds the Wrangellia composite terrane on the southeast is a late-stage strike-slip or oblique-slip fault, as has been suggested, for example, along strike in the Matanuska Valley (Little and Naeser, 1989).

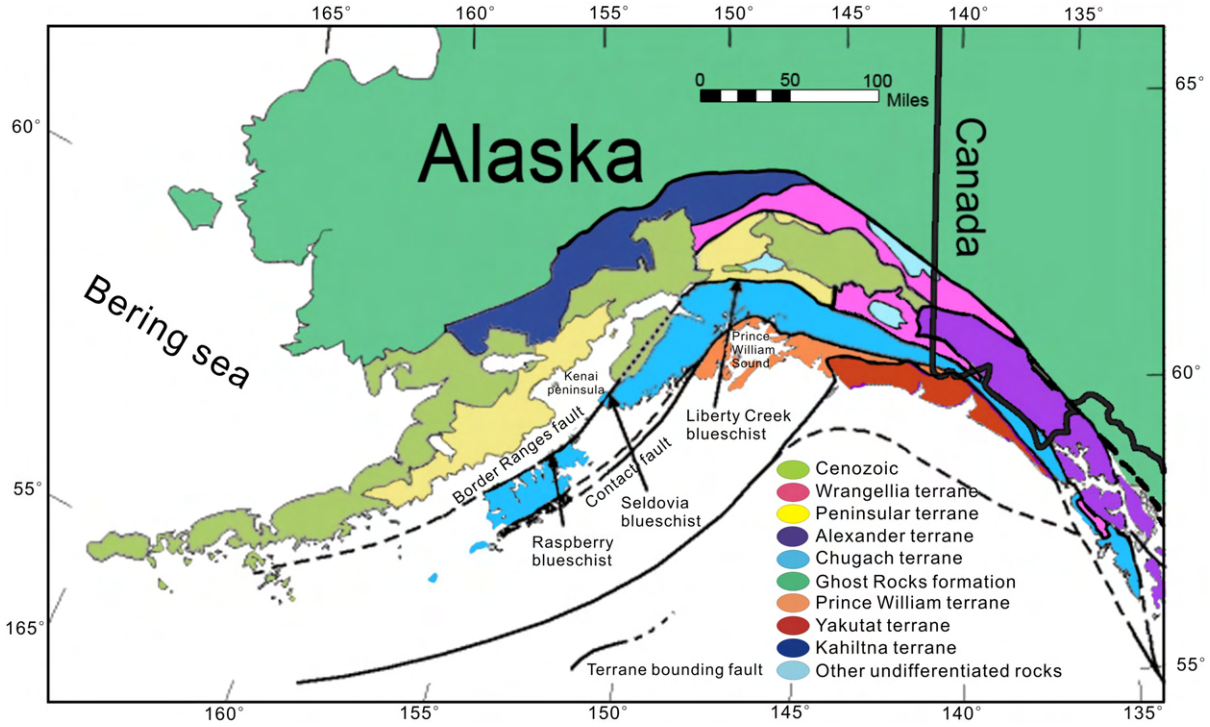

Fig. 1. Map of southern Alaska (modified alter Kusky et al., 1997a).

The southern Alaska convergent margin contains several small belts of sedimentary and volcanic rocks metamorphosed to blueschist facies, located along the Border Ranges fault on the contact between the Wrangellia and Chugach terranes. These include the Raspberry Schist on Kodiak Afognak, Shuyak, and several small islands, the Seldovia blueschist on the Kenai Peninsula, and the Liberty Creek schist in the Chugach Mountains (Carden and Decker, 1977; Carden and Forbes, 1976; Roeske, 1986; Roeske et al., 1989). These belts are significant in that they are the most inboard, and thus probably contain the oldest record of Triassic–Jurassic northward-directed subduction beneath Wrangellia. Here we present a description of the structural, lithological, and petrological relationships in the Seldovia and Liberty Creek metamorphic belts, and discuss what these relationships might mean for the tectonic evolution and PT conditions during early stages of subduction along the southern Alaskan convergent margin.

3. Field observations

Several months of field work were carried out in the Seldovia and Liberty Creek blueschist belts to determine the main lithologies present and the structural history of the rock units. In this contribution we summarize this field work from both belts, then focus our petrological studies on the lawsonite and epidote blueschists from the Liberty Creek belt.

3.1. Seldovia blueschist belt

The Seldovia blueschist forms a narrow belt that is best exposed in and northwest of the village of Seldovia on the southern Kenai Peninsula (Fig. 2). Based on our mapping (Bradley et al., 1999, 2000) we subdivide the belt into three main lithological segments, including a fragmental volcaniclastic unit in the east (Fig. 3G–H), a metacarbonate unit in the west, and a mixed metapelitic and volcaniclastic unit between the two (Fig. 3A–C). The lithological descriptions in the following section follow a general north to south direction, starting at Outside Beach south of Seldovia Point, and continuing to the village of Seldovia. Important locations are noted on Fig. 2.

3.1.1. Description of rock exposures

3.1.1.1. Outside Beach, north end. Outcrops at Outside Beach north of Seldovia include, from south to north (1) graywacke blocks in argillite matrix; (2) basalt; and (3) radiolarian chert (Figs. 2 and 3E–F) belonging to the McHugh Complex. About 300 m north along the beach, a prominent seastack exposes an argillite-matrix melange containing blocks of greenstone, limestone, pebbly graywacke, and chert. This particular limestone is undated but is typical of the limestone blocks in the McHugh Complex that have yielded Permian fossils of Tethyan affinity (Bradley et al., 1999). Still farther north, at the beginning of a long section of cliffs that continues to the end of the beach, is a belt of melange containing blocks of sandstone and pebbly sandstone that are reminiscent of the Valdez Group (moderately sorted, dominant quartz and feldspar framework grains), and quite different from typical sandstones of the McHugh Complex (poorly sorted, matrix-rich, dominant chert and volcanic framework grains). This resemblance suggests that these blocks and their matrix might have been injected upward along a fault zone from underthrust Valdez Group rocks (Fig. 3D).

3.1.1.2. Outside Beach, south end. High-pressure metamorphic rocks of the Seldovia blueschist belt stretch from the southern end of Outside Beach to Watch Point in Seldovia, a linear distance of about 1.5 km. A variety of metamorphic rocks are exposed, including greenstone (metamorphosed basalt and associated volcaniclastic rocks), schist (metamorphosed pelite), thin-bedded quartzite (metachert), and marble. Various types of schists include common biotite–amphibole schist, epidote–chlorite–albite schist, glaucophane/riebeckite–epidote–chlorite blueschist, and blue-green hornblende–garnet–epidote schist. The various rock types are typically separated by steep faults. Throughout the Seldovia blueschist belt small-scale structures include superb early intrafolial folds, later tight to isoclinal folds, strong mineral and intersection lineations, kink bands, and late sulfide-rich shear zones, and even later brittle fault zones. Hornblende and white mica separates from two schist samples have yielded $^{40}Ar/^{39}Ar$ plateau ages of 191–192 Ma (Fig. 4: A. Till, pers. Comm.). This age falls in the Early Jurassic (Pliensbachian according to the DNAG time scale) and, as noted previously, is believed to date subduction zone metamorphism.

Between Outside Beach and the marble quarry there is an interesting wave-washed outcrop best viewed at low-tide, and during calm-water conditions. At this outcrop the fragmental nature of one of the distinctive units in the blueschist belt can be observed. The layers in the metamorphic rocks here are very flattened defining the foliation, and the protolith is questionable. In some places, the fragments resemble volcaniclastic conglomerate clasts (or perhaps pillow breccia), whereas in other places the apparently fragmental nature of the outcrop can be ascribed to dismemberment of isoclinal folds. There are some obvious fold hinges here, and we favor an origin by early isoclinal folding of a volcaniclastic conglomerate/sandstone unit, similar to units in the McHugh Complex, and in less-deformed parts of the Seldovia blueschist belt. Excellent examples of less-deformed volcaniclastic conglomerate are present in coastal exposures north of Watch Point.

3.1.1.3. Marble quarry. The old marble quarry is unfortunately mostly filled in, but numerous blocks and a few outcrops showing interesting structures and minerals remain. There are bright green (fuchsitic?) micas, chloritized garnets with beautiful pressure shadows, and infolded graphitic (carbonaceous) schist and layers of amphibolite still visible. The foliation in the metapelite and metabasite layers is clearly folded, whereas the marble shows evidence for grain-scale recrystallization and polyphase folding. A late stylolitic cleavage truncates both F1 and F2 folds.

3.1.1.4. Gray Cliff. Further southwest at Gray Cliff, units of limestone and dolostone are interlayered, and are in fault contact with adjacent metabasite and interlayered quartzites (recrystallized chert?). Just south of Gray Cliff, beautiful quartz–garnet–mica schists display tight to isoclinal folds, and are cut by late brittle faults.

3.1.2. Structural synthesis of Seldovia blueschist belt

Detailed observations of outcrops of the Seldovia blueschist belt has enabled us to construct a structural history of the belt. Beds and foliations strike to the northeast, generally parallel to the belt, and most mineral lineations plunge moderately to the northeast (Fig. 2). Rocks of the metamorphic terrane preserve numerous folds. Many of these contain limited information on ages, but in some cases fold overprinting relationships have enabled us to establish the geometry and style of F1 and F2 structures. F1 folds are tight to isoclinal structures, some of which form intrafolial relationships with the main foliation. F1 folds are nearly all northeast striking with moderately to steeply NE plunging hinges (parallel to the main mineral lineation), although a rare NW striking F1 fold was noted. In the marble quarry, F1 folds are also NE striking, but have south to southwest plunging hinges (Fig. 2).

F2 folds are more open to tight structures, with north-northeast to north–northwest striking axial surfaces, and northeast plunging hinges (also parallel to the mineral lineation). In the marble quarry, F2 folds strike northeast and have gently southwest plunging hinges (Fig. 2).

Unclassified folds (Fig. 2), whose generation could not be established, strike northeast and have generally shallow NE or SW plunging hinges.

In addition to the fold overprinting relationships, we were able to establish that the main tectonic foliation is cut by kink bands, and by

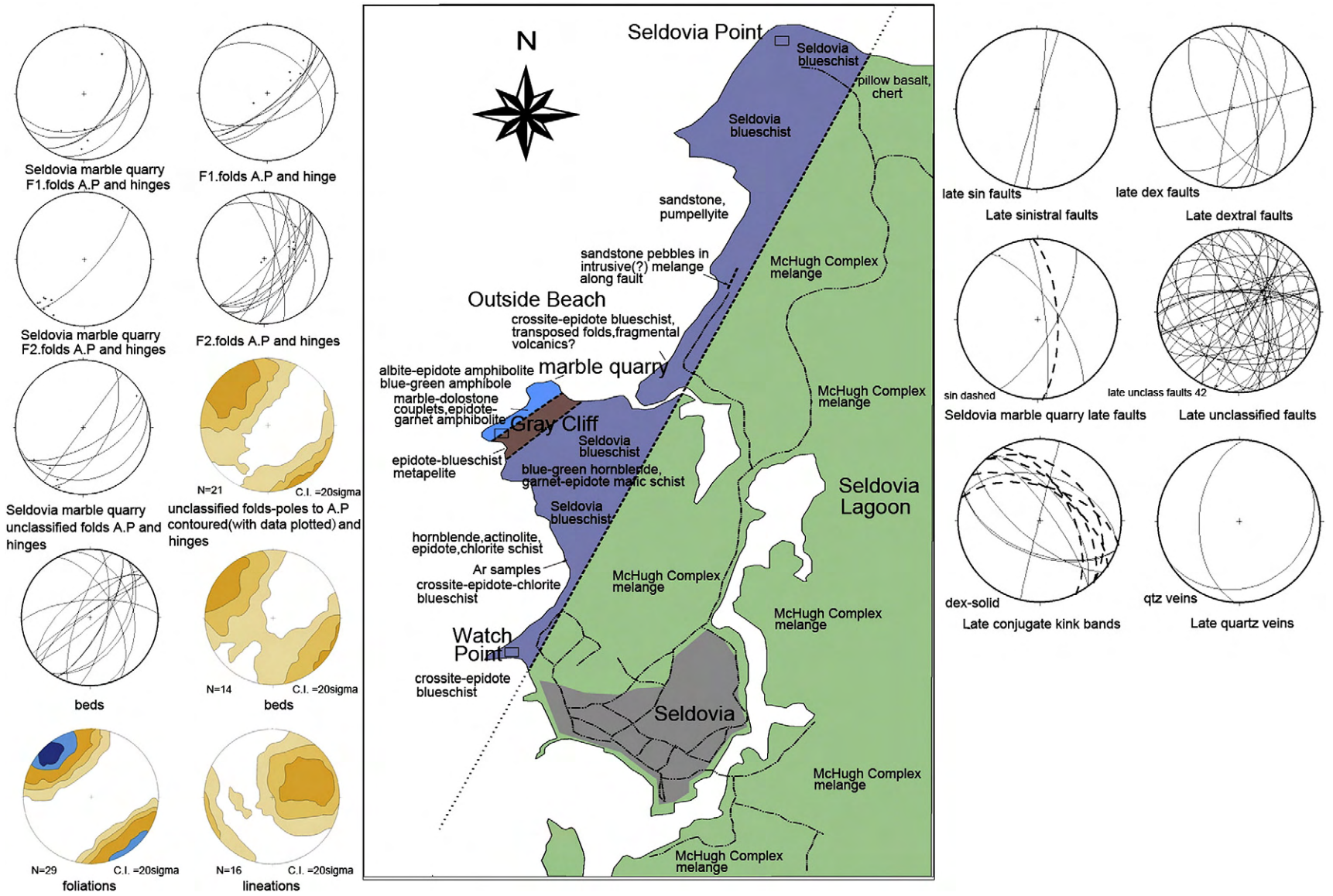

Fig. 2. Detailed map of Seldovia schist (after Bradley et al., 2000). Stereoplots of beds, foliations, lineations, fold and late fault data from the Seldovia schist are shown.

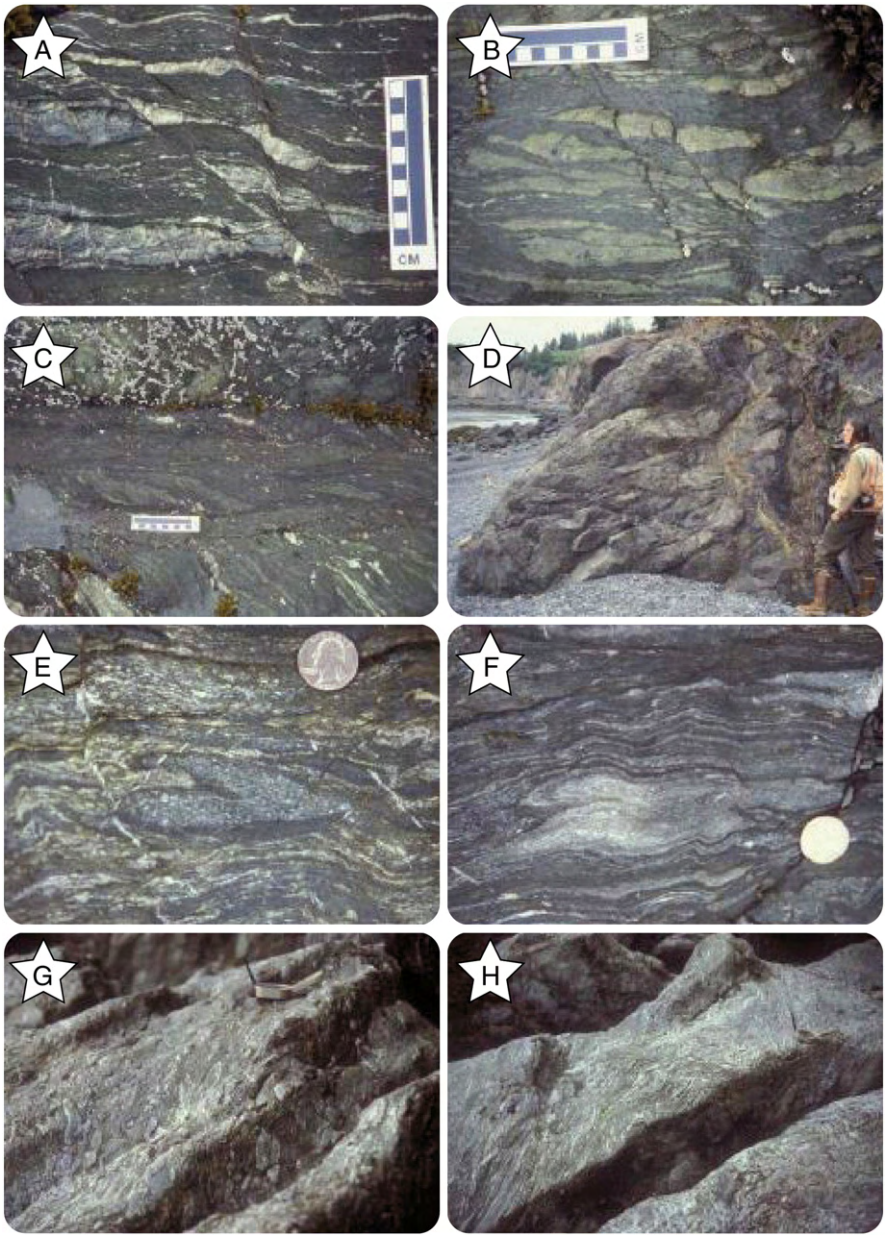

Fig. 3. A,B,C, Blueschist photos showing strong foliation, and interlayered metapelitic and metabasic varieties. D, Photo of McHugh melange showing near-vertical fractures with clasts of sandstone along the fractures. E–F, photos of intrafolial folds from Outside Beach. G–H, photos of fragmental Rocks, see text for discussion.

late faults and cataclastic fault zones. Late sulfide-rich shear zones also truncate the tectonic foliation and the kink bands, and further north in the Chugach terrane we were able to date similar structures, and correlate them with a period of faulting and mineralization associated with Paleocene passage of a triple junction along the southern margin of the Chugach–Prince William terrane (Bradley et al., 2003; Kusky et al., 1997a, 2003).

3.2. Liberty Creek schist

In the northern Chugach Mountains, the Liberty Creek schist forms the oldest and most landward portion of the Chugach terrane. It is composed of very fine-grained blueschist and greenschist derived from argillite and mafic tuff, and lesser mafic flows (Fig. 5). The Liberty Creek schist forms a narrow, fault-bounded slab, about 13 km wide in a north–south direction, and about 28 km long in an east–west direction, and is correlated with the high-*P*/*T* Seldovia blueschist belt on the Kenai Peninsula and the high-*P*/*T* Raspberry schist on Kodiak Island. The protolith age of the Liberty Creek schist is pre-Early Cretaceous, based on the oldest K–Ar whole rock apparent age for the schists (Plafker et al., 1989) and may be pre-Middle Jurassic, which is the Ar/Ar age of metamorphism of the correlative (?) blueschist of Iceberg Lake (Sisson and Onstott, 1986).

The Libert Creek schist is bordered on the north by the highly deformed and metamorphosed Haley Creek assemblage (Fig. 5), interpreted as the southern margin of the Wrangellia terrane. The Haley Creek metamorphic complex was thrust at least 40 km southward onto the northern Chugach terrane, forming a large outlying nappe to the south of the Liberty Creek schist in the area of Fig. 5. The Haley Creek metamorphic complex is composed of two units. An older unit, the Strelna Formation, consists of highly deformed and metamorphosed metasedimentary and metavolcanic rocks that are, at least in part, of Early Pennsylvanian age. The other younger unit, the Uranatina River metaplutonic assemblage, consists of highly deformed and metamorphosed gabbro, diorite, tonalite and granodiorite and trondhjemite of Middle Pennsylvanian and Late Jurassic age. A U–Pb sphene age of

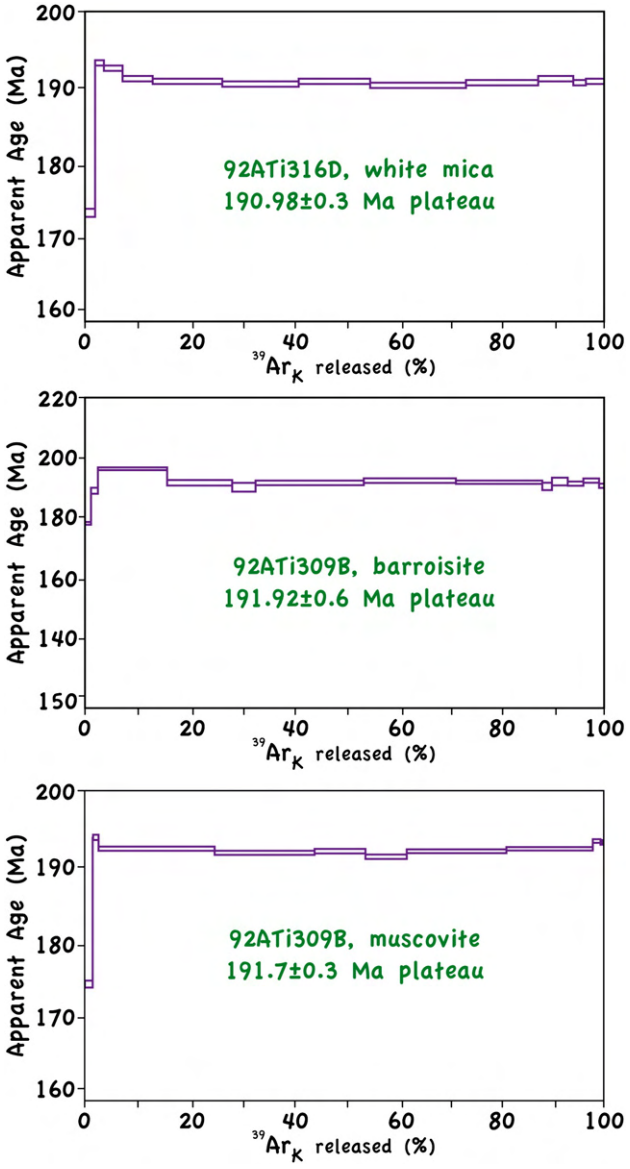

Fig. 4. Ar–Ar plateaus from the Seldovia schist, provided by A. Till (USGS).

156 Ma for a Pennsylvanian metaganodiorite and U–Pb zircon age of 153 Ma for a schistose granodiorite, indicate that Uranatina River metaplutonic rocks intruded the Late Jurassic Tonsina magmatic arc. The strong linear fabric and the increase of metamorphic grade, to upper amphiboltie facies near the Uranatina River metaplutonic assemblage, indicate Late Jurassic syntectonic intrusion of these plutons.

The Liberty Creek schists are transitional blueschist to greenschist grade metamorphic rocks that crop out along the northern edge of Chugach terrane adjacent to the Border Ranges fault. The blueschist belt is bounded by the Tonsina ultramafic complex to the northwest (Fig. 5), the oblique dextral-thrust Second Lake fault to the south and Taral fault (outside of map in Fig. 5) to the east (Nokleberg et al., 1994). Reconnaissance studies by Plafker and Berg (1994) and our own mapping reveal that rock types include blueschist, greenschist, muscovite and actinolite schist, siliceous schist, metachert, metabasalt, and graphitic schist. In some places units reveal compositional layering defined by chlorite, feldspar, actinolite, epidote, and crosstie rich layers. The protolith was mostly basaltic pillow flows, tuffs, tuff breccias, and volcaniclastic rocks with minor chert, carbonate, and argillaceous rocks; some faint primary structures at Liberty Creek suggest a breccia or pillow breccia origin, similar to the exposures in the Seldovia blueschist belt. Very fine-grained blue amphibole, mostly glaucophane/riebeckite with rarely occurring lawsonite, occurs at some levels. The protolith age is pre-early Cretaceous based on K–Ar whole rock analysis (Plafker et al., 1989). Early Cretaceous (123–107 Ma) K–Ar whole rock ages have been determined from Liberty Creek but these ages are uncertain due to fine grain size of the amphiboles. The geochemistry of the metabasalts in the Liberty Creek are N type MORB (Plafker et al., 1989).

The Liberty Creek schist is poly-deformed (Fig. 5). Well-developed foliation has variable dips ranging from gently to the northwest, to steeply west and northeast, with SE and NW trending mineral lineations (Fig. 5a,b). At least two generations of folds exist in the Liberty Creek Schist. The first generation folds are mostly symmetrical, 5–20 cm in size and tight to isoclinal with axial planar foliation parallel to the main foliation in the unit. A few of these folds show asymmetry to south. The second generation folds are upright E–W trending crenulation folds, locally showing a northward vergence. All these structures are truncated by Cenozoic brittle faults (Fig. 5c) that create very prominent, steeply dipping fracture surfaces (Nokleberg et al., 1989), striking mostly the NW.

In this study, samples were collected during mapping of the Liberty Creek blueschist. We selected one outcrop (Fig. 5) for detailed petrologic study, based on the presence of well-preserved blueschist facies minerals, and a variety of protoliths.

4. Metamorphic evolution

4.1. Petrography and mineral chemistry

We classified the Liberty Creek schists into two types based on their mineral parageneis: (1) lawsonite blueschists (LBS, sample 110.430); and (2) epidote blueschists (EBS, samples 110.431, 110.432, 110.433 and 110.434). The LBS are metapelites and contain lawsonite + phengite + chlorite + titanite + albite ± apatite ± carbonates and quartz. The EBS comprises both metapelites and metabasites with basaltic composition (Table 5, Plafker and Berg, 1994). The metapelites contain epidote + phengite + chlorite + albite + titanite ± carbonates and quartz. The metabasites are composed of Na-amphiboles (Mg-riebeckite), Na–Ca amphiboles (winchite), and Ca-amphiboles (Fe-hornblende, Fe-Tsermackite and actinolite) + epidote + phengite + chlorite + albite + titanite + magnetite + carbonates and quartz (Fig. 6).

These rocks are intensely foliated. The texture varies from lepidoblastic in the metapelitic samples, defined by preferred orientation of phengite and chlorite (samples 110.430 and 110.434; Fig. 7.1–8), to nematoblastic or nemato-lepidoblastic in the metabasite sample 110.431 where the orientation is marked by amphiboles and chlorites (Fig. 7C, D). The texture in samples 110.432–110.433 is grano-lepidoblastic (Fig. 7A, E). The regional foliation is locally transitional to mylonite (Fig. 7.1, 4).

Chemical analyses of the major minerals in five representative samples were carried out with a JEOL-Superprobe JXA-8900M microprobe equipped with five spectrometers at the Luis Bru Electronic Microscopy Centre (Universidad Complutense de Madrid). The operating parameters were: 15 kV accelerating voltage, 20 nA beam current, between 1 and 5 μm of beam diameter and 10 s counting time. Some of the microprobe analyses do not show the ideal total probably due to the small grain size of the samples, which forced us to use a 1 μm beam diameter. In these conditions, a small part of elements such as Na_2O may escape making the sum of the corresponding phases slightly lower than normal. Representative mineral compositions are listed in Tables 1–4. Mineral abbreviations in all figures and tables are after Kretz (1983) and Holland and Powell (1998).

4.1.1. Phengites

Phengite is present in both EBS and LBS. It is fine-grained, up to 0.5 mm long and tends to grow as orientated lepidoblasts in the

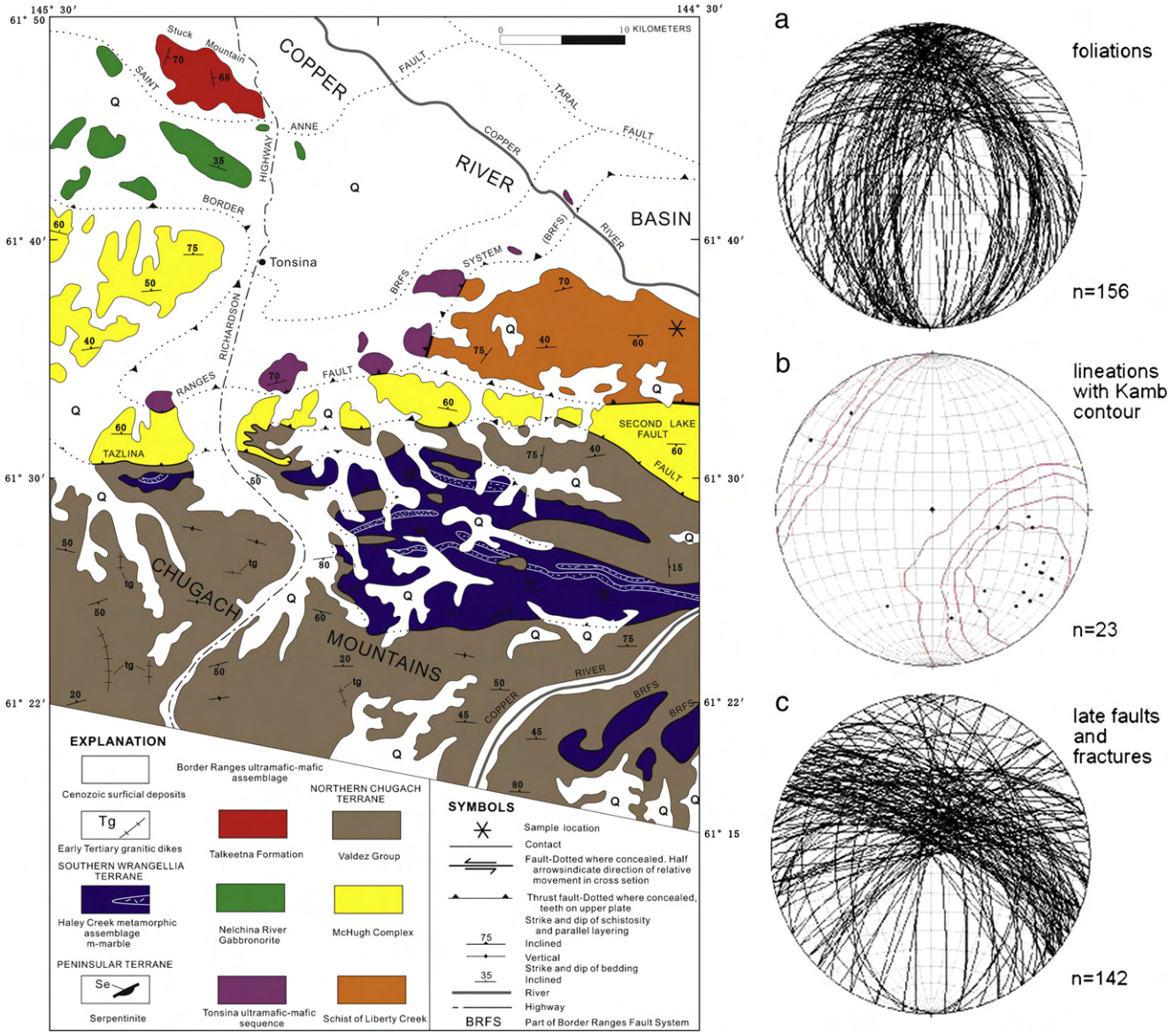

Fig. 5. Map of Eastern Chugach Mountains, showing structural/tectonic setting of Liberty Creek blueschist (after Nokleberg et al., 1994). Steroplots of structural data from the Liberty Creek schist showing (a) foliations, (b) lineations, and (c) late faults and fractures.

matrix (Fig. 7.5–8 and H), rarely tabular in shape (Fig. 7.5, 6). It is well oriented defining the foliation together with the chlorite in all samples. The silica content in the phengites is relatively high, ranging between 3.18 and 3.58 c.p.f.u. (calculated on the basis of 11 oxygens). X_{Mg} varies among the different samples with $X_{Mg} \approx 0.64–0.67$ in LBS and X_{Mg} 0.85–0.88 in EBS (Fig. 8A, Tables 1–4). Na contents are very low (Fig. 8D), reaching the maximum in LBS (sample 110.430). The ratio Na/(Na + K) is 0.02 in LBS and up to 0.01 in EBS (Tables 1–4). All phengite compositions plot below the Tschermak substitution line (Fig. 8C), indicating that part of the Fe is in a trivalent state, being substituted by Al. In the diagram FeO_T–Al_2O_3 (Fig. 8B), all the white micas are classified as metamorphic micas from glaucophane schists (Miyashiro, 1973).

4.1.2. Amphibole

Amphiboles are present only in the mafic schists (samples 110.432–433). The composition of blue amphibole in the Libery Creek rocks is Mg-riebeckite with a $X_{Al} = Al/(Al + Fe^{3+})$ ranging from 0.36 (samples 110.432–110.433) up to 0.50 (sample 110.431) and a $X_{Mg} = Mg/(Mg + Fe^{2+})$ that varies from 0.57 up to 0.75, respectively

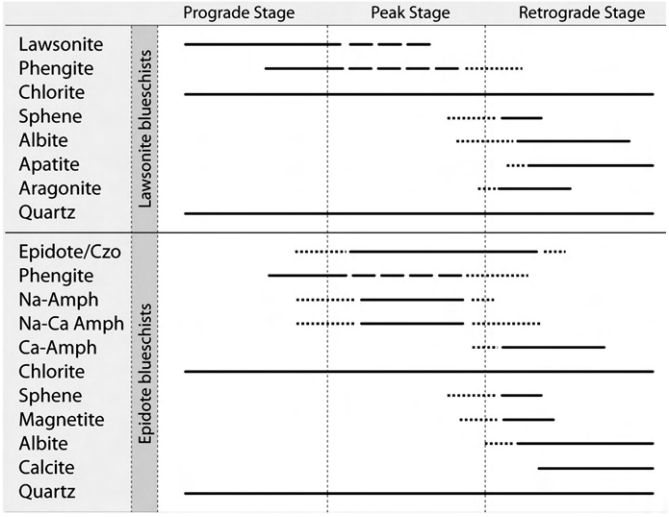

Fig. 6. Phase crystallization diagram showing the mineral stability along the metamorphic path of the Liberty Creek Schists.

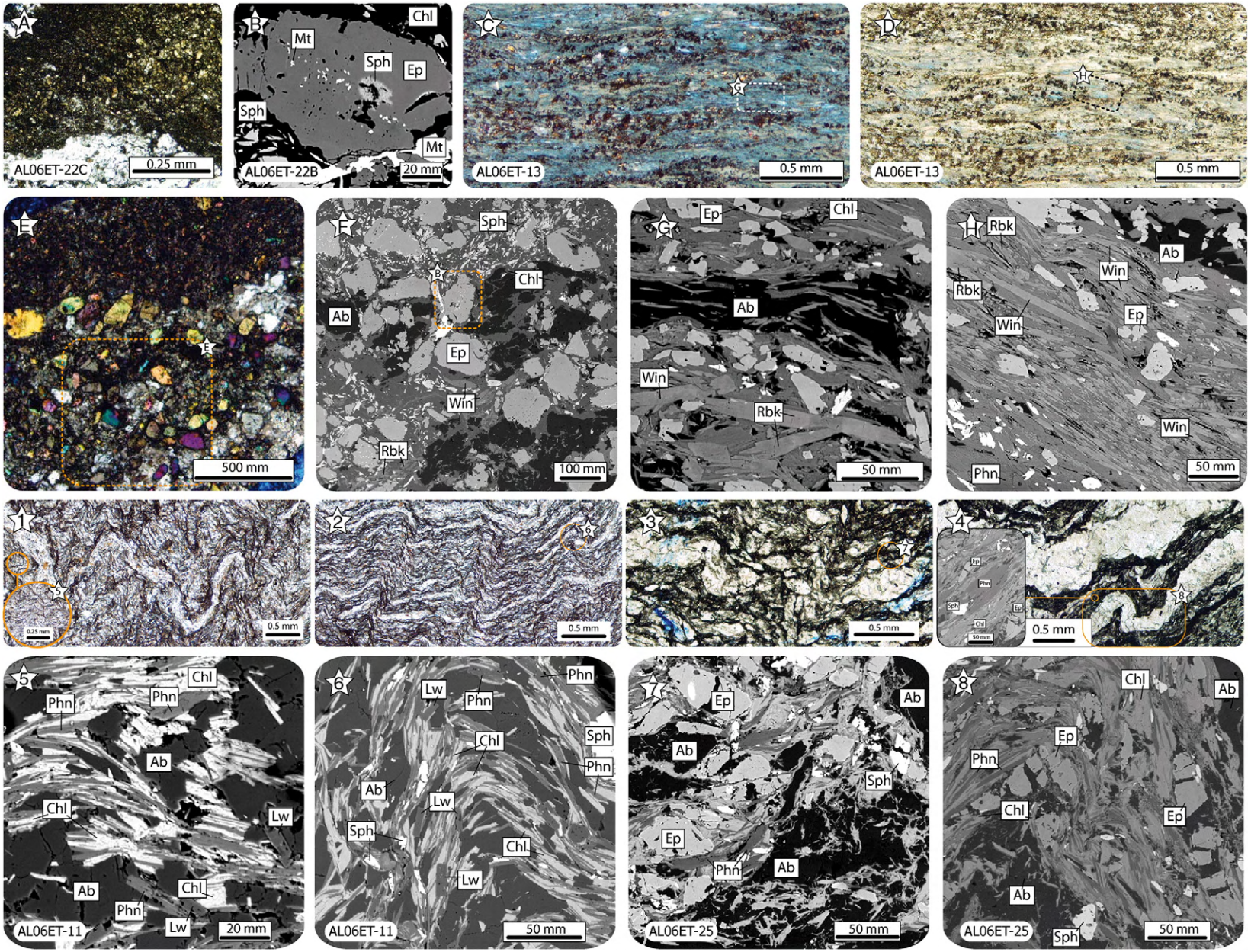

Fig. 7. 1–8, Microphotographs of the Liberty Creek pelitic Schist. 1–2 and 5–6 are lawsonite blueschists at different scales; 3–4 and 7–8 are epidote blueschists: sample location in Figs. 1 and 5. 1–4, thin section images showing the lepidoblastic texture and the highly deformed fabric. 5–8, corresponding EMP images inquiring some details of the Lw-deformed rhombs (5 and 6), and the late-Ab porphyroblasts growth. Lw: lawsonite; Ep: epidote; Phn: phengite; Chl: chlorite; Ab: albite; Sph: sphene. A–H, Microphotographs of the Liberty Creek mafic Schist at different scales; sample location in Figs. 1 and 5. A, E and F show the granoblastic texture defined by the abundant allotriomorphic epidote grains. B shows the magnetite inclusions in a corroded epidote crystal. C and D are thin section images showing the nematoblastic texture and the intensely deformed foliation. G and H are the corresponding EMP images. Win: winchite; Rbk: riebeckite; Ep: epidote; Chl: chlorite; Ab: albite; Sph: sphene; Mt: magnetite.

Table 1
Representative microprobe analysis of Lw-blueschists minerals (sample 110.430); phengites (Phn), chlorites (Chl), albite (Ab), lawsonite (Lw) and sphene (Sph). X_{Mg} = Mg/(Mg + Fe) (Chl, Lw, Sph); X_{Fe} = Fe/(Fe + Mg) (Phn); X_{Na} = Na/(Na + K) (Phn); An = [Ca/(Ca + Na + K)]100, Ab = [Na/(Ca + Na + K)]100, Or = [K/(Ca + Na + K)]100.

Sample	110,430											
Mineral	Phn	Phn	Chl	Chl	Chl	Chl	Ab	Ab	Lw	Lw	Sph	Sph
Analysis	5-4	4	2	71	31	32	6	3	5-3	16	13	4
SiO_2	53.21	50.26	25.98	25.41	32.11	30.25	66.02	64.75	39.02	37.71	33.14	30.54
TiO_2	0.03	0.10	0.01	0.01	0.03	0.04	0.08	0.06	0.13	0.20	33.55	37.04
Al_2O_3	25.90	28.08	21.53	20.62	19.69	23.03	20.25	21.51	30.54	30.51	3.33	2.17
Cr_2O_3	0.00	0.01	0.04	0.06	0.07	0.00	0.05	0.03	0.05	0.03	0.00	0.00
Fe_2O_3	0.00	0.01	0.00	0.00	0.00	0.00	0.87	1.06	0.00	0.00	0.00	0.00
FeO	2.39	2.65	27.01	26.93	23.94	20.41	0.00	0.00	0.25	2.75	0.27	0.35
MnO	0.00	0.04	0.10	0.46	0.37	0.4	0.02	0.00	0.00	0.09	0.00	0.00
MgO	2.75	2.71	11.79	12.18	10.28	9.24	0.49	0.78	0.07	0.91	0.04	0.02
CaO	0.00	0.00	0.02	0.01	0.03	0.01	0.04	0.01	16.38	14.98	26.13	28.11
Na_2O	0.13	0.16	0.01	0.02	0.02	0.07	10.73	8.10	0.42	0.04	0.06	0.01
K_2O	9.52	9.99	0.08	0.01	0.44	3.03	0.59	2.93	0.19	0.20	0.16	0.12
Total	93.93	94.01	86.57	85.71	86.97	86.48	99.14	99.23	87.03	87.40	96.67	98.35
Data calculated with AX software (Holland and Powell, 1998)												
Si	3.56	3.39	2.79	2.77	3.33	3.15	2.93	2.88	2.59	2.52	1.10	1.01
Ti	0.00	0.01	0.00	0.00	0.00	0.00	0.00	0.00	0.01	0.01	0.84	0.92
Al	2.04	2.23	2.72	2.65	2.40	2.83	1.06	1.13	2.39	2.40	0.13	0.08
Cr	0.00	0.00	0.00	0.01	0.01	0.00	0.00	0.00	0.00	0.00	0.00	0.00
Fe^{3+}	0.00	0.00	0.00	0.00	0.00	0.00	0.03	0.04	0.00	0.00	0.00	0.00
Fe^{2+}	0.13	0.15	2.43	2.45	2.07	1.78	0.00	0.00	0.01	0.15	0.01	0.01
Mn	0.00	0.00	0.01	0.04	0.03	0.04	0.00	0.00	0.00	0.00	0.00	0.00
Mg	0.27	0.27	1.89	1.98	1.59	1.43	0.03	0.05	0.01	0.09	0.00	0.00
Ca	0.00	0.00	0.00	0.00	0.00	0.00	0.00	0.00	1.16	1.07	0.93	1.00
Na	0.02	0.02	0.00	0.00	0.00	0.01	0.92	0.70	0.05	0.00	0.00	0.00
K	0.81	0.86	0.01	0.00	0.06	0.40	0.03	0.17	0.02	0.02	0.01	0.01
X_{Mg}			0.44	0.45	0.43	0.45			0.33	0.37	0.21	0.10
X_{Na}	0.02	0.02										
X_{Fe}	0.33	0.36										
An							0.21	0.00				
Ab							96.24	80.72				
Or							3.55	19.28				

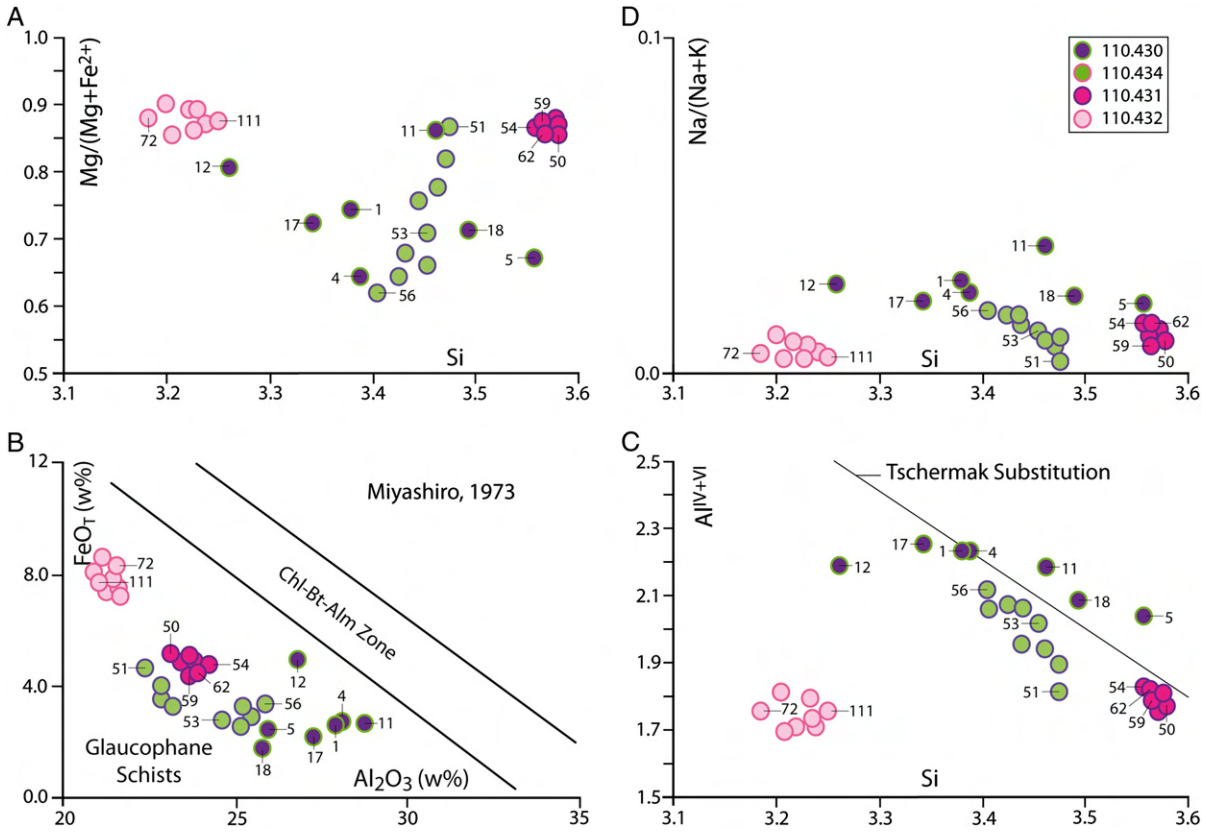

Fig. 8. Compositional variation of phengite in terms of different elements. (A) Si–[Mg/(Mg + Fe)]; (B) white mica classification diagram based on metamorphic origin (Miyashiro, 1973); (C) Si–[Na/(Na + K)] and (D) Si *vs.* Al_T. Cation numbers are calculated for 11 oxygens. Pointed numbers correspond to EMP analysis listed in Tables 1–4.

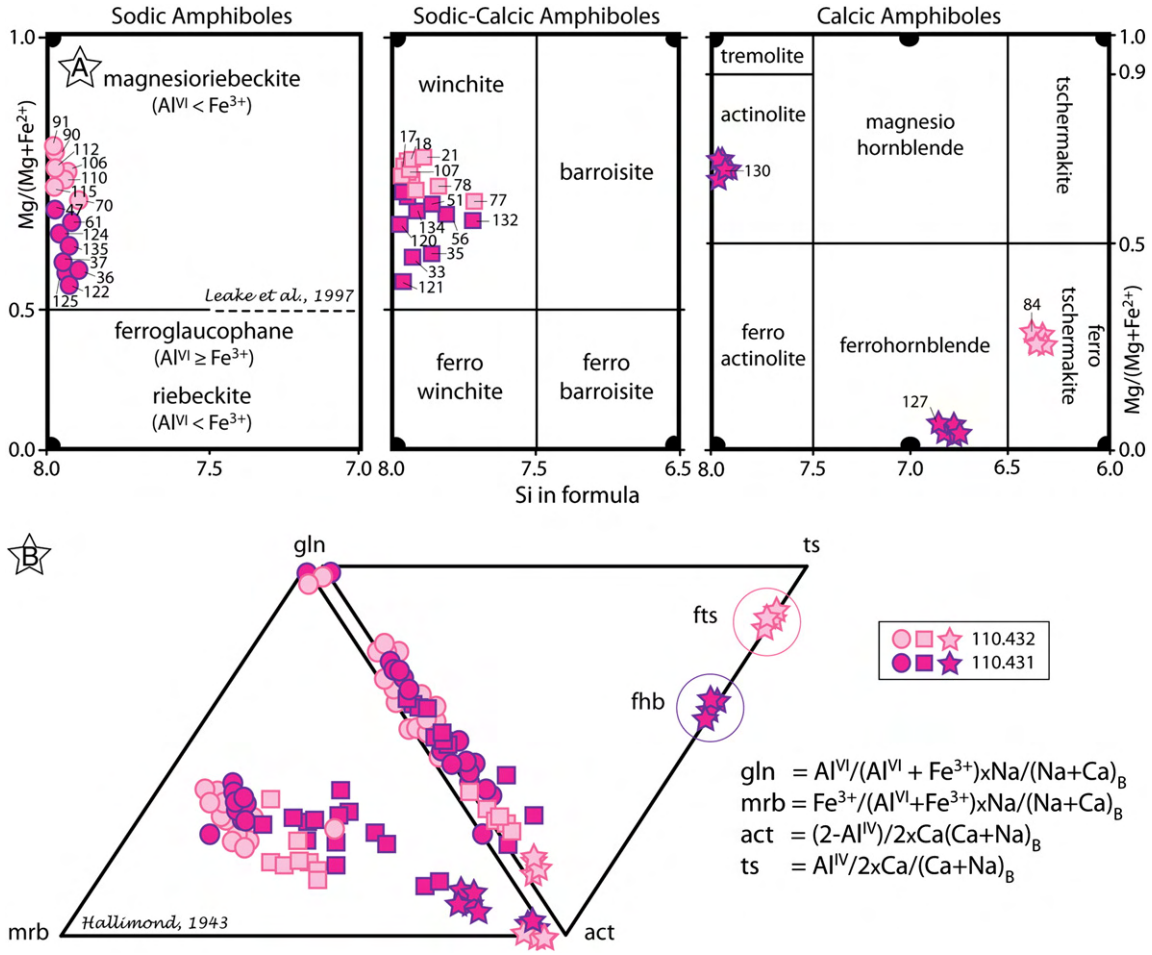

Fig. 9. (A) Chemical compositions of sodic, sodic–calcic and calcic amphiboles plotted in the classification diagrams of Leake et al. (1997); (B) Compositional variations of Na, Na–Ca and Ca amphibole from mafic schists at Liberty Creek expressed in the glaucophane–magnesioriebeckite–actinolite–tschermakite system of Hallimond diagrams (Hallimond, 1943). gln: glaucophane; mrb: magnesioriebeckite; act: actinolite; ts: tschermakite; fts: ferrotschermakite; fhb: ferrohornblende. Pointed numbers correspond to EMP analysis listed in Tables 1–4.

(Fig. 9A, Tables 3 and 4). Variation of X_{Al} contents in the blue amphibole probably derived from the variation in the bulk chemistry of the rock, and no zoning in individual crystals was found. The Na–Ca amphiboles are winchites with a $X_{Al} = Al/(Al + Fe^{3+}) \approx 0.31–0.65$ and a $X_{Mg} = Mg/(Mg + Fe^{2+}) \approx 0.59–0.74$ (Fig. 9A, Tables 3 and 4). The third type of amphibole ranges in composition from Fe-hornblende to actinolite (sample 110.431) and Fe-tschermakite (samples 110.432–110.433). Amphiboles in mafic schists contain almost no Ti. The compositional variation of Na–Ca amphiboles from the Liberty Creek schists is shown in Fig. 9B expressed in the glaucophane–magnesioriebeckite–actinolite–tschermakite system (Hallimond, 1943).

4.1.3. Lawsonite

Fresh prismatic lawsonite (≈20–30 μm long) in rocks with a strong foliation was identified in LBS metapelites (sample 110.430) with a nearly end-member composition (Table 1). No evidence of pseudomorphs of this mineral could be identified in the rest of the samples, probably due to the strong retrogression to greenschist facies observed in all the rocks, except sample 110.430.

4.1.4. Epidote group minerals

Epidote is a major mineral phase in the metabasalts of Liberty Creek. The mineral usually occurs in the pelitic schists as disrupted matrix porphyroblasts of 0.5–1 mm length, in the form of elongated and frequently broken prisms. It also forms clusters in the matrix. In mafic schists the epidote appears as corroded crystals that commonly contain magnetite inclusions and titanite along fractures. According to the nomenclature of Armbuster et al. (2006), all analyses in epidote group minerals of the EBS metapelites (sample 110.434) are classified as clinozoisites. Their $X_{Ps} = 0.19$ [Ps = pistacite, $Fe^{3+}/(Fe^{3+} + Al)$] and no compositional zoning was detected (Table 2). Epidote group minerals in EBS metabasalts are classified as epidotes rich in Fe ($X_{Ps} = 0.31$) with no core-rim zonation (Tables 3 and 4). The ternary diagram Al–Fe^{3+}–Ca shows that there is no compositional variation in the epidotes from the mafic schist's. The epidotes in pelitic schists from Liberty Creek are much less ferric than the previous ones. Epidote and clinozoisite occur as a matrix phase in blueschists without lawsonite. Due to the strong retrogression into greenschist facies conditions of the LBS/EBS, we could not distinguish primary from retrograde epidote/clinozoisite. All samples show evidence for retrograde metamorphism including the presence of texturally late white micas and chlorites. Considering that the less retrogressed sample contains abundant lawsonite, it seems very likely that part of the epidote/clinozoisite could be the product of retrograde metamorphism after lawsonite, although unquestionable pseudomorphs of this mineral were not found.

4.1.5. Chlorite

Chlorite, together with phengite, is the dominant phase in the matrix of the Liberty Creek schists. From the textural point of view, there is only one chlorite generation. However in the LBS samples, it is possible to detect a decrease in Fe^{2+} (2.45 up to 1.78 c.p.f.u), with a corresponding increase in Mg (1.98 up to 1.43 c.p.f.u), from two different trends of analyses that are texturally mixed, but chemically grouped (Table 1, Fig. 10). In some of the very fine grain grained varieties, chlorite forms

Table 2
Representative microprobe analysis of Ep-blueschists minerals (sample 110.434); phengites (Phn), chlorites (Chl), albite (Ab), clinozoisite (Czo), calcite (Cc) and sphene (Sph). X_{Mg} = Mg/(Mg + Fe) (Chl, Sph); X_{Fe} = Fe/(Fe + Mg) (Phn); X_{Fe} = Fe^{3+}/(Fe^{3+} + Al) (Czo); X_{Na} = Na/(Na + K) (Phn); An = [Ca/(Ca + Na + K)]100, Ab = [Na/(Ca + Na + K)] 100, Or = [K/(Ca + Na + K)]100.

Sample	110,434							
Mineral	Phn	Phn	Phn	Czo	Chl	Ab	Cc	Sph
Analysis	51	53	56	54	52	69	71	58
SiO_2	50.26	49.57	49.02	38.05	27.00	68.62	0.00	30.22
TiO_2	0.11	0.09	0.11	0.07	0.06	0.00	0.03	37.76
Al_2O_3	22.33	24.55	25.86	25.73	18.38	19.95	0.03	1.66
Cr_2O_3	0.06	0.08	0.02	0.09	0.07	0.01	0.01	0.05
Fe_2O_3	3.38	0.00	0.00	9.58	0.00	0.14	0.00	0.00
FeO	1.31	2.72	3.30	0.09	23.73	0.00	0.38	0.34
MnO	0.07	0.13	0.00	0.12	0.41	0.00	0.00	0.09
MgO	4.85	3.73	3.00	0.07	16.02	0.00	0.00	0.01
CaO	0.02	0.01	0.01	22.76	0.04	0.02	51.98	28.00
Na_2O	0.03	0.09	0.13	0.00	0.00	11.89	0.00	0.01
K_2O	10.37	10.95	10.98	0.03	0.11	0.02	0.03	0.07
Total	92.79	91.93	92.43	96.59	85.81	100.63	52.46	98.23
Data calculated with AX software (Holland and Powell, 1998)								
Si	3.48	3.46	3.41	3.02	2.89	2.98	0.00	1.00
Ti	0.01	0.01	0.01	0.00	0.01	0.00	0.00	0.94
Al	1.82	2.02	2.12	2.41	2.32	1.02	0.00	0.07
Cr	0.00	0.00	0.00	0.01	0.01	0.00	0.00	0.00
Fe^{3+}	0.18	0.00	0.00	0.57	0.00	0.00	0.00	0.00
Fe^{2+}	0.08	0.16	0.19	0.01	2.12	0.00	0.01	0.01
Mn	0.00	0.01	0.00	0.01	0.04	0.00	0.00	0.00
Mg	0.50	0.39	0.31	0.01	2.56	0.00	0.00	0.00
Ca	0.00	0.00	0.00	1.94	0.01	0.00	1.99	1.00
Na	0.00	0.01	0.02	0.00	0.00	1.00	0.00	0.00
K	0.92	0.97	0.97	0.00	0.02	0.00	0.00	0.00
X_{Mg}			0.62		0.55			0.04
X_{Na}	0.00	0.01	0.02					
X_{Fe}	0.13	0.29	0.38	0.19				
An						0.10		
Ab						99.80		
Or						0.10		

porphyroblasts and is associated with relatively low Si phengitic white mica (Si = 3.2 a.p.f.u.) (Fig. 7.4). Within the metapelites, in sample 110.430 chlorites show less X_{Mg} (0.43 apfu) than the chlorites in sample 110.434 (X_{Mg} = 0.55). In the mafic schists, the chlorites are notably more magnesian (X_{Mg} = 0.67–0.72) than in the pelitic schist (Tables 1–4). This slight increase in the X_{Mg} content is related with the mafic composition.

4.1.6. Plagioclase

Plagioclase is almost exclusively albite in all the samples. The mineral occurs as millimeter-sized porphyroblasts and as late-stage veins and is found closely intergrown with chlorite. In LBS, the albite and orthoclase content varies from 81 to 96 wt.% and 3.5 to 19 wt.%, respectively. Plagioclases in the EBS are nearly pure albite, reaching a maximum of 99.9 wt.% in albite content (Tables 1–4).

4.1.7. Titanite and magnetite

Titanite appears as allotriomorphic matrix grains (≈20 μm long) in LBS and EPS. In the EBS metabasites, it occurs as disordered aggregates in calcite veins (≈15–30 μm long) and partially replacing epidote crystal rims and fractures. The titanites do not show chemical zoning and are characterized by low Al_2O_3 contents, reaching a maximum of 2.17 wt.% in the LBS. The accessory magnetite inclusions are small, averaging 1–3 μm or less in diameter. Magnetite forms micro inclusions in epidote grains in EBS metabasites (see Fig. 7B).

4.1.8. Carbonates and apatite

The X-ray diffraction analyses carried out in this study have provided the identification of the high-pressure carbonate phase aragonite, typically associated with well-preserved low temperature blueschist parageneses. The aragonite grains are only in the LBS, whereas in the EBS the carbonates are calcite crystals and veins. Apatite is present only in the LBS, where it constitutes the most abundant accessory mineral. The sub-idiomorphic crystals do not exceed 25 μm in length. Fl and Cl have not been detected in the grains.

4.2. Phase equilibria modeling

Pressure–temperature (*P–T*) pseudosections were calculated with the PERPLE_X computer program package (Connolly, 1990; 2005, updated July, 2010) for the *P–T* range of 5–20 kbar and 200–600 °C using the thermodynamic data set of Holland and Powell (1998, updated 2004) for mineral end members. The following solid solution models for pseudosection calculation were chosen from the most updated solution file (solution_model.dat): Mica(CHA) for white mica (Auzanneau et al., 2010; Coggon and Holland, 2002), Chl(HP), Ctd (HP) and Ep(HP) for chlorite, chloritoid and epidote, respectively (Holland and Powell, 1998), cAmph(DP) for amphibole (Diener et al., 2007), Omph(GHP) for clinopyroxene (Green et al., 2007), Gt(WHP) for garnet (White et al., 2000), IlHm(A) and MtUl(A) for ilmenite and magnetite (Andersen and Lindsley, 1988), Bio(TCC) for biotite (Tajcmanová et al., 2009), and Ab(h) for plagioclase (Newton et al., 1980). The fluid phase was fixed as pure H_2O in excess based on the tectonic setting of these rocks within a hydrous subduction regime. CO_2 has been excluded from the calculations and SiO_2 is considered to be in excess.

Bulk compositions were determined by whole rock analyses of the same five samples used for petrographic studies using X-ray Fluorescence Spectroscopy (XRF). A representative slab of each sample was chosen: one LBS (sample 110.430) and four EBS (samples 110.431–434). The *P–T* pseudosections were computed for the system Na_2O–CaO–K_2O–FeO–MgO–Al_2O_3–SiO_2–TiO_2–Fe_2O_3 (NCKFMASHTO). The original compositions of the studied rocks were simplified to fit this system (Table 5).

The final pseudosections (Figs. 11 and 12) were redrawn as demonstrated by Connolly (2005). The compositional isopleths for Si and Fe content in phengite were generated using *werami* program from Perple_X package and plotted with *pscontor* and *Python* programs. W*erami* program has been used also to get the composition of each phase at particular *P–T* conditions.

Estimating the *P–T* conditions of the schists from Liberty Creek by conventional methods is problematic since no suitable geothermobarometer can be applied to these rocks. Moreover, the strong re-equilibration into greenschist and epidote–amphibolite facies assemblages displayed by all samples, and their small grain size, compounds this problem. In this work, we therefore addressed this issue by calculating the *P–T* conditions by pseudosections. However it is important to make some preliminary considerations based on the mineral assemblages. The absence of garnet in all the samples indicates a low temperature setting for the initial high-pressure event (*ca.* ≥400 °C). The presence of lawsonite in sample 110.430 is also a key indicator of the high pressure nature of these rocks. This hydrous mineral is stable over a wide *P–T* range in the low-*T* blueschist facies, but rarely preserved.

We computed *P–T* pseudosections for four representative samples from the Liberty Creek schists: two pelitic schists (LBS; sample 110.430, EPB; sample 110.434) and two mafic schists (EBS; samples 110.431–110.432). The results are shown in Figs. 11 and 12 were thick continuous and dashed lines indicate the stability field of diagnostic phases and thick black lines represents the proposed *P–T* path. Jd + Qtz → Ab reaction (Holland, 1980) is shown as reference. White fields are divariant and increasing variance is shown with progressively darker shades of grey. Mineral abbreviations are after Kretz (1983), Holland and Powell (1998) and Whitney and Evans (2010).

Table 3
Representative microprobe analysis of Ep-blueschists minerals (sample 110.431); phengites (Phn), chlorites (Chl), albite (Ab), epidote (Ep), ferrohornblende (Fe-Hb), actinolite (Act), magnesioriebeckite (Mrb), winchite (Win) and sphene (Sph). $X_{Mg} = Mg/(Mg + Fe)$ (Chl, Sph, Amph); $X_{Fe} = Fe/(Fe + Mg)$ (Phn); $X_{Fe} = Fe^{3+}/(Fe^{3+} + Al)$ (Ep); $X_{Na} = Na/(Na + K)$ (Phn); $X_{Al} = Al/(Al + Fe^{3+})$ (Amph), An = [Ca/(Ca + Na + K)]100, Ab = [Na/(Ca + Na + K)]100, Or = [K/(Ca + Na + K)]100.

Sample	110,431												
Mineral	Phn	Phn	Chl	Chl	Ab	Ep	Fe-Hb	Act	Mrb	Mrb	Win	Win	Sph
Analysis	50	54	40	57	58	131	127	130	36	37	35	39	44
SiO_2	55.02	55.51	27.77	28.36	68.99	37.71	42.51	54.64	53.05	54.54	53.80	55.46	30.60
TiO_2	0.06	0.03	0.00	0.04	0.00	0.07	0.08	0.03	0.07	0.05	0.17	0.07	36.19
Al_2O_3	23.09	24.20	17.97	19.02	19.68	21.91	19.69	1.54	3.99	3.55	3.64	1.83	1.74
Cr_2O3	0.00	0.03	0.06	0.04	0.00	0.02	0.04	0.03	0.03	0.03	0.07	0.05	0.06
Fe_2O_3	3.67	3.39	4.69	0.00	0.47	14.85	14.28	1.79	6.36	7.24	3.01	6.50	0.00
FeO	1.42	1.31	16.88	19.60	0.00	0.13	0.00	11.28	13.14	12.38	13.81	8.36	1.15
MnO	0.00	0.06	0.06	0.04	0.00	0.08	0.10	0.25	0.03	0.00	0.12	0.04	0.00
MgO	4.65	4.67	19.66	19.00	0.00	0.00	0.73	15.14	9.65	9.57	11.08	13.31	0.07
CaO	0.43	0.04	0.03	0.02	0.01	22.30	19.80	9.18	1.82	2.53	4.60	5.61	28.00
Na_2O	0.06	0.09	0.00	0.00	12.17	0.09	0.02	1.84	6.47	6.20	5.06	3.17	0.05
K_2O	8.37	8.95	0.01	0.00	0.01	0.01	0.00	0.05	0.00	0.03	0.04	0.01	0.05
Total	96.77	98.28	87.13	86.12	101.33	97.17	97.25	95.77	94.61	96.12	95.40	94.41	97.91
Data calculated with AX software (Holland and Powell, 1998)													
Si	3.58	3.56	2.45	2.94	2.98	3.04	6.17	7.96	7.92	7.99	7.94	8.09	1.02
Ti	0.00	0.00	0.00	0.00	0.00	0.00	0.01	0.00	0.01	0.01	0.02	0.01	0.91
Al	1.77	1.83	3.44	2.32	1.00	2.08	3.37	0.26	0.70	0.61	0.63	0.32	0.07
Cr	0.00	0.00	0.01	0.00	0.00	0.00	0.01	0.00	0.00	0.00	0.01	0.01	0.00
Fe^{3+}	0.18	0.16	0.57	0.00	0.02	0.90	1.56	0.20	0.72	0.80	0.33	0.71	0.00
Fe^{2+}	0.08	0.07	2.29	1.70	0.00	0.01	0.00	1.37	1.64	1.52	1.71	1.02	0.03
Mn	0.00	0.00	0.01	0.00	0.00	0.01	0.01	0.03	0.00	0.00	0.02	0.01	0.00
Mg	0.45	0.45	4.76	2.93	0.00	0.00	0.16	3.29	2.15	2.09	2.44	2.90	0.00
Ca	0.03	0.00	0.01	0.00	0.00	1.93	3.08	1.43	0.29	0.40	0.73	0.88	1.00
Na	0.01	0.01	0.00	0.00	1.02	0.02	0.01	0.52	1.87	1.76	1.45	0.90	0.00
K	0.69	0.73	0.00	0.00	0.00	0.00	0.00	0.01	0.00	0.01	0.01	0.00	0.00
X_{Mg}			0.67	0.63			1.00	0.71	0.57	0.58	0.59	0.74	0.10
X_{Na}	0.01	0.01						0.27	0.87	0.82	0.67	0.51	
X_{Fe}	0.15	0.14				0.30	0.32	0.43	0.50	0.57	0.35	0.69	
X_{Al}						0.70	0.68	0.57	0.50	0.43	0.65	0.31	
An					0.00								
Ab					99.90								
Or					0.10								

4.3. P–T paths and discussion

The *P–T* pseudosection for the LBS is shown in Fig. 11A. The coexistence of lawsonite and high silica phengite (3.56 c.p.f.u) marks a high-*P* limit around 19 kbar, constraining a maximum pressure for the LBS and confirming the high-*P* nature of this paragenesis. However, no chloritoid or carpholite are present. The intersection between the Si (3.56 c.p.f.u.) and the Fe (0.33–0.36 c.p.f.u) isopleths in phengites provides another approximation for the maximum pressures reached, at 15–16 kbars. At these pressures magnesiocarpholite is still predicted as a stable phase in the paragenesis. However it has not been observed in the natural assemblage. Currently there is no a solid solution model for carpholite, being always considered for the petrologic modeling as pure (ideal solid solution). The stability of this phase is restricted to a narrow temperature window (300–400 °C) at elevated pressures (Mottana and Schreyer, 1977) so it may appear in the considered *P–T* range. The predicted presence of this mineral in the pseudeosection for the LBS can be explained by the limitations resulting from the absence of a proper solid solution model for this phase, which would affect to the actual extension of its stability field, or more probably to its consumption during retrograde reactions. The absence of the other phases predicted in the pseudosection and now not present in the LBS are equally interpreted as a result of retrograde metamorphism. For example, jadeite probably have been consumed during retrograde metamorphism to form albite according to the reaction Jd + Qtz = Ab (Holland, 1980). No paragonite was found in these rocks. The boundary reaction between paragonite and albite is Gln + Zo + Pg + H_2O = Chl + Law + Ab (e.g. Heinrich and Althaus, 1988). Therefore, the possible interpretations are that paragonite was never present or it was consumed completely to form albite. The last hypothesis will also explain the absence of sodic amphibole in these rocks. However, the diagram predicts the presence of amphibole as a stable phase. According to the stability of lawsonite + phengite and the intersection of isopleths for Si and Fe content in white mica, the *P–T* conditions can be estimated as 220–280 °C and 14–15 kbar. Garnet-free LBS with similar *P–T* conditions and mineralogy have been reported in other high-pressure terranes (see i.e. L. Zhang et al., 2009; Z. Zhang et al., 2009).

In the pelitic EBS rocks (Fig. 11B), epidote is present in the matrix assemblage. The Si (3.46–3.48 c.p.f.u) and the Fe (0.13–0.29 c.p.f.u) content in phengites suggests approximate *P–T* conditions of 18 kbar and 400 °C. However, no lawsonite has been found in these rocks. Clinozoisite could be a product of retrograde metamorphism replacing earlier lawsonite. Based on the presence of clinozoisite in the natural paragenesis the *P–T* path could evolve to the 4-variant field chl-ph-pg-czo-jd-ru. But paragonite, jadeite and rutile are absent in these rocks. The presence of albite and sphene and the lack of biotite suggests a rapid decompression at 10 kbar with a slightly decrease in temperature from 450 to 400 °C. Again; the presence of amphiboles, clinopyroxene and paragonite in the intermediate fields does not conform to the petrographic observations. The mode of rutile in all the assemblages is very low (up to a maximum of 0.15%). The lack of this phase could be explained due to its fine-grained size precluding detection by routine microprobe techniques. In the case of clinopyroxenes and paragonite the same reactions explained previously could take place, justifying the absence of these phases. Regarding omphacite alternate possibilities are that the mineral could have been totally consumed to form carbonates, or that it was never present.

The mafic EBS pseudosections are shown in Fig. 12A and B. Lawsonite is the only high-*P* phase predicted that has not been observed either as inclusions or in the matrix. However, this mineral has been

Table 4
Representative microprobe analysis of Ep-blueschists minerals (sample 110.432); phengites (Phn), chlorites (Chl), albite (Ab), epidote (Ep), ferrotschermakite (Fe-Ts), magnesioriebeckite (Mrb), winchite (Win) and sphene (Sph). $X_{Mg} = Mg/(Mg + Fe)$ (Chl, Sph, Amph); $X_{Fe} = Fe/(Fe + Mg)$ (Phn); $X_{Fe} = Fe^{3+}/(Fe^{3+} + Al)$ (Ep); $X_{Na} = Na/(Na + K)$ (Phn); $X_{Al} = Al/(Al + Fe^{3+})$ (Amph), An = [Ca/(Ca + Na + K)]100, Ab = [Na/(Ca + Na + K)]100, Or = [K/(Ca + Na + K)]100.

Sample	110,432											
Mineral	Phn	Phn	Chl	Chl	Ab	Ep	Fe-Ts	Mrb	Mrb	Win	Win	Sph
Analysis	72	111	66	88	113	22	84	106	110	77	78	25
SiO_2	45.53	45.83	30.05	28.86	68.23	37.13	40.29	55.25	55.15	52.67	53.23	30.53
TiO_2	0.09	0.07	0.00	0.00	0.04	0.00	0.04	0.08	0.03	0.02	0.28	38.27
Al_2O_3	21.30	20.98	18.11	17.37	19.49	21.43	19.74	3.17	3.13	5.31	4.37	0.91
Cr_2O_3	0.14	0.08	0.07	0.05	0.02	0.07	0.02	0.07	0.08	0.06	0.08	0.04
Fe_2O_3	5.97	5.52	0.00	0.00	0.16	15.10	14.14	8.70	8.38	6.87	5.54	0.00
FeO	2.30	2.13	15.51	15.99	0.00	0.14	0.00	7.31	8.05	10.16	9.40	0.77
MnO	0.11	0.10	0.36	0.48	0.02	0.00	0.20	0.17	0.13	0.19	0.11	0.00
MgO	9.64	8.44	21.53	22.61	0.01	0.02	4.64	12.32	12.16	12.42	12.82	0.05
CaO	0.01	0.05	0.04	0.01	0.02	22.00	16.30	2.85	2.79	1.49	2.91	27.60
Na_2O	0.03	0.02	0.01	0.00	11.99	0.03	0.03	5.63	5.81	5.86	5.33	0.02
K_2O	8.23	8.45	0.57	0.00	0.02	0.00	0.00	0.02	0.07	0.07	0.01	0.07
Total	93.35	91.67	86.25	85.37	100.00	95.92	95.40	95.57	95.78	95.12	94.08	98.26
Data calculated with AX software (Holland and Powell, 1998)												
Si	3.18	3.25	3.05	2.97	2.99	3.03	5.94	7.98	7.97	7.71	7.83	1.01
Ti	0.01	0.00	0.00	0.00	0.00	0.00	0.00	0.01	0.00	0.00	0.03	0.96
Al	1.75	1.75	2.17	2.11	1.01	2.06	3.43	0.54	0.53	0.92	0.76	0.04
Cr	0.01	0.00	0.01	0.00	0.00	0.00	0.00	0.01	0.01	0.01	0.01	0.00
Fe^{3+}	0.31	0.30	0.00	0.00	0.01	0.93	1.57	0.95	0.91	0.76	0.61	0.00
Fe^{2+}	0.13	0.13	1.32	1.38	0.00	0.01	0.00	0.88	0.97	1.24	1.16	0.02
Mn	0.01	0.01	0.03	0.04	0.00	0.00	0.03	0.02	0.02	0.02	0.01	0.00
Mg	1.00	0.89	3.26	3.47	0.00	0.00	1.02	2.65	2.62	2.71	2.81	0.00
Ca	0.00	0.00	0.00	0.00	0.00	1.93	2.57	0.44	0.43	0.23	0.46	0.98
Na	0.00	0.00	0.00	0.00	1.02	0.00	0.01	1.58	1.63	1.66	1.52	0.00
K	0.73	0.77	0.07	0.00	0.00	0.00	0.00	0.00	0.01	0.01	0.00	0.00
X_{Mg}	0.88	0.88	0.71	0.72			1.00	0.75	0.73	0.69	0.71	
X_{Na}	0.01	0.00					0.00	0.78	0.79	0.88	0.77	
X_{Fe}	0.12	0.12				0.31	0.31	0.64	0.63	0.45	0.45	
X_{Al}						0.69	0.69	0.36	0.37	0.55	0.55	
An					0.10							
Ab					99.80							
Or					0.10							

found in the associated pelitic schists from Liberty Creek. Also we consider the possibility that some of the abundant crystals of zoisite/clinozoisite found in the matrix of the mafic schists could have been formed at the expense of earlier lawsonite in the rock. The growth of late albite porphyroblasts in some levels indicates a dramatic decompression from the fields with lawsonite to the fields with stable albite. Further constraints can be placed from the fact that the samples contain Na-amphibole and phengite, indicating that the *P–T* path should first pass through the fields with this assemblage and then through those with albite. In sample 110.431 the fields that best fits the petrographic data comprises the shaded area between 5–9 kbar and 250–350 °C (Figs. 12A and 13). The intersection between the Si (3.58 c.p.f.u) and the Fe (0.15 c.p.f.u) isopleths in phengites support this data. However, the mode of lawsonite and pyroxene in these parageneses is extremely high compared with that of epidote, besides the absence of calcic amphiboles. Therefore, in this case the intersection of the silica isopleths cannot be considered as a reliable barometer (see i.e. Massone and Schreyer, 1987). Based on the highest silica content analyzed in phengites (3.58 c.p.f.u) the *P–T* path that best fits with the petrographic observations would start in the 4-variance field jd-chl-ph-law-ilm-ru evolving through jd-chl-ph-law-ep-ru, reporting the first occurrence of epidote coexisting with lawsonite, crossing the field omp-chl-ph-ep-ru, to enter in the 3-variance field omp-chl-ep-ph-pg-sph-ru (with the formation of paragonite and sphene and the consumption of ilmenite), going finally to omp-chl-ep-ph-sph-ab, from the EBS fiels to the GS field. The resulting *P–T* path suggests strong isothermal decompression from *ca.* 17 kbar to 7 kbar, with a temperature peak around 425 °C. The mode of each phase in the parageneses bear out this trajectory, and the presence of biotite limit the temperature to a maximum value of 450 °C. However the absence of amphiboles in all the area does not conform to the natural assemblages. In sample 110.432 the presence of epidote and the silica isopleths in phengite (3.25 c.p.f.u) points to maximum pressure conditions at about 18 kbar and 450 °C in the 4-variance field omp-chl-ep-ph-pg-ru. The *P–T* path could have reached higher pressures starting in the EBS field, but no petrographic evidence of this fact can support this hypothesis. The evidence of sodic and sodic–calcic amphiboles suggests that the *P–T* path evolves to a temperature of 500 °C crossing the fields omp-Namp-ep-ph-pg-ru and omp-NCamp-ep-ph-ab-ru, where albite appears and paragonite disappears. Finally from 500 °C to 400 °C the path crosses the 4-variance field omp-NCamp-ep-ph-sph-ab in the epidote–amphibolite facies to end in the omp-Camp-chl-ep-ph-sph-ab field, with the appearance of calcic amphibole, as corroborated by petrographic data.

A synthesis of the results is shown in Fig. 13 where thick black line represents the calculated *P–T* paths.

5. Petrologic modeling conclusions

Comparing the pseudosection calculations with the petrographic observations some important considerations can be concluded. Currently analytical techniques cannot identify how many Fe_2O_3 and FeO of the FeO_T comes from re-equilibration or is primary. These uncertainties are directly connected with the results when using particular solid solution models (i.e. amphiboles, epidote group minerals or Ti and Fe^{2+}/Fe^{3+} rich-oxides) as they are extremely sensitive in terms of the proportion of certain elements. However, although the strong re-equilibration into greenschist and epidote–amphibolite facies assemblages displayed by all samples influences the final mineralogy, the *P–T* diagrams are not affected and show the whole metamorphic evolution.

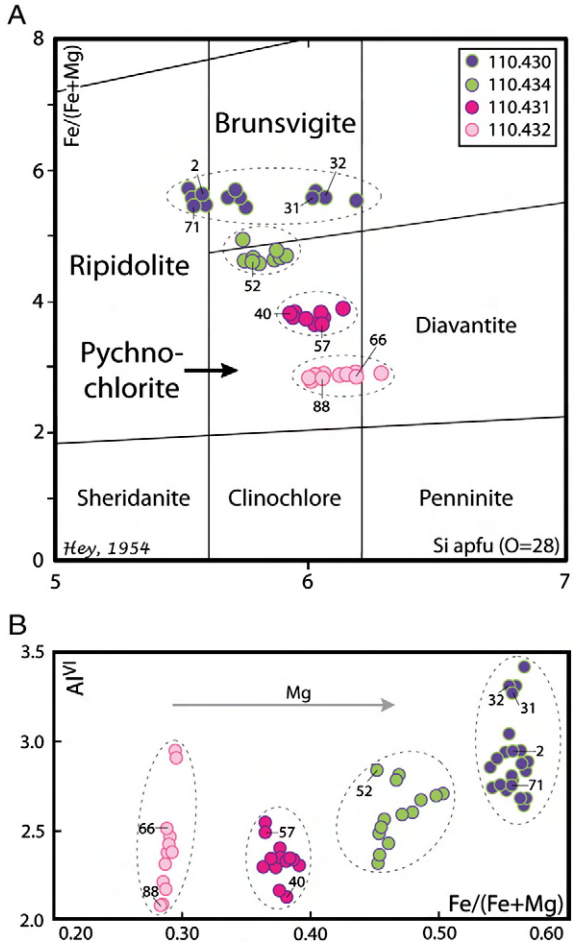

Fig. 10. (A) Chemical composition of chlorites in the Liberty Creek Schists plotted in Hey' s diagram (Hey, 1954). (B) Compositional variations of chlorite in terms of [Fe/(Fe + Mg)] *vs.* Al^{VI}. Pointed numbers correspond to EMP analysis listed in Tables 1–4.

Since calculations are performed in the NCKFMASHTO chemical frame, our model system considers two tricky components – TiO_2 and Fe_2O_3 – because of 1) the incomplete knowledge of the thermodynamic properties of Fe^{3+}-end members in the available solid solution models and 2) the remaining uncertainties on the effect of TiO_2, mainly in amphiboles and pyroxenes, as its solid solution models do not contain this component. Thus, when involving TiO_2 in the calculations it does not work for some bulk-rock compositions because: 2.1) the stability field of amphibole is suppressed or becomes irregular senseless shapes. 2.2) The stability field of pyroxenes shown in the diagrams is unrealistic in nature. 2.3) Considering TiO_2 avoids reducing the CaO bulk content which is involved in titanite but on the other hand, 2.4) the stability of Ti-rich phases such as rutile and ilmenite is overestimated.

The presence of lawsonite is crucial for the evaluation of the mechanisms of exhumation of these rocks (e.g. L. Zhang et al., 2009; Z. Zhang et al., 2009, with references therein). In the Liberty Creek Schists lawsonite has been found only in sample 110.430 and all observed epidote was present alone. As demonstrated by Davis and Whitney (2006) in all pseudosections when epidote and lawsonite coexists it is in a phase field rather than on a univariant line. The reaction glaucophane + lawsonite = albite + clinozoisite + clinochlore + quartz + H_2O can tightly constrain the metamorphic temperatures rather than the stability of lawsonite or epidote alone. This equilibrium is one of the many describing the transition from lawsonite blueschists to epidote blueschists (Evans, 1990) that can be followed in all diagrams. Therefore, we consider the possibility that some of the abundant crystals of epidote found in the matrix of samples 110.431–110.434 could have been formed at the expense of earlier lawsonite.

Finally, the growth of late albite porphyroblasts in all samples suggests a dramatic decompression, as also evidenced in the general trend of all paths in the calculated pseudosections.

6. General Conclusions

The Liberty Creek Schist outcrops over an area 28 km long and up to 13 km wide. The blueschist-bearing metamorphic rocks occur

Table 5
Bulk-rock composition from XRF analyses of the five representative samples. For comparison, some reference bulk-rock compositions are also included: N-MORB (Viereck et al., 1989), BHVO-2 corresponds to a basalt from the Hawaiian Volcanic Observatory (http://minerals.cr.usgs.gov/geo_chem_stand/basaltbhvo2.pdf), North American Pelite (Atherton and Brotherton, 1982) and aluminous Scottish Dalradian Pelite (Atherton and Brotherton, 1982). Bulk 1–5 normalized for H_2O in excess conditions. The $Fe_2O_{3(T)}$ is measured by the XRF and the FeO is measured by titration. The Fe_2O_3 is a calculation taking the converting: [total iron/1.43 − (FeO/1.286) * 1.43]. All the oxides are expressed in wt.%.

	110,430 AL06ET-11	110,431 AL06ET-13	110,432 AL06ET-22B	110,433 AL06ET-22C	110,434 AL06ET-25	N-MORB	BHVO-2	NAP	Al-SDP
						model bulk compositions			
SiO_2	59.96	51.70	47.93	46.14	57.65	49.8–51.66	49.90	61.54	59.88
TiO_2	0.84	1.05	1.26	1.16	0.86	1.36–1.62	2.73	0.82	1.03
Al_2O_3	16.20	12.88	14.09	16.49	15.94	14.32–16.28	13.50	16.95	19.15
FeO	6.25	8.87	4.56	4.46	5.48			3.90	5.15
Fe_2O_3	0.72	2.98	5.94	5.87	1.90			2.56	2.49
FeO_T	6.97	11.85	10.50	10.33	7.38	8.91–11.02	12.30	6.46	
MnO	0.10	0.17	0.18	0.17	0.14	0.16–0.20			0.12
MgO	3.10	8.67	6.29	4.32	3.54	6.09–8.06	7.23	2.52 ± 1.91	2.34
CaO	1.95	4.65	8.65	10.65	3.94	11.07–11.95	11.40	1.76 ± 2.03	1.03
Na_2O	2.23	1.23	2.88	3.37	3.98	2.20–2.65	2.22	1.84 ± 1.18	2.10
K_2O	2.56	1.26	1.17	1.40	1.01	0.08–0.52	0.52	3.45 ± 1.32	3.50
P_2O_5	0.22	0.10	0.10	0.15	0.24	0.11–0.15	0.27		
NiO	0.00	0.00	0.00	0.00	0.00				
Cr_2O_3	0.03	0.05	0.05	0.07	0.02				

	NCKFMASHTO (H_2O in excess)								
	Na_2O	CaO	K_2O	FeO	MgO	Al_2O_3	SiO_2	TiO_2	Fe_2O_3
110,430	2.52	2.07	1.90	6.09	5.38	11.13	69.86	0.74	0.32
110,431	1.35	5.48	0.91	8.39	14.62	8.59	58.50	0.89	1.27
110,432	3.27	10.70	0.88	4.47	10.99	9.74	56.21	1.11	2.62
110,433	3.87	13.26	1.06	4.42	7.62	11.51	54.62	1.03	2.61
110,434	4.45	4.48	0.74	5.29	6.09	10.84	66.53	0.75	0.83

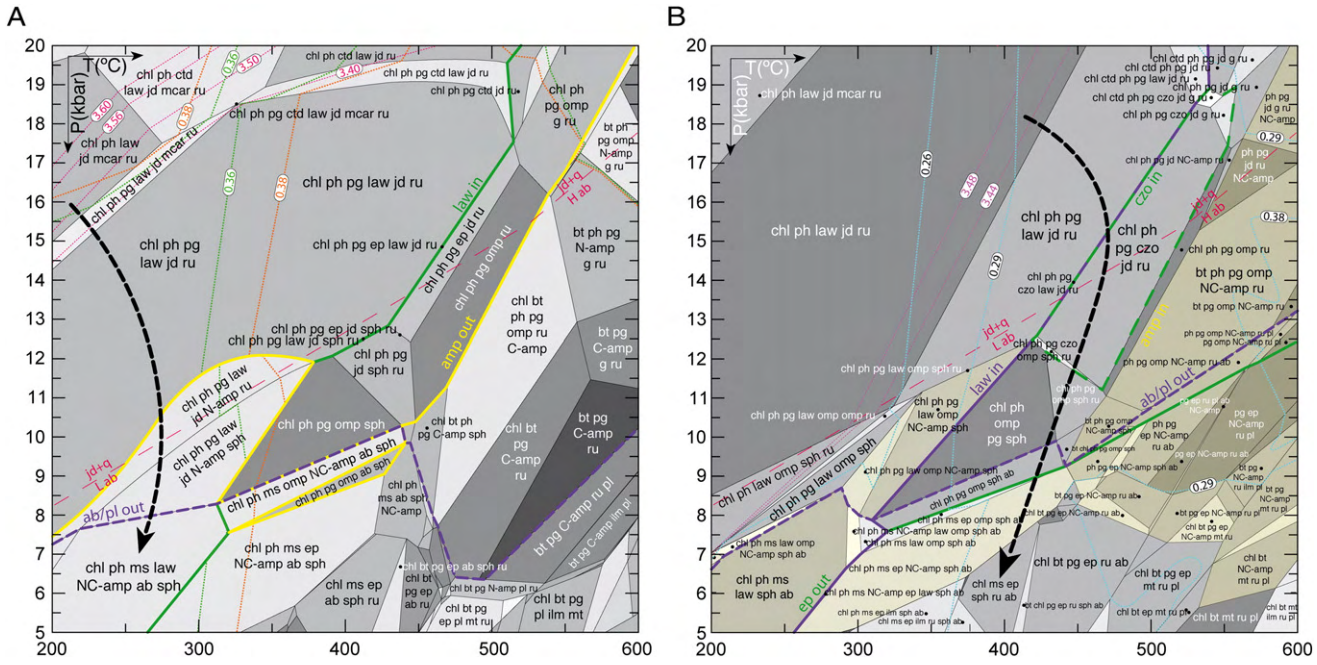

Fig. 11. Pseudosections calculated in the NCKFMASHTO system for representative bulk-rock composition (Table 5) of; A) Lw-pelitic blueschist (sample 110.430) and B) Ep-pelitic blueschist (sample 110.434). Thin dashed lines correspond to Fe^{2+} and Si isopleths in phengites (c.p.f.u.).

near the Border Ranges Fault in the eastern Valdez quadrangle of the northern Chugach Mountains. The rock types are mostly greenschist and blueschist, and also include muscovite and actinolite schist, siliceous schist, metachert, and graphitic schist. The protolith was mostly basaltic pillow flows, tuffs, tuff breccias, and volcaniclastic rocks with minor chert, carbonate, and argillaceous rocks; some faint primary structures at Liberty Creek suggest breccia or pillow breccia. At least two generations of folds exist in the Liberty Creek Schist—an earlier south-verging set of folds overprinted by younger, north-verging folds and a later brittle-shearing event mid-Cretaceous or younger. The metamorphic minerals have been isotopically dated, giving Late Triassic to mid-Cretaceous crystallization ages, which would have occurred during deep subduction (Plafker and Berg, 1994) reaching to 50–55 km.

The Liberty Creek schist is correlative with the Seldovia blueschist belt on the Kenai Peninsula, as well as the Raspeberry Schist on Kodiak, Afognak and Shuyak islands.

The Seldovia, Liberty Creek, and Raspberry schists preserve typical subduction zone blueschist facies metamorphic assemblages in a complexly deformed volcanic-sedimentary sequence that has clear affinities with the McHugh Complex. The circa 190 Ma (Early Jurassic) age of metamorphism likely records an early stage of subduction beneath Wrangellia, but there could be up to 40 million years between the

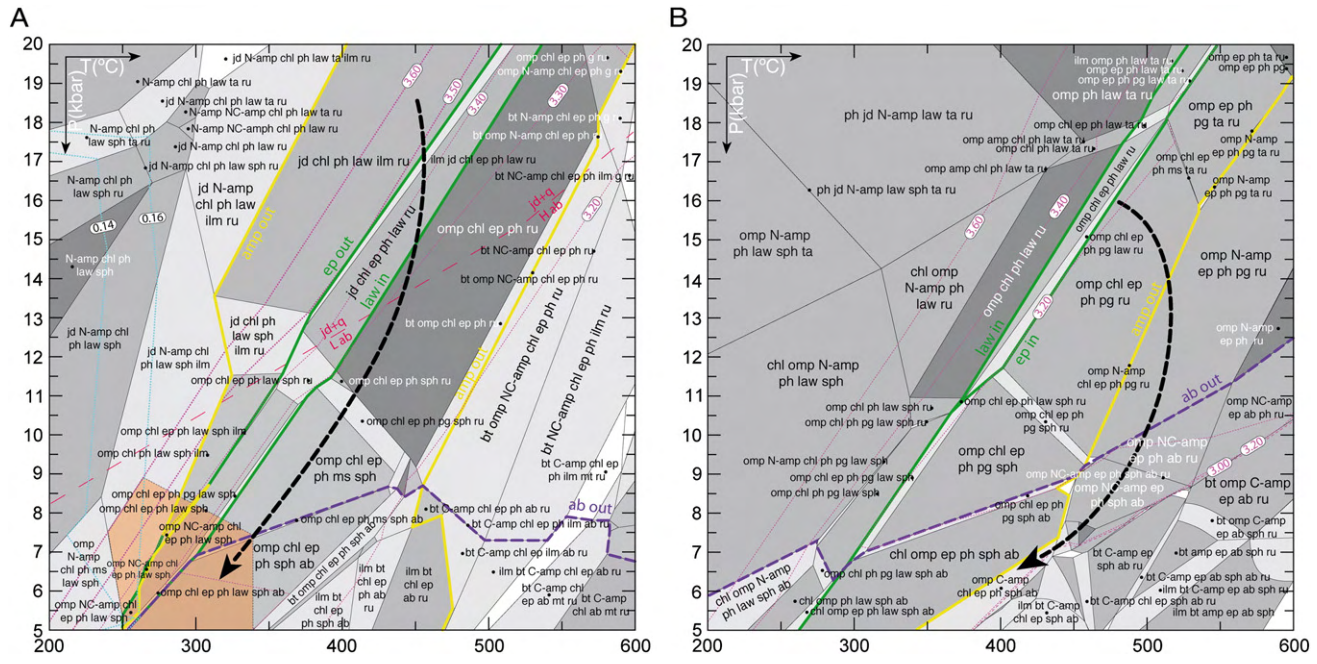

Fig. 12. Pseudosections calculated in the NCKFMASHTO system for representative bulk-rock composition (Table 5) of; A) Ep-mafic blueschist (sample 110.431) and B) Ep-mafic blueschist (sample 110.432). Thin dashed lines correspond to Fe^{2+} and Si isopleths in phengites (c.p.f.u.).

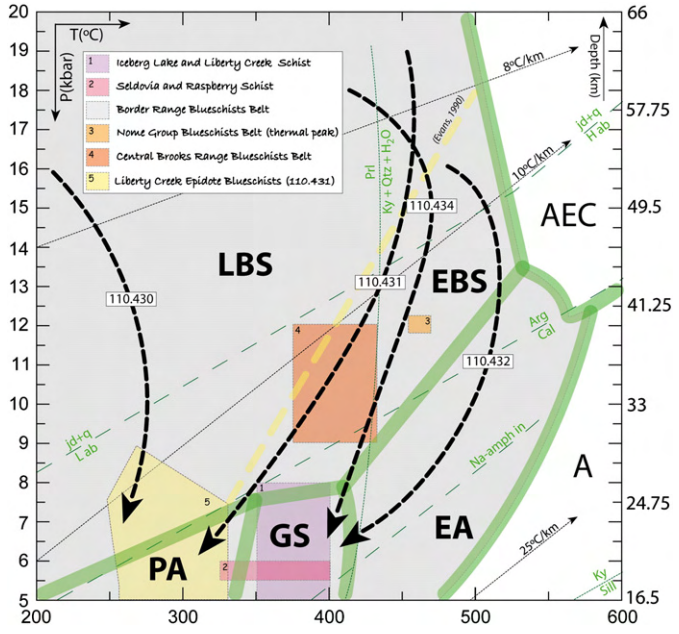

Fig. 13. *P–T* diagram showing the metamorphic paths of the Liberty Creek Schists. Dashed thin lines refer to different diagnostic reactions: Jd + Qtz → Ab (Holland, 1980); Prl → Ky + Qtz + H_2O and aluminosilicate stability fields after Holdaway (1971). Arg = Cal (Johannes and Puhan, 1971), Na-amph in (Maresch (1977), are also shown for reference. Continuous thick lines separate facies fields simplified after Maruyama et al. (1996) and Evans (1990). Thick continuous lines represent the calculated *P–T* paths. Facies field abbreviations: PA, pumpellyite–actinolite facies; GS, greenschist facies; EA, epidote–amphibolite facies; A, amphibolite facies; LBS, lawsonite blueschist facies; EBS, epidote blueschist facies and AEC, amphibole eclogite facies. For comparison, previous *P–T* estimations for the Liberty Creek Schist are shown; *P–T* paths from Iceberg Lake (Sisson and Onstott, 1986); Seldovia and Raspberry Schist (Carden et al., 1977); Border Range Blueschists Belt (Roeske, 1986; Roeske et al., 1989); Nome Group Blueschists Belt (Patrick and Evans, 1989); Central Brooks Range Blueschists Belt (Patrick, 1995) are also included.

initiation of subduction and the metamorphism in the blueschist belts. This estimate is based on the difference in age between the 230 Ma (Norian) U/Pb age of the Halibut cove SSZ ophiolite crust (Kusky and Glass, 2007), and 230 Ma tuffs in Port Graham formation, and the190 Ma age of the Seldovia and Liberty Creek metamorphism. So, if it took a maximum of 40 Ma to subduct the protoliths of the Seldovia and Liberty Creek blueschist to depths of perhaps 50–55 km, we estimate a minimum vertical component of subduction of 1.2–1.5 cm/year. True rates are likely to be faster.

More interestingly, we speculate on why blueschist facies rocks only appear to be preserved in a few very narrow fault-bounded strips adjacent to the Border Ranges fault. Several ideas are possible and require testing. First, the Border Ranges fault may be responsible for exhuming the blueschist facies rocks from depth, and they are only preserved adjacent to the fault because this is the only place they were brought close to the surface. Second, it is possible that blueschist facies assemblages are preserved because the Border Ranges fault marks the site of the initial subduction, where a cold oceanic slab thermally insulated material brought to about 50–55 km depth before they were returned (buoyantly?) to the surface. The Border Ranges fault is now largely a major strike-slip fault (Little and Naeser, 1989; Pavlis and Roeske, 2007), but the correlation of the blueschists with the trace of the fault support its earlier history as a subduction thrust (Plafker and Berg, 1994; Plafker et al., 1989). It is also interesting in this respect that all three preserved blueschist belts in this setting are long and narrow lens-shaped bodies, perhaps aiding their rapid return to the surface as demonstrated by the fast isothermal decompression documented in this study, and suggested for other HP terrains around the world (e.g., Wang et al., 2010).

Acknowledgements

Field work in the Seldovia quadrangle was the Alaska Mineral Resource Assessment Program of the USGS. Tim Kusky received funding, in addition, from the National Science Foundation Grants EAR-9304647 and EAR-9706699. Additional funds were provided by the National Natural Science Foundation of China (Grant 40821061) and the Ministry of Education of China (B07039). Laboratory work was financially supported by the CGL2007-65338-C02-01 project provided by the Spanish Ministry of Science and Innovation. We thank our colleagues Dwight Bradley, Alison Hill, and George Plafker of the USGS, and Erkan Toroman, for collaboration in the field and sharing samples and data. We also thank the Co-editor Dr. Ian Buick, Dr. Stephen T. Johnston and Dr. Lucie Tajcmanova for their constructive revisions that significantly improved the quality of this manuscript.

References

Andersen, D.J., Lindsley, D.H., 1988. Internally consistent solution models for Fe–Mg–Mn–Ti oxides — Fe–Ti oxides. American Mineralogist 73, 714–726.
Armbuster, T., Bonazzi, P., Akasaka, M., Bermanex, V., Chopin, C., Giere, R., Heuss-Assbichler, Liebscher, A., Menchettic, S., Pan, Y., Pasero, M., 2006. Recommended nomenclature of epidote-group minerals. European Journal of Mineralogy 18, 551–567.
Atherton, M.P., Brotherton, M.S., 1982. Major element composition of the pelites of the Scottish Dalradian. Geological Journal 17, 185–221.
Auzanneau, E., Schmidt, M.W., Vielzeuf, D., Connolly, J.A.D., 2010. Titanium in phengite: a geobarometer for high temperature eclogites. Contributions to Mineralogy and Petrology 159, 1–24.
Bradley, Dwight C., Kusky, Timothy M., Karl, Susan M., Haeussler, Peter J., 1997. Field guide to the Mesozoic accretionary complex along Turnagain Arm and Kachemak Bay, south-central Alaska. In: Karl, S.M., Vaughan, N.R., Ryherd, T.J. (Eds.), 1997 Guide to the Geology of the Kenai Peninsula, Alaska: Alaska Geological Society, Anchorage, Alaska, pp. 2–12.
Bradley, D.C., Kusky, T.M., Haeussler, P., Karl, S.M., Donley, D.T., 1999. Geologic map of the Seldovia Quadrangle, U.S. Geological Survey open file report 99-18, scale 1:250,000, with marginal notesAlso available as an internet publication: http://wrgis.wr.usgs.gov/open-file/of99-18/1999.
Bradley, Dwight C., Kusky, Timothy M., Karl, Susan M., Till, Alison, Haeussler, Peter J., 2000. Field guide to the Mesozoic Accretionary Complex in Kachemak Bay and Seldovia. South-Central Alaska, Alaska Geological Society and British Petroleum, Anchorage, Alaska, May 12–15, 2000.
Bradley, D.C., Kusky, T.M., Haeussler, P., Rowley, D.C., Goldfarb, R., Nelson, S., 2003. Geologic signature of early ridge subduction in the accretionary wedge, forearc basin, and magmatic arc of south-central Alaska. In: Sisson, V.B., Roeske, S., Pavlis, T.L. (Eds.), Geology of a Transpressional Orogen Developed during a Ridge–Trench Interaction along the North Pacific Margin: Geological Society of America Special Paper, 371, pp. 19–50.
Carden, J.R., Decker, J.E., 1977. Tectonic significance of the Knik River schist terrane, south-central Alaska, in short notes on Alaskan geology: Alaska Division of Geological and Geophysical Surveys. Geologic Report 55, 7–9.
Carden, J.R., Forbes, R.B., 1976. Discovery of blueschists in Kodiak Islands, Alaska, in short notes on Alaskan geology: Alaska Division of Geological and Geophysical Surveys. Geologic Rep. 51, 19–22.
Carden, J.R., Connelly, W., Forbes, R.B., Turner, D.L., 1977. Blueschists of the Kodiak Islands, Alaska: an extension of the Seldovia schist terrane. Geology 5, 529–533.
Coggon, R., Holland, T.J.B., 2002. Mixing properties of phengitic micas and revised garnet–phengite thermobarometers. Journal of Metamorphic Geology 20, 683–696.
Coney, P.J., Jones, D.L., Monger, J.W.H., 1980. Cordilleran suspect terranes. Nature 288, 329–333.
Connolly, J.A.D., 1990. Multivariable phase diagrams; an algorithm based on generalized thermodynamics. American Journal of Science 290, 666–718.
Connolly, J.A.D., 2005. Computation of phase equilibria by linear programming: a tool for geodynamic modeling and its application to subduction zone decarbonation. Earth and Planetary Science Letters 236, 524–541.
Davis, P.B., Whitney, D.L., 2006. Petrogenesis of lawsonite and epidote eclogite and blueschist, Sivrihisar Massif, Turkey. Journal of Metamorphic Geology 24, 823–849.
Diener, J.F.A., Powell, R., White, R., Holand, T.J.B., 2007. A new thermodynamic model for clino- and orthoamphiboles in the system Na_2O–CaO–FeO–MgO–Al_2O_3–SiO_2–H_2O–O. Journal of Metamorphic Geology 25, 631–656.
Ernst, W.G., 2010. Subduction-zone metamorphism, calc-alkaline magmatism, and convergent-margin crustal evolution. Gondwana Research 18, 8–16.
Evans, B.W., 1990. Phase relations of epidote-blueschists. Lithos 25, 3–23.
Green, E.C.R., Holland, T.J.B., Powell, R., 2007. An order–disorder model for omphacitic pyroxenes in the system jadeite–diopside–hedenbergite–acmite, with applications to eclogite rocks. American Mineralogist 92, 1181–1189.
Hallimond, A.F., 1943. On the graphical representation of the calciferous amphiboles. American Mineralogist 28 (2), 65–89.
Heinrich, W., Althaus, E., 1988. Experimental determination of the reaction 4 lawsonite + 1 albite = 1 paragonite + 2 zoisite + 2 quartz + 6 H_2O and 4 lawsonite + 1

jadeite = 1 paragonite + 2 zoisite + 1 quartz + 6 H_2O. Neues Jahrbuch fu¨r Mineralogie Monatshefte 11, 516–528.
Hey, M.H., 1954. A new review of the chlorites. Mineralogical Magazine 30, 277–292.
Holdaway, M.J., 1971. Stability of andalusite and the aluminum silicate phase diagram. American Journal of Science 211, 97–131.
Holland, T., 1980. The reaction albite = jadeite + quartz determined experimentally in the range 600–1200 °C. American Mineralogist 65, 125–134.
Holland, T.J.B., Powell, R., 1998. An internally consistent thermodynamic data set for phases of petrological interest. Journal of Metamorphic Geology 16, 309–343.
Isozaki, Y., Aoki, K., Nakama, T., Yanai, S., 2010. New insight into a subduction-related orogen: a reappraisal of the geotectonic framework and evolution of the Japanese Islands. Gondwana Research 18, 82–105. doi:10.1016/j.gr.2010.02.015.
Johannes, W., Puhan, D., 1971. The calcite–aragonite transition, reinvestigated. Contributions to Mineralogy and Petrology 31, 225–228.
Kadarusman, A., Maruyama, S., Kaneko, Y., Ota, T., Ishikawa, A., Sopaheluwakan, J., Omori, S., 2010. World's youngest blueschist belt from Leti Island in the non-volcanic Banda outer arc of Eastern Indonesia. Gondwana Research 18, 189–204. doi:10.1016/j.gr.2010.02.009.
Kretz, R., 1983. Symbols for rock-forming minerals. American Mineralogist 68, 277–279.
Kusky, T.M., Bradley, D.C., 1999. Kinematics of mélange fabrics: examples and applications from the McHugh Complex, Kenai Peninsula, Alaska. Journal of Structural Geology 21 (12), 1773–1796.
Kusky, T.M., Glass, A., 2007. Structure, Cr-chemistry, and age of the border ranges ultramafic/mafic complex: a suprasubduction zone ophiolite complex. Geological Society of America, Special Paper 431 on the Tectonic Growth of a Collisional Continental Margin: Crustal Evolution of Southern Alaska, pp. 207–225. doi:10.1130/2007.2431(09).
Kusky, T.M., Bradley, D.C., Haeussler, P.J., 1997a. Progressive deformation of the Chugach accretionary complex, Alaska, during a Paleogene ridge-trench encounter. Journal of Structural Geology 19, 139–157.
Kusky, T.M., Bradley, D.C., Haeussler, P., Karl, S., 1997b. Controls on accretion of flysch and mélange belts at convergent margins: evidence from the Chugach Bay thrust and Iceworm mélange, Chugach Terrane, Alaska. Tectonics 16 (6), 855–878.
Kusky, T.M., Bradley, D.C., Donley, D.T., Rowley, D., Haeussler, P., 2003. Controls on intrusion of near-trench magmas of the Sanak-Baranof belt, Alaska, during Paleogene ridge subduction, and consequences for forearc evolution. In: Sisson, V.B., Roeske, S., Pavlis, T.L. (Eds.), Geology of a Transpressional Orogen Developed During a Ridge–Trench Interaction Along the North Pacific Margin: Geological Society of America Special Paper, 371, pp. 269–292.
Leake, B.E., Woolley, A.R., Arpes, C.E.S., et al., 1997. Nomenclature of amphiboles: report of the Subcommittee on amphiboles of the International Mineralogical Association, Commission on New Minerals and Mineral Names. American Mineralogist 82, 1019–1037.
Little, T.A., Naeser, C.W., 1989. Tertiary tectonics of the Border Ranges fault system, Chugach Mountains, Alaska: deformation and uplift in a forearc setting. Journal of Geophysical Research 94, 4333–4359.
López-Carmona, A., Abati, J., Reche, J., 2010. Petrologic modeling of chloritoid–glaucophane schists from the NW Iberian Massif. Gondwana Research 17, 377–391.
Maresch, W., 1977. Experimental studies on glaucophane: an analysis of present knowledge. Tectonophysics 43, 109–125.
Maruyama, S., Liou, J.G., Terabayashi, M., 1996. Blueschists and eclogite of the world and their exhumation. International Geological Review 38, 485–594.
Maruyama, S., Hasegawa, A., Santosh, M., Kogiso, T., Nakamura, H., Kawai, K., Zhao, D., 2009. The dynamics of big mantle wedge, magma factory, and metamorphic-metasomatic factory in subduction zones. Gondwana Research 16, 414–430.
Massone, H.J., Schreyer, W., 1987. Phengite geobarometry based on the limiting assemblage with K-feldspar, phlogopite and quartz. Contributions to Mineralogy and Petrology 96, 212–214.
Miyashiro, A., 1973. Metamorphism and Metamorphic Belts. G. Allen and Unwin Publications, London.
Mottana, A., Schreyer, W., 1977. Carpholite crystal chemistry and preliminary experimental stability. Neues Jahrbuch für Mineralogie 129, 113–138.
Newton, R.C., Charlu, T.V., Kleppa, O.J., 1980. Thermochemistry of the high structural state plagioclases. Geochemica and Cosmochimica Acta 44, 933–941.
Nilsen, T.H., Zuffa, G.G., 1982. The Chugach terrane, a Cretaceous trench-fill deposit, southern Alaska. Geological Society of London. Special Publication 10, 213–227.
Nokleberg, W.J., Foster, H.L., Aleinikoff, J.N., 1989. Geology of the northern Copper River basin, eastern Alaska Range, and southern Yukon-Tanana Basin, southern and east-central Aslaska. In: Nokleberg, W.J., Fisher, M.A. (Eds.), Alaskan Geological and Geophysical Transect: International Geological Congress, 27th, Guidebook T104, pp. 34–64.
Nokleberg, W.J., Plafker, G., Wilson, F.H., 1994. Geology of south-central Alaska. In: Plafker, G., Berg, H.C. (Eds.), The Geology of Alaska, Decade of North American Geology vol. G-1: Geological Society of America, pp. 311–366.
Omori, S., Kita, S., Maruyama, S., Santosh, M., 2009. Pressure–temperature conditions of ongoing regional metamorphism beneath the Japanese Islands. Gondwana Research 16, 458–469.
Ota, T., Kaneko, Y., 2010. Blueschists, eclogites, and subduction zone tectonics: Insights from a review of Late Miocene blueschists and eclogites, and related high-pressure metamorphic rocks. Gondwana Research 18, 167–188. doi:10.1016/j.gr.2010.02.013.
Patrick, B.E., 1995. High pressure-low temperatura metamorphism of granitic orthogneisses in the Brooks Range, northern Alaska. Journal of Metamorphic Geology 13, 111–124.
Patrick, B.E., Evans, B.W., 1989. Metamorphic evolution of the Seward Peninsula blueschist terrane. Journal of Petrology 30, 531–555.
Pavlis, T.L., Roeske, S.M., 2007. The Border Ranges fault system, southern Alaska. In: Ridgeway, K.D., Trop, J.M., Glen, J.M.G., O'Oneill, J.M. (Eds.), Tectonic Growth of a Collisional Continental Margin: Crustal Evolution of Southern Alaska: Geological Society of America Special Paper, 431, pp. 95–127.
Plafker, G., Berg, H.C., 1994. Overview of the Geology and Tectonic Evolution of Alaska. In: Plafker, G., Berg, H. (Eds.), The Geology of North America: The Geology of Alaska, Geological Society of America, vol. G-1, pp. 989–1021. Chapter 33.
Plafker, G., Nokleberg, W.J., Lull, J.S., 1989. Bedrock geology and tectonic evolution of the Wrangellia, Peninsular, and Chugach terranes along the Trans-Alaska Crustal Transect in the Chugach Mountains and southern Copper River basin. Journal of Geophysical Research 94, 4255–4295.
Poli, S., Schmidt, M.W., 2002. Petrology of subducted slabs. Annual Review of Earth and Planetary Sciences 30, 207–235.
Roeske, S.M., 1986. Field relations and metamorphism of the Raspberry Schist, Kodiak Islands, Alaska. Blueschists and eclogites. In: Evans, B.W., Brown, E.H. (Eds.), Geological Society of America Memoir, 164, pp. 169–184.
Roeske, S.M., Mattison, J.M., Armstrong, R.L., 1989. Isotopic ages of glaucophane schist on the Kodiak Islands, southern Alaska, and their implications for the Mesozoic tectonic history of the Border Ranges Fault system. Geological Society of America Bulletin 101, 1021–1037.
Sisson, V.B., Onstott, T.C., 1986. Dating blueschist metamorphism; a combined 40Ar/39Ar and electron microprobe approach. Geochimica et Cosmochimica Acta 50, 2111–2117.
Tajcmanová, L., Connolly, J.A.D., Cesare, B., 2009. A thermodynamic model for titanium and ferric iron solution in biotite. Journal of Metamorphic Geology 27, 153–164.
Tsujimori, T., Sisson, V.B., Liou, J.G., Harlow, G.E., Sorensen, S.S., 2006. Very-low-temperature record of the subduction process: a review of worldwide lawsonite eclogites. Lithos 92, 609–624.
Viereck, L.G., Flower, M.F.J., Hertogen, J., Schmincke, H.-U., Jenner, G.A., 1989. The genesis and significance of N-MORB sub-types. Contributions to Mineralogy and Petrology 102, 112–126.
Wang, Lu., Kusky, T., Li, S.Z., 2010. Structural geometry and evolution of an exhumed ultra-high pressure eclogite massif, Yangkou Bay, Sulu Belt, China. Journal of Structural Geology 32, 423–444.
White, R., Powell, R., Holland, T.J.B., Worley, B.A., 2000. The effect of TiO_2 and Fe_2O_3 on metapelitic assemblages at greenschist and amphibolite facies conditions: mineral equilibria calculations in the system K_2O–FeO–MgO–Al_2O_3–SiO_2–H_2O–TiO_2–Fe_2O_3. Journal of Metamorphic Geology 18, 497–511.
Whitney, D.L., Evans, B.W., 2010. Abbreviations for names of rock-forming minerals. American Mineralogist 95, 185–187.
Zhang, L., Wang, Q., Song, S., 2009a. Lawsonite blueschist in Northern Qilian, NW China: *P–T* pseudosections and petrologic implications. Journal of Asian Earth Sciences 35, 354–366.
Zhang, Z., Zhu, W., Shu, L., Wan, J., Yang, W., Su, J., Zheng, B., 2009b. Apatite fission track thermochronology of the Precambrian Aksu blueschist, NW China: implications for thermo-tectonic evolution of the north Tarim basement. Gondwana Research 16, 182–188.

3.3.3 *Partial Conclussions*

PETROLOGIC MODELLING CONCLUSIONS

1. Comparing the pseudosection calculations with the petrographic observations some important considerations can be concluded. Currently analytical techniques cannot identify how many Fe_2O_3 and FeO of the FeO_T comes from re-equilibration or is primary. These uncertainties are directly connected with the results when using particular solid solution models (i.e. amphiboles, epidote group minerals or Ti and Fe^{2+}/Fe^{3+} rich-oxides) as they are extremely sensitive in terms of the proportion of certain elements. However, although the strong re-equilibration into greenschist and epidote–amphibolite facies assemblages displayed by all samples influences the final mineralogy, the P–T diagrams are not affected and show the whole metamorphic evolution. Since calculations are performed in the NCKFMASHTO chemical frame, our model system considers two tricky components – TiO_2 and Fe_2O_3 – because of 1) the incomplete knowledge of the thermodynamic properties of Fe^{3+}-end members in the available solid solution models and 2) the remaining uncertainties on the effect of TiO_2, mainly in amphiboles and pyroxenes, as its solid solution models do not contain this component. Thus, when involving TiO_2 in the calculations it does not work for some bulk-rock compositions because: 2.1) the stability field of amphibole is suppressed or becomes irregular senseless shapes. 2.2) The stability field of pyroxenes shown in the diagrams is unrealistic in nature. 2.3) Considering TiO_2 avoids reducing the CaO bulk content which is involved in titanite but on the other hand, 2.4) the stability of Ti-rich phases such as rutile and ilmenite is overestimated.

2. The presence of lawsonite is crucial for the evaluation of the mechanisms of exhumation of these rocks (e.g. L. Zhang *et al.*, 2009; Z. Zhang *et al.*, 2009, with references therein). In the Liberty Creek Schists lawsonite has been found only in sample 110.430 and all observed epidote was present alone. As demonstrated by Davis and Whitney (2006) in all pseudosections when epidote and lawsonite coexists it is in a phase field rather than on a univariant line. The reaction glaucophane + lawsonite = albite + clinozoisite + clinochlore + quartz + H_2O can tightly constrain the metamorphic temperatures rather than the stability of lawsonite or epidote alone. This equilibrium is one of the many describing the transition from lawsonite blueschists to epidote blueschists (Evans, 1990) that can be followed in all diagrams. Therefore, we consider the possibility that some of the abundant crystals of epidote found in the matrix of samples 110.431–110.434 could have been formed at the expense of earlier lawsonite.

3. Finally, the growth of late albite porphyroblasts in all samples suggests a dramatic decompression, as also evidenced in the general trend of all paths in the calculated pseudosections.

GENERAL CONCLUSIONS

1. The Liberty Creek Schist outcrops over an area 28 km long and up to 13 km wide. The blueschist-bearing metamorphic rocks occur near the Border Ranges Fault in the eastern Valdez quadrangle of the northern Chugach Mountains. The rock types are mostly greenschist and blueschist, and also include muscovite and actinolite schist, siliceous schist, metachert and graphitic schist. The protoliths were mostly basaltic pillow flows, tuffs, tuff breccias and volcaniclastic rocks with minor chert, carbonate, and argillaceous rocks; some faint primary structures at Liberty Creek suggest breccia or pillow breccia.

2. At least two generations of folds exist in the Liberty Creek Schist, an earlier south verging set of folds overprinted by younger, north-verging folds and a later brittle-shearing event mid-Cretaceous or younger. The metamorphic minerals have been isotopically dated, giving Late Triassic to mid Cretaceous crystallization ages, which would have occurred during deep subduction (Plafker & Berg, 1994) reaching to 50–55 km.

3. The Liberty Creek schist is correlative with the Seldovia blueschist belt on the Kenai Peninsula, as well as the Raspeberry Schist on Kodiak, Afognak and Shuyak islands. The Seldovia, Liberty Creek, and Raspberry schists preserve typical subduction zone blueschist facies metamorphic assemblages in a complexly deformed volcanic-sedimentary sequence that has clear affinities with the McHugh Complex. The circa 190 Ma (Early Jurassic) age of metamorphism likely records an early stage of subduction beneath Wrangellia, but there could be up to 40 million years between the initiation of subduction and the metamorphism in the blueschist belts. This estimate is based on the difference in age between the 230 Ma (Norian) U/Pb age of the Halibut cove SSZ ophiolite crust (Kusky & Glass, 2007), and 230 Matuffs in Port Graham formation, and the190 Ma age of the Seldovia and Liberty Creek metamorphism. So, if it took a maximumof 40 Ma to subduct the protoliths of the Seldovia and Liberty Creek blueschist to depths of perhaps 50–55 km, we estimate a minimum vertical component of subduction of 1.2–1.5 cm/year. True rates are likely to be faster.

4. More interestingly, we speculate on why blueschist facies rocks only appear to be preserved in a few very narrow fault-bounded strips adjacent to the Border Ranges fault. Several ideas are possible and require testing. First, the Border Ranges fault may be responsible for exhuming the blueschist facies rocks from depth, and they are only preserved adjacent to the fault because this is the only place they were brought close to the surface. Second, it is possible that blueschist facies assemblages are preserved because the Border Ranges fault marks the site of the initial subduction, where a cold oceanic slab thermally insulated material brought to about 50–55 km depth before they were returned (buoyantly?) to the surface. The Border Ranges fault is now largely a major strike-slip fault (Little & Naeser, 1989; Pavlis & Roeske, 2007), but the correlation of the blueschists with the trace of the fault support its earlier history as a subduction thrust (Plafker & Berg, 1994; Plafker *et al.*, 1989). It is also interesting in this respect that all three preserved blueschist belts in this setting are long and narrow lens-shaped bodies, perhaps aiding their rapid return to the surface as demonstrated by the fast isothermal decompression documented in this study, and suggested for other HP terrains around the world (*e.g.*, Wang *et al.*, 2010).

CHAPTER 4

Correlation of the nappe stack in the Ibero-Armorican Arc

4. CORRELATIONS ACROSS THE IAA

Correlation of the nappe stack in the Ibero-Armorican arc across the Bay of Biscay: a joint French-Spanish project

MICHEL BALLÈVRE[1]*, JOSÉ RAMÓN MARTÍNEZ CATALÁN[2], ALICIA LÓPEZ-CARMONA[1-3], JACOBO ABATI[3], RUBÉN DÍEZ FERNÁNDEZ[2], CÉLINE DUCASSOU[4], PAVEL PITRA[1], RICARDO ARENAS[3], VALÉRIE BOSSE[5], PEDRO CASTIÑEIRAS[3], JAVIER FERNÁNDEZ-SUÁREZ[3], JUAN GÓMEZ BARREIRO[2], JEAN-LOUIS PAQUETTE[5], JEAN-JACQUES PEUCAT[1], MARC POUJOL[1], GILLES RUFFET[1] & SONIA SÁNCHEZ MARTÍNEZ[3].

SUBMITTED TO THE GEOLOGICAL SOCIETY OF LONDON (under review)

[1] Géosciences Rennes - UMR-CNRS 6118- Université de Rennes I, 35042 Rennes Cedex, France
[2] Departamento de Geología, Universidad de Salamanca, 37008 Salamanca, Spain
[3] Departamento de Petrología y Geoquímica e Instituto de Geociencias (UCM-CSIS), Universidad Complutense, 28040 Madrid, Spain
[4] Department of Applied Geosciences, German University of Technology in Oman (GUtech), PO Box 1816, Athaibah, PC 130, Sultanate of Oman
[5] Laboratoire Magmas et Volcans, Université Blaise-Pascal Clermont-Ferrand, 5 rue Kessler, 63000 Clermont-Ferrand, France
*Corresponding author (e-mail: michel.ballevre@univ-rennes1.fr)

ABSTRACT

A correlation among allochthonous units exposed in the NW Iberian Massif and the southern Armorican Massif is carried out based on lithological associations, structural position, age and geochemistry of protoliths, and tectonometamorphic evolution. The units in both sides of the Bay of Biscay are succesfully grouped in three different ensembles called the Upper, Middle and Lower Allochthons, while an underlying allochthonous thrust sheet with stratigraphic and petrologic affinities with its relative autochthon, is also identified in both massifs, and is referred to as the Parautochthon.

The Lower Allochthon represents a fragment of the outermost edge of Gondwana that underwent continental subduction shortly after the closure of a Palaeozoic ocean which, in turn, is represented by the Middle Allochthon. The oceanic domain consists of supra-subduction type ophiolites and metasedimentary sequences alternating with basic, MORB-type volcanics, with inheritances suggesting the proximity of a continental domain. Sea-floor spreading began at the Cambro-Ordovician boundary and oceanic crust was still formed during the Late Devonian, covering, the time interval of existence of the Rheic Ocean, which is a clear candidate for being represented by the Middle Allochthon. The opening of the oceanic domain was related to pulling apart of a peri-Gondwanan continental arc, which is represented by the Upper Allochthon.

4.1 INTRODUCTION

The existence of an arc in the north of the Iberian Massif was made evident for the first time in the map published by Gillermo Schulz (1858, map dated at 1857, reproduced in Truyols & Marcos 1978) about the geology of Oviedo province. The map, which was modified in successive editions (Gillermo Schulz 1900, 1901, 1930), shows the Devonian beds and the Carboniferous limestones delineating an arc, concave toward the east, which is currently known as the Asturian knee and the Asturian or Cantabrian arc. Eduard Suess, in the second book of "Das antlitz der Erde" (1885-1909, 1904-1909), proposed the continuation of the Asturian arc to the north in the Hercynian (Variscan) mountains of Brittany. The work of Suess was followed by many other contributions (Stille 1924, 1951; Kossmat 1921; Choubert 1935; Lotze 1929, 1954-1955; Carey 1955; Cogné 1967), and the so-called Armorican or Ibero-Armorican arc has received a wide acceptance by geologists for more than a century.

Different relationships have been envisaged between the Iberian and French structures and zones in both sides of the Bay of Biscay or Cantabrian Sea. The structures of the Variscan belt in NW Iberia have been continued into the British Isles (Baker, 1936), the Pyrenees (Holmes 1929; Llopis Lladó 1966), or the basement of Aquitaine and the French Massif Central (Matte 1968). Most authors, however, have linked NW Iberia with the Armorican Massif. The latter correlation, first established by Suess (1885-1909), has been always the most popular and became fully accepted after the work of Bard *et al.* (1971), which called Ibero-Armorican virgation to the large arc whose core is occupied by the Asturian knee. That contribution was soundly founded, based on the distribution of Precambrian and Palaeozoic sedimentary facies, for which they divided the Iberian Massif in nine zones, and continued most of them in Western France. The authors also established a tectonic zoning comparable in both sides of the Bay of Biscay, and did the same with the metamorphic belts and the distribution of Variscan granitoids.

Palaeomagnetic and structural data indicate that the arc dates from the latest Carboniferous-earliest Permian (305-295 Ma; Weil 2006, Alonso *et al.* 2009, Merino-Tomé *et al.* 2009, Weil *et al.* 2010), and that it bends structures that were previously linear or almost linear (*e.g.* Bonhommet *et al.* 1981; Weil, 2006). These include a huge nappe stack built during the early phases of the Variscan orogeny, folds, and late-Variscan strike-slip shear zones (Fig. 1). Stratigraphic correlations have been established between both sides of the Bay of Biscay for the Neoproterozoic and Palaeozoic series of the autochthonous domains (Cogné 1974; Robardet *et al.* 1990; Young 1990; Chantraine *et al.* 1994; Eguíluz *et al.* 2000), and also for some structures, namely strike-slip shear zones (Martínez Catalán *et al.* 2007). Similitudes between the allochthonous units have been put forward too (Iglesias *et al.* 1983, Ballèvre *et al.* 2009), but a detailed comparison has never been attempted.

Our aim is to establish a correlation of the units forming the nappe stack on both sides of the Bay of Biscay, and therefore to unify the terminology when describing them. Field work has been made in common by members of the French and Spanish teams for checking whether or not

lithologies, structures, and the metamorphic evolution were similar. The following account relies on detailed mapping made in the Armorican Massif and NW Iberia, the two sections having weaknesses as well as strengths. The section along the northern coast of Spain is of exceptional quality, aided by high relief and improved with information from the interior of NW Spain and Northern Portugal, but the allochthonous nappe stack there includes a suture whose root is never seen on land. On the French side, adding to the relatively poor quality of most outcrops, the South-Armorican shear zone cuts across significant portions of the nappe stack, and therefore displaces the suture zone, whose occurrence and location is a matter of discussion.

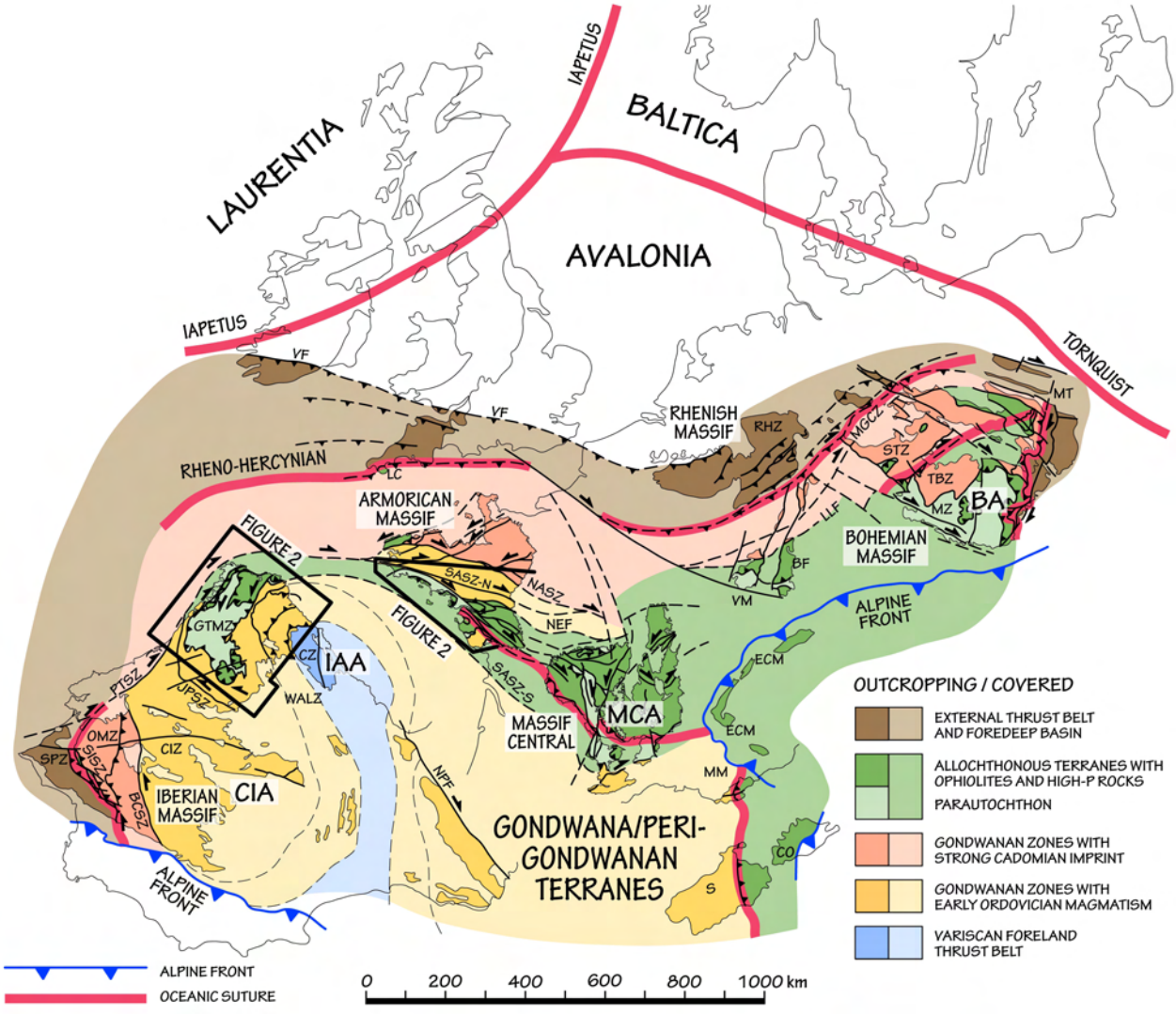

Fig. 1. Sketch of the Variscan belt, modified from Martínez Catalán *et al.* (2007). Arcs: BA- Bohemian; CIA- Central Iberian; IAA- Ibero-Armorican; MCA- Massif Central. Zones: CIZ- Central Iberian; CZ- Cantabrian; GTMZ- Galicia-Trás-os-Montes; MGCZ- Mid-German Crystalline; MZ- Moldanubian; OMZ- Ossa-Morena; RHZ- Rheno-Hercynian; SPZ- South Portuguese; STZ- Saxo-Thuringian; TBZ- Teplá-Barrandian; WALZ- West Asturian-Leonese. Shear zones and faults: BCSZ- Badajoz-Córdoba; JPSZ- Juzbado-Penalva; LLF- Layale-Lubine; MT- Moldanubian thrust; NASZ- North Armorican; NEF- Nort-sur-Erdre; NPF- North Pyrenean; PTSZ- Porto-Tomar; SASZ- South Armorican (N and S- northern and southern branches); SISZ- Southern Iberian; VF- Variscan front. Other: BF- Black Forest; CO- Corsica; ECM- External crystalline massifs of the Alps; LC- Lizard Complex; MM- Maures Massif; S- Sardinia; VM- Vosges Massif.

4.2 GEOLOGICAL SETTING

The geology of both, the Armorican Massif and NW Iberia is characterised by an autochthonous domain overlain by a parautochthonous thrust sheet and an allochthonous nappe stack (Fig. 2). The Autochthon consists of a sedimentary succession and accompanying volcanics deposited during the Neoproterozoic and Palaeozoic. Sedimentation of the Neoproterozoic succession took place during the last stages of the Cadomian-Pan-African events in an active continental margin, a Gondwanan peripheral orogenic belt (Murphy & Nance 1991; Fernández-Suárez *et al.* 1998; Gutiérrez-Alonso *et al.* 2004a), and also during its transition to an early Cambrian passive continental margin (Valladares *et al.* 2000).

The Palaeozoic witnesses the evolution of a relatively stable continental margin from the early Cambrian to the Early Devonian, broken by an unconformity marking a middle Cambrian to Early Ordovician phase of extension. The unconformity reflects continental rifting and drifting away of peri-Gondwanan terranes, and the opening of the Rheic Ocean. Extension is also indicated by magmatism, bimodal and covering the time span from Cambrian to Silurian, but voluminous only during the Early Ordovician: Ollo de Sapo Fm and granitic orthogneisses in Spain, "porphyroïdes" in France (Le Hébel *et al.* 2002, 2007). They derived from partial melting of a source that includes a significant Cadomian component, and are dated at about 490-470 Ma and (Díez Montes *et al.* 2010; Ballèvre *et al.* 2012). Faunal evidence (Robardet, 2002, 2003) and detrital zircon age populations (Ugidos *et al.*, 2003; Martínez Catalán *et al.* 2004; Bea *et al.*, 2010) point to a palaeogeographic position of the Autochthon in the northern margin of Gondwana.

The Parautochthon represents a distal part of the Gondwanan continental margin (Martínez Catalán *et al.* 2009) and, as in the Autochthon, deformation and metamorphism are Variscan. It is also known as the Schistose Domain in NW Iberia, where it is formed by a thick succession of Ordovician, Silurian and Early Devonian metasediments and volcanics, with stratigraphic and igneous affinities with the Iberian Autochthon (Marquínez García 1984; Farias *et al.* 1987; Farias and Marcos, 2004; Valverde-Vaquero *et al.*, 2005; Dias da Silva *et al.*, 2012, this volume). The affinities are also supported by detrital zircon age populations (Díez Fernández *et al.* 2012d; Dias da Silva,2013). Early Carboniferous syn-orogenic flysch deposits in NW Iberia have been preserved in both the Autochthon and Parautochthon (Martínez Catalán *et al.*,2004, 2008; Meireles,2011; Dias da Silva, 2013).

The allochthonous nappe stack is formed by different units characterised by their lithologic association and tectonometamorphic evolution. They are grouped according to their lithological affinities, evolution and relative position in the original nappe pile, and are separated from each other by thrusts, extensional detachments, and strike-slip shear zones and faults. These units have been grouped in three ensembles, called the Lower, Middle, and Upper Allochthons (Table 1), and are the objective of our correlation.

TABLE 1. Correlations between the allochthonous units in NW Iberia and the Armorican Massif. See text for sources of data.

		NW IBERIAN MASSIF				ARMORICAN MASSIF		
		BRAGANÇA-MORAIS	MALPICA-TUI	ÓRDENES	CABO ORTEGAL	AUDIERNE	CHAMPTOCEAUX	VENDÉE
UPPER ALLOCHTON	LOW-GRADE UNITS			Betanzos			Mauges (basement + Palaeozoic cover)	Roc-Cervelle (basement + Palaeozoic cover)
	IP UNITS	Lagoa		Monte Castelo, Corredoiras, A Silva, O Pino	Cariño	Penhors		
	HP UNITS	Core of Bragança Complex and three small slices in Morais Complex		Sobrado, Melide, Belmil, Fornás	Cedeira, A Capelada	Keramoine, Kergroaz		Essarts
MIDDLE ALLOCHTON (OCEANIC DOMAIN)	DEVONIAN OPHIOLITES	Morais-Talhinhas		Careón	Purrido, Moeche		Drain - le Hâvre	
	CAMBRO-ORDOVICIAN OPHIOLITES	Izeda-Remondes		Villa de Cruces, Bazar	Somozas	Audierne (Ty Lan, Peumerit, Tréogat)	les Folies Siffait	Saint-Martin-des-Noyers
	CAMBRO-ORDOVICIAN OCEANIC SUPRACRUSTALS	Pombais	Ceán	Lamas de Abad, Cercio				Ile-de-Groix, Bois-de-Cené
LOWER ALLOCHTHON	HP UNITS	Centro-Transmontane sub-Domain, Macedo de Cavaleiros	Malpica-Tui	Agualada, Santiago, Forcarei, Lalín	Espasante	Audierne	Champtoceaux, Saint-Mars-du-Désert, Cellier, Mauves-sur-Loire	Sainte-Pazanne - Mervent
PARAUTOCHTON (GONDWANA)		Schistose Domain				Nerly		

4.3 LOWER ALLOCHTHON

This ensemble includes a terrigenous sequence of latest Proterozoic age intruded by Cambrian and Early Ordovician plutons (500-470 Ma), displaying a wide range of chemistries, including metaluminous, calc-alkaline rocks largely dominating over alkaline and peralkaline bodies. These are recognised from Portugal to the Massif Central. A coeval or younger set of mafic bodies (mainly doleritic dikes) cuts across the granitoids and their country rocks. The units of this group represent the farther sections of a continent facing a Cambro-Ordovician Ocean that was involved in an accretionary prism at the onset of the Variscan cycle.

4.3.1 THE LOWER ALLOCHTHON IN NW IBERIA

This group is well represented in the Portuguese complexes of Morais and Bragança, in the Centro-Transmontane sub-Domain, especially in the Macedo de Cavaleiros Unit. In Galicia (NW Spain; Fig. 2) it includes the Espasante Unit, in the eastern border of the Cabo Ortegal Complex, the Agualada, Santiago, Forcarei, and Lalín units in the southern and western rims of the Órdenes Complex, and the elongated Malpica-Tui Unit in western Galicia (Fig. 3).

All these units consist of metasediments alternating with igneous rocks. The metasediments include phyllites, schists, metagreywackes and paragneisses, normally with high plagioclase content. Schists with albite-oligoclase porphyroblasts of albite and oligoclase are rather common. Quartzites, carbonaceous schists, cherts, and calc-silicate rocks occur occasionally. Detrital zircon age populations suggest a late Ediacaran age for the lower sequence, as well as a relationship with a Neoproterozoic Avalonian-Cadomian arc (Díez Fernández *et al.* 2010; ; Fuenlabrada *et al.* 2012).

The igneous rocks of the Centro-Transmontane sub-Domain form a bimodal suite of rhyolitic tuffs, intrusive porphyries, metadiabases and greenschists derived from basic rocks (Ribeiro 1974; Ribeiro, 1991). In Galicia, granitic orthogneisses alternate with amphibolites forming rather continuous bodies, flattened, stretched, and subsequently folded during the Variscan deformation (Díez Fernández & Martínez Catalán 2009; Díez Fernández *et al.*, 2011). The granitoids have meta- to peraluminous character, and calc-alkaline, alkaline and peralkaline compositions. The amphibolites have tholeiitic compositions, although some of them might correspond to alkali basalts (Marquínez García 1984). The alkaline and peralkaline orthogneisses are A-type granitoids derived from the mantle and probably linked genetically to alkali basalts (Floor 1966; Ribeiro & Floor 1978; Pin *et al.* 1992; Montero 1993).

Granitic and peralkaline orthogneisses have yielded U-Pb ages of 495-470 Ma (Santos Zalduegui *et al.* 1995; Rodríguez *et al.* 2007; Montero *et al.* 2009; Abati *et al.* 2010; Díez Fernández *et al.* 2012c). The granitic orthogneisses are the older, because they were intruded by basic dikes which are absent in the peralkaline orthogneisses. The bimodal, partially alkaline

Correlation of the nappe stack across the Bay of Biscay

Fig. 2. Geological maps of NW Iberia and the Southern Armorican Massif showing the distribution of the autochthonous, parautochthonous and allochthonous domains and the correlation established for the units of the latter. Large strike-slip shear zones disrupting the different domains are shown. For location, see Fig. 1.

magmatism reflects a late Cambrian-Early Ordovician episode of rifting (Ribeiro & Floor 1987; Pin *et al.* 1992). As the Lower Allochthon is not separated from the Parautochthon by ophiolites (Fig. 4), it is assumed to belong to Gondwana, and because the ophiolitic units overlie it, it is viewed as a fragment of the most external edge of the Gondwanan continental margin. Rifting probably preceded the separation of a peri-Gondwanan terrane.

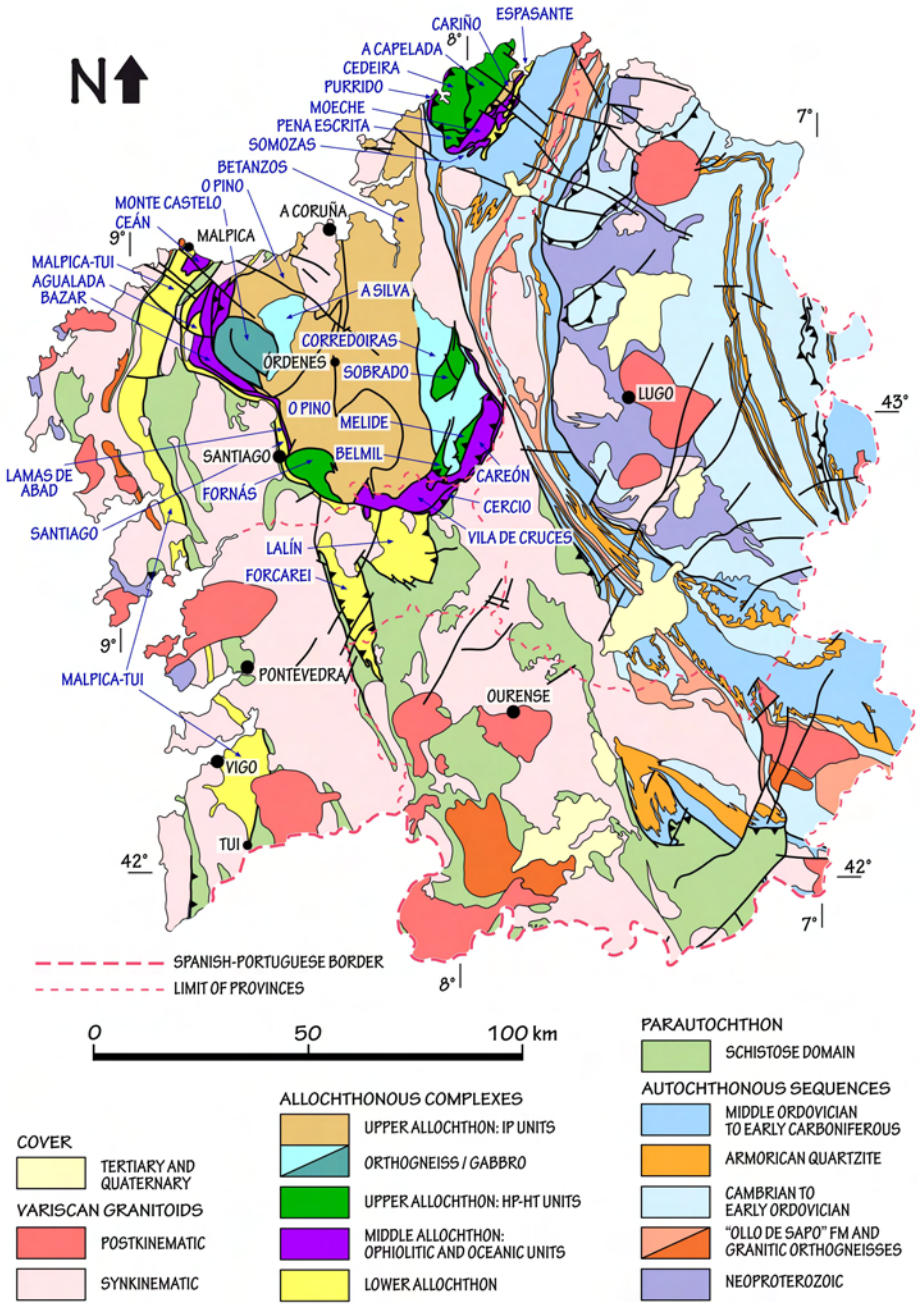

Fig. 3. Geological map of Galicia, NW Spain, with the names and location of the allochthonous units indicated.

The Lower Allochthon is characterised by bearing the imprint of early Variscan high-pressure (HP) metamorphism (Fig. 5), interpreted as a result of continental subduction. The HP event is identified by the presence of eclogites, jadeite-bearing orthogneisses, and blueschists, and has been quantified by thermo-barometry in metabasites and metapelites (Ribeiro 1976;Wegen 1978; Munhá *et al.* 1984; Schermerhorn & Kotsch 1984; Gil Ibarguchi & Ortega Gironés 1985; Gil Ibarguchi 1995; Arenas 1991; Arenas *et al.* 1995, 1997; Rubio Pascual *et al.* 2002; Rodríguez *et al.* 2003; Rodríguez Aller 2005).

The metamorphic conditions for that initial event vary according to the position occupied in the subduction zone. In the Órdenes Complex, estimated pressure peaks are in the range 1-1.65 GPa (Arenas *et al.* 1995; Rubio Pascual *et al.* 2002). The P-T metamorphic gradient varies along the units of Santiago, Lalín and Forcarei (Fig. 5a), forming a continuum folded by a huge recumbent anticline which overprints the HP event. Unfolding the anticline shows that both P and T increased toward the west, and thereby, a west-directed subduction zone (in present-day coordinates) has been deduced (Martínez Catalán *et al.* 1996). For the Malpica-Tui Unit, a minimum pressure of 1.6 GPa was established in a jadeite-bearing metagranitoid (Gil Ibarguchi 1995), and a maximum pressure of 2.6 GPa in eclogite boudins (Rodríguez *et al.* 2003).

According to $^{40}Ar/^{39}Ar$, Rb-Sr, and U-Pb data, continental subduction may have started slightly before 370 Ma ago and ended at ca. 365 Ma (Santos Zalduegui *et al.* 1995; Rodríguez *et al.* 2003; Abati *et al.* 2010). After pressurization, the P-T paths were governed by strong decompression, related to exhumation by thrusting and tectonic denudation. Exhumation was nearly isothermal in some units, but underwent moderate to strong heating in the Lalín Unit, and moderate decreasing temperature over the upper structural sections (Díez Fernández, 2011). These units show an inverted metamorphic gradient, implying that some heat source lay above them. It has been attributed to the mantle wedge above the subduction zone, which would have come into contact with the Lower Allochthon, either by an out-of-sequence thrust fault or an extensional detachment (Arenas *et al.* 1995; Martínez Catalán *et al.* 1996).

4.3.2 THE LOWER ALLOCHTHON IN NW FRANCE

This group is well represented in the Armorican Massif, especially in its southwestern part, including the basal units of the Champtoceaux Complex (Marchand 1981) and the Essarts Complex (Godard 2001).

In the Champtoceaux Complex, it includes a thick sequence of albite-bearing micaschists (the Mauves Unit), thought to derive from late Neoproterozoic immature sediments (greywackes). Although these were ascribed to the Parautochton (e.g. Ballèvre *et al.* 2009; Pitra *et al.* 2010), we now attribute the Mauves Unit to the Lower Allochton because of its similarity with the Spanish outcrops. Overlying these micaschists there are fine-grained

leucocratic gneisses containing eclogite lenses, followed by garnet micaschists, sometimes bearing graphite (Cellier Unit). Finally, another sequence of leucocratic orthogneisses and plagioclase-bearing miscaschists occurs (Saint-Mars-du-Désert Unit).

Petrological and geochemical data allow the distinction of two main lineages amongst the orthogneisses, namely garnet-epidote-muscovite orthogneisses of calc-alkaline composition, and biotite-amphibole orthogneisses of alkaline chemistry. U-Pb data on these two types of orthogenisses has provided Early Ordovician ages for their protoliths, namely 485±11 Ma for the calc-alkaline Saint-Mars orthogneiss (Paquette *et al.* 1984) and 481+6/-5 Ma for an alkaline body within the Cellier Unit (Ballèvre *et al.* 2002). Most orthogneisses show well-developed layering, at a scale from decimetre to metre, which would favour their origin as tuffs or ignimbrites, or their epiclastic equivalents. However, some orthogneisses display relics of igneous textures indicating derivation from a medium- to coarse-grained granitoid (Lasnier *et al.* 1973), consistent with the occurrence of a few pre-orogenic hornfelses.

Metre-sized eclogite lenses are dispersed within the orthogneisses from the Cellier Unit. These are very-fine to fine-grained rocks essentially consisting of garnet, omphacite and rutile. The eclogites display relics of doleritic textures (Godard 1988) and have a rather homogeneous bulk-rock chemistry of tholeiitic basalts. Their REE patterns are similar to E-MORB (Paquette 1987). They are therefore interpreted as former doleritic dikes intruding the Early Ordovician granitoids and the associated felsic volcanics.

The early Variscan, HP metamorphism is recorded in many different lithologies from the Cellier Unit (Figs. 5b and 6). Indeed, not only mafic bodies are transformed into eclogites (Lacroix 1891; Godard 1988), but HP parageneses are also recorded in some orthogneisses as garnet coronas around magmatic biotite (Lasnier *et al.* 1973), in felsic gneisses displaying garnet-jadeite-quartz or garnet-omphacite-kyanite-quartz assemblages, and in the overlying metapelites (Ballèvre *et al.* 1987, 1989). An interesting point is the observed change in mineral parageneses along strike within the Cellier Unit, documenting lower grade conditions in the east (garnet-omphacite with late glaucophane porphyroblasts in the metabasites (Godard *et al.* 1981), garnet-chloritoid-chlorite in the metapelites) compared to higher grade conditions in the west (garnet-omphacite-kyanite in the metabasites, garnet-kyanite with prograde chloritoid-staurolite inclusions in the metapelites) (Ballèvre & Marchand 1991; Bosse *et al.* 2000). This is interpreted as a gradient in peak P-T conditions during the eclogite-facies event (from about 1.5-2.0 to about 2.5 GPa). Taking into account the late folding of the nappe stack, this indicates a continental subduction dipping to the north or nothwest (in present-day geographic coordinates).

The HP event is dated at around 360 Ma using an array of isotopic methods in a glaucophane-bearing eclogite, including U-Pb data on zircon (356±8 Ma), a Sm-Nd isochron on

garnet-omphacite-whole-rock (362±25 Ma) (Paquette 1987; Bosse *et al.* 2000). $^{40}Ar/^{39}Ar$ data on phengite in the same eclogite have given ages of about 350 Ma, whereas the same method applied on deformed samples from the surrounding micaschsits and gneisses have given slightly younger ages, ranging from 350 to 340 Ma (Bosse *et al.* 2000; Maurel *et al.* 2003).

Following the HP event, decompression took place at nearly isothermal or even decreasing temperature (Figs. 5b and 6) (Godard *et al.* 1981, Ballèvre *et al.* 1989). This stage is associated to the main stacking of the different units, contemporaneous with an inverted metamorphism (Pitra *et al.* 2010). Because both Rb-Sr and $^{40}Ar/^{39}Ar$ data give similar ages in samples on both sides of the main thrust, cooling is considered as a relatively efficient and fast process taking place at about 340-330 Ma (Pitra *et al.* 2010). After the nappe stack was built (the exposed outcrops along the Loire River reveal a crustal section that was at about 0.8 GPa, i.e. 25 km depth at the time of thrusting), it has been reworked during later events. These include (i) a ductile normal fault zone at the boundary with the overlying Mauges Unit, possibly during deposition of the Ancenis Formation, and (ii) transcurrent shearing along its northern boundary, associated to development of small pull-apart basins and contemporaneous large-scale folding during dextral movement along the South-Armorican Shear Zone (Fig. 6).

Further south, in the Essarts Complex (Vendée), a discontinuous belt of intensely deformed orthogneisses runs southwest of the Essarts Unit, from Sainte-Pazanne in the north to Mervent in the south, i.e. along a total length of about 200 km (Godard 2001). This Sainte-Pazanne-Mervent Unit is considered as a representative of the Lower Allochthon (Ballèvre *et al.* 2009). Despite rather poor outcrops, the mineralogy and chemistry of this orthogneiss display typical calc-alkaline characteristics. Its age has been established using the U-Pb method on zircon, in two different localities (495+37/-14 Ma: unpublished data from C. Guerrot quoted in Godard 2001; 486+15/-11: Diot *et al.* 2007).

4.4 MIDDLE ALLOCHTHON

This ensemble consists of dismembered slices of oceanic derivation that locally display a blueschist-to eclogite-facies overprint during the Variscan orogeny. These include a diverse array of well-characterised oceanic complexes, with ages clustering around the Cambro-Ordovician boundary and in the Devonian. Some are true ophiolitic units, while others are better interpreted as accretionnary prisms derived from an Early Ordovician ocean, or an ocean-continent transitional domain related either to the Lower or the Upper Allochthon.

4.4.1 THE MIDDLE ALLOCHTHON IN NW IBERIA

The old units with more clear oceanic affinity are represented in Galicia by the Vila de Cruces and Bazar units, in the SE and west of the Órdenes Complex respectively, and by the Moeche Unit in Cabo Ortegal (Fig. 3). In Northern Portugal, these units are represented by the Izeda-Remondes Unit of the Morais Complex. A group of units of similar age, formed by Ceán, Cercio and Lamas de Abad, have been interpreted either as forming part of the Lower Allochthon (Díez Fernández *et al.* 2010; Gómez Barreiro *et al.* 2010) or as oceanic units (Rodríguez Aller 2005). They are not ophiolitic in a strict sense, as they are essentially metasedimentary, but due to their transitional character and the fact that comparable units in France are considered oceanic, they will be included in the Middle Allochthon. Finally, an early Variscan ophiolitic mélange, the Somozas Unit, which includes Cambro-Ordovician protoliths, is exposed to the east of the Cabo Ortegal Complex (Arenas *et al.* 2009).

The younger ophiolites are represented by the Careón Unit in the SE of the Órdenes Complex, the Purrido and Moeche units in the western and eastern parts of the Cabo Ortegal Complex, respectively, and the Morais-Talhinhas Unit in the Morais Complex. When units of both groups occur together, the older units occupy a lower structural position which, according to the mode of imbrication during accretion, would imply proximity to the margin of Gondwana in relation to the younger and structurally upper units (Martínez Catalán *et al.* 1996; Pin *et al.* 2006).

4.4.1.1 CAMBRO-ORDOVICIAN OPHIOLITES

The Vila de Cruces Unit consists of a tectonically repeated succession of metabasites and metapelitic phyllites and schists, with scarce and thin layers of granitic orthogneisses, serpentinites and metacherts. The dominant lithologies are greenschist-facies metabasites exhibiting an intense deformation, though the occasional preservation of igneous textures suggests a metabasaltic origin with minor presence of coarse- to medium-grained gabbros. Metapelites dominate in the upper part, and greenschists in the middle and lower parts (Fig. 4). The main body of orthogneiss intruded in the mafic sequence has yielded a U-Pb age of 497±4 Ma (Arenas *et al.* 2007a, b). It can be considered as a reference for the Formation of the Unit, although zircon ages around 1.2 Ga in metagabbros of the same Unit point to inheritances or even to an origin as a composite terrane. The Moeche Unit, to the east of the Cabo Ortegal Complex, shows the same dominant lithologies as the Vila de Cruces Unit.

Most of the basic rocks plot in the fields of the island-arc tholeiites, supra-subduction zone basalts, or destructive plate-margin basalts (Arenas *et al.* 2007b). The granitic orthogneisses plot into the field of volcanic arc granitoids and are also related to a destructive plate margin. Abundances of the most immobile trace elements in metagabbros mimic those of the greenschists, suggesting a similar tectonic setting. Both show a marked negative Nb

anomaly, characteristic of magmas generated in a subduction zone (Pearce & Peate 1995; Pearce 1996). For the orthogneisses, the immobile trace elements are typical of granitoids generated in volcanic arcs or supra-subduction zones (Pearce *et al.* 1984).

The Vila de Cruces Unit developed during back-arc spreading above a Cambro-Ordovician subduction zone in the northern margin of Gondwana. It shares some characteristics with the Ceán and Cercio units, such as part of the lithological association and HP metamorphism (Arenas *et al.* 2007b), and overlies the Cercio Unit, suggesting that both where close and adjacent to each other. Vila de Cruces probably represents a transitional Unit between the outermost attenuated continental margin and truly oceanic crust, and remained attached to the margin of Gondwana during spreading of the back-arc that created a peri-Gondwanan ocean, possibly the Rheic Ocean. No ages are available for the HP metamorphic event, which probably was Late Devonian, coeval with that on the Lower Allochthon. Subsequent greenschists facies conditions have been dated at 366.8±0.4 Ma in Vila de Cruces (Dallmeyer *et al.* 1997) and 370.2±0.6 Ma in comparable rocks in the Morais Complex (Dallmeyer *et al.* 1991).

The Bazar Unit is located in the west of the Órdenes Complex (Figs. 3 and 4). Though its internal structure is poorly known, its thickness, up to 5000 m, and the presence of several thrust faults suggest that it is an imbricate. It is made up of monotonous metagabbroic amphibolite, with a relatively undeformed layer of gabbro, leucogabbro, pegmatoid gabbro, pyroxenite, and ultramafic rocks located toward the bottom of the Unit (Díaz García 1990; Abati 2002). The Unit was affected by an early high temperature (HT) metamorphism, which formed mafic granulites transitional between the low- and medium-pressure types. U-Pb zircon ages yield two populations with mean values of 495±2 Ma and 475±2 Ma, interpreted as the ages of the gabbroic protolith and of the granulitic metamorphism respectively (Sánchez Martínez 2009). The origin and meaning of this HT metamorphic event are not clear, but it can be tentatively interpreted as related to subduction of very young oceanic lithosphere, culminating with subduction of a mid-ocean ridge (Arenas *et al.* 2007a; Sánchez Martínez 2009; Sánchez Martínez *et al.*, 2012).

A fragment of oceanic lithosphere formed at a mid-ocean ridge might have been preserved in Portugal, where a remnant of oceanic lithosphere has been reported in the Morais Complex (Pin *et al.* 2006). According to these authors, the Izeda-Remondes Unit shows elemental and Nd isotope similarities with oceanic basalts formed in normal mid-ocean ridge settings, without any recognizable interaction with components derived from the continental crust. An imprecise 447±24 Ma Sm-Nd whole rock isochron age is tentatively interpreted by these authors to date their generation in a mature oceanic basin, apparently free from the influence of a subduction zone.

NW
SE
W
E
NW
SE
MALPICA-TUI COMPLEX
ÓRDENES COMPLEX
CABO ORTEGAL COMPLEX
CEÁN UNIT
LAMAS DE ABAD UNIT
AGUALADA UNIT
BAZAR UNIT
O PINO UNIT
MONTE CASTELO UNIT
A SILVA UNIT
BETANZOS UNIT
PONTE CARREIRA DETACHMENT
CORREDOIRAS UNIT
PURRIDO UNIT
CEDEIRA UNIT
A CAPELADA UNIT
CARIÑO UNIT
ESPASANTE UNIT
PARAUTOCHTHON
SOMOZAS UNIT
BELMIL UNIT
MELIDE UNIT
SANTIAGO UNIT
NEGREIRA GRANODIORITE
MALPICA-TUI UNIT
PICO SACRO DETACHMENT
SANTIAGO UNIT
FORNÁS UNIT
CAMPO MARZO SLICE
FORCAREI UNIT
LALÍN UNIT
PARAUTOCHTHON
CAREÓN UNIT
PICO SACRO DETACHMENT
CERCIO UNIT
OUT-OF-SEQUENCE THRUSTS
"OLLO DE SAPO" ANTICLINORIUM
LALÍN-FORCAREI THRUST
CARRIO ANTICLINE
VILA DE CRUCES UNIT
0
10
20
30
40 km
UPPER ALLOCHTHON
IP AND LOW-GRADE UNITS
LOW-GRADE SLATES AND GREYWACKES
MEDIUM-GRADE SCHISTS AND PARAGNEISSES
ORTHOGNEISSES
METAGABBROS AND AMPHIBOLITES
HP-HT AND HP UNITS
PARAGNEISSES
ECLOGITES, GRANULITES AND AMPHIBOLITES
ULTRAMAFIC ROCKS
MIDDLE ALLOCHTHON
SCHISTS, CARBONACEOUS SCHISTS AND AMPHIBOLITES
AMPHIBOLITES
FLASERGABBROS AND AMPHIBOLITES
ULTRAMAFIC ROCKS
LOW-GRADE METAPELITES
LOW-GRADE METABASITES

NNE
SSW
NE
SW
NORMAL OR STRIKE-SLIP
EXTENSIONAL DETACHMENT
THRUST FAULT
MAUGES UNIT
PALAEOZOIC COVER
PROTEROZOIC BASEMENT
LANVAUX UNIT
ST GEORGES-SUR-LOIRE UNIT
ANCENIS BASIN
DRAIN UNIT
MORTAGNE LEUCOGRANITE
ST MARTIN-DES-NOYERS UNIT
ESSARTS UNIT
STE PAZANNE-MERVENT UNIT
BOIS-DE-CENÉ UNIT
ST GILLES UNIT
SAUZAIE UNIT
MESOZOIC OF THE AQUITAINE BASIN
CHAMPTOCEAUX
BRÉTIGNOLLES THRUST
SABLES D'OLONNE AND ILE D'YEU ORTHOGNEISSES
10 km
20 km
NORT-SUR-ERDRE FAULT
MAUVES UNIT
CELLIER UNIT
ST MARS UNIT
LES FOLIES-SIFFAIT UNIT
SOUTH-ARMORICAN SHEAR ZONE
ESSARTS COMPLEX
CHAMPTOCEAUX COMPLEX
0
10
20
30
40 km
LOWER ALLOCHTHON
SCHISTS AND PARAGNEISSES
ORTHOGNEISSES
AMPHIBOLITES
PARAUTOCHTHON
ORDOVICIAN-EARLY DEVONIAN: SCHISTS, METASANDSTONES AND VOLCANICS
AUTOCHTHON
SILURIAN: GREY AND CARBONACEOUS SLATES
MIDDLE AND LATE ORDOVICIAN: GREY SLATES AND QUARTZITES
EARLY ORDOVICIAN: ARMORICAN QUARTZITE
MIDDLE CAMBRIAN-EARLY ORDOVICIAN: SLATES AND QUARTZITES
EARLY ORDOVICIAN: "OLLO DE SAPO" FORMATION AND GRANITIC ORTHOGNEISSES
VARISCAN GRANITOIDS
TWO-MICA SYNKINEMATIC GRANITES
SYNKINEMATIC GRANODIORITES

Fig 4. Representative geological sections of the Galician and Armorican allochthons. a) Composite section across the complexes of Malpica-Tui, Órdenes and Cabo Ortegal. b) Schematic section of the allochthonous complexes in the SW part of the Armorican massif. The Nort-sur-Erdre Fault marks the northern boundary of the nappe stack. To the south of this fault, the nappe stack is sheared along the branches of the South-Armorican Shear Zones, delineating two main stacks (Champtoceaux Complex, Essarts Complex). Location of sections shown in Fig. 2.

The units of Ceán, in the northern part of the Malpica-Tui Complex, and Lamas de Abad and Cercio, in the west and southeast of the Órdenes Complex (Figs. 3 and 4), probably represent the cover of a transitional to oceanic crust. They consist of a mainly pelitic sequence which intercalates mafic igneous rocks which, in Ceán, have N-MORB affinity (Rodríguez Aller 2005). The Ceán Unit has a late Cambrian maximum depositional age, according to its youngest zircon age population, and represents a distal palaeoenvironment in a back-arc basin behind a Cambro-Ordovician volcanic arc (Díez Fernández *et al.* 2010; 2013). The Pombais Unit, in the eastern part of the Morais Complex occurs in the same structural position and consists of up to four slices of mafic metavolcanics with a typical MORB signature (Oliveira *et al.* 2003, Pereira *et al.* 2003).

The HP event has been identified in the Ceán Unit by the presence of blueschists, and has been quantified by conventional thermo-barometry in metapelites (Fig. 5a). Pressures of 1.4-1.8 GPa for temperatures below 550°C were estimated for blueschist facies metamorphism by Rodríguez *et al.* (2003) and Rodríguez Aller (2005), whereas López-Carmona *et al.* (2010; 2013) have confirmed slightly higher pressures of 1.9-2.1 GPa and lower temperatures of 420-460 °C using pseudosection approach.

The Ceán, Lamas de Abad and Cercio units are sandwiched between the Lower Allochthon and the Cambro-Ordovician ophiolitic units of the Middle Allochthon. The contacts are always of tectonic origin, mostly extensional detachments which either reactivate or overprint earlier thrust faults (Gómez Barreiro *et al.* 2010). The lithologic association of these units and the metamorphic evolution established for Ceán make them akin to the Ile-de-Groix Unit, to the south of the Armorican Massif. As for the Lower Allochthon, the P-T paths underwent strong decompression during thrusting, and underwent moderate heating in the Lamas de Abad Unit (Arenas *et al.* 1995).

The Somozas Unit is a tectonic mélange cropping out at the base of the Cabo Ortegal Complex (Figs. 3 and 4). It includes two different series of igneous rocks, namely a group of basic to acid rocks of calc-alkaline affinity, and a group of metabasites with chemical compositions of island arc tholeiites (Arenas *et al.* 2009). According to these authors, the protoliths were probably generated in a mature volcanic arc located along the periphery of Gondwana between ca. 527 and 485 Ma. The mélange developed during the Upper Devonian in a Variscan subduction zone in northern Gondwana beneath an ensemble of exhumed HP units.

4.4.1.2 EARLY DEVONIAN OPHIOLITES

The Careón Unit is an incomplete but well exposed ophiolitic sequence occurring to the SE of the Órdenes Complex (Figs. 3 and 4). It consists of three tectonic imbricates (Díaz García *et al.* 1999), the best preserved of which consists of 600 m of metagabbros overlying 500 m of ultramafics of harzburgitic composition. The transition between imbricates is abrupt, without significant deformation, and intruded by numerous gabbroic and diabase dikes, and is considered the petrological paleo-Moho. The gabbroic section is formed by a complex network of multiple intrusions of gabbroic rocks, wehrlite and wehrlite-gabbro transitional terms, and diabasic to pegmatoid dikes.

The metabasites have compositions equivalent to tholeiitic basalts and, according to their immobile trace elements, show transitional characteristics between N-MORB and island-arc tholeiites (Sánchez Martínez *et al.* 2007). Their immobile trace element patterns normalised to the average composition of N-MORB vary from flat and close to one to slightly fractionated or more depleted patterns. A negative Nb anomaly indicates an origin in a supra-subduction zone setting (Pearce 1996). A plagioclase-rich gabbro was dated by U-Pb geochronology at 395±2 Ma, considered the crystallisation age of the gabbro and evidence for oceanic crust generation by Early Devonian time (Díaz García *et al.* 1999). A similar age of 395±3 Ma was obtained in the Careón Unit by Pin *et al.* (2002), with εNd values for that age implying that these rocks were derived from a depleted mantle reservoir at the time of their Formation, and are therefore juvenile.

Thermobarometric estimations on a metamorphic sole yielded 650°C and 1.15 GPa, pointing to a subductive environment for ophiolite imbrication (Díaz García *et al.* 1999). A well-foliated amphibolite was dated at 376.8±0.4 Ma (Dallmeyer *et al.* 1997), interpreted as a cooling age following the metamorphic thermal peak. This is slightly younger than the 390-380 Ma age reported for amphibolite facies metamorphism in ophiolitic units from Cabo Ortegal and the Portuguese complexes (Peucat *et al.* 1990; Dallmeyer *et al.* 1991).

The Purrido Unit is exposed in cliffs along the west part of the Cabo Ortegal Complex, where it consists of 300 m of lithologically homogeneous, medium-grained and well-foliated massive nematoblastic amphibolites, occasionally with garnet-bearing types (Vogel, 1967). Geochemically, they can be classified as island-arc tholeiites, which suggests generation in a supra-subduction zone setting (Sánchez Martínez 2009). U-Pb zircon ages show a dominant Mesoproterozoic population with an age of 1155±14 Ma and younger ages of 395±3 interpreted as those of crystallisation (Sánchez Martínez *et al.* 2006, 2011). Hf isotope data show that most Devonian zircons crystallised from a juvenile depleted mantle source, although some Devonian crystals show evidence of mixing with the Mesoproterozoic zircons. Whole rock Sm-Nd isotope data indicate also heterogeneity in composition only compatible

with the generation from two different sources. The Devonian mantle-derived magmatic source shows interaction with some Mesoproterozoic basement, either generated at a continent-ocean transition, or being the plutonic section of an arc-related ophiolite. Amphiboles of the prograde nematoblastic fabric were dated at 391±6.6 Ma (Peucat *et al.* 1990; $^{40}Ar/^{39}Ar$ in a hornblende).

The Moeche Unit, in the eastern part of the Cabo Ortegal Complex, shows the same dominant lithologies as the Vila de Cruces Unit, namely a sequence of greenschists with some alternations of phyllites and inclusions of metagabbros and serpentinites. However, U-Pb, LA-ICP-MS ages of zircons from a sample of mafic greenschist have yielded a maximum age of 400±3 Ma (Arenas *et al.* 2013). Together with the 364 Ma $^{40}Ar/^{39}Ar$ age of its mylonitic fabric (Dallmeyer *et al.* 1997), the zircon ages suggest that Moeche belongs to the group of Early Devonian units of oceanic affinity. The pervasively mylonitised character of Moeche and Vila de Cruces units masks their primary features, making them look similar to each other and suggesting a correlation that is not supported by age data.

The Morais-Talhinhas Unit occurs in the northern half of the Morais Complex. It consists largely of metaperidotites together with gabbroic rocks and minor felsic veins, whose U-Pb zircon ages range from 405±1 Ma to 396±1 Ma (Pin *et al.* 2006). According to these authors, rocks from this Unit have high Th/Nb ratios and elevated εNd values, reflecting generation above an intraoceanic subduction zone. The tectonometamorphic overprinting of the ophiolitic units, including imbrication with high- and medium-grade nappe units was completed prior to ca. 385 Ma (Dallmeyer *et al.* 1991).

4.4.2 THE MIDDLE ALLOCHTHON IN NW FRANCE

Units of undisputable oceanic affinity are represented in Brittany and Vendée by the Audierne and Drain units, respectively. By contrast with their Spanish counterparts, the French ophiolitic complexes are very poorly exposed and are therefore much less known.

4.4.2.1 CAMBRO-ORDOVICIAN OPHIOLITES

The Audierne Unit displays serpentinised peridotites (Ty Lan Formation) with rare chromite pods up to 0.4 m thick (Bouladon & Chauris 1965), metagabbros (Peumerit Formation), and greenschists (Tréogat Formation) that most probably derive from basaltic lava flows and tuffs (Peucat 1973; Peucat & Cogné 1974; Hanmer 1977). According to their geochemistry, the metagabbros and the greenschists belong to a tholeiitic suite, and have compositions similar to those of MORB (Bernard-Griffiths and Cornichet 1985; Lucks *et al.* 2002). The Audierne Unit is cut by the South-Armorican Shear Zone, but has a distinct magnetic signature that can be followed offshore for about 50 km in a NE-SW direction (de Poulpiquet 1988). The age of the ophiolite complex is now considered to be Early Ordovician, because a plagiogranite from the Peumerit Formation has been dated at 482±3 Ma (Paquette *et al.* in prep.).

The metamorphic history of the Audierne Unit is characterized by an intense deformation under amphibolite-facies conditions, estimated at about 0.6 GPa at 600°C (Lucks *et al.* 2002). Altough HP parageneses have been found in some metabasites from this area (e.g. garnet-diopside and garnet-plagioclase-omphacite mafic granulites, garnet-kyanite felsic granulites) (Velde 1972; Lucks *et al.* 2002), these rocks do not belong to the ophiolitic complex, but represent thin slices located along the tectonic boundary above the ophiolitic complex. They are therefore interpreted as belonging to a strongly dismembered HP Unit attributed to the Upper Allochthon.

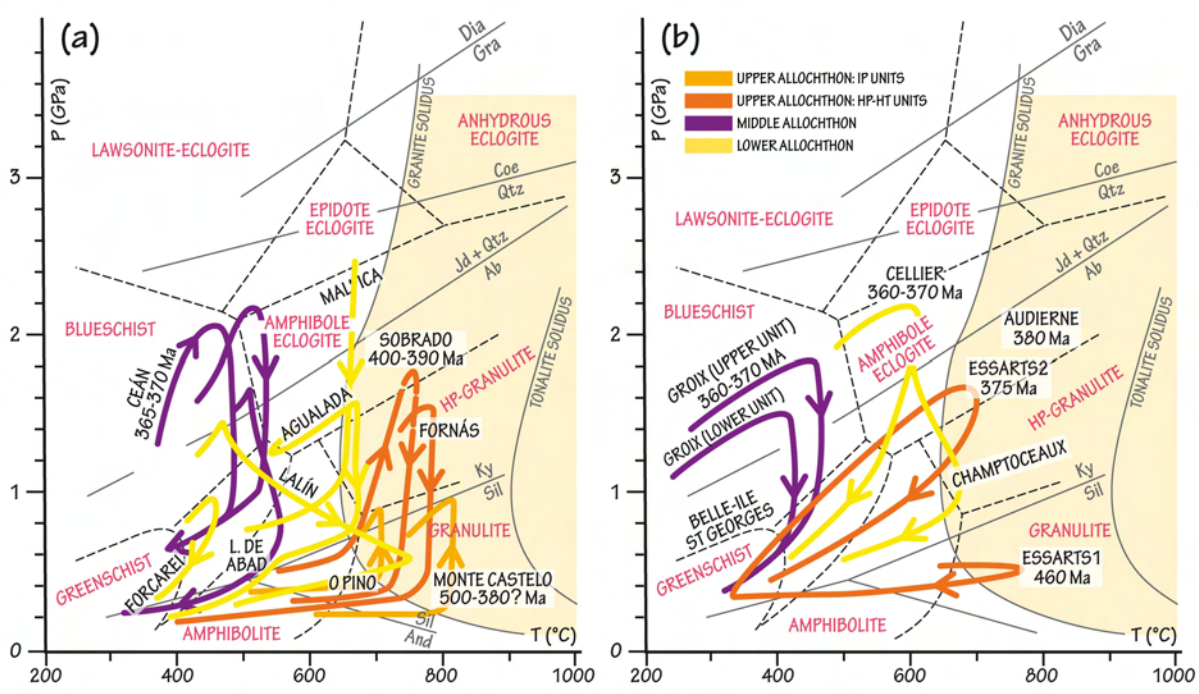

Fig. 5. A summary of the P-T paths from the allochthonous units. a) Galicia, NW Spain. The Lower Allochthon generally records monocyclic P-T paths with pressurization followed by nearly isothermal decompression, but the Santiago and Lalín unit registered heating from an overlying hot source, probably the mantle wedge above the subduction zone. Some units of the Middle Allochthon (Ceán, Lamas de Abad, Vila de Cruces) record HP metamorphism too. The Upper Allocthon records pressurization after strong heating in the IP units (Monte Castelo, O Pino), and strong pressurization following a subductive-type path, followed by nearly isothermal decompression, in the HP/HT units (Sobrado, Fornás). b) Armorican Massif. The Lower Allochthon (Cellier, Champtoceaux) and the Middle Allochthon (Groix) record monocyclic P-T paths, while the Upper Allochthon (Essarts) records a polyclyclic P-T path. Note that the ages for the HP event cluster at around 375-360 Ma (i.e. Late Devonian). Early partial melting (at about 350 Ma) following the HP event is only found in the Champtoceaux Unit, but is more commonly observed in the Autochthon (at around 320-300 Ma).

Other rocks of oceanic affinity include the blueschist-facies metabasites and micaschists from the Ile-de-Groix (Barrois 1883) and Bois-de-Cené units. These occupy similar structural positions, being considered as a klippe on top of the Parautochton (Ile-de-Groix) or coring a synformal fold (Bois-de-Cené). The lithologies are essentially made of metapelites and metabasites, the latter deriving from basaltic lava flows or sills, eventually reworked by submarine turbidity currents and mixed with a terrigeneous detrital component (Bernard-Griffiths *et al.* 1986; El Korh *et al.* 2009, 2012). Geochemical data on the mafic rocks have

revealed an extensive alteration of the basaltic protoliths during oceanic hydrothermalism, the basalts having affinities with E-MORB. The oceanic character of the sequence is also testified by the occurrence of a few serpentinites associated to chlorite schists, the latter being interpreted as sheared and metasomatised gabbroic rocks. In addition, oceanic sediments include (i) cherts interlayered within the micaschists or capping some lava flows, (ii) manganiferous nodules (up to 1 m in diameter) dispersed in some micaschists (Kiénast & Triboulet 1973; Cornen 1999), and (iii) a unique ferriferous layer (Dudek & Kiénast 1989).

The age of this sequence is constrained by rare layers of fine-grained, felsic gneisses most probably derived from tuffs or dikes, which have provided U-Pb ages on zircon of 481±5 Ma (El Korh *et al.* 2012). Zircons extracted from the chlorite schists in both the Ile-de-Groix and Bois-de-Cené units have recently provided La-ICP-MS ages of about 490 Ma (Paquette *et al.* in prep.), interpreted as the age of crystallisation of their gabbroic ancestors.

The metamorphic history of the Ile-de-Groix and Bois-de-Cené units is dominated by an extensive blueschist-facies overprint, with garnet-chloritoid-chlorite to chloritoid-chlorite assemblages in the metapelites, and garnet-glaucophane-epidote (+/- lawsonite or omphacite) in the metabasites (Kiénast & Triboulet 1972, Triboulet 1974, Dudek & Kiénast 1989, Bosse *et al.* 2002, Ballèvre *et al.* 2003, El Korh *et al.* 2009). The metamorphic zonation of the Ile-de-Groix Unit (Triboulet 1974) has been re-interpreted as due to the abnormal superposition of two units that slightly differ in their P-T paths (Fig. 5b), although they share similar lithologies (Bosse *et al.* 2002, Ballèvre *et al.* 2003). Alternative models, such as those explaining the zonation by the superimposition of a pervasive fluid flow at the scale of the island (Barrientos & Selverstone 1993) and/or of several deformation episodes (Philippon *et al.* 2009) are considered less likely (for a discussion, see El Korh *et al.* 2013).

The Rb-Sr and $^{40}Ar/^{39}Ar$ data indicate that the HP event took place 360-370 Ma ago, while cooling was achieved in rocks overprinted by the greenschist-facies metamorphism at about 350-340 Ma (Bosse *et al.* 2005). U-Pb data on titanite extracted from a felsic gneiss (366±33 Ma), although imprecise due to a large amount of common Pb, have recently confirmed the Late Devonian (Famennian) age of the HP event (El Korh *et al.* 2012).

The poorly-known les Folies-Siffait Unit (less than 500 m thick but at least 30 km long), in the Champtoceaux Complex, is made of intensely deformed amphibolites and metaperidotites (Pitra *et al.* 2010), which are thought to derive from an ophiolitic complex. Its age is, however, unkown. Eclogite-facies relics have not been observed in this Unit, characterized by an amphibolite-facies foliation developed in both the mafic and the ultramafic rocks.

The Saint-Martin-des-Noyers Unit in Vendée constitutes a narrow belt (from a few hundred metres to 3 km in thickness) extending about 200 km long from Sainte-Pazanne in the northwest to Mervent in the southeast (Godard 2001). This Unit is essentially made of amphibolites, ranging from massive, homogeneous dark rocks of basaltic composition to leucocratic banded gneisses of rhyodacitic composition. Geochemical data indicate that this suite belongs to a tholeiitic trend, and has been interpreted as a volcanic or hypovolcanic

sequence that might have been erupted in an island-arc or fore-arc setting (Thiéblemont *et al.* 1987a). Taking into account that the latter point needs to be re-evaluated using modern techniques, it has been proposed that the Saint-Martin-des-Noyers Unit could belong to the Middle Allochthon (Ballèvre *et al.* 2009). The metamorphism of the Saint-Martin-des-Noyers Unit is characterized by the lack of eclogite-facies relics (as distinct from the overlying Essarts Unit), and by peak P-T conditions at about 0.7 GPa at 470 to 550°C (Thiéblemont *et al.* 1988). Both the age of the protoliths and their metamorphism has not been investigated, and they are here tentatively considered as Early Ordovician in age.

One major uncertainty in the structure of the South-Armorican domain is the root zone of the Ile-de-Groix and Bois-de-Cené units. For geometrical reasons, they may be rooted along the contact at the base of les Folies-Siffait or Saint-Martin-des-Noyers units. According to an alternative hypothesis, the Ile-de-Groix and Bois-de-Cené units would represent accretionnary prims developed at an early stage of the subduction.

4.4.2.2 LATE DEVONIAN OPHIOLITES

The Drain Unit, on top of the Champtoceaux complex, is essentially made of serpentinised peridotites (with some chromite) and metagabbros. Some of the latter still diplay well-preserved magmatic textures and mineralogy (olivine-plagioclase-clinopyroxene), including relics of early, layered gabbro-norites and norites cut across by dikes of isotropic microgabbros displaying chilled margins (Lasnier 1974). Spinel coronas around olivine are found in some gabbros (Lasnier 1974), while garnet coronas developed in the most Fe-rich lithologies, recording isothermal cooling (Carlier 1978). However, most metagabbros have been severely deformed during an amphibolite-facies event, producing a foliation that is parallel to the main regional structures of the underlying Champtoceaux Complex.

The internal structure of the Drain Unit is poorly known, but peridotites (up to 500 m thick) appear to be confined to its SW part, while gabbros (from 800 m to less than 200 m thick) constitute the main body. It has been proposed that the greenschists and the micaschists from the Hâvre Unit, occupying the same structural position than the Drain Unit along the northern flank of the Champtoceaux complex, would represent the upper part of an oceanic crust. According to geochemical data, the metagabbros show compositions akin to cumulates (with positive Eu* anomalies) or to liquids similar to N-type MORB (Bernard-Griffths & Cornichet 1985; Paquette 1987). U-Pb data from the Drain metagabbro indicate an age of 371±3 Ma for the magmatic protolith (Paquette 1987). Further studies on the same sample using the LA-ICP-MS have confirmed this data, providing a new age at 379±2 Ma (Paquette *et al.* in prep.). The Drain metagabbro therefore belongs to a late Devonian ophiolite, and is the youngest protolith involved in the nappe stack of the Champtoceaux Complex (Fig. 6).

Like in Iberia, the ophiolitic complexes in western France present large differences in age, ranging from the Early Ordovician to the Late Devonian. For the moment, it is difficult to ascertain these results derive from a sampling bias (via tectonic processes operating during the Variscan Orogeny) of a single, long-lived ocean, or whether the two age groups reveal the existence of two different kinds (and age) of oceanic domains.

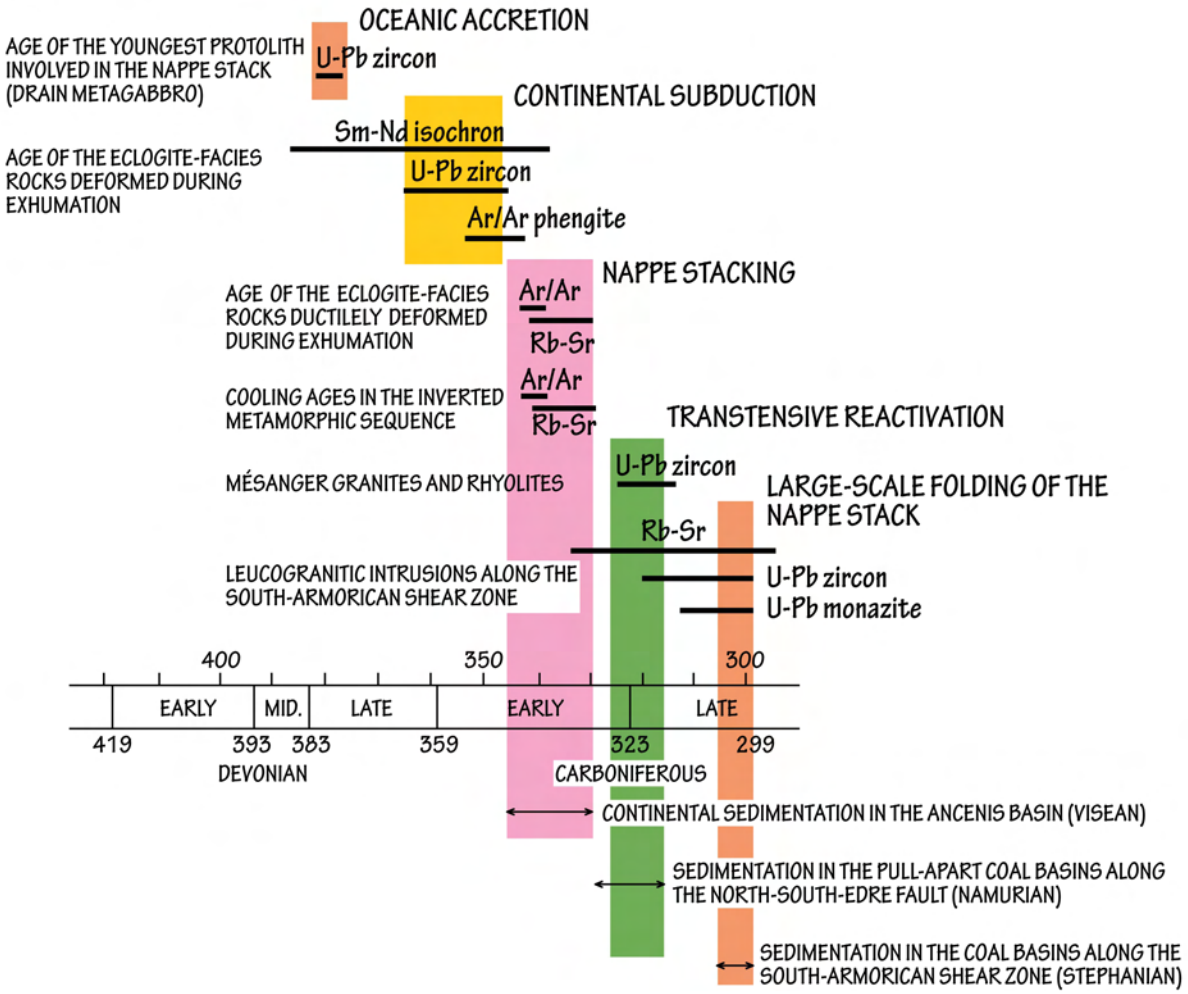

Fig. 6. Geochronological constraints on the evolution of the Champtoceaux Complex, from oceanic accretion during the Late Devonian to the late folding of the nappe stack in the latest Carboniferous. The sources of the data are explained in the text, except for the age of the Mésanger granites and rhyolites (Ducassou *et al.* 2011b) and the leucogranites along the South-Armorican Shear Zone (Tartèse *et al.* 2011a, 2011b).

4.5 UPPER ALLOCHTHON

The Upper Allochthon derives from a late Cambrian, continental (ensialic) arc developed at the northern margin of Gondwana, and comprises two groups of units. Occupying the lower structural position, the first group preserves evidences of a HP and HT, granulite to eclogite-facies, early-Variscan metamorphic event. The upper group displays granulite, amphibolite, or greenschist facies metamorphism, characterized by a gradient of intermediate-pressure type (IP), whose age has been reported in NW Iberia as pre-Variscan.

4.5.1 THE UPPER ALLOCHTHON IN NW IBERIA

The upper assemblage of allochthonous units in NW Iberia has been subdivided in two groups, the HP-HT and IP units, each occupying a distinct position in the nappe pile. The HP-HT group occupies the lower structural position (Fig. 4), and includes the units of Cedeira and A

Capelada in the Cabo Ortegal Complex (Marcos *et al.* 2002), Belmil, Melide, Sobrado, and Fornás in the Órdenes Complex (Van Zuuren 1969; Hubregtse 1973; Martínez Catalán *et al.* 2002; Gómez Barreiro *et al.* 2007), the core of the Bragança Complex, and three small slices in the Morais Complex (Vale da Porca in the NW, Caminho Velho in the west, and Vinhas in the SE; Ribeiro 1974, Ribeiro *et al.* 1990). The overlying group of IP units is represented by the Cariño Unit in the Cabo Ortegal Complex, but it is in Órdenes and Morais where it occupies a large extension at the core of both complexes.

4.5.1.1 HP-HT UNITS

The allochthonous units of this group share similar characteristic in the four complexes where they occur (all but that of Malpica-Tui). They consist of paragneisses and basic and ultrabasic metaigneous rocks. The most characteristic rocks are metabasites, commonly garnet-clinopyroxene granulites and eclogites, retrograded to the amphibolite facies (Vogel 1967; Hubregtse 1973). Gabbros occur in several stages of transformation, from practically undeformed and scarcely affected by the metamorphism, to coronitic metagabbros, HP granulites and amphibolites (Arenas & Martínez Catalán, 2002). In the less deformed gabbros, subophitic and diabase textures have been preserved, indicating an emplacement at relatively shallow crustal levels. The metagabbros are of tholeiitic composition, and their geochemical signature has been compared to MORB (Gil Ibarguchi *et al.* 1990) and related to continental rifting (Galán & Marcos, 1997). However, geochemical studies of the ultramafic rocks of Cabo Ortegal are consistent with the hypothesis that these rocks were generated in an arc environment (Santos *et al.* 2002).

Early Palaeozoic ages (490-480 Ma) were obtained by Peucat *et al.* (1990) in metabasic rocks, and interpreted as dating the HP and HT metamorphism. More recent analyses have yielded 520-480 Ma, viewed as protolith ages (Ordóñez Casado *et al.* 2001), although they might also reflect the imprint of a nearly contemporaneous metamorphic event (Fernández-Suárez *et al.* 2002, 2007). But the main tectonothermal event, the HP granulite and eclogite facies metamorphism, occurred later, and has been dated at 400-390 Ma (Schäfer *et al.* 1993; Santos Zalduegui *et al.* 1996; Ordóñez Casado *et al.* 2001; Fernández-Suárez *et al.* 2007). This HP Early-Middle Devonian metamorphic event, which implied subduction (Gil Ibarguchi *et al.* 1999), was followed by decompression and partial melting (Fig. 5a) and then, successively, by a penetrative mylonitisation in the amphibolite facies, recumbent folding, and thrusting in the greenschist facies (Vogel 1967; Marcos *et al.* 1984; Gil Ibarguchi *et al.* 1990; Girardeau & Gil Ibarguchi 1991; Mendia Aranguren, 2000). The retrograde amphibolite-facies metamorphism has been dated at 390-380 Ma (Dallmeyer *et al.* 1991, 1997; Valverde –Vaquero & Fernández, 1996; Gómez Barreiro *et al.* 2006).

4.5.1.2 IP UNITS

The uppermost allochthonous units are composed by a thick terrigenous sequence intruded by Cambro-Ordovician gabbros and granitoids. In the Órdenes Complex, metamorphism ranges from granulite facies in the structurally lower Unit of the group (Monte Castelo Unit), to amphibolite facies in the middle units (Corredoiras and O Pino), and

greenschist facies in the culminating Unit (Betanzos; Figs. 3 and 4). Changes in metamorphic grade are abrupt and occur at extensional detachments (Díaz García 1990; Abati 2002; González Cuadra 2007).

The Monte Castelo Unit is a massive two-pyroxene gabbro cropping out to the west of the Órdenes Complex. Three major compositional types have been distinguished, olivine gabbronorites, amphibole gabbronorites, and biotite gabbronorites. Textures vary from granular to intergranular and ophitic. The presence of olivine and the common ophitic textures point to a relatively shallow emplacement. The chemical composition is tholeiitic, with the majority of analysed samples plotting into the field of island arc tholeiites (Andonaegui *et al.* 2002). Near its bottom, the gabbro is cut by a prograde shear zone in the granulite facies, which produced a complete recrystallisation of the igneous components. Furthermore, granoblastic aluminous granulites occur in small metapelitic enclaves sparsely distributed in the gabbro (Abati *et al.* 2003). Thermobarometric studies show an increase in pressure of between 0.2 and 0.4 GPa at a nearly constant temperature of 800-825ºC during granulitization (Fig. 5a). U-Pb analyses on zircon give a precise age of 499±2 Ma for the crystallisation of the protolith. Monazite included within biotite in a granulite-facies metapelite yielded an age of 498± Ma, whereas rutiles in the same sample gave ages of 380-390 Ma, about 100 Ma younger than the monazites (Abati *et al.* 1999).

The Corredoiras Unit is a coarse-grained orthogneiss of granodioritic to tonalitic composition that crops out in the eastern limb of the Órdenes Complex (Figs. 3 and 4). U-Pb dating on zircon yielded concordant ages of 500±2 Ma according to Abati et al.,(1999), and 492±3 after Andonaegui *cr _j,** (2012). The massif is variably gneissified and kilometre-scale xenoliths of hornfelses and migmatites occur inside the orthogneisses. The hornfelses reflect contact metamorphism, whereas migmatization indicates a regional metamorphic event. The latter has been supposedly dated with monazite at 493±2 and 484±2 Ma, closely following the intrusion (Abati *et al.* 1999), but the possibility that these ages reflect the thermal influence of the intrusion cannot be ruled out. A few metapelites show a well-preserved granulitic association (González Cuadra 2007), and small bodies of gabbro, some of which with a granulitic association, and diabase dikes occur sparsely distributed inside the Unit. A Silva Unit is a granodioritic orthogneiss that may represent the continuation of the Corredoiras Unit in the western limb of the large synform forming the Órdenes Complex, and has yielded a slightly older but imprecise age around 510 Ma (Castiñeiras *et al.* 2010). A comparable granodioritic massif forms the Lagoa Unit, in the Morais Complex, dated at 496±3 Ma (Dallmeyer & Tucker 1993). The chemistry of the Corredoiras orthogneiss point to a generation above a subduction zone for tonalitic and gabbroic rocks, and to crustal influence in the case of granodiorites, all suggesting an ensialic island arc environment.

The O Pino Unit is a thick sequence of monotonous mesozonal schists and paragneisses intruded by relatively small bodies of gabbro and granitoids that overlie the high-grade metaigneous massifs of Monte Castelo and Corredoiras. The Cariño Unit, in the Cabo Ortegal Complex, is comparable to that of O Pino in the Órdenes Complex, and is intruded by the San Xiao composite massif (gabbro, granodiorite and granite), calc-alkaline and characteristic of a volcanic arc setting (Castiñeiras *et al.* 2002; Castiñeiras 2005). O Pino and Cariño units underwent mesozonal metamorphism, with zones ranging from almandine to sillimanite (Castiñeiras 2005). Kyanite is found replacing andalusite pseudomorphs in O Pino, indicating pressurization after heating, as in the Monte Castelo and Corredoiras units (Fig. 5a). Monazites from semipelitic paragneisses of the sillimanite zone yielded ages of 493±1.3 and 496±3 Ma (Abati *et _j,** 1999), interpreted as reflecting late Cambrian, IP regional metamorphism.

The Betanzos Unit culminates the nappe stack in the Órdenes Complex, and consists of 2000-3000 m of metapelites and greywackes, with alternations of grey to black quartzites and a few conglomerates. The facies and sedimentary structures indicate a turbiditic character (Matte & Capdevila 1978). Greywackes are feldspathic and rich in volcanic components which, when considered together with the geochemistry of gabbros and orthogneisses, suggest a volcanic arc setting. The Unit probably represents a forearc or back-arc basin fill. The metagreywackes have been investigated for detrital zircon ages, yielding a maximum depositional age of 510-530 Ma and suggesting derivation from the West African craton and surrounding Cadomian belts. (Fernández-Suárez *et al.* 2003; Fuenlabrada *et al.* 2010). Diabase dikes are common in the Betanzos Unit, and one of them yielded a U-Pb zircon age of 510 Ma (Díaz García *et al.* 2010). The Lagoa schists are the equivalent in the Morais Complex of the O Pino and Betanzos units.

4.5.2 THE UPPER ALLOCHTHON IN NW FRANCE

The upper assemblage of allochthonous units in NW France consists of two types of units. The lower ones are characterized by an eclogite-facies event (the Essarts Unit, a few slices in the Audierne Bay), while the upper ones display a low-grade basement unconformably overlain by Cambrian to Carboniferous sediments (the Mauges Unit, and possibly the Roc-Cervelle Unit).

4.5.2.1 HP UNITS

The Essarts Unit is world famous because of its beautiful eclogites (Lacroix 1891, Brière 1920). These constitute lenses a few hundred metres thick and up to a few kilometres long derived from metagabbros forming a tholeiitic suite (Godard 1988, 2001). From the less to the most evolved magmatic protoliths, one can distinguish (i) Mg-rich kyanite-bearing quartz-free eclogites, (ii) kyanite-bearing quartz-poor eclogites, (iii) quartz-bearing eclogite and (iv) ferro-titanian quartz-bearing eclogite. Banded fine-grained gneisses interlayered with eclogite

are thought to derive from plagiogranites. Geochemical data show compositions similar to MORB, and therefore these eclogites are classically considered as derived from an oceanic crust (Montigny & Allègre 1974, Godard 1983, 1988, Bernard-Griffiths & Cornichet 1985).

U-Pb data on zircon from the Essarts eclogites have been obtained a long time ago by Peucat *et al.* (1982). Based on these data, it has been frequently argued that the oceanic crust could have been Proterozoic (about 1.3 Ga), while the eclogite-facies event would have been Early Silurian (436+15/-12 Ma). However, it should be stressed that these data are now obsolete for two main reasons. We now know that the conventional method used by Peucat and co-workers cannot resolve the details of the mixing arising from different populations having inherited cores and/or one or several stages of overgrowths. Moreover, the oceanic crust would have registered a rather peculiar tectonic history (see for instance Paquette 1987), because the difference in age between crystallisation of the protoliths and subduction of the crust would have been to large (about 1000 Ma!). In order to solve this issue, the sample has been redated using the LA-ICP-MS method, which has provided evidence for inherited cores and a protolith age at 487±12 Ma (Paquette *et al.* in prep.).

The Essarts Unit also displays some orthogneisses, one of them being dated at 483±4 Ma (la Roche-aux-Lutins at Rocheservière; Lahondère *et al.* 2009). Moreover, polycyclic gneisses nicely record a HT metamorphism predating the eclogite-facies event (Godard 2001, 2009). The early, HT event (Fig. 5b) is recorded by migmatitic, cordierite-bearing gneisses that also show some evidence of cooling (cordierite alteration into pinite). The HP overprint results in coronitic and/or pseudomorphic reactions, notably the replacement of cordierite by garnet-kyanite-quartz. Two generations of monazite have been identified on a petrographical ground (Godard, 2001), and have been dated using the La-ICP-MS method (Bosse *et al.* 2010). The first generation of monazite, associated to the HT event, has provided an age of 460 Ma (i.e. slightly youger than the gabbroic and granitic intrusions), whereas the second generation gives an age of 375 Ma, potentially dating the HP event exhumation of the Unit (Fig. 5b).

To sum up, the Essarts Unit now appears to be made of nearly contemporaneous gabbroic and granitic intrusions. The HT metamorphism could result from either a regional event resulting from the heat supply associated to the Ordovician intrusions, or to an unrelated event. After cooling, all rock types together were subjected to an eclogite-facies event recording the Late Devonian subduction of a piece of thinned, continental crust. An alternative scenario, advocated by Godard (1983, 1988, 2001, 2009), involves a tectonic mélange between pieces of oceanic and continental crust during the subduction event.

In the Audierne Bay, a few slices of small size (not more than 100 m in thickness) display garnet-diopside mafic granulites (Keramoine Unit; Velde 1972; Lucks *et al.* 2002) and garnet kyanite gneisses and mafic eclogites (Kergroaz Unit; Marchand 1982; Lucks *et al.* 2002). These slices are found on top of the ophiolite complex and they are separated from the underlying ophiolite complex by an intensely deformed orthogneiss (Languidou orthogneiss), (Ballèvre *et al.* 1994). This mylonite zone might represent a ductile extensional detachment similar to those cutting across the nappe pile in Iberia. All slices record a HP and HT metamorphism (up to about 1.8-2.0 GPa, 800-900°C for the Kergroaz Unit). U-Pb data on zircons (Peucat 1983, Paquette *et al.* 1985) suggest an Early Ordovician age for the protoliths of the garnet-kyanite granulites (480±8 Ma) and the Languidou orthogneiss (470±7 Ma).The age of the HP event is constrained by U-Pb data on zircons from a garnet granulite at 384±6 Ma. Altough reasonable, these geochronological data should be used with caution, because they have been obtained by dissolution of zircon populations. The Penhors Unit is essentially made of metagreywackes and interlayered amphibolites. The age of the protoliths is unknown. Their metamorphic grade belongs to the albite-epidote amphibolite facies. Because it has been rarely studied, the affinity of this Unit is still unclear. However, it should belong to the Upper Allochthon due to its structural position above the ophiolite complexes.

4.5.2.2 LOW-GRADE UNITS

In the Armorican Massif, two low-grade units are found in an uppermost structural position, namely the Mauges Unit (overthrusting the Champtoceaux Complex, including the ophiolite Drain Unit), and the Roc-Cervelle Unit, overthrusting the Essarts Complex. The Mauges Unit is a prime example of the Upper Allochton because it displays both the Proterozoic basement and its Palaeozoic cover

The Proterozoic basement is essentially made of low-grade schists, displaying only a few lithological markers, namely a layer of black cherts ("phtanites") associated to mafic volcanics. An increasing grade of metamorphism is recorded towards the contact with the underlying Drain Unit, with a km-thick sequence of mylonitized amphibolite-facies gneisses.

The Palaeozoic cover of the Mauges Unit consists, to the south, of a sequence of conglomerates and schists that have provided a few Cambrian trilobites (Cavet *et al.* 1966). These are overlain and partly intruded by a complex of hypovolcanic and volcanic rocks of mafic to felsic chemistry, dated at 519+14/-10 Ma and 521±7 Ma (Thiéblemont et al. 1987b, 2001). Along the northern boundary of the Mauges Unit (Ducassou 2010), the Neoproterozoic basement is unconformably overlain by reddish siltstones of Early Ordovician age (Cavet *et al.* 1971). The Cambrian volcanics (Perroud & van der Voo 1985) and the Early Ordovician siltstones (Perroud *et al.* 1986) have provided palaeomagnetic evidence for a

position of the Mauges Unit, hence the Upper Allochthon, at high southerly latitudes, consistent with linkage to the northern Gondwana margin at this time.

Two types of sedimentary sequences are in fact observed in the Mauges Unit (Cavet *et al.* 1971, Ducassou *et al.* 2011a). In the proximal sequence (known as the Châteaupanne sequence), the red siltstones are succeeded by Middle to Upper Ordovician slates and sandstones (Lardeux *et al.* 2008). These are unconformably overlain by the Chalonnes Formation, with a basal sandstone member recording the oldest terrestrial plants of the Armorican (and Iberian) massifs (Strullu-Derrien *et al.* 2010; Gerrienne *et al.* 2011). Most of the Chalonnes Formation consists of reefal limestones of Emsian age (Le Maître 1934), that are overlain by immature sandstones rich in plant debris (Ducassou *et al.* 2009). These sandstones, of late Emsian to early Eifelian age (Ballèvre *et al.* 2010), are interpreted as turbiditic deposits at the front of a delta prograding into a shallow sea.

In a more distal sequence, known as the Tombeau Leclerc sequence, the Early and Middle Ordovician are unknown. Upper Ordovician sediments display the typical glaciomarine sequences found all along the northern Gondwana palaeomargin, and are covered by graptolite-rich cherts (Piçarra *et al.* 2002, 2009), then pelites and finally pelagic carbonates of Emsian age.

Both Devonian sequences are in turn unconformably overlain by the mudstones, sandstones and conglomerates of the Ancenis Formation (Rivière 1977, Ballèvre et Lardeux, 2005, Ducassou 2010). Although its stratigraphy is still largely unknown, due to the lack of good lithological markers and the scarcity of the fauna and flora, the Ancenis Formation may have been deposited in a deep lake which was progressively filled in by deltaic then alluvial deposits.

The Roc-Cervelle Unit is located in the southwestern part of the Armorican Massif, and it is partly covered by the Mesozoic sediments of the Aquitaine basin. It consists of low-grade schists whose deformation may be Proterozoic (i.e. Cadomian) in age (Bouton & Branger 2007, Bouton & Camuzard 2012) rather than Variscan as generally thought. A Devonian sequence outcrops nearby, and may have been deposited on top of the Roc-Cervelle schists. This sequence starts with fluviatile sandstones followed by shales and reefal limestones of Givetian age (Le Maître 1937). It therefore records a marine transgression during the Middle Devonian, and also the proximity of an emerged land, because of the presence of well-preserved compressions of terrestrial plants (Camuzard *et al.* 1968, 1969).

To sum up, the low-grade units of the Upper Allochthon in the Armorican Massif are key pieces for understanding the early history of the Variscan orogeny, because they record the sedimentary evolution at the beginning of the convergence in the upper plate close to the former plate boundary. Because the sediments contain a huge amount of volcanic-derived material, and using detrital thermochronology to constrain their age (Ducassou *et al.* this

volume), it is possible to suggest that the Upper Allochthon was part of a volcanic arc during the late Early to Middle Devonian part of a volcanic arc.

4.6 AN ATTEMPT TO SYNTHETISE THE GEODYNAMIC EVOLUTION

The nappe stack of units representing different geotectonic realms in NW Iberia and the Armorican Massif permits a qualitative palinspastic reconstruction. Assuming that the Autochthon represents the Gondwana mainland, successively higher units in the pile can be interpreted as having travelled from progressively more external positions during thrusting. This, together with the data on lithologic associations, chemical affinities, metamorphic evolution and ages, is the base for the following interpretation, which is incomplete, and leaves several points unexplained or open to debate.

4.6.1 PERI-GONDWANAN TERRANE DISPERSION

The IP units of the Upper Allochthon in NW Iberia provide keys on the existence of a late Cambrian, continental (ensialic) magmatic arc. A bimodal, calc-alkaline suite dated at 500±10 Ma intruded a terrigenous succession deposited in a peri-Gondwana realm, with volcanic components, and a maximum depositional age of 510-530 Ma. For the underlying HP-HT units, the arc signature is less clear, as gabbros ca. 500 Ma old have MORB affinity and point to continental rifting. Only the ultramafic rocks beneath suggest a supra-subduction environment.

As the IP units overlie the HP-HT units, the rule of thumb "higher means farther" suggests an explanation for the arc vs. rift paradox: the IP units represent the leading edge of the continental arc facing a subduction zone, while the underlying HP-HT units represent the trailing edge behind, facing a back-arc opened following rifting and pulling apart of the arc (Fig. 7a).

The development of a volcanic arc at a continental margin and its subsequent pulling apart by slab roll-back requires a wide ocean with old oceanic lithosphere. As an example, the Cambro-Ordovician was a time of widespread arc development in Iapetus (van Staal *et al.* 1998; Winchester *et al.* 2002; van Staal 2005). Iberia and the Southern Armorican Massif lay to the south of the Iapetus suture at the end of the Varican cycle (Fig. 1). But as they were displaced by late Variscan dextral strike-slip shear zones, they could have occupied a more eastward position, to the south of the Tornquist suture. So, the arc developed ca. 500 Ma ago at the Gondwanan side of either the Iapetus or Tornquist oceans, both opened around 100 Ma before between Gondwana, on one side, and Laurentia or Baltica respectively on the other. The subsequent widening of the back-arc developed at its trailing edge (Fig. 7b, c, d) may have created the Rheic Ocean (Martínez Catalán *et al.* 2007, 2009).

The development of a volcanic arc at a continental margin and its subsequent pulling apart by slab roll-back requires a wide ocean with old oceanic lithosphere. As an example, the Cambro-Ordovician was a time of widespread arc development in Iapetus (van Staal *et al.* 1998;

Winchester *et al.* 2002; van Staal 2005). Iberia and the Southern Armorican Massif lay to the south of the Iapetus suture at the end of the Varican cycle (Fig. 1). But as they were displaced by late Variscan dextral strike-slip shear zones, they could have occupied a more eastward position, to the south of the Tornquist suture. So, the arc developed ca. 500 Ma ago at the Gondwanan side of either the Iapetus or Tornquist oceans, both opened around 100 Ma before between Gondwana, on one side, and Laurentia or Baltica respectively on the other. The subsequent widening of the back-arc developed at its trailing edge (Fig. 7b, c, d) may have created the Rheic Ocean (Martínez Catalán *et al.* 2007, 2009).

Generation of oceanic lithosphere starting at ca. 500 Ma (Vila de Cruces, Izeda-Remondes, Audierne, Groix, Bois de Cené), deposition of back-arc sequences (Ceán, Lamas de Abad, Cercio and possibly Ile-de-Groix), and diabase dikes in the Upper and Lower Allochthon support the opening of the back-arc. It would have occurred shortly after voluminous arc-type felsic and intermediate plutonism in the Upper Allochthon (500±10 Ma), as diabase dikes intruded the granitic massifs, and one of them has been dated at 510 Ma. Ages are somewhat younger in the Lower Allochthon: 495-470 Ma for the orthogneisses (Fig. 7a, b), of which only those of granitic composition were cut by basic dikes, whereas the younger peralkaline orthogneisses post-date dike injection.

The Lower Allochthon would represent the outer edge of the conjugate margin of the back-arc, on the Gondwanan side, whereas more continental domains are represented by the Parautochthon and Autochthon. Protolith ages younger here than in the Upper Allochthon may reflect diachronism in the opening of the back-arc. This suggests that although on opposite sides, they were not in front to each other, but located in a different position along the marginal basin opened in the northern margin of Gondwana. Detrital zircon age populations suggest that the Iberian Upper Allochthon derives from a westward position with respect to the Lower Allochthon, Parautochthon and Autochthon (Díez Fernández *et al.* 2010, 2012d). These data support the diachronous opening of the Rheic Ocean, proceeding from west to east in the northern periphery of Gondwana, as proposed by Linnemann *et al.* (2008).

Turning back to the Upper Allochthon, its separation from Gondwana at the Cambro-Ordovician boundary makes it a lateral equivalent to Avalonia, although it was a separate terrane, possibly accreted to the south of Laurussia prior to the collision with Gondwana (Gómez Barreiro *et al.* 2007; Martínez Catalán *et al.* 2007, 2009). If granulite facies metamorphism in the IP units in Iberia occured shortly after voluminous bimodal magmatism (ca. 500-490 Ma), it could reflect magmatic underplating, deformation, and crustal thickening related to the dynamics of the arc (Abati *et al.* 2003). But no structures associated to granulite facies metamorphism have been found. This event, not described in the underlying units, was perhaps masked by the early Variscan HP-HT event,

although some monazite and zircon ages, around 500-480 Ma (Fernández-Suárez *et al.* 2002), can be related with equivalent monazite ages in the IP units. The data from the Essarts Unit in the Armorican Massif suggest that a Cambro-Ordovician HT event was widespread in the Upper Allochthon, except in the low-grade units (Betanzos, Mauges, Roc-Cervelle). But the IP event in the Órdenes Complex is perhaps more reasonably related to early Variscan convergence. Then, pressurization after strong heating, as drawn in the Monte Castelo and O Pino P-T paths (Fig. 5a) would be an artifact, and things would be more like for the Essarts Unit (Fig. 5b, Essarts 1 and 2), which records a polyclyclic P-T path.

The mafic granulites of the ophiolitic Bazar Unit, of LP-MP type, and dated at ca. 500 Ma (protolith) and ca. 485 Ma (metamorphism) are probably related to the evolution of the arc. Subduction of a mid-ocean ridge may have implied a change in plate dynamics around the arc (Fig. 7b), which did not register any further magmatic or metamorphic event in the next 85 Ma.

In the SW Armorican Massif, the Mauges Unit, representative of the uppermost allochthon, preserves Cambrian or Early Ordovician sedimentary rocks unconformably overlying low-grade schists. Subsequent discontinuous sedimentation records the Hirnantian glaciation, the Silurian anoxic event, and finally, the establishment of a carbonate platform close to an emerged land during the Early Devonian.

The unconformity marks the erosion of a basement, possibly that of the peri-Gondwanan arc, and glaciomarine deposits suggest proximity to Gondwana by the Late Ordovician, but little is known about its subsequent evolution until Devonian times. It might have remained close to Gondwana, or travelled passively with the Iapetus or Torquist oceanic lithosphere until their closure during the Silurian, around 440-420 Ma (Hossack & Cooper 1986; van Staal *et al.* 1998; Winchester *et al.* 2002). In the latter case, the marginal basin opened behind the arc would have spread to create the ~3000 km wide Rheic Ocean (Winchester *et al.* 2002). Otherwise, the continental arc should have stayed around together with other peri-Gondwanan terranes, forming part of a complex Rheic oceanic realm involving several oceanic branches.

4.6.2 EARLY VARISCAN CONVERGENCE

The first evidences of convergence related to the Variscan cycle are generation of intraoceanic, suprasubduction zone ophiolites at 405-395 Ma (Careón, Morais-Talhinhas), and HP-HT metamorphism producing eclogites at 400-390 Ma in the lower group of the Upper Allochthon (Fig. 7d, e). This Early-Middle Devonian metamorphic event implied subduction of the part of the continental arc corresponding to its trailing edge, but not of the IP units interpreted as its leading edge, where no HP event occurred. However, It is possible that IP

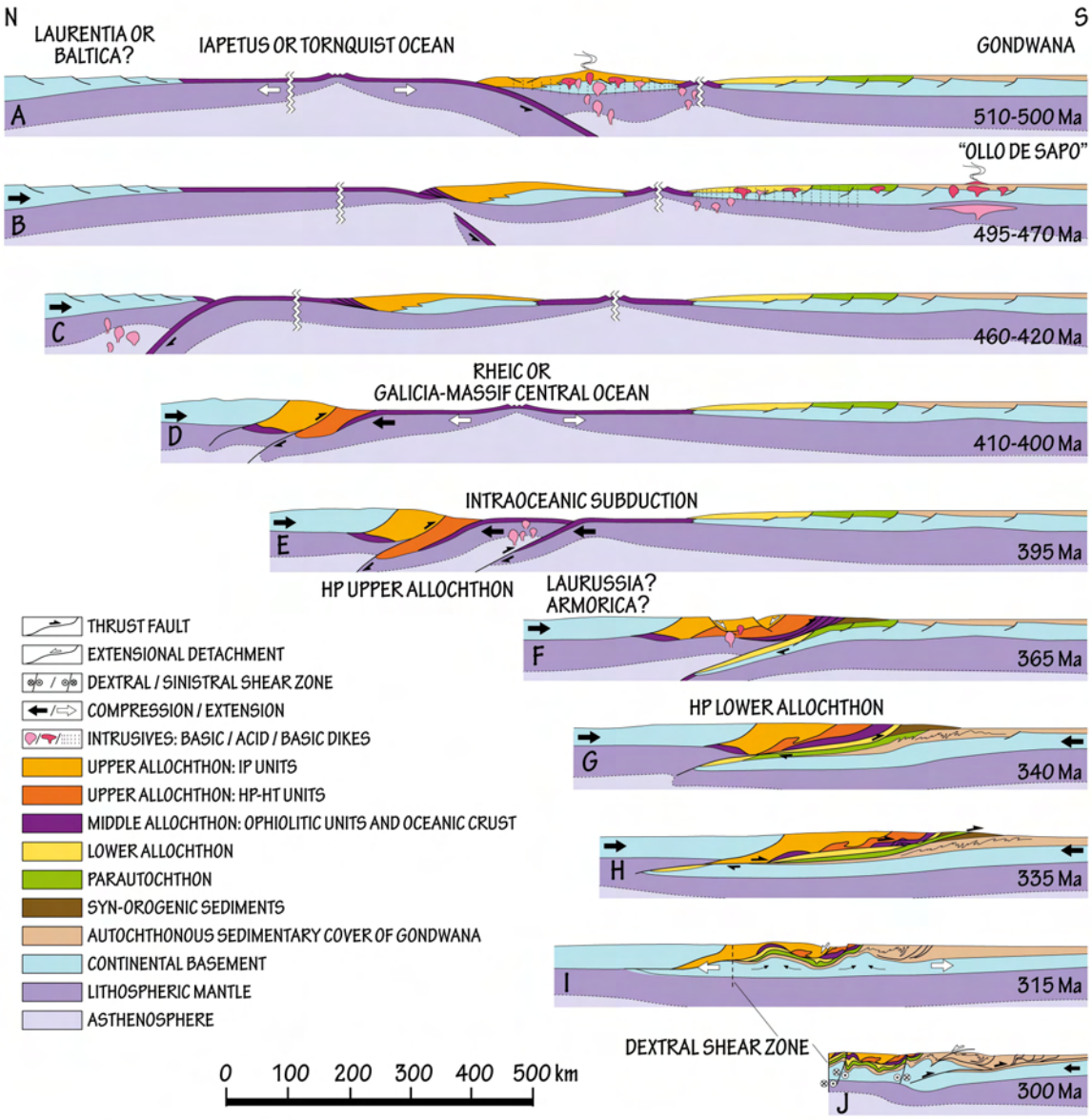

Fig. 7. Suggested stages in the tectonic evolution of NW Iberia and the Southern Armorican Massif. a) Formation of a continental arc during the late Cambrian to Early Ordovician and its individualization of a peri-Gondwanan terrane by slab rollback. b) Subduction of a mid-ocean ridge at the leading edge of the arc. c) Separation of the continental arc pulled by subduction to the north and opening of an intervening ocean. d) Building of an accretionary prism by underthrusting and imbrication of the peri-Gondwanan terrane, whose trailing edge reached eclogite-facies conditions. e) Progressive closure of the ocean by intraoceanic subduction. f) Subduction of outer edge of Gondwana. g) Thrusting of Allochthon over the Parautochthon. h) Out-of-sequence thrusting of the Middle and Upper Allochthons over the Lower Allochthon, and thrusting the Parautochthon, with imbrication of the syn-orogenic deposits. i) Thrusting of more external parts of the belt, and collapse and extension of the thickened crust, with Formation of extensional detachments and domes. j) Late upright folding, strike-slip faulting, and hin-skinned tectonics in the foreland with underthrusting of its basement.

metamorphism in the Iberian uppermost allochthon was actually coeval with the HP event of the underlying units. Then, the Cambro-Ordovician monazite ages would represent only a thermal event related to magmatic underplating in the continental arc. The possible existence of an arc during the late Early to Middle Devonian in the Upper Allochthon of the Armorican Massif (Ducassou *et al.* this volume) would also reflect early Variscan convergence.

Intraoceanic and arc subduction reflect Gondwana-Laurussia convergence (Fig. 7e), although the polarities have not been established. Arc subduction might reflect accretion to Laurussia (Martínez Catalán *et al.* 2007, 2009), a hypothesis not backed up with the presence of Laurussia- or Avalonia-derived units on top of the allochthonous nappe stack.

Independently of the buttress against which the different terranes collided, accretion of the old continental arc was followed by that of the Middle Allochthon (Early Devonian and Cambro-Ordovician suprasubduction zone ophiolites and related units) at 390-380 Ma, and of the Lower Allochthon at >370-365 Ma (Fig. 7f). For the latter, the subduction polarity has been established in the NW Iberian Massif, to the west or SW in present coordinates (Martínez Catalán *et al.* 1996; Díez Fernández *et al.* 2011, 2012a, b) and in the Armorican Massif, to the north or NW in present coordinates (Ballèvre & Marchand 1991). This means continental subduction outward from Gondwana and toward Laurussia and/or Armorica.

In France, intrusion in the Upper Allochthon of gabbro-dioritic bodies of calc-alkaline affinity, dated at ca. 380-360 Ma ("ligne tonalitique du Limousin" in the French Massif Central) (Bernard-Griffiths *et al.* 1985, Bertrand *et al.* 2001), is related to north-vergent subduction of an oceanic domain. This magmatism extends to the west in the Vendée area, where it is represented by the Moncoutant and le Tallud diorites (373+6/-11 Ma; Cuney *et al.* 1993). Also, it may be associated to the development of a back-arc basin, poorly-dated but surely Devonian, represented by mafic volcanics of the Chantonnay syncline (Wyns *et al.* 1989), and extensive felsic volcanism with massive sulfides developed during the Famennian-Visean from the Morvan (Delfour, 1989) to the Vosges (Lefèvre *et al.* 1994; Krecher *et al.* 2007).

Progressive accretion of the Middle and Lower allochthons (oceanic units and outer margin of Gondwana respectively) produced exhumation of the overlying Upper Allochthon, accompanied by decompression and partial melting. This was in turn overprinted by penetrative mylonitisation in the amphibolite facies, dated at 390-380 Ma. These were followed in Iberia by recumbent folding and thrusting under greenschist facies conditions, dated at ca. 365 Ma in the Middle Allochthon.

4.6.3 VARISCAN COLLISION

Once continental subduction became locked, shortening began in the inner parts of the continental platform, giving rise first to recumbent folds, and then to large thrust sheets (Fig. 7g, h). In NW Iberia, the cleavage related to the folds is dated at 359 Ma close to the allochthonous complexes, and 336 Ma to the east (Dallmeyer *et al.* 1997), showing that shortening was diachronous and younger toward the external zones. Folding resulted from pushing of the stacked accretionary prism against Gondwana as a backstop. But the prism was finally emplaced onto the Gondwanan platform some 15 Ma after the generation of the

first recumbent folds, forming the allochthonous terranes limited at its bottom by a weakly-dipping sole thrust.

In France, thrusting of the Upper Allochthon over the Middle and Lower Allochthon resulted in the development of an inverted metamorphism, with synkinematic biotite-staurolite-kyanite parageneses indicating P-T conditions of about 0.8 GPa and 600ºC just below the main thrust contact, dated at about 350-340 Ma (early Carboniferous). In NW Iberia, thrusting of the Lower Allochthon over the Parautochthon was followed by out-of-sequence thrusting of the Upper and Middle Allochthon over the Lower Allochthon, which also resulted locally in an inverse metamorphic gradient. About the same time, thrusting of the Parautochthon over the Autochthon took place, while thick syn-orogenic flysch deposits ("Culm") were laid down in depocenters in front of the active thrusts, becoming imbricated as they progressed (Fig. 7h). Flysch deposition spans 380-330 Ma whereas active thrusts involving the Allochthon and Parautochthon took place at 345-335 Ma. Then, thrusting propagated toward more external parts of the belt, while the hinterland underwent gravitational collapse and attenuation giving rise to migmatitic domes and extensional detachments (Fig. 7i, j).

Reworking of the suture zone resulted in the deposition of thick (2-3 km) detrital sequences in fault-bounded, deep lakes located in transtensional basins (Ancenis basin, of probable late Visean age i.e., 340-330 Ma) on top of the nappe pile. Similar deposits occur in Iberia, normally along Late Variscan transcurrent faults in the inner zones, and as syn-orogenic deposits involved in thin-skinned thrust belts in the external zones of the Iberian Massif (Fig. 1).

Strike-slip faulting and late upright folding developed in the Armorican Massif (Jégouzo 1980, Jégouzo & Rossello 1988, Ducassou *et al.* 2011b, Tartèse *et al.* 2012) and Iberia around 320-300 Ma, roughly contemporaneous with oroclinal bending which formed the Ibero-Armorican and Central Iberian arcs between 315 and 295 Ma (Weil 2006; Weil *et al.* 2010; Martínez Catalán 2012).

4.7 CONCLUDING REMARKS

A straightforward correlation is established among the allochthonous units on both sides of the Bay of Biscay, which have been grouped in three different ensembles called the Upper, Middle and Lower Allochthons (Table 1). An intermediate Unit, allochthonous but with stratigraphic and petrologic affinities with its relative autochthon, has been also identified in NW Iberia and the south of the Armorican Massif, and is referred to as the Parautochthon.

The Lower Allochthon represents a fragment of the outermost edge of Gondwana (or of a Gondwana-derived terrane), that underwent A-type subduction after the closure of a Palaeozoic ocean to the north. That ocean is represented by the Middle Allochthon, whose protoliths cover the

time lapse between 500 and 395 Ma, similar to that of existence of the Rheic Ocean (Winchester *et al.* 2002). These are mostly supra-subduction type ophiolites or metasedimentary sequences alternating with basic, MORB-type volcanics, with inheritances pointing to their generation at a continent-ocean transition. The ocean began to open around the Cambro-Ordovician boundary, during the separation of a continental arc which is represented by the Upper Allochthon.

The correlation has been carried out on the basis of lithological associations, relative structural position, age and geochemistry of protoliths, and tectonometamorphic evolution, which includes P-T conditions and time. In terms of the number and quality of fitting criteria, correlation is excellent for the Lower Allochthon and the units of the Middle Allochthon forming a supracrustal, probably oceanic sequence. For the rest of the Middle Allochthon, (ophiolitic units), it is reasonably good taking into account the limited outcropping conditions in the Armorican Massif. For the Upper Allochthon, correlation is good for the structurally lower units characterized by HP, early Variscan metamorphism.

For the overlying units, especially those of low metamorphic grade, the correlation is problematic, as while the age of metamorphism seems Cadomian for the Mauges and Roc-Cervelle units, the maximum depositional age for metasediments of the Betanzos Unit appears as early to middle Cambrian. This does not preclude that they form part of the same peri-Gondwanan terrane, but they may represent different parts of it: a Cadomian basement and a Cambrian forearc or back-arc basin fill respectively.

There is a wide consensus among the authors of this contribution on the correlation between individual allochthonous units in NW Iberia and Armorican Massif, and also about the relevance of the three groups established. However, the adscription of some units to a particular group has been a matter of discussions and a full agreement has not been reached. The units supposedly representing a supracrustal oceanic sequence have been included in the Middle Allochthon according to the opinion of the French team and part of the Spanish team, while the rest would have preferred to keep them in the Lower Allochthon based on their reasonable continuity, continental inheritances and comparable metamorphic evolution. Another problem is the MORB signature of some HP units of the Upper Allochthon, which indicates an oceanic affinity and might be included in the Middle Allochthon. These aspects primarily reflect the transitional character of some units, but also different points of view concerning palaeogeographic and orogenic evolution, and perhaps insufficient knowledge.

Notwithstanding, the correlation of the allochthonous units confirms the continuation of the Asturian arc to the north in Brittany, as proposed by Suess (1885-1909). With all its complexities, the Allochthon represents the suture zone of one and the same oceanic tract. Furthermore, it is an accretionary prism assembled in an early stage of the Variscan convergence which was followed by the Variscan collision. Not only the different allochthons can be compared, but also the relative autochthon is thought to be the same to both sides of the Bay of Biscay.

Several other questions closely related to palaeogeography remain open: What was the buttress or backstop against which the accretionary prism was built? What ocean was closed to form the suture? Did the Autochthon form part of the northern margin of Gondwana at the time of emplacement?

For the backstop, the options are either the great continent to the north (Baltica or the yet amalgamated Laurussia; Martínez Catalán *et al.* 2007, 2009), or a peri-Gondwanan, isolated terrane (Armorica; Ballèvre *et al.* 2009). For the ocean, it may have been the wide Rheic Ocean (Martínez Catalán 1990; Martínez Catalán *et al.* 2007, 2009), or a narrower ocean separating Gondwana and the Armorica microplate (Massif Central, Galicia-South Brittany or Galicia-Brittany-French Massif Central Ocean; Matte 1986, 1991, Matte 2001, 2002, 2007). For the Autochthon, the alternative to Gondwana is the ribbon hypothesis, defended by Stampfli & Borel (2002), Stampfli *et al.* (2002), and von Raumer *et al.* (2009), according to which it was part of a continental strip separated from Gondwana by the Palaeotethys.

These questions are not the subject of this communication, as it seems that understanding the dynamics of the northern peri-Gondwanan domain would require more data from the whole Variscan belt to constrain the models and reach a consensus. Meanwhile, to establish sound correlations along the Variscan belt is viewed as a tool to progress in the knowledge of the Palaeozoic dynamics of Central and Western Europe.

The Spanish team has been funded by the research projects CGL2007-65338-C02-01 and 02/BTE, and CGL2011-22728 of the Spanish Ministry of Science and Innovation, as part of the National Program of Projects in Fundamental Research, in the frame of the VI National Plan of Scientific Research, Development and Technologic Innovation 2008-2011. The first two projects were co-financed by European Funds of Regional Development (FEDER). JGB appreciates financial support by the Spanish Ministry of Science and Innovation through the Ramón y Cajal program.

CHAPTER 5

Conclusions

5. CONCLUSIONS

The conclusions of this research have been presented and discussed in detail throughout the manuscript, especially in Chapters 3 and 4. The main insights of this PhD thesis concern to the numerical modelling of blueschist-facies rocks and to the geological and geochronological knowledge of the Malpica-Tui Complex. The following paragraphs summarise the major contributions of this research.

5.1 *Inverse and forward modelling of the blueschist-facies rocks from the MTC*

BLUESCHIST-FACIES PELITIC ROCKS

The metamorphic evolution of the Ceán Schists has been widely investigated by both conventional and multiequilibrium thermobarometry. Classical inverse modelling provided a first approach, whereas the thorough study has been implemented by numerical modelling on phase equilibria through pseudosection approach.

Conventional techniques using micro-inclusion compositions indicate peak conditions of 19–22 kbar and 500 °C. The same calculations using the matrix minerals yield approximate values of 16–20 kbar and 440–515 °C. P–T values obtained with the average P–T method of THERMOCALC are compatible with the conventional thermobarometry results, but show significantly lower pressures for the matrix foliation (13–14 kbar and 495–500 °C).

Attempting to obtain a model that satisfactorily describe the high complexity of the paragenetic succession observed in this rocks, the effects of progressively adding new components to the chemical system have been monitored in the course of this investigation. Thereby, pseudosection approach has been performed in the KFMASH, MnNCKFMASH and MnNCKFMASHTO chemical systems. The P–T pseudosection calculated in the KFMASH system resulted overly simplified to make geologically reasonable inferences. Although it does not permit going further on the interpretation of the crystallization sequence along the P–T path, it provided an initial approach that allowed deducing a coherent interval for the peak P–T conditions, refined by the isopleths barometry using the Si content in phengitic muscovite and constrained at P> 20 kbar and T< 550°C. Petrological modelling in the MnNCKFMASH system provided a minimum pressure limit for the paragenesis chloritoid + glaucophane at P>17 kbar, confirming the HP stability of this assemblage in pelitic rocks. But the whole reaction history and a coherent model that fully describes the metamorphic evolution of the Ceán schists have been obtained investigating their P–T–X evolution in the MnNCKFMASHTO chemical system.

Inferences attained from this petrologic model suggest that the Upper Sheet of the MTC recorded a three-stage metamorphic evolution involving (i) Early subduction-related medium-pressure/LT metamorphism (M_1) roughly constrained at 350–380 °C and 12–14 kbar, exclusively preserved in the basal part of the sequence. (ii) Subduction-related blueschist facies prograde metamorphism (M_2) going from 19 kbar and 400 °C to 21 kbar and 460 °C at the base of the sequence, and from 16 kbar, 430 °C to 21–22 kbar, 520 °C in the middle part of the sequence. (iii) Exhumation-related metamorphism (M_3) is characterized by a decompression to 8–10 kbar and 470–490 °C at the base of the sequence. This decompression is also recorded in the middle part, but it was not possible to estimate precise P–T conditions.

The results obtained from numerical modelling calculations yielded first-order constraints for geodynamic models that may have a general application in the investigation of rocks with similar composition. The uncertainty associated to the role of water and the state of oxidation of Fe is mostly related to the difficulty of estimating their original proportions in the rock through quantitative analytical techniques. Using pseudosection approach it has been possible to estimate the existing proportion of both components during the prograde evolution of the Ceán Schists. (i) H_2O content appear to be a critical factor in the metamorphic evolution of blueschist facies metapelites. When modelling HP rocks, fluid(H_2O)-saturation is commonly assumed during metamorphism. Although reasonable for other environments, this research suggests subduction zone metamorphism may occur in H_2O-undersaturated conditions induced by the crystallization of a significant modal amount of lawsonite, and the transition from lawsonite blueschist to amphibolite-greenschist facies may involve significant hydration, principally as a result of lawsonite breakdown. However, rocks with low modal amounts of lawsonite (such as low-Ca metapelites) would not reach H_2O-depletion and the rock would remain H_2O-saturated during the prograde evolution. (ii) The proportion of ferric iron also has a strong influence on phase equilibrium. The analysed values of Fe_2O_3 may not reflect the oxidation state during the main metamorphic evolution and are probably easily modified by superficial alteration even in apparently fresh samples. The use of P–T–X(Fe_2O_3) pseudosections together with petrographic observations is then necessary to estimate the real oxidation state of the rocks and correctly evaluate the P–T conditions.

RETROGRESSED BLUESCHISTS

Based on the results obtained from the investigation of the Ceán schists, the metamorphic evolution of the Cambre metabasic rocks was explored through P–T–X(H_2O /Fe_2O_3) pseudosections in the NCKFMASHTO chemical system, with the aim to better establish the P–T evolution for the Ceán Unit in the MTC, and associate it with the different stages of the subduction- vs. exhumation-related metamorphism. Because activity-composition relations for Mn-bearing solid solutions are poorly constrained and the studied

sample has a low MnO content, which is exclusively concentrated in the garnet cores, MnO was not included in the chemical model system.

The composition of mafic rocks is favourable for the growth of high modal proportions of lawsonite and, predictably, the effect of lawsonite growth on the H_2O availability emerged as crucial for the interpretation of mineral assemblages. Thus, prograde metamorphism in the Cambre metabasic rocks is also characterized by a H_2O-undersaturated P–T evolution (induced by the crystallization of lawsonite) in the lawsonite blueschist/LT-eclogite-facies conditions peaking at P = 22 kbar and T = 550–560 °C (M_2). Exhumation-related metamorphism is characterized by a nearly isothermal decompression from the lawsonite-bearing fields to fields with stable albite at P = 10 kbar (M_3). This led to the pseudomorphism of lawsonite crystals in the early decompression stages, and a subsequent amphibolite-greenschist facies overprint at P < 8 kbara and T = 440–480 °C (post-M_3).

The results obtained from the numerical modelling on phase equilibrium in blueschist-facies rocks from the Ceán Unit account reasonably well for the first-order petrographic observations in both the Ceán pelitic schists and the Cambre metabasic rocks. Nevertheless, phase diagram modelling failed to reproduce some of the petrographic observations. This research reveals that uncertainties on the P–T estimates when modelling rocks in the HP–LT pelitic or mafic system are related either to the incomplete knowledge of the thermodynamic properties of Mn/Ti/Fe^{3+}-end members in the available solid solution models, to problems with the identification of the effective bulk composition or both. Nevertheless, a thorough petrographic investigation, together with an extensive knowledge on the mineral chemistry and the textural relationships, frequently helps to identify and overcome these problems. This is, in turn, related to the correct identification of the effective bulk rock composition, decisive since the pseudosection would be only valid for such election.

The lithologies constituting the Ceán Unit show systematic changes in texture and mineral composition that are spatially related depending on deformation. Thus, choosing the "right" bulk composition has been one of the most complex challenges. Compositionally unlayered rocks (such as metapelitic and metabasic rocks at the base of the sequence) have been successfully modelled using the bulk rock composition analysed by XRF of a crushed rock-slab corresponding to a representative domain (at thin-section scale). However, the pelitic schists located in the middle part of the sequence are compositionally layered low-Ca metapelites. In certain layers, fractionating the bulk composition (using the "rbi" facility of THERMOCALC) to reflect porphyroblasts growth was necessary. These layers became effectively inert domains while deformation progressed, whereas other layers were recrystallized and the XRF analysis of a representative rock-slab was applicable for modelling these domains.

Through this research the mixing models for solid solutions in glaucophane, paragonite, and Ti-rich phases, particularly titanite, does not faithfully reproduce the naturals stability of such phases in the predicted models. Even using the most recent and comprehensive clinoamphibole (Diener & Powell, 2012) and white mica (Smye et al., 2010) models, only results in minor differences in the pseudosection topology, and does not solve the inconsistencies. In general, regardless of the nature of the modelled HP-rock, glaucophane is "too" stable, in particular with respect to paragonite, over an excessively wide range of P-T conditions. Paragonite is frequently absent or shows a very restricted stability, unless it is forced in excess in an effectively reduced model system. The stability of titanite in all pseudosections is limited to low pressures, whereas it is a common phase in all assemblages, as inclusions and in the matrix. This may be explained by the fact that titanite is considered as a pure end-member in the model, whereas analysed titanite crystals has small, but non negligible, substitutions of Al and Fe that possibly will significantly extend its stability.

Nevertheless, ongoing improvements in the internally consistent thermodynamic datasets and a-x relationships coupled with continued advance in analytical methods ensure expansion of modelling capacity into larger and more accurate model chemical systems.

5.2 *Metamorphic evolution of the Ceán Unit*

Petrological analysis involving P-T-X pseudosections in the MnNCKFMASHTO chemical system in both metapelitic and metabasic rocks shows that the Ceán Unit recorded a three-stage metamorphic evolution. The first episode (M_1) represents the early subduction-related stages and is only preserved in the lower structural levels of the sequence. M_1 is characterized by the relics of a former assemblage partially preserved as S_1 inclusions (ep-sph-ru-q) in the core of large garnet porphyroblasts, and has been roughly constrained at ≈ 12-14 kbar and 350-380 °C. The second metamorphic stage, M_2, is evidenced by the syntectonic development of an assemblage including lawsonite, glaucophane, a second generation of garnet and a foliation (S_2) consisting of ep-act/bar-o-mu-ru/ilm-sph-q in the metabasic rocks and ctd-chl-mu-pa-ru/ilm-q in the metapelites. This assemblage is preserved at the base and in the middle part of the Ceán Unit. M_2 represents the subduction-related blueschist/LT-eclogite facies facies prograde metamorphism and is characterized by a H_2O-undersaturated prograde P-T path peaking at 19-22 kbar, corresponding to a maximum burial of ca. 65-70 km. The temperatures recorded by the metapelitic and the metabasic rocks differ slightly. Within the Ceán schists, the temperature of the pressure peak is of ca. 460°C at the base and of ca. 520°C in the intermediate part of the sequence. The temperature estimated for the Cambre metabasic rocks is slightly higher and constrained at ca. 560 °C. Finally, M_3 is best developed at the top of the sequence. It is characterized by the growth of syntectonic albite porphyroblasts and a foliation S_3 containing ep-act-hb-chl-mu±ilm-sph-q in the metabasic rocks, and ep-chl-mu-pa-bi-ru/ilm-sph-q±g±win/bar in the metapelites. The exhumation-related

metamorphism is characterized by a nearly-isothermal decompression to ca. 10 kbar (M_3) and an amphibolite-greenschist facies overprint from 10 to 5 kbar and from T < 560 to 380 °C (post-M_3).

5.3 *Advances in geochronology*

Timing constraints on the P-T evolution of HP terranes are essential to understand the subduction-exhumation process. Whilst the ages of various events of the Lower Allochthon of the MTC have been extensively studied, the data for the Middle Allochthon are limited to only one $^{40}Ar/^{39}$ Ar age on muscovite of 348 ± 8 Ma (Rodríguez Aller et al. 2003).

The age of the HP event in the blueschist-facies conditions in the Ceán Unit can be constrained at a minimum age ca. 363 ± 2 Ma. Peak P-T conditions of 19-22 kbar and 460 - 560 °C correspond to an approximate depth of 65-70 km and a geothermal gradient of 6-7 °C km^{-1}, typical of relatively cold subduction zones. $^{40}Ar/^{39}Ar$ dating of muscovite from the quartzo-feldspathic mylonites of the Bembibre-Ceán detachment, at the base of the Ceán Unit, yields an age of ca. 337±3 Ma, interpreted as the age that marks the beginning of the post-nappe extensional tectonics that led to the gravitational collapse of the orogen (at ca. 350-340 Ma). Differences between the HP/LT event, and the beginning of the post-nappe tectonics, confirms that the exhumation of the MTC lasted ca. 15-20 Ma. A nearly isothermal decompression from ca. 22 to ca. 10 kbar provides an exhumation rate of ca. 2-2.5 mm/year from ca. 70 to ca. 30 km, characteristic of slow and long-lasting accretionary-wedge subdution type. Afterward, during the orogenic collapse, a fast cooling may follow the slow exhumation. Therefore, last stages of exhumation from 10 to 5 kbar occurred within a period of ca. 10-15 Ma (from ca. 350 to ca. 335-340 Ma), suggesting that decompression occurred in two stages (1) a slow exhumation stage with little temperature change over a large depth interval and (2) a phase of fast cooling once the rocks have reached an upper crustal level.

The age of the peak blueschist-facies metamorphism support the equivalence of the Ceán Unit and its counterpart in the Armorican Massif, the Upper Unit of Ile de Groix, and suggest that both terranes share a blueschist-facies event constrained at ca. 360-370 Ma, that may represent the Late Devonian-Early Carboniferous subduction of the northern margin of Gonwana beneath Laurussia, at the onset of the Variscan collision.

5.4 *Correlations across the Ibero-Armorican Arc*

Similitudes between the allochthonous units at both sides of the Bay of Biscay have been suggested since the nineteenth century, but a detailed comparison has never been attempted. The work of many authors throughout several years is collected in this PhD thesis in the form of a scientific publication that aims to establish a correlation of the units forming the nappe

stack on both sides of the Bay of Biscay and to unify the terminology when describing them. Correlation between the units exposed in the NW Iberian Massif and the southern Armorican Massif has been established based on lithological associations, structural position, age and geochemistry of protoliths, and tectonometamorphic evolution. Similar allochthonous units in both sides of the Bay of Biscay have been grouped in three different ensembles called the Upper, Middle and Lower Allochthons. The Lower Allochthon has been interpreted as a fragment of the outermost margin of Gondwana that underwent continental subduction shortly after the closure of a Palaeozoic ocean which, in turn, is represented by the Middle Allochthon. The oceanic domain consists of supra-subduction type ophiolites and metasedimentary sequences alternating with basic and MORB-type volcanics, with inheritances suggesting the proximity of a continental domain. Sea-floor spreading began at the Cambro-Ordovician boundary and lasted until Late Devonian, coinciding with the time interval of existence of the Rheic Ocean, which is a clear candidate for being represented by the Middle Allochthon. Finally, the Upper Allochthon represents the pull apart of a peri-Gondwanan continental arc that led to the opening of the oceanic domain.

5.5 *Conclusions*

From this research we can conclude that:

1. The Ceán Unit recorded a three-stage metamorphic evolution involving (i) Early subduction-related MP/LT metamorphism (M_1) roughly constrained at 350–380 °C and 12–14 kbar, which is only preserved in the basal part of the sequence. (ii) Subduction-related blueschist/LT-eclogite-facies prograde metamorphism (M_2) characterized by a H_2O-undersaturated prograde P–T path peaking at 19–22 kbar, corresponding to a maximum burial of ca. 65–70 km. (iii) Exhumation-related metamorphism (M_3/post- M_3) occurred in two stages (1) a nearly isothermal decompression from ca. 70 to ca. 30 km, characteristic of slow and long-lasting accretionary-wedge subdution type and (2) a phase of fast cooling once the rocks have reached an upper crustal level.

2. The results obtained from numerical modelling calculations on the effects of H_2O and Fe_2O_3 in the metamorphic evolution of blueschist-facies rocks yielded first-order constraints for geodynamic models that may have a general application in the investigation of rocks with similar composition. (i) This research proposes that subduction zone metamorphism may occur in H_2O-undersaturated conditions induced by the crystallization of a significant modal amount of lawsonite. Then, the transition from lawsonite blueschist-facies to amphibolite-greenschist facies may involve significant hydration, principally as a result of lawsonite breakdown. (ii) The proportion of ferric iron has a strong influence on phase equilibrium. The analysed values of Fe_2O_3 may not reflect the oxidation state during the main metamorphic evolution and are probably easily modified by superficial alteration even in apparently fresh samples.

3. The use of P-T-X(H_2O/Fe_2O_3) pseudosections together a thorough petrographic investigation, and an extensive knowledge on the mineral chemistry and the textural relationships is then necessary to estimate the extent of fluid-saturation during subduction zone metamorphism and the real oxidation state of the rocks to correctly evaluate the P-T conditions.

4. The age of the peak blueschist-facies metamorphism has been constrained at ca. 363±2 Ma by $^{40}Ar/^{39}Ar$ step-heating of phengitic muscovite from the pelitic schists. $^{40}Ar/^{39}Ar$ dating of muscovite from the quartzo-feldspathic mylonites of the Bembibre-Ceán detachment, at the base of the Ceán Unit, yields an age of ca. 337±3 Ma, interpreted as the age that marks the beginning of the post-nappe extensional tectonics that led to the gravitational collapse of the orogen. Differences between the HP/LT event, and the beginning of the post-nappe tectonics, suggest an exhumation rate of 2-2.5 mm/year for the Malpica-Tui Complex. These ages support the equivalence of the Ceán Unit and its counterpart in the Armorican Massif, the Upper Unit of Ile de Groix, and suggest that both terranes share a blueschist-facies event constrained at ca. 360-370 Ma, that may represent the Late Devonian-Early Carboniferous subduction of the northern margin of Gondwana beneath Laurussia, at the onset of the Variscan collision.

CHAPTER 6

References

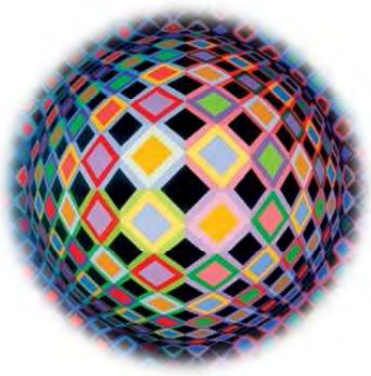

ABATI, J. & DUNNING, G.R. (2002). Edad U–Pb en monacitas y rutilos de los paragneisses de la Unidad de Agualada (Complejo de Órdenes, NW del Macizo Ibérico). Geogaceta 32, 95–98

ABATI, J. (2002). Petrología metamórfica y geocronología de la unidad culminante del Complejo de Órdenes en la región de Carballo (Galicia, NW del Macizo Ibérico). Nova Terra, 20, 1–269

ABATI, J., ARENAS, R., MARTÍNEZ CATALÁN, J.R. & DÍAZ GARCÍA, F. (2003). Anticlockwise P–T path of granulites from the Monte Castelo Gabbro (Órdenes Complex, NW Spain). Journal of Petrology, 44 305–327

ABATI, J., DUNNING, G.R., ARENAS, R., DÍAZ GARCÍA, F., GONZÁLEZ CUADRA, P., MARTÍNEZ CATALÁN, J.R. & ANDONAEGUI, P. (1999). Early Ordovician orogenic event in Galicia (NW Spain): evidence from U–Pb ages in the uppermost unit of the Órdenes Complex. Earth Planetary Science Letters 165, 213–228

ABATI, J., GERDES, A., FERNÁNDEZ SUÁREZ, J., ARENAS, R., WHITEHOUSE, M.J. & DÍEZ FERNÁNDEZ, R. (2010). Magmatism and early–Variscan continental subduction in the northern Gondwana margin recorded in zircons from the basal units of Galicia, NW Spain. Geological Society of America Bulletin 122, 219–235

ABLE, L. & BRADY, J.B. (2001). Lawsonite pseudomorphs in the schists of Syros, Greece: Geological Society of America, Abstracts with Programs 33, p.A9

AERDEN, D.G.A.M. (2004). Correlating deformation in Variscan NW Iberia using porphyroblasts: Implications for the Ibero–Armorican Arc. Journal of Structural Geology 26, 177–196

AGARD, P., YAMATO, P., JOLIVET, L. & BUROV, E. (2009). Exhumation of oceanic blueschists and eclogites in subduction zones: Timing and mechanisms. Earth–Science Reviews 92, 53–79

ALBERT ROPER, R., ARENAS, R., SÁNCHEZ MARTÍNEZ, S. & GERDES, A. (2012). The eclogite facies gneisses of the Cabo Ortegal Complex (NW Iberian Massif): Tectonothermal evolution and exhumation model. Journal of Iberian Geology 38, 389–406

ALCOCK, J., ARENAS, R. & MARTÍNEZ CATALÁN, J.R. (2005). Shear stress in subducting continental margin from high–pressure, moderate–temperature metamorphism in the Órdenes Complex, Galicia, NW Spain. Tectonophysics 397,181–194

ALLEMAND, P. & LARDEAUX, J.M. (1997). Strain partitioning and metamorphism in a deformable orogenic wedge: application to the Alpine belt. Tectonophysics 280, 157–169

ALONSO, J.L. & GONZ.LEZ, J.C. (1982). Mapa Geológico de España, E. 1:50000, hoja número 44 (SISARGAS–CARBALLO). Instituto Geológico y Minero de España (IGME).

ALONSO, J.L., MARCOS, A. & SUAREZ, A. (2009). Paleogeographic inversion resulting from large out of sequence breaching thrusts: The León Fault (Cantabrian Zone, NW Iberia). A new picture of the external Variscan Thrust Belt in the Ibero–Armorican Arc. Geologica Acta 7, 451–473

ANDERSEN, D.J. & LINDSLEY, D.H. (1988). Internally Consistent Solution Models for Fe–Mg–Mn–Ti Oxides–Fe–Ti Oxides. American Mineralogist 73, 714–26

ANDONAEGUI, P., CASTIÑEIRAS, P., GONZÁLEZ CUADRA, P., ARENAS, R., SÁNCHEZ MARTÍNEZ, S., ABATI, J., DÍAZ GARCÍA, F. & MARTÍNEZ CATALÁN, J.R. (2012). The Corredoiras orthogneiss (NW Iberian Massif): Geochemistry and geochronology of the Paleozoic magmatic suite developed in a peri–Gondwanan arc. Lithos 128–131, 84–99

ANDONAEGUI, P., GONZÁLEZ DEL TÁNAGO, J., ARENAS, R., ABATI, J., MARTÍNEZ CATALÁN, J.R., PEINADO, M. & DÍAZ GARCÍA, F. (2002). Tectonic setting of the Monte Castelo gabbro (Órdenes Complex, northwestern Iberian Massif): evidence for an arc–related terrane in the hanging wall to the Variscan suture. In: MARTÍNEZ CATALÁN, J.R., HATCHER, R.D., ARENAS, R. & DÍAZ GARCÍA, F. (eds). Variscan–Appalachian Dynamics: The Building of the Late Paleozoic Basement. Geological Society of America Special Paper 364, 37–56

ANTHONIOZ, P. & FERRAGNE, A. (1978). Le Precambrien polymétamorphique allochtone du nord-ouest de la Peninsule Ibérique, temoin d'une nappe de charriage caledonienne?. In: Geología de la parte N del Macizo Ibérico. O Castro, La Coruña, 23-41

ARENAS, R. & MARTÍNEZ CATALÁN, J.R. (2002). Prograde development of corona textures in metagabbros of the Sobrado window (Ordenes Complex, NW Iberian Massif). In: Martínez Catalán, J.R., Hatcher Jr., R.D., Arenas, R. & Díaz García, F. (eds). Variscan-Appalachian Dynamics: The Building of the Late Paleozoic Basement, Geological Society of America Special Paper 364, 73-88

ARENAS, R. (1991). Opposite P-T-t paths of Hercynian metamorphism between the upper units of the Cabo Ortegal Complex and their substratum (northwest of the Iberian Massif). Tectonophysics 191, 347-364

ARENAS, R., ABATI, J., MARTÍNEZ CATALÁN, J.R., DÍAZ GARCÍA, F. & RUBIO PASCUAL, F.J. (1997). P-T evolution of eclogites from the Agualada Unit (Órdenes Complex, NW Iberian Massif, Spain): Implications for crustal subduction. Lithos 40, 221-242

ARENAS, R., DÍAZ GARCÍA, F., MARTÍNEZ CATALÁN, J.R., ABATI, J., CASTIÑEIRAS, P., FERNÁNDEZ-SUÁREZ, J., GÓMEZ-BARREIRO, J., ANDONAEGUI, P., GONZÁLEZ CUADRA, P. & GONZÁLEZ DEL TÁNAGO, J. (2004a). Zona de Galicia-Trás-os-Montes: Complejos alóctonos de Galicia-Trás-os-Montes, Unidades superiores. In: VERA, J.A. (ed). Geología de España, Sociedad Geológica de España-Instituto Geológico y Minero de España (SGE-IGME), Chapter 2, 154-162

ARENAS, R., FARIAS, P., GALLASTEGUI, G., GIL IBARGUCHI, J.I., GONZÁLEZ LODEIRO, F., KLEIN, E., MARQUÍNEZ, J., MARTÍN PARRA, L.M., MARTÍNEZ CATALÁN, J.R., ORTEGA, E., DE PABLO MACÍA, J.G., PEINADO, M. & RODRÍGUEZ-FERNÁNDEZ, L.R. (1988). Características geológicas y significado de los dominios que componen la Zona de Galicia-Trás-os-Montes. II Congreso Geológico de España. Simposios, 75-84

ARENAS, R., GIL IBARGUCHI, J.I., GONZÁLEZ LODEIRO, F., KLEIN, E., MARTÍNEZ CATALÁN, J.R., ORTEGA GIRONÉS, E., DE PABLO MACÍA, J.G. & PEINADO, M. (1986): Tectonostratigraphic units in the complexes with mafic and related rocks of the NW of the Iberian Massif. Hercynica 2, 87-110

ARENAS, R., MARTÍNEZ CATALÁN, J.R., SÁNCHEZ MARTÍNEZ, S., DÍAZ GARCÍA, F., ABATI, J. & FERNÁNDEZ-SUÁREZ, J. (2004b). Ofiolitas paleozoicas de la sutura varisca de Galicia (NW del Macizo Ibérico, España): distribución, características y significado. In: PEREIRA, E.S., CASTROVIEJO, R. & ORTIZ, F. (eds). Complejos ofiolíticos en Iberoamérica. Guías de prospección para metales preciosos, CYTED, Madrid, 203-230

ARENAS, R., MARTÍNEZ CATALÁN, J.R., SÁNCHEZ MARTÍNEZ, S., DÍAZ GARCÍA, F., ABATI, J., FERNÁNDEZ-SUÁREZ, J., ANDONAEGUI, P. y GÓMEZ-BARREIRO, J. (2007a). Paleozoic ophiolites in the Variscan suture of Galicia (northwest Spain): distribution, characteristics and meaning. In: HATCHER, R.D., CARLSON, M.P., MCBRIDE, J.H. & MARTÍNEZ CATALÁN, J.R. (eds). 4-D Framework of Continental Crust, Boulder, Colorado. Geological Society of America Memoir 200, 425-444

ARENAS, R., MARTÍNEZ CATALÁN, J.R., SÁNCHEZ MARTÍNEZ, S., FERNÁNDEZ-SUÁREZ, J., ANDONAEGUI, P., PEARCE, J.A. & CORFU, F. (2007b). The Vila de Cruces Ophiolite: A remnant of the early Rheic Ocean in the Variscan suture of Galicia (NW Iberian Massif). Journal of Geology 115, 129-148

ARENAS, R., RUBIO PASCUAL, F.J., DÍAZ GARCÍA, F. & MARTÍNEZ CATALÁN, J.R. (1995). High pressure micro-inclusions and development of an inverted metamorphic gradient in the Santiago Schists (Ordenes Complex, NW Iberian Massif, Spain): evidence of subduction and syncollisional decompression. Journal of Metamorphic Geology 13, 141-164

ARENAS, R., SÁNCHEZ MARTÍNEZ, S., CASTIÑEIRAS, P., JEFFRIES, T.E., DÍEZ FERNÁNDEZ, R. & ANDONAEGUI, P. (2009). The basal tectonic mélange of the Cabo Ortegal Complex (NW Iberian Massif): a key unit in the suture of Pangea. Journal of Iberian Geology 35, 85-125

ARMBUSTER, T., BONAZZI, P., AKASAKA, M., BERMANEX, V., CHOPIN, C., GIERE, R., HEUSS-ASSBICHLER, LIEBSCHER, A., MENCHETTIC, S., PAN, Y., & PASERO, M. (2006). Recommended nomenclature of epidote-group minerals. European Journal of Mineralogy 18, 551-567

ARPS, C.E.S. (1970). Petrology of a part of the Western Galicia Basement between the río Jallas and the Ría de Arosa (NW Spain) with emphasis on zircon investigations. Leidse Geologische Mededelingen 46, 57-155

ARPS, C.E.S. (1981). Amphibolites and other mafic rocks of the Blastomylonitic Graben in Western Galicia, NW Spain: Field relations and petrography. Leidse Geologische Mededelingen 52, 57-71

ATHERTON, M. P. & BROTHERTON, M. S. (1982). Major element composition of the pelites of the Scottish Dalradian. Geological Journal 17, 185-221

ATHERTON, M.P. (1968). The variation in garnet, biotite, and chlorite composition in medium grade pelitic rocks from the Dalradian, Scotland, with particular reference to the zonation in garnet. Contributions to Mineralogy and Petrology 18, 347-371

AUDREN C. & LEFORT, J.P. (1977). Géologie du plateau continental sud armoricain entre les îles de glénan et noirmoutier: implications géodynamiques. Bulletin de la Société Géologique de France, XIX. 395-404

AUDREN, C., TRIBOULET, C., CHAURIS, L., LEFORT, J.P., VIGNERESSE, J.L., AUDRAIN, J., et al. (1993). Notice explicative de la feuille Ile de Groix à 1/25000 (carte géologique). BRGM, Orléans.

AUZANNEAU, E. VIELZEUF, D. & SCHMIDT, M.W. (2006). Experimental evidence of decompression melting during exhumation of subducted continental crust. Contributions to Mineralogy and Petrology 152, 125-148

AUZANNEAU, E., SCHMIDT, M.W. VIELZEUF, D. AND CONNOLLY, J.A.D. (2010). Titanium in phengite: a geobarometer for high temperature eclogites. Contributions to Mineralogy and Petrology 159, 1-24

AVÉ LALLEMANT, H.G. (1965). Petrology, petrofabrics and structural geology of the Sierra de Outes-Muros Region (Prov. La Coru.a, Spain). Leidse Geologische Mededelingen 33, 147-175

BABIST, J., HANDY, M. R., KONRAD-SCHMOLKE, M. & HAMMERSCHMIDT, K. (2006). Precollisional, multistage exhumation of subducted continental crust: The Sesia Zone, western Alps. Tectonics 25: TC6008

BAILEY, E.H. (1962). Metamorphic facies of the Franciscan Formation of California and their geologic significance [abstract]. Geological Society of America Special Paper 68, 4-5

BAKER, H.B. (1936). Structural features crossing Atlantic Ocean. Pan-American Geology LXVI, 1-2

BALDWIN, J. A., BOWRING, S. A. & WILLIAMS, M. L. (2003). Petrological and geochronological constraints on high pressure, high temperature metamorphism in the Snowbird tectonic zone, Canada. Journal of Metamorphic Geology 21, 81-98

BALDWIN, J. A., BOWRING, S. A., WILLIAMS, M. L. & WILLIAMS, I. S. (2004). Eclogites of the Snowbird tectonic zone: petrological and U-Pb geochronological evidence for Paleoproterozoic high-pressure metamorphism in the western Canadian Shield. Contributions to Mineralogy and Petrology 147, 528-548

BALLÈVRE, M. & LARDEUX, H. (2005). Signification paléoécologique et paléogéographique des bivalves du Carbonifère inférieur du bassin d'Ancenis (Massif armoricain). Comptes Rendus Palevol 4, 109-121

BALLÈVRE, M. & MARCHAND, J. (1991). Zonation du métamorphisme éclogitique dans la nappe de Champtoceaux (Massif armoricain, France). Comptes-Rendus de l'Académie des Sciences de Paris II-312, 705-711

BALLÈVRE, M., BOSSE, V., DUCASSOU, C. & PITRA, P. 2009. Palaeozoic history of the Armorican Massif: Models for the tectonic evolution of the suture zones. Comptes Rendus Geosciences 34, 174-201

BALLÈVRE, M., CAPDEVILA, R., GUERROT, C. & PEUCAT, J.J. (2002). Discovery of an alkaline orthogneiss in the eclogite-bearing Cellier Unit (Champtoceaux Complex, Armorican Massif): a new witness of the Ordovician rifting, Comptes Rendus Geoscience 334, 303-311

BALLÈVRE, M., DUCASSOU, C., LARDEUX, H. & RÉGNAULT, S. (2010). A revised age (Emsian-Eifelian) for the Sainte-Anne Formation (Armorican Massif, France): implications for the onset of mountain building in the Variscan belt. Neues Jarhbuch für Geologie und Paläontologie Abhandlungen 255, 237-254

BALLÈVRE, M., FOURCADE, S., CAPDEVILA, R., PEUCAT, J.J., COCHERIE, A. & FANNING, C.M. (2012). Geochronology and geochemistry of Ordovician felsic volcanism in the Southern Armorican Massif (Variscan belt, France): Implications for the breakup of Gondwana. Gondwana Research 21, 1019-1036

BALLÈVRE, M., KIÉNAST, J.R. & PAQUETTE, J.L. (1987). Le métamorphisme éclogitique dans la nappe hercynienne de Champtoceaux (Massif armoricain). Comptes-rendus de l'Académie des Sciences de Paris II-305, 127-131

BALLÈVRE, M., MARTÍNEZ CATALÁN, J.R., LÓPEZ-CARMONA, A., ABATI, J., DÍEZ FERNÁNDEZ, R., DUCASSOU, C., PITRA, P., ARENAS, R., BOSSE, V., CASTIÑEIRAS, P., FERNÁNDEZ-SUÁREZ, J., GÓMEZ BARREIRO, J., PAQUETTE, J.L., PEUCAT, J.J., POUJOL, M., RUFFET, G. & SÁNCHEZ MARTÍNEZ, S. (submitted). Correlation of the nappe stack in the Ibero-Armorican arc across the Bay of Biscay: a joint French-Spanish project. In: Schulmann, K., Oggiano, G., Lardeaux, J.M., Janousek, V., Martínez Catalán, J.R. & Scrivener, R. (eds). The Variscan Orogeny: Extent, Timescale and the Formation of the European Crust. London: Geological Society of London Special Publication

BALLÈVRE, M., PINARDON, J.L., KIÉNAST, J.R. & VUICHARD, J.P. (1989). Reversal of Fe-Mg partitioning between garnet and staurolite in eclogite-facies metapelites from the Champtoceaux nappe (Brittany, France). Journal of Petrology 30, 1321-1349

BALLÈVRE, M., PITRA, P. & BOHN, M. (2003). Lawsonite growth in the epidote blueschists from the Ile de Groix (Armorican Massif, France): a potential geobarometer. Journal of Metamorphic Geology 21, 723-735

BALLY, A. W. (1975). A geodynamic scenario for hydrocarbon occurrences: Tokyo, 9th World Petroleum Congress 2, 33-44

BANNO, S. & CHII, S. (1978). A model to explain the Mn-enrichment in the rim of zoned garnet. Geochemical Journal, 12, 253-257

BARBER, A. (1982). Interpretations of the tectonic evolution of Southwest Japan. Proceedings of the Geologists' Association 93, 131-145

BARD, J.P., CAPDEVILA, R. & MATTE, P. (1971). Structure de la chaîne hercynienne de la Meseta Ibérique: Comparaison avec les segments voisins. In: Histoire structurale du Golfe de Gascogne. Publ Inst Francais Pétrole, Technip, Paris, Symp CNEXO I, vol 4, 1-68

BARRIENTOS, X. & SELVERSTONE, J. (1993). Infiltration vs. thermal overprinting of epidote blueschists, Ile de Groix, France. Geology 21, 69-72

BARROIS, C. (1883). Mémoire sur les schistes métamorphiques de Ile de Groix. Annales de la Société Géologique Du Nord XI, 18-71

BARTH, T. F. W. (1936). Structural and petrologic studies in Dutchess County, New York. II. Geological Society of America Bulletin 47,775-850.

BEA, F., MONTERO, P., TALAVERA, C., ABU ANBAR, M., SCARROW, J.H., MOLINA, J.F. & MORENO, J.A. (2010). The palaeogeographic position of Central Iberia in Gondwana during the Ordovician: evidence from zircon chronology and Nd isotopes. Terra Nova 22, 341-346

BEANE, R.J., & LIOU, J.G. (2005). Metasomatism in Serpentinite Melange Rocks from the High-Pressure Maksyutov Complex, Southern Ural Mountains, Russia. International Geology Review 47, 24-40

BEARTH, P. (1959). Ueber Eklogit, Glaukophanschiefer und metamorphe Pillowlaven. Schweizer Mineralogische und Petrographische Mitteilungen 39,267-86

BEHR, H. J., ENGEL, W., FRANKE, W., GIESE, P. & WEBER, K. (1984). The Variscan Belt in Central Europe: Main structures, geodynamic implications, open questions. Tectonophysics, 109, 15-40

BELLIDO, F. BRANDLE, J.L., LASALA, M. & REYES, J. (1992). Consideraciones petrológicas y cronológicas sobre las rocas graníticas hercínicas de Galicia. Cuadernos del Laboratorio Xeologico de Laxe 17, 241-261

BENTLEY, 2010 http://mountainbeltway.wordpress.com/

BERMAN, R.G. (1988) Internally-consistent thermodynamic data for minerals in the system Na20-K20-Ca0-Mg0-Fe0-Fe203-Al203-Si02-Ti02-H20-C02. Journal of Petrology, 29, 445-522.

BERMAN, R.G. (1991). Thermobarometry using multi-equilibrium calculations: a new technique, with petrological applications. In: Gordon, T.M. & Martin, R.F. (eds). Quantitative methods in petrology: an issue in honor of Hugh J. Greenwood. Canadian Mineralogist 29, 833-855

BERMAN, R.G. (2007). WinTWQ (version 2.3): a software package for performing internally-consistent thermobarometric calculations, Geological Survey of Canada, Open File 5462, (ed. 2.32), 41 p.

BERNARD-GRIFFITHS, J. & CORNICHET, J. (1985). Origin of eclogites from South Brittany, France: A Sm-Nd isotopic and REE study. Chemical Geology 52, 185-201

BERNARD-GRIFFITHS, J., CARPENTER, M.S.N., PEUCAT, J.-J. & JAHN, B.-M. (1986). Geochemical and isotopic characteristics of blueschist facies rocks from the Ile de Groix, Armorican Massif (northwest France). Lithos 19, 235-253

BERNARD-GRIFFITHS, J., CARPENTER, M.S.N., PEUCAT, J.J. & JAHN, B.M. (1986). Geochemical and isotopic characteristics of blueschist facies rocks from the Ile de Groix, Armorican Massif (northwest France). Lithos 19, 235-253

BERNARD-GRIFFITHS, J., GEBAUER, D., GRÜNENFELDER, M. & PIBOULE, M. (1985). The tonalite belt of Limousin (French Central Massif): UPb zircon ages and geotectonic implications. Bulletin de la Société Géologique de France (8) I, 523-529

BERTRAND, J.M., LETERRIER, J., CUNEY, M., BROUAND, M., STUSSI, M., DELAPERRIERE, E. & VIRLOGEUX, D. (2001). Géochronologie UPb sur zircons de granitoïdes du Confolentais, du massif de Charroux-Civray (seuil du Poitou) et de Vendée. Géologie de la France 2001(1-2), 167-189

BLACK, P.M. (1973). Mineralogy of New Caledonian metamorphic rocks. II. Amphiboles from the Ouegoa District. Contributions to Mineralogy and Petrology 39, 55-64

BLACKWELL, D. D. (1971). The Structure and Physical Properties of the Earth's Crust. In: J.G. Heacock & D.D. Blackwell (eds). The Thermal Structure of the Continental Crust. American Geophysical Union, 169-184

BLANCO-QUINTERO, I.F., GARCÍA-CASCO, A. & GERYA, T. (2011b). Tectonic blocks in serpentinite melange (eastern cuba) reveal large-scale convective flow of the subduction channel. Geology 39, 79-82

BLANCO-QUINTERO, I.F., GERYA, T., GARCÍA-CASCO, A. & CASTRO, A. (2011c). Subduction of young oceanic plates: A numerical study with application to aborted thermal-chemical plumes. Geochemistry, Geophysics and Geosystems, Q10012

BLANCO-QUINTERO, I.F., LÁZARO, C., GARCÍA-CASCO, A., PROENZA, J. & ROJAS-AGRAMONTE, Y. (2011d). Barium-rich fluids and melts in the subduction environment (La Corea and Sierra del Convento mélanges, eastern Cuba). Contributions to Mineralogy and Petrology 162, 395-413

BLANCO-QUINTERO, I.F., PROENZA, J.A. GARCÍA-CASCO, A., TAULER, E. & GALÍ, S. (2011a). Serpentinites and serpentinites within a fossil subduction channel: La Corea mélange, eastern Cuba. Geologica Acta 9, 389-405

BLOXAM, T. W & ALLEN, J. B. (1960). Glaucophane-schist, eclogite and associated rocksm from Knockormal in the Girvan-Ballantrae complex, south Ayrshire. Transactions of the Royal Society of Edinburgh 64,1-27

BLOXAM, T. W. (1956). Jadeite-bearing metagreywackes in California. American Mineralogist 41, 488-96

BOGER, S. D. & HANSEN, D. (2004). Metamorphic evolution of the Georgetown Inlier, northeast Queensland, Australia; evidence for an accreted Palaeoproterozoic terrane?. Journal of Metamorphic Geology, 22, 511-527.

BOHLEN, S. R. & LIOTTA, J. J. (1986). A Barometer for Garnet Amphibolites and Garnet Granulites. Jounal of Petrology, 27, 1025-1034.

BONHOMMET, N., COBBOLD, P.R., PERROUD, H., RICHARDSON, A. (1981). Palaeomagnetism and cross-folding in a key area of the Asturian arc (Spain). Journal of Geophysical Research 86, 1873-1887

BOSSE, V., BALLÈVRE, M. & VIDAL, O. (2002). Ductile thrusting recorded by the garnet isograd from blueschist-facies metapelites of the Ile de Groix, Armorican Massif, France. Journalof Petrology 43, 485-510

BOSSE, V., FÉRAUD, G., BALLÈVRE, M., PEUCAT, J.J. & CORSINI, M. (2005). Rb-Sr and $^{40}Ar/^{39}Ar$ ages in blueschists from the Ile de Groix (Armorican Massif, France): Implications for closure mechanisms in isotopic systems. Chemical Geology 220, 21-45.

BOSSE, V., FÉRAUD, G., RUFFET, G., BALLÈVRE, M., PEUCAT, J.-J. & DE JONG, K. (2000). Late Devonian subduction and early orogenic exhumation of eclogite-facies rocks from the Champtoceaux complex (Variscan belt, France). Geological Journal 35, 297-325

BOSSE, V., GODARD, G., SHEA, T. & PAQUETTE, J.L. (2010). Datations des évènements polymétamorphiques: intérêts majeurs de l'analyse in situ par ablation laser dans la monazite (Complexe des Essarts, Vendée) [abstract]. Réunion des Sciences de la Terre, XXIII, Bordeaux, 34-35

BOULADON, J. & CHAURIS, L. (1965). Contribution à l'étude des indices métallifères du Massif Armoricain. III – La minéralisation en chromite de Peumerit (Finistère). Bulletin de la Société Géologique et Minéralogique de Bretagne 1962-1963, 105-112

BOUSQUET R., EL MAMOUN, R., SADDIQI, O. & GOFFÉ, B. (2008). Mélanges and ophiolites: was the Bou-Azzer's ophiolite suite (Morocco) a Franciscan-type wedge during the Pan-African orogeny?. In: The Boundaries of the West African Craton. Ennih, N. & Liégois, J.P. (eds). Geological Society, London, Special Publications 297, 233-247

BOUSQUET, R. (2008). Metamorphic heterogeneities within a same HP unit: overprint effect or metamorphic mix?. Lithos 103, 46-69

BOUSQUET, R., GOFFÉ B., HENRY P., LE PICHON X. & CHOPIN C. (1997). Kinematic, thermal and petrological model of the Central Alps: Lepontine metamorphism in the upper crust and eclogitisation of the lower crust. In: Touret, J.R.L. & Austrheim, H. (eds). Collision Orogens: Zones of Active Transfers between Crust and Mantle. Tectonophysics 273, 105-127

BOUSQUET, R., GOFFÉ, B., LE PICHON, X., DE CAPITANI, C., CHOPIN, C. & HENRY, P. (2005). Comment on Subduction factory - 1. Theoretical mineralogy, densities, seismic wave speeds, and H_2O contents by B.R. Hacker, G.A. Abers and S.M. Peacock. Journal of Geophysical Research-Solid Earth 110(B2), B02206

BOUTON, P. & BRANGER, P. (2007). Notice explicative de la carte géologique de France au 1:50000, feuille Coulonges-sur-l'Autize (587). BRGM, Orléans, 134 p.

BOUTON, P. & CAMUZARD, J.P (2012). Le Givétien de la Villedé d'Ardin (Sud du Massif armoricain, France): une série discordante sur un socle cadomien?. Annales de la Société Géologique du Nord 19, 25-34

BRADLEY, D.C., & KUSKY, T.M. (1992). Deformation history of the McHugh Complex, Seldovia quadrangle, south-central Alaska. In: Bradley, D.C. & Ford, A.B. (eds). Geologic Studies in Alaska by the U.S. Geological Survey, 1990. Geological Survey Bulletin, 17-32

BRADLEY, D.C., KUSKY, T.M., HAEUSSLER, P., KARL, S.M. & DONLEY, D.T. (1999). Geologic Map of the Seldovia Quadrangle, U.S. Geological Survey Open File Report 99-18, scale 1:250,000, with marginal notes. Also available as an internet publication: http://wrgis.wr.usgs.gov/open-file/of99-18/

BRADLEY, D.C., KUSKY, T.M., HAEUSSLER, P., ROWLEY, D.C., GOLDFARB, R. & NELSON, S. (2003). Geologic signature of early ridge subduction in the accretionary wedge, forearc basin, and magmatic arc of south-central Alaska, in: Sisson, V.B., Roeske, S. & Pavlis, T.L. (eds). Geology of a Transpressional Orogen Developed During a Ridge-Trench Interaction Along the North Pacific Margin, Geological Society of America Special Paper 371, 19-50

BRADLEY, D.C., KUSKY, T.M., KARL, S.M., TILL, A. & HAEUSSLER, P.J. (2000). Field guide to the Mesozoic Accretionary Complex in Kachemak Bay and Seldovia, South-Central Alaska, Alaska Geological Society and British Petroleum, Anchorage, Alaska, May 12-15, 2000.

BRADLEY, DWIGHT C., KUSKY, TIMOTHY M., KARL, SUSAN M. & HAEUSSLER, PETER J. (1997). Field guide to the Mesozoic accretionary complex along Turnagain Arm and Kachemak Bay, south-central Alaska. In: Karl, S.M., Vaughan, N.R. & Ryherd, T.J. (eds). Guide to the Geology of the Kenai Peninsula, Alaska. Alaska Geological Society, Anchorage, Alaska, 2-12

BRIÈRE, Y. (1920). Les éclogites françaises. Leur composition minéralogique et chimique. Leur origine. Bulletin de la Société Française de Minéralogie 43, 72-222

BROTHERS, R. N. (1954). Glaucophane schists from the North Berkeley Hills, California. American Journal of Science 252, 614-26

BROWN, M. (2009). Metamorphic patterns in orogenic systems and the geological record. In: Accretionary Orogens in Space and Time. Cawood, P.A. & Kröner, A. (eds). Geological Society, London, Special Publications 318, 37-74

BROWN, M. (2010). Paired metamorphic belts revisited. Gondwana Research 18, 46-59

BRUN, J.P. & BURG, J.P. 1982. Combined thrusting and wrenching in the Ibero-Armorican arc: a corner effect during continental collision. Earth and Planetary Science Letters 6, 319-332

BRUN, J.P. & FACCENNA, C. (2008). Exhumation of high-pressure rocks driven by slab rollback. Earth and Planetary Science Letters 272, 1-7.

BUCHER, K. & FREY, M. (2002). Petrogenesis of Metamorphic Rocks. Berlin, Heidelberg, New York: Springer-Verlag, 7th ed, 341 pp.

BUROV, E., FRANCOIS, T., YAMATO, P. & WOLF, S. (2012). Mechanisms of continental subduction and exhumation of HP and UHP rocks. Gondwana Research http://dx.doi.org/10.1016/j.gr.2012.09.010

BUROV, E., JOLIVET, L., LE POURHIET, L. & POLIAKOV, A. (2001). A thermomechanical model of exhumation of high pressure (HP) and ultra-high pressure (UHP) metamorphic rocks in Alpine-type collision belts. Tectonophysics 342,113-136

CABY, R. (1994). Precambrian coesite from nothern Mali: first record and implications for plate tectonics in the trans-Saharan segment of the Pan-African belt. European Journal of Mineralogy, 6, 235-244

CADDICK, M.J., THOMPSON, A.B., (2008) Quantifying the tectono-metamorphic evolution of pelitic rocks from a wide range of tectonic settings: Mineral compositions in equilibrium. Contributions to Mineralogy and Petrology 56, 177-195

CAMUZARD, J.P., LARDEUX, H., PILLET, J. & RIVIÈRE, L.M. (1969). Données nouvelles sur les calcaires givétiens de la Villedé-d'Ardin au gisement de la fontaine de la Marbrière. Bulletin de la Société d'Etudes Scientifiques de l'Anjou VII, 41-52

CAMUZARD, J.P., MATHIEU, G., PILLET, J. & RIVIÈRE, L.M. (1968). Nouvelles découvertes fossilifères dans le Givétien de la Marbrière de la Villedé-d'Ardin. Comptes-Rendus de l'Académie des Sciences de Paris D-267, 471-472

CARDEN, J.R. & DECKER, J.E. (1977). Tectonic significance of the Knik River schist terrane, south-central Alaska, in short notes on Alaskan geology: Alaska Division of Geological and Geophysical Surveys, Geologic Report 55, 7-9

CARDEN, J.R., & FORBES, R.B. (1976). Discovery of blueschists in Kodiak Islands, Alaska, in short notes on Alaskan geology: Alaska Division of Geological and Geophysical Surveys, Geologic Report 51, 19-22.

CARDEN, J.R., CONNELLY, W., FORBES, R.B. & TURNER, D.L. (1977). Blueschists of the Kodiak Islands, Alaska: An extension of the Seldovia schist terrane, Geology, 5, 529-533.

CAREY, S.W. (1955). The orocline concept in geotectonics. Royal Society of Tasmania Proceedings 89, 255-288

CARLÉ, W. (1945): Ergebnisse geologischer Untersuchungen im Grundgebirge von Galicien. (Nordwest Spanien). Geotektonische Forschungen 6:,13-36

CARLIER, G. (1978). Etude des associations réactionnelles à structures coronitiques dans les métagabbros de la région nantaise. PhD thesis, University of Paris VI, 185 p.

CARMAN, J.H. & GILBERT, C.M. (1983). Experimental studies on glaucophane stability. American Journal of Science 283, 414-437

CARMAN, J.H. (1974). Preliminary data on the P-T stability of synthetic glaucophane. EOS Transactions of the American Geophysical Union 55, 481p.

CARSWELL, D.A. (1990). Eclogite facies rocks. Blackie, Glasgow and London: 396p.

CASTIÑEIRAS, P. (2005). Origen y evolución tectonotermal de las unidades de O Pino y Cariño (Complejos Alóctonos de Galicia). Laboratorio Xeolóxico de Laxe, Serie Nova Terra 28, 279 p.

CASTIÑEIRAS, P., ANDONAEGUI, P., ARENAS, R. & MARTÍNEZ CATALÁN, J.R. (2002). Descripción y resultados preliminares del plutón compuesto de San Xiao, Complejo de Cabo Ortegal (noroeste del Macizo Ibérico). Geogaceta 32, 111-114

CASTIÑEIRAS, P., DÍAZ GARCÍA, F. & GÓMEZ BARREIRO, J. (2010). REE-assisted U-Pb zirconage (SHRIMP) of an anatectic granodiorite: constraints on the evolution of the A Silva granodiorite, Iberian Allochthonous Complexes. Lithos, 116, 153-166

CAVET, P., GRUET, M. & PILLET, J. (1966). Sur la présence du Cambrien à Paradoxides à Cléré-sur-Layon (M.-et-L.) dans le Nord-Est du Bocage Vendéen (Massif armoricain). Comptes-Rendus de l'Académie des Sciences de Paris D-263, 1685-1688

CAVET, P., LARDEUX, H. & PHILIPPOT, A. (1971). Ordovicien et Silurien aux environs de Montjean et Chalonnes (Maine-et-Loire, Sud-Est du Massif armoricain). Mémoires du Bureau de Recherches Géologiques et Minières 73, 199-212

CHÁB, J. & VRÁNA, S. (1979). Crossite-actinolite amphiboles of the Krkonoše-Jizera crystalline complex and their geological significance. Věštník Ústředního ústavu geologického, Bulletin of the Geological Survey of Prague 54, 143-150

CHAKRABORTY, S. & GANGULY, J. (1991). Compositional zoning and cation diffusion in aluminosilicate garnets. In: Ganguly, J. (ed). Diffusion, atomic ordering and mass transport: selected problems in geochemistry. Springer-Verlag, New York, 120-170

CHANTRAINE, J., AUVRAY, B., BRUN, J.P., CHAUVEL, J.J. & RABU, D. (1994=. The Cadomian Orogeny in the Armorican Massif. Introduction. In: Keppie, J.D. (ed). Pre-Mesozoic Geology in France and related áreas. Springer-Verlag, Berlin, 75-80

CHEMENDA, A.I., MATTAUER, M., MALAVIEILLE, J. & BOKUN, A.N. (1995). A mechanism for syn-collisional deep rock exhumation and associated normal faulting: results from physical modeling. Earth and Planetary Science Letters 132, 225-232

CHERNOFF, C.B. & CARLSON, W.D. (1997). Disequilibrium for Ca during growth of pelitic garnet. Journal of Metamorphic Geology 15(4), 421-438

CHOPIN, C. (1981). Talc-phengite: a widespread assemblage in high-grade pelitic blueschists of the Western Alps. Journal of Petrology 22, 628-650

CHOPIN C. (1984): Coesite and pure pyrope in high-grade blueschists of the western Alps: a first record and some consequences. Contributions to Mineralogy and Petrology 86, 107-118

CHOPIN, C. (2003). Ultrahigh-pressure metamorphism: tracing continental crust into the mantle. Earth and Planetary Science Letters 212, 1-14

CHOUBERT, B. (1935). Recherches sur la genèse des chaînes paléozoiques et antecambriennes. Revue de Géographie Physique et Géologie Dynamique 8, 1-50

CLARK, A.H., ARCHIBALD, D.A., LEE, A.W., FARRAR, E. & HODGSON, C.J. (1998). Laser Probe $^{40}Ar/^{39}Ar$ ages of early- and Late-stage alteration assemblages, Rosario porphyry copper-molybdenum deposit, Collahuasi District, I Region, Chile. Economic Geology 93, 326-337.

CLARKE, G. L., AITCHISON, J. C. & CLUZEL, D. (1997). Eclogites and blueschists of the Pam Peninsula, NE New Caledonia: a reappraisal. Journal of Petrology 38, 843-876

CLARKE, G. L., DACZKO, N. R. & NOCKOLDS, C. (2001). A method for applying matrix corrections to X-ray intensity maps using the Bence-Albee algorithm and Matlab. Journal of Metamorphic Geology 19, 635-644

CLARKE, G.L., POWELL, R. & FITZHERBERT, J.A. (2006) The lawsonite paradox: a comparison of field evidence and mineral equilibria modelling. Journal of Metamorphic Geology 24, 715-725

CLOOS, M. (1982). Flow melanges: Numerical modeling and geologic constraints on their origin in the Franciscan subduction complex, California. Geological Society of America Bulletin 93, 330-344

CLOOS, M. (1985). Thermal evolution of convergent plate-margins: Thermal modelling and re-evaluation of isotopic Ar-ages for blueschists in the Franciscan complex of California. Tectonics 4, 421-433

COGGON, R. & HOLLAND, T. J. B. (2002). Mixing properties of phengitic micas and revised garnet-phengite thermobarometers. Journal of Metamorphic Geology 20, 683–696

COGNÉ , J., JEANNETTE, D. & RUHLAND, M. (1966). L'Ile de Groix: étude structurale d'une série métamorphique à glaucophane en Bretagne méridionale. Bulletin du Service de la Carte Géologique d'Alsace–Lorraine, 19, 41–95

COGNÉ, J. (1967). Zones stables et zones mobiles au cours de l'orogènese hercynienne dans le massif Armoricain. In: Contribution de la carte gravimétrique de la géologie du Massif Armoricain. Mémoires du Bureau de Recherches Géologiques et Minières 52, 15–23

COGNÉ, J. (1974). Le Massif Armoricain. In: Debelmas, J. (ed). Géologie de la France. Doin, Paris, France 1, 105–161

COKE, C. & RIBEIRO, A. (2000). Malpica–Lamego shear zone; A major crustal discontinuity in the Iberian Variscan fold belt, Program and Abstracts – International Conference on Basement Tectonics 15, 208–210

COLEMAN, R.G. & LEE, D.G. (1963). Glaucophane–bearing metamorphic rock types of the Cazadero area, California. Journal of Petrology 4, 260– 301

COLEMAN, R.G. (1972). Blueschist metamorphism and plate tectonics: 24th International Geological Congress, section 2, 19–26

COLL.E, A.L.G. (1964). The geology of the coastal section from Cabo de S. Adrian to Playa de Baldayo (Galicia). Leidse Geologische Mededelingen 30, 121–130

COLLEMAN, R.G., TATSUMOTO, M. COLES, D.G. HEDGE, C.E., & MAYS, M.E. (1974). Red Sea Basalts. EOS Transactions of the American Geophysical Union 54, 1001–1002

COMODI P. & ZANAZZI P. F. (1996). Effects of temperature and pressure on the structure of lawsonite, Piazza University, Perugia, Italy. American Mineralogist 81, 833–841

COMPAGNONI, R. & MAFFEO, B. (1973). Jadeite–bearing metagranite l.s. and related rocks in the Monte Mucrone area (Sesia Lanzo zone, Western Italian Alps). Schweizer Mineralogische und Petrographische Mitteilungen 53, 355–377

CONEY, P.J., JONES, D.L., & MONGER, J.W.H. (1980). Cordilleran suspect terranes: Nature 288, 329–333

CONNELLY, W. (1978). The Uyak Complex, Kodiak Islands, Alaska: A Cretaceous subduction complex: Geological Society of America Bulletin 89, 755–769

CONNOLLY, J.A.D. & KERRICK, D.M. (1987). An algorithm and computer program for calculating composition phase diagrams. Calphad–computer Coupling of Phase Diagrams and Thermochemistry (CALPHAD) 11, 1–55

CONNOLLY, J.A.D. (1990). Multivariable phase diagrams; an algorithm based on generalized thermodynamics. American Journal of Sciences 290, 666–718

CONNOLLY, J.A.D. (2005). Computation of phase equilibria by linear programming: a tool for geodynamic modeling and its application to subduction zone decarbonation. Earth and Planetary Science Letters 236, 524–541

COOMBS, D.S. (1960). Lawsonite metagraywackes in New Zealand. American Mineralogist 45, 454–455

COOMBS, D.S. (1972) Progressive metamorphism from prehnite–pumpellyite to greenschist facies in the Dansy Pass area, Otago, New Zealand. Geological Society of America Bulletin 83, 3177–3198

CORNEN, G. (1999). Occurrence of HP relics in the manganese–ore of Groix island (South Brittany, France). European Union of Geosciences Meeting X. Journal of Conference Abstracts 4, 475

CORONA, J. C., JENKINS, D. M., & HOLLAND, T. J. B. (2013) Constraints on the upper pressure stability of blueschist facies metamorphism along the reaction: glaucophane = talc + 2 jadeite in the Na_2O–MgO–Al_2O_3–SiO_2–H_2O system. American Journal of Science (in revision for publication)

CRAWFORD, W. A. & FYFE, W. S. (1965). Lawsonite equilibria. American Journal of Science 263, 262–270

CUNEY, M., STUSSI, J.M., BROUAND, M., DAUTEL, D., MICHARD, A., GROS, Y., PONCET, D., BOUTON, P., COLCHEN, M. & VERVIALLE, J.P. (1993). Géochimie et géochronologie UPb des diorites quartziques du Tallud et de Montcoutant: nouveaux arguments pour une extension de la «Ligne Tonalitique Limousine» en Vendée. Comptes–rendus de l'Académie des Sciences de Paris II–316, 1383–1390

CYMERMAN, Z., PIASECKI, M. A. J. & SESTON, R. (1997). Terranes and terrane boundaries in the Sudetes, Northeast Bohemian Massif. Geological Magazine 134, 717–725

DALLMEYER, R.D. & TUCKER, R.D. (1993). UPb zircon age for the Lagoa augen gneiss, Morais Complex, Portugal: tectonic implications. Journal of the Geological Society of London150, 405–410

DALLMEYER, R.D., MARTÍNEZ CATALÁN, J.R., ARENAS, R., GIL IBARGUCHI, J.I., GUTIÉRREZ ALONSO, G., FARIAS, P., ALLER, J. & BASTIDA, F. (1997). Diachronous Variscan tectonothermal activity in the NW Iberian Massif: Evidence from 40Ar/39Ar dating of regional fabrics. Tectonophysics 277, 307–337

DALLMEYER, R.D., RIBEIRO, A. & MARQUES, F. (1991). Polyphase Variscan emplacement of exotic terranes (Morais and Bragança Massifs) onto Iberian successions: Evidence from 40Ar/39Ar mineral ages. Lithos 27, 133–144

DANA, J.D. (1849). Geology, in Wilkes, C., United States Exploring Expedition, 10: Philadelphia (C. Sherman), with Atlas: New York, Putnam.

DAVIS, P.B. & WHITNEY, D.L. (2006). Petrogenesis of lawsonite and epidote eclogite and blueschist, Sivrihisar Massif, Turkey. Journal of Metamorphic Geology 24, 823–849

DE CAPITANI C. & BROWN T.H. (1987): The computation of chemical equilibrium in complex systems containing non–ideal solutions. Geochimica et Cosmochimica Acta 52, 639–2652

DE POULPIQUET, J. (1988). Etude magnétique et sismique du massif basique et ultrabasique de la Baie d'Audierne (Massif armoricain). Géologie de la France 1988–4, 11–22

DE ROEVER, W. P. (1955a). Genesis of jadeite by low–grade metamorphism. American Journal of Science 253, 283–98

DE ROEVER, W.P. & BEUNK, F.F. (1976). Blue Amphibole–Albite–Chlorite Assemblages from Fuscaldo (S Italy) and the Role of Glaucophane in Metamorphism. Contributions to Mineralogy and Petrology 58, 221–234

DE ROEVER, W.P. (1955b). Some remarks concerning the origin of glaucophane in the North Berkeley Hills, California. American Journal of Science 253, 240–244

DE ROEVER, W.P. (1956). Some differences between post-Paleozoic and older regional metamorphism. Netherlands Journal of Geosciences - Geologie en Mijnbouw 18, 123–127

DE ROEVER, W.P. (1972b). Glaucophane problems. Schweizer Mineralogische und Petrographische Mitteilungen 18, 64–75

DEER, W. A., HOWIE, R. A. & ZUSSMAN, J. (1992). An Introduction to the Rock–Forming Minerals. Prentice Hall, London.

DELANOË Y., GALENNE B., LASNIER B. & PINOT J.P. (1972). Découverte par carottage sous–marin d'une association pétrographique de micaschistes à chloritoïde et de schistes à glaucophane autour de la Baz

Moullek, à 11 km au SE de l'Ile de Groix (Morbihan). Comptes-rendus de l'Académie des Sciences de Paris 274, 644-646

DELFOUR J. (1989). Données lithostratigraphiques et géochimiques sur le Dévono-Dinantien de la partie sud du faisceau du Morvan (nord-est du Massif central français). Géologie de la France 4, 49-77

DEN TEX, E. & FLOOR, P. (1967). A blastomylonitic and polymetamorphic "graben" in western Galicia (NW Spain). In: "Etages Tectoniques", La Bacconière, Neuchatel, 169-178

DEN TEX, E. (1981a). Basement evolution in the northern Hesperian Massif: A preliminary survey of results obtained by the Leiden Research Group. Leidse Geologische Mededelingen 52, 1-21

DEN TEX, E. (1981b). A geological section across the Hesperian Massif in western and central Galicia. Geologie Mijnbouw 60, 33-40

DESMONS, J. & SMULIKOWSKI, W. (2007). High P/T metamorphic rocks. Recommendations by the IUGS Subcommission on the Systematics of Metamorphic Rocks: Web version of 01.02.07, http://www.bgs.ac.uk/scmr/home.html. SCMR website (www.bgs.ac.uk/SCMRH)

DESMONS, J., SMULIKOWSKI, W. & SCHMID, R. (1997). High-P/T rock terms: Definitions proposed by SCMR. 4th International Eclogite Conference, Ascona.

DESMONS, J., SMULIKOWSKI, W. & SCHMID, R. (2001). High-P/T rock terms: definitions proposed by SCMR. Mineralogical Society of Poland – Special papers 19, 36-38

DEWEY, J. F., RYAN, P. D. & ANDERSEN, T. B. (1993). Orogenic uplift and collapse, crustal thickness, fabrics and metamorphic phase changes: the role of eclogites. Geological Society of London, Special Publication 76, 325-343

DEWEY, J.F. & BIRD, J.M. (1970). Mountain belts and new global tectonics. Journal of Geophysical Research 75, 2625-2685

DIAS DA SILVA, Í. (2013). Geología de las Zonas Centro Ibérica y Galicia-Trás-osMontes en la parte oriental del Complejo de Morais, Portugal/España. Unpublished PhD thesis, Universidad de Salamanca, 424 p.

DIAS DA SILVA, Í., VALVERDE-VAQUERO, P., GONZÁLEZ CLAVIJO, E., DÍEZ MONTES. A. & MARTÍNEZ CATALÁN, J.R. (2012). Structural and stratigraphical significance of UPb ages from the Saldanha and Mora volcanic complexes (NE Portugal, Iberian Variscides). In: Length scales, times scales and relative contribution of Variscan orogenic events to formation of European crust. Géologie de la France 2012-1, 105-106

DÍAZ GARC.A, F., ARENAS, R., MARTÍNEZ CATALÁN, J.R., GONZÁLEZ DEL TANAGO, J. y DUNNING, G. (1999). Tectonic evolution of the Care.n ophiolite (Northwest Spain): a remnant of oceanic lithosphere in the Variscan belt. Journal of Geology 107, 587-605

DÍAZ GARCÍA, F. (1990). La geología del sector occidental del Complejo de Ordenes (Cordillera Hercínica, NW de España). Nova Terra 3, A Coruña. 230 p.

DÍAZ GARCÍA, F., ARENAS, R., MARTÍNEZ CATALÁN, J.R., GONZÁLEZ DEL TÁNAGO, J. & DUNNING, G. (1999). Tectonic evolution of the Careón ophiolite (Northwest Spain): a remnant of oceanic lithosphere in the Variscan belt. Journal of Geology 107, 587-605

DÍAZ GARCÍA, F., SÁNCHEZ MARTÍNEZ, S., CASTIÑEIRAS P., FUENLABRADA J.M. & ARENAS, R. (2010). A peri-Gondwanan arc in NW Iberia. II: Assessment of the intra-arc tectonothermal evolution through U-Pb SHRIMP dating of mafic dykes. Gondwana Research 17, 352-362

DIENER, J. F. A., POWELL, R., WHITE, R. W. & HOLLAND, T. J. B. (2007). A new thermodynamic model for clino- and orthoamphiboles in the system Na_2O-CaO-FeO-MgO-Al_2O_3-SiO_2-H_2O-O. Journal of Metamorphic Geology 25, 631-656

DIENER, J.F.A. & POWELL, R. (2010). Influence of ferric iron on the stability of mineral assemblages. Journal of Metamorphic Geology 28, 599–613

DIENER, J.F.A. & POWELL, R. (2012). Revised activity–composition models for clinopyroxene and amphibole. Journal of Metamorphic Geology 30, 131–142

DIENER, J.F.A., POWELL, R. & WHITE, R.W. (2008). Quantitative phase petrology of cordierite–orthoamphibole gneisses and related rocks. Journal of Metamorphic Geology 26, 795–814

DÍEZ FERNÁDEZ, R., MARTÍNEZ CATALÁN, J. R., ARENAS, R. & ABATI, J. (2011). Tectonic evolution of a continental subduction–exhumation channel: Variscan structure of the basal allochthonous units in NW Spain. Tectonics 30: TC3009

DÍEZ FERNÁNDEZ, R. & MARTÍNEZ CATALÁN, J. R. (2009). 3D Analysis of an Ordovician igneous ensemble: A complex magmatic structure hidden in a polydeformed allochthonous Variscan unit. Journal of Structural Geology 31, 222–236

DÍEZ FERNÁNDEZ, R. & MARTÍNEZ CATALÁN, J.R. (2012). Stretching lineations in high–pressure belts: the fingerprint of subduction and subsequent events (Malpica–Tui Complex, NW Iberia). Journal of the Geological Society of London 169, 531–543

DÍEZ FERNÁNDEZ, R. (2011). Evolución estructural y cinemática de una corteza continental subducida: la Unidad de Malpica–Tui (NO del Macizo Ibérico). Nova Terra 40, A Coruña.

DÍEZ FERNÁNDEZ, R., CASTIÑEIRAS, P. & GÓMEZ–BARREIRO, J. (2012). Age constraints on Lower Paleozoic convection system: Magmatic events in the NW Iberian Gondwana margin. Gondwana Research 21, 1066–1079 [reference cited in Chapter 4 as Díez Fernández *et al.*, 2012c]

DÍEZ FERNÁNDEZ, R., MARTÍNEZ CATALÁN, J. R., ARENAS, R. & ABATI, J. (2012a). The onset of the assembly of Pangaea in NW Iberia: Constraints on the kinematics of continental subduction. Gondwana Research 22, 20–25 [reference cited in Chapter 4 as Díez Fernández *et al.*, 2012b]

DÍEZ FERNÁNDEZ, R., MARTÍNEZ CATALÁN, J.R., ARENAS, R., ABATI, J., GERDES, A. & FERNÁNDEZ SUÁREZ, J. (2012c). U–Pb detrital zircon analysis of the lower allochthon of NW Iberia: age constrains, provenance and links with the Variscan mobile belt and Gondwanan cratons. Journal of the Geological Society 169, 655–665 [reference cited in Chapter 4 as Díez Fernández *et al.*, 2012d]

DÍEZ FERNÁNDEZ, R., MARTÍNEZ CATALÁN, J.R., GERDES, A., ABATI, J., ARENAS, R., & FERNÁNDEZ–SUÁREZ, J. (2010). U–Pb ages of detrital zircons from the Basal allochthonous units of NW Iberia: Provenance and paleoposition on the northern margin of Gondwana during the Neoproterozoic and Paleozoic. Gondwana Research 18, 385–399

DÍEZ FERNÁNDEZ, R., MARTÍNEZ CATALÁN, J.R., GÓMEZ BARREIRO, J. & ARENAS, R. (2012b). Extensional flow during gravitational collapse: a tool for setting plate convergence (Padrón migmatitic dome, Variscan belt, NW Iberia). Journal of Geology 120, 83–103

DÍEZ MONTES, A., MARTÍNEZ CATALÁN, J.R. & BELLIDO MULAS, F. (2010). Role of the Ollo de Sapo massive felsic volcanism of NW Iberia in the Early Ordovician dynamics of northern Gondwana. Gondwana Research 17, 363–376

DIOT H., FEMENIAS, O., MOREAU, C., GAUFRIAU A., ROY C. & KARNAY, G. (2007). Notice explicative de la carte géologique de France au 1:50000, feuille Fontenay–le–Conte (586). BRGM, Orléans, 96 p.

DIPPLE, G.M. & FERRY, J.M. (1992). Fluid flow and stable isotopic alteration in rocks at elevated temperatures with applications to metamorphism. Geochimica et Cosmochimica Acta 56, 3539–3550

DIXON, J. E. (1968). The metamorphic rocks of Syros, Greece. Unpublished PhD thesis, Cambridge University

DOBRETSOV, N. L., SOBOLEV, V. S., SOBOLEV, N. V. & KHLESTOV, V. V. (1974). The Facies of Regional Metamorphism at High Pressure. Moscow, 328 p. (English translation by D.A. Brown, 1975, ANU Press, Camberra)

DODSON, M.H. (1973). Closure temperature in geochronological and petrological systems. Contributions to Mineralogy and Petrology 40, 259-274

DROOP, G.T.R. (1987). A general equation for estimating Fe^{3+} in ferromagnesian silicates and oxides from microprobe analysis, using stoichiometric criteria. Mineralogical Magazine 51, 431-437

DU TOIT, A.L. (1937). Our Wandering Continents. Edinburgh, Oliver and Boyd, 366 p.

DUCASSOU, C. (2010). Age et origine des premiers reliefs de la chaîne varisque: Le Dévono-Carbonifère du Bassin d'Ancenis. Mémoires de Géosciences Rennes135, 513 p.

DUCASSOU, C., BALLÈVRE, M., LARDEUX, H. & ROBIN, C. (2011a). Evidence for pre-orogenic, Early Devonian rifting in the Variscan belt: stratigraphy and structure of the Palaeozoic cover of the Mauges Unit (Upper Allochthon, Armorican massif, France). International Journal of Earth Sciences 100, 1451-1476

DUCASSOU, C., POUJOL, M., HALLOT, E., BRUGUIER, O. & BALLÈVRE, M. (2011b). Petrology and geochronology of the high-K calc-alkaline Mésanger magmatism (Armorican Massif, France): a ca. 320 Ma old volcanoPlutonic association. Bulletin de la Société Géologique de France 182, 467-477

DUCASSOU, C., STRULLU-DERRIEN, C., BALLÈVRE, M., DABARD, M.P., GERRIENNE, P., LARDEUX, H. & ROBIN, C. (2009). Age and depositional environment of the Sainte-Anne Formation (Armorican Massif, France): the oldest (Emsian) evidence for mountain erosion in the Variscan belt. Bulletin de la Société Géologique de France 180, 529-544

DUCHÊNE, S., LARDEAUX, J.M. & ALBARÈDE, F. (1997) Exhumation of eclogites: insights from depth-time path analysis. Tectonophysics 280, 125-140

DUDEK, K. & KIÉNAST J.R. (1989). Deerite from ile de Groix, Brittany, France. Mineralogical Magazine 53, 603-612

DUFFY, T. S. (2008). Some recent advances in understanding the mineralogy of Earth's deep mantle. Philosophical Transactions of the Royal Society of London. Series A. Mathematical, Physical and Engineering Sciences 366, 4273-4293

DUMOULIN, J.A. (1988). Sandstone petrographic evidence and the Chugach-Prince William terrane boundary in sothern Alask. Geology 16, 456-460

EGUÍLUZ, L., GIL IBARGUCHI, J.I., ABALOS, B. & APRAIZ, A. (2000). Superposed Hercynian and Cadomian orogenic cycles in the OssaMorena zone and related areas of the Iberian Massif. Geological Society of America Bulletin 112, 1398-1413

EL KORH, A., SCHMIDT, S.T., BALLÈVRE, M., ULIANOV, A. & BRUGUIER, O. (2012). Discovery of an albite gneiss from the Ile de Groix (Armorican Massif, France): geochemistry and LA-ICP-MS U-Pb geochronology of its Ordovician protolith. International Journal of Earth Sciences 101, 1169-1190

EL KORH, A., SCHMIDT, S.T., ULIANOV, A. & POTEL S. (2009). Trace element partitioning in HP-LT metamorphic assemblages during subduction-related metamorphism, Ile de Groix, France: a detailed LA-ICPMS study. Journal of Petrology 50, 1107-1148

EL KORH, A., SCHMIDT, S.T., VENNEMANN, T. & BALLÈVRE, M. (2013). Trace element and isotopic fingerprints in HP-LT metamorphic rocks as a result of fluid-rock interactions (Ile de Groix, France). Gondwana Research 23, 880-900

ELLENBERGER, F. (1960). Sur une paragenèse éphémère à lawsonite et glaucophane dans le métamorphisme alpin de Haute-Maurienne (Savoie). Bulletin de la Société Géologique de France 7, 190-194

EL-SHAZLY, A. K. & LIOU, J. G. (1991). Glaucophane chloritoid-bearing assemblages from NE Oman: petrologic significance and a petrogenetic grid for high P metapelites. Contributions to Mineralogy and Petrology 107, 180-201

ENAMI, M., SUZUKI, K., LIOU, J.G., & BIRD, D.K. (1993). Al-Fe^{3+} and F-OH substitutions in titanite and constraints on their P-T dependence. European Journal of Mineralogy 5, 219-231.

ENGLAND, P.C. & THOMPSON, A.B. (1984). Pressure-temperaturetime paths of regional metamorphism. Heat transfer during the evolution of regions of thickened continental crust. Journal of Petrology 25, 894-928.

ENGLAND, P.C. (1987). Diffuse continental deformation: length scales. Rates and metamorphic evolution. Philosophical Transactions of the Royal Society of London A 321, 3-22

ENGVIK, A.K., AUSTRHEIM, H. & ANDERSEN, T.B. (2000). Structural, mineralogical and petrophysical effects on deep crustal rocks of fluid limited polymetamorphism, Western Gneiss Region, Norway. Journal of the Geological Society London 157, 121-134

ERNST, W.G. (1961). Stability relations of glaucophane. American Journal of Science 259,735-65

ERNST, W.G. (1963). Petrogenesis of glaucophane schist. Journal of Petrology 4, 1-30

ERNST, W.G. (1971). Metamorphic zonations on presumably subducted lithospheric plates from Japan, California and the Alps. Contributions to Mineralogy and Petrology 34, 43-59

ERNST, W.G. (1972). Possible Permian oceanic crust and plate junction in central Shikoku: Tectonophysics 15, 233-239

ERNST, W.G. (1973). Blueschists Metamorphism and P-T Regimes in Active Subduction Zones. Tectonophysics 17, 255-272

ERNST, W.G. (1988). Tectonic history of subduction zones inferred from retrograde blueschist P-T paths. Geology, 16, 1081-1084

ERNST, W.G. (1999). Hornblende, the continent maker-evolution of H_2O during circum-Pacific subduction versus continental collision. Geology 27, 675-678

ERNST, W.G. (2001). Subduction, ultrahigh-pressure metamorphism, and regurgitation of buoyant crustal slices-implications for arcs and continental growth. Physics of the Earth and Planetary Interiors 127, 253-275

ERNST, W.G. (2010). Subduction-zone metamorphism, calc-alkaline magmatism, and convergent- margin crustal evolution. Gondwana Research 18, 8-16

ERNST, W.G., MARUYAMA, S. & WALLIS, S. (1997). Buoyancy-driven, rapid exhumation of ultrahigh-pressure metamorphosed continental crust. Proceedings of the National Academy of Sciences 94, 9532-9537

ESKOLA, P. (1920). The mineral facies of rocks. Norsk Geol. Tidsskr. 6, 143-94

ESKOLA, P. (1922). On contact phenomena between gneiss and limestone in western Massachusetts. The Journal of Geology. 30, 265-94

ESKOLA, P. (1929). Om Mineralfacies. Geol. Fören. Stockholm, Förh. 51, 157-71

ESKOLA, P. (1939). Die Entstehung der Gesteine (Barth-Correns, Eskola), Berlin

ESSENE, E. J., FYFE, W.S. (1967). Omphacite in Californian metamorphic rocks. Contributions to Mineralogy and Petrology 15, 1–23

ESSENE, E.J. (1982). Geologic thermometry and barometry. In: Ferry, J.M. (ed). Characterization of Metamorphism Through Mineral Equilibria. Reviews in Mineralogy,Mineralogical Society of America, Washington, 153–206

ESSENE, E.J. (1989). The current status of thermobarometry in metamorphic rocks. Geological Society, London, Special Publications, 43, 1–44

EVANS, B. W. (1990). Phase relations of epidote–blueschists. Lithos 25, 3–23

EVANS, T. P. (2004a). A method for calculating effective bulk composition modification due to crystal fractionation in garnet–bearing schist: implications for isopleth thermobarometry. Journal of Metamorphic Geology 22, 547–557

EVANS, T. P. (2004b). Reconciling the structural and metamorphic record of orogeny in central western New Hampshire through microstructure and garnet isopleth thermobarometry. Unpublished PhD Thesis, James Cook University, 89 p.

FARIAS, P. & MARCOS, A. (2004). Dominio Esquistoso de Galicia–Trás–osMontes. In: Vera, J.A. (ed). Geología de España, Sociedad Geológica de España–Instituto Geológico y Minero de España (SGE-IGME), Chapter 2, 135–138

FARIAS, P., GALLASTEGUI, G., GONZÁLEZ LODEIRO, F., MARQUÍNEZ, J., MARTÍN–PARRA, L.M., MARTÏNEZ CATALÁN, J.R., DE PABLO MACIÁ, J.G. & RODRÍGUEZ–FERNÁNDEZ, L.R. (1987). Aportaciones al conocimiento de la litoestratigraf.a y estructura de Galicia Central. Mem.rias da Faculdade de Ciencias, Museu e Laborat.rio Mineral.gico e Geol.gico, Universidade do Porto 1, 411–431

FARYAD, S. W. & KACHLÍK, V. (2013). New evidence of blueschist facies rocks and their geotectonic implication for Variscan suture(s) in the Bohemian Massif. Journal of Metamorphic Geology 31, 63–82

FAURE M., BE MÉZÈME E., DUGUET M., CARTIER C. & TALBOT, J.Y. (2005). Paleozoic tectonic evolution of medio–Europa from the example of the French Massif Central and Massif Armoricain. In: Carosi R., Dias R., Lacopini D. & Rosenbaum G. (eds). The southern Variscan belt, Journal of the Virtual Explorer, Electronic Edition, Volume 19, Paper 5, 1441–8142

FAURE M., MEZEME E.B., COCHERIE A., ROSSI P., CHEMENDA A. & BOUTELIER D. (2008). Devonian geodynamic evolution of the Variscan Belt, insights from the French Massif Central and Massif Armoricain. Tectonics 27: TC2005

FELIX, C. (1972). Etude structuro–minéralogique des pseudomorphes de présumée Lawsonite des glaucophanoschistes de Ile de Groix (Bretagne–France): considération sur la possibilité d'une paragénèse à Glaucophane–Lawsonite. Annales de la Socié té Geologique de Belgique 95, 345–391

FERNÁNDEZ–SUÁREZ, J., ARENAS, R., ABATI, J., MARTÍNEZ CATALÁN, J. R., WHITEHOUSE, M. J. AND JEFFRIES, T. (2007). U–Pb Chronometry of polimetamorphic high–pressure granulites: An example from the allochthonous terranes of the NW Iberian Variscan belt. In: 4–D framework of continental crust (eds). Hatcher, R. D. J., Carlson, M. P., McBride, J. H. and Martínez Catalán, J. R.), 469–488, The Geological Society of America Memoir.

FERNÁNDEZ–SUÁREZ, J., CORFU, F., ARENAS, R., MARCOS, A., MARTÍNEZ CATALÁN, J.R., DÍAZ GARCÍA, F., ABATI, J. & FERNÁNDEZ, F.J. (2002). UPb evidence for a polyorogenic evolution of the HP–HT units of the NW Iberian Massif. Contributions to Mineralogy and Petrology 143, 236–253

FERNÁNDEZ–SUÁREZ, J., DÍAZ GARCÍA, F., JEFFRIES T.E., ARENAS, R. & ABATI, J. (2003). Constraints on the provenance of the uppermost allochthonous terrane of the NW Iberian Massif: Inferences from detrital zircon UPb ages. Terra Nova 15,138–144

FERNÁNDEZ-SUÁREZ, J., GUTIÉRREZ-ALONSO, G., JENNER, G.A. & JACKSON, S.E. (1998). Geochronology and geochemistry of the Pola de Allande granitoids (northern Spain). Their bearing on the Cadomian/Avalonian evolution of NW Iberia. Canadian Journal of Earth Sciences 35, 1439-1453

FERRY, J.M. (1982). Characterization of Metamorphism through Mineral Equilibria. Reviews in Mineralogy 10. The Mineralogical Society of America. 397 p.

FITZHERBERT, J.A., CLARKE, G.L. & POWELL, R. (2003). Lawsonite-omphacite-bearing metabasites of the Pam Peninsula, NE New Caledonia: Evidence for disrupted blueschist-to eclogite-facies conditions. Journal of Petrology 44, 1805-1831

FLOOR, P. (1966). Petrology of an aegirine-ribeckite gneiss-bearing part of the Hesperian Massif: The Galiñeiro and surrounding areas, Vigo, Spain. Leidse Geologische Mededelingen 36, 1-204

FORBES, R. B., EVANS, B. W. & THURSTON, S. P. (1984). Regional progessive high-pressure metamorphism, Seward Peninsula, Alaska. Journal of Metamorphic Geology 2, 43-54

FORNERIS, J. & HOLLOWAY, J. (2004). Evolution of mineral compositions during eclogitization of subducting basaltic crust. American Mineralogist 89, 1516-1524

FRANZ, G. & SPEAR, F.S. (1985). Aluminious titanite (sphene) from the Eclogite zone, south-central Tauern Window, Austria. Chemical Geology 50, 33-46

FREY, M., DE CAPITANI, C. & LIOU, J.G. (1991) A new petrogenetic grid for low-grade metabasites. Journal of Metamorphic Geology 9, 497-509

FROST, B.R. & TRACY, R.J. (1991). P-T paths from zoned garnets: Some minimum criteria. American Journal of Science 291, 917-939

FRYER, P. & G. J. FRYER (1987). Origins of non-volcanic seamounts in forearc environments. In: Keating et al. (eds). Seamount Islands and Atolls. AGU Monograph Series 43, 61-69

FUENLABRADA, J. M., ARENAS, R., DÍEZ FERNÁNDEZ, R., SÁNCHEZ MARTÍNEZ, S., ABATI, J. & LÓPEZ-CARMONA, A. (2012). Sm/Nd isotope geochemistry and tectonic setting of the metasedimentary rocks from the basal allochthonous units of NW Iberia (Variscan suture, Galicia). Lithos 148, 196-208

FUENLABRADA, J.M., ARENAS, R., SÁNCHEZ MARTÍNEZ, S., DÍAZ GARCÍA, F. & CASTIÑEIRAS, P. (2010). A peri-Gondwanan arc in NW Iberia. I: isotopic and geochemical constraints to the origin of the arc -the sedimentary approach. Gondwana Research 17, 338-351

FYFE, W.S. & TURNER, F.J. (1966). Reappraisal of the metamorphic facies concept. Contributions to Mineralogy and Petrology 12, 354-364

FYFE, W.S., TURNER, F. J. & VERHOOGEN, J. (1958). Metamorphic reactions and metamorphic facies. The Geological Society of America. Memoir 73

GALÁN, G. & MARCOS, A. (1997). Geochemical evolution of highPressure mafic granulites from the Bacariza formation (Cabo Ortegal complex, NW Spain): an example of a heterogeneous lower crust. Geologische Rundschau 86, 539-355

GALLASTEGUI, G. (1993). Petrología del macizo granodiorítico de Baio-Vigo (Pontevedra, España). Unpublished PhD thesis, Universidad de Oviedo. 356 p.

GARCÍA-CASCO, A. & TORRES ROLDAN, R.L. (1996). Disequilibrium induced by fast decompression in St-Bt-Grt-Ky-Sil-And metapelites from the Betic Belt (Southern Spain). Journal of Petrology 37, 1207-1239

GARCÍA-CASCO, A. (2007). Magmatic paragonite in trondhjemites from the Sierra del Convento melange, Cuba. American Mineralogist 92, 1232-237

GARCÍA-CASCO, A., LÁZARO, C., ROJAS-AGRAMONTE, Y., KRÖNER, A., TORRES ROLDÁN, R. L., NUÑEZ, K., MILLÁN, G., NEUBAURER, F. & QUINTERO, I. (2008). Partial melting and counterclockwise P-T path of subducted oceanic crust (Sierra del Convento, E Cuba). Journal of Petrology 49, 129-161

GARCÍA-CASCO, A., TORRES ROLDAN, R.L., ITURRALDE-VINENT, M.A., MILLÁN, G. NÚÑEZ CAMBRA, K., LÁZARO, C. & RODRÍGUEZ VEGA, A. (2006). High pressure metamorphism of ophiolites in Cuba. Geologica Acta 4, 63-88

GERRIENNE, P., GENSEL, P.G., STRULLU-DERRIEN, C., LARDEUX, H., STEEMANS, P. & PRESTIANNI, C. (2011). A simple type of wood in two Early Devonian plants. Science 333, 837 p.

GERYA, T.V. & STÖCKHERT, B. (2006). Two-dimensional numerical modeling of tectonic and metamorphic histories at active continental margins. International Journal of Earth Sciences 95, 250-274

GERYA, T.V., STÖCKHERT, B. & PERCHUK, A.L. (2002). Exhumation of high-pressure metamorphic rocks in a subduction channel -a numerical simulation. Tectonics 21, 6-1-6-19

GHENT, E. D. (1965). Glaucophane-schist facies metamorphism in the Black Butte area, northern Coast Ranges, California. American Journal of Science, 263-400

GIL IBARGUCHI, J.I. & DALLMEYER. R.D. (1991). Hercynian blueschist metamorphism in North Portugal: tectonotherrnal implications. Journal of Metamorphic Geology 9, 539-549

GIL IBARGUCHI, J.I. & ORTEGA GIRONÉS, E. (1985). Petrology, structure and geotectonic implications of glaucophane-bearing eclogites and related rocks fromthe Malpica-Tuy unit, Galicia, northwest Spain. Chemical Geology 50, 145-162

GIL IBARGUCHI, J.I. (1995). Petrology of jadeite-Metagranite and associated orthogneiss from the Malpica-Tuy allochthon (Northwest Spain). European Journal of Mineralogy 7, 403-415

GIL IBARGUCHI, J.I., ABALOS, B., AZCÁRRAGA, J. & PUELLES, P. (1999). Deformation, high-pressure metamorphism and exhumation of ultramafic rocks in a deep subduction/collision setting (Cabo Ortegal, NW Spain). Journal of Metamorphic Geology 17, 747-764

GIL IBARGUCHI, J.I., MENDIA, M., GIRARDEAU, J. & PEUCAT, J.J. (1990). Petrology of eclogites and clinopyroxene-garnet metabasites from the Cabo Ortegal Complex (northwestern Spain). Lithos 25, 133-162

GILBERT, M.C. & POPP, R.K. (1973). Properties and stability of glaucophane at high pressure. Eos, Transactions American Geophysical Union 54, p. 1223

GILBERT, S.A., CASEY, J.F., BRADLEY, D. & KUSKY, T.M. (1992). Geochemistry of siliciclastic rocks in the Peninsular, Chugach, and Prince William Terranes: Implications for the tectonic evolution of south central Alaska. Geological Society of America, Abstracts with Programs 24 (7), p. A305

GILLET, P., REYNARD, B. & TEQUI, C. (1989). Thermodynamic properties of glaucophane; new data from calorimetric and spectroscopic measurements. Physics and Chemistry of Minerals 16, 659-667

GIRARDEAU, J. & GIL IBARGUCHI, J.I. (1991). Pyroxenite-rich peridotites of the Cabo Ortegal Complex (Northwestern Spain): Evidence for large-scale upper mantle heterogeneity. Journal of Petrology 32, 135-154

GLEISSNER, P., GLODNY, J. & FRANZ, G. (2007). Rb-Sr isotopic dating of pseudomorphs after lawsonite in metabasalts from the Glockner nappe, Tauern Window, Eastern Alps. European Journal of Mineralogy 19, 723-734

GODARD, G. (1983). Dispersion tectonique des éclogites de Vendée lors d'une collision continent–continent. Bulletin de Minéralogie 106, 719–722

GODARD, G. (1988). Petrology of some eclogites in the Hercynides: The eclogites from the southern Armorican Massif, In: Smith, D.C. (ed). Eclogites and eclogite–facies rocks, Elsevier, Amsterdam, 451–519

GODARD, G. (2001). The Les Essarts eclogite–bearing metamorphic Complex (Vendée, southern Armorican Massif, France): Pre–Variscan terrains in the Hercynian belt? Géologie de la France 2001–1–2, 19–51

GODARD, G. (2009). Two orogenic cycles recorded in eclogite–facies gneiss from the southern Armorican Massif (France). European Journal of Mineralogy 21, 1173–1190

GODARD, G., KIÉNAST, J.R. & LASNIER, B. (1981). Retrogressive development of glaucophane in some eclogites from the "Massif Armoricain" (east of Nantes, France). Contributions to Mineralogy and Petrology 78, 126–135

GOLDSCHMIDT, V. M. (1911). Die Kontaktmetamorphose im Kristianiagebiet. Vidensk. Skrifter. I Mat.–Naturv. K. (1911) 11

GÓMEZ BARREIRO, J. (2007). La Unidad de Fornás: Evolución tectonometamórfica del SO del Complejo de Órdenes. Nova Terra 32, 291 p.

GÓMEZ BARREIRO, J., MARTÍNEZ CATALÁN, J.R., ARENAS, R., CASTIÑEIRAS, P., ABATI, J., DÍAZ GARCÍA, F.& WIJBRANS, J.R. (2007). Tectonic evolution of the upper allochthon of the Órdenes Complex (northwestern Iberian Massif): structural constraints to a polyorogenic peri–Gondwanan terrane. In: Linnemann, U., Nance, R.D., Kraft, P. & Zulauf, G. (eds). The Evolution of the Rheic Ocean: from Avalonian–Cadomian Active Margin to Alleghenian–Variscan Collision. Geological Society of America, Special Papers 423, 315–332

GÓMEZ BARREIRO, J., MARTÍNEZ CATALÁN, J.R., DÍEZ FERNÁNDEZ, R., ARENAS, R. & DÍAZ GARCÍA, F. (2010). Upper crust reworking during gravitational collapse: the Bembibre–Pico Sacro detachment system (NW Iberia). Journal of the Geological Society of London 167, 769–784.

GÓMEZ BARREIRO, J., WIJBRANS, J.R., CASTIÑEIRAS, P., MARTÍNEZ CATALÁN, J.R., ARENAS, R., DÍAZ GARCÍA, F. & ABATI, J. (2006). $^{40}Ar/^{39}Ar$ laserprobe dating of mylonitic fabrics in a polyorogenic terrane of the NW Iberia. Journal of the Geological Society, London, 163, 61–73.

GÓMEZ–PUGNAIRE, M.T., VLSONA D. & FRANZ, G. (1985). Kyanite, margarite and paragonite in pseudomorphs in amphibolitized eclogites from the betic Cordilleras, Spain. Chemical Geology 50, 129–141.

GONZÁLEZ CUADRA, P. (2007). La Unidad de Corredoiras (Complejo de Órdenes, Galicia): Evolución estructural y metamórfica. Nova Terra 33, 254 p.

GONZÁLEZ LODEIRO, F., HERNÁNDEZ URROZ, J., MARTÍNEZ CATALÁN, J.R., NAVAL BALBIN, A., ORTEGA GIRONES, E., & PABLO MACIA, G. (1984). Mapa Geológico de España E. 1:200.000, Santiago de Compostela (7). Instituto Geológico y Minero de España (IGME)

GOTTARDI, R., KAO, P.H., SAAR, M. O. & TEYSSIER, C. (2013). Effects of permeability fields on fluid, heat, and oxygen isotope transport in extensional detachment systems. Geochemistry, Geophysics, Geosystems 14, 1493–1522

GRASEMANN, B., RATSCHBACHER, L. & HACKER, B.R. (1998). Exhumation of ultrahigh–pressure rocks: Thermal boundary conditions and cooling history. In: When Continents Collide: Geodynamics and Geochemistry of Ultrahigh–Pressure Rocks. Hacker, B.R. & Liou, J.G. (eds). Springer, New York, 117–139

GREEN, D. H., LOCKWOOD, J. P. & KISS, E. (1968). Eclogite and almandine–jadeite–quartz rock from the Guajira Peninsula, Colombia, South America. American Mineralogist 53, 1320–1335

GREEN, E.C.R, HOLLAND, T.J.B. & POWELL, R. (2007). An order–disorder model for omphacitic pyroxenes in the system jadeite–diopside–hedenbergite–acmite, with applications to eclogite rocks. American Mineralogist 92, 1181–1189

GRESENS, R.L. (1969). Blueschist alteration during serpentinization. Contributions To Mineralogy and Petrology 24, 93–113

GROPPO, C. & CASTELLI, D., (2010). Prograde P–T evolution of a lawsonite eclogite from the Monviso metaophiolites (Western Alps): dehydration and redox reactions during subduction of oceanic FeTi–oxide gabbro. Journal of Petrology 51, 2489–2514

GUILLOT, S., HATTORI, K., AGARD, P., SCHWARTZ, S. & VIDAL, O. (2009). Exhumation Processes in Oceanic and Continental Subduction Contexts: A Review. In: Subduction Zone Geodynamics. Lallemand, S. & Funiciello, F. (eds). Frontiers in Earth Sciences V, 175–205. doi:10.1007/978–3–540–87974–9 10, 2009.

GUILLOT, S., HATTORI, K., DE SIGOYER, J., NÄGLER, T. & AUZENDE, A.L. (2001). Evidence of hydration of the mantle wedge and its role in the exhumation of eclogites. Earth and Planetary Science Letters 193, 115–127

GUIRAUD, M. & BURG, J.P. (1984). Mineralogical and petrological study of a blueschist metatulf from the Železný Brod Crystalline Complex. Czechoslovakia. Neues Jahrbuch für Mineralogie Abhandlungen 149, 1–12

GUIRAUD, M. & POWELL, R. (2006). P–V–T relationships and mineral equilibria in inclusions in minerals. Earth and Planetary Science Letters 244, 683–694

GUIRAUD, M., BURG, J.P. & POWELL, R. (1987). Evidence for a Variscan suture zone in the Vendée, France: a petrological study of blueschist facies rocks from Bois de Cené. Journal of Metamorphic Geology 5, 225–237

GUIRAUD, M., HOLLAND, T. & POWELL, R. (1990). Calculated mineral equilibria in the greenschist–blueschist–eclogite facies in Na_2O–FeO–MgO–Al_2O_3–SiO_2–H_2O: methods, results and geological applications. Contributions to Mineralogy and Petrology 104, 85–98

GUIRAUD, M., POWELL, R. & REBAY, G. (2001). H_2O in metamorphism and unexpected behaviour in the preservation of metamorphic mineral assemblages. Journal of Metamorphic Geology 19, 445–454

GUIRAUD, R., BELLION, Y., BENKHELIL, J. & MOREAU, C. (1987). Post–hereynian tectonies in Northern and Western Africa, Geological Journal 22, 433–466

GUTIÉRREZ–ALONSO, G., FERNÁNDEZ–SUÁREZ, J. & JEFFRIES, T.E. (2004). Age and setting of the Upper Neoproterozoic Narcea Antiform volcanic rocks (NW Iberia). Geogaceta 35, 79–82 [reference cited in Chapter 4]

GUTIÉRREZ–ALONSO, G., FERNÁNDEZ–SUÁREZ, J., & WEIL, A.B. (2004). Orocline triggered lithospheric delamination. Geological Society of America Special Paper 383, 121–131 [reference cited in Chapter 2]

GUTIÉRREZ–ALONSO, G., FERNÁNDEZ–SUÁREZ, J., JEFFRIES, T.E., JOHNSTON, S.T., PASTOR–GALÁN, D., MURPHY, J.B., FRANCO, M.P. & GONZALO, J.C. (2011a). Diachronous post–orogenic magmatism within a developing orocline in Iberia, European Variscides: Tectonics 30: TC5008

GUTIÉRREZ–ALONSO, G., FERNÁNDEZ–SUÁREZ, J., WEIL, A.B, MURPHY, J.B, NANCE, R.D., CORFU, F., JOHNSTON, S.T. (2008). Self–subduction of the Pangean global plate. Nature Geoscience 1, 549–553

GUTIÉRREZ–ALONSO, G., MURPHY, J.B., FERNÁNDEZ–SUÁREZ, J., WEIL, A.B., FRANCO, M.P. & GONZALO, J.C. (2011b). Lithospheric delamination in the core of Pangea: Sm–Nd insights from the Iberian mantle. Geology 39, 155–58

GUTIÉRREZ-ALONSO, G., FERNÁNDEZ-SUÁREZ, J., JEFFRIES, T.E., JENNER, J.E., TUBRETT, M.N., COX, R. & JACKSON, S.E. (2003). Terrane accretion and dispersal in the Northern Gondwana margin: an Early Paleozoic analogue of a long-lived active margin. Tectonophysics 365, 221–232

HACKER, B.R. & PEACOCK, S.M. (1994). Creation, preservation, and exhumation of coesite-bearing, ultrahigh–pressure metamorphic rocks. In: Coleman, R.G. & Wang, X. (eds). Ullrahigh Pressure Melamorphism, Cambridge University Press, Cambridge, United Kingdom

HACKER, B.R. (2001). http://www.geol.ucsb.edu/faculty/hacker/geo102C/lectures/part14.html

HACKER, B.R. (2006). Pressures and temperatures of ultrahigh–pressure metamorphism: Implications for UHP tectonics and H_2O in subducting slabs. International Geology Review 48, 1053–1066

HACKER, B.R., ABERS, G.A. & PEACOCK, S.M. (2003). Subduction factory - 1. Theoretical mineralogy, densities, seismic wave speeds, and H_2O contents. Journal of Geophysical Research-Solid Earth 108(B1), 2029

HAISSEN, F., GARCÍA-CASCO, A., TORRES-ROLDÁN, R.L. & AGHZER, A. (2004). Decompression reactions and P–T conditions in high–pressure granulites from Casares–Los Reales units of Betic–Rift belt (S Spain and N Morocco). Journal of African Earth Sciences 39, 375–383

HALLIMOND, A.F. (1943). On the graphical representation of the calciferous amphiboles. The American Mineralogist 28, 65–89

HANMER, S. (1977). Age and tectonic implications of the Baie d'Audierne basic–ultrabasic complex. Nature 270, 336–338

HANMER, S. (1977). Age and tectonic implications of the Baie d'Audierne basic–ultrabasic complex. Nature 270, 336–338

HARKER, A. (1932). Metamorphism. Methuen, London, 360 p.

HARLOV, D., TROPPER, P., SEIFERT, W., NIJLAND, T. & FÖRSTER, H.J. (2006). Formation of Al–rich titanite ($CaTiSiO_4O$–$CaAlSiO_4OH$) reaction rims on ilmenite in metamorphic rocks as a function of f H_2O and f O_2. Lithos 88, 72–84

HARRISON, T., CÉLÉRIER, J., AIKMAN, A., HERMANN, J. & HEIZLER, J. (2009). Diffusion of ^{40}Ar in muscovite. Geochimica et Cosmochimica Acta 73, 1039–1051

HARTE, B. & HUDSON, N.F.C. (1979). Pelite facies series and the temperatures and pressures of Dalradian metamorphism in E Scotland. In: Harris, A.L., Holland, C.H. & Leake, B.E. (eds). The Caledonides off the British Isles–Reviewed. The Geological Society of London Special Publication 8, 323–336

HASEBE, K., FUJII, N. & UYEDA, S. (1970). Thermal processes under island arcs. Tectonophysics 10, 335–355

HEINRICH, W. & ALTHAUS, E. (1988). Experimental determination of the reactions 4 lawsonite + 1 albite = 1 paragonite + 2 zoisite + 2 quartz + 6 H_2O and 4 lawsonite + 1 jadeite = 1 paragonite + 2 zoisite + 1 quartz + 6 H_2O. Neues Jahrbuch für Mineralogie Monatshefte 11, 516–528

HEMINGWAY, B.S., BOHLEN, S.R, HANKINS W.B., WESTRUM E.F.J. & KUSKOV O.L. (1998). Heat capacity and thermodynamic properties for coesite and jadeite, reexamination of the quartz–coesite equilibrium boundary. American Mineralogist 83, 409–418

HENSEN, B.J. (1971). Theoretical phase relations involving garnet and cordierite in the system MgO–FeO–Al_2O_3–SiO_2 . Contributions to Mineralogy and Petrology 33, 191–214

HEY, M.H. (1954). A new review of the chlorites. Mineralogical Magazine 30, 277–292

HILLERT, M. (1985). Principles of phase diagrams. International Metals Reviews, 30, 45–67

HIRAJIMA, T. & COMPAGNONI, R. (1993). Petrology of a jadeite–quartz/coesite almandine– phengite fels with retrograde ferro–nyböite from the Dora–Maira Massif, Western Alps. European Journal of Mineralogy 5, 943–955

HIRSCH, D.M., PRIOR, D.J. & CARLSON, W.D. (2003). An overgrowth model to explain multiple, dispersed high-Mn regions in the cores of garnet porphyroblasts. American Mineralogist 88, 131–141

HODGES, K.W. (1991). Pressure–tempeture–time paths. Annual Review of Earth and Planettary Science 19, 207–236

HOLDAWAY, M. J. (1971) .Stability of andalusite and the aluminosilicate phase diagram. American Joumal of Science 271, 97–131

HOLDAWAY, M. J. (2001). Recalibration of the GASP geobarometer in light of recent garnet and plagioclase activity models and versions of the garnet–biotite geothermometer. American Mineralogist 86, 1117–1129

HOLDAWAY, M. J., DUTROW, B. L. & HINTON, R. W. (1988). Devonian and Carboniferous metamorphism in west–central Maine; the muscovite–almandine geobarometer and the staurolite problem revisited. American Mineralogist 73, 20–47

HOLÉNYI, K. & ANNERSTEIN, H. (1987). Iron in titanite: a Mössbauer–spectroscopy study. Canadian Mineralogist 25, 429–433

HOLLAND, T. J.B. (1980). The reaction albite = jadeite + quartz determined experimentally in the range 600–1200°C. American Mineralogist 65, 125–134

HOLLAND, T.J. B. & POWELL, R. (2011). An improved and extended internally consistent thermodynamic dataset for phases of petrological interest, involving a new equation of state for solids. Journal of Metamorphic Geology 29, 333–383

HOLLAND, T.J.B. & POWELL, R. (1985). An internally consistent thermodynamic dataset with uncertainties and correlations : 2. Data and results. Journal of Metamorphic Geology 3, 343–370

HOLLAND, T.J.B. & POWELL, R. (1990). An enlarged and updated internally consistent thermodynamic dataset with uncertainties and correlations: the system K_2O–Na_2O–CaO–MgO–MnO–FeO–Fe_2O_3–Al_2O_3–TiO_2–SiO_2–C–H_2–O_2. Journal of Metamorphic Geology 8, 89–124

HOLLAND, T.J.B. & POWELL, R. (1998). An internally consistent thermodynamic data set for phases of petrological interest. Journal of Metamorphic Geology 16, 309–343

HOLLAND, T.J.B. & POWELL, R. (2000) In: POWELL, R. & HOLLAND, T.J.B. (2002). Course Notes for THERMOCALC Workshop 2002: Calculating Metamorphic Phase Equilibria (Barcelona). CD–ROM.

HOLLAND, T.J.B. & POWELL, R. (2003). Activity–composition relations for phases in petrological calculations: an asymmetric multicomponent formulation. Contributions to Mineralogy and Petrology 145, 492–501.

HOLLAND, T.J.B., BAKER, J. & POWELL, R. (1998). Mixing properties and activity–composition and relationships of chlorites in the system MgO–FeO–Al_2O_3–SiO_2–H_2O. European Journal of Mineralogy 10, 395–406.

HOLLISTER, L. S. (1966). Garnet zoning: an interpretation based on the Rayleigh fractionation model. Science 154, 1647–1651

HOLLOWAY, J.R. & WOOD, B.J. (1988). Simulating the Earth: Experimental Geochemistry. Winchester Ma: Unwin Hyman, 181 p.

HOLMES, A. (1929). A review of the continental drift hypothesis. Mineralogical Magazine 40, 1–16

HOLUB, F. & SOUČEK, J. (1994). Blueschist–greenschist metamorphism of metabasites in the Krušné Hory (Erzgebirge) Mts. Zentralblatt für Geoologie und Paläontologie 1, 815–826

HOSSACK, J.R. & COOPER, M.A. (1986). Collision tectonics in the Scandinavian Caledonides. In: Coward, M.P. & Ries, A.C. (eds). Collision Tectonics. Geological Society, Special Publication 19, 287–304

HUBREGTSE, J.J.M.W. (1973). Petrology of the Mellid area, a Precambrian polymetamorphic rock complex, Galicia, N.W. Spain. Leidse Geologische Mededelingen 49, 9–31

HUDSON, N.F.C. & HARTE, B. (1985). K_2O–poor, aluminous assemblages from the Buchan Dalradian, and the variety of orthoamphibole assemblages in aluminous bulk compositions in the amphibolite facies. American Journal of Science 285, 224–266.

HUDSON, N.F.C. (1980). Regional metamorphism of some Dalradian pelites in the Buchan Area, NE Scotland. Contributions to Mineralogy and Petrology 73, 39–51

HYNDMAN, D.W. (1972). Petrolagy of Igneous and Metarnorphic Rocks: McGraw–Hill, New York, 533 p.

HYNES, A. & FOREST, R. C. (1988). Empirical garnet–muscovite geothermometry in low–grade metapelites, Selwyn Range (Canadian Rockies). Journal of Metamorphic Geology 6, 297–309

IGLESIAS, M., RIBEIRO, M.L. & RIBEIRO, A. (1983). La interpretación aloctonista de la estructura del Noroeste peninsular. In: Comba J.A. (ed). Geología de España (Libro Jubilar J.M.Rios), Tomo I, Instituto Geológico y Minero de España (IGME), Madrid, 459–467

ISOZAKI, Y., AOKI, K., NAKAMA, T. & YANAI, S. (2010). New insight into a subduction–related orogen: A reappraisal of the geotectonic framework and evolution of the Japanese Islands. Gondwana Research 18, 82–105

JAHN, B.M., CABY, R. & MONIÉ, P. (2001). The oldest UHP eclogites of the World: age of UHP metamorphism, nature of protoliths and tectonic implications. Chemical Geology 178, 143–158

JANJOU, D. (1998). Notice explicative, Carte géologique France (1/50000), feuille Segré (422). Avec la collaboration de Lardeux, H., Chantraine, J., Callier, L. & Etienne, H. BRGM, Orléans, 68p.

JÉGOUZO, P. & ROSSELLO, E.A. (1988). La Branche Nord du Cisaillement sud–armoricain (France): un essai d'évaluation du déplacement par l'analyse des mylonites. Comptes–rendus de l'Académie des Sciences de Paris II–307, 1825–1831

JÉGOUZO, P. (1980). The South Armorican Shear Zone. Journal of Structural Geology 2, 39–47

JÉGOUZO, P., PEUCAT, J.J. & AUDREN, C. (1986). Caractérisation et signification géodynamique des orthogneiss calco–alcalins d'âge ordovicien de Bretagne Méridionale. Bulletin de la Societe Geologique de France 8, 839–848

JOHANNES, W. & PUHAN, D. (1971). The calcite–aragonite transition, reinvestigated. Contributions to Mineralogy and Petrology 31, 225–228

JOHNSON, C.M., MCLENNAN, S.M, MCSWEEN, H.Y. & SUMMONS, R.E. (2013). Smaller, better, more: Five decades of advances in geochemistry. In: Bickford, M.E. (ed). The Web of Geological Sciences: Advances, Impacts, and Interactions: Geological Society of America Special Paper 500, in press

JOLIVET, L., FACCENNA, C., GOFFÉ, B., BUROV, E. & AGARD, P. (2003). Subduction tectonics and exhumation of high–pressure metamorphic rocks in the Mediterranean orogens. American Journal of Science 303, 353–409

JOWHAR, T.N. (2012). Computer Programs for P–T History of Metamorphic Rocks using Pseudosection Approach. International Journal of Computer Applications 41,18–25

JULIVERT, M. (1971). L'évolution structurale de l'Arc Asturien, en Histoire structurale du Golfe de Gascogne. Collection Colloques et séminaires, 22. Paris

JULIVERT, M., FONTBOTÉ, J.M., RIBEIRO, A. & NABAIS-CONDE, L.E. (1972). Mapa tectónico de la Península Ibérica y Baleares. Escala 1:1.000.000. Instituto Geológico y Minero de España (IGME), Madrid

JULIVERT, M., FONTBOTÉ, J.M., RIBEIRO, A. & NABAIS-CONDE, L.E. (1980). Mapa tectónico de la Península Ibérica y Baleares a escala 1:1.000.000 y memoria explicative. Instituto Geológico y Minero de España (IGME), Madrid. Madrid, 113 p.

KADARUSMAN, A., MARUYAMA, S., KANEKO, Y., OTA, T., ISHIKAWA, A., SOPAHELUWAKAN, J. & OMORI, S. (2010). World's youngest blueschist belt from Leti Island in the non-volcanic Banda outer arc of Eastern Indonesia. Gondwana Research 18, 189-204

KANISSAWA, S. (1964). Metamorphic rocks of the southwestern part of the Kitakami mountainland, Japan. The science reports of the Tohoku University, 3rd series IX, 155-98

KATAGAS, C. (1980). Ferroglaucophane and chloritoid-bearing metapelites from the phyllite series, southern Peloponnes, Greece. Mineralogical Magazine 43, 975-978

KELLEY, J.S. (1980). Environment of deposition and petrography of Lower Jurassic volcaniclastic rocks, southwestern Kenai Peninsula, Alaska Ph.D. disseration, Univ. of California, Davis, 304 p.

KELLEY, J.S. (1985). Geology of the southwestern tip of the Kenai Peninsula, Alaska. In: Sisson, A. (ed). Guide to the Geology of the Kenai Peninsula, Alaska. Alaska Geological Society Guidebook, 50-68

KENNEDY, C.S. & KENNEDY, G.C. (1976). The equilibrium boundary between graphite and diamond. Journal of Geophysical Research 81, 2467-2470

KEPPIE, D.F., CURRIE, C.A. & WARREN, C. (2009). Subduction erosion modes: comparing finite element numerical models with the geological record. Earth and Planetary Science Letters 287, 241-254

KIÉNAST, J. R. & TRIBOULET, C. (1972). Le chloritoïde dans les paragenèses à glaucophane, albite ou paragonite. Bulletin de la Societe Francaise Minéralogie et de Cristallographie 95, 565-573

KIÉNAST, J.R. & TRIBOULET, C. (1973). Sur la piémontite de l'Île de Groix (Morbihan, France). Comptes-rendus de l'Académie des Sciences de Paris D-276, 1377-1379

KONRAD-SCHMOLKE, M., O'BRIEN, P.J. & ZACK, T. (2011). Fluid migration above a subducted slab. Constraints on amount, pathways and major element mobility from partially overprinted eclogite-facies rocks (Sesia Zone, Western Alps). Journal of Petrology 52, 457-486

KOONS, P. O. (1982). An experimental investigation of the behavior of amphibole in the system Na_2O-MgO-Al_2O_3-SiO_2-H_2O at high pressure. Contributions to Mineralogy and Petrology 79, 258-267

KOONS, P.O. & THOMPSON, A.B. (1985). Non-mafic rocks in the greenschist, blueschist and eclogite facies. Chemical Geology 50, 3-30

KORHONEN, F.J., POWELL, R. & STOUT, J.H. (2012). Stability of sapphirine + quartz in the oxidized rocks of the Wilson Lake terrane, Labrador: calculated equilibria in NCKFMASHTO. Journal of Metamorphic Geology 30, 21-36.

KORNPROBST, J. (2002). Metamorphic rocks and their geodynamic significance. Kluwer Academic Publishers, Dordrecht/Boston/London, 208 p.

KOSSMAT, F. (1921). Die mediterranen Kettengebirge in ihrer Beziehung zum Gleichgewichtszustande der Erde. Abhandlungen der Sächsische Akademie der Wissenschaften, Mathematisch-Physischen Kl., 38 (2), Leipzig

KOZIOL, A.M. (1989) Recalibration of the garnet–plagioclase–Al2Si05–quartz (GASP) geobarometer and application to natural parageneses. American Geophysical Union Spring Meeting, Baltimore, Maryland, EOS 70, p. 493

KREBS M., GERYA, T.V., MARESCH, W.V., SCHERTL, H.P., STÖCKHERT, B. & DRAPER, G. (2001). Serpentinite melanges of the northern Caribbean: records of complex material flow in a subduction zone, Beiheft 1. European Journal of Mineralogy 13, 104

KRECHER, M., BEHRMANN, J.H. & MÜLLER–SIGMUND, H. (2007). Sedimentology and tectonic setting of Devonian–Carboniferous turbidites and debris–flow deposits in the Variscan Vosges Mountains (Markstein Group, NE–France). Zeitschrift der Deutschen Gesellschaft für Geowissenschaften158, 1063–1087

KRETZ, R. (1973). Kinetics of the crystallization of garnet at two localities near Yellowknife. Canadian Mineralogist 12, 1–20

KRETZ, R. (1983). Symbols for rock–forming minerals. American Mineralogist 68, 277–279

KROGH, E.I., OH, C.W. & LIOU, J.G. (1994). Polyphase and anticlockwise , P–T evolution for Franciscan eclogites and blueschists from Jenner, California, USA. Journal of Metamorphic Geology 12, 121– 134

KRÖNER, A. & STERN, R.J. (2004). AFRICA. Pan–African Orogeny. Encyclopedia of Geology 1, 1–12

KRYZA, R. & PIN, C. (2010). The Central–Sudetic ophiolites (SW Poland): petrogenetic issues, geochronology and palaeotectonic implications. Gondwana Research 17, 292–305

KRYZA, R., MUSZYNSKI, A. & VIELZEUF, D. (1990). Glaucophanebearing assemblage overprinted by greenschist–facies metamorphism in the Variscan Kaczawa Complex, Sudetes, Poland. Journal of Metamorphic Geology, 8, 345–355.

KRYZA, R., WILLNER, A.P., MASSONNE, H.J., MUZSYNSKI, A. & SCHERTEL, H.P. (2011). Blueschist–facies metamorphism in the Kaczawa Mountains (Sudetes, SW Poland) of the Cental–European Variscides: P–T constraints from a jadeite–bearing metatrachyte. Mineralogical Magazine 75, 241–263

KURATA, H. & BANNO, S. (1974). Low–grade Progressive Metamorphism of Pelitic Schists of the Sazare area, Sanbagawa Metamorphic Terrain in central Sikoku, Japan. Journal of Petrology 15, 361–382

KUSKY, T. M. & POLAT, A. (1999). Growth of granite–greenstone terranes at convergent margins, and stabilization of Archeans cratons. Tectonophysics 305, 43–73

KUSKY, T.M. & BRADLEY, D.C. (1999). Kinematics of mélange fabrics: Examples and Applications from the McHugh Complex, Kenai Peninsula, Alaska. Journal of Structural Geology 21, 1773–1796

KUSKY, T.M. & GLASS, A. (2007). Structure, Cr–Chemistry, and Age of the Border Ranges Ultramafic/Mafic Complex: A Suprasubduction Zone Ophiolite Complex. In: on the Tectonic Growth of a Collisional Continental Margin: Crustal Evolution of Southern Alaska. Geological Society of America, Special Paper 431, 207–225

KUSKY, T.M., BRADLEY, D.C. & HAEUSSLER, P.J. (1997b). Progressive deformation of the Chugach accretionary complex, Alaska, during a Paleogene ridge–trench encounter. Journal of Structural Geology 19, 139–157

KUSKY, T.M., BRADLEY, D.C., DONLEY, D.T., ROWLEY, D. & HAEUSSLER, P. (2003). Controls on intrusion of near–trench magmas of the Sanak–Baranof belt, Alaska, during Paleogene ridge subduction, and consequences for forearc evolution. In: Sisson, V.B., Roeske, S., & Pavlis, T.L. (eds). Geology of a Transpressional Orogen Developed During a Ridge–Trench Interaction Along the North Pacific Margin. Geological Society of America, Special Paper 371, 269–292

KUSKY, T.M., BRADLEY, D.C., HAEUSSLER, P. & KARL, S. (1997a). Controls on accretion of flysch and mélange belts at convergent margins: Evidence from The Chugach Bay thrust and Iceworm mélange, Chugach Terrane, Alaska. Tectonics 16, 855–878

KYLANDER-CLARK, A.R.C., HACKER, B.R. & MATTINSON, J.M. (2008). Slow exhumation of UHP terranes; titanite and rutile ages of the Western Gneiss region, Norway. Earth and Planetary Science Letters 272, 3–4

LACROIX, A. (1891). Etude pétrographique des éclogites de la Loire–Inférieure. Bulletin de la Société des Sciences Naturelles de l'Ouest de la France I, 81–114

LAHONDÈRE, D., CHEVREMONT, P., BECHENNEC, F., BOUTON, P., GODARD, G., STUSSI, J.M. avec la collaboration de VIAUD, J.M., ROY, C., COCHERIE, A. & REBAY, G. (2009). Notice explicative de la carte géologique de France au 1:50000, feuille Palluau (535). BRGM, Orléans, 176 p.

LAMOUCHE COLONEL (1929). Etude tectonique de lle de Groix. Bulletin de la Société de Sciences Naturelles de l'Ouest de la France 4 (IX), 70–87

LARDEUX, H., BECQ–GIRAUDON, J.–F., BAILLAT, A., BEAULIEU, G., DAVID, J., LARDEUX, F. & RÉGNAULT, S. (2008). Trilobites et brachiopodes des «Schistes à Dicellograptus» de la carrière de Châteaupanne (Ordovicien supérieur, sud–est du Massif armoricain). Bulletin de la Société des Sciences Naturelles de l'Ouest de la France 30, 63–79

LASNIER, B. (1974). Origine du corindon secondaire dans les gabbros, norites et pyroxénolites à spinelle du Pont de Louen, Bretagne méridionale, France. Bulletin de la Société Géologique et Minéralogique de Bretagne (C) VI, 109–130

LASNIER, B., LEYRELOUP, A. & MARCHAND, J. (1973). Découverte d'un granite charnockitique au sein de gneiss oeillés: perspectives nouvelles sur l'origine de certaines leptynites du Massif armoricain méridional. Contributions to Mineralogy and Petrology 41, 134–144

LE BAYON, B., PITRA, P., BALLÈVRE, M., & BOHN, M. (2006). Reconstructing P–T paths during continental collision using multi–stage garnet (Gran Paradiso nappe, Western Alps). Journal of Metamorphic Geology 24, 477–496

LE HÉBEL, F., FOURCADE, S., BOIRON, M.C., CATHELINEAU, C., CAPDEVILA, R. & GAPAIS, D. (2007). Fluid history during deep burial and exhumation of oil–bearing volcanics, Hercynian belt of southern Brittany, France. American Journal of Science 307, 1096–1125

LE HÉBEL, F., VIDAL, O., KIENAST, J.R. & GAPAIS, D. (2002). Les "Porphyroïdes" de Bretagne méridionale: une unité de HP–BT dans la chaîne Varisque. Comptes Rendus Geoscience 334, 205–211

LE MAÎTRE, D. (1934). Etudes sur la faune des calcaires dévoniens du bassin d'Ancenis (calcaire de Chaudefonds et calcaire de Chalonnes, Maine–etLoire). Mémoires de la Société Géologique du Nord XII, 1–267

LE MAÎTRE, D. (1937). Étude de la faune corallienne des calcaires givétiens de la Ville–Dé d'Ardin (Deux–Sèvres). Bulletin de la Société Géologique de France (5) VII, 105–128

LEAKE, B.E., WOOLLEY, A.R., ARPS, C.E.S., BIRCH, W.D., GILBERT, M.C., GRICE, J.D., HAWTHORNE, F.C., KATO, A., KISCH, H.J., KRIVOVICHEV, V.G., LINTHOUT, K., LAIRD, J., MANDARINO, J., MARESCH, W.V., NICKEL, E.H., ROCK, N.M.S., SCHUMACHER, J.C., SMITH, D.C., STEPHENSON, N.C.N., UNGARETTI, L., WHITTAKER, E.J. W. & YOUZHI, G. (1997). Nomenclature of amphiboles: report of the Subcommittee on amphiboles of the International Mineralogical Association, Commission on New Minerals and Mineral Names. American Mineralogist 82, 1019–1037

LEFÈVRE C., LAKHRISSI M. & SCHNEIDER J.L. (1994). Les affinités magmatiques du volcanisme dinantien des Vosges méridionales (France): approche géochimique et interprétation. Comptes Rendus de l'Académie des Sciences de Paris II–319, 79–86

LEFORT, J.P. & RIBEIRO, A. (1980). La faille Porto-Badajoz-Cordou a-t-elle contrôlé l'évolution de l'océan Paléozoique sud-armoricain?. Bulletin de la Societé Géologique de France 22, 455-462

LEFORT, J.P. & Vigneresse, J.L. (1992). Le lever magnétique et gravimétrique de Groix : une aide pour comprendre les structures profondes de l'ile et son mode de mise en place. Bulletin de la Societé Géologique de France 163, 3-11

LILLIE, A. R. (1975). Structures in the lawsonite-glaucophane schists of New Caledonia. Geological Magazine 112, 225-340

LINNEMANN, U., PEREIRA, F., JEFFRIES, T.E., DROST, K. AND GERDES, A. (2008). The Cadomian Orogeny and the opening of the Rheic Ocean: The diacrony of geotectonic processes constrained by LA-ICPMS U-Pb zircon dating (OssaMorena and Saxo-Thuringian Zones, Iberian and Bohemian Massifs). Tectonophysics 461, 21-43

LIOU, J.G. (1971). P-T stabilities of laumontite, wairakite, lawsonite, and related minerals in the system $CaO-Al_2O_3-SiO_2-H_2O$. Journal of Petrology 12, 379-411

LIOU, J.G. (1981). Petrology of metamorphosed oceanic rocks in the Central Range of Taiwan. Memoir of the Geological Society of China 4, 291-342

LIOU, J.G., HACKER, B.R. & ZHANG, R.Y. (2000). Into the Forbidden Zone. Science 287, 1215-1216

LIOU, J.G., MARUYAMA, S., WANG, X., GRAHAM, S.A. (1990). Precambrian blueschist terranes of the world. Tectonophysics 181, 97-111

LIOU, J.G., TSUJIMORI, T., ZHANG, R.Y., KATAYAMA, I. & MARUYAMA, S. (2004). Global UHP Metamorphism and Continent Subduction/Collision: The Himalayan Model. International Geology Review 46, 1-27

LIOU, J.G., ZHANG, R. Y., EIDE, E.A., MARUYAMA, S., WANG, X. & EMST, W.G. (1996). Metamorphism and tectonics ofhigh-P and ultrahigh-P belts in Dabie-Sulu Regions, eastem central China. In: Yin, A. & Harrison, T.M. (eds). The Teclonic Evolution of Asia, Rubey Volume IX, Cambridge University Press, Cambridge, United Kingdom, 300-343

LIOU, J.G., ZHANG, R.Y., ERNST, W.G., RUMBLE, D. III. & MARUYAMA, S. (1998). High pressure minerals from deeply subducted metamorphic rocks. In: Hemley, R.J. (ed). Ultrahigh-Pressure Mineralogy: Physics and Chemistry of the Earth's Deep Interior. Reviews in Mineralogy 37, 33-96

LITTLE, T.A. & NAESER, C.W. (1989). Tertiary of the Border Ranges fault system, Chugach Mountains, Alaska: Deformation and uplift in a forearc setting. Journal of Geophysical Research 94, 4333-4359

LLANA-FÚNEZ, S. & MARCOS, A. (2002). Structural record during exhumation and emplacement of high-pressure-low-to intermediate-temperature rocks in the Malpica-Tui unit (Variscan Belt of Iberia). In: Martínez Catalán J.R., Hatcher Jr, R.D., Arenas, R & Díaz García, F. (eds). Variscan-Appalachian dynamics: The building of the late Paleozoic bassamen. Geological Society of America, Special Paper 125-142.

LLANA-FÚNEZ, S. (2001). La estructura de la unidad de Malpica-Tui (Cordillera varisca en Iberia). Serie de Tesis Doctorales 1. Madrid, Instituto Geológico y Minero de España (IGME)

LLOPIS LLADO, N. (1966). Sur la structure hercynienne de l'Espagne et ses rapports avec la Chaîne hercynienne en Europe occidentale. Comptes Rendus de l'Académie des Sciences de Paris D-262, 2581-2584

LÓPEZ-CARMONA, A., ABATI, J. & RECHE, J. (2008). Phase equilibrium modelling in the KFMASH system to show the Metamorphic Evolution of the Ceán Schists (Malpica-Tui Unit, NW Iberian Massif). Geogaceta 44, 27-30

LÓPEZ-CARMONA, A., ABATI, J. & RECHE, J. (2010). Petrologic modeling of chloritoid-glaucophane schists from the NW Iberian Massif. Gondwana Research 17, 377-391

LÓPEZ-CARMONA, A., ABATI, J., PITRA, P. & LEE, J.K.W. Retrogressed lawsonite blueschists from the NW Iberian Massif: P-T constraints from numerical modelling and $^{40}Ar/^{39}Ar$ geochronology. Submitted to Contributions to Mineralogy and Petrology

LÓPEZ-CARMONA, A., KUSKY, T.M, SANTOSH, M & ABATI, J. (2011). P-T and structural constraints of lawsonite and epidote blueschists from Liberty Creek and Seldovia: Tectonic implications for early stages of subduction along the southern Alaska convergent margin. Lithos 121, 100-116

LÓPEZ-CARMONA, A., PITRA, P. & ABATI, J. (2013). Blueschist-facies metapelites from the Malpica-Tui Unit (NW Iberian Massif): phase equilibria modelling and H_2O and Fe_2O_3 influence in high-pressure assembalges. Journal of Metamorphic Geology 31, 263-280

LÓPEZ-CARMONA, A., ABATI, J. & RECHE, J. (2007). Evolución Metamórfica de los Esquistos de AP/BT de Ceán (Unidad de Malpica-Tui, NW del Macizo Ibérico). Geogaceta 43, 3-6.

LOTZE, F. (1929). Stratigraphie und Tektonik des Keltiberischen Grundgebirges (Spanien). Beitrage zur Geologie der westlichen Mediterrangebiete 3, Berlin

LOTZE, F. (1954-1955). Estratigrafía y tectónica de las cadenas paleozoicas celtibéricas. Publicaciones extranjeras sobre geología de España, Instituto Lucas Mallada, Consejo Superior de Investigaciones Científicas (CSIC), Madrid, VIII, 313 p. Translated by M. San Miguel de la Cámara.

LUCKS, H., SCHULZ, B., AUDREN, C. & TRIBOULET C. (2002). Variscan pressure-temperature evolution of garnet-pyroxenites and amphibolites in the Baie d'Audierne metamorphic series, Brittany (France). In: Martínez Catalán, J.R., Hatcher Jr., R.D., Arenas, R. & Díaz García, F. (eds). Variscan-Appalachian Dynamics: The Building of the Late Paleozoic Basement. Geological Society of America, Special Paper 364, 89-103

LYUBETSKAYA, T. & AGUE, J.J. (2009). Modeling the magnitudes and directions of regional metamorphic fluid flow in collisional orogens. Journal of Petrology 50, 1505-1531

MAEKAWA, H., SHOZUI, M., ISHII, T., FRYER, P. & PEARCE. J.A. (1993). Blueschist metamorphism in an active subduction zone. Nature 364, 520-523

MAGOON, L.B., ADKISON, W.L. & EGBERT, R.M. (1976). Map showing geology, wildcat wells, Tertiary plant fossil localities, K-Ar age dates, and petroleum operations, Cook Inlet area, Alaska: U.S. Geological Survey Miscellaneous Investigations Series Map I-1019, scale 1:250,000

MAHAR, E. M., BAKER, J. M., POWELL, R., HOLLAND, T. J. B. & HOWELL, N. (1997). The effect of Mn on mineral stability in metapelites. Journal of Metamorphic Geology 15, 223-238

MANNING, C.E., MENOLD, C.A. & YIN, A. (2001). Metamorphism and exhumation of ultrahigh-pressure eclogites and gneisses, north Qaidam, China, GSA Annual Meeting

MANON, M.R. (2008). Heat capacity of high pressure minerals and phase equilibria of Cretan blueschists. Michigan. Unpublished PhD thesis, University of Michigan. 192 p.

MARCHAND, J. (1981). Ecaillage d'un «mélange tectonique» profond: le complexe cristallophyllien de Champtoceaux (Bretagne méridionale). Comptes-rendus de l'Académie des Sciences de Paris II-293, 223-228

MARCOS, A. & FARIAS, P. (1999). La estructura de las láminas inferiors del Complejo de Cabo Ortegal y su autóctono relativo (Galicia, NO de España). Universidad de Oviedo, Trabajos de Geología 21, 201-218

MARCOS, A., FARIAS, P., GALÁN, G., FERNÁNDEZ, F.J. & LLANA-FÚNEZ, S. (2002). Tectonic framework of the Cabo Ortegal Complex: A slab of lower crust exhumed in the Variscan orogen (northwestern Iberian

Peninsula). In: Martínez Catalán, J.R., Hatcher Jr., R.D., Arenas, R. & Díaz García, F. (Eds.), Variscan–Appalachian Dynamics: The Building of the Late Paleozoic Basement, Geological Society of America, Special Paper 364, 125–142

MARCOS, A., MARQUÍNEZ, J., PÉREZ–ESTAÚN, A., PULGAR, J.A. & BASTIDA, F. (1984). Nuevas aportaciones al conocimiento de la evolución tectonometamórfica del Complejo de Cabo Ortegal (NW de España). Cuadernos do Laboratorio Xeolóxico de Laxe 7, 125–137

MARESCH, W.M. (1973) New data on the synthesis and stability relations of glaucophane. Earth and Planettary Science Letters 20, 385–390

MARESCH, W.M. (1977). Experimental studies on glaucophane: an analysis of present knowledge. Tectonophysics 43, 109–125

MARMO, B.A., CLARKE, G.L. & POWELL, R. (2002). Fractionation of bulk rock composition due to porphyroblast growth: effects on eclogite facies mineral equilibria, Pam Peninsula, New Caledonia. Journal of Metamorphic Geology 20, 151–165

MARQUÍNEZ GARCÍA, J.L. (1984). La geología del área esquistosa de Galicia Central (Cordillera Herciniana, NW de España). Memorias del Instituto Geológico y Minero de España (IGME) 100, 231 p.

MARTÍNEZ CATALÁN, J. R., ARENAS, R., DÍAZ GARCÍA, F., RUBIO PASCUAL, F.J., ABATI, J. & MARQUÍNEZ, J. (1996). Variscan exhumation of a subducted Paleozoic continental margin: The basal units of the Ordenes Complex, Galicia, NW Spain. Tectonics 15, 106–121

MARTÍNEZ CATALÁN, J.R. (1990). A non–cylindrical model for the northwest Iberian allochthonous terranes and their equivalents in the Hercynian belt of Western Europe. Tectonophysics 179, 253–272

MARTÍNEZ CATALÁN, J.R. (2011). Are the oroclines of the Variscan belt related to late Variscan strike–slip tectonics?. Terra Nova 23, 241–247

MARTÍNEZ CATALÁN, J.R. (2012). The Central Iberian arc, an orocline centered in the Iberian Massif and some implications for the Variscan belt. International Journal of Earth Sciences 101, 1299–1314

MARTÍNEZ CATALÁN, J.R., ARENAS, R., ABATI, J., SÁNCHEZ MARTÍNEZ, S., DÍAZ GARCÍA, F., FERNÁNDEZ–SUÁREZ, J., GONZÁLEZ CUADRA, P., CASTIÑEIRAS, P., GÓMEZ–BARREIRO, J., DÍEZ MONTES, A., GONZÁLEZ CLAVIJO, E., RUBIO PASCUAL, F.J., ANDONAEGUI, P., JEFFRIES, T. E., ALCOCK, J. DÍEZ FERNÁNDEZ, R. & LÓPEZ–CARMONA, A. (2009). A rootless suture and the loss of the roots of a mountain chain: The Variscan belt of NW Iberia. Comptes Rendus Geosciences 341, 114–126

MARTÍNEZ CATALÁN, J.R., ARENAS, R., DÍAZ GARCÍA, F. & ABATI, J. (1997). Variscan acretionary complex of northwest Iberia: Terrane correlation and succession of tectonothermal events. Geology 27, 1103–1106

MARTÍNEZ CATALÁN, J.R., ARENAS, R., DÍAZ GARCÍA, F. y ABATI, J. (1999). Allochthonous units in the Variscan belt of NW Iberia. Terranes and accretionary history. In: Sinha, A.K. (ed). Basement Tectonics. Kluwer Academic Publishers13, 65–84

MARTÍNEZ CATALÁN, J.R., ARENAS, R., DÍAZ GARCÍA, F., GONZÁLEZ CUADRA, P., GÓMEZ–BARREIRO, J., ABATI, J., CASTIÑEIRAS, P., FERNÁNDEZ–SUÁREZ, J., SÁNCHEZ MARTÍNEZ, S., ANDONAEGUI, P., GONZÁLEZ CLAVIJO, E., DÍEZ MONTES, A., RUBIO PASCUAL, F.J. & AGUADO, B.V. (2007). Space and time in the tectonic evolution of the northwestern Iberian Massif: Implications for the Variscan belt. Geological Society of America Memoirs 200, 403–423

MARTÍNEZ CATALÁN, J.R., DÍAZ GARCÍA, F., ARENAS, R., ABATI, J., CASTIÑEIRAS, P., GONZÁLEZ CUADRA, P., GÓMEZ BARREIRO, J. & RUBIO PASCUAL, F.J. (2002). Thrust and detachment system in Órdenes Complex (northwestern Spain): Implications for the Variscan–Appalachian Dynamics: the Building of the late Paleozoic Basement. Geological Society of América Special Paper 364, 163–182

MARTÍNEZ CATALÁN, J.R., FERNÁNDEZ-SUÁREZ, J., JENNER, G.A., BELOUSOVA, E. & DÍEZ MONTES, A. (2004). Provenance constraints from detrital zircon UPb ages in the NW Iberian Massif: implications for Paleozoic plate configuration and Variscan evolution. Journal of the Geological Society of London 161, 461–473

MARTÍNEZ CATALÁN, J.R., FERNÁNDEZ-SUÁREZ, J., MEIRELES, C., GONZÁLEZ CLAVIJO, E., BELOUSOVA, E. & SAEED, A. (2008). UPb detrital zircon ages in synorogenic deposits of the NW Iberian Massif (Variscan belt): interplay of Devonian–Carboniferous sedimentation and thrust tectonics. Journal of the Geological Society of London 165, 687–698

MARUYAMA, S. & LIOU, J.G. (1998). Initiation of ultrahigh-pressure metamorphism and its significance on the Proterozoic–Phanerozoic boundary. Island Arc 7, 6–35

MARUYAMA, S. (1997). Pacific-type orogeny revisited: Miyashiro-type orogeny proposed. Island Arc 6, 91–20

MARUYAMA, S., CHO, M., LIOU, J.G. (1986). Experimental investigations of blueschist–greenschist transition equilibria: pressure dependence of Al_2O_3 contents in sodic amphiboles –a new geobarometer. Geological Society of America Memoir 164, 1–16

MARUYAMA, S., HASEGAWA, A., SANTOSH, M., KOGISO, T., NAKAMURA, H., KAWAI, K. & ZHAO, D. (2009). The dynamics of big mantle wedge, magma factory, and metamorphic–metasomatic factory in subduction zones. Gondwana Research 16, 414–430

MARUYAMA, S., ISOZAK, Y., KIMURA, G. & TERABAYASHI, M. (1997). Paleogeographic maps of the Japanese islands: plate tectonics synthesis from 750 Ma to the present. Island Arc 6,121–142

MARUYAMA, S., LIOU, J. & TERABAYASHI, M. (1996). Blueschists and eclogites of the world and their exhumation. International Geology Review 38, 485–594

MASAGO, H., OMORI, S. & MARUYAMA, S. (2009). Counter-clockwise prograde P–T path in collisional orogeny and water subduction at the Precambrian–Cambrian boundary: The ultrahigh-pressure pelitic schist in the Kokchetav massif, northern Kazakhstan. Gondwana Research 15, 137–150

MASSONE, H. J. & SCHREYER, W. (1987). Phengite geobarometry based on the limiting assemblage with K-feldspar, phlogopite and quartz. Contributions to Mineralogy and Petrology 96, 212–214

MATSUDA, T. & UYEDA, S. (1971), On the Pacific-type orogeny and its model: extension of the paired belts concept and possible origin of marginal seas. Tectonophysics 11, 5–27

MATTE, P. & CAPDEVILA, R. (1978). Tectonique en grands plis couchés et plissements superposés d'âge hercynien dans la série de Ordenes–Betanzos (Galice Occidentale). Cuadernos del Seminario de Estudios Cerámicos de Sargadelos 27, 193–201

MATTE, P. (1968). La structure de la virgation hercynienne de Galice (Espagne). Revue de Géologie Alpine 44, 1–128

MATTE, P. (1986). Tectonics and plate tectonics model for the Variscan belt of Europe, Tectonophysics 126, 329–374

MATTE, P. (1991). Accretionary history and crustal evolution of the Variscan belt in Western Europe. Tectonophysics 196, 309–337

MATTE, P. (2001). The Variscan collage and orogeny (480–290 Ma) and the tectonic definition of the Armorica microplate: a review. Terra Nova 13, 112–128

MATTE, P. (2002). Variscides, between the Appalachians and the Urals: Similarities and differences between Paleozoic subduction and collision belts. In: Martínez Catalán, J.R., Hatcher Jr., R.D., Arenas, R. & Díaz García, F. (eds). Variscan–Appalachian Dynamics: the Building of the Late Paleozoic Basement, Geological Society of America Special Paper 364, 237–248

MATTE, P. (2007). Variscan thrust nappes, detachments, and strike-slip faults in the French Massif Central: Interpretation of the lineations. In: Hatcher Jr., R.D., Carlson, M.P., McBride, J.H. & Martínez Catalán, J.R. (eds). 4-D framework of continental crust. Geological Society of America Memoir, 200, 391-402

MAUREL, O., MONIE, P., RESPAUT, J.P., LEYRELOUP, A.F. & MALUSKI, H. (2003). Pre-Metamorphic $^{40}Ar/^{39}Ar$ and U-Pb ages in HP metagranitoids from the Hercynian belt (France). Chemical Geology 193, 195-214

MEINHOLD, G. (2010). Rutile and its application in earth sciences. Earth Science Reviews 102, 1-28

MEIRELES, C.A.P. (2011). Litoestratigrafia do Paleozóico do Sector a Nordeste de Bragança (Trás-osMontes). Unpublished PhD thesis, Universidade do Porto, 470 p.

MENDIA ARANGUREN, M.S. (2000). Petrología de la Unidad Eclogítica del Complejo de Cabo Ortegal (NW de España). Nova Terra 16, 424 p.

MERINO-TOMÉ, O.A., BAHAMONDE, J.R., COLMENERO, J.R., HEREDIA, N., VILLA, E. & FARIAS, P. (2009). Emplacement of the Cuera and Picos de Europa imbricate thrust system at the core of the Iberian-Armorican arc (Cantabrian zone, north Spain): New precisions concerning the timing of arc closure. Geological Society of America Bulletin121, 729-751

MILLER, C., SATIR, M. & FRANK, W. (1980). High pressure metamorphism in the Tauern Window. Mitteilungen der Österreichischen Geologischen Gesellschaft 71, 89-97

MIYASHIRO, A. & BANNO, S. (1958). Nature of glaucophanitic metamorphism. American Journal of Science 256, 97-110

MIYASHIRO, A. & SEKI, Y. (1958). Mineral assemblages and subfacies of the glaucophane schist facies. Japanese Journal of Geology and Geography 29, 199-208

MIYASHIRO, A. (1961). Evolution of metamorphic belts. Journal of Petrology 2, 277-311

MIYASHIRO, A. (1967). Orogeny, regional metamorphism and magnetism in the Japanese islands. Meddelelser fra Dansk Geologisk Forening 17, 390-446

MIYASHIRO, A. (1973). Metamorphism and metamorphic belts. John Wiley & Sons, New York, 492 p.

MIYASHIRO, A. (1981). Tectonic and petrologic aspects of Asia. Geological Society of China (Taiwan) Memoir 4, 1-32

MIYASHIRO, A. (1994). Metamorphic Petrology. Oxford University Press, New York, 404 p.

MÖLLER, A., APPEL, P., MEZGER, K. & SCHENK, V. (1995). Evidence for 2 Ga subduction zone- Eclogites in the Usagaran belt of Tanzania. Geology 23, 1067-1070

MÖLLER, A., MEZGER, K. & SCHENK, V. (1998). Crustal age domains and the evolution of the continental crust in the Mozambique Belt of Tanzania: Combined Sm-Nd, Rb-Sr, and Pb-Pb isotopic evidence. Journal of Petrology 39, 749-783

MOLNAR, P. & TAPPONNIER, P. (1975). Cenozoic Tectonics of Asia: Effects of a Continental Collision. Science 189, 419-426

MONTERO, P. (1993). Geoquímica y petrogénesis del complejo peralcalino de la Sierra del Galiñeiro (Pontevedra, España). Unpublished PhD thesis, Universidad de Oviedo, 318 p.

MONTERO, P., BEA, F., CORRETGÉ, L.G., FLOOR, P. & WHITEHOUSE, M.J. (2009). UPb ion microprobe dating and Sr and Nd isotope geology of the Galiñeiro Igneous Complex. A model for the peraluminous/peralkaline duality of the Cambro-Ordovician magmatism of Iberia. Lithos 107, 227-238

MONTIGNY, R. & ALLÈGRE, C. (1984). A la recherche des océans perdus: les éclogites de Vendée témoins métamorphisés d'une ancienne croûte océanique. Comptes-rendus de l'Académie des Sciences de Paris D-279, 543-545

MOONEY, W.D., LASKE, G. & MASTERS, G. (1998). CRUST 5.1: A global crustal model at 5°x5°. Journal of Geophysical Research 103, 727-747

MOTTANA, A. & SCHREYER, W. (1977). Carpholite crystal chemistry and preliminary experimental stability. Neues Jahrbuch für Mineralogie 129,113-138

MUNHÁ, J. M. & RIBEIRO, M. L. (1984). Blueschists in the Iberian Variscan chain (Trás-os-Montes, NE Portugal). Comunicados do Serviço Geologico do Portugal 70, 31-53.

MURPHY, J.B. & NANCE, R.D. (1991). Supercontinent model for the contrasting character of Late Proterozoic orogenic belts. Geology 31, 873-876

MURPHY, J.B., GUTIÉRREZ-ALONSO, G., NANCE, R.D., FERNANDEZ-SUAREZ, J., KEPPIE, J.D., QUESADA, C., DOSTAL., J. & BRAID, J.A. (2009b). Rheic Ocean mafic complexes: overview and synthesis. In: Murphy, J.B., Keppie, J.D. & Hynes, A. (eds). Ancient Orogens and Modern Analogues. Geological Society of London Special Publication 327, 343-369

MURPHY, J.B., NANCE, R.D. & CAWOOD, P.A. (2009a). Contrasting modes of supercontinent formation and the conundrum of Pangea. Gondwana Research 15, 408-420

NELSON, S.W., BLOME, C.D., HARRIS, A.G., REED, K.M. & WILSON, F.H. (1986). Late Paleozoic and Early Jurassic fossil ages from the McHugh Complex. In: Bartsch-Winkler, S. & Reed, K.M. (eds). Geologic Studies in Alaska by the U.S. Geological Survey during 1985. U.S. Geological Survey Circular 978, 60-64

NEUMAN, R.B. & MAX, M.D. (1989). Penobscottian-Grampian-Finnmarkian orogenies as indicators of terrane linkages. In: Dallmeyer, R.D. (ed). Terranes in the Circum-Atlantic Paleozoic Orogens. Geological Society of America, Special Paper 230, 31-45

NEWTON, R.C., & FYFE, W.S. (1976). High-pressure metamorphism. In: Bailey, D.K., & Macdonald, R. (eds). The evolution of the crystalline rocks. Academic Press, London, 101-186

NEWTON, R.C., CHARLU, T.V. & KLEPPA, O.J. (1980). Thermochemistry of the high structural state plagioclases, Geochemica and Cosmochimica Acta 44, 933- 941

NILSEN, T.H. & ZUFFA, G.G. (1982). The Chugach terrane, a Cretaceous trench-fill deposit, southern Alaska. Geological Society of London, Special Publication 10, 213-227

NOKLEBERG, W.J., FOSTER, H.L. & ALEINIKOFF, J.N. (1989). Geology of the northern Copper River basin, eastern Alaska Range, and southern Yukon-Tanana Basin, southern and east-central Aslaska. In: Nokleberg, W.J. & Fisher, M.A. (eds). Alaskan geological and geophysical transect, International Geological Congress, 27th, Guidebook T104, 34-64

NOKLEBERG, W.J., PLAFKER, G. & WILSON, F.H. (1994). Geology of south-central Alaska. In: Plafker, G. & Berg, H.C. (eds). The Geology of Alaska, Decade of North American Geology, Geological Society of America vol. G-1, 311-366

NORDSTROM, D. K. & MUNOZ, J. L. (1994). Geochemical Thermodynamics. 2nd edition. Blackwell, Cambridge, 493 p.

NORRISH, K. & HUTTON, J.T. (1969). An accurate X-ray spectrographic method for the analysis of a wide range of geological samples. Geochimica et Cosmochimica Acta, 33, 431-453

O´BRIEN, P.J. & RÖTZLER, J. (2003). High-pressure granulites: formation, recovery of peak conditions, and implications for tectonics. Journal of Metamorphic Geology 21, 1, 3-20

OGILVIE, P. (2010). Metamorphic studies in the Vredefort Dome, South Africa. Unpublished PhD thesis, University of the Witwatersrand, Johannesburg.

OKAMOTO, K. & MARUYAMA, S. (1999). The high pressure stability limits of lawsonite in the MORB+H_2O system. American Mineralogist 84, 362–373

OKAY, A.I. (1982). Incipient blueschist metamorphism and metasomatism in the Tavsanh region, northwest Turkey. Contributions to Mineralogy and Petrol ogy79, 361–67

OKRUSCH, M., SEIDEL, E. & DAVIS, E.N. (1978). The assemblage jadeite–quartz in the glaucophane rocks of Sifnos (Cyclades Archipelago, Greece). Neues Jarhbuch für Mineralogie Abhandlungen 132, 284–308

OMORI, S., KITA, S., MARUYAMA, S. & SANTOSH, M. (2009). Pressure–temperature conditions of ongoing regional metamorphism beneath the Japanese Islands. Gondwana Research 16, 458–469

ONSTOTT, T.C. & PEACOCK, M.W. (1987). Argon retentivity of hornblendes; a field experiment in a slowly cooled metamorphic terrane. Geochimica et Cosmoehimica Acta 51, 2891–2903

ORDÓÑEZ CASADO, B., GEBAUER, D., SCHÄFER, H.J., GIL IBARGUCHI, J.I. & PEUCAT, J.J. (2001). A single Devonian subduction event for the HP/HT metamorphism of the Cabo Ortegal complex within the Iberian Massif. Tectonophysics 332, 359–385

ORTEGA GIRONÉS, E. & GIL IBARGUCHI, J.I. (1983). La Unidad de Malpica–Tuy ("Complejo Antiguo"–"Fosa Blastomilonítica"). In: Comba J.A. (ed). Geología de España (Libro Jubilar J.M.Rios), Tomo I, Instituto geológico y Minero de España (IGME), Madrid, 430–440

ORTEGA, E. (1980). Aportaciones a la estructura geológica de los alrededores de Malpica, extremo septentrional de la Fosa Blastomilonítica, La Coruña. Cuadernos del Laboratorio Xeológico de Laxe, 1, 177–186

ORTEGA–GUTIÉRREZ F., SOLARI L. A., SOLÉ. J., MARTENSB, U., GÓMEZ–TUENA, A., MORÁN–ICALA S. & REYES–SALASA, M. (2004). Polyphase, high–temperature eclogite–facies metamorphism in the Chuacus Complex, central Guatemala; petrology, geochronology, and tectonic implications. International Geology Review 46, 445–70

OTA, T. & KANEKO, Y. (2010). Blueschists, eclogites, and subduction zone tectonics: Insights from a review of Late Miocene blueschists and eclogites, and related high–pressure metamorphic rocks. Gondwana Research 18, 167–188

OXBURGH, D.L. & TURCOTTE, E.R. (1970). Thermal Structure of Island Arcs. Geological Society of America Bulletin 81, 1665–1688

PAQUETTE, J. L. (1987). Comportement des systèmes isotopiques U–Pb et Sm–Nd dans le métamorphisme éclogitique. Chaîne hercyniene et chaine alpine. Mem. Doc. Centre Arm. Struct. Socles14, Rennes, 190 p.

PAQUETTE, J.L., MARCHAND, J. & PEUCAT, J.J. (1984). Absence de tectonique cadomienne dans le complexe de Champtoceaux (Bretagne méridionale)? Comparaison des systèmes Rb–Sr et U–Pb d'un métagranite. Bulletin de la Société Géologique de France (7) XXV, 907–912

PAQUETTE, J.L., PEUCAT, J.J., BALLÈVRE, M., BOSSE, V., CAPDEVILA R. & CORNEN G. (in preparation). From oceanic spreading to continental subduction: Geochronology (and geochemistry) of mafic rocks from the Southern Armorican Massif (Variscan belt, France).

PARGA PONDAL, I. (1953a). Mapa geológico de España. Explicación de la hoja 43 (Lage). Instituto Geológico y Minero de España (IGME), Madrid

PARGA PONDAL, I. (1953b). Mapa geológico de España. Explicación de la hoja 44 (Carballo). Instituto Geológico y Minero de España (IGME), Madrid

PARGA PONDAL, I. (1953c). Mapa geológico de España. Explicación de la hoja 261 (Tuy–Valença). Instituto Geológico y Minero de España (IGME), Madrid

PARGA PONDAL, I. (1956). Nota explicativa del mapa geol.gico de la parte NO de la provincia de La Coruña. Leidse Geologische Mededelingen 21, 467–484

PARRISH, R., GOUGH, S.J., SEARLE, M. & DAVE, W. (2006). Plate velocity exhumation of ultrahigh-pressure eclogites in the Pakistan Himalaya. Geology 34, 989–992

PASTOR–GALÁN, D., GUTIERRÉZ–ALONSO, G., & WEIL, A.B. (2011). Orocline timing through joint analysis: Insights from the Ibero–Armorican Arc. Tectonophysics 507, 31–46

PASTOR–GALÁN, D., GUTIÉRREZ–ALONSO, G., ZULAUF, G. & ZANELLA, F. (2012). Analogue modeling of lithospheric–scale orocline buckling: Constraints on the evolution of the Iberian–Armorican Arc. Geological Society of America Bulletin 124, 1293–1309

PATIÑO DOUCE, A. (2011). Thermodynamics of the Earth and Planets. Cambridge University Press, Cambridge, 709 p.

PATOČKA, F., PIVEC, E. & OLIVERIOVÁ , D. (1997). Mineralogy and petrology of mafic blueschist from the Ry´ chory Mts. Crystalline Complex (Western Sudetes, Bohemian Massif). Neues Jahrbuch für Mineralogie Abhandlungen 170, 313–330

PATRICK, B. E. & EVANS, B. W. (1989). Metamorphic evolution of the Seward Peninsula Blueschist terrane. Journal of Petrology 30, 531–555

PATRICK, B.E. (1995). High pressure–low temperatura metamorphism of granitic orthogneisses in the Brooks Range, northern Alaska. Journal of Metamorphic Geology 13, 111–124

PAVLIS, T.L. & ROESKE, S.M. (2007). The Border Ranges fault system, southern Alaska. In: Ridgeway, K.D., Trop, J.M., Glen, J.M.G. & O'Oneill, J.M. (eds). Tectonic Growth of a Collisional Continental Margin: Crustal Evolution of Southern Alaska. Geological Society of America Special Paper 431, 95–127

PAWLEY, A. R. (1994). The pressure and temperature stability limits of lawsonite: implications for H_2O recycling in subduction zones. Contributions to Mineralogy and Petrology 118, 99–108

PEACOCK, S. M. (1987). Thermal effects of metamorphic fluids in subduction zones. Geology 15, 1057–1060

PEACOCK, S. M. (1989). Thermal effects of metamorphic fluids in subduction zones. Geology 15,1057–1060

PEACOCK, S. M. (1996). Thermal and petrologic structure of subduction zones. In: Bebout, G.E., et al., (eds). Subduction: Top to Bottom. American Geophysical Union Geophysical Monograph 96, 119–133

PEARCE, J.A. & PEATE, D.W. (1995). Tectonic implications of composition of volcanic arc magmas. Annual Review of Earth Planetary Sciences 23, 251–285

PEARCE, J.A. (1996). A user's guide to basalt discrimination diagrams. In: Wyman, D.A. (ed). Trace Element Geochemistry of Volcanic Rocks: Applications for Massive Sulphide Exploration. Short Course Notes. Geological Association of Canada 12, 79–113

PEARCE, J.A., HARRIS, N.G. & TINDLE, A.G. (19849. Trace element discrimination diagrams for the tectonic interpretation of granitic rocks. Journal of Petrology 25, 956–983

PERCHUK, L.L., KROTOV, A.V. & GERYA, T.V. (1999). Petrology of amphibolites of the Tanaelv Belt and granulites of the Lapland complex. Petrology 7, 539–563

PEREIRA, M.F., APRAIZ, A., CHICHORRO, M. , SILVA, J.B. & ARMSTRONG, R.A. (2010). Exhumation of high-pressure rocks in northern Gondwana during the Early Carboniferours (Coimbra-Cordoba shear zone, SW Iberian

Massif): tectonothermal analysis and U-Th-Pb SHRIMP in-situ zircon geochronology. Gondwana Research 17, 2–4

PEREIRA, M.F., SILVA, J.B., CHICHORRO, M., MOITA, P., SANTOS, J.F., APRAIZ, A. & RIBEIRO, C. (2007). Crustal growth and deformational processes in the northern Gondwana margin: Constraints from the Evora Massif (Ossa-Morena zone, southwest Iberia, Portugal). Geological Society of America Special Paper 423, 333–358

PERROUD, H. & VAN DER VOO, R. (1985). Paleomagnetism of the late Ordovician Thouars massif, Vendée province, France. Journal of Geophysical Research 90, 4611–4625

PERROUD, H., BONHOMMET, N. & THEBAULT, J.P. (1986). Palaeomagnetism of the Ordovician Moulin de Chateaupanne Formation, Vendée, western France. Geophysical Journal of the Royal Society of Astronomy 85, 573–582

PEUCAT, J.J. & COGNE, J. (1974). Les schistes cristallins de la Baie d'Audierne (Sud Finistère): un jalon intermédiaire entre la Meseta ibérique et les régions sud-armoricaines. Comptes-rendus de l'Académie des Sciences de Paris D-278, 1809–1812

PEUCAT, J.J. (1973). Les schistes cristallins de la baie d'Audierne: étude pétrographique et structurale. Unpublished PhD thesis, Université de Rennes. 108 p.

PEUCAT, J.J., BERNARD-GRIFFITHS, J., GIL IBARGUCHI, J.I., DALLMEYER, R.D., MÉNOT, R.P., CORNICHET, J. & IGLESIAS PONCE DE LEÓN, M. (1990). Geochemical and geochronological cross section of the deep Variscan crust: The Cabo Ortegal highPressure nappe (northwestern Spain). Tectonophysics 177, 263–292

PEUCAT, J.J., VIDAL, P., GODARD, G. & POSTAIRE, B. (1982). Precambrian UPb zircon ages in eclogites and garnet pyroxenites from south Brittany (France): an old oceanic crust in the west European Hercynian belt? Earth and Planetary Science Letters 60, 70–78

PHILIPPON, M., BRUN, J.P. & GUEYDAN, F. (2009). Kinematic records of subduction and exhumation in the Ile de Groix Blueschist (Hercynian belt; Western France). Journal of Structural Geology 31, 1308–1321

PHILIPPON, M., BRUN, J.P. & GUEYDAN, F. (2009). Kinematic records of subduction and exhumation in the Ile de Groix blueschists (Hercynian belt; Western France). Journal of Structural Geology 31, 1308–1321

PHILIPPON, M., GUEYDAN, F., PITRA, P. & BRUN, J. P. (2013). Preservation of subduction-related prograde deformation in lawsonite pseudomorph-bearing rocks. Journal of Metamorphic Geology 31, 571–583

PIÇARRA, J.M., ROBARDET, M., BOURAHROUH, A., PARIS, F., PEREIRA, Z., LE MENN, J., GOURVENNEC, R., OLIVEIRA, T. & LARDEUX, H. (2002). Le passage Ordovicien-Silurien et la partie inférieure du Silurien (Sud-Est du Massif armoricain, France). Comptes Rendus Geoscience 334, 1177–1183

PIÇARRA, J.M., ROBARDET, M., OLIVEIRA, J.T., PARIS, F. & LARDEUX, H. (2009). Graptolite faunas of the Llandovery «phtanites» at Les Fresnaies (Chalonnes-surLoire, southeastern Armorican Massif): Palaeontology and biostratigraphy. Bulletin of Geosciences 84, 41–50

PIN, C. & VIELZEULF, D. (1988). Les granulites de haute pression d´Europe moyenne témoins d´une subuctionéo-hercynienne. Implications surl´orgine des groupes leptyno- amphiboliques. Bulletin de la Societé Géologique de France 1, 13–20

PIN, C., ORTEGA CUESTA, L. A. & GIL IBARGUCHI, J.I. (1992). Mantle-derived, early Paleozoic A-type metagranitoids from the NW Iberian massif: Nd isotope and trace-element constraints. Bulletin de la Societe Geologique de France 163, 483–494

PIN, C., PAQUETTE, J.L., .BALOS, B., SANTOS ZALDUEGUI, J.F. & GIL IBARGUCHI, J.I. (2006). Composite origin of an early Variscan transported suture: Ophiolitic units of the Morais Nappe Complex (north Portugal). Tectonics 25: TC5001

PIN, C., PAQUETTE, J.L., SANTOS ZALDUEGUI, J.F. & GIL IBARGUCHI, J.I. (2002). Early Devonian supra-subduction zone ophiolite related to incipient collisional processes in the Western Variscan Belt: The Sierra de Careón unit, Ordenes Complex, Galicia. In: Martínez Catalán, J.R., Hatcher Jr., R.D., Arenas, R. & Díaz García, F. (eds). Variscan-Appalachian Dynamics: The Building of the Late Paleozoic Basement, Geological Society of America Special Paper 364, 57-71

PITRA P., KOUAMELAN A.N., BALLÈVRE M., PEUCAT J.J. (2010b). Palaeoproterozoic high-pressure granulite overprint of the Archaean continental crust: evidence for homogeneous crustal thickening (Man Rise, Ivory Coast). Journal of Metamorphic Geology 28, 41-58

PITRA, P. & GUIRAUD, M. (1996). Probable anticlockwise P-T evolution in extending crust: Hlinsko region, Bohemian Massif. Journal of Metamorphic Geology 14, 49-60

PITRA, P. (2011). Numerical modelling of phase equilibria and its contribution to understanding orogenic processes. Mémoire présenté en vue d´obtenir l´Habilitation à diriger des recherches. 66 p. Unpublished. http://tel.archives-ouvertes.fr/docs/00/61/17/28/PDF/HDR-Pitra.pdf

PITRA, P., BALLÈVRE, M. & RUFFET, G. (2010a). Inverted metamorphic field gradient towards a Variscan suture zone (Champtoceaux Complex, Armorican Massif, France). Journal of Metamorphic Geology 28, 183-208

PLAFKER, G. & BERG. H.C. (1994). Overview of the Geology and Tectonic Evolution of Alaska. In: Plafker, G. & Berg, H. (eds). The Geology of North America G-1, Chapter 33, The Geology of Alaska, Geological Society of America, 989-1021

PLAFKER, G. NOKLEBERG, W. J. & LULL, J. S. (1989). Bedrock geology and tectonic evolution of the Wrangellia, Peninsular, and Chugach terranes along the Trans-Alaska Crustal Transect in the Chugach Mountains and southern Copper River basin: Journal of Geophysical Research 94, 4255-4295

PLATT, J. P. (1993). Exhumation of high-pressure rocks: a review of concepts and processes. Terra Nova 5, 119-133

PLATT, J.P. (1986). Dynamics of orogenic wedges and the uplift of high-pressure metamorphic rocks. Geological Society of America Bulletin 97, 1037-1053

POLI, S. & FUMAGALLI, P. (2003). Mineral assemblages in ultrahigh pressure metamorphism: a review of experimentally determined phase diagrams. In: Ultrahigh Pressure Metamorphism, Carswell, D.A., Compagnoni, R. (eds). EMU n. 5, Eötvös University Press: Budapest, 307-340

POLI, S. & SCHMIDT, M. (2002). Petrology of subducted slabs. Annual Review of Earth and Planetary Sciences 30, 207-235

POLI, S. & SCHMIDT, M.W. (1995). Water transport and release in subduction zones: experimental constraints on basaltic and andesitic systems. Journal of Geophysical Research 100, 22299-22314

POWELL, R. & HOLLAND, T.J.B. (1985). An internally consistent thermodynamic dataset with uncertainties and correlations : 1. Methods and a worked example. Journal of Metamorphic Geology 3, 327-342

POWELL, R. & HOLLAND, T.J.B. (1988). An internally consistent dataset with uncertainties and correlations: 3. Applications to geobarometry, worked examples and a computer program. Journal of Metamorphic Geology 6, 173-204

POWELL, R. & HOLLAND, T.J.B. (1990). Calculated mineral equilbria in the pelite system, KFMASH. American Mineralogist 75, 367-380

POWELL, R. & HOLLAND, T.J.B. (1994) Optimal geothermometry and geobarometry. American Mineralogist 79, 120–133

POWELL, R. & HOLLAND, T.J.B. (2008). On thermobarometry. Journal of Metamorphic Geology 26, 155–179

POWELL, R. (1978). Equilibrium thermodynamics in petrology (An Introduction). Harper & Row, London, 284 p.

POWELL, R. GUIRAUD, M. & WHITE, R.W. (2005). Truth and beauty in metamorphic mineral equilibria: conjugate variables and phase diagrams. Canadian Mineralogist 43, 21–33

POWELL, R., HOLLAND, T.J.B. & WORLEY, B. (1998). Calculating phase diagrams involving solid solutions via nonlinear equations, with examples using THERMOCALC. Journal of Metamorphic Geology 16, 577–588

PROYER, A. (2003). Metamorphism of pelites in NKFMASH–a new petrogenetic grid with implications for the preservation of high–pressure mineral assemblages during exhumation. Jornal of Metamorphic Geology 21, 493–509

PROYER, A., DACHS, E. & MCCAMMON, C. (2004). Pitfalls in geothermobarometry of eclogites: Fe^{3+} and changes in the mineral chemistry of omphacite at ultrahigh pressures. Contributions to Mineralogy and Petrology 147, 305–318

RÅHEIM, A. (1977). Petrology of the Strathgordon area, western Tasmania: Si4+–content of phengite mica as a monitor of metamorphic grade. Journal of the Geological Society of Australia 24, 329–338

RANSOME, F. L. (1895). On lawsonite, a new rock–forming mineral from the Tiburon Peninsula, Marin County, California. California University Department of Geology Bulletin 1, 301–312

RAPP, R. P., SHIMIZU, N. & NORMAN, M. D. (2003). Growth of early continental crust by partial melting of eclogite. Nature 425, 605–609

RAVNA, E.J.K., ANDERSEN, B., JOLIVET, L. & DE CAPITANI, C. (2010). Cold subduction and the formation of lawsonite eclogite–constraints from prograde evolution of eclogitized pillow lava from Corsica. Journal of Metamorphic Geology 28, 381–395.

REBAY, G., POWELL, R. & DIENER, J.F.A. (2010). Calculated phase equilibria for a MORB composition in a P–T range, 450–650°C and 18–28 kbar: the stability of eclogite. Journal of Metamorphic Geology 28, 635–645

REDDY, P. R., RAJENDRA PRASAD, B., VIJAYA RAO, V., SAIN, K., PRASAD RAO, P., KHARE, P. & REDDY, M.S. (2003). Deep seismic reflection and refraction/wideangle reflection studies along kuppam–palani transect in the southern granulite terrain. Memoir – Geological Society of India 50, 79–106

REICHEN, L.E. & FAHEY, J.J. (1962). An improved method for the determination of FeO in rocks and minerals including garnet. In: Contributions to Geochemistry. Geological Survey Bulletin 144–B. United States Government Printing Office, Washington, B1–B5 p.

REYNARD, B. & BALLÈVRE, M. (1988). Coexisting amphiboles in an eclogite from the Western Alps: new constraints on the miscibility gap between sodic and calcic amphiboles. Journal of Metamorphic Geology 6, 333–350

RIBEIRO, A. (1974). Contribution a l'étude tectonique de Trás–osMontes Oriental. Memória dos Serviços Geologicos de Portugal, 24 (Nova Série), 179 p., 8 fold maps

RIBEIRO, A., DIAS, R. & BRANDAO SILVA, J. (1995). Genesis of the Ibero–Armorican arc. Geodinamica Acta 8, 173–184

RIBEIRO, A., PEREIRA, E. & DIAS, R. (1990). Structure in the Northwest of the Iberian Peninsula. In: Dallmeyer, R.D. & Martínez García, E. (eds). Pre–Mesozoic geology of Iberia. Springer–Verlag, Heidelberg, 220–236

RIBEIRO, M. L. (1976). Consideracões sobre a ocorrência de crossite em Trás-os-Montes oriental, Mem. Not. Publ. Mus. Lab. Mineral. Geol. Univ. Coimbra 82, 1-16

RIBEIRO, M.L. & FLOOR, P. (1987). Magmatismo peralcalino no Macico Hesperico: Sua distribuico e significado geodinamico, geologia de los granitoides y rocas asociadas del Macizo Hesperico. Libro Homenaje a L.C. García de Figuerola, 211-222 p.

RIES, A. C. & SHACKLETON, R. M. (1971). Catazonal complexes of North-West Spain and North Portugal, remnants of a Hercynian thrust plate. Nature 234, 65-69

RING, U., BRANDON, M.T., WILLET, S.D. & LISTER, G.S. (1999). Exhumation processes. In: RING, U., BRANDON, M.T., LISTER, G.S. & WILLET, S.D. (eds). Exhumation Processes: Normal Faulting, Ductile Flow and Erosion. Geological Society of London, Special Publication 154, 1-27

RIVIÈRE, L.M. (1977). Le Culm frasno-dinantien du synclinal d'Ancenis (S.E. du Massif armoricain) au Nord de la Loire. Bulletin de la Société Géologique et Minéralogique de Bretagne (C) IX, 19-57

ROBARDET, M. (2002). Alternative approach to the Variscan Belt of southwestern Europe: Preorogenic paleobiogeographical constraints. In: Martínez Catalán, J.R., Hatcher Jr., R.D., Arenas, R. & Díaz García, F. (Eds.), Variscan-Appalachian Dynamics: The Building of the Late Paleozoic Basement, Geological Society of America, Special Paper, 364, 1-15.

ROBARDET, M. (2003). The Armorica 'microplate': fact or fiction? Critical review of the concept and contradictory paleobiogeographical data. Palaeogeography, Palaeoclimatology, Palaeoecology 195, 125-148

ROBARDET, M., PARIS, F. & RACHEBOEUF, P.R. (1990). Paleogeographic evolution of southwestern Europe during Early Paleozoic times. In: McKerrow, W.S. & Scotese, C.R. (Eds.), Paleozoic palaeogeography and biogeography. Geological Society of London Memoir 12, 411-419

ROBIE, R.A., HEMINGWAY, B.S., GILLET, P. & REYNARD, B. (1991). On the entropy of glaucophane $Na_2Mg_3Al_2Si_8O_{22}(OH)_2$. Contributions to Mineralogy and Petrology 107, 484-486

RODDICK, J.C. (1983). High-precision intercalibration of 40Ar-39Ar standards. Geochimica et Cosmochimica Acta 47, 887-898

RODRÍGUEZ, J. (2005). Recristalización y deformación de litologías supracorticales sometidas a metamorfismo de alta presión (Complejo de Malpica-Tui, NO del Macizo Ibérico). Nova Terra 29, 410 p.

RODRÍGUEZ, J., COSCA, M.A., GIL IBARGUCHI, J.I., & DALLMEYER, R.D. (2003). Strain partitioning and preservation of $^{40}Ar/^{39}Ar$ ages during Variscan exhumation of a subducted crust (Malpica-Tui complex, NW Spain). Lithos 70, 111-139

RODRÍGUEZ, J., PAQUETTE, J.L., & GIL IBARGUCHI, J.I. (2007). U-Pb dating of Coger Ordovician alkaline magmatism in the Gondwana margin (Malpica-Tui Complex, Iberian Massif): Latest continental events before oceanic spreading. In: Arenas, R., Martínez Catalán, J.R. & Abati, J. (eds). The rootless Variscan suture of NW Iberia (Galicia, Spain): Field trip guide and conference abstracts: International Geological Correlation Programme 497, The Rheic Ocean: Its origin, evolution and correlatives: Publicaciones del Instituto Geológico y Minero de España (IGME), 163-164

ROESKE, S.M. (1986). Field relations and metamorphism of the Raspberry Schist, Kodiak Islands, Alaska. In: B.W. Evans, B.W. & Brown, E.H. (eds). Blueschists and eclogites. Geological Society of America Memoir 164, 169-184

ROESKE, S.M., MATTISON, J.M. & ARMSTRONG, R.L. (1989). Isotopic ages of glaucophane schist on the Kodiak Islands, southern Alaska, and their implications for the Mesozoic tectonic history of the Border Ranges Fault system. Geological Society of America Bulletin 101, 1021-1037

ROEVER, E.W.F. (1972). Lawsonite–albite–facies metamorphism near Fascaldo, Calabria (Southern Italy), its geological significance and petrological aspects. GUA Papers of Geology 1, nº 3

RUBIO PASCUAL, F. J., ARENAS, R., DÍAZ GARCÍA, F., MARTÍNEZ CATALÁN, J. R. & ABATI, J. (2002). Eclogites and eclogite–amphibolites from the Santiago Unit (Ordenes Complex, NW Iberian Massif, Spain): a case study of contrasting high–pressure metabasites in a context of crustal subduction. In: Martínez Catalán, J. R., Hatcher, R. D., Arenas, R. & Díaz García, F. (eds). Variscan–Appalachian Dynamics: the Building of the Late Paleozoic Basement: Geological Society of America Special Paper, 105–124

SÁNCHEZ MARTÍNEZ, S. (2009): Geoquímica y geocronología de las Ofiolitas de Galicia. Nova Terra 37, 351 p.

SÁNCHEZ MARTÍNEZ, S., ARENAS, R., ANDONAEGUI, P., MARTÍNEZ CATALÁN, J.R. & PEARCE, J.A. (2007b). Geochemistry of two associated ophiolites from the Cabo Ortegal Complex (Variscan Belt of NW Spain). In: Hatcher, R.D., Jr., Carlson, M.P., McBride, J.H. & Martínez Catalán, J.R. (eds). The 4D Framework of Continental Crust. Geological Society of America Memoir 200, 425–444

SÁNCHEZ MARTÍNEZ, S., ARENAS, R., DÍAZ GARCÍA, F., MARTÍNEZ CATALÁN, J.R., GÓMEZ–BARREIRO, J. & PEARCE, J.A. (2007a). Careón ophiolite, NW Spain: Suprasubduction zone setting for the youngest Rheic Ocean floor. Geology 35, 53–56

SÁNCHEZ MARTÍNEZ, S., ARENAS, R., FERNÁNDEZ–SUÁREZ, J. & JEFFRIES, T.E. (2009). From Rodinia to Pangaea: ophiolites from NW Iberia as witness for a long–lived continental margin. Geological Society of London, Special Publication 327, 317–341

SÁNCHEZ MARTÍNEZ, S., ARENAS, R., GERDES, A., CASTIÑEIRAS, P., POTREL, A. & FERNÁNDEZ–SUÁREZ, J. (2011). Isotope geochemistry and revised geochronology of the Purrido Ophiolite (Cabo Ortegal Complex, NW Iberian Massif): Devonian magmatism with mixed sources and involved Mesoproterozoic basement. Journal of the Geological Society of London 168, 733–750

SÁNCHEZ MARTÍNEZ, S., JEFFRIES, T., ARENAS, R., FERNÁNDEZ–SUÁREZ, J. & GARCÍA–SÁNCHEZ, R. (2006). A preRodinian ophiolite involved in the Variscan suture of Galicia (Cabo Ortegal Complex, NW Spain). Journal of the Geological Society of London163, 737–740

SANDIFORD, M. (2010). Why are the continents just so...?. Journal of Metamorphic Geology 28, 569–577

SANLOUP, C. (2012). High–pressure experimental geosciences: state of the art and prospects. Bulletin Société Géologique de France 183, 73–185

SANTOS ZALDUEGUI, J.F., SCHÄRER, U. & GIL IBARGUCHI, J. I. (1995). Isotope constraints on the age and origin of magmatism and metamorphism in the Malpica–Tuy allochthon, Galicia, NW–Spain. Chemical Geology 121, 91–103

SANTOS ZALDUEGUI, J.F., SCHÄRER, U., GIL IBARGUCHI, J.I. & GIRARDEAU, J. (1996). Origin and evolution of the Paleozoic Cabo Ortegal ultramaficMafic complex (NW Spain): U–Pb, Rb–Sr and Pb–Pb isotope data. Chemical Geology 129, 281–304

SANTOS ZALDUEGUI, J.F., SCHÄRER, U., GIL IBARGUCHI, J.I. & GIRARDEAU, J. (2002): Genesis of pyroxenite–rich peritotite at Cabo Ortegal (NW Spain): geochemical and Pb–Sr–Nd isotope data. Journal of Petrology 43, 17–43

SANTOSH, M. & KUSKY, T.M. (2010). Origin of paired high pressure–ultrahigh–temperature orogens: a ridge subduction and slab window model. Terra Nova 22, 35–42

SANTOSH, M., MARUYAMA, S. & SATO, K. (2009). Anatomy of a Cambrian suture in Gondwana: Pacific–type orogeny in southern India? Gondwana Research 16, 321–341

SCHÄFER, H.J., GEBAUER, D., GIL IBARGUCHI, J.I. & PEUCAT, J.J. (1993). IonMicroprobe UPb zircon dating on the HP/HT Cabo Ortegal Complex (Galicia, NW Spain): preliminary results. Terra Abstracts 5, 4, 22

SCHERMERHORN, L.G. & KOTSCH, S. (1984). First occurrence of lawsonite in Portugal and tectonic implications. Comunicados do Serviço Geologico do Portugal 70, 23-29

SCHLIESTEDT, M. & MATTHEWS, A. (1987). Transformation of blueschist to greenschist facies rocks as a consequence of fluid infiltration, Sifnos (Cyclades), Greece. Contributions to Mineralogy and Petrology 9, 237-250

SCHMIDT, M. W. (1995). Lawsonite: upper pressure stability and formation of higher density hydrous phases. American Mineralogist 80, 1286-1292.

SCHMIDT, M.W. & POLI, S. (1994). The stability of lawsonite and zoisite at high-pressure: experiments in CASH to 92 kbar and implications for the presence of hydrous phases in subducted lithosphere. Earth and Planetary Science Letters 124, 105-118

SCHREYER, W. & BALLER, T. (1977). Tale-muscovite: synthesis of a new high-pressure phyllosilicate assemblage. Neues Jahrbuch für Mineralogie Monatshefte 9, 421-425

SCHULMANN, K. LEXA, O., ŠTÍPSKÁ, P., RACEK, M. TAJČMANOVÁ, L., KONOPÁSEK, J., EDEL, J.B., PESCHLER, A. & LEHMANN, J. (2008). Vertical extrusion and horizontal channel flow of orogenic lower crust: key exhumation mechanisms in large hot orogens?. Journal of Metamorphic Geology 26, 273-297

SCHULTE, B. & SINDERN, S. (2002). K-rich fluid metasomatism at high-pressure metamorphic conditions: Lawsonite decomposition in rodingitized ultramafite of the Maksyutovo Complex, Southern Urals (Russia). Journal of Metamorphic Geology 20, 529-541

SCHULZ, G. (1858). Descripción geológica de la provincia de Oviedo. escala 1:400 000, Madrid. 138 p.

SCHULZ, G. (1900). Descripción geológica de la provincia de Oviedo, (2nd edition). Imprenta La Cantábrica (Navarro hermanos). 162 p.

SCHULZ, G. (1901). Descripción geológica de Asturias, (3rd edition). Biblioteca Bascongada de Fermín Herrán, 55, 238 p.

SCHULZ, G. (1930). Descripción geológica de la provincia de Oviedo, (4th edition). Gráficas Reunidas, Madrid, 176 p.

SCHÜRMANN, H.M.E. (1951). Beitrage zur Glaucophanfrage (1). Neues Jahrbuch für Mineralogie Monatshefte 49-68

SCHÜRMANN, H.M.E. (1953). Beitrage zur Glaucophanfrage (2). Neues Jahrbuch für Mineralogie Abhandlungen 85, 303-394

SCHÜRMANN, H.M.E. (1956). Beitrage zur Glaucophanfrage (3). Ibid 89, 41-85

SCOTESE, C.R. (1997). Continental Drift Flip Book, 7th edition, Arlington, Texas, 80 p.

SEKI, Y. (1958). Glaucophanitic regional metamorphism in the Kanto Mountains, central Japan. Japanese Journal of Geology and Geography 29,233-58

SENGÖR, A. M. C. (1999). Continental interiors and cratons: any relation?. Tectonophysics 305, 1-42

SERRANO-PINTO, M., CASQUET, C., IBARROLA, E., CORRETGÉ, L.G. & PORTUGAL-FERREIRA, M. (1988). Sintese geocronológica dos granitoides do macizo hesperico. In: Bea, F. et al. (eds). Geologia de los granitoides y rocas asociadas del macizo Hespérico, Rueda, Madrid, 69-86

SHAW, J., JOHNSTON, S.T., GUTIÉRREZ-ALONSO, G. & WEIL, A.B. (2012). Oroclines of the Variscan orogen of Iberia: Paleocurrent analysis and paleogeographic implications: Earth and Planetary Science Letters 329-330, 60-70

SHELLEY, D. & BOSSIÈRE, G. (1999). Ile de Groix: retrogression and structural developments in an extensional régime. Journal of Structural Geology 21, 1441–1445

SHI, G.H., CUI, W.Y., TROPPER, P., WANG, C.Q., SHU, G.M. & YU, H. (2003). The petrology of a complex sodic and sodic–calcic amphibole association and its implications for the metasomatic processes in the jadeitite area in northwestern Myanmar, formerly Burma. Contributions to Mineralogy and Petrology 145, 355–376

SISSON, V.B. & ONSTOTT, T.C. (1986). Dating blueschist metamorphism; a combined 40Ar/ 39Ar and electron microprobe approach: Geochimica et Cosmochimica Acta 50, 2111–2117

SMELIK, E. A. & VEBLEN, D. R. (1992). Exsolution of Ca-amphibole from glaucophane and the miscibility gap between sodic and calcic amphiboles. Contributions to Mineralogy and Petrology 112, 178–195

SMITH, C.A., SISSON, V.B., AVE´ LALLEMANT, H.G. & COPELAND, P. (1999). Two contrasting pressure–temperature–time paths in the Villa de Cura blueschist belt, Venezuela: Possible evidence for Late Cretaceous initiation of subduction in the Caribbean. Geological Society of America Bulletin 111, 831–848

SMITH, D.C. (1984). Coesite in clinopyroxene in the Caledonides and its implicalions for geodynamics. Nature 310, 641–644

SMULIKOWSKI, W. (1995). Evidence of glaucophane-schist facies metamorphism in the East Karkonosze Complex, West Sudetes, Poland. Geologische Rundschau 84, 720–737

SMULIKOWSKI, W., DESMONS, J., FETTES, D.J., HARTE, B., SASSI, F.P. & SCHMID R. (2007). Types, grade and facies of metamorphism. In: Fettes D. & Desmons J. (eds). Metamorphic rocks: A classifi cation and glossary of terms: Recommendations of the International Union of Geological Sciences Subcommission on the Systematics of Metamorphic Rocks. Cambridge University Press, Cambridge, 16–24

SMYE, A.J., GREENWOOD, L.V. & HOLLAND, T.J.B. (2010). Garnet–chloritoid–kyanite assemblages: eclogite facies indicators of subduction constraints in orogenic belts. Journal of Metamorphic Geology 28, 753–768

SOBOLEV, N.V. & SHATSKY, V.S. (1990). Diamond inclusions in garnets from metamorphic rocks: A new environment for diamond formation. Nature 343, 742–746

SONG, S.G., YANG, J.S., LIOU, J.G., WU, C.L., SHI, R.D. & XU, Z.Q. (2003). Petrology, geochemistry and isotopic ages of eclogites in the Dulan UHPM terrane, the North Qaidam, NW China. Lithos 70, 195–211

SONG, S.G., ZHANG, L.F., NIU, Y., WEI, C.J., LIOU, J.G. & SHU, G.M. (2007). Eclogite and carpholite-bearing metasedimentary rocks in the North Qilian suture zone, NW China: implications for Early Palaeozoic cold oceanic subduction and water transport into mantle. Journal of Metamorphic Geology 25, 547–563

SOUCHE, A., MEDVEDEV, S., ANDERSEN, T.B. & DABROWSKI, M. (2013). Shear heating in extensional detachments: implications for the thermal history of the Devonian basins of W Norway. Tectonophysics. doi: 10.1016/j.tecto.2013.07.005

SPANDLER, C., HERMANN, J., ARCULUS, R. & MAVROGENES, J. (2003). Redistribution of trace elements during prograde metamorphism from lawsonite blueschist to eclogite facies; implications for deep subduction–zone processes. Contributions to Mineralogy and Petrology 146, 205–222.

SPEAR, F. & CHENEY, J. (1989). A petrogenetic grid for pelitic schists in the system SiO_2–Al_2O_3–FeO–MgO–K_2O–H_2O. Contributions to Mineralogy and Petrology 101, 149–164

SPEAR, F.S. & MARKUSSEN, J.C. (1997). Mineral zoning, P–T–X–M phase relations, and metamorphic evolution of some Adirondack granulites, New York. Journal of Petrology 38, 757–783

SPEAR, F.S. & MENARD, T. (1989). Program GIBBS: A generalized Gibbs method algorithm. American Mineralogist 74, 942–943

SPEAR, F.S. (1988). The Gibbs method and Duhem's theorem: The quantitative relationships among P, T, chemical potential, phase composition and reaction progress in igneous and metamorphic systems. Contributions to Mineralogy and Petrology 99, 249–256

SPEAR, F.S. (1991). On the interpretation of peak metamorphic temperatures in light of garnet diffusion during cooling. Journal of Metamorphic Geology, 9, 379–388

SPEAR, F.S. (1993). Metamorphic Phase Equilibria and Pressure–Temperature–Time Paths. 1st edition. Mineralogical Society of America, Washington, D.C., 799 p.

SPEAR, F.S. (1995). Metamorphic Phase Equilibria and Pressure–Temperature–Time Paths. 2nd edition. Mineralogical Society of America, Washington, D.C., 799 p.

SPEAR, F.S., Kohn, M.J., Florence, F. & Menard, T. (1990). A model for garnet and plagioclase growth in pelitic schists: Implications for thermobarometry and P–T path determinations. Journal of Metamorphic Geology 8, 683–696

SPEAR, F.S., SELVERSTONE, J., HICKMOTT, P., CROWLEY, P. & HODGES, K.V. (1984). P–T paths from garnet zoning: a new technique for deciphering tectonic processes in crystalline terranes. Geology 12, 87–90

SPERRY, A. (2000). Pseudomorphs after lawsonite as an indication of pressure–temperature evolution in blueschists from Syros, Greece. 13th Keck Research Symposium in Geology Proceedings. The Keck Geology Consortium, Carleton College, Northfield, MN.

STAMPFLI, G.M. & BOREL, G.D. (2002). A plate tectonic model for the Paleozoic and Mesozoic constrained by dynamic plate boundaries and restored synthetic oceanic isochrones. Earth and Planetary Sciences Letters 196, 17–33

STAMPFLI, G.M., VON RAUMER, J.F. & BOREL, G.D. (2002). Paleozoic evolution of pre–Variscan terranes: From Gondwana to the Variscan collision. In: Martínez Catalán, J.R., Hatcher Jr., R.D., Arenas, R. & Díaz García, F. (eds). Variscan–Appalachian Dynamics: The Building of the Late Paleozoic Basement. Geological Society of America Special Paper 364, 263–280

STAUB, R. (1926). Gedanken zur Tektonik Spaniens. Vierteljahrsschrift der. Naturforschenden Gesellschaft in Zurich 71, 196–261

STECK, A., EPARD, J.L.. VANNAY, J.C., HUNZIKER, J., GIRARD, M., MORARO, A. & ROBYR, M. (1998). Geological transect across the Tso Morari and Spiti areas: The nappe structures of the Tethys Himalaya, Eclogae Geologicae Helvetiae 91, 103–121

STEIGER, R.H. & JÄGER, E. (1977). Subcommission on geochronology: Convention on the use of decay constants in geo– and eosmochronology. Earth and Planetary Science Letters 36, 359–362

STERN, R. J. (2002). Subduction Zones. Reviews of Geophysics. doi:10.1029/2001RG000108

STERN, R. J. (2004). Subduction initiation: spontaneous and induced. Earth and Planetary Science Letters 226, 275–292

STERN, R.J., (2005). Evidence from ophiolites, blueschists, and ultrahigh–pressure metamorphic terranes that the modern episode of subduction tectonics began in Neoproterozoic time. Geology 33, 557–560

STEVENS, C.H., DAVYDOV, V.I. & BRADLEY, D.C. (1997). Permian Tethyan fusilinids from the Kenai Peninsula, Alaska. Journal of Paleontology 71, 985–994

STEVENSON, D.J. (2003). Planetary magnetic fields. Earth and Planetary Science Letters Frontiers 208, 1–11.

STILLE, H. (1924). Grundfragen der Vergleichenden. Tectonik, Gebrueder Borntragen. Berlin

STILLE, H. (1951). Das mitteleuropäische variszische Grundgebirge im Bilde des gesamatenropäischen. Beihefte Geologischen Jahrbuch 2, 138 p.

ŠTÍPSKÁ, P., PITRA, P. & POWELL, R. (2006). Separate or shared metamorphic histories of eclogites and surrounding rocks? An example from the Bohemian Massif. Journal of Metamorphic Geology 24, 219–240

STOBER, I. & BUCHER, K. (2004) Fluid sinks within the earth's crust. Geofluids 4, 143–151

STRULLU–DERRIEN, C., DUCASSOU, C., BALLÈVRE, M., DABARD, M.P., GERRIENNE, P., LARDEUX, H., LE HÉRISSÉ, A., ROBIN, C., STEEMANS, P. & STRULLU, D.G. (2010). The early land plants from the Armorican Massif: sedimentological and palynological considerations on age and environment. Geological Magazine 147, 830–843

STUWE, K. & POWELL, R. (1995). P–T paths from modal proportions: application to the Koralm Complex, Eastern Alps. Contributions to Mineralogy and Petrology 119, 83–93

STÜWE, K. (1997). Effective bulk composition changes due to cooling: a model predicting complexities in retrograde reaction textures. Contributions to Mineralogy and Petrology 129, 43–52

SUESS, E. (1888). Das Antlitz der Erde, Volume 2: Vienna, Tempsky, 704 p.

SUESS, E. (1909). The Face of the Earth, translated from German (Suess, E., 1885. Das antlitz der erde. F. Tempsky, Vienna) by H.B.C. Sollas & W.J. Sollas: Oxford, Clarendon, 672 p.

SUZUKI, J. (1930). Petrological study of the crystalline schist system of Shikoku, Japan. Journal of Faculty of Science, Hokkaido Imperial University , 4, 27–111

SYMMES, G. H. & FERRY, J. M. (1992). The effect of whole–rock MnO content on the stability of garnet in pelitic schists during metamorphism. Journal of Metamorphic Geology 10, 221–237

TAJČMANOVÁ, L., CONNOLLY, J.A.D. & CESARE, B. (2009). A thermodynamic model for titanium and ferric iron solution in biotite. Journal of Metamorphic Geology 27, 153–64

TAJČMANOVÁ, L., KONOPÁSEK, J. & CONNOLLY, J. (2007). Diffusion–controlled development of silica–undersaturated domains in felsic granulites of the Bohemian Massif (Variscan belt of Central Europe). Contributions to Mineralogy and Petrology 153, 237–250

TAKCUCHI, H. & UYEDA, S. (1965). A possibility of present–day regional metamorphism. Tectonophysics 2, 59–68

TALIAFERRO, W. L. (1943). Franciscan–Knoxville problem. American Association of Petroleum Geologists Bulletin 27, 109–219

TARTÈSE, R., BOULVAIS, P., POUJOL, M., CHEVALIER, T., PAQUETTE, J.L., IRELAND, T.R. & DELOULE, E. (2012). Mylonites of the South Armorican Shear Zone: Insights for crustal–scale fluid flow and water–rock interaction processes. Journal of Geodynamics 56–57, 86–107

TARTÈSE, R., POUJOL, M., RUFFET, G., BOULVAIS, P., YAMATO, P. & KOSLER, J. (2011a). New UPb zircon and 40Ar/39Ar muscovite age constraints on the emplacement of the Lizio syn–tectonic granite (Armorican Massif, France). Comptes Rendus Geoscience 343 443–453

TARTÈSE, R., RUFFET, G., POUJOL, M., BOULVAIS, P. & IRELAND, T.R. (2011b). Simultaneous resetting of the muscovite K–Ar and monazite UPb geochronometers: a story of fluids. Terra Nova 23, 390–398

THEYE, T., SEIIDEL, E. & VIDAL, O. (1992). Carpholite, sudoite and chloritoid in low-grade high-pressure metapelites from Crete and the Peloponnese, Greece. European Journal of Mineralogy 4, 487-507

THIÉBLEMONT, D., CABANIS, B. & LE MÉTOUR, J. (1987b). Etude géochimique d'un magmatisme de distension intracontinentale: la série bimodale ordovico-silurienne du Choletais (Massif vendéen). Géologie de la France 1987-1, 65-76

THIÉBLEMONT, D., CABANIS, B., WYNS, R. & TREUIL, M. (1987a). Etude géochimique (majeurs et traces) de la formation amphibolitique de SaintMartin-des-Noyers (complexe cristallophyllien des Essarts, Vendée). Mise en évidence d'un paléo-arc insulaire dans la partie interne de l'orogensèe varisque. Bulletin de la Société Géologique de France (7) II, 371-378

THIÉBLEMONT, D., GUERROT, C., LE MÉTOUR, J. & JÉZÉQUEL, P. (2001). Le complexe de Cholet-Thouars: un ensemble volcano-plutonique cambrien moyen au sein du bloc précambrien des Mauges. Géologie de la France 2001 (1-2), 7-17

THIÉBLEMONT, D., TRIBOULET, C. & GODARD, G. (1988). Mineralogy, petrology and P-T-t path of Ca-Na amphibole assemblages, Saint-Martin des Noyers Formation, Vendée, France, Journal of Metamorphic Geology 6, 697-716

THIÉBLEMONT, D., TRIBOULET, C. & GODARD, G. (1988). Mineralogy, petrology and P-T-t paths of Ca-Na amphibole assemblages, SaintMartin-des-Noyers formation, Vendée, France. Journal of Metamorphic Geology 6, 697-715

THOMPSON, A.B., SCHULMANN, K., JEŽEK, J. (1997). Extrusion tectonics and elevation of lower crustal metamorphic rocks in convergent orogens. Geology 25, 491-494

THOMPSON, J. B. J., LAIRD, J. & THOMPSON, A. B. (1982). Reactions in amphibolite, greenschist and blueschist. Journal of Petrology 23, 1-27

THOMPSON, J.B. (1959). Local equilibrium in metasomatic processes. In: Abelson, P.H. (ed.). Researches in Geochemistry, Wiley, New York, 427- 457

TINKHAM, D. K., ZULUAGA, C. A. & STOWELL, H. H. (2003). Metapelite phase equilibria modeling in MnNCKFMASH: The effect of variable Al_2O_3 and MgO/(MgO + FeO) on mineral stability. American Mineralogist 88, 117

TINKHAM, D.K. & GHENT, E.D. (2005). Estimating P-T conditions of garnet growth with isochemical phase diagram sections and the problem of effective bulk-composition. Canadian Mineralogist 43, 35-50

TIREL, C., BRUN, J.P., BUROV, E., WORTEL, M. J.R. & LEBEDEV, S. (2013). A plate tectonics oddity: Caterpillar-walk exhumation of subducted continental crust. Geology 41, 555-558

TRACY, R.J. (1982). Compositional zoning and inclusions in metamorphic minerals. In: Ferry, J.M. (ed). Characterization of metamorphism through mineral equilibria. Mineralogical Society of America, Washington, 355-397

TRIBOULET, C. (1974). Les glaucophanites et roches associées de l'Île de Groix (Morbihan, France): étude minéralogique et pétrogénétique. Contributions to Mineralogy and Petrology 45, 65-90

TRIBOULET, C. (1974). Les glaucophanites et roches associéesde Ile de Groix (Morbihan, France): étude minéralogique et pétrologique. Contributions to Mineralogy and Petrology 45, 65-90

TRIBOULET, C. (1991). Etude geothermo-barométrique comparée des schistes bleus paléozoïques de l'ouest de la France (Ile de Groix, Bretagne méridionale et bois de Céné, Vendé e). Comptes Rendus de l'Académie des Sciences 312, 1163-1168

TROPPER, P., MANNING, C.E. & ESSENE, E.J. (2002). The substitution of Al and F in titanite at high pressure and temperature: experimental constraints on phase relations and solid solution properties. Journal of Petrology 43, 1787- 814

TRUYOLS, J. & MARCOS, A. (1978). La cartografía geológica de Asturias desde Guillermo Schulz a nuestros días. Trabajos de Geología, Universidad de Oviedo 10, 5-18

TSUJIMORI, T., SISSON, V.B., LIOU, J.G., HARLOW, G.E. & SORENSEN, S.S. (2006). Very-low temperature record of the subduction process: a review of worldwide lawsonite eclogites. Lithos 92, 609-624

TURNER, F.J. (1948). Mineralogical and structural evolution of the metamorphic rocks. Geological Society of America Memoirs 30, 1-342

TURNER, F.J. (1968). Metamorphic petrology, mineralogical, field and tectonic aspects. 1st edition. McGraw-Hill, New York. 403 p.

TURNER, F.J. (1981). Metamorphic petrology, mineralogical, field and tectonic aspects. 2nd edition. McGraw-Hill, New York. 524 p.

UGIDOS, J.M., BILSTRÖM, K., VALLADARES, M.I. & BARBA, P. (2003). Geochemistry of the Upper Neoproterozoic and Lower Cambrian siliciclastic rocks and U-Pb dating on detrital zircons in the Central Iberian Zone, Spain. International Journal of Earth Sciences 92, 661-676

VALLADARES, M.I., BARBA, P., UGIDOS, J.M., COLMENERO, J.R. & ARMENTEROS, I. (2000). Upper NeoproterozoicLower Cambrian sedimentary successions in the Central Iberian Zone (Spain): sequence stratigraphy, petrology and chemostratigraphy. Implications for the other European zones. International Journal of Earth Sciences 89, 2-20

VALVERDE- VAQUERO, P. & FERNÁNDEZ, F.J. (1996). Edad de enfriamiento U/Pb en rutilos del Gneis de Chímparra (Cabo Ortegal, NO de España). Geogaceta 20, 475-478

VALVERDE-VAQUERO, P., MARCOS, A., FARIAS, P. & GALLASTEGUI, G. (2005). UPb dating of Ordovician felsic volcanism in the Schistose Domain of the Galicia-Trás-osMontes Zone near Cabo Ortegal (NW Spain). Geológica Acta 3, 27-37

VAN CALSTEREN, P.W.C, BOBLRIJK, N.A.I.M., HEREDA, E.H., PRIEM, H.N.A., DENTEX, VERDURMEN, E.A.T.H. & VERSCHURE, R.H. (1979). Isotopic dating of older elements (including the Cabo Ortegal mafic-ultramafic complex) in the Hercynian Origen of NW Spain: manifestations of a presumed Early Paleozoic mantle-plume. Chemical Geology 24, 35-56

VAN CALSTEREN, P.W.C. (1977). Geochronological, geochemical and geophysical investigations in the highgrade mafic-ultramafic complex at Cabo Ortegal and other preexisting elements in the Hercynian basement of Galicia (NW Spain). Unpublished PhD thesis, Leiden University. 74 p.

VAN DER LAAN, S.R. & KOSTER VAN GROOS, A.F. (1991). PtFe alloys in experimental petrology applied to high-pressure research on Fe-bearing systems. American Mineralogist 76, 1940-1949

VAN DER PLAS, L. (1959). Petrology of the northern Adula region, Switzerland (with particular reference to glaucophane-bearing rocks). Leidse Geologische Mededelingen 24, 415-602

VAN DER WEGEN, G. (1978). Garnet-bearing metabasites from the Blastomylonitic Graben, western Galicia, Spain. Scripta Geologica, 45, Rijksmuseum van Geologie en Mineralogie, Leiden, 95 p.

VAN DER WEGEN, G. (1978). Garnet-bearing metabasites from the Blastomylonitic Graben, Western Galicia, Spain. Scripta Geologica 45, 1-95

VAN DINTHER, Y., MORRA, G., FUNICIELLO, F., ROSSETTI, F. & FACCENNA, C. (2012). Exhumation and subduction erosion in orogenic wedges: Insights from numerical models. Geochemistry Geophysics Geosystems 13, doi: 10.1029/2011GC004011.

VAN KEKEN, P.E., KIEFER, B. & PEACOCK, S.M. (2002). High-resolution models of subduction zones: Implications for mineral dehydration reactions and the transport of water to the deep mantle. Geochemistry, Geophysics, Geosystems 3, doi:10.1029/2001GC000256

VAN STAAL, C.R. (2005). The Northern Appalachians. In: Selley, R.C., Cocks, L.R.M. & Plimer, I.R. (Eds.), Encyclopedia of Geology, Elsevier, Oxford, 81–91

VAN STAAL, C.R., CURRIE, K.L., ROWBOTHAM, G., ROGERS, N. & GOODFELLOW, W. (2008). Pressure–temperature paths and exhumation of Late Ordovicianâ€"Early Silurian blueschists and associated metamorphic nappes of the Salinic Brunswick subduction complex, northern Appalachians. Geological Society of America Bulletin 120, 1455–1477

VAN STAAL, C.R., DEWEY, J.F., MACNIOCAILL, C. & MCKERROW, W.S. (1998). The Cambrian–Silurian tectonic evolution of the northern Appalachians and British Caledonides: history of a complex, west and southwest Pacific–type segment of Iapetus. In: Blundell, D.J. & Scott, A.C. (eds). Lyell: the past is the key to the present. Geological Society of London Special Publication,143, 199–242

VAN ZUUREN, A. (1969). Structural petrology of an area near Santiago de Compostela (NW Spain). Leidse Geologische Mededelingen 45, 1–71

VANCE, D. & HOLLAND, T.J.B. (1993). A detailed isotopic and petrological study of a single garnet from the Gassetts Schist, Vermont. Contributions to Mineralogy and Petrology 114,101–18

VANCE, D. & MAHAR, E. (1998). Pressure–temperature paths from P–T pseudosections and zoned garnets: potential, limitations and examples from the Zanskar Himalaya, NW India. Contributions to Mineralogy and Petrology,132, 225–245

VEGA–GRANILLO, R., TALAVERA–MENDOZA, O., MEZA–FIGUEROA, D., RUIZ, J., GEHRELS, G.E., LÓPEZ–MARTÍNEZ, M. & DE LA CRUZ–VARGAS, J.C. (2007). Pressure–temperature–time evolution of Paleozoic high–pressure rocks of the Acatlán Complex (southern Mexico): Implications for the evolution of the Iapetus and Rheic Oceans. Geological Society of America Bulletin 119, 1249–1264

VELDE, B. (1972). The origin of some granulite facies rocks from the Baie d'Audierne, Finistère. Bulletin de la Société Géologique et Minéralogique de Bretagne (C) IV, 91–95

VERNON R.H. & CLARKE, G.L. (2008). Principles of Metamorphic Petrology. Cambridge University Press, New York, 446 p.

VIERECK, L.G., FLOWER M.F.J., HERTOGEN, J., SCHMINCKE, H.U. & JENNER, G.A. (1989). The genesis and significance of N–MORB sub–types. Contributions to Mineralogy and Petrology 102, 112–126

VILLA, J.E., HERMANN, I.M., MÜNTENER, O. & TROMMSDORFF, V. (2000). ^{40}Ar–^{39}Ar dating of multiply zoned amphibole generations (Malenco, Italian Alps). Contributions to Mineralogy and Petrology 140, 363–381

VITALE BROVARONE, A., GROPPO, C., HETÉNYI, G., COMPAGNONI, R. & MALAVIEILLE, J. (2011). Coexistence of lawsonite–bearing eclogite and blueschist: phase equilibria modelling of Alpine Corsica metabasalts and petrological evolution of subducting slabs. Journal of Metamorphic Geology 29, 583–600

VOGEL, D.E. (1967). Petrology of an eclogite –and pyrigarnite– bearing polymetamorphic rock Complex at Cabo Ortegal, NW Spain. Leidse Geologische Mededelingen 40, 121–213

VOGT, T. (1927). Sulitelmafeltets geologi og petrografi. Norges geologiske undersøkelser 121, 560 p.

VON RAUMER, J.F. & STAMPFLI, G.M. (2008). The birth of the Rheic Ocean–Early Palaeozoic subsidence patterns and subsequent tectonic plate scenarios. Tectonophysics 46, 9–20

VON RAUMER, J.F., BUSSY, F., STAMPFLI, G.M. & BOREL, G. (2009). The Variscan evolution in the External massifs of the Alps and place in their Variscan framework. Comptes Rendus Geoscience 341, 239–252

WAKABAYASHI, J. (1990). Counterclockwise P–T–t paths from amphibolites, Franciscan Complex, California: relics from the early stages of subduction zone metamorphism. Journal of Geology 98, 657–680

WALKER, J.D., GEISSMAN, J.W., BOWRING, S.A., & BABCOCK, L.E., compilers. (2012). Geologic Time Scale v. 4.0: Geological Society of America, doi: 10.1130/2012.CTS004R3C

WANG, L., KUSKY, T. & LI, S.Z. (2010). Structural Geometry and Evolution of an Exhumed Ultra–High Pressure Eclogite Massif, Yangkou Bay, Sulu Belt, China. Journal of Structural Geology, DOI: 10.1016/j.jsg.2010.01.012

WARREN, C. J. & MILLER, J. M. (2007). Structural and stratigraphic controls on the origin and tectonic history of a subducted continental margin, Oman. Journal of Structural Geology 29, 541–558

WARREN, C.J. & WATERS, D.J. (2006). Oxidized eclogites and garnet–blueschists from Oman: P–T path modeling in the NCFMASHO system. Journal of Metamorphic Geology 24, 783–802

WARREN, C.J. (2013). Exhumation of (ultra–)high–pressure terranes: concepts and mechanisms. Solid Earth 4, 75–92

WARREN, C.J., BEAUMONT, C. & JAMIESON, R.A. (2008a). Deep subduction and rapid exhumation: Role of crustal strength and strain weakening in continental subduction and ultrahigh–pressure rock exhumation. Tectonics 27: TC6002

WARREN, C.J., BEAUMONT, C. & JAMIESON, R.A. (2008b). Modelling tectonic styles and ultrahigh pressure (UHP) rock exhumation during the transition from oceanic subduction to continental collision. Earth and Planetary Science Letters 267, 129–145

WARREN, C.J., BEAUMONT, C. & JAMIESON, R.A. (2008c). Formation and exhumation of UHP rocks during continental collision: Role of detachment in the subduction cannel. Geochemistry, Geophysics, Geosystems 9: Q04019

WARREN, C.J., HANKE F. & KELLEY, S.P. (2012). When can muscovite $^{40}Ar/^{39}Ar$ dating constrain the timing of metamorphic exhumation?. Chemical Geology 291, 79–86

WEI, C.J. & POWELL, R. (2003). Phase relations in high–pressure metapelites in the system KFMASH (K_2O–FeO–MgO–Al_2O_3–SiO_2–H_2O) with application to natural rocks. Contributions to Mineralogy and Petrology 145, 301–315

WEI, C.J. & POWELL, R. (2004). Calculated Phase Relations in High–Pressure Metapelites in the System NKFMASH (Na_2O–K_2O–FeO–MgO–Al_2O_3–SiO_2–H_2O). Journal of Petrology 45, 183–202

WEI, C.J. & POWELL, R. (2006). Calculated phase relations in the system NCKFMASH (Na_2O–CaO–K_2O–FeO–MgO–Al_2O_3–SiO_2–H_2O) for high–pressure metapelites. Journal of Petrology 47, 385–408

WEI, C.J. & SONG, S.G. (2008). Chloritoid–glaucophane schist in the north Qilian orogen, NW China: phase equilibria and P–T path from garnet zonation. Journal of Metamorphic Geology 26, 301–316

WEI, C.J., POWELL, R. & ZHANG, L.F. (2003). Eclogites from the south Tianshan, NW China: petrological characteristic and calculated mineral equilibria in the Na_2O–CaO–FeO–MgO–Al_2O_3–SiO_2–H_2O system. Journal of Metamorphic Geology 21,169–179

WEI, C.J., YANG, Y., SU, X.L., SONG, S.G. & ZHANG, L.F. (2009). Metamorphic evolution of low-T eclogite from the north Qilian orogen, NW China: Evidence from petrography and calculated phase equilibrium in the system NCKFMASHO. Journal of Metamorphic Geology 27, 55-70

WEIL, A. B., GUTIÉRREZ-ALONSO, G., JOHNSTON, S. T. & PASTOR-GALÁN, D. (2013). Kinematic constraints on buckling a lithospheric-scale orocline along the northern margin of Gondwana.: A geologic synthesis. Tectonophysics 582, 25-49

WEIL, A.B. (2006). Kinematics of orocline tightening in the core of an arc: Paleomagnetic analysis of the Ponga Unit, Cantabrian Arc, northern Spain. Tectonics 25: TC3012

WEIL, A.B., GUTIÉRREZ-ALONSO, G., & CONAN, J. (2010). New time constraints on lithospheric-scale oroclinal bending of the Ibero-Armorican arc: a palaeomagnetic study of earliest Permian rocks from Iberia. Journal of the Geologic Society of London 167, 127-143

WEIL, A.B., VAN DER VOO, R., & VAN DER PLUIJM, B.A. (2001). Oroclinal bending and evidence against the Pangea megashear: The Cantabria-Asturias arc (northern Spain). Geology 29, 991-994

WEIL, A.B., VAN DER VOO, R., VAN DER PLUIJM, B.A. & PARES, J.M. (2000). The formation of an orocline by multiphase deformation: a paleomagnetic investigation of the Cantabria-Asturias Arc (northern Spain). Journal of Structural Geology 22, 735-756

WHITE, R.W. & POWELL, R. (2002). Melt loss and the preservation of granulite facies mineral assemblages. Journal of Metamorphic Geology 20, 621-632

WHITE, R.W., POMROY, N.E. & POWELL, R. (2005). An in-situ metatexite-diatexite transition in upper amphibolite facies rocks from Broken Hill, Australia. Journal of Metamorphic Geology 23, 579-602

WHITE, R.W., POWELL, R. & CLARKE, G.L. (2002). The interpretation of reaction textures in Fe-rich metapelitic granulites of the Musgrave Block, central Australia: Constraints from mineral equilibria calculations in the system K_2O-FeO-MgO-Al_2O_3-SiO_2-H_2O-TiO_2-Fe_2O_3. Journal of Metamorphic Geology 20, 41-55

WHITE, R.W., POWELL, R. & HOLLAND, T.J.B. (2001). Calculation of partial melting equilibria in the system CaO-Na_2O-K_2O-FeO-MgO-Al_2O_3-SiO_2-H_2O (CNKFMASH). Journal of Metamorphic Geology 19, 139-153

WHITE, R.W., POWELL, R. & HOLLAND, T.J.B. (2007). Progress relating to calculation of partial melting equilibria for metapelites. Journal of Metamorphic Geology 25, 511-527.

WHITE, R.W., POWELL, R., HOLLAND, T.J.B. & WORLEY, B. (2000). The effect of TiO_2 and Fe_2O_3 on metapelitic assemblages at greenschist and amphibolite facies conditions: mineral equilibria calculations in the system K_2O-FeO-MgO-Al_2O_3-SiO_2-H_2O-TiO_2-Fe_2O_3. Journal of Metamorphic Geology 18, 497-511

WHITNEY, D.L. & EVANS, B.W. (2010). Abbreviations for names of rock-forming minerals. American Mineralogist 95, 185-187

WILL, T., OKRUSCH, M., SCHMÄDICKE, E. & CHEN, G. (1998). Phase relations in the greenschist-blueschist-amphibolite-eclogite facies in the system Na_2O-CaO-FeO-MgO-Al_2O_3-SiO_2-H_2O (NCFMASH), with application to metamorphic rocks from Samos, Greece. Contributions to Mineralogy and Petrology 132, 85-102

WILLNER, A.P., GLODNY, J., GERYA, T.V., GODOY, E. & MASSONNE, H.J. (2004). A counterclockwise P-T-t path of high-pressure/low-temperature rocks from the Coastal Cordillera accretionary complex of south-central Chile: constraints for the earliest stage of subduction mass flow. Lithos 75, 283-310

WILSON, A. D. (1955). A new method for the determination of ferrous iron in rocks and minerals : Bulletin of the Geological Survey of Great Britain 9, 56-58

WINCHESTER, J.A., PHARAOH, T.C. & VERNIERS, J. (2002). Palaeozoic amalgamation of Central Europe: an introduction and synthesis of new results from recent geological and geophysical investigations. In: Winchester, J.A., Pharaoh, T.C. & Verniers, J. (eds). Palaeozoic Amalgamation of Central Europe. Geological Society Special Publication 201, 1–18

WINDLEY, B.F. (1995). The evolving continents. 3rd edition. John Wiley & Sons, Chichester ,526 p.

WING, B. A. & FERRY, J. M. (2002). Three-dimensional geometry of metamorphic fluid flow during Barrovian regional metamorphism from an inversion of combined petrologic and stable isotope data. Geology 30, 639–642

WING, B. A., & FERRY, J. M. (2007). Magnitude and geometry of reactive fluid flow from direct inversion of spatial patterns of geochemical alteration. American Journal of Science 307, 793–832

WINKLER, H. G. F. (1965). Petrogenesis of metamorphic rocks. 1st edition. Springer-Verlag, New York, 220 p.

WINKLER, H. G. F. (1967). Petrogenesis of metamorphic rocks. 2nd edition. Springer-Verlag, New York, 237 p.

WINTER, J.D. (2001). An introduction to igneous and metamorphic petrology. Prentice Hall, Upper Saddle River, New Jersey, 697 p.

WOOD, B.J. & FRASER, D.G. (1977). Elementary Thermodynamics for Geologists. Oxford University Press, Cary, North Carolina, 318 p.

WU, H.Q., FENG, Y.M. & HOU, Y. (1990). The discovery of Ordovician lawsonite-glaucophane schist in the middle section of the Northern Qianlian Mountains, Sunan County, Gansu Province, and its significance (in Chinese with English abstract). Geological Review 3, 277–280

WYNS, R., LARDEUX, H. & WEYANT, M. (1989). Présence de Dévonien dans le Groupe de Réaumur (synclinal de Chantonnay, Vendée). Conséquence sur l'évolution géodynamique de la Vendée. Comptes Rendus de l'Académie des Sciences de Paris II–308, 855–860

YAKOVLEV, L.Y. (1993). The role of metamorphism of the basaltic basement of sedimentary basins in crustal evolution. International Geology Review 35, 27–47

YARDLEY, B.W.D. (1989). An introduction to Metamorphic Petrology. Longman Scientific & Technical, London, 248 p.

YOUNG, T.P. (1990). Ordovician sedimentary facies and faunas of Southwest Europe: palaeogeographic and tectonic implications. In: McKerrow, W.S. & Scotese, C.R. (eds). Palaeozoic Palaeogeography and Biogeography. Geological Society Memoir 12, 421–430

ZACK, T., RIVERS, T., BRUMM, R. & KRONZ, A. (2004). Cold subduction of oceanic crust: implications from a lawsonite eclogite from the Dominican Republic. Eur opean Journal of Mineralogy 16, 909–916

ZÁČKOVÁET, E., KONOPÁSEK, J., JEŘÁBEK, P., FINGER, F. & KOŠLER, J. (2010). Early Carboniferous blueschist facies metamorphism in metapelites of the West Sudetes (Northern Saxothuringian Domain, Bohemian Massif. Journal of Metamorphic Geology 28, 361–379

ZHANG, J.X. & MENG, F.C. (2006). Lawsonite-bearing eclogites in the north Quilian and north Altyn Tagh: evidence for cold subduction of oceanic crust. Chinese Science Bulletin 51, 1238–1244

ZHANG, L., WANG, Q. & SONG, S. (2009). Lawsonite blueschist in Northern Qilian, NW China: P–T pseudosections and petrologic implications. Journal of Asian Earth Sciences 35, 354–366

ZHANG, Z., ZHU, W., SHU, L., WAN, J., YANG, W., SU, J. & ZHENG, B. (2009). Apatite fission track thermochronology of the Precambrian Aksu blueschist, NW China: Implications for thermo-tectonic evolution of the north Tarim basement. Gondwana Research 16, 182–188.

ZUCALI, M. & SPALLA, M.I. (2011). Prograde lawsonite during the flow of continental crust in the Alpine subduction: Strain vs. metamorphism partitioning, a field-analysis approach to infer tectonometamorphic evolutions (Sesia-Lanzo zone, Western Italian Alps). Journal of Structural Geology 33, 381–398

ZULUAGA, C.A., STOWELL, H.H. & TINKHAM, D.K. (2005). The effect of zoned garnet on metapelite pseudosection topology and calculated metamorphic P–T paths. American Mineralogist 90, 1619–1628

ANNEXES

ANNEX I (R.D. 1393/2007)

ANNEX II (l´Arrêté 6 janvier 2005/Article 11)

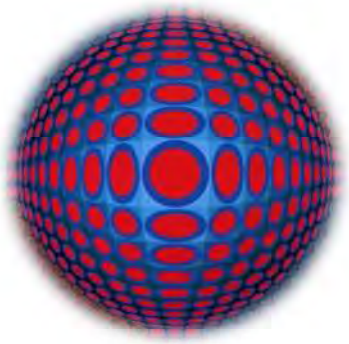

ANNEX I

1. *Introducción*

El hundimiento de material litosférico frío y denso en las zonas de subducción es el principal motor de las placas tectónicas. El descenso del material cortical a profundidades mantélicas constituye el origen de las rocas metamórficas de alta presión (AP) y baja-media temperatura (B/M-T), conocidas como los esquistos azules y las eclogitas. Estas rocas afloran frecuentemente en las zonas de sutura de los cinturones orogénicos y se conciben como marcadores de zonas de subducción, extintas y activas. Las asociaciones minerales que las constituyen almacenan mucha información relacionada con los procesos de convergencia entre los bordes de placa, proporcionando valiosas pistas para la comprensión de la historia termal del Planeta Tierra. En este contexto, el estudio de la paleogeografía y la dinámica de las placas litosféricas durante el Paleozoico en el entorno peri-Gondwánico ha sido el marco de numerosos trabajos a lo largo de las últimas décadas, siendo aún muchos los interrogantes que quedan por resolver. El conocimiento de las características de esta subducción, su polaridad, su cronología, las condiciones físicas máximas alcanzadas o la geometría y características de sus trayectorias P-T aportaría nuevos datos para el conocimiento de la evolución de estos terrenos durante la colisión varisca.

2. *Objetivos y metodología*

La investigación llevada a cabo en esta tesis doctoral ha consistido en 1) un estudio petrológico y termobarométrico detallado, mediante pseudosecciones, de las rocas en facies de esquistos azules del Complejo de Malpica-Tui (MTC; Galicia, España), (2) un estudio geocronológico empleando el método del $^{40}Ar/^{39}Ar$ en dichas rocas y (3) la correlación del MTC con terrenos equivalentes en el dominio sur armoricano (Macizo Armoricano, Francia).

Los objetivos específicos son:

(1) Un estudio petrológico y termobarométrico detallado de los esquistos de Ceán y las metabasitas de Cambre usando la siguiente metodología:

- Recopilación y revisión bibliográfica de la zona de estudio, así como del resto de los Complejos Alóctonos del NO peninsular, con el fin de obtener una visión amplia del marco geológico regional.

- Muestreo y recopilación de datos de campo.

- Estudio petrográfico de las láminas delgadas correspondientes a las muestras tomadas en campo.

- Análisis de la composición química de los minerales de interés termobarométrico mediante microsonda electrónica y microscopio electrónico de barrido. Los análisis minerales así como los mapas de rayos-X se han realizado con una microsonda JEOL-Superprobe JXA-8900M, equipada con cinco espectrómetros ubicada en el Centro Nacional de Microscopía Electrónica de la Universidad Complutense de Madrid (http://www.cnme.es). Las imágenes de electrones secundarios se obtuvieron con un microscopio electrónico de barrido JEOL JSM-820 equipado con un microanalizador EDX ubicado en el Centro de Asistencia a la Investigación de Técnicas Geológicas de la Facultad de Ciencias Geológicas de la Universidad Complutense de Madrid (http://www.ucm.es/centros/webs/cai5134).

- Análisis de geoquímica de roca total de las litologías más representativas mediante espectrometría de fluorescencia de rayos-X (XRF). La proporción de FeO (vs. Fe_2O_3) se determinó mediante análisis volumétrico ("titration"). Los análisis químicos se realizaron en Activation Laboratories Ltd. (Actlabs, Canada; http://www.actlabs.com). Los métodos empleados para la obtención de los análisis de roca total (XRF y "titration") se detallan en la sección 1.2 del Capítulo 1.

- Modelización numérica del equilibrio de fases empleando herramientas de software científico como THERMOCALC (Powell & Holland, 1988) y Perple_X (Connolly, 1990).

(2) El establecimiento de la trayectoria P–T detallada de dichas litologías con el fin de caracterizar los procesos de subducción y su evolución posterior.

(3) Proporcionar un marco temporal a los resultados termobarométricos obtenidos mediante el método de datación $^{40}Ar/^{39}Ar$ usando la técnica del "step heating" en concentrados y cristales individuales de mica blanca.

(4) Teniendo en cuenta los datos anteriores, estudiar las implicaciones de la evolución metamórfica de la Unidad de Ceán para la evolución del cinturón varisco europeo y compararla con terrenos equivalentes en el dominio sur armoricano.

La metodología empleada para la modelización petrológica y para la datación $^{40}Ar/^{39}Ar$ usando la técnica del "step heating" se detalla en las secciones 1.5.2 y 3.2.2, respectivamente.

Las especificaciones analíticas referentes a los parámetros establecidos para el uso de la microsonda electrónica se detallan para cada litología a lo largo del Capítulo 3.

3. *Enfoque de la investigación y aportaciones*

Esta tesis doctoral se presenta como compendio de publicaciones e incluye tres artículos publicados en revistas indexadas (SCI; Artículos 1, 2 y 4) y dos artículos en fase de revisión (Artículos 3 y 5). En cuatro de los artículos el autor de la memoria es el primer firmante.

La presente investigación comprende cuatro etapas. Cada una de las tres primeras representa una sección del Capítulo 3, mientras que la cuarta etapa cubre la totalidad del Capítulo 4.

La primera etapa se centra en el estudio de los esquistos de Ceán. El estudio de esta litología constituye la continuación natural del trabajo iniciado para la obtención del DEA. Los esquistos pelíticos de los niveles estructurales inferiores de la secuencia volcanosedimentaria contienen numerosos porfiroblastos de granate que preservan las foliaciones más antiguas descritas en estas rocas. Las inclusiones preservadas en la primera generación de crecimiento de granates hacen de esta litología la más adecuada para el estudio de las condiciones P-T y de las fases de deformación asociadas a la subducción. La segunda generación de granates contiene una paragénesis en la que destaca la asociación cloritoide-glaucofana, que se caracteriza por ser uno de los indicadores de condiciones de AP en rocas metapelíticas, y que se ha identificado en numerosos terrenos de esquistos azules en el mundo (ej. Kiénast & Triboulet, 1972; Kryza *et al.*, 1990; Katagas, 1980; Theye *et al.*, 1992; Chopin, 1981; Song *et al.*, 2007; Wei & Song, 2008; El-Shazly & Liou, 1991; Warren & Waters, 2006). Sin embargo, esta asociación mineral no se había descrito con anterioridad en los terrenos del NO del Macizo Ibérico. Por tanto, uno de los objetivos de este estudio es documentar la existencia de la paragénesis cloritoide-glaucofana en los esquistos pelíticos del Complejo de Malpica-Tui mediante un estudio petrológico y termobarométrico detallado (ARTÍCULO 1).

Los resultados obtenidos de la investigación anterior incluyen una aproximación inicial a la cuantificación de las condiciones P-T de los esquistos de Ceán, así como una propuesta de evolución metamórfica. Sin embargo, en el trascurso de dicho estudio surgieron interesantes incógnitas que conciernen a los efectos de componentes químicos clave en la evolución metamórfica de esta litología como el H_2O o el Fe_2O_3. Al igual que en las metabasitas, las asociaciones de AP en las metapelitas son extremadamente sensibles a las variaciones en las proporciones de ambos óxidos. Con el fin de obtener resultados que reflejen los efectos de estos componentes en la modelización petrológica de los esquistos de Ceán, así como unas condiciones P-T lo más precisas posibles, se han estudiado los efectos del H_2O y del Fe_2O_3. La incertidumbre asociada al papel del fluido (en este caso el agua) y del estado de oxidación del hierro está íntimamente relacionada con la dificultad para cuantificar las proporciones reales de ambos componentes mediante los métodos analíticos existentes (ej. Guiraud *et al.*, 2001; Diener & Powell, 2010; Rebay *et al.*, 2010). A través de la construcción de pseudosecciones en

distintos sistemas químicos ha sido posible estimar las proporciones de ambos óxidos durante la etapa prograda de la evolución metamórfica de los esquistos de Ceán, y los resultados obtenidos de la modelización numérica permiten establecer estimaciones de primer orden en los modelos geodinámicos que podrían tener una aplicación general en la investigación de rocas con una composición "similar" (ARTÍCULO 2).

La segunda etapa de investigación en la presente tesis doctoral se centra en el estudio de las metabasitas de Cambre. Esta litología se interpreta como esquistos azules fuertemente retrogradados a anfibolitas y esquistos verdes que preservan pseudomorfos de lawsonita (Rodríguez, 2005). La lawsonita es un silicato hidratado de calcio y aluminio que cristaliza en condiciones de M/AP y BT (ej. Crawford & Fyfe, 1965; Liou, 1971; Pawley, 1994; Schmidt & Poli, 1994; Schmidt, 1995; Comodi *et al.*, 1996). Por tanto, es otro de los minerales clave que se ha usado como indicador de condiciones de esquistos azules y, con menos frecuencia, de eclogitas de BT, en numerosos cinturones de AP (ej. Maruyama *et al.*, 1996; Tsujimori *et al.*, 2006). Durante la descompresión la lawsonita se desestabiliza fácilmente a minerales secundarios (en general a minerales del grupo de la epidota, micas blancas, clorita y albita). Por tanto, es más común la presencia de pseudomorfos de lawsonita que encontrar cristales frescos preservados de dicho mineral. Por su alto contenido en H_2O, la lawsonita constituye la mayor fuente y reservorio de agua en los sistemas máficos de AP–BT, desempeñando un papel fundamental en el transporte de dicho fluido en las zonas de subducción. Al modelizar rocas de AP frecuentemente se asumen condiciones de saturación en agua durante la subducción, sin embargo, estudios recientes (Ballèvre *et al.*, 2003; Clarke *et al.*, 2006; incluyendo la investigación llevada a cabo en los esquistos de Ceán; López-Carmona *et al.*, 2013) sugieren que la cristalización de la lawsonita puede conducir, en determinadas ocasiones, a que la evolución prograda de la roca suceda en condiciones de subsaturación en H_2O. En consecuencia, la evolución metamórfica de los esquistos azules retrogradados se ha investigado mediante el cálculo de pseudosecciones, evaluando la posibilidad de que experimentasen un metamorfismo subductivo en condiciones de subsaturación en agua inducidas por la cristalización de la lawsonita así como investigando los cambios en el estado de oxidación que afectan al equilibrio químico durante el metamorfismo. La riqueza de asociaciones minerales en las metabasitas de Cambre y su compleja química mineral favorecen la idoneidad de esta litología para evaluar sus condiciones P–T. Los resultados alcanzados en este estudio complementan, y son consistentes, con los obtenidos para las rocas metapelíticas, lo que ha permitido establecer una historia P–T para el Alóctono Medio del MTC. De forma complementaria, la edad del evento de AP obtenida mediante el método del $^{40}Ar/^{39}Ar$ en los esquistos pelíticos y la edad del despegue basal que separa los Alóctonos Inferior y Medio en el MTC se presentan en esta sección. Las dataciones absolutas en la evolución P–T de los terrenos de AP son esenciales para entender los procesos de subducción-exhumación. Mientras que la cronología de varios eventos del Alóctono Inferior del MTC se ha estudiado extensamente, las dataciones absolutas

de los eventos establecidos en el Alóctono medio se limitan a una edad $^{40}Ar/^{39}Ar$, y la edad del despegue de Bembibre-Ceán permanecía indeterminada. Por tanto, la datación de las milonitas ha permitido establecer la edad de las fases extensionales tempranas que condujeron al colapso del orógeno en los Complejos Alóctonos del NO de la Península Ibérica. Por último, en base a la petrografía, a las condiciones P–T y a la edad, se han propuesto correlaciones a pequeña escala entre litologías similares dentro del Alóctono Medio a través del Arco Ibero-Armoricano (ARTÍCULO 3).

El objetivo de la tercera etapa de este estudio ha consistido en la investigación de los esquistos azules Mesozoicos de Liberty Creek (en el terreno de Chugach, Alaska), que contienen abundantes anfíboles sódicos y lawsonita fresca. A pesar de que esta unidad no presenta una relación geológica con el área de estudio localizada en el NO del Macizo Ibérico, la investigación de esta litología empleando los mismos métodos citados anteriormente (ver apartado 2) ha proporcionado una perspectiva muy útil al trabajo desarrollado en la presente tesis doctoral. El estudio de los esquistos de Liberty Creek ha sido fundamental para entender las relaciones texturales de las litologías de AP del MTC. En comparación con los esquistos azules Paleozoicos del NO de Iberia, donde la mineralogía original ha sido modificada por los procesos de exhumación y/o retrogradación, o aparece preservada únicamente en los porfiroblastos de los minerales más resistentes, los esquistos de Liberty Creek representan un libro abierto a un universo de texturas originales (casi) inalteradas. Por tanto, su estudio ha constituido un complemento excelente a la investigación detallada en las dos primeras etapas de esta tesis doctoral. El margen convergente localizado al Sur de Alaska se compone de varios cinturones de dimensiones reducidas constituidos por rocas sedimentarias y volcánicas. Estas rocas presentan un metamorfismo en condiciones de esquistos azules y se disponen a lo largo de las Border Ranges, que separan los terrenos de Wrangellia y Chugach. La importancia de estos cinturones reside en su localización, constituyen los afloramientos más internos de este margen y por ello posiblemente preserven los vestigios de la subducción Triásico-Jurásica del terreno de Chugach bajo Wrangellia. En esta sección se presenta una descripción estructural, litológica y petrológica de los cinturones metamórficos de Seldovia y Liberty Creek junto con edades $^{40}Ar/^{39}Ar$, además de un estudio termobarométrico detallado mediante pseudosecciones de los tipos litológicos de esquistos de Liberty Creek. Finalmente, se incluye una discusión centrada en la evolución tectonothermal de los estadios tempranos de la subducción a lo largo del margen convergente de Alaska, en la que se proponen hipótesis para explicar la morfología de los afloramientos y su relación con las tasa de exhumación, que podrían extrapolarse a otros terrenos de AP (ARTÍCULO 4).

Por último, la cuarta etapa recoge las conclusiones de un proyecto conjunto Hispano-Francés que refleja los resultados del trabajo de numerosos autores durante varios años. Esta colaboración surge en el marco del convenio de codirección de esta tesis doctoral firmado entre

la Universidad Complutense de Madrid (UCM) y la Universidad de Rennes 1, y se ha llevado a cabo durante el progreso de la presente investigación, financiada por una beca asociada al proyecto CONSOLIDER (CGL2007-65338-C02-01) integrado por miembros de la UCM y de la Universidad de Salamanca, así como ha recibido apoyo económico del departamento de Géosciencies de la Universidad de Rennes 1. El objetivo principal de este proyecto ha sido establecer las correlaciones existentes entre las unidades alóctonas que afloran en el NO del Macizo Ibérico y en el Sur del Macizo Armoricano, tratando de unificar la terminología y su descripción. Las correlaciones se han establecido en base a las asociaciones litológicas, a la posición estructural, a la edad, a la geoquímica de los protolitos y a la evolución tectonothermal de las distintas unidades. El trabajo de campo se llevó a cabo en equipos mixtos con el fin de determinar si las litologías, estructuras, y evolución metamórfica de las distintas unidades eran o no similares a ambos lados de la bahía de Vizcaya, concluyéndose que se pueden agrupar en tres terrenos que se han denominado Alóctonos Inferior, Medio y Superior, que se disponen sobre una lámina alóctona que presenta características estratigráficas y afinidad petrológica con su autóctono relativo, habiéndose identificado en ambos macizos, y que se conoce como el Parautóctono (ARTÍCULO 5).

4. *Conclusiones*

De esta investigación se puede concluir que:

1. La Unidad de Ceán registra una evolución metamórfica en la que se pueden distinguir tres etapas: (i) un evento de MP-BT (M_1) asociado al comienzo de la subducción que únicamente ha quedado registrado en la parte basal de la secuencia, cuyas condiciones P-T aproximadas se han establecido en 350-380°C y 12-14 kbar. (ii) El metamorfismo progrado asociado a la subducción se desarrolló en facies de esquistos azules/eclogitas de BT (M_2) y se caracteriza por una evolución subsaturada en H_2O. Las condiciones del pico bárico se han establecido en 19-22 kbar, correspondientes a un enterramiento máximo de ca. 65-70 km. (iii) El metamorfismo asociado a la exhumación de la unidad (M_3/post-M_3) se desarrolló en dos etapas: (1) una etapa de descompresión casi isotérmica desde ca. 70 a ca. 30 km de profundidad, característica de una subducción lenta y prolongada, y (2) una fase de enfriamiento rápido una vez las rocas han alcanzado los niveles corticales superiores.

2. Los resultados obtenidos de la modelización petrológica en relación a los efectos del H_2O y del Fe_2O_3 en la evolución metamórfica de las rocas en facies de esquistos azules permiten establecer estimaciones de primer orden en los modelos geodinámicos que podrían tener una aplicación general en la investigación de rocas con una composición "similar". (i) Esta investigación propone que en presencia de una

proporción modal significativa de lawsonita el metamorfismo prograd en zonas de subducción puede tener lugar en condiciones de subsaturación en in H_2O. Posteriormente, la transición entre la facies de esquistos azules con lawsonita y la facies de esquistos verdes podría implicar una importante liberación de H_2O durante la retrogradación, que procedería de la desestabilización de dicho mineral. (ii) La proporción de hierro férrico considerada en la modelización petrológica influencia notablemente el equilibrio de fases minerales. El porcentaje estimado de Fe_2O_3 mediante el análisis de roca total podría no reflejar el estado de oxidación real de la roca durante la evolución metamórfica principal. Este estudio propone que la proporción analizada podría ser el resultado de la sensibilidad de dicho componente a variaciones ambientales tales como la alteración superficial de la roca, incluso en muestras aparentemente frescas.

3. Por tanto, el cálculo de pseudosecciones P–T–X(H_2O/Fe_2O_3), combinado con un estudio petrográfico exhaustivo, además de un amplio conocimiento de la química mineral y las relaciones texturales, resulta necesario para establecer si existieron condiciones de subsaturación en H_2O (u otro/s fluidos) durante la etapa prograda de la evolución metamórfica de la roca, así como para determinar una aproximación razonable a su estado de oxidación real, lo que posibilitará establecer de forma precisa la evolución de las condiciones P–T.

4. La edad del pico metamórfico en facies de esquistos azules se ha estimado en ca. 363±2 Ma mediante $^{40}Ar/^{39}Ar$ en fengitas de los esquistos pelíticos. El mismo método aplicado en moscovitas de las milonitas cuarzo-feldespáticas que representan el despegue de Bembibre-Ceán, en la base de la Unidad de Ceán, proporcionó una edad de ca. 337±3 Ma, interpretada como la edad que marca el comienzo de la tectónica extensional tras el apilamiento de las láminas alóctonas, y que condujo al colapso gravitacional del orógeno. Las diferencias entre el evento de AP–BT y el comienzo de la tectónica extensional, sugieren que el Complejo de Malpica-Tui se exhumó a una velocidad de 2-2.5 mm/año. Los datos obtenidos apoyan la equivalencia establecida entre la Unidad de Ceán y el terrreno homólogo en el Macizo Armoricano, la Unidad Superior de la Isla de Groix. Ambos terrenos experimentaron una evolución en facies de esquistos azules datada en ca. 360–370 Ma, que se interpreta como la subducción durante finales del Devónico-comienzos del Carbonífero del margen norte de Gondwana bajo Laurussia, al comienzo de la colisión Varisca.

ANNEX II

1. *Introduction*

L'affaissement du froid et dense matériel lithosphérique dans les zones de subduction est le principal moteur de la tectonique des plaques. La diminution de la matière corticale à des profondeurs mantéliques est à l'origine des roches métamorphiques de haute pression (HP) et de la température faible à moyenne (B/M-T), comme schistes bleus et éclogites. Ces roches affleurent souvent dans les zones de suture de la ceinture orogénique et sont considérés comme des marqueurs des zones de subduction, actifs et inactifs. Les associations de minéraux qui sont stockés plus de renseignements concernant le processus de convergence entre les frontières de plaques, en fournissant de précieux indices pour comprendre l'histoire thermique de la planète Terre. Dans ce contexte, l'étude de la paléogéographie et la dynamique des plaques lithosphériques au cours de l'environnement péri-Gondwana Paléozoïque a été le cadre de nombreux travaux au cours des dernières décennies, de nombreuses questions demeurent. La connaissance des caractéristiques de cette subduction, sa polarité, sa chronologie, les conditions physiques de pointe a atteint ou de la géométrie et les caractéristiques des chemins P-T fourniraient de nouvelles données pour comprendre l'évolution de ces terrains au cours de la collision varisque.

2. *Objectifs et méthodologie*

Cette thèse Le travail présenté dans cette thèse comprend 1) une étude pétrologique détaillée, à l'aide des pseudosections, des roches du faciès des schistes bleus du Complexe de Malpica-Tui (MTC; Galice, Espagne), 2) une étude géochronologique par la méthode $^{40}Ar/^{39}Ar$ de ces roches et 3) une corrélation entre les unités du MTC avec leurs équivalents dans le domaine sud-armoricain.

Les objectifs spécifiques sont :

(1) Une étude pétrologique et thermobarométrique détaillée des schistes de Ceán et des métabasites de Cambre, à l'aide des méthodes suivantes:

- Une revue bibliographique de la région étudiée ainsi que des autres Complexes Allochtones du NO de l'Espagne, afin d'obtenir une perspective large du contexte géologique.

- Echantillonage et collection des données de terrain.

- Etude pétrographique de plusieurs lames minces pour chacun des échantillons sélectionnés.

- Etude de la composition chimique de minéraux à l'aide d'une microsonde électronique et d'un microscope électronique à balayage. Les analyses minérales et les cartes aux rayons X ont été effectuées avec une microsonde JEOL-Superprobe JXA-8900M, équipée de cinq spectromètres à l'ICTS-National Electronic Microscopy Centre de l'Université Complutense de Madrid (Centro Nacional de Microscopía Electronica; http://www.cnme.es). Les images en électrons secondaires ont été obtenues avec une microscope électronique à balayage JEOL JSM-820 équipé d'un microanalyseur EDX au Research Assistance Centre of Geological Techniques de l'Université Complutense de Madrid (CAI de Técnicas Geológicas de la UCM; http://www.ucm.es/centros/webs/cai5134).

- Analyses géochimiques roches totales de chacun des échantillons représentatifs par fluorescence X (X-ray fluorescence spectroscopy – XRF). FeO (vs. Fe_2O_3) a été déterminé par titration. Toutes les analyses ont été effectuées par Activation Laboratories Ltd. (Actlabs, Canada; http://www.actlabs.com). Les méthodes utilisées pour l'analyse de roche totale (XRF et titration) sont décrites dans la section 1.2 du Chapitre 1.

- Modélisation numérique des équilibres de phases par la construction de pseudosections à l'aide du programme THERMOCALC (Powell & Holland, 1988) et Perple_X (Connolly, 1990).

(2) d'établir une trajectoire P–T détaillée pour ces unités afin de caractériser le processus de subduction et l'évolution consécutive.

(3) Contraindre ces processus en temps par l'utilisation de la datation $^{40}Ar/^{39}Ar$ par étape de température sur population de grains ou grains individuels de muscovite.

(4) Comparer l'évolution métamorphique de ces unités à celle de leurs équivalents dans le domaine sud armoricain et intégrer les données obtenues dans l'évolution de la chaîne varisque européenne.

Les méthodologies de la modélisation pétrologique et de la datation $^{40}Ar/^{39}Ar$ par étape de température sont détaillées respectivement dans les sections 1.5.2 et 3.2.2.

Les détails analytiques, comme les paramètres des analyses à la microsonde électronique, sont décrits en détail pour chaque type de roche en Chapitre 3.

3. *Approche de recherche et contributions*

Cette thèse est présentée sous forme d'une compilation de publications qui ont été publiées (articles 1, 2 et 4) ou soumises (articles 3 et 5) dans des revues internationales à comité de lecture.

Le travail de recherche a été divisé en quatre étapes. Les trois premières étapes sont présentées sous forme de sections dans le Chapitre 3, la quatrième dans le Chapitre 4.

La première étape concerne l'étude des schistes de Ceán. Elle représente la continuation du travail initié lors de mon stage de Master 2. Les schistes pélitiques des niveaux inférieurs de la série contiennent de nombreux porphyroblastes de grenat qui préservent les foliations les plus anciennes décrites dans ces roches. Les inclusions dans la première génération de grenat permettent d'étudier la phase de déformation et les conditions P–T liées à la subduction. La seconde génération de grenat contient une paragenèse initiale à chloritoïde-glaucophane qui est l'un des principaux indicateurs de haute pression dans les métapélites (p.ex. Kiénast & Triboulet, 1972; Kryza *et al.*, 1990; Katagas, 1980; Theye *et al.*, 1992; Chopin, 1981; Song *et al.*, 2007; Wei & Song, 2008; El-Shazly & Liou, 1991; Warren & Waters, 2006). Cette paragenèse n'a jamais été décrite auparavant dans le Massif Ibérique. L'un des but de cette étude était donc de documenter cette paragenèse et ses caractéristiques pétrologiques et conditions P–T de formation (ARTICLE 1).

Les résultats de cette première étape de recherche comprennent une première estimation des conditions P–T et de leur évolution dans les schistes de Ceán. Néanmoins, ils soulèvent également des questions intéressantes sur le rôle clé des constituants chimiques tels que H_2O ou Fe_2O_3. Comme dans les roches métabasiques, les assemblages de haute pression dans les roches métapélitiques sont très sensibles à la quantité disponible de ces constituants. Afin d'obtenir des réponses à ces questions et d'affiner les conditions P–T et leur évolution dans les schistes de Ceán, l'effet de ces constituants a été étudié plus en détail. Les incertitudes associées au rôle de H_2O et de l'état d'oxydation du fer sont principalement liées à la difficulté d'estimer correctement leurs proportions initiales par des techniques d'analyse quantitative (p.ex. Guiraud *et al.*, 2001; Diener & Powell, 2010; Rebay *et al.*, 2010). L'utilisation des pseudosections calculées dans des systèmes chimiques variés a permis d'estimer la proportion des deux constituants pendant l'évolution prograde des schistes de Ceán et les résultats ont donné des contraintes de premier ordre pour les modèles géodynamiques qui peuvent avoir une application générale pour l'étude des roches similaires (ARTICLE 2).

La deuxième étape est centrée sur l'étude des roches métabasiques de Cambre. Cette lithologie a été interprétée comme des schistes bleus fortement rétromorphosés, contenant

des pseudomorphes de lawsonite (Rodríguez, 2005). La lawsonite est un silicate hydraté de calcium et aluminium qui cristallise dans des conditions de moyenne à haute pression et basse température (p.ex. Crawford & Fyfe, 1965; Liou, 1971; Pawley, 1994; Schmidt & Poli, 1994; Schmidt, 1995; Comodi *et al.*, 1996). C'est donc un autre minéral typique des terrains de haute pression, indicateur d'un métamorphisme dans le faciès des schistes bleus et, plus rarement, éclogite (p.ex. Maruyama *et al.*, 1996; Tsujimori *et al.*, 2006 et leurs références). Pendant la décompression, la lawsonite se décompose facilement en minéraux secondaires (épidote, micas blancs, chlorite et albite) et est donc plus souvent trouvée sous forme de pseudomorphes que de cristaux frais. A cause de sa forte teneur en H_2O, la lawsonite est une source majeure d'eau dans les systèmes mafiques de HP/BT et joue un rôle clé dans le transport de l'eau dans les zones de subduction. Lors de la modélisation numérique des équilibres de phases, la saturation en H_2O est souvent assumée, y compris dans des conditions de HP. Néanmoins, des études récentes (Ballèvre *et al.*, 2003; Clarke *et al.*, 2006; López-Carmona *et al.*, 2013) ont montré que la cristallisation de la lawsonite pouvait mener à une sous-saturation en H_2O lors de l'évolution prograde. L'évolution métamorphique des roches métabasiques rétromorphosées à pseudomorphes de lawsonite a donc été étudiée en utilisant des pseudosections et tenant compte de la possibilité d'une évolution prograde sous-saturée en H_2O. Les effets de la variation d'oxydation du fer ont également été examinés. La richesse minéralogique des métabasites de Cambre permet une bonne estimation de leur évolution P–T. Les résultats obtenus sont cohérents avec ceux obtenus des roches métapélitiques et les complètent, permettant ainsi d'établir l'histoire complète d'Allochtone moyen du Complexe de Malpica-Tui. Sont présentés dans cette section aussi les âges $^{40}Ar/^{39}Ar$ obtenus pour l'événement de HP dans les schistes métapélitiques et dans le détachement de base qui sépare les Allochtones moyen et inférieur du Complexe de Malpica-Tui. Alors que la chronologie des différents événements dans Allochtone inférieur du MTC a été largement étudiée, les données pour Allochtone moyen se limitaient jusqu'à ce jour à un âge $^{40}Ar/^{39}Ar$, et l'âge du détachement de Bembibre-Ceán n'était pas contraint. La datation de ces mylonites a permis de dater des phases précoces du collapse gravitationnel de l'orogène dans les Complexes Allochtones du NO ibérique. Finalement, toutes ces données ont permis de proposer des corrélations avec des lithologies similaires à travers l'arc Ibéro-Armoricain (ARTICLE 3).

La troisième étape concerne l'étude des schistes bleus mésozoïques de Liberty Creek en Alaska qui contiennent des amphiboles bleus et de la lawsonite fraîche. Bien que ces unités ne soient pas géologiquement liées au principal terrain d'étude dans le NO ibérique, leur investigation a été très profitable pour une meilleure compréhension de nombreuses caractéristiques des roches de HP de Galice. Comparés aux schistes bleus paléozoïques du Massif Ibérique, dont la minéralogie d'origine est masquée par des processus d'exhumation et de rétromorphose, les schistes de Liberty Creek offre une vue imprenable sur des textures et relations minérales quasi immaculées. La marge convergente de l'Alaska sud contient plusieurs

petites chaînes de roches sédimentaires et volcaniques métamorphisées dans le faciès des schistes bleus, localisées le long de la faille de Border Ranges, au contact entre les terrains de Wrangellia et Chugach. Ces terrains contiennent probablement le plus ancien enregistrement de la subduction triaso-jurassique sous la Wrangellia. Est présentée une description des relations structurales, lithologiques et pétrologiques dans les chaînes métamorphiques de Seldovia et Liberty Creek ainsi qu'une thermobarométrique étude détaillée, basée sur la modélisation des schistes bleus à lawsonite et épidote de Liberty Creek à l'aide des pseudosections. Finalement, une discussion de l'évolution tectonique et des conditions P-T pendant les phases précoces de la subduction le long de la marge sud de l'Alaska a permis de formuler des hypothèses qui peuvent être extrapolées aux autres terrain de HP pour expliquer la préservation de la forme des affleurements de schistes bleus et les relations avec les vitesses d'exhumation (ARTICLE 4).

Finalement, une quatrième étape montre les résultats d'un projet franco-espagnol, le fruit du travail d'un grand nombre de participants sur plusieurs années. Ce projet a été initié dans le cadre de cette thèse en cotutelle entre l'Université Complutense de Madrid et l'Université Rennes 1. Ce projet a été supporté par un financement du projet CONSOLIDER (CGL2007-65338-C02-01) incluant également des participants de l'Université de Salamanque et a également reçu un support financier de Géosciences Rennes. Le but de ce projet était d'établir une corrélation entre les unités allochtones exposées au NO du Massif Ibérique et au sud de Massif Armoricain. La corrélation a été établie sur la base des associations lithologiques, la position structurale, âge et géochimie des protolithes ainsi que l'évolution tectono-métamorphique. Les unités des deux côtés du Golfe de Gascogne sont regroupées en trois ensembles nommés Allochtone Supérieur, Moyen et Inférieur. Une unité allochtone sous-jacente qui présente des affinités stratigraphiques et pétrologiques avec son autochtone a également été identifiée dans les deux domaines et désignée par le terme Parautochtone (ARTICLE 5).

4. *Conclusions*

Ce travail de recherche a abouti aux conclusions suivantes:

1. L'unité de Ceán a enregistré une évolution en trois étapes: (i) un métamorphisme précoce (M_1) de type MP-BT, lié à la subduction, approximativement contraint à 350-380°C et 12-14 kbar, et qui est uniquement préservé dans la partie basale de la séquence. (ii) Un métamorphisme prograde de type schistes bleus / éclogites de BT (M_2), associé à la subduction. Il est caractérisé par une évolution sous-saturée en H_2O qui culmine à 19-22 kbar, ce qui correspond à un enfouissement maximum de ca. 65-70 km. (iii) Un métamorphisme associé à l'exhumation (M_3/post-M_3) qui s'est développé en deux sous-étapes : (1) une décompression sub-

isotherme de ca. 70 à ca. 30 km de profondeur, caractéristique d'une subduction lente, de longue durée et (2) une phase de refroidissement rapide au moment où les roches ont atteint les niveaux crustaux supérieurs.

2. Les résultats obtenus de la modélisation numérique des effets de H_2O et Fe_2O_3 sur l'évolution métamorphique des roches du faciès des schistes bleus donnent des contraintes de premier ordre sur les modèles géodynamiques et peuvent avoir une application générale pour des roches de composition "similaire". (i) Ce travail propose que le métamorphisme dans les zones de subduction peut avoir lieu dans des conditions de sous-saturation en H_2O, liées à la cristallisation de la lawsonite. La subséquente transition du faciès des schistes bleus dans le faciès des amphibolites/schistes verts implique une importante hydratation qui résulte de la déstabilisation de la lawsonite. (ii) La proportion de fer ferrique dans les roches a une forte influence sur les équilibres de phases. Les valeurs analysées de Fe_2O_3 ne reflètent pas nécessairement l'état oxydation pendant l'évolution métamorphique et sont probablement facilement modifiées lors de l'altération superficielle même dans des échantillons en apparence frais.

3. L'utilisation de pseudosections P-T-X(H_2O/Fe_2O_3) ensemble avec une analyse pétrographique détaillée et une étude approfondie de la composition chimique des minéraux et de leurs relations texturales est nécessaire pour estimer le taux de saturation en fluides et le degré oxydation pendant le métamorphisme dans les zones de subduction. Sans ces informations, les conditions P-T du métamorphisme ne peuvent pas être correctement estimées.

4. L'âge du pic du métamorphisme schistes bleus a été contraint à 363±2 Ma par la méthode $^{40}Ar/^{39}Ar$ par paliers de température sur muscovite phengitique des schistes pélitiques. La datation $^{40}Ar/^{39}Ar$ de la muscovite des mylonites quartzo-feldspathiques du détachement de Bembibre-Ceán, situé à la base de l'unité de Ceán, a donné un âge de ca. 337±3 Ma, interprété comme le début de la tectonique extensive post-nappe qui a conduit au collapse gravitationnel de l'orogène. La différence d'âge entre l'événement HP-BT et le début de la tectonique post-nappe suggère une vitesse d'exhumation de 2-2.5 mm/an pour le Complexe de Malpica-Tui. D'autre part, ces âges supportent l'équivalence entre l'unité de Ceán et l'unité supérieure de l'Ile de Groix dans le Massif Armoricain et suggèrent que les deux terrains partagent le même événement en faciès des schistes bleus vers 360-370 Ma qui peut représenter la subduction tardi-dévonienne-carbonifère précoce de la marge nord du Gondwana sous le Laurussia, au début de la tectonique varisque.